

**Petrologic and geochemical characteristics of  
the Krivaja-Konjuh ophiolite complex (NE Bosnia and Herzegovina) –  
petrogenesis and regional geodynamic implications**

**INAUGURAL-DISSERTATION**

zur Erlangung der Doktorwürde der  
Mathematisch-Naturwissenschaftlichen Gesamtfakultät  
der Ruprecht-Karls-Universität Heidelberg

vorgelegt von  
**Diplom-Geologe**  
**Branimir Šegvić**  
aus Zadar, Kroatien

Tag der mündlichen Prüfung: 05. Februar 2010



**Petrologic and geochemical characteristics of  
the Krivaja-Konjuh ophiolite complex (NE Bosnia and Herzegovina) –  
petrogenesis and regional geodynamic implications**

**INAUGURAL-DISSERTATION**

zur Erlangung der Doktorwürde der  
Mathematisch-Naturwissenschaftlichen Gesamtfakultät  
der Ruprecht-Karls-Universität Heidelberg

vorgelegt von

**Diplom-Geologe**

**Branimir Šegvić**

aus Zadar, Kroatien

**Gutachter:**

Prof. Dr. Rainer Altherr (Universität Heidelberg)

Prof. Dr. Alan Woodland (Universität Frankfurt)

Tag der mündlichen Prüfung: 05. Februar 2010



***Mojim roditeljima***

**(Meinen Eltern)**



# TABLE OF CONTENTS

<b>ABSTRACT</b>	1
<b>KURZFASSUNG</b>	5
<b>1. INTRODUCTION</b>	9
1.1. Prologue	9
1.2. Aims of dissertation	10
1.3. Structure of the thesis	10
<b>2. GEOGRAPHICAL SETTING</b>	13
<b>3. GEOLOGICAL SETTING</b>	17
3.1. A modern conception of Tethyan ophiolites	17
3.2. The Central Dinaridic Ophiolite Belt (CDOB)	19
3.3. Geology of the Krivaja-Konjuh Ophiolite Complex (KKOC)	21
<b>4. PETROGRAPHY AND MINERAL CHEMISTRY OF THE KKOC ROCKS</b>	27
4.1. Sampling locations	27
4.2. Ultramafic rocks	30
4.2.1. Rock types, textures and structures	30
4.2.1.1. Plagioclase lherzolite	31
4.2.1.2. Spinel lherzolite	33
4.2.1.3. Plagioclase lherzolite with pyroxene streaks	35
4.2.1.4. Plagioclase lherzolite with poikiloblastic texture	35
4.2.1.5. Equigranular spinel lherzolite	35
4.2.1.6. Spinel-olivine websterite	35
4.2.1.7. Dunite (cumulate ultramafic rocks)	36
4.2.1.8. Podiform chromitite	36
4.2.1.9. Summary of petrographic features	36
4.2.2. Mineral chemistry	38
4.2.2.1. Olivine	38
4.2.2.2. Orthopyroxene	39
4.2.2.3. Clinopyroxene	44
4.2.2.4. Spinel	47
4.2.2.5. Plagioclase	50
4.2.2.6. Other phases	51

<b>4.3. Metamorphic sole</b>	52
<b>4.3.1. Rock types, textures and structures</b>	52
4.3.1.1. Granoblastic amphibolites	54
4.3.1.1.1. <i>Clinozoisite-sapphirine amphibolite</i>	54
4.3.1.1.2. <i>Corundum amphibolite</i>	54
4.3.1.1.3. <i>Epidote-ilmenite amphibolite</i>	56
4.3.1.1.4. <i>Amphibolite</i>	58
4.3.1.2. Porphyroblastic garnet-diopside amphibolite	59
4.3.1.2.1. <i>Rutile-garnet-diopside amphibolite</i>	59
4.3.1.2.2. <i>Contact Opx-bearing garnet-diopside amphibolite</i>	59
4.3.1.2.3. <i>Titanite-garnet-diopside amphibolite</i>	60
4.3.1.2.4. <i>Garnet-diopside amphibolite</i>	61
4.3.1.3. Garnet-diopside-hypersthene amphibolite	61
4.3.1.3.1. <i>Porphyroblastic garnet-diopside-hypersthene amphibolite</i>	61
4.3.1.3.2. <i>Granoblastic garnet-diopside-hypersthene amphibolite</i>	61
4.3.1.4. Diopside-amphibolite gneiss	62
4.3.1.5. Plagioclase-garnet-diopside gneiss	62
<b>4.3.2. Mineral chemistry</b>	68
4.3.2.1. Amphibole	68
4.3.2.2. Garnet	71
4.3.2.3. Plagioclase	73
4.3.2.4. Clinopyroxene	75
4.3.2.5. Orthopyroxene	76
4.3.2.6. Other phases	77
<b>5. GEOCHEMISTRY OF KKOC ROCKS</b>	81
<b>5.1. Ultramafic rocks</b>	81
<b>5.1.1. Peridotites</b>	81
<b>5.1.2. Olivine websterites and dunites</b>	93
<b>5.2. Metamorphic sole</b>	97
<b>6. DISCUSSION</b>	107
<b>6.1. Geothermobarometry</b>	107
<b>6.1.1. Introduction</b>	107
<b>6.1.2. Peridotites</b>	110
6.1.2.1. Geothermometers	110
6.1.2.2. Geobarometer	112
<b>6.1.3. Metamorphic rocks</b>	113
6.1.3.1. Geothermometers	113
6.1.3.2. Geobarometers	117
<b>6.2. Petrogenesis of peridotitic rocks</b>	127
<b>6.2.1. Mantle peridotites</b>	127
6.2.1.1. Composition and equilibration of KKOC upper mantle	127



6.2.1.2.	Nature of upper mantle dynamics	131
6.2.1.3.	KKOC geotectonic setting and regional implications	135
<b>6.2.2.</b>	<b>Pyroxenites, dunites, and chromitites</b>	140
<b>6.3.</b>	<b>Petrogenesis of metamorphic rocks</b>	150
<b>6.3.1.</b>	<b>Protolith and its original geotectonic setting</b>	150
<b>6.3.2.</b>	<b>Conditions and model of metamorphism</b>	157
6.3.2.1.	Metamorphic evolution recorded in petrographic characteristics	157
6.3.2.2.	Mineral assemblages and P-T conditions of metamorphism	160
6.3.2.3.	<i>P-T-t</i> path of metamorphism	164
6.3.2.4.	Geodynamic significance of metamorphism	166
<b>7.</b>	<b>CONCLUSIONS</b>	169
<b>8.</b>	<b>REFERENCES</b>	173
<b>APPENDIX</b>		193
A.	Materials	193
B.	Analytical techniques	195
C.	Mineral chemistry	201
D.	Bulk-rock geochemistry	298

## ABSTRACT

Based on its petrological and geochemical characteristics, the Krivaja-Konjuh Ophiolite Complex (KKOC) and the surrounding ophiolitic mélange make an integral part of the Central Dinaridic Ophiolite Belt (CDOB) of the Internal Dinarides. The Jurassic ultramafic and mafic sequences form about 80 % of the KKOC, whereas the rest belongs to the metamorphic sole, which is found concentrating in the northwestern and southern margins. Due to the emplacement processes, the main peridotite mass is reported to possess a highly dismembered block-like structure.

The KKOC ultramafic rocks, comprising lherzolites, pyroxenites, dunites, along with rocks from the metamorphic sole and chromitites were subjected to an extensive analytical investigation, which included electron microprobe analysis (EMPA), secondary electron microscopic (SEM) studies, x-ray fluorescence (XRF) analysis and inductively coupled plasma mass spectrometry (ICP-MS), in order to reveal their mineralogical, geochemical and petrological characteristics.

The lherzolitic modal mineralogy consists of olivine, orthopyroxene, clinopyroxene, spinel and occasionally plagioclase. Most of the analysed samples are characterised by a mantle porphyroclastic texture and a foliated structure. With respect to clear differences in modal mineralogy, as well as in phase and bulk-rock chemistry, one is able to distinguish two main varieties among the KKOC lherzolites. The first one renders spinel lherzolites, whilst the second variety is known as plagioclase lherzolites.

Geothermometric estimations yielded the main equilibration range, for both spinel and plagioclase lherzolites, to range from 809 to 1012 °C (T1). The Fe-Mg exchange between olivine and spinel provided a temperature range of 550 to 682 °C (T2), which is found to be indicative for subsolidus re-equilibration processes. Using the oceanic and rift-ridge geotherms, the equilibration pressures extending from 1.2 to 2.0 GPa (ca. 40-65 km depth) were inferred for T1 temperatures. The final equilibration level marked by the T2 temperatures happened under pressures below 1.0 GPa.

Numerous geochemical parameters are pointing to the KKOC lherzolites as fertile solid residues, which, before metamorphism, underwent low to moderate degrees of MOR melting. The mineral chemistry of spinel and the REE normalisation levels (relative to chondrite) yielded an average batch melting degree of ~ 7.7 % for spinel lherzolites. Based on this estimation and constant values of melt production rate and depth of melting onset, the KKOC oceanic crust thickness is calculated, having been around 5.4 km. This crustal thickness would imply a ridge spreading rate of 32 mm/year, which defines the KKOC ridge system to have been relatively slow-spreading (< 55 mm/year). The modern analogues of such MOR settings exist in the Northern Atlantic and the Indian Ocean. The most-eastern segment of the KKOC is, however reported to deviate from the MOR fertile geochemistry.

The occurrence of pargasitic amphibole, coupled with a Cr-enriched spinel, call for enhanced mantle melting (~ 15 %) in a SSZ-type of setting. Contrary to the amphibole formation in a SSZ mantle wedge, geochemical evidences clarify the growth of plagioclase through sub-solidus equilibration (T2) and melt metasomatism of the lithospheric mantle at a MOR-type setting. It can be concluded that the main part of the KKOC lherzolites presents a

segment of mantle column, which experienced relatively fast and continuous adiabatic ascent under the spreading MOR environment. The main stage of equilibrium (T1) for the coarse-grained and porphyroclastic lherzolites is advocated to have occurred shortly after partial melting. By further ascent, the KKOC mantle portion passed the dry solidus having experienced different mineralogical adjustments (equilibration) (T2), ensued by melt metasomatism, which had led to plagioclase formation.

Pyroxenites (olivine websterites) are reported to crop out sporadically in the NW part of KKOC, where they form lenses up to 20 cm wide. They are always associated with dominant plagioclase lherzolites. Mineral paragenesis of pyroxenites comprises big euhedral grains of ortho- and clinopyroxene, which define a recondite cumulate texture. The intercumulus space is occupied by small to medium-grained mosaic olivine and rarely spinel. Occasionally, a mesh of altered plagioclase rims the spinel grains. Petrological and geochemical evidences suggest that the KKOC pyroxenites formed under high pressures and temperatures as 'deeply originated' ultramafic cumulates. This required higher melting degrees of an already depleted MORB source. It is suggested that crystallisation took place in thermal conduits, located under the ocean ridge system, where significant cooling of conductive melt occurs. The corresponding clinopyroxene mineral characteristics of pyroxenites and surrounding plagioclase lherzolites imply that both rocks underwent a common late-stage metasomatic path.

Dunites were recovered from two locations placed on the western and eastern margins of KKOC. They possess a typical cumulate texture, containing major olivine (~ 90 vol.%) and some minor clinopyroxene and spinel. The most striking geochemical and textural characteristics are a concave-upward 'U'-shaped REE pattern with a clear Eu positive anomaly and coarse, massive euhedral grains of olivine. These features define the KKOC dunites as highly refractory ultramafic rocks that underwent partial melting, accompanied by a 'boninitic fluid' impregnation process. A chromitite body is reported from the Duboštica locality (western KKOC), characterised by a high Cr content in spinel ( $Cr\# \approx 80$ ). This calls upon for the influence of the subduction-related, most probably boninitic melts as well, as parental to this mineralization. It is inferred that the KKOC dunites and associated chromitites actually represent the uppermost part of the transitional zone (crust-mantle transition) formed by crystal fractionation from a hypothesised crustal magma chamber. Mineralogical and geochemical evidences further suggest that this process was followed by a sizable melt-rock metasomatism. Initially, the chromitites segregated from the invading (boninitic) melt, which subsequently percolated neighbouring rocks, producing dunites.

Between the two major KKOC peridotite blocks, an elongated metamorphic domain is located. The northern part of the domain actually comprises only small, scattered metamorphic occurrences, whereas the main metamorphic portion is found southwards, around the villages of Duboštica and Vijaka. Within the KKOC metamorphic unit, a variety of metamorphic paragenesis, textures and structures was recognised. Textures are either crystalloblastic or porphyroblastic. The rock structures are more often than not parallel, showing an alternation of 'white' and 'black' rock segments. The differences in modal mineralogy reflect discrepancies in the protolith geochemistry, but they also witness different conditions of metamorphism. Based on the general classification criteria set for

metamorphic rocks, the following petrographic varieties among the KKOC metamorphic rocks were distinguished: (1) *granoblastic amphibolite*, (2) *garnet-diopside amphibolite*, (3) *garnet-diopside-hypersthene amphibolite*, (4) *diopside amphibolites* and (5) *plagioclase-garnet-diopside gneiss*. Major and trace element geochemistry, as well as petrographic data show that two-thirds of KKOC metamorphic rocks bear geochemical signatures of mafic to ultramafic gabbroic rocks, whereas the rest corresponds to more evolved basalts of tholeiitic affinity. In the case of metacumulates, a supra-subduction-zone (SSZ) type of geotectonic setting was inferred, whereas for metabasalts the MORB-type of geotectonic affiliation was evident.

Geothermobarometric calculations, based on the phase chemistry of different coexisting minerals, yielded ranges of temperature and pressure for the different KKOC petrographic varieties, as follows: (a) ~ 880 °C and 0.90-1.30 GPa for granoblastic amphibolites, (b) 802-1028 °C and 0.94-1.40 GPa for garnet-diopside amphibolites, (c) for garnet-diopside-hypersthene amphibolites the metamorphic conditions are analogue to the previous variety, recording slightly reduced pressure values, (d) 0.84-0.89 GPa for diopside amphibolites, with no temperature data, and (e) 729-890 °C and 1.10-1.60 GPa for plagioclase-garnet-diopside gneisses. Based on geothermobarometric calculations and textural characteristics of the rocks, hypothetical clockwise *P-T-t* paths or trajectories were constructed, suggesting that the plagioclase-garnet-diopside gneisses present the deepest parts of the subducted slab (~ 30-42 km), followed by the garnet-diopside and garnet-diopside-hypersthene amphibolites (~ 24-35 and ~ 24-30 km, respectively). The shallowest domains of the metamorphosed oceanic crust belong to the granoblastic amphibolites, approximating from 4 to 30 km depths.

Due to the striking similarities of CDOB with ophiolitic complexes in Albania and Greece, the geodynamic evolution of KKOC is bound to the Mesozoic evolution of the Pindos Ocean, a Tethyan back-arc type of ocean. The generation of KKOC commenced in the Late Triassic by Pindos opening and subsequent Late Triassic to Early Jurassic ocean-spreading and detachment of the Drina-Ivanjica element from the Adriatic microplate. This extensional processes might have lasted for some 30 to 40 Ma, when in the Early to Middle Jurassic (Bajorcian-Taorcian period), due to the continuous northwards movement of Africa, an intra-oceanic NE dipping subduction took place, indicating an overall space shortening. Strong petrological and geochemical evidences imply the proximity of a Dinaridic intra-oceanic subduction zone and a KKOC mantle domain. Furthermore, in order to reconcile the features of two contrasting geotectonic settings (MOR and SSZ) displayed by almost all KKOC lithological units, one suggests that a subducted slab must have been placed under the Krivaja-Konjuh mantle domain. Such a scenario is logical with respect to the presence of dunites, which are normally bound to SSZ boninitic melts. The existence of an island arc should be expected, but the direct proof has not been relieved yet. The metamorphic sole is also related to such a defined intra-oceanic subduction and underplating of the cold oceanic crust under the hot mantle wedge. Part of the oceanic crust is found deeply subducted, having recorded the highest metamorphic grades. During the late Jurassic to early Cretaceous transition period, the subduction trench collided with the Adriatic microplate, and the KKOC among other CDOB ultramafic complexes was thrust southwestwards on the

Adriatic carbonate platform. Throughout the emplacement, the eastern KKOC mantle portion was most probably tectonically exhumed along the ancient subduction channels, causing an erosion of the above placed plagioclase-containing lithospheric mantle (impregnation zone). This resulted in the present-day placement of spinel lherzolites of the Konjuh domain at the same attitude with the plagioclase lherzolites of the western Krivaja segment, whereas the metamorphic sole rocks are found situated in-between the two.

## KURZFASSUNG

Der Krivajah-Konjuh Ophiolith-Komplex (KKOC) und die umgebende Ophiolithische Mélange sind wichtige Bestandteile des Zentral-Dinaridischen Ophiolith-Gürtels (CDOB) der internen Dinariden. Diese jurassischen ultramafischen und mafischen Gesteinssequenzen bilden ca. 80 % des KKOC; der restliche Teil besteht aus Gesteinen der „metamorphic sole“, die vor allem in den nordwestlichen und südlichen Randbereichen des KKOC zu finden sind. Auf Grund des Platznahme-Prozesses ist die peridotitische Hauptmasse des KKOC „dismembered“, d.h. in zahlreiche tektonische Blöcke zerlegt.

Die ultramafischen Gesteine des KKOC umfassen Lherzolithe, Pyroxenite und Dunite. Diese wurden zusammen mit den Gesteinen der „metamorphic sole“ und Chromititen im Detail untersucht, wobei neben der Polarisationsmikroskopie auch die Elektronenstrahl-Mikrosonde (EMPA), das Rasterelektronenmikroskop (SEM), das Röntgenfluoreszenzspektrometer (XRF) und das ICP-MS zum Einsatz kamen.

Der Modalbestand von Lherzolithen umfasst Olivin, Orthopyroxen, Clinopyroxen, Spinell und manchmal auch Plagioklas. Die meisten der untersuchten Proben sind foliiert und porphyroklastisch. Innerhalb der Lherzolite lassen sich auf Grund des Mineralbestandes, der Mineralchemie und der Gesamtgesteinschemie zwei unterschiedliche Typen unterscheiden: Spinell-Lherzolithe und Plagioklas-Lherzolithe.

Geothermometrische Abschätzungen zeigen, dass die Gleichgewichtstemperaturen für beide Lherzolithtypen bei 809 – 1012 °C liegen (T1). Der Fe-Mg-Austausch zwischen Olivin und Spinell liefert deutliche geringere Temperaturen von 550 – 682 °C (T2). Dies ist durch eine Reäquilibration im Subsolidus-Bereich bedingt. Unter Zuhilfenahme der ozeanischen Rift-Geotherme ergeben sich für T1 Drücke von 1.2 – 2.0 GPa, was einer Tiefenlage von 40 – 65 km entspricht. Den T2 Temperaturen entsprechen Drücke von weniger als 1.0 GPa.

Zahlreiche geochemische Parameter belegen einen fertilen Charakter der KKOC-Lherzolithe, die nur einem geringen Aufschmelzgrad unterlagen. Sowohl der Chemismus des Spinells als auch die REE-Gehalte weisen auf einen durchschnittlichen ehemaligen Gleichgewichts-Aufschmelzgrad („batch melting“) von ~ 7.7 % für die Spinell-Lherzolithe hin. Basierend auf diesem Wert ergibt sich eine Krustenmächtigkeit von ca. 5.4 km, wenn man eine konstante Schmelzmenge und Tiefe des Schmelzbeginns annimmt. Eine derartige Krustenmächtigkeit impliziert eine Spreading-Rate von 32 mm/a, d.h. das KKOC Ridge-System war durch eine langsame Spreizung charakterisiert. Moderne Analoga solcher MOR existieren im Nordatlantik und im Indischen Ozean. Das östlichste Segment des KKOC ist allerdings stärker verarmt.

Das gleichzeitige Auftreten von pargasitischem Amphibol mit einem Cr-reichen Spinell sprechen für einen stärkeren Aufschmelzgrad (~15 %) in einem Suprasubduktions-Setting (SSZ). Im Gegensatz zur Amphibolbildung in einem SSZ-Mantelkeil, wird das Auftreten von Plagioklas durch Subsolidusreaktion und Metasomatose in einem MOR-Setting erklärt. Man kann annehmen, dass die KKOC-Lherzolithe aus einem Segment der Mantelsäule stammen, das unter einem Ozeanrücken relativ schnell adiabatisch aufgestiegen ist. Die Hauptäquilibration der grobkörnigen und porphyroklastischen Lherzolithe (T1) wird relativ rasch

nach dem partiellen Schmelzprozess stattgefunden haben. Beim Aufstieg reagierten die Lherzolithe zunächst noch durchgreifend auf die fallenden  $P$ - $T$ -Bedingungen und danach wurden bei ca. 1020-800 °C viele Gleichgewichte zwischen den Mineralphasen eingefroren. Lediglich die auch bei niedrigeren Temperaturen ablaufenden Elementaustauschprozesse (z.B. Mg-Fe zwischen Spinell und Olivin) zeigen noch eine Überprägung bei niedrigeren Temperaturen. Auch die Bildung von Plagioklas in einigen Lherzolithen erfolgte wahrscheinlich bei relativ niedrigen Temperaturen.

Pyroxenite, i.e. Olivin-Websterite sind vereinzelt im NW-Teil des KKOC aufgeschlossen und bilden Linsen, die selten mehr als 20 cm mächtig sind. Diese Gesteine sind immer mit Plagioklas-Lherzolithen vergesellschaftet. Die Paragenese der Olivin-Websterite besteht aus großen, nahezu idiomorphen Körnern von Ortho- und Clinopyroxen, die eine Kumulattextur definieren. Als Interkumulusphasen treten fein- bis mittelkörniger Olivin und seltener auch Spinell auf. Manchmal ist Spinell von Plagioklas umwachsen. Die KKOC-Pyroxenite (Olivin-Websterite) wurden bei höheren Drücken und Temperaturen gebildet. Es handelt sich um Kumulate. Wahrscheinlich sind sie durch weiteres Aufschmelzen eines bereits an MORB verarmten Lherzoliths entstanden. Die Kristallisation dieser Magmen fand wahrscheinlich in thermischen „conduits“ und dem mittelozeanischen Rücken statt, wo die Schmelzen stark auskühlen und stecken bleiben können. Die Clinopyroxene der Olivin-Websterite und der Plagioklas-Lherzolithe sind ähnlich zusammengesetzt, was auf eine späte gemeinsame metasomatische Überprägung hinweist.

Dunite wurden an zwei Orten, entlang des westlichen und östlichen Randes des KKOC gefunden. Diese Gesteine besitzen eine typische Kumulattextur, enthalten hauptsächlich Olivin (~ 90 %) neben Cpx und Spinel und zeichnen sich durch zwei Besonderheiten aus. Einerseits besitzen sie nach oben konkave, „U-förmige“ REE-Muster mit einer deutlichen positiven Eu-Anomalie, andererseits enthalten sie grobkörnigen, nahezu idiomorphen Olivin. Diese Eigenschaften definieren die KKOC-Dunite als hoch refraktäre ultramafische Gesteine, die als Reste einer partiellen Schmelzbildung eventuell durch „boninitische Fluide“ imprägniert wurden. Bei Duboštica im westlichen KKOC ist ein Chromitkörper aufgeschlossen, der durch Chromit mit einem hohen Cr#-Wert von ca. 80 charakterisiert ist. Auch bei der Entstehung derartiger Spinell könnten boninitische Schmelzen beteiligt gewesen sein. Es wird vermutet, dass die Dunite und assoziierten Chromitite den obersten Teil der Übergangszone zwischen Mantel und Kruste darstellen, d.h. sie sind wahrscheinlich durch Kristallisation aus einer Magmakammer entstanden. Dieser Prozess war von einer durchgreifenden Metasomatose durch Schmelze begleitet.

Zwischen den beiden grossen KKOC-Blöcken ist ein langgestrecktes Areal metamorpher Gesteine aufgeschlossen. Der nördliche Teil dieses Areals enthält nur wenige und relativ kleine Vorkommen von basischen Metamorphiten, während diese Gesteine im südlichen Bereich um die Orte Duboštica und Vijaka sehr häufig sind. Insgesamt sind die metamorphen Gesteine sehr unterschiedlich, mit kristalloblastischen oder porphyroklastischen Gefügen. Relativ weit verbreitet sind Gesteine, die abwechselnd aus hellen und dunkleren Lagen aufgebaut sind. Die unterschiedliche mineralogische Zusammensetzung beruht nicht nur auf unterschiedlichem Chemismus, sondern auch auf unterschiedlichem Metamorphosegrad. Insgesamt wurden folgende Gesteinstypen unterschieden: (1) *Granoblastische Amphibolite*, (2) *Granat-Diopsid-*

*Amphibolite*, (3) *Granat-Diopsid-Hypersthen-Amphibolite*, (4) *Diopsid-Amphibolite* und (5) *Plagioklas-Granat-Diopsid-Gneise*. Der Chemismus dieser Gesteine sowie ihre petrographischen Eigenheiten legen nahe, dass sie überwiegend (ca. 2/3) aus mafischen oder ultramafischen gabbroiden Gesteinen entstanden sind. Das restliche Drittel entspricht eher differenzierten Basalten tholeiitischer Affinität.

Geothermobarometrische Berechnungen zeigen, dass diese Gesteine bei unterschiedlichen P-T-Bedingungen entstanden sind: (a) Granoblastische Amphibolite lieferten ~ 880 °C und 0.9-1.3 GPa; (b) Granat-Diopsid-Amphibolite sind bei 802-1028 °C und 0.94-1.40 GPa entstanden; (c) Granat-Diopsid-Hypersthen-Amphibolite weisen nahezu die gleichen Entstehungsbedingungen auf wie (b), lediglich die Drücke sind etwas geringer; (d) für die Diopsid-Amphibolite liessen sich nur Druckwerte von 0.84-0.89 GPa, aber keine Temperaturwerte ermitteln; (e) die Plagioklas-Granat-Diopsid-Gneise entstanden bei 729-890 °C und 1.10-1.60 GPa. Aufbauend auf diesen Werten wurden für die verschiedenen Gesteinstypen metamorphe *P-T-t*-Pfade konstruiert. Sehr wahrscheinlich nahmen die Plagioklas-Granat-Diopsid-Gneise in der Liegendplatte die tiefste Position ein (~ 30-42 km), nach oben gefolgt von den Granat-Diopsid- und Granat-Diopsid-Hypersthen-Amphiboliten (~ 24-35 and ~ 24-30 km). Aus dem flachsten Bereich (4-30 km) stammen die granoblastischen Amphibolite.

Auf Grund der auffälligen Gemeinsamkeiten des CDOB mit den Ophiolithkomplexen Albanien und Griechenlands (nicht Kreta und östliche Bereiche), wird auch der KKOC mit der mesozoischen Entwicklung des Pindos-Ozeans als einem Back-arc Ozean in Verbindung gebracht. Die Bildung des KKOC begann in der späten Trias durch die Öffnung des Pindos-Ozeans und dem "Spreading" im Zeitraum späte Trias bis früher Jura. In dieser Zeit wurde auch das Drina-Ivanjica-Terrain von der adriatischen Mikroplatte abgespalten. Dieser extensionale Prozess dauerte für ungefähr 30 bis 40 Millionen Jahre an, bis um die Grenze zwischen dem Unteren und Mittleren Jura (Bajorcian-Toarcian), als eine intraozeanische nach NE einfallende Subduktionszone entstand und von Einengungsprozessen gefolgt wurde. Es gibt wichtige petrologische und geochemische Hinweise darauf, dass eine solche intra-ozeanische Subduktionszone im Bereich des KKOC dokumentiert ist. So weisen die Gesteine des KKOC darauf hin, dass sie in einem späteren Stadium über einer Subduktionszone gelegen sind. Hierauf weisen unter anderem die Dunite hin, die normalerweise mit SSZ verknüpften Boniniten vergesellschaftet sind. Allerdings kann man die Existenz eines Inselbogens nur vermuten, da direkte Hinweise (z.B. Kalkalkalivulkanite) fehlen. Das Vorkommen von Gesteinen der "metamorphic sole" kann ebenfalls mit einer intraozeanischen Subduktion in Verbindung gebracht werden. Während des späten Jura bis in die frühe Kreide kollidierte der Subduktions-Trench mit der Adriatischen Mikroplatte und der KKOC wurde neben anderen Ophiolithvorkommen des CDOB südwestwärts auf die Adriatische Karbonatplattform über-schoben. Während der Platznahme wurde vor allem der östliche Teil des KKOC (Konjuh-Segment) tektonisch abgetragen. Daher fehlt hier das plagioklas-peridotische Stockwerk des lithosphärischen Mantels, während dieser vor allem im Westen (Krivaja-Segment) anzutreffen ist. Die Gesteine der "metamorphic sole" sind vor allem im zentralen Bereich des Gesamt-komplexes anzutreffen.





# 1. INTRODUCTION

## 1.1. Prologue

The key to the origin of igneous and metamorphic rocks lies in the study of their structural, textural and mineralogical characteristics (including phase chemistry) and their bulk-rock chemistry (including trace element concentrations). The science that interprets these characteristics is usually called petrology. It offers possible answers to the genesis of igneous and metamorphic rocks. In particular, a study of ophiolitic rocks may help to constrain the genesis of mid-ocean ridge basalts (MORBs) and to understand the tectonic progression from an oceanic ridge to a suprasubduction setting.

This thesis presents a petrogenetic study of Bosnian ophiolites. More precisely, it deals with the large ophiolite complex of eastern Bosnia and Herzegovina, called the Krivaja-Konjuh ophiolite complex (KKOC).

Ophiolites represent slivers of ancient oceanic lithosphere obducted onto the continental or oceanic crust (Bodinier and Godard 2003). Ophiolitic rocks are spread worldwide and they can be found in all collisional belts. The exact definition of an ophiolite has been controversial for many years. However, during the well-known Penrose Conference in 1972, a global consensus was attained over the ophiolite definition (e.g. Coleman 1977). It states that in a completely developed ophiolite, the rock types are spatially arranged in the following upward sequence: (1) metamorphic sole rocks, (2) ultramafic complex (mantle rocks), (3) ultramafic cumulates (crustal rocks), (4) gabbroic complex, (5) mafic sheeted dike complex, (6) mafic volcanic complex (pillow lavas) and (7) oceanic sediments (e.g. radiolarites, shales, pelagic carbonates). The following decades of petrological research fully ascertained an oceanic lithosphere origin of ophiolite complexes. Today, the term ophiolite clearly means fossil oceanic lithosphere, normally found tectonically emplaced onto the continental margin. Most commonly, after the emplacement, only parts of the ophiolite sequence is found preserved, being associated with different sedimentary rocks. Together they form an ophiolitic *mélange* (e.g. Miyashiro 1975, Dimitrijević and Dimitrijević 1973).

The Dinarides were formed during the Alpine evolution of the present-day area of SE Europe. They show a regular zonation, visible in the spatial distribution of distinctive Mesozoic-Palaeogene tectonostratigraphic units (Pamić and Tomljenović 1998). One of these zones is the Central Dinaridic Ophiolite Belt (CDOB) comprising dismembered ophiolite blocks and related sedimentary formations. The Krivaja-Konjuh ophiolite complex renders the biggest block of the CDOB. Its size, intriguing lithological diversity and field relations, outcrop accessibility, as well as lack of modern comprehensive petrologic studies, make it a prominent choice for an attractive petrogenetic research. This thesis focuses on the ultramafic and metamorphic parts of the Krivaja-Konjuh ophiolite complex, whereas the mafic segment is the subject of another thesis, which was defended at the University of Tuzla, Bosnia and Herzegovina in 2009 (Babajić 2009).

The purpose of this dissertation is to present a detailed petrologic and geochemical overview of metamorphic and ultramafic rocks of the KKOC. Strong accent is put on its

genesis in the context of regional geodynamics of the Dinarides, a part of the Mesozoic Tethys.

## 1.2. Aims of dissertation

The aims of the thesis are thoroughly summarised as follows:

- (1) Optical study of a large number of thin sections (~ 110) in order to select the most representative samples for further analytical treatment.
- (2) Provide detailed petrographic descriptions of the selected samples.
- (3) Determine phase (mineral) compositions by electron microprobe.
- (4) Interpret mineral compositions, in particular chemical zoning patterns, with respect to changing pressure-temperature ( $P$ - $T$ ) conditions (geothermobarometry).
- (5) Define the character and provenance of ultramafic rocks and estimate the degree of partial melting.
- (6) Determine potential metasomatic processes and reequilibration effects.
- (7) Determine possible protoliths of metamorphic sole rocks.
- (8) Determine the  $P$ - $T$  conditions of the metamorphic sole rocks, and envision a grid of the important metamorphic reactions.
- (9) Describe the chromite occurrence (podiform type) in peridotite.
- (10) Offer a critical overview of the petrogenesis of the Krivaja-Konjuh ophiolite complex, including its geodynamic development and emplacement on the continental margin.
- (11) Correlate petrogenetic results with other areas of the Central Dinaridic Ophiolite Belt and compare it with genetically linked areas of the Pindos Ocean in Serbia, Kosovo, Albania and Greece. Underline the differences with geographically proximal rocks of the Vardar Zone in Serbia and Croatia.

## 1.3. Structure of the thesis

This thesis is partitioned in 7 chapters (without References), with an appendix at the end. The chapters form a sequence where the foregoing chapter renders a logical precursor to the following one. The thesis commences with an already presented general introduction accompanied with a list of dissertation's aims. Literature is considered up to the publication date of December 2009. **Chapter 2** offers detailed insight in the geographical position of investigated area. Furthermore, sampling spots are indicated on a comprehensive geological map of the Krivaja-Konjuh ophiolite complex (KKOC). **Chapter 3** begins with an overview of the modern Tethyan ophiolite theory. Apart from the classic ophiolite sequence, this presentation also includes related rocks forming metamorphic soles. As well, a brief note on the supra subduction zone (SSZ) Mesozoic Tethys ophiolites is presented here. In the mid-subchapter one can find an introductory insight to the Geology of the Central Dinaridic Ophiolite Belt. The chapter ends with a detailed outline of the geological features of the Krivaja-Konjuh Ophiolite Complex (KKOC), which also includes the general petrography

and geochemistry of ultramafic and metamorphic rocks. In **Chapter 4**, one finds the description of the sampling locations. The following subchapter presents a detailed petrography and mineral chemistry of the investigated ultramafic rocks. Great accent is given to rock textures. Thereupon, the same is given for the rocks forming the metamorphic sole. **Chapter 5** offers data on whole-rock compositions. Several subchapters treat main elements, trace elements and rare earth elements for ultramafic and metamorphic rocks, respectively. **Chapter 6** starts with geothermobarometric calculations defining equilibration of ultramafic rocks and *P-T* conditions for the rocks forming the metamorphic sole. This is followed by the discussion on petrogenesis and provenance of ultramafic rocks and by speculations on plausible protoliths of metamorphic rocks. Further considerations deal with the original geotectonic setting of protolith formation and present the most possible model of the metamorphic event. Final thoughts go to the KKOC genesis and correlation of its geodynamic history with adjacent ophiolitic realms of Serbia, Kosovo, Albania and Greece. **Chapter 7** includes an outline of all results and conclusions of this research. In **Chapter 8**, the referred bibliography of this thesis is listed. The following items are found in the **Appendix**: (a) Materials, (b) Analytical technique, (c) Mineral phase chemistry and (d) Bulk-rock geochemistry.



## 2. GEOGRAPHICAL SETTING

The Krivaja-Konjuh ophiolite complex (KKOC) is the biggest ophiolite occurrence in Dinarides. It presents a tectonic sheet (~ 1 km thick) indicating a synclinal structure (Roksandić 1971). The complex is situated in the northeastern part of Bosnia and Herzegovina (Fig. 1), occupying the southern part of the Tuzla district, possessing a WNW-ESE Dinaridic elongation and covering approximately 650 km<sup>2</sup>. Its longer axis is ~ 40 km, and the shorter axis is ~ 20 km long. The closest large town is Tuzla (~15 km), whilst the distance to Sarajevo approximates 100 km.

Northwards and northwestwards, the KKOC merges with the Ozren ultramafic massif, whereas to the south, it is bordered by the town of Vareš and by the Ravan and Zvijezda mountains. The main state road, connecting Sarajevo and Tuzla, crosses the KKOC at the Karaula locality. The furthest western frontier renders the valley of river Bosna (Pamić 1978). The river Krivaja flows through the mid section of the KKOC, intersecting the complex along its longest axis. To the southwest of the river, the area comprises almost ubiquitous ultramafic rocks. To the northeast of the river, the mountainous area of Konjuh is also made of ultramafic rocks. Therefore, in the literature this entire area is known as the Krivaja-Konjuh ophiolite complex, with Petković (1961) who introduced the term.

As already mentioned, the dominant constituents of the KKOC are ultramafic rocks, accompanied by smaller outcrops of gabbro, dolerite, diabase, and meta-morphic rocks such as granulite, amphibolite, and amphibolite gneisses. Together with greywacke, sandstone and claystone, these crystalline rocks form the Jurassic 'magmatic-sedimentary' complex. If one considers KKOC being part of the above-mentioned complex, then together with the adjacent sediment formations, it covers an area of approximately 1000 km<sup>2</sup>.



## Europe



## Bosnia and Herzegovina



## Krivaja-Konjuh Ophiolitic Complex

**Fig. 1.** Geographical map of Europe indicating the position of Bosnia and Herzegovina. The study area of the Krivaja-Konjuh ophiolite complex is marked and depicted in the lower left corner. Maps from [www.bih-x.com/bhinfo/mape](http://www.bih-x.com/bhinfo/mape)





### 3. GEOLOGICAL SETTING

#### 3.1. A modern conception of Tethyan ophiolites

Nowadays, the term 'ophiolite' includes sizeable ultramafic (and mafic) sections of fossil oceanic lithosphere that were obducted onto the continental (or oceanic) crust. Many years of scientific debate passed since the compromise on the ophiolite rock-suite definition was reached at the Penrose Conference in 1972. Modern ophiolite geochemical classification distinguishes different types of ophiolites through the simple classification scheme based on their fertility. Italian internal Ligurides (fertile) and Semail ophiolites in Oman (refractory) are found to be type localities, presenting two opposite compositional points regarding the discussed criterion (e.g. Nicolas and Boudier 2003).

Mildly refractory ophiolite mantle material of *lherzolitic* composition is interpreted to present an embryonic oceanic crust developed at the ocean ridge setting (e.g. Bodinier et al. 1986a). Apart from the Ligurian ophiolites, dominantly lherzolitic mantle sequences are reported from several other ophiolite localities, such as the eastern Dinarides and Hellenides (e.g. Lugović et al. 1991, Nicolas et al. 1999, Cvetković et al. 2007). A common feature of all these mantle rocks is a strong to moderate serpentinisation, whilst textural evidences, which indicate their mantle tectonite's origin, are occasionally preserved. The genesis of the lherzolitic sequence is attributed to lower degrees of partial melting relative to harzburgitic mantle sections. This issue is usually explained by a slow-spreading rate at the mid-ocean ridge (e.g. Moores et al. 2000).

Strongly refractory mantle material, e.g. tectonite *harzburgite* is generally more frequently encountered and more occasionally preserved as complete ophiolitic sequences. It comprises thick mantle sections up to 10 km (e.g. Semail ophiolite in Oman, Trodos ophiolite on Cyprus, Zlatibor and Varda complexes in Dinarides) (Lippard et al. 1986, Pamić and Desmons 1989). The harzburgite tectonites are featured by coarse-grained porphyroclastic textures recording high temperatures (> 1200 °C) and implying that ductile deformation occurred during asthenospheric mantle flow. The foliation is well pronounced with generally flat trends being parallel to the Mohorovičić discontinuity. The genesis of this kind of highly refractory ophiolites has been widely debated since the supra-subduction zone (SSZ) geotectonic setting came forward as a most liable origin environment (e.g. Miyashiro 1975, Moores et al. 2000, Shervais 2001). Consensus exists over the fact that the harzburgite's refractive character is due to a high degree of melt extraction. However, the cause of this process is still in discussion, ascribing it either to hydrous melting in the SSZ mantle wedges, or to decompression melting at fast-spreading mid-ocean ridges (e.g. Coleman 1977, Boudier and Nicolas 1985).

The actual regional geotectonic models of Tethyan development differ considerably. Notwithstanding, many characteristics are found to be in common. They are envisaged in fact that the present day Tethyan orogens render succession of continental plate collisions that supervened multi-phase dissolution of Gondwana and repeated cycles of ocean basins openings and closures (Stampfli et al. 2000, Flower and Dilek 2003). Since Late Palaeozoic onward, the northward drift of Gondwana fragments encompassed at least three opening cycles. The last one indicates Neotethys opening, which commenced in Early Triassic, with

separation of the Pelagonian mass, i.e. different detached continental blocks, such as Tauride-Anatolide, Lhasa, Burma, Apulia, Adria, etc. Still, there is no sharp line between Neotethys and older Palaeotethys oceanic realms, since the two oceanic systems evolved from one to another (Robertson 2002). Today, the Neotethys ophiolites refer to those rifted in the Early Mesozoic and being emplaced on the continental margins by the end of Cretaceous. As outcome of Tethyan development, the ophiolites are known in the literature as Tethyan ophiolites, today spread from the French Alps up to the Himalayas (Fig. 2.). Almost by the rule, these ophiolites are all preserved in a highly dismembered state forming blocks of ultramafic and mafic rocks tectonically emplaced on (sediment) rock sequences. If the ophiolite suite rocks are found in a strongly mixed state, they are referred to form an ophiolitic mélange.

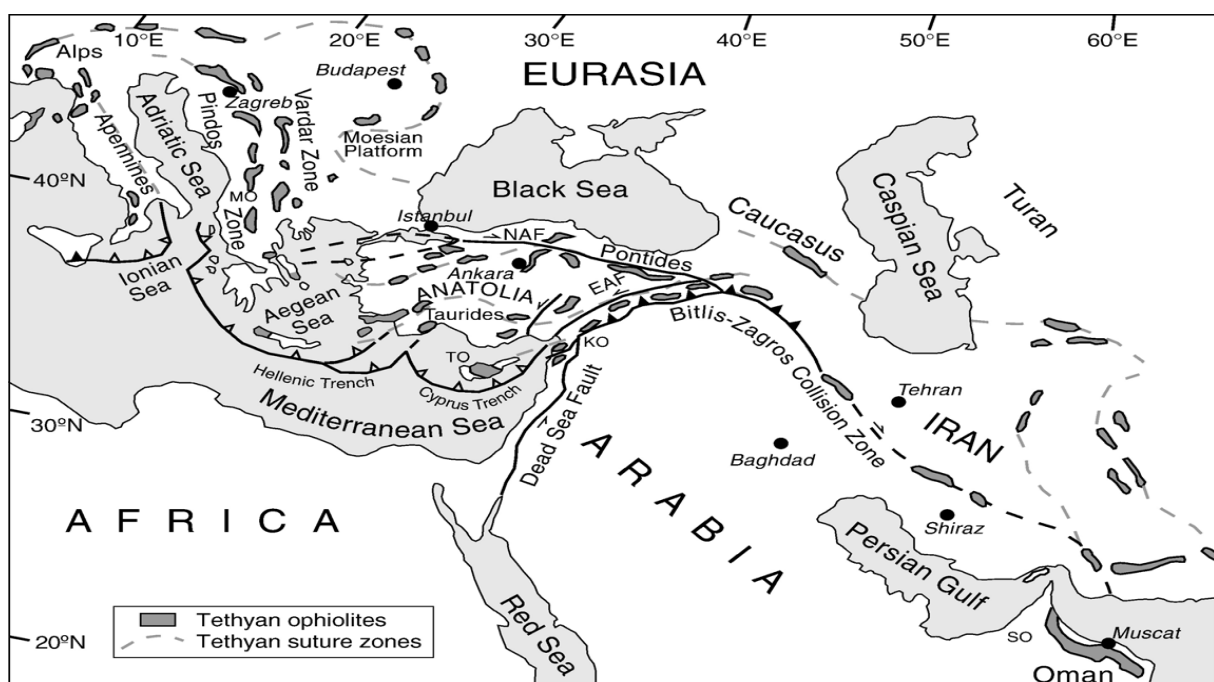


**Fig. 2.** Map showing the stretching of Tethyan ophiolites throughout Eurasia (after Dilek et al. 2008).

Regarding the ophiolite genesis itself, two principal concepts came through as the most probable. These are (a) ocean-ridge, and (b) subduction-related origin (SSZ) concepts. The first hypothesis advocates ophiolite formation along the sea-floor spreading zones. The second hypothesis argues that ophiolites are formed in a supra-subduction zone setting (SSZ) and thus underwent a relatively high degree of partial melting, enhanced by volatile influx released from the subducted slab. Both hypotheses have some deficiencies. For instance, two parallel ophiolitic belts stretching throughout the Western Tethyan Ophiolites (Dinarides, Albanides and Hellenides) greatly differ in the refractory nature of their ultramafic sequences. The western belt is not so depleted, since it is mainly of lherzolitic composition, in marked contrast to the eastern belt, which is more depleted (harzburgitic). Therefore, such 'high fertility' cannot be interpreted by the simple SSZ hypothesis. On the other hand, development of geochemical discrimination techniques based on the comparison of ophiolite extrusive rocks with oceanic volcanics of modern tectonic settings (e.g. Pearce 1980)

indicated that some ophiolites previously believed to be of MOR origin are unambiguously SSZ affiliated.

In light of the above-mentioned concepts, the new geotectonic concepts on Tethyan ophiolite development have started to conceal both hypotheses (Dilek and Flower 2003, Robertson 2002). It speculates with Mesozoic Tethyan ophiolites affiliated to slow spreading mid-ocean ridges often evolved into the SSZ type peridotites. The lithological and structural ophiolite diversities are due to progressive incorporation of magmatic and metamorphic ridge, arc and back-arc domains into soon to be obducted ophiolite sequences.

Metamorphic rocks known as metamorphic sole accompany most of the Tethyan ophiolite complexes. They are featured by an inverted metamorphic gradient with amphibolite to granulite facies metamorphic rocks formed at temperatures of up to 1000 °C (e.g. Guilmette et al. 2005, Šegvić et al. 2006). The metamorphic gradient tends to drop structurally downwards, attaining greenschist-facies conditions at the lowermost levels. The pressure conditions are subjected to great oscillation depending on physical properties of the overridden rock sequences. The overlying rock is an ophiolitic peridotite (e.g. cases of Oman or Bosnia, Pamić et al. 1977, Gnos and Peters 1993). Today there is general agreement that oceanic spreading and metamorphic sole formation are synchronous or at least form two closely sequential events occurred at the collapsed spreading ridges or in hypothetical back-arc realm of Tethyan marginal basins (Dilek and Flower 2003).

### **3.2 The Central Dinaridic Ophiolite Belt (CDOB)**

The Dinarides form part of the Alpine-Himalaya Tethyan orogenic belt. They possess a NW-SE strike with a south-westward vergence. In the NW, the Dinarides merge with the Southern Alps, whilst in the SE they are continued as Hellenides and Albanides. The overall elongation covers ca. 700 km stretching throughout Slovenia, Croatia, Bosnia-Herzegovina, Serbia, Montenegro and Kosovo. In the NE-SW crosscutting profile, a characteristic regular zonal pattern in the spatial distribution of Mesozoic-Early Tertiary tectonostratigraphic units is recognised (Pamić et al. 1998a) (Fig. 3). Thus, going from the Adriatic microplate to the NE, the following units are distinguished: (1) the Adriatic-Dinaridic carbonate platform of External Dinarides, (2) Jurassic-Cretaceous passive continental margins of Apulia known as 'flysch Bosniaques' or Bosnian nappe (Aubouin et al. 1970), (3) ophiolites and genetically related sedimentary formations, which together form the Central Dinaridic Ophiolite Belt (CDOB), (4) a Late Cretaceous sequence composed of sedimentary, magmatic and metamorphic rocks related to the Vardar zone (VZ-western belt), thrust on the CDOB sequence, and (5) Paleozoic-Triassic nappes of Eastern Dinarides as defined by Rampnoux (1970), which are found thrust on internal units of the Eastern Dinarides. Referring to the division presented here, the Vardar zone ophiolites render the most internal units of the Dinarides. Units defined as (2) to (4) forming the Internal Dinarides *sensus-stricto* are sometimes also called the 'Supradinaric' (Herak 1986).

The Dinaride ophiolites are reported to belong either to CDOB or to VZ (also called IDOB = Inner Dinaridic ophiolite belt). In both cases, they are found associated with different sedimentary formations. Their main differences happen to be: (a) diverse genetic model of

origin, (b) different ages of formation, and (c) dissimilar structures, especially concerning their relations to underlying and overstepping sedimentary sequences. Dismembered CDOB ophiolites are related to the ocean-ridge geotectonic setting, whereas patches of the VZ ophiolite occurrences are SSZ affiliated (Pamić et al. 2002, Bazylev et al. 2009).

The Central Dinaridic Ophiolite Zone (CDOB) (Fig. 3) is in the literature also known as the Dinaride Ophiolite Zone (DOZ), Dinaride Ophiolite Belt (DOB) or formerly, as the Bosnian serpentine zone. The CDOB stretches from Zagreb and the Banovina region in Croatia, across all northern and central Bosnia to southern Serbia, with further prolongations to the Hellenides. As stated above, the CDOB rocks are associated with different sedimentary rock formations. Thus, they form an ophiolitic *mélange* known as the Jurassic magmatic-sedimentary formation (Pamić 1974).

Main components of the CDOB are individual ophiolite fragments, ranging from small ones (up to 1 km) to extensively large ones (up to several decades of km). Their principal lithological constituent is tectonic (or cumulate) lherzolite (spinel peridotite). Smaller blocks can also be composed of different varieties of gabbro, dolerite, diabase, spilite and metamorphic sole rocks. Mafic rocks make up to 5 % of the ophiolite complexes. The larger ultramafic complexes as, for instance, the KKOC, are divided in several smaller blocks, which display peculiar structural features (e.g. strike and dip of foliation). Apart from ultramafic and mafic rocks and associated metamorphic rocks, the ophiolitic *mélange* is composed of a shaly to silty matrix, which embeds fragments of greywacke, radiolarite and exotic limestone of different Jurassic-Cretaceous ages. Sometimes the matrix also embeds fragments of gabbro, diabase, basalt, ultramafics, tuff, amphibolite, chert and schist. Rarely one encounters completely preserved ophiolite profiles. More often, they are chaotically dispersed and found as ophiolitic *mélange* (Pamić and Desmons 1989, Dimitrijević and Dimitrijević 1973). An ophiolitic *mélange* of the CDOB transgressively overrides sedimentary sequences (up to 2000 m thick). This sequence is known as Pogari formation. It is mainly composed of conglomerates and breccias (Jovanović 1957). Clasts of this sequence are formed of ophiolitic fragments as well as some granitoids of presumed Variscan age. The Pogari formation is determined to be of Late Cretaceous age. Hence, it is the youngest possible age of all rocks belonging to the CDOB.

So far, the ophiolitic *mélange*, shales and greywackes in particular, do not exhibit any characteristic index fossils. Based on the peculiar fauna of platy limestone their Jurassic age is hypothesized. This correlates with results of radiometric measurements on metamorphic sole rocks (Lanphere et al. 1975, Majer et al. 1979, Lugović et al. 1991). One infers that fossil limestone content, radiometric ages and the age of the Pogari formation define the age of the CDOB spanning the Early Jurassic to Early Cretaceous.

Inside the CDOB (Fig. 3), besides the KKOC, one can distinguish five other ophiolite complexes: (1) Kozara ophiolite complex (e.g. Pamić et al. 2002, Karamata et al. 2005, Ustaszewski et al. 2006), (2) Ljubić and Čavka ophiolite complex (e.g. Majer and Jurković 1963, Pamić 1983, Lugović et al. 1991), (3) Ozren ophiolite complex (e.g. Sijarić and Šibenik-Studen 1989, Lugović et al. 1991, Bazylev et al. 2009), (4) Borje and Mahnjača ophiolite complex (e.g. Džepina 1970, Pamić and Majer 1974, Lugović et al. 1991), and (5) Vardar and Zlatibor ophiolite area (e.g. Trubelja et al. 1974, Pamić and Desmons 1989,

Popević et al. 1993, Korikovski et al. 1996). The interested reader is referred to the bibliography provided and references therein.

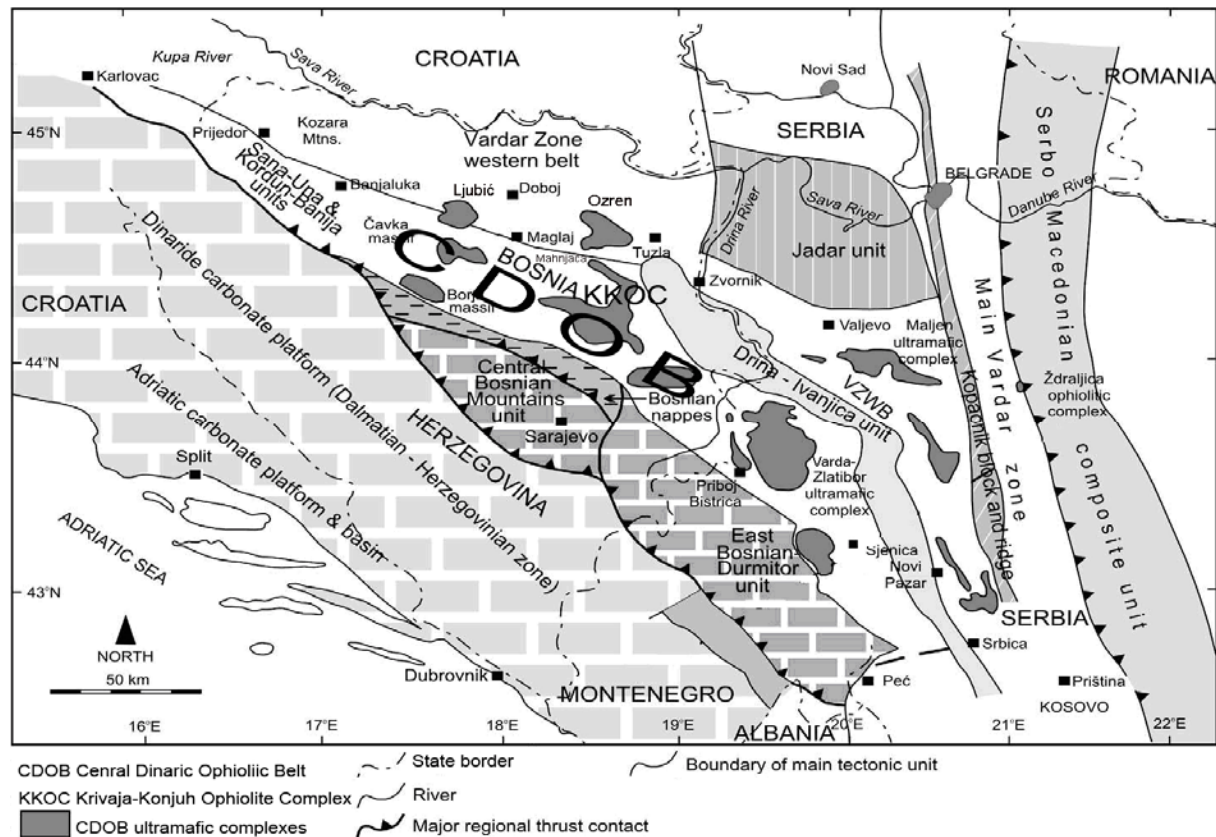


**Fig. 3.** Map showing the position of CDOB and VZ ophiolites in Dinarides (modified after Robertson et al. 2009).

### 3.3. Geology of the Krivaja-Konjuh Ophiolite Complex (KKOC)

Comprehensive geological investigations on the KKOC began in the late 19<sup>th</sup> century by the Croatian scientist Kišpatić (1897, 1902) in his work on the Bosnian Serpentinite Zone. After the second world war the research dealing with KKOC was published by Đorđević (1958), Trubelja (1961), Ristić and Mudrinić (1965), Sunarić-Pamić and Olujić (1968), Pamić and Keppeler (1971) and others. During the work on the basic geological map of the former Socialist Federative Republic of Yugoslavia, much fruitful petrologic information on the KKOC rocks has been gathered. This information can be found in the legends of the following map-sheets: Zavidovići, Vareš and Vlasenica (Pamić 1968, 1970, Đorđević and Pamić 1972). The first modern comprehensive investigation of the KKOC rock suite is given in Pamić et al. (1977). A treatise on the ophiolitic mélangé problematics of the Dinaridic ophiolite is given in Dimitrijević and Dimitrijević (1973). A very detailed report on the KKOC mineral phase chemistry is provided in Maksimović and Majer (1981) and Maksimović and Kolomejceva-Jovanović (1987). The results of extensive studies on the CDOB Jurassic ophiolites and associated metamorphics origin are reported in Lugović et al. (1991), Trubelja et al. (1995), Operta (2004) and Bazylev et al. (2009).

*Ultramafic rocks* form about 80 % of the KKOC, whereas the rest are mafic and metamorphic rocks, which are found concentrating in the NW part and along the southern margins of the complex, respectively (Fig. 4). Other lithologies are reported extremely rare. The ophiolite sequence is highly dismembered due to its emplacement on the continental margin. It is estimated that the present sedimentary succession of the KKOC was deposited during or prior to the emplacement. This formation is usually referred as ophiolitic *mélange* or magmatic-sedimentary formation, also known in the literature as the diabase-chert formation. The *ultramafic* part of the KKOC covers an area of 500 km<sup>2</sup>. The composition is uniform, consisting almost entirely of lherzolite. However, one can distinguish rather large areas of dunites with subordinate pyroxenites outcropping along the southern margins of the complex, especially in the vicinity of Vijaka and Duboštica villages. Chromitite appearances inside the peridotite bodies are not unusual. Nevertheless, they are found rather disseminated without depicting any significant accumulation. The contact with Jurassic podiform sediments is purely tectonic, since signs of sediment metamorphism have not been reported. Serpentinisation is recorded not only along the marginal areas of the ultramafic mass, but also in its central parts (Pamić et al. 1977). According to geophysical data, the ultramafic segment of the KKOC forms a slightly concave sheet (Roksandić 1971) with an estimated maximal thickness of 2000 m. By the dismembering of the ophiolite sequence it acquired the block-like structure. So, inside the structure of the KKOC two comparatively large blocks can be recognised. The western block is further segmented by faulting, while the eastern one is homogeneous with a syn-shaped form. The tectonic movements are echoed in the peridotite structural and textural features. However, they are reported not to overlap with those of the surrounding Jurassic sediments (Nicolas et al. 1971, Pamić et al. 1977). This implies separate geological evolutions of these units, which is further corroborated by the lack of contact metamorphism of sediments. *Gabbro* makes the main KKOC mafic component. Compared to the ultramafics it is found as a minor constituent concentrated either along margins or in the central areas of the complex. Thus, it renders the transitional zone to the Jurassic sediments. Main outcrops are reported in the upper flow of the river Gostovića and at the hill of Romanovac. Overall, the gabbro surface in these localities is approximately 25 km<sup>2</sup>. The contact of the gabbro mass and lherzolite is not open, but the broader area is featured by many gabbro veins. Sometimes, enclaves of lherzolite are perceived inside gabbro. Mineral compositions of enclaved and surrounding peridotite are practically identical (Pamić and Antić 1964). Very often the gabbro displays cumulative structural features, observed as a foliation. By comparing the pyroxene lineation of the gabbros with those of the ultramafics, one can infer the intrusive contact of the gabbro mass with the neighbouring lherzolites (Pamić et al. 1977). Therefore, it is estimated that the basic lavas intruded the ultramafic complex before its tectonic emplacement. This is endorsed by the lack of intrusive relation between gabbro and Jurassic sediments. *Dolerite-diabase* rocks form the third most abundant lithological unit often observed inside the KKOC with the biggest surface occurrence recorded along the northern slopes of the complex near the small town of Banovići. There, these rocks comprise an area of ~ 25 km<sup>2</sup>. The dolerite-diabase body is made of a variety of coarse-grained dolerites and medium to small-grained diabases. The contact to the Jurassic sediment is sharp and clearly indicates an intrusive

event (Karamata and Pamić 1960). *Metamorphic rocks* are reported to occupy the southern margins of the KKOC, outcropping mostly in the vicinity of the Vijaka and Duboštica localities. They form separated zones of up to 10 km long and several hundred metres in width. Besides the stated outcrop localities, metamorphics are observed inside the complex, particularly along the main longitudinal fault, dividing the complex into two large blocks (Fig. 4). The contact of metamorphic and ultramafic rocks is mostly hidden. However, an intimate gradation between the two units is noticed. Duboštica and Vijaka metamorphic rocks present the biggest ophiolite-related occurrence of metamorphic rocks in the Dinarides. They comprise an area of approximately 40 km<sup>2</sup>. It is a lithologically diverse terrain comprising rocks from greenschist to granulite facies (Pamić and Keppeler 1971, Operta 2004). However, amphibolites prevail depicting variable mineralogical compositions as well as structural and textural characteristics. Their textural attributes are to a certain degree highly correlated with those of the ultramafics and mafics (Pamić et al. 1977). On the other hand, the relation to Jurassic sediments is solely tectonic. The *sedimentary* rocks belonging to KKOC are not homogeneous. The dominant lithological units are small-to-medium grained greywackes and dark greyish to black claystones accompanied by significant amounts of breccias and limestones (Jovanović 1957, Pamić et al. 1977).





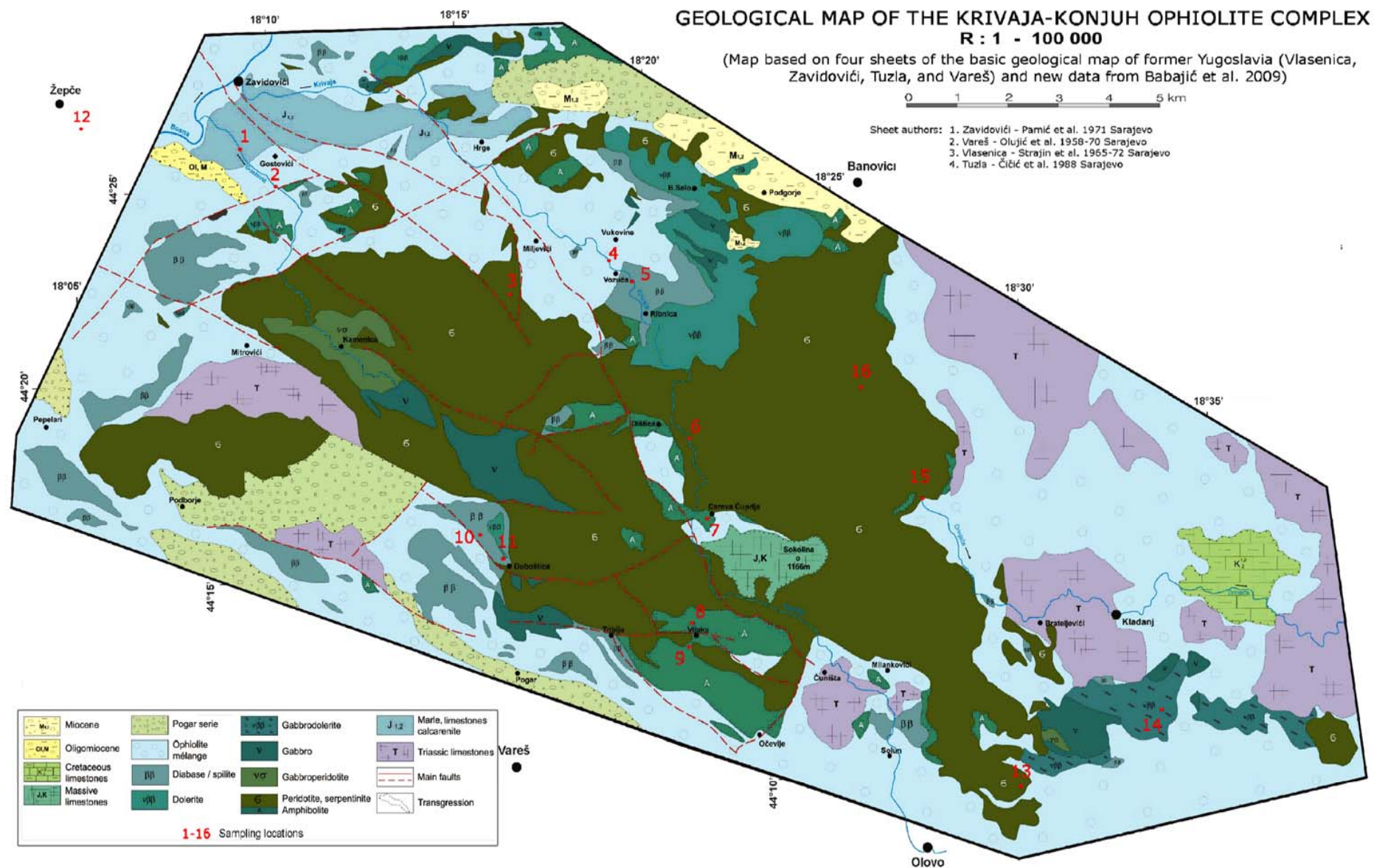


Fig. 4. Geological map of the Krivaja-Konjuh ophiolite complex with indicated sampling localities.



## 4. PETROGRAPHY AND MINERAL CHEMISTRY OF THE KKOC ROCKS

### 4.1. Sampling locations

After a comprehensive KKOC terrain prospecting, 16 localities were chosen as the most appropriate to be sampled from. They are briefly summarised in Table 1. The sampling date, spot signs in the enclosed geological map of the KKOC (Fig. 4) and basic terrain and rock lithology are shown in the same Table. The lithology is inferred from field observation and the basic geological map of Bosnia and Herzegovina (e.g. Pamić 1970). Where available, GPS coordinates are provided.

*Stipanovići* and *Gostovića Rijeka* are localities placed along the banks of the river Gostovića around 10 kilometres upstream from its confluence. The distance between these two localities is approximately 2 km. Samples of peridotite and garnet pyroblastite were taken from the southern banks. The area is composed of Jurassic sediments, mostly sandstones. Based on the rock fragments' size and shape, it is believed that these boulders originate from the relatively small ultramafic bodies tectonically displaced from the main ophiolitic mass in the area located south and west of Gostovići village. The *Manastir* locality is situated in the mid-part of the northern rim of a large Krivaja ultramafic body. The distance to the river Krivaja totals ~ 10 km south-westwards. Samples of fresh foliated peridotite are very nicely exposed, eroded by the hill's stream (Fig. 5). *Krivaja* and *Krivaja Vozuća* localities are placed on the southern bank of the Krivaja river (Fig. 5). These localities are a few kilometres apart and both are found inside the Jurassic magmatic-sedimentary formation. Metamorphic rocks sampled here most probably originate from upstream Dištica and Careva Ćuprija metamorphic areas, which mark the northern portion of the Krivaja and Konjuh ophiolite segment junction.



**Fig. 5.** *Manastir* (left) and *Krivaja* (right) localities.

The next sampling spot, called *Maoče* (Fig. 6), is located further upstream the river Krivaja. Here, the riverbed is made of fresh peridotite of different structures, whereas amongst shore pebbles, one can encounter high-grade metamorphic rocks from nearby metamorphic terrains. *Careva Ćuprija* locality is placed further upstream, in the Olovo direction. The locality is named after the village situated inside the metamorphic terrain as shown on the geological map. It was hard to find a suitable outcrop for sampling. A sample of high-grade pyroblastite was taken near the city bridge at the river's shore. The localities *Vijaka*

*Stream* and *Vijaka* are located some 10 km southwards. They are placed north and south of the *Vijaka* village, respectively. The distance between these localities approximates one kilometre. Pebbles of metamorphics were gathered from *Vijaka* Stream, whereas the *Vijaka* locality is presented by an outcrop of in-situ metamorphic rocks. The metamorphic terrain of the *Vijaka* area represents the main metamorphic mass inside the KKOC, featured by particular pargasite schists. Some twenty kilometres westwards, *Duboštica* and *Duboštica North* localities are placed (Fig. 6).



**Fig. 6.** *Maoče* (left) and *Duboštica* (right) localities.

The hamlet of *Duboštica* can be reached passing the *Pogari* plateau in the direction of *Vareš*. The localities are found about 5 km uphill from the hamlet. Although the area is covered by sediments, the riverbed of the *Duboštica* creek and pebbles recovered therein, offer the best collection of ophiolite-related rocks in whole KKOC. Cumulate peridotite, tectonite lherzolite (in contact with chromitite), amphibolite and granulite were sampled there. Granulite was taken from the outcrop, whereas the peridotite is found just above it, in primary contact with its metamorphic sole. Before entering the hamlet, one can see a steep abandoned side road for the nearby *Rakovac* locality. In former times the chromite ore was exploited there.



**Fig. 7.** *Muška Voda* (left) and *Karaula* (right) localities.

**Table 1.** Locality overview with sampling time, map signs, samples' names, Gauss-Krüger coordinates, and main lithology from field observation and geological map.

Locality name	Time of sampling (month/year)	Sign on the map (Fig. 4.)	Samples gathered	GPS coordinates (X, Y)	Field remarks
Stipanovići	07/2007	1	GR2	4 919 625, 6 512 175	Pebbles of ultramafic & metam. rocks - terrain made of
Gostovića Rijeka	09/2006, 07/2007	2	GR12	4 917 125, 6 514 420	Jurassic magmat.-sedimentary mélange.
Manastir	09/2006, 07/2007	3	U4, M2	4 910 160, 6 520 200	Ultramafic terrain. Nice samples of layered peridotite.
Krivaja	07/2007	4	MK2	4 910 405, 6 520 980	Pebbles of high grade metamorphic rocks gathered along river bank.
Krivaja – Vozuća	09/2006	5	U29, U30	n.a.	
Maoče	old samples	6	R8, R/	4 905 700, 6 534 230	Ultramafic terrain of fresh peridotite having different texture.
Careva Čuprija	07/2007	7	CC1	4 900 280, 6 530 540	Metamorphic terrain with no well exposed outcrops.
Vijaka Stream	09/2006, 07/2007	8	V1, U40	4 890 840, 6 530 510	Main metamorphic mass inside KKOC. Terrain is featured by distinctive pargasite schists.
Vijaka South	07/2007	9	V4, X1	4 890 685, 6 53 0440	
Duboštica North	07/2007	10	U22, D5	4 900 270, 6 520 595	Stream-pebbles of igneous and metamorphic lithologies.
Duboštica	09/2006, 04 and 07/ 2007, old samples	11	U23, DU5, U19, D16, D17, D18	4 900 060, 6 520 510	Contact of ultramafics and metamorphic sole.
Žepče	09/2006, old samples	12	10D, 11C, Z1C, 1C, 2A, 4A	Not available	Fresh peridotite terrain. Metamorphics-ultramafics contact.
Olovo	07/2007	13	O2	4 880 660, 6 540 710	Porphyroblastic peridotite sampling.
Karaula	09/2006, 07/2007	14	K1	4 893 084, 6 553 138	Predominantly mafic terrain. Ultramafic cumulate sampled.
Muška Voda	09/2006	15	U35	4 902 750, 6 546 375	Ophiolite mélange terrain. Composite peridotite taken.
Zlaća	07/2007	16	Z4	4 910 720, 6 545 198	Heart of Konjuh ultramafic terrain. Porphyroblastic peridotite.

Around fifty kilometres to the west from the hamlet of Duboštica, on the state road Doboj - Zenica, the city of Žepče is located. It is surrounded by relatively small ophiolite terrains, which are believed to be tectonically detached from the main KKOC ophiolite mass. The sampling spot named *Žepče* comprises one hundred metres of sampling along the canyon of the river Ograjna, found in the vicinity of the city. The area is composed of fresh lherzolite with pyroxenite veins. Samples of peridotite and of a peridotite-pyroxenite contact were taken there. Further up the canyon, one encounters the contact of altered peridotite and metamorphic rocks. The contact is partially parallel with the foliation of metamorphic rocks. Along the contact fault zone, plenty of peridotite inclusions are found inside the metamorphic rocks. Samples of felsic and mafic granulite were taken from the contact area. As one gets away from the contact, metamorphic lithology changes into magmatic (mafic), probably presenting the metamorphic protolith. On the far opposite eastern side of the KKOC, at the slopes of the Konjuh hill, the city of Olovo is located.

The *Olovo* locality is found a few kilometres to the north, following the main road to Tuzla. There, nice samples of porphyroclastic peridotite were taken. Twenty kilometres further north up the road, the locality of *Karaula* is situated. This whole area is formed of mafic rocks with the primitive gabbro quarry placed just aside the road (Fig. 7). By carefully observing, the good samples of cumulate plagioclase-rich peridotite were recovered. Further northwest, following the Drinjača stream, at the rim of the ultramafic Konjuh body, the locality of *Muška Voda* is located. It is a mountain spring, in a terrain made mostly of ophiolitic *mélange*. A sample of peridotite, cut by mafic veins was taken from a nearby creek (Fig. 7). Around 15 km towards the centre of the Konjuh ultramafic mount is the *Zlača* locality. There, nice outcrops of porphyroclastic peridotite are exposed.

## **4.2. Ultramafic rocks**

### **4.2.1. Rock types, textures and structures**

The great majority of the KKOC ultramafic rocks show characteristic granular or porphyroclastic textures (Pamić et al. 1977). Granular textures are not frequently reported, since these normally pertain to less abundant cumulate olivine-rich lherzolite and pyroxenite, both having massive homogeneous structures with uniformly distributed mineral phases (Fig. 8). Such a distinct granular texture can easily be distinguished from immanent banded and foliated tectonite peridotites, marked by characteristic mantle (metamorphic) texture (Fig. 9). Banded peridotite structures are characterised by alternating layers of olivine- and pyroxene-rich domains, with clear and sharp boundaries. This peridotite structure type is relatively rare and crops out near the Duboštica village where peridotites are associated with chromite mineralizations. On the other hand, about 90 % of KKOC lherzolite possesses a foliated peridotite structure (Pamić 1968, 1970, Đorđević and Pamić 1972) where one can notice elongated pyroxene clusters imbedded in a medium to small grained olivine matrix, which underwent a certain degree of serpentinisation (e.g. Fig. 11g). This lherzolite texture variety is in south Slavic geological literature referred as 'bobičasti lercolit'.

A detailed characterisation of the KKOC mantle rock (tectonite) subtypes, which is based on their textural and structural features as well as on modal mineral composition, requires comprehensive thin-section analyses. The petrographic descriptions given in here follow textural classifications proposed by Mercier and Nicolas (1975) and Basu (1977) for porphyroclastic peridotites and Wager and Brown (1968) for cumulate ultramafic rocks. Eight rock-subtypes are reported within the ultramafic segment of the Krivaja-Konjuh ophiolite taking into account: (a) rocks' primary mineral paragenesis, (b) estimated phase abundances, (c) rocks' textures and (d) observed rocks' alteration degrees, complex (Table 2). However, it needs to be added that modal mineralogy estimations are scarcely accurate due to the combined effects of alteration and sample heterogeneity, partly induced by extensive mantle deformations.

#### 4.2.1.1. Plagioclase lherzolites

A transitional type of protogranular to porphyroclastic texture characterises this ultramafic rock subtype represented by samples D5, GR2, GR12 and M2 recovered from the NW part of the KKOC (Fig. 4, Table 2). Mineral constituents are olivine, orthopyroxene (Opx), and in lesser quantities, clinopyroxene (Cpx) and spinel, whereas plagioclase is an uncommon phase. Porphyroclasts are sporadically found, being mostly isometric or occasionally slightly flattened subhedral Opx (~5 mm across). The grains show an intracrystalline deformation history reflected in serrated grain boundaries, heavily kinked subgrains and polygonisation (Fig. 10c). As well, cleavage planes, diopside exsolution lamella and undulose extinction are occasionally reported. The matrix is composed of equant grains of olivine, Opx and Cpx (~ 2 mm across). Olivine is most abundant and it is preserved in insular forms due to progressive serpentinisation, enhanced by the copious cracks and grain-ruptures. Former grain boundaries between olivine and pyroxene are clearly curvilinear, occasionally converging to triple points. Sometimes, peculiar olivine grains are found as chada-crysts in pyroxene (sample GR12). Euhedral to subhedral Opx grains found in the matrix are lamellae free, every so often marked by cleavage and polygonization. Clinopyroxene is not so frequent as olivine and orthopyroxene. It has subhedral grains, usually marked by cleavage and exsolution lamellae. Incipient polygonisation is occasionally reported. Within this texture one can rarely notice strain-free pyroxene neoblasts formed by syntectonic recrystallisation and/or post-deformational annealing. Spinel is disseminated throughout the sample, either as small anhedral blebs (~ 0.01 mm across) insulated in olivine/Opx and encircling porphyroclasts or, as characteristic xenomorphic or holly-leaf shapes with dimensions of up to 1.5 mm (Fig. 10a). Plagioclase is reported rarely, as a subhedral matrix phase, with average grain size of ~ 0.8 mm across. This rock type experienced comparatively low deformation, which is particularly supported in a coarse-grained matrix and lack of neoblasts.





**Fig. 8a-d.** Photographs showing ultramafic cumulate rocks having granular texture and homogeneous structure, which form the smaller portion of the KKOC ultramafic segment: textures seen in saw-intersection smooth surfaces (a and b); textures seen in natural rock surfaces (c and d).

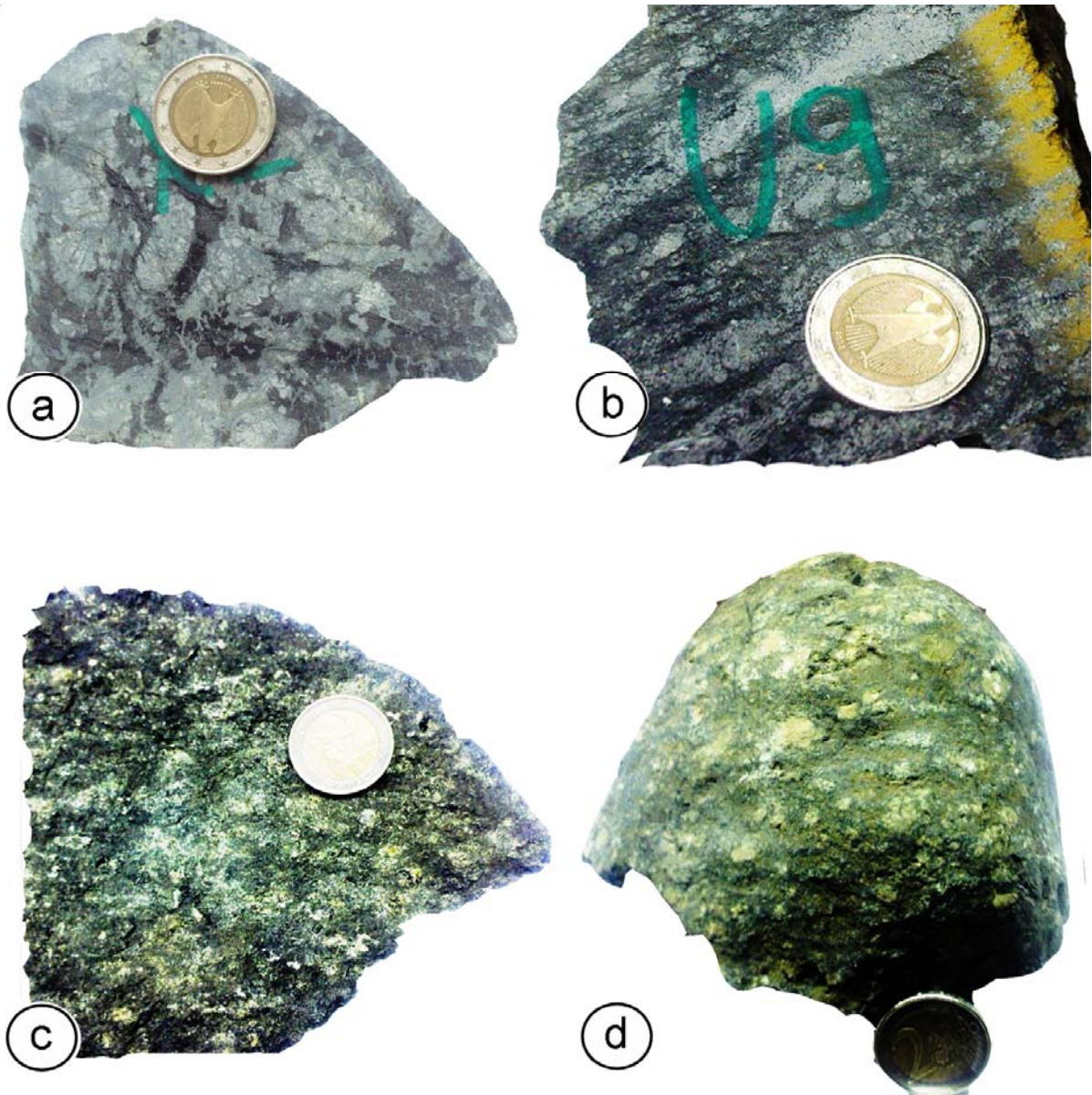


**Fig. 9a-d.** Photographs showing the KKOC ultramafic tectonite rocks having porphyroclastic texture and banded or foliated structure: porphyroclastic textures in the saw-intersection smooth surfaces with foliated (a) and banded (b) structures; textures in the normal rock surfaces (c and d).

#### 4.2.1.2. Spinel lherzolites

This subtype is generally characterised by porphyroclastic textures, comprising a suite of samples (O2, Z2, Z4, U35) that were recovered from the eastern slopes of Konjuh (Fig. 4, Table 2). The paragenesis comprises olivine, orthopyroxene, clinopyroxene, two kinds of spinel and occasionally amphibole (samples Z4 and U35). Numerous porphyroclasts consist of orthopyroxene, sometimes found randomly flattened (~ 5 mm across, with sample U35 having ~ 2 mm across). The deformation effects are echoed in undulose extinction, cleavage planes, intra-grain ruptures, kink-bands, subgrains and sporadically in pressure lamellae (sample Z4) and insulated phases (olivine in Z2 and spinel in U35, Fig. 10d). Often, the strain-free neoblasts are found to encircle large porphyroclasts (Fig. 10e).

**Table 2.** The Krivaja-Konjuh ultramafic rocks' subtypes and their modal mineralogy estimation (vol.%)

Ultramafic rock subtype	Rock samples	Mineral paragenesis	Modal mineralogy estimation (vol.%)					
			olivine	Opx	Cpx	Pl	spinel	minor phases
<b>Coarse-grained PI Iherzolite – Type A</b>	D5, GR2, GR12, and M2	OI, Opx, Cpx, Pl, Sp, Srp, and Tc	60-65	10-15	7-10	5-7	2-4	5-10
<b>Spinel Iherzolite – Type B</b>	O2, Z2, Z4, and U35	OI, Opx, Cpx, Sp, Srp, Amp, and Chl	68-72	14-20	4-8	-	0-2	5-10
<b>Pyroxene rich PI Iherzolite – Type C</b>	U4	OI, Opx, Cpx, Pl, Sp, Tc, and Srp	50	20	15	3	2	10
<b>Poikiloblastic Iherzolite – Type D</b>	4A	OI, Opx, Cpx, Pl, Sp, Srp, Pec and Chl	65	15	5	3	2	10
<b>Equigranular mylonitised Sp Iherzolite – Type E</b>	R7	OI, Opx, Cpx, Sp, and Srp	70	12	4	-	4	10
<b>Spinel olivine websterite – Type F</b>	1C and 2A	OI, Opx, Cpx, Sp, Chl, Srp, and Grt	20-25	30-35	20-30	-	2-4	10-15
<b>Dunite (cumulate) – Type G</b>	U19 and K1	OI, Cpx, Sp, Chl, Amp, Grt and Prh	82-88	-	0-3	-	4-6	5-10
<b>Podiform chromitite – Type H</b>	D16, D17, and D18	Sp, Srp, and OI	0-2	-	-	-	95-100	0-5

*Mineral abbreviations after Kretz (1983), extended by Bucher and Frey (1994).*

Olivine, ortho- and clinopyroxene grains found in a recrystallised matrix are all of similar dimensions (~ 1 mm across). Olivine is the most abundant phase, mostly subhedral, featured by kink-band boundaries, ruptures and serpentinisation. Many olivine grains display undulose extinction and occasionally curvilinear grain boundaries. The obvious reduction in olivine grain size as compared to rock type A is due to an enhanced matrix recrystallisation. Subhedral to anhedral clinopyroxene is quantitatively subordinate, recording minimal strain (Fig. 10f). Spinel often emerges as an anhedral chadacryst in olivine (~ 0.2 mm across) or has an elongate xenomorphic shape (~ 0.8 mm across) (Fig. 11b). In sample Z4, secondary actinolite is developed in form of rectangular bars after orthopyroxene porphyroclasts. On the other hand, microprobe analyses of sample U35 record the minute growth of the primary metasomatic amphibole along OI-Opx-Cpx triple points (Fig. 11h).

#### 4.2.1.3. Plagioclase lherzolites with pyroxene streaks

Sample U4 recovered from the western segment of Konjuh defines this rock subtype. Its texture is practically analogue to that of subtype A, with an exception of pyroxene streaks or lenses, which are unique for this type. They make up to 30 vol.% of the sample. In most cases, the streaks are composed of both pyroxenes (~ 1 mm across) reported to be free of strains or to decipher minimum deformation (Fig. 11g). The average streak size is ~ 4 mm across. Similar garnet-free pyroxenite lenses in peridotites of the Western Alps are explained through segregation and small-scaled transport of near-solidus partial melts from the host peridotites (e.g. Shervais 1979, Bodinier et al. 1986b). Occasionally, talc formation after pyroxene is reported.

#### 4.2.1.4. Plagioclase lherzolites with poikiloblastic texture

This textural subtype includes sample 4A recovered from the Žepče area (Fig. 4, Table 2). Its mineral paragenesis comprises olivine, Opx, Cpx, spinel and completely altered plagioclase. Except the presence of plagioclase and large poikiloblasts, all other petrographic features appear to be highly similar to rock type B. Hence, the peculiarity of this sample are orthopyroxene porphyroclasts with incorporated olivine, clinopyroxene and pectolite chadacrysts, as well as spinel holly-leaf grains found insulated by serpentinised olivine (Fig. 10g, Fig. 11c). As it was the case with other samples from the Žepče region (pyroxenite, rock type F), the formation of hydrous phases, such as pectolite, is interpreted to be due to rodingitisation.

#### 4.2.1.5. Equigranular spinel lherzolites

Sample R7 from the Maoče locality, situated inside the KKOC central fault zone, defines this rock subtype (Fig. 4, Table 2). The paragenesis is primarily composed of olivine, whereas pyroxene and spinel are subordinate phases. The average size of rare euhedral orthopyroxene porphyroclasts is ~ 4 mm across, being remarkably parallel and elongated, which clearly defines the rock's fabric. The elongation of orthopyroxene is due to the strong strain reflected in translation gliding under asthenospheric conditions (Gueguen and Nicolas 1980). Grains are also featured by undulose extinctions, cleavage and transversal cracks, whereas diopside exsolution lamellae and encircling strain-free neoblasts are occasionally observed. The fine-grained matrix (~ 0.05 mm across) is peculiar, linking this rock to high-stress shear zones (Fig. 11f). Its main phase is olivine, followed by pyroxenes. Cr-spinel forms a minor phase being regularly scattered. All mineral phases, which form the fine-grained rock matrix, are devoid of deformation. They are anhedral to subhedral and have straight boundaries. Secondary magnetite was formed during enhanced mesh-like serpentinisation.

#### 4.2.1.6. Spinel-olivine websterites

This rock type covers the pyroxenite rocks (samples 1C and 2A) recovered from the western displaced segment of the KKOC in the Žepče region. The paragenesis comprises

big euhedral to subhedral grains of Opx and Cpx (~ 4 mm and ~ 3 mm across, respectively) (Fig. 11d). Grain size reduction at the grain boundaries has led to the development of many strain-free matrix phases (~ 1 mm across) forming a mosaic texture with clear triple junctions (Fig. 10h). Within the matrix, the main phases are olivine, spinel and garnet, whilst pyroxene is rare. Spinel is occasionally particularly coarse (~ 2 mm across), possessing a corona of needle-shaped secondary phases like chlorite and amphibole. Otherwise, spinel is xenomorphic and scarcely distributed (~ 0.05 mm across). Porphyroclasts are full of cracks and ruptures, regularly polygonated and sometimes containing olivine chadacrysts. Additionally, some of them are featured by undulose extinction and banded exsolution lamellae. Sample 2A records the formation of hydrogarnet (hybschite) and one other Ca-rich unknown phase in the matrix zone between pyroxene grains. This nucleation is due to the metasomatic processes that caused serpentinisation.

#### 4.2.1.7. Dunites (cumulate ultramafics)

This granular rock comprises samples with a clear cumulate texture. Samples U19 and K1 (Fig. 10b) were recovered from Duboštica and Karaula localities, respectively (Fig. 4, Table 2). Inside a heteroadcumulate texture, olivine and spinel are cumulus phases, whereas in the intercumulus interstices, one can notice plagioclase, Cpx, spinel and secondary phases like amphibole, chlorite, prehnite (sample U19) and magnetite (sample K1). Olivine cumulus grains are subhedral to anhedral, clearly isometric, polygonated and highly serpentinised (especially K1 sample). Average grain size is ~ 2 mm across. Olivine makes around 70 vol.% of these rocks. Cumulus spinel is ~ 1 mm across often being encircled by altered plagioclase coronae (Fig. 11e). Dark-brown anhedral intercumulus spinel (~ 0.2 mm across) is ubiquitously dispersed over the sample. Intercumulus plagioclase is regularly altered, mostly to prehnite. Careful microprobe investigations revealed clinopyroxene and occasionally olivine as xenomorphic intercumulus phases (~ 0.05 mm across). Detected secondary chlorite and amphibole are pseudomorphs of orthopyroxene.

#### 4.2.1.8. Podiform chromitite

A podiform chromitite deposit occurs near the Duboštica locality at the southern slopes of the Konjuh ultramafic domain (Fig. 4, Table 2). Three samples (D16, D17 and D18) were taken from this locality. The chromite grains are closely packed, having narrow interstices filled with silicate phases in samples D16 and D17. Sample D18 is devoid of silicate minerals; it was recovered away from the peridotite host rock. The chromitite texture is massive, with coarse-grained chromite comprising more than 90 vol.% chromite. The grains are ~ 4 mm across, being all anhedral with no reaction signs.

#### 4.2.1.9. Summary of petrographic features

The most characteristic features of primary petrogenetic phases in the analysed ultramafic rocks of the Krivaja-Konjuh ophiolitic complex are summarised and provided as follows:

**Olivine** is widely affected by alteration processes resulting occasionally in well-developed mesh-texture nets of serpentine. The following olivine morphologies are recognised:

- Relatively coarse, euhedral to subhedral olivine grains (~ 2 mm across) recovered from plagioclase lherzolite and cumulate ultramafics, which show signs of undulose extinction, serpentinisation and disintegration (cracks and intragrain ruptures).
- Subhedral, partly recrystallised, undulatory medium-sized olivine grains (~ 1 mm across) marked by weak kinking (KBB) and irregularly curvilinear boundaries and polygonisation. This olivine morphology is reported mostly in spinel lherzolites but is also found in plagioclase-bearing peridotites.
- Plausible strain-free grains recovered from olivine websterite and mylonitised lherzolite featured by polygonal shapes and fragment triple-point grain boundaries. The common size is ~ 0.3 mm.

Chadacrysts of olivine occur occasionally in porphyroclasts of pyroxene and spinel.

**Orthopyroxene** is mostly found as porphyroclast or matrix phase but other morphological varieties are also common. So, one can distinguish the following morphologies:

- Mainly subhedral rounded or slightly elongated porphyroclasts with grain sizes of 4-6 mm. Deformation features are echoed in undulose extinction, cleavage, kink-bands, and sporadically in pressure lamellae.
- Flattened porphyroclasts recovered from mylonitised lherzolite with an average grain size of 1-4 mm. Apart from mineral deformation effects, grain size reductions are ubiquitous.
- Matrix related small grains (~ 1 mm), mostly recording moderate deformation effects.
- Mosaic anhedral strain-free grains (~ 0.2 mm across) recovered from mylonitised lherzolite.
- Aggregates of polygonal grains (~ 0.5 mm across), often with converging triple point boundaries are noticed clustering along surfaces of (elongate) porphyroclasts together with recrystallised clinopyroxene and olivine.

Most of the Opx porphyroclasts include insulated phases such as olivine and hydrous minerals. When significantly elongated, they define the rock texture, i.e. the foliation plane which is typical for the solid-state flow deformation in the mantle.

**Clinopyroxene** appears as:

- Coarse subhedral isometric grains (~ 3 mm across) found in olivine websterite. The grains are marked by numerous cracks and fractures.
- Rounded or weakly elongated grains (up to ~ 2 mm across, including porphyroclasts), depicting significant strain-deformation such as exsolution lamellae, cleavage and polygonisation.
- Polycrystalline clinopyroxene aggregates reported as pyroxene streaks in plagioclase lherzolite. Strain-free grains have ~ 1 mm grain size, forming up to ~ 4 mm long streaks.

- Tiny clinopyroxene crystals (~ 0.02 mm across) formed either in mylonitised lherzolite matrix and bigger orthopyroxene porphyroclasts, or as an inter-cumulus phase in cumulate ultramafics.
- Exsolution lamellae parallel to (100) in orthopyroxene.

Cpx porphyroclasts are always smaller than Opx porphyroclasts, recording less deformation results. Fresh and colourless postkinematic grains, which occur in intergranular matrix positions, might represent products of sub-solidus crystallisation processes, or an outcome of local melting events as suggested by Nicolas et al. (1980).

**Cr-spinel** is irregularly distributed and found in almost all analysed KKOC ultramafic rocks. Various grain morphologies are recognised, mostly depending on the textures of associated silicate phases:

- Disseminated anhedral grains (~ 0.02 mm across) found inside all silicate phases, but mostly in olivine and/or orthopyroxene (porphyroclasts).
- Elongated amoeboidal grains (~ 0.8 mm across) or disseminated anhedral grains occurring inside the serpentinised matrix.
- Skeletal holly-leaf spinel grains marked by their lobate structure (~ 1.5 mm across), situated inside the rock matrix, occasionally occurring as porphyroclasts (~ 2.5 mm across) which include olivine chadacrysts.
- Relatively isometric to xenomorphic spinel grains (~ 1 mm across) found as cumulus phase in dunites. A peculiarity of this spinel shape is the development of secondary coronas encircling the spinel grains. The coronae are composed of plagioclase alteration products.

Generally, it can be concluded that spinel occurs either in form of small xenomorphic blebs (~ 0.02 mm across) within insulated silicates or they are reported to possess elongated, mostly irregular hook-shaped forms (~ 1 mm across).

## 4.2.2. Mineral chemistry

### 4.2.2.1. Olivine

Olivine is the most abundant and ubiquitous phase, occurring in all KKOC ultramafic lithological types. A comprehensive data set of olivine analyses is given in Appendix C (Table A-1–A-13). Olivine grains from the analysed KKOC ultramafics have a narrow compositional span of Fo<sub>87.4–92.3</sub> indicating a moderately depleted nature of the upper mantle peridotites. The minimum Fo value corresponds to ultramafic rocks having cumulate textures (dunites), whereas the maximum Fo value is measured in chromitite interstitial olivine. Olivine from the KKOC ultramafic rocks is classified either as forsterite or as chrysolite (Deer et al. 1992). The forsterite value in plagioclase and spinel lherzolites varies from 89.1 to 90.7 and from 88.8 to 91.9, respectively. This chemical homogeneity is attributed to balanced partial melting of large areas of upper mantle, which resulted in a compositional continuity, specifically in Fo content, throughout sections of depleted mantle up to several hundred square kilometres in size (Arai 1994). Presented data are in correlation with Fo values of tectonite peridotites

from the Vardar zone and the Central Dinaride Ophiolite Belt (e.g. Lugović 1986, Maksimović and Kolomejceva-Jovanović 1987, Lugović et al. 1991, Majer 1993, Bazylev et al. 2009). Olivine from olivine websterites has Fo values of 89.1 to 90.4, whereas Ol in dunites and chromitites is marked by Fo values of 87.5–89.1 and 91.5–92.2, respectively. Elevated Mg# values in olivines recovered from chromitites are due to the olivine subsolidus Mg-Fe exchange with volumetrically dominant host chromite (e.g. Roeder et al. 1979, Lehmann 1983). Forsterite proportions in olivine from the KKOC minor lithological units correspond well to similar ophiolitic and MORB domains found worldwide (e.g. olivine pyroxenites of Southwest Indian Ridge, Dantas et al. 2007; dunites from Nan Uttaradit ophiolite, Oberger et al. 1995; chromitites from the Luobusa ophiolite, Zhou et al. 2005).

NiO contents vary from 0.28 to 0.56 wt%, with a minimum recorded in olivine websterites, whereas the maximum value is found in chromitite interstitial olivine. Plagioclase and spinel lherzolites have NiO values of 0.32 to 0.46 wt%. Based on the NiO and Fo values in olivine, a discrimination diagram is constructed, which distinguishes tectonite ultramafic from cumulate and replacive ultramafic rocks (Leblanc et al. 1984). Regardless of host rock petrography, all analysed olivine grains from the KKOC ultramafic segment are classified as originating from tectonite ultramafic rocks (i.e. mantle rocks showing a metamorphic overprint) (Fig. 12). In plagioclase and spinel lherzolites, no systematic change in Fo values or NiO abundances are reported with respect to modal abundances of pyroxene. Occasionally, in cumulate textured dunites, the detectable NiO depletion follows the FeO enrichment. The CaO content and its fluctuations are low (0.01–0.04 wt%) for both peridotite types. However, in the olivine websterites and dunites, CaO abundances are significantly higher, reaching 0.19 wt%. Low TiO<sub>2</sub> values (~ 0.01 wt%) of all analysed olivine grains are within the normal peridotite values (e.g. Burgath et al. 1997).

#### 4.2.2.2. Orthopyroxene

Microprobe analyses of different orthopyroxene varieties detected in the KKOC spinel and plagioclase lherzolites as well as olivine websterites are listed in Appendix C (Table B-1–B-5, Table C-1–C-6). The analyses refer to porphyroclasts (88), deformed and undeformed smaller matrix-grains (107), and exsolution lamellae (3).

The data show similar Mg# for porphyroclasts (88.2–90.9) and smaller grains (88.2–90.5). Opx has a high range of Al<sub>2</sub>O<sub>3</sub>, i.e. 1.56–6.21 wt% in porphyroclasts and 1.40–6.21 wt% in smaller grains, indicating a moderately depleted nature of upper mantle peridotites (Fig. 14). Cr<sub>2</sub>O<sub>3</sub> abundances are within 0.27–0.97 wt% for porphyroclasts and 0.14–0.95 wt% for smaller grains, whereas the CaO proportion in all Opx varieties varies from 0.32–3.23 wt% (Fig. 13). There are no significant differences between Opx from spinel and plagioclase lherzolites and Opx recovered from olivine websterites. Even though, unusually elevated TiO<sub>2</sub>, Al<sub>2</sub>O<sub>3</sub> or Cr<sub>2</sub>O<sub>3</sub> contents in Opx from the KKOC pyroxenites are in accordance with published data on the chemistry of pyroxenite recovered from similar lherzolite massifs (e.g. Lherz, French Pyrenees; Bodinier et al. 1986b).



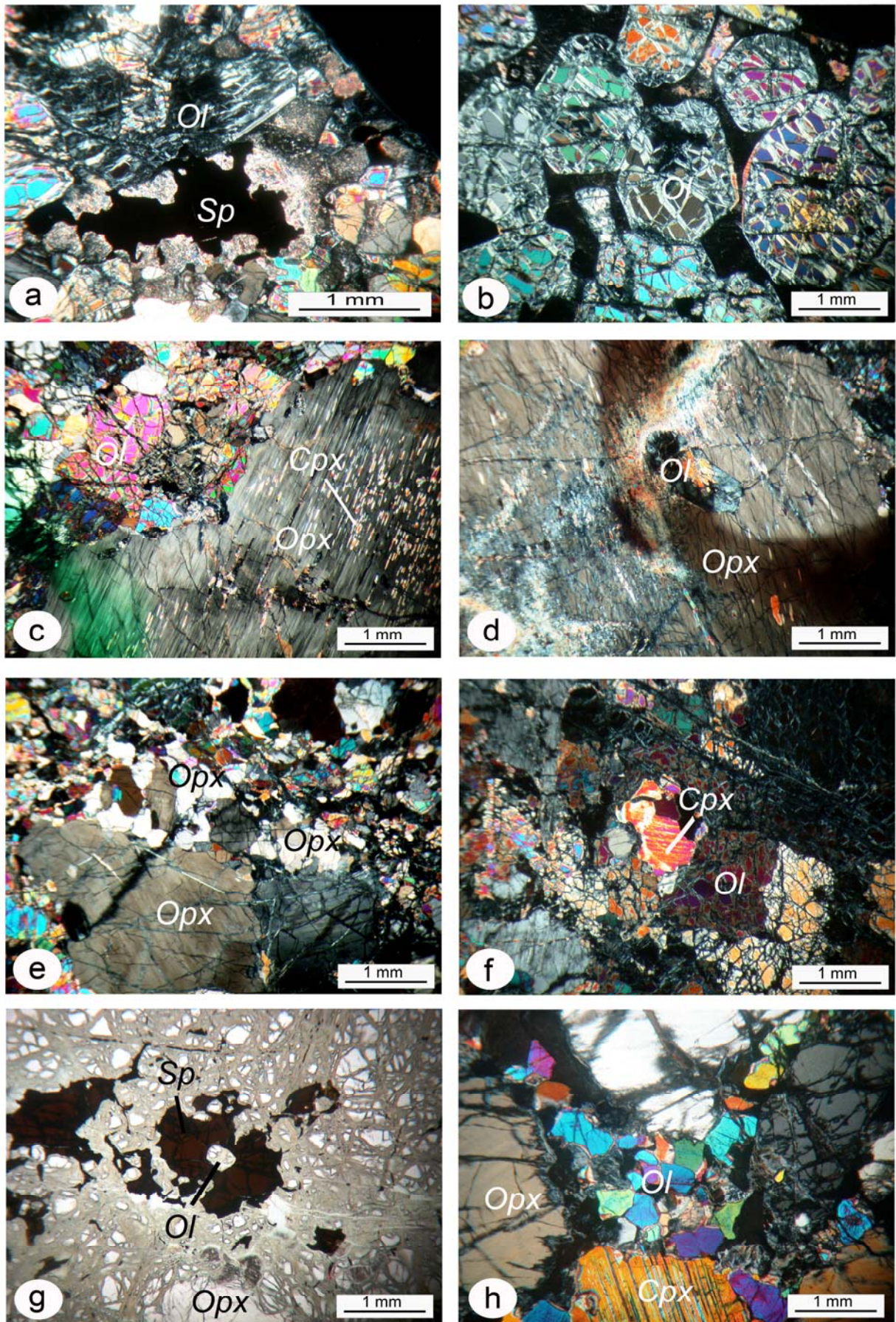


**Fig. 10a-h.** Selected microphotographs of analysed ultramafic rocks. For details see text (subchapter 4.2.1.); Ol = olivine, Sp = spinel, Opx = orthopyroxene, Cpx = clinopyroxene.

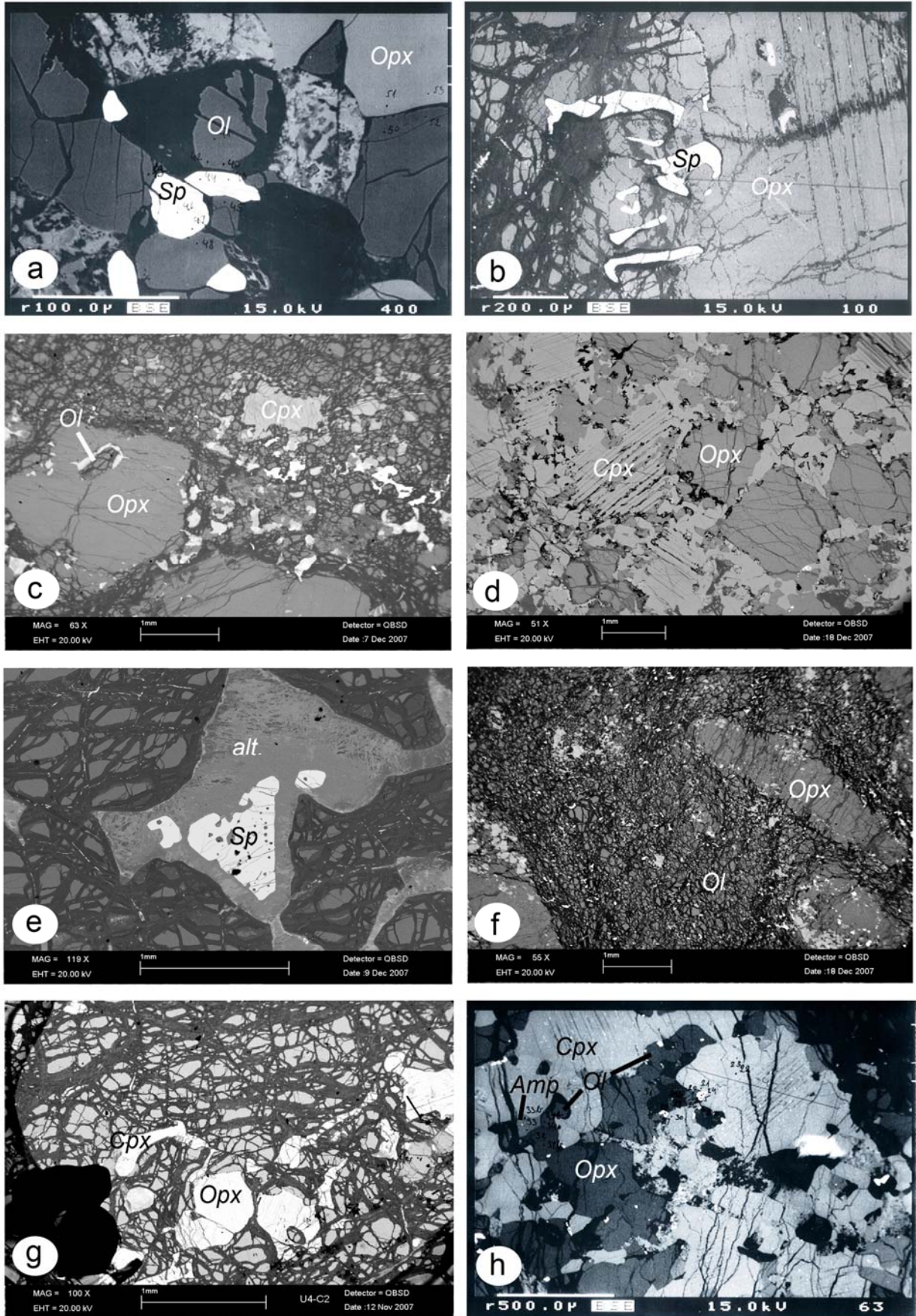


**Fig. 11a-h.** Selected BSE pictures of analysed ultramafic rocks. Description in text - subchapter 4.2.1. Numbers in microprobe BSE pictures refer to the respective mineral chemistry analyses (Appendix C, mineral chemistry); signs like in Fig. 8a-h, alt = alteration products. Abbreviations after Kretz (1983).

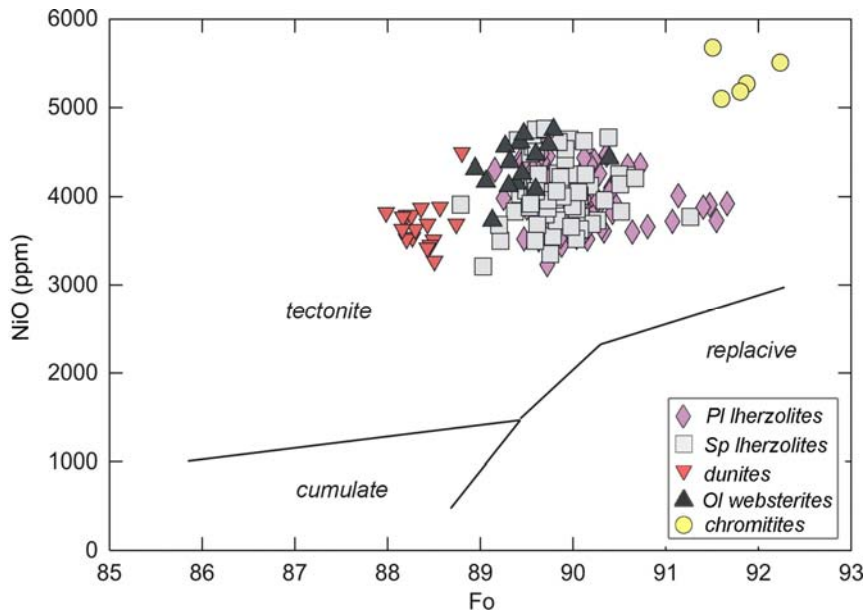


**Fig. 12.** Variation of NiO with Fo content in olivine used to distinguish between cumulate and tectonite ultramafics (adapted from Leblanc et al. 1984). Legend shows studied rock type based on its petrography (see Chapter 4.2.1.).

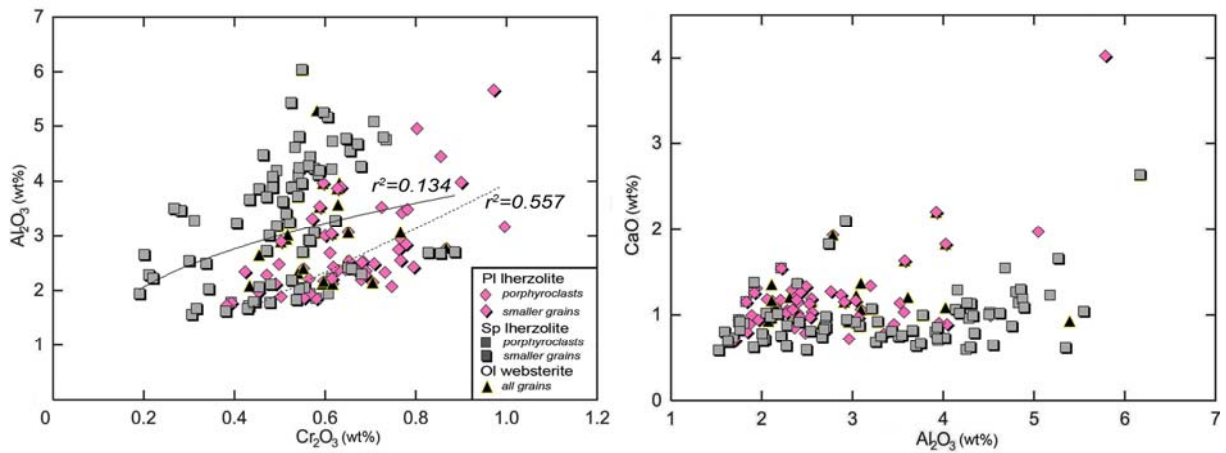


**Fig. 13.**  $Al_2O_3$  vs  $Cr_2O_3$  in orthopyroxene from different KKOC ultramafic rock lithologies (left);  $CaO$  vs  $Al_2O_3$  in orthopyroxene from different KKOC ultramafic rock lithologies (right).

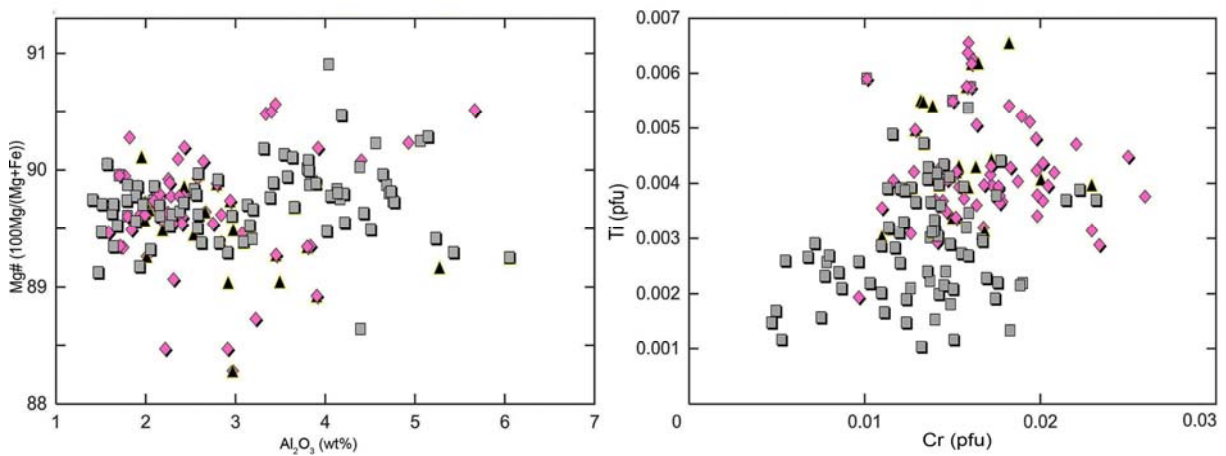


**Fig. 14.** Mg# vs  $Al_2O_3$  in orthopyroxene from different KKOC ultramafic rock lithologies (left); Ti vs Cr in orthopyroxene from different KKOC ultramafic rock lithologies (right). For symbols see Fig. 11.

Al<sub>2</sub>O<sub>3</sub> and Cr<sub>2</sub>O<sub>3</sub> abundances in Opx are positively correlated, displaying a higher correlation for plagioclase lherzolites ( $r^2 = 0.56$ ) as compared to spinel lherzolites ( $r^2 = 0.13$ ) (Fig. 13). Analyses having the highest values of both elements belong to the large orthopyroxene grains that are free of clinopyroxene exsolutions. Opx featured by spinel blebs and Cpx exsolution lamellae show the lowest Al<sub>2</sub>O<sub>3</sub> and Cr<sub>2</sub>O<sub>3</sub> values. Generally higher Al<sub>2</sub>O<sub>3</sub> abundances of Opx from spinel lherzolites as compared to Al<sub>2</sub>O<sub>3</sub> values in Opx from plagioclase lherzolites are consistent with experimental values for spinel and plagioclase lherzolite stability fields (e.g. Borghini et al. 2007). Relatively high CaO values and Al<sub>2</sub>O<sub>3</sub>/Cr<sub>2</sub>O<sub>3</sub> ratios of analysed KKOC orthopyroxene is typical for high temperature dry systems that are devoid of major pressure influences (Sachtleben and Seck 1981, Werner and Pilot 1997).

The Ti-Cr diagramme (Fig. 14) reveals higher titanium values for orthopyroxene from plagioclase lherzolites, compared to spinel lherzolites. Plagioclase lherzolite shows similar or higher Al<sub>2</sub>O<sub>3</sub> contents, ranging within the same Mg# span like those of spinel lherzolites (Fig. 14). Furthermore, Ti-poor Opx porphyroclast cores are the richest in alumina at the given CaO values, whereas the bulk of CaO values are elevated in Opx from plagioclase lherzolites compared to orthopyroxene from spinel lherzolite (Fig. 13). All discussed features might suggest that plagioclase lherzolites have undergone compositional changes due to interaction with metasomatic fluids or impregnating melts (Cannat et al. 1990).

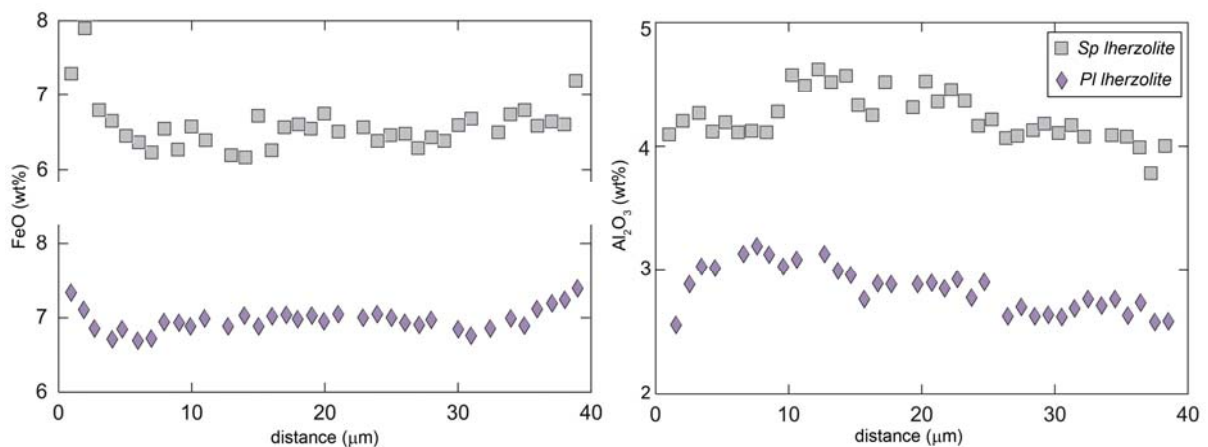


**Fig. 15.** Selected profiles for FeO (left) and Al<sub>2</sub>O<sub>3</sub> (right) made through the orthopyroxene porphyroclasts from plagioclase and spinel lherzolites

Most of the profiles of Opx porphyroclasts in both, plagioclase and spinel lherzolites, show a clear tendency in the FeO distribution toward higher abundances in the grain rims compared to the abated values in their cores (Fig. 15). Conversely, the content of Al<sub>2</sub>O<sub>3</sub> is found elevated inside the grains. CaO and Cr<sub>2</sub>O<sub>3</sub> behave irregular. The compositional patterns of Opx porphyroclasts are best explained through the process of sub-solidus reequilibration here seen as an impoverishment of alumina within the grain's rim due to cooling (e.g. Cannat et al. 1990).

#### 4.2.2.3. Clinopyroxene

Clinopyroxene is found in all major KKOC ultramafic subtypes including olivine websterites, dunites and podiform chromitites. Its comprehensive microprobe analyses are provided in Appendix C, comprising 90 analyses of clinopyroxene porphyroclasts (Table D-1-D-5), 45 analyses of smaller and postkinematic grains as well as 8 analyses of clinopyroxene inclusions and lamellae (Table E-1-E-3).

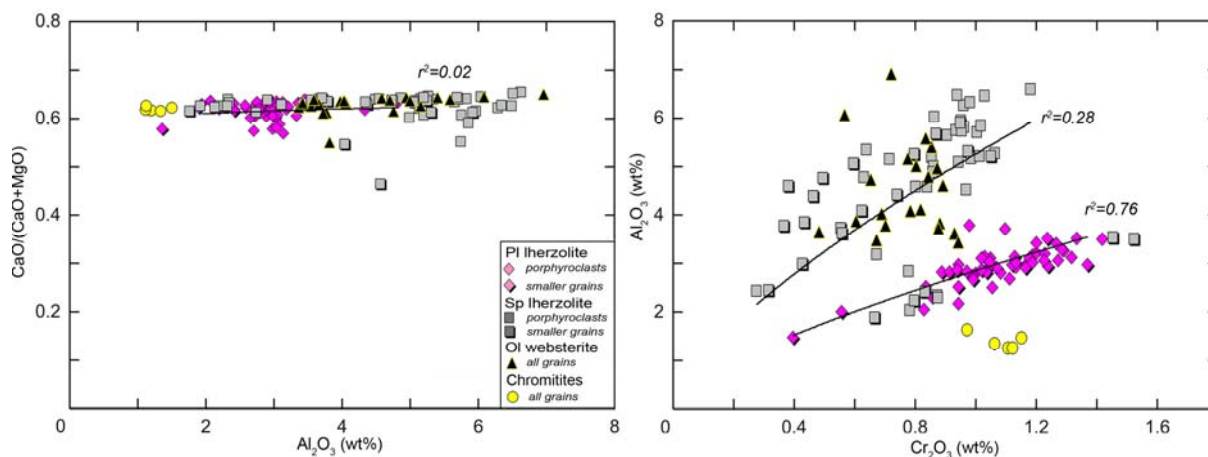


**Fig. 16.**  $Al_2O_3$  vs  $CaO/(CaO+MgO)$  in clinopyroxene from different KKOC ultramafic rock lithologies (left);  $Cr_2O_3$  vs  $Al_2O_3$  in clinopyroxene from different KKOC ultramafic rock lithologies (right). For symbols, see left picture.

The Mg# of clinopyroxene in lherzolites varies considerably, both for prekinematic and postkinematic grains (88.2-93.4 and 88.2-94.4, respectively). Taking into account the average Mg# values of all clinopyroxene varieties being around 91, the KKOC clinopyroxene host rocks are referred to less-depleted peridotites (Michael and Bonatti 1985, Cannat et al. 1990). As well, in both morphological cases, the Mg# of Cpx is obviously higher than that of Opx. Like in Opx, the  $Al_2O_3$  content of Cpx is wide-ranging, fitting 1.45-7.16 wt% for prekinematic and 1.22-6.11 wt% for postkinematic grains. One can notice that Cpx from spinel lherzolite has almost twice as much  $Al_2O_3$  as Cpx from plagioclase lherzolite (Fig. 16). Other main components decipher considerable variability, e.g. CaO ranges from 18.1 to 24.3 wt% and  $Cr_2O_3$  from 0.06 to 1.72 wt% (Fig. 16). MgO is higher in postkinematic grains (15.3-21.4 wt%), than in prekinematic ones (14.4-18.5 wt%), while FeO concentration shows a different trend with porphyroclasts having a broader compositional range (2.04-4.08 wt%) as compared to smaller grains and Cpx inclusions and lamellae. Minor element oxides, such as  $TiO_2$ , MnO and  $Na_2O$ , are also found to have a high compositional span. The presented mineral chemistry defines the analysed clinopyroxenes as aluminium to chromium diopsides.

In olivine websterites, the Mg# values of clinopyroxene range from 89.5 to 97.7. These clinopyroxenes are highly aluminous, with  $Al_2O_3$  contents ranging from 3.70 to 7.16 wt%. Their  $TiO_2$  and  $Na_2O$  abundances are also high, reported to be within the ranges of 0.35-0.55 and 0.41-0.62 wt%, respectively. The  $Cr_2O_3$  concentration is relatively elevated, reported within the span of 0.57-0.94 wt%. Main element abundances in Cpx from olivine websterites are similar to those of fertile lherzolite subtypes, as is shown in Figures 16-18. An exception is  $TiO_2$ , which is significantly higher than in its lherzolite host counterparts (Fig.

18). The analysed clinopyroxene chemistry is very similar to Cpx from pyroxenites from the Mid-Atlantic Ridge at the Kane Fracture Zone (e.g. Juteau et al. 1990) or those from the Southwest Indian Ridge (Dantas et al. 2007). Partly they correspond to those of the Alpine pyroxenite bodies (e.g. Lherz, Bodinier et al. 1986a, b), whereas they are considerably richer in  $\text{TiO}_2$ ,  $\text{Al}_2\text{O}_3$  and  $\text{Na}_2\text{O}$  with respect to Cpx of pyroxenite of several ophiolite domains found worldwide (e.g. Troodos, Oman, Appalachian, and Thailand; Augé 1983, Ernewein et al. 1988, Hébert and Laurent 1989, Oberger et al. 1995, and references therein).

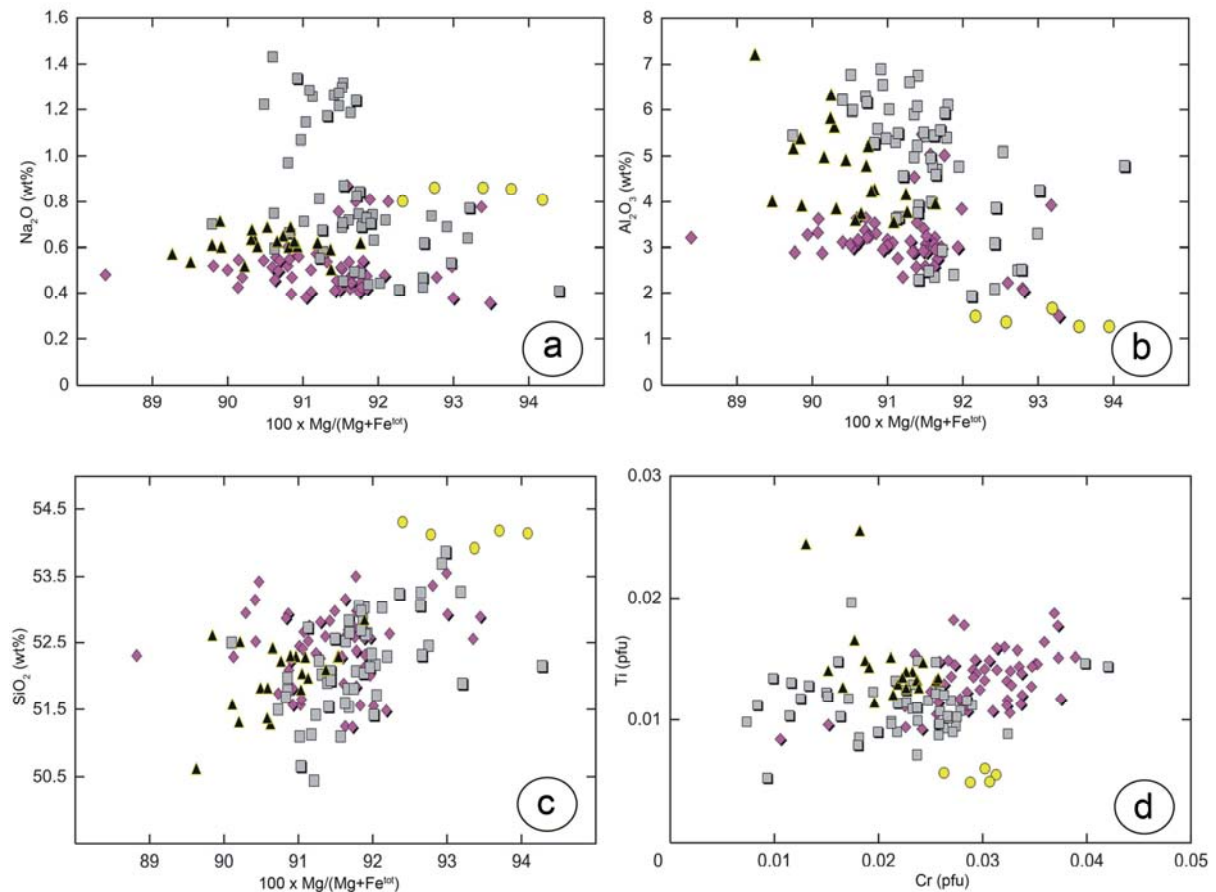


**Fig. 17a-d.** (a)–(c)  $\text{Na}_2\text{O}$ ,  $\text{Al}_2\text{O}_3$  and  $\text{SiO}_2$  vs Mg-number in analysed clinopyroxenes from different KKOC ultramafic rock lithologies; (d) Ti vs Cr in clinopyroxene from the different KKOC ultramafic rock lithologies. For symbols, see Fig. 14.

Clinopyroxene occurs sporadically in dunites and chromitites as minor interstitial constituent. Its  $\text{Al}_2\text{O}_3$  content ranges from 1.45 to 4.75 wt% and from 1.22 to 1.49 wt%, respectively.  $\text{TiO}_2$  ranges from 1.57 to 2.05 and from 0.06 to 0.10 wt% for dunite and pyroxenite host varieties, respectively. It is interesting to remark that clinopyroxene in the chromitites have higher  $\text{SiO}_2$  but lower  $\text{Al}_2\text{O}_3$  and FeO in comparison to those originating from lherzolites and pyroxenites. This ratio is reversed for dunite clinopyroxene. It is noteworthy to say that interstitial clino-pyroxene of cumulate dunites is characterised by high Mg# values ( $\sim 93.2$ ), which might be diagnostic for subsolidus melt impregnation (Rampone et al. 1997). Cpx found in chromitite shows similarities with Cpx reported from chromitite transition zones of certain ophiolitic domains (e.g. Luobusa ophiolite, Zhou et al. 2005).

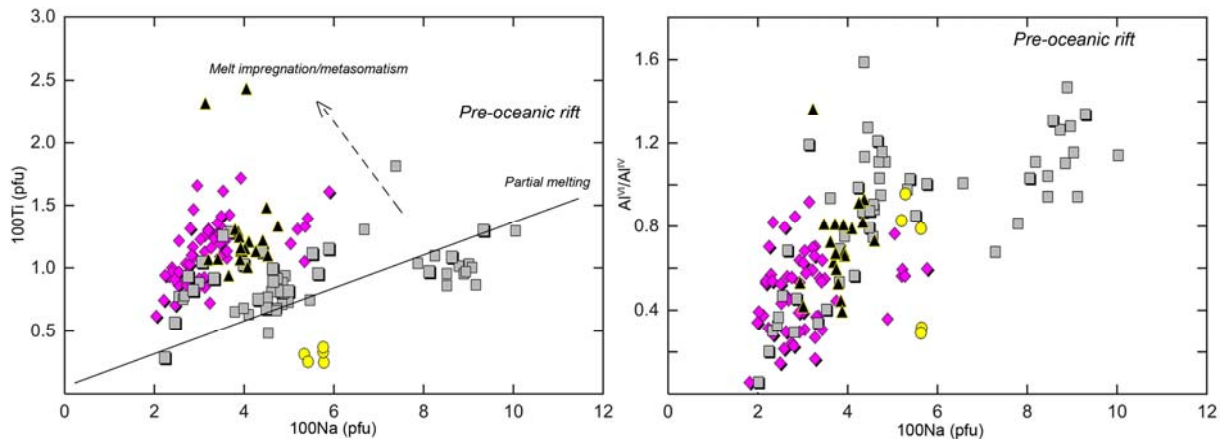


**Fig. 18.** 100Ti vs 100Na for clinopyroxene from different KKOC ultramafic rock lithologies (left);  $Al^{VI}/Al^{IV}$  for clinopyroxene from different KKOC ultramafic rock lithologies (right). For symbols, see Fig. 14.

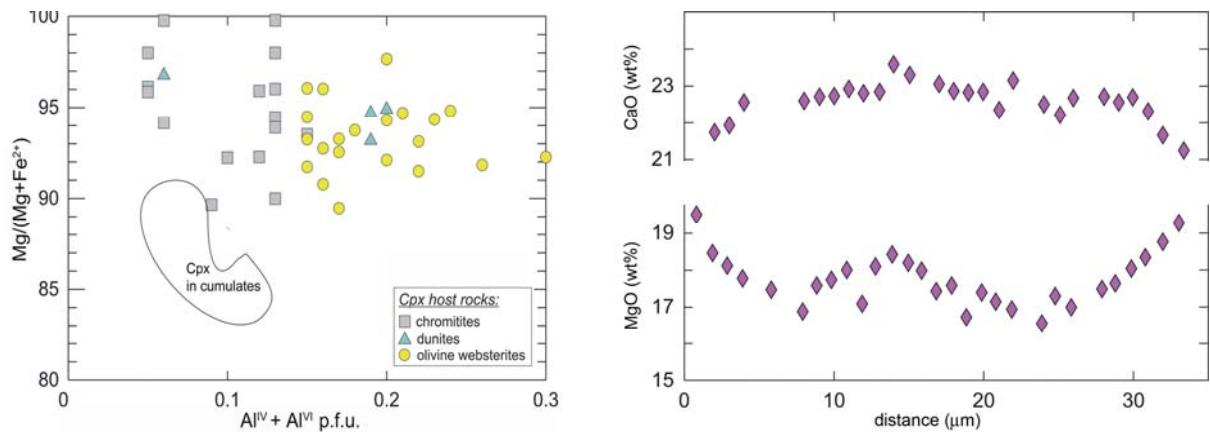


**Fig. 19.** Minor lithologies' clinopyroxene plotted in the  $Mg/(Mg+Fe^{2+})$  vs Al diagramme. Clinopyroxene in cumulates, data from Orberger et al. (1995) and references therein (left); Selected profiles for CaO and MgO across a typical clinopyroxene porphyroclast from plagioclase lherzolites of KKOC (right).

Assuming that (at least part of) the KKOC ultramafic rocks have an ocean-ridge origin, 100Ti vs 100Na and 100Ti vs  $Al^{VI}/Al^{IV}$  plots were used, originally constructed for discrimination of ridge-affiliated suboceanic peridotites (e.g. Girardeau and Francheteau 1993, Niida 1997) (Fig. 18). One can notice that the chemistry of parts of Cpx from the KKOC spinel lherzolites bounds its host rocks to the near pre-rift oceanic peridotite setting, nowadays recovered along the American-Antarctic ridge (Dick 1989). The rest of clinopyroxene from spinel lherzolites is comparatively impoverished in Na and Ti, implying that those host rocks underwent higher (moderate) degrees of partial melting. The bulk of clinopyroxenes from the KKOC plagioclase lherzolites and olivine websterites is, due to its Ti content, shifted from the solid line, which presents a peridotite partial melting trend. The shift, marked by a dashed line, is aimed to the array of metasomatically influenced peridotites (Fig. 18). As shown in Fig. 18 (right), the range of  $Al^{VI}/Al^{IV}$  values of clinopyroxenes that originate from spinel lherzolite (0.05-1.60) is generally twice as high than the range belonging to clinopyroxene from plagioclase lherzolites or from olivine websterites (0.05-0.80). This suggests deeper equilibration depths of spinel lherzolite pyroxenes, whereas Cpx

from plagioclase lherzolite and pyroxenite host rocks reequilibrated at shallower levels. Furthermore, the Na content of Cpx from spinel lherzolites is evidently higher for porphyroclasts than for smaller post-kinematic grains. The Cpx group enriched in Na corresponds to clinopyroxene from peridotites of an early stage of pre-oceanic rifting (e.g. SW Australia, Nicholls et al. 1981).

The grain profile variations demonstrate a weak trend of opposite distribution of MgO and CaO in Cpx porphyroclasts recovered from plagioclase lherzolites. The rims are enriched in MgO and impoverished in CaO, whereas the cores are impoverished in MgO and enriched in CaO (Fig. 19). FeO behaves similar like MgO, whereas Al<sub>2</sub>O<sub>3</sub> records a completely unpredictable pattern. For clinopyroxene from spinel lherzolite, no significant grain zonation is reported with respect to CaO and MgO/FeO. The Al<sub>2</sub>O<sub>3</sub> abundances oscillate through the grain.

In Fig. 19, the composition of Cpx that originates from minor ultramafic lithologies of the Krivaja-Konjuh ophiolite complex (olivine websterite, dunite and chromitite) is depicted with respect to its Mg# and total Al per formula unit. It is indicative that clinopyroxene from these rocks has significantly higher magnesia and alumina values compared to clinopyroxene from several world's ultramafic cumulate complexes (e.g. Dantas et al. 2007, Oberger et al. 1995 and references therein). Thus, although many of the analysed dunites and pyroxenites possess a cumulate texture, a stationary cumulate settling from basaltic magmas was not the sole mechanism of formation of these rocks.

#### 4.2.2.4. Spinel

211 microprobe analyses of spinel, an integral but irregularly distributed mineral in KKOC ultramafic rocks, are listed in Appendix C, Tables F-1–F-12. The analyses cover spinel recovered from spinel and plagioclase lherzolites, pyroxenites, dunites and chromitites.

In spinel lherzolites, spinel is mainly yellowish to brownish, whereas in plagioclase lherzolites, it is more brownish having a composition of chromium picotite. As well, in dunites spinel has a picotite composition, whilst in pyroxenites it contains more alumina (Deer et al. 1992; Figs. 20 and 21). Generally, spinel chemistry is dominated by a strong Cr-Al trend, ranging from Al rich spinel grains of 'high-pressure' spinel lherzolites to Al- and Fe<sup>3+</sup>-poor spinel grains of chromitite podiform bodies. Roughly, the bulk of spinel grains from the KKOC ultramafic rocks show a continuous geochemical transition within the ocean-floor compositional range, whereas spinel grains from chromitites, and partly also from dunites, show an arc-related affinity (Fig. 20). It is known that Al is rapidly removed from the spinel lattice due to alteration, whereas Fe is added into the structure (e.g. Barnes and Röder 2001). Therefore, the grain rim analyses are usually excluded from further consideration. However, in case of the KKOC ultramafic rocks, the spinel composition was not significantly altered by serpentinisation (Fig. 20).

Spinel mineral chemistry is very informative regarding petrogenesis. The Chromium number (Cr#) is a sensitive indicator of partial melting, while the Mg# indicates exchange reaction temperatures with neighbouring silicates, whereas the ferric number (Fe<sup>3+</sup>#)



depends on the sub-solidus oxygen fugacity (e.g. Dick and Bullen 1984, Hellebrand et al. 2001). The lowest Cr# is 7.2, recorded in spinel from spinel lherzolite, and its maximum is 78.1 found in spinel from podiform chromitites. The compositional ranges of Cr# of spinel originating from different ultramafic lithologies cluster from 7 to 50, 30 to 50, 15 to 32, 40 to 60, and 70 to 80 for spinel and plagioclase lherzolites, spinel websterites, dunites, and podiform chromitites, respectively (Fig. 21). Spinel grains with Cr# > 40 also have considerably elevated Fe<sup>3+</sup># and TiO<sub>2</sub> contents (Fig. 22). The Mg# clusters from 40 to 80, and Fe<sup>3+</sup># from 1 to 16. Cr# and Fe<sup>3+</sup># values of spinel from spinel lherzolites plot inside the compositional field defined by abyssal and alpine spinel peridotites, as shown in Fig. 21 (e.g. Dick and Bullen 1984, Bonnati et al. 1992).

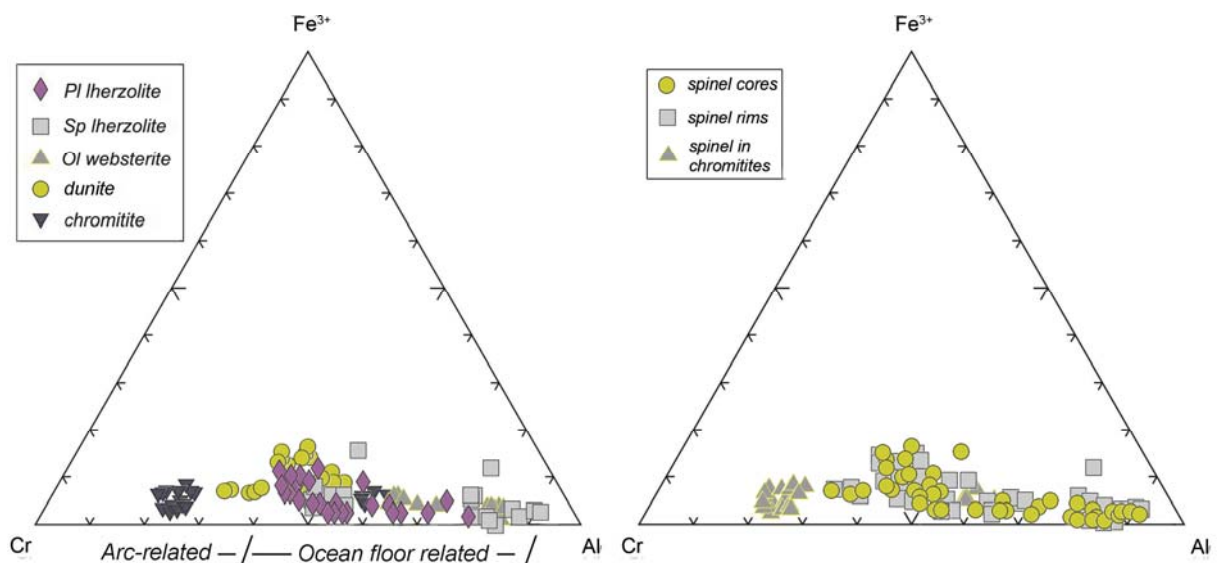


**Fig. 20.** Trivalent ion classification plot for spinel from different KKOC ultramafic rock lithologies (left); Trivalent ion composition of spinel grain rims and cores (right). The bulk of spinel grains from the KKOC show a continuous geochemical transition in the ocean floor compositional range. Spinel in chromitites shows an arc-related affinity.

According to the equation proposed by Hellebrand et al. (2001), the degree of partial melting of primary spinel lherzolite of MOR settings is ~ 7.7 %. Spinel from plagioclase lherzolite is found inside the compositional area defined by the arc-related harzburgites, whereas spinel from dunites is found in both, the arc harzburgites' and dunites' compositional fields (Ishii et al. 1992). Cr-rich spinel from chromitites is found ideally corresponding to the field defined by chromitites (Barnes and Röder 2001), and spinel grains from olivine websterites display a non-uniform, broad range of composition, showing the highest match with spinel of spinel lherzolites (Figs. 20 and 21).

Spinel from all ultramafic lithological units is featured by peculiar TiO<sub>2</sub> abundances. Its average abundances in spinel from plagioclase and spinel lherzolites, olivine websterites, dunites, and chromitites are 0.48, 0.10, 0.36, 1.84 and 0.28 wt%, respectively (Tables F-1-F-12). Taking into account general criteria and the large current analytical dataset for residual peridotites in the world, it is inferred that only spinel with TiO<sub>2</sub> under 0.12 wt% is considered as primary (Bazylev et al. 2009).

Accordingly, only the spinel from plagioclase-free spinel lherzolites is a primary MOR-related phase. Hence, low Ti in spinel supports the absence of plagioclase and testifies the rock's primary (residual) nature (e.g. Hellebrand et al. 2002). Both, the elevated  $\text{TiO}_2$  contents and the high Cr# values of spinel from plagioclase lherzolites are symptoms of sub-solidus metasomatic processes that might have influenced these rocks (e.g. Takahashi 2001). In Fig. 21a, one can notice that Ti enriched spinel originating from the minor ultramafic lithologies is shifted from the general trend of partial melting of MOR associated rocks (Niida 1997). This shift of spinel chemistry from the MOR trend is also explained by lowered Mg# of associated silicates or from lowered closure temperature of the Fe-Mg olivine-spinel exchange (Dick and Bullen 1984). Such a tendency is characteristic for non-MOR peridotites of (fore-)arc affinity (Ishii et al. 1992, Zanetti et al. 2006).

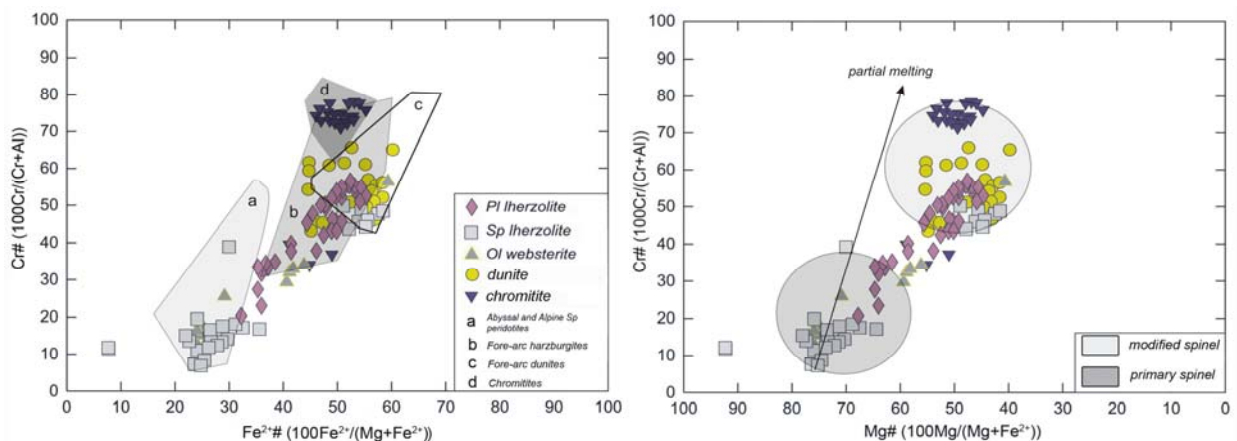


**Fig. 21.**  $\text{Cr}/(\text{Cr}+\text{Al})$  vs  $\text{Fe}^{2+}/(\text{Fe}^{2+}+\text{Mg})$  in spinels from the different KKOC ultramafic rock lithologies. Fields are according to Dick and Bullen (1984), Ishii et al. (1992) and Barnes and Röder (2001) (left);  $\text{Cr}/(\text{Cr}+\text{Al})$  vs  $\text{Mg}/(\text{Mg}+\text{Fe}^{2+})$  for spinels from different KKOC ultramafic rock lithologies (right). For symbols, see left picture.

In Fig. 22, the geotectonic setting of the minor lithologies spinel host rocks is further treated by discussing spinel  $\text{TiO}_2$  vs.  $\text{Fe}^{3+}$ - and Cr-number proportions. Highly chromiferous spinel, low in  $\text{TiO}_2$  is characteristic for chromitites derived from boninite magmas or for those formed by an interaction with magmas of boninite affinities (e.g. Oberger et al. 1995, Peck and Keays 1990). Large  $\text{Fe}^{3+}$ #,  $\text{TiO}_2$ , and moderately Cr# and Mg# variations characterise spinel from the dunite paragenesis. They need to be ascribed to the subsolidus partitioning with the host olivine. An increase in Cr# is accompanied by decrease in Mg#, since Mg enforces Al to enter the structure of spinel (e.g. Sack 1982). Such a broad compositional span of dunite-originated spinel suggests island-arc tholeiitic magma took part in their formation as already previously suggested (Arai et al. 2007). Spinel hosted in olivine websterite has relatively high Mg# (58-77), along with low  $\text{Fe}^{3+}$ # and Cr# values, suggesting a within-limit overlap with the boninite spinel field (Fig. 22). Nevertheless, this indication is due to a significant increase in Al and decrease in Fe of pyroxenite spinel, whereas the Cr abundances are altered moderately, which strongly suggests a MOR origin of spinel in pyroxenites (Fig. 22, e.g. Dantas et al. 2007).

Correlation trends of Cr# of analysed spinel grains were tested with respect to the Mg# and  $\text{Al}_2\text{O}_3$  contents of the neighbouring silicates (Ol, Cpx and Opx) (Fig. 23). The phase chemistry of coexisting olivine and spinel define its host rocks as tectonites, with only part of the dunites additionally defined as cumulates. The upper part of the tectonite field portion in

the diagramme Cr# vs Fo is occupied by the arc or melt impregnation-related lithological units (chromitites and plagioclase lherzolites), whereas the lower part belongs to the impregnation-unaffected MOR rocks, here being spinel lherzolites and pyroxenites. Fo content in olivine shows a weak correlation with the Cr# of spinel, whereas the Al<sub>2</sub>O<sub>3</sub> contents of both clinopyroxene and orthopyroxene show a clear negative correlation with Cr# of neighbouring spinel. It is known that the alumina content of peridotite pyroxenes is sensitive to the degrees of mantle melting regularly declining as the refractory nature of peridotite increases (e.g. Dick and Natland 1986). On the other hand, spinel gets richer in Cr as mantle melting advances.

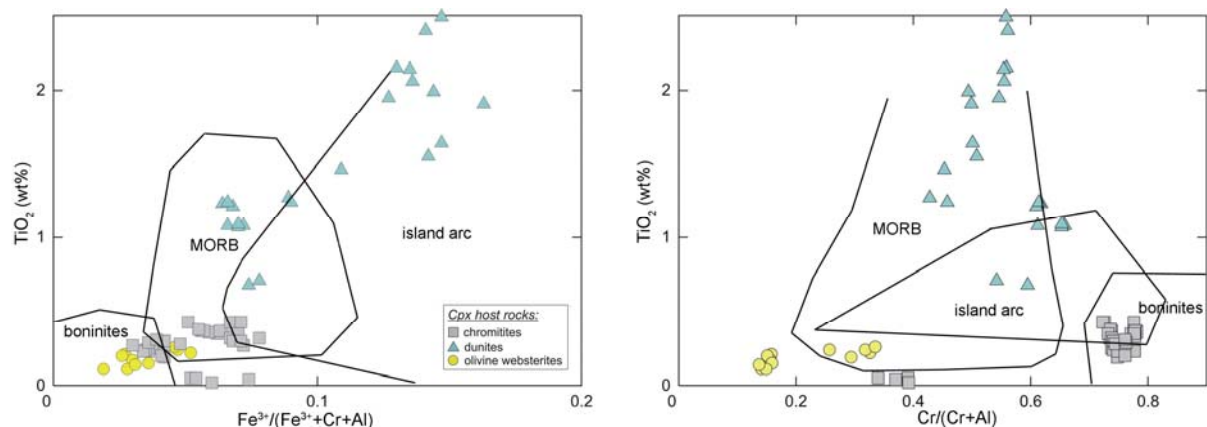


**Fig. 22.** TiO<sub>2</sub> vs Fe<sup>3+</sup>/(Fe<sup>3+</sup>+Cr+Al) plot for spinels from subordinate KKOC ultramafic lithologies (left); TiO<sub>2</sub> vs Cr/(Cr+Al) of spinel from minor KKOC ultramafic lithologies (right); Geotectonic setting fields from Oberger et al. (1995), Arai (1992) and references therein. For symbols, see the first picture.

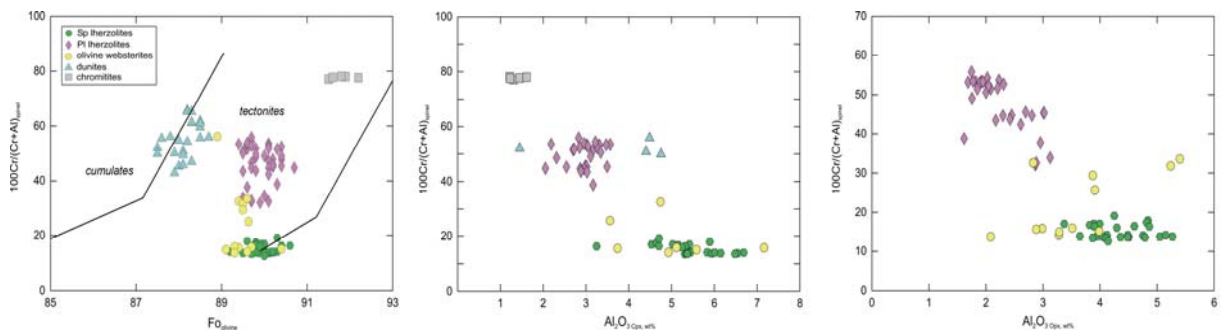


**Fig. 23.** Cr# (spinel) vs Fo (olivine) of coexisting Sp-Ol pairs (left); Cr# (spinel) vs Al<sub>2</sub>O<sub>3</sub> (Cpx) for coexisting Sp-Cpx pairs (center); Cr# (spinel) vs Al<sub>2</sub>O<sub>3</sub> (Opx) of coexisting Sp-Opx pairs (right). For symbols, see the first picture.

#### 4.2.2.5. Plagioclase

Plagioclase is reported occasionally, most often as rare fine-grained granoblastic aggregates (plagioclase lherzolites), or in the form of alteration-generated marginal aggregated substance formed around spinel of picotite composition (olivine websterites). The complete plagioclase compositional dataset can be found in Appendix C, Table G-1.

The compositional span of plagioclase is narrow, being mostly bytownite (Fig. 24). Within bigger grains, a moderate Na-Ca zoning is noticed, often featured by a rimward increase of the An component, whereas the rest shows oscillatory saw-tooth zoning as described in Takahashi (2001)(Fig. 24). Described An enrichment along plagioclase margins, along with the oscillatory zoning pattern, invoke to upper mantle melt migration processes triggered by clear decompression processes (Ozawa and Takahashi 1995, Takahashi 2001).

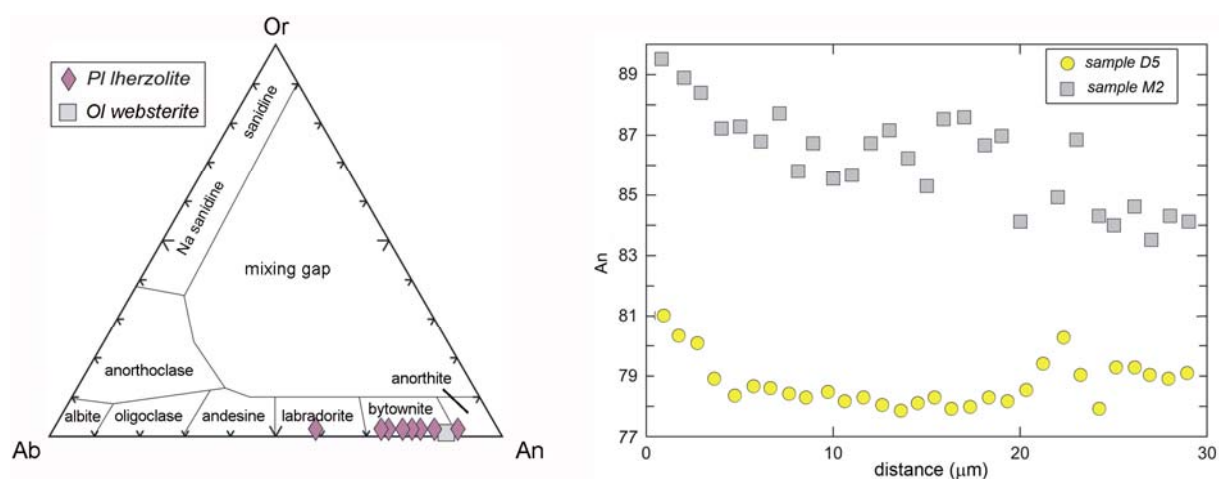


**Fig. 24.** Ab-Or-An classification diagramme for feldspar from plagioclase Iherzolites and olivine websterites from the KKOC complex (Deer et al. (1992) (left); Line profiles of An mol% ( $100Ca/(Ca+Na+K)$ ) in plagioclase from the KKOC Pl Iherzolites (right).

#### 4.2.2.6. Other phases

Comprehensive microprobe analyses of minor phases are provided in Appendix C, Tables H1-H2. In the KKOC ultramafic rocks, amphibole is either the primary or most often secondary phase and it shows wide compositional variations (Fig. 25). The compositions of secondary interstitial amphibole in dunites and olivine websterites range from tschermakite to pargasite, whereas the secondary amphibole in spinel Iherzolites is of actinolite/tremolite composition. The primary amphibole is detected in one sample of spinel Iherzolite, always along Ol-Opx-Cpx triple points (sample U35, Fig. 11h). It has the composition of pargasitic hornblende with Mg# fitting the range of 96.1-97.1. Concentrations of  $K_2O$  range from 0.08-0.10 wt% and the  $TiO_2$  content is 1.45-1.53 wt%. Nowadays the primary-textured amphibole is a feature widely accepted to indicate one or more metasomatic events, through fluid or melts infiltration (e.g. Erlank et al. 1987, Grégoire et al. 2005). In sample U35 the suggested metasomatic overprint is highly consistent to erstwhile geochemical parameters, especially the spinel chromium number.

Chlorite is a frequent secondary phase. According to the classification proposed by the CMS committee for nomenclature (Bailey 1988), the analysed chlorites fit the range marked by clinochlore and shamozite. Alternatively, they are classified as clinochlore or picnochlorite (Hey 1954). Pectolite, a Ca-rich phase ( $CaO \sim 34$  wt%) of the wollastonite group is found as inclusion in Opx porphyroclasts due to the ongoing rodingitisation (e.g. Sabzehei 2002, Sample 4A).

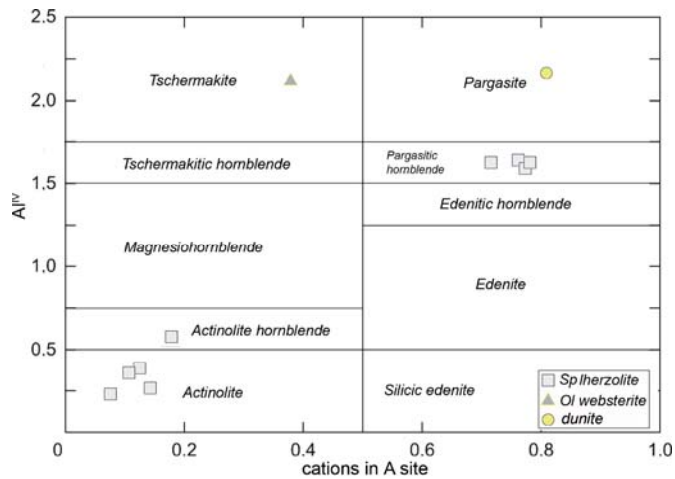


**Fig. 25.** Discrimination diagramme for the classification and nomenclature of Ca-amphiboles (Leake et al. 1997). Samples from the KKOC different ultramafic lithologies.

In pyroxenites, within the pyroxene intragrain reaction space (sample 2A), sub-solidus hydrogarnet of hibschite composition was detected. The ubiquitous alteration phase is serpentine, recorded in all samples; it is a dark green antigorite with Mg# of 88-93. Secondary prehnite is recorded in sample U19 and pyrite in sample 2A.

### 4.3. Metamorphic sole

#### 4.3.1. Rock types, textures and structures

As it was already outlined, the Krivaja-Konjuh ophiolite complex is composed of two great individual blocks. Metamorphic rocks can be traced as small patches found within the blocks' junction zone (Krivaja, Maoče and Careva Čuprija localities), whereas their main portion pertains to the great amphibolite mass (Duboštica and Vijaka localities), which forms the southern rim of the KKOC western segment.

Metamorphic textures are crystalloblastic being mostly granoblastic or nematoblastic, defined by the amphibole elongation (Figs. 26a, c, e). In rocks that contain garnet porphyroblasts, an adequate rock texture is reported as porphyroblastic (Figs. 26b,d). Rock structures are either massive (homogenous) or parallel. The massive structure is rare and was found in the Maoče and Careva Čuprija localities of the KKOC junction zone (Figs. 26a, b). Parallel structures (lineations, foliations) are more common, in particular in the Duboštica-Vijaka amphibolite mass. Such parallel texture is more precisely described as banded with an alternation of 'bright' and 'dark' rock domains. Bright domains are dominantly composed of plagioclase, whereas dark ones are foliated to lineated and consist of dark to pale-green amphibole, having a broad chemical composition. An average grain size in these metamorphic rocks is 0.5 to 1.0 mm across. Compiling results of this research with previous work of Pamić et al. (1977) and Operta (2004), four main rock groups are to be distinguished according to their macroscopic structural and textural criterions. They are provided as follows, according to their occurrence frequency:

- group with pronounced banded and foliated structure and porphyroblastic texture (Fig. 26d, e.g. Duboštica locality)
- group with pronounced banded and foliated structure and granular to nematoblastic texture (Figs. 26c, e, e.g. Vijaka locality)
- group with pronounced massive (homogenous) structure and porphyroblastic texture (Fig. 26b, e.g. Careva Ćuprija locality)
- group with pronounced massive (homogenous) structure and granular to nematoblastic texture (Fig. 26a, e.g. Maoče locality)

In addition to metabasites, one has reported the sporadic occurrence of metasediments, mostly marbles and hornfels, within the suite of ophiolitic sole rocks, probably presenting the uppermost (clastic) segment of the metamorphosed oceanic crust column (Fig. 26f). Hornfels and metabasites, when occurring together, both show a well-developed foliation, thus indicating the thrust plane. Furthermore, due to the fact that the KKOC metamorphic rocks' pile was affected by a dynamic process of obduction, the mineral constituents of analysed rocks are often found stretched which may be informative for the direction of transport.

The granular to nematoblastic, banded Vijaka amphibolites show a characteristic pale to dark-green colour, where subidiomorphic amphibole grains define the foliation of the rock (Figs. 26c,e). Other textural groups are characterised by a dark-green or more often black colour having inclusions of pink rounded garnet grains (0.2–10 mm) embedded in a fine-grained homogenous or parallel matrix composed of amphibole, clinopyroxene and plagioclase (Figs. 26a,b,d). In none of the analysed metabasites, neither aluminous phases such as kyanite and sillimanite, nor primary calcite were reported corroborating their igneous non-altered (spilitised) origin (Dessai et al. 2004, Ćelik and Delaloye 2006).

Taking into account the above-discussed structural and textural features of the analysed rocks, along with other criteria established for the metamorphic rocks' classification (modal mineral composition, foreseen protolith and appropriate special name, Yardley 1989), the following metabasite rock varieties and their subtypes in the Krivaja-Konjuh ophiolite complex may be recognised:

- *Granoblastic amphibolites*
  - a) *Clinzoisite-sapphirine amphibolites (sample U30)*
  - b) *Corundum amphibolites (sample U29)*
  - c) *Epidote-ilmenite amphibolites (sample 11C)*
  - d) *Normal amphibolites (samples R8 and U23)*
- *Porphyroblastic garnet-diopside amphibolites*
  - a) *Rutile-garnet-diopside amphibolites (sample CC1)*
  - b) *Contact Opx-bearing garnet-diopside amphibolites (MK2, GR7 and V1)*
  - c) *Titanite-garnet-diopside amphibolites (sample DU5)*
  - d) *Garnet-diopside amphibolites (sample U22)*
- *Garnet-diopside-hypersthene amphibolites*
  - a) *Porphyroblastic Garnet-Diopside-Hypersthene amphibolites (Samples U22 and U40)*

#### *b) Granoblastic Garnet-diopside-hypersthene amphibolites (Sample V4)*

- *Diopside-amphibole gneisses*
- *Plagioclase-garnet-diopside gneisses*

#### 4.3.1.1. Granoblastic amphibolites

##### *4.3.1.1.1. Clinozoisite-sapphirine amphibolite*

This amphibolite subtype contains amphibole, plagioclase, clinozoisite, sapphirine and Cr and Al spinel (sample U30 recovered from the Krivaja-Vozuća locality; Table 3). The rock is of nematoblastic texture, but retains some igneous (gabbroic) texture characteristics. It is defined by the prevailing medium- to coarse-grained polygonated and partly elongated colourless amphibole of pargasite to tschermakite composition (~ 0.3 mm) (Fig. 27a). The amphibole interstitial space is filled by An-rich plagioclase, having clear tapered twinning and oriented granoblastic polygonal forms, which are due to the tendency to reduce mineral interface area during the polygonisation process (Paterson et al. 1989). Secondary clinozoisite may also be a relatively abundant constituent, forming flattened lenses that are oriented according to the rock's general fabric. Its origin is partly due to the late instability of anorthite (Fig. 29a). Further retrogression induces epidote, which develops on the clinozoisite substrate as aggregated, optically inactive film. The same picture (Fig. 29a) records a relatively coarse (~ 0.7 mm) isometric blast of relict chromium spinel, rimmed by a narrow reaction assemblage composed of Al-rich spinel, clinozoisite and sapphirine. As a rule, sapphirine emerges as blue pleochroitic medium-sized blast (~ 0.5 mm), commonly including Cr-rich spinel cores, apparently completely resorbing them (Fig. 27b). The overall texture of dominant amphibole and anorthite is depicted by mineral equilibrium with simple grain boundaries and triple-point contacts. However, sapphirine and especially clinozoisite single crystals record textural disequilibrium due to extensive grain boundary migration (Fig. 29b). Chemical prerequisites for sapphirine formation in silica unsaturated systems presume the high aluminous environment at high grades of metamorphism (e.g. Williams 1984, Gnos and Kurz 1994). Thus, sapphirine formation at the expense of spinel records changing conditions of temperature and pressure, coupled with the progressive silification, during or shortly after the peak-metamorphism event (Deer et al. 1992).

##### *4.3.1.1.2. Corundum amphibolite*

The paragenesis of this rock subtype comprises amphibole, plagioclase, corundum as major, and clinopyroxene, clinozoisite, Al- and Cr-spinel, clintonite, Al-pumpellyite, and calcite as accessory phases. Attractive corundum bearing amphibolite has been recovered from the Krivaja-Vozuća locality (sample U29, Table 3), but one also reports its presence more southwards, near the Vijaka village. However, former works decipher slightly different mineral assemblages (e.g. Operta et al. 2003).

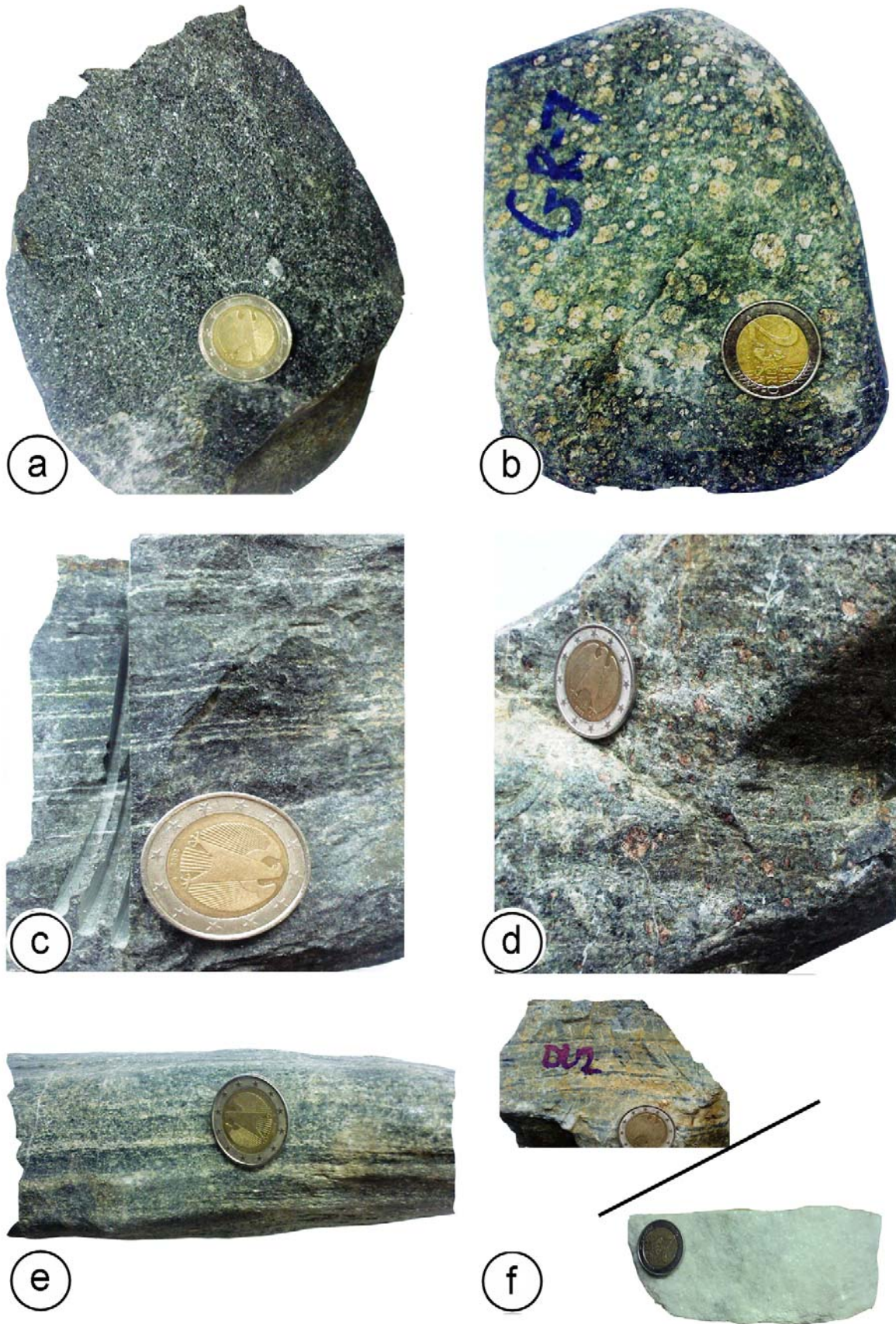


**Fig. 26a-f.** Photographs showing KKOC metamorphic sole rocks: (a) granoblastic to nematoblastic massive amphibolite, (b) porphyroblastic massive granulite, (c) granoblastic to nematoblastic banded amphibolite, (d) porphyroblastic banded granulite, (e) granoblastic to nematoblastic banded structure of pale-green Cr-pargasite amphibolite and (f) hornfels and marble, which form the metasediment portion of the metamorphic sole profile.



Grains of medium-sized amphibole and corundum (~ 0.15 mm) define the rocks' granoblastic to porphyroblastic textures (former gabbroic), with inner-space occupied by relics of euhedral calcic plagioclase from peak metamorphism, and anhedral albite and clinozoisite crystals formed during retrogression (Fig. 27c). Small relicts of igneous pyroxene (Al<sub>2</sub>O<sub>3</sub> contents of 6.5-11.3 wt%) exhibit no clear shape due to the epitaxial metamorphic amphibole growth (Fig. 29d). Prismatic hornblende is a pale-green pargasite having no pronounced pleochroism, rarely showing a weak fabric. The appearance of idiomorphic to hypidiomorphic Cr-spinel inclusions within the amphibole porphyroblasts is frequently reported. Occasionally, inclusions of Cr-spinel are accompanied by blebs of clinozoisite, Al-pumpellyite, clinopyroxene, plagioclase and calcite. Matching geochemical parameters, like the spinel Cr-number and TiO<sub>2</sub> content from both sources, strongly indicate so (Table Y-1-Y-2, Morishita and Arai 2001). Corundum commonly appears as subhedral rod-shaped crystals, characterised by many cracks with no cleavages (Fig. 27d). Corundum prismatic granoblasts are always mantled by Mg-Al green spinel and occasional pronounced resorption of the core phase (Fig. 29c). Such phenomenon is usually explained by reaction of corundum and Mg-rich calcite yielding spinel and carbon dioxide (Nitch et al. 1985, Liati 1988). A further peculiarity of this sample is the formation of Al-rich mica, clintonite, in some domains emerging as corundum's second (outer) rim. The spinel and clintonite occurrence are clearly related to peak metamorphic conditions, being additionally coupled with higher water activity that enhanced formation of both phases in such a peraluminous environment. Like in the case of sapphirine-bearing amphibolite, recovered from the same locality as this one, the high metamorphic conditions are hypothesised with an igneous mafic precursor sufficiently rich in alumina, e.g. troctolite or gabbro (Morishita and Arai 2001).

#### 4.3.1.1.3. *Epidote-ilmenite amphibolite*

This basic metamorphic rock has amphibole, plagioclase and epidote/clinozoisite as major, as well as ilmenite, titanite, chlorite, prehnite, apatite, albite, Fe- to Al- pumpellyite and clinopyroxene as accessory phases. This paragenesis is confined to sample 11C, which was recovered from the displaced Žepče ophiolite area (Table 3). As in the previous amphibolite subtypes, the texture is relict gabbroic marked by dominant polygonate amphibole crystalloblasts (~ 0.4 mm), while the interstitial space is occupied by xenomorphic plagioclase alteration products (saussuritisation). Amphibole is green magnesio-hornblende to edenite, featured by strong light absorption parallel to elongation (dark-greenish to brownish colour). Commonly, it contains bleb-shaped titanite inclusions. Since titanite is an anisotropic phase, the reported ellipsoidal form in this rock variety is the most adequate low-energy inclusion shape (Vernon and Clarke 2008). Plagioclase shows complete obliteration by late alteration(s), characterised by widespread formation of clinozoisite- and prehnite-rich aggregates (Fig. 29f). Although plagioclase boundaries are not always clear, due to the ongoing alteration and twinning absence, one can notice that they are not straight with respect to amphibole. It may imply disequilibrium during peak-metamorphism. Clinopyroxene occurs rarely, mostly in form of small patches or nucleation seeds surrounding and interpenetrating amphibole host grains (Fig. 29f).

**Table 3.** The Krivaja-Konjuh metamorphic sole rocks and their estimated modal mineralogy (vol.%)

Metamorphic rock variety and subtype	Rock samples	Mineral paragenesis	Modal mineralogy estimation (vol.%)					
			Grt	Amp	Cpx	Opx	Pl	Other phases
<b>1. AMPHIBOLITE</b>								
Clinozoisite – sapphirine-amphibolite - Subtype A	U30	Amp, Pl, Czo, Spr, Sp	0	60-70	0	0	10-20	Czo (10-20) Spr (0-5)
Corrundum amphibolite - Subtype B	U29	Amp, Pl, Crn, Czo, Cpx, Ct, Pmp, Cc, Cpx, Sp	0	40-50	5	0	25-30	Crn(10-20) Czo (5-10)
Epidote-ilmenite amphibolite - Subtype C	11C	Amp, Pl, Ep, Prh, Ilm, Cpx, Ttn, Ap, Pmp, Chl	0	40-45	5	0	15-20	Ep (15-20) Ilm (5-10) Prh (10-15)
Amphibolite - Subtype D	R8, U23	Amp, Pl, Ttn, Ilm, Ap, Chl, Prh	0	50-70	0	0	25-40	Ttn (5) Prh (5) Others (5)
<b>2. GARNET-DIOPSIDE AMPHIBOLITE</b>								
Rutile amphibolite - Subtype A	CC1	Grt, Amp, Pl, Cpx, Ttn, Rt, Cc, Ilm	20-30	20-30	20-25	0	10-15	Rt (0-5) Other (0-5)
Contact Opx amphibolite - Subtype B	MK2, GR7, V1	Grt, Amp, Pl, Cpx, Opx, Mt	10-15	20-40	10-30	0-5	20-30	0-5
Titanite amphibolite - Subtype C	DU5	Grt, Amp, Pl, Cpx, Ttn, Xo	25-30	35-40	15-20	0	0-5	Ttn (5-10) Other (0-5)
Grt-Di amphibolite - Subtype D	U22	Grt, Amp, Pl, Cpx, Chl	10-15	20-25	30-35	0	15-25	0-5
<b>3. GARNET-DIOPSIDE-HYPERSTHENE AMPHIBOLITE</b>								
Porphyroblastic amphibolite - Subtype A	X1, U40	Grt, Cpx, Pl, Amp, Opx, Rt, Mt	10-20	20-25	25-35	5-15	20-25	0-5
Granoblastic amphibolite - Subtype B	V4	Grt, Cpx, Pl, Amp, Opx, Mt	10-15	45-50	0-5	5-10	25-30	0-5
<b>4. DIOPSIDE AMPHIBOLITE GNEISS</b>								
Diopside amphibolite gneiss	10D	Amp, Cpx, Pl, Ttn, Ilm, Ap, Prh	0	35-40	25-30	0	20-25	0-5
<b>5. PLAGIOCLASE-GARNET-DIOPSIDE GNEISS</b>								
Plagioclase - garnet - diopside gneiss	Z1C	Grt, Cpx, Pl, Sp, Opx, Ttn, Ilm	5-10	0	40-45	0	25-30	Ilm (5-10) Sp (0-5)

It is important to mention that this clinopyroxene stands as the only documented occurrence of potential metamorphic clinopyroxene (diopside, Al<sub>2</sub>O<sub>3</sub> content up to 1.9 wt% in the rim, and 0.5 wt% in the core) within the analysed metamorphic rocks of the Krivaja-Konjuh ophiolite complex. The first appearance of clinopyroxene in metabasites is usually used to trace the boundary of the upper amphibolite facies (~ 750 °C, 0.8 GPa, El-Naby et al. 2000) where Ts-amphibole is no longer a stable phase. A portion of the analysed sample was affected by a most pronounced regression; this part of the rock probably served as the late fluid conduit space. It contains relative coarse grains of ilmenite (~ 0.5 mm), and the surrounding ground mass is characterised by a secondary paragenesis of blue interfering zoisite, Fe- to Al-pumpellyite, prismatic shaped apatite and dark-green chlorite (Fig. 27e). Zoisite and pumpellyite form numerous rod-shaped crystals clearly formed at the expense of plagioclase. Within the ilmenite crystalloblasts, one can perceive regular titanite exsolutions, being nicely depicted in the related BSE photograph (Fig. 29e). The clear coalescing history of the depicted grain indicates that this phenomenon was facilitated by deformation, which affected this rock domain. Since the titanite mineral chemistry reveals a high water content per formula unit (analyses total to ~ 97.5 wt%), the ilmenite replacement by titanite is most often ascribed to retrogressive changes induced by hydration, which may follow a breakdown of upper-amphibolite- or granulite-facies assemblage (e.g. Ilnicki 2002).

#### 4.3.1.1.4. Amphibolite

This is an amphibolite *sensus stricto*, which is characteristic for samples R8 and U23, recovered from the Maoče and Duboštica localities respectively (Table 3). Both samples record a mineral assemblage of prevailing hornblende and plagioclase with minor titanite, prehnite, ilmenite, chlorite, and apatite. Rock texture in sample R8 is relict gabbroic defined by isometric hornblende crystalloblasts (~ 0.5 mm) having often obscure grain boundaries (Fig. 27f). In the case of sample U23, the rock texture is described as granoblastic to nematoblastic illustrated by the lobe-shaped, polygonal hornblende (~ 2 mm) having perfectly straight grain boundaries (Fig. 27g). Former textural features were recognised in genetically related subophiolitic rocks from the Greek island of Evia, being reported as the granoblastic relict cumulate texture type (Gartzos et al. 2009). Xenomorphic and isomorphic plagioclase grains fill the remaining interstitial space. The sample from Duboštica (U23) also records weak fabric shown in partial subparallel alignment of amphibole crystalloblasts. In both samples, amphibole is the fresh green typomorphic hornblende, having more pronounced pleochroism in the sample from the Maoče locality (R8). Plagioclase is of intermediate, andesine to labradorite composition. Often, it is obliterated by a regression testifying formation of the aggregated neoalbite and prehnite. Titanite is the most abundant accessory mineral indicating moderate temperature conditions. It is usually found scattered within large hornblende crystalloblasts in form of undersized ellipsoidal blebs. Ilmenite, in form of isometric, lobate and opaque mineralization, is perceived ubiquitously disseminated throughout samples. The more altered rock domains are featured by a dark-green chlorite mineralization.

#### 4.3.1.2. Porphyroblastic garnet-diopside amphibolite

##### 4.3.1.2.1. *Rutile-garnet-diopside amphibolite*

This metamorphic rock variety has been recovered from the Careva Ćuprija locality, placed in the central part of the Krivaja-Konjuh ophiolite complex (sample CC1). Its mineral paragenesis comprises garnet, amphibole, clinopyroxene, and plagioclase as major phases, whilst rutile, titanite, ilmenite and calcite appear as minor constituents (Table 3). The texture is typically porphyroblastic, defined by a medium- to coarse-grained isometric garnet (up to 2 mm across), and medium grained sub-rounded clinopyroxene and partly elongated amphibole crystalloblasts (up to 1 mm across) (Fig. 27h). The matrix is homogenous, consisting of polygonated fine granoblasts of amphibole, clinopyroxene, plagioclase and minor phases. Such a diverse matrix composition, as well as brittle deformation features and kink-bands reported within porphyroblasts, imply that the recrystallisation was highly advocated by varying degrees of cataclasis. The garnet crystalloblasts correspond to the pyrope-almandine compositional span. They are frequently marked by inclusions of clinopyroxene, plagioclase, rutile and titanite, indicating that garnet grew at the expense of the main assemblage (e.g. Guilmette et al. 2008). Moderately developed kelyphitic coronas around garnet are commonly observed, having an average width of 30  $\mu\text{m}$ . Amphibole is a pale-green edenite to pargasite of striking pleochroism. In the matrix, amphibole is found in intimate contact with clinopyroxene developing after it (Fig. 29g). Clinopyroxene is an igneous relict ( $\text{Al}_2\text{O}_3$  content of 4.7 to 6.5 wt%) being entirely pseudomorphed, or recording the incipient amphibole rimming around larger crystalloblasts. Plagioclase occurs as small polygonal interstitial grains, which record nice twinning and no alteration. Small euhedral grains (up to 0.05 mm long) of brown rutile and black ilmenite are ubiquitous and commonly considered to be a part of the peak high-pressure paragenesis (e.g. Meinhold et al. 2008). However, the presence of rutile in the high-grade metabasites may be linked to  $\text{TiO}_2$ -rich incipient melts and subsequent rutile precipitation during decompression and cooling (e.g. Finger et al. 2003).

##### 4.3.1.2.2. *Contact Opx-bearing garnet-diopside amphibolite*

This rock type has been ascribed to the samples MK2, GR7 and V1 recovered from the Krivaja, Gostovića Rijeka and Vijaka localities, respectively. Major phases are garnet, amphibole, clinopyroxene and plagioclase, whereas accessory phases are orthopyroxene and magnetite (Table 3). Furthermore, all samples all characterised by extremely large garnet crystalloblasts (up to 10 mm across), thus marking the rocks' textures as porphyroblastic. Other major phases are more often than not equidimensional and granoblastic ( $\sim 0.1$  mm), occasionally attaining larger proportions ( $\sim 1.5$  mm). Garnet is essentially composed of pyrope-almandine components. Commonly, it embeds clinopyroxene and amphibole inclusions implying garnet growth on their account. In sample MK2, certain garnet domains are featured by a system of rutile needles with an apparent crystallographic orientation ( $\{111\}$  direction of garnet) (Fig. 28a). Retrograde metamorphism heterogeneously overprinted garnet-bearing prograde paragenesis, being clearly indicated by up to 0.2 mm wide coronas found around garnet. Kelyphitic rims are composed of secondary phases (albite, orthopyroxene, hornblende

and magnetite), which grew at the expense of primary garnet. Such vermicular and radial symplectites of orthopyroxene, plagioclase and magnetite (Fig. 29h) without any preferred orientation, are commonly attributed to alteration effects of silica saturated, oxidising fluids which may enhance the garnet decompression breakdown through the reaction  $\text{Grt} + \text{Cpx} + \text{silica (from fluid)} = \text{Opx} + \text{Pl} + \text{Mt}$  (e.g. Prakash et al. 2007). Clinopyroxene is of igneous origin ( $\text{Al}_2\text{O}_3$  content  $\approx 6$  wt%), sometimes weakly coloured and partly recrystallised, sporadically reporting epitaxial overgrowth of hornblende or tiny orthopyroxene reaction rims. All samples within this rock type have similar amphibole edenitic to pargasitic composition. The colour is pale-green to green showing clear pleochroism. Plagioclase depicts more elongated forms than other phases and highly basic compositions, which may be indicative to the magmatic origin (Vernon and Clarke 2008). Orthopyroxene is a pinkish coloured hypersthene occurring almost exclusively as small radial intergrowth within the garnet kelyphitic coronas. Occasionally it emerges in form of small spots ( $\sim 50 \mu\text{m}$ ) attached to plagioclase faces. Both occurrences reflect metamorphic retrogression (Fig. 30a). The explanation of the aforementioned rutile needles in garnet has been debated for a long time. Most recent work on the subject offers a cleaving/healing garnet theory as the most liable clarification of this unique phenomenon (Hwang et al. 2007). The garnet  $\{110\}$  microparting is underlined as a response to the strain events within the ultra-high pressures metabasite rocks. Micro-scale partial melts, characteristic for such high-grade metamorphics during peak or immediate post-peak metamorphism, might have had reacted with the garnet host, hence precipitating the oriented rutile needles. The Ti source is hypothesised as external due to the moderately low garnet  $\text{TiO}_2$  content ( $\sim 0.07$  wt%).

#### 4.3.1.2.3. Titanite-garnet-diopside amphibolite

This rock type has been recognised in the sample DU5 recovered from the Duboštica locality. Garnet, amphibole, clinopyroxene and titanite form the principal mineral assemblage, whereas ilmenite is an accessory phase (Table 3). Apart from garnet inclusions, no plagioclase has been reported. The texture is characterised by ubiquitous and uniformly positioned garnet grains ( $\sim 1.5$  mm), which nicely define the rock's granoblastic texture and homogenous structure. The inner space matrix is composed of prevailing granular amphibole mixed with the other two main phases. (Fig. 28c). Kelyphitic coronas around garnet are hardly developed, recording a formation of Ca-Si hydrous silicate, xonotlite, emerging in form of cloudy aggregated mineral patches. Garnet is usually observed incorporating, engulfing, or coalescing with clinopyroxene relicts, thus testifying that it grew on the clinopyroxene account (Figs. 28d and 30b). Amphibole is a greenish to pale-brownish Ti-rich pargasite (up to 1.9 wt%  $\text{TiO}_2$ ), having an accentuated pleochroism. The igneous clinopyroxene (up to 6.5 wt%  $\text{Al}_2\text{O}_3$ ) records an unusually high degree of deformation via kink bands, bent cleavages and undulose extinction. The proportion of titanite is elevated. It depicts xenomorphic shapes, and it is often found embedded by garnets or along the weak lineation defined by amphibole crystalloblasts. Occasionally, ilmenite is intergrown with titanite, which may raise the conclusion on titanite origin through ilmenite hydration or oxidation via reactions with clinopyroxene and amphibole, respectively (Harlov et al. 2006). The same hydrothermal event may be considered as a trigger to the formation of xonotlite crystallite agglomerations,

which rim garnet porphyroblasts (Hacker and Mosenfelder 1996). Plagioclase is reported to be a metastable relict, preserved only within porphyroblasts of garnet. Such an insular textural position protected the grain from sub-solidus metamorphic processes, having affected the rest of plagioclase found in matrix (Fig. 28d).

#### 4.3.1.2.4. *Garnet-diopside amphibolite*

This rock subtype is classified as garnet-diopside amphibolite *sensu stricto* and it is confined to the sample U22 recovered from the Duboštica locality. The mineral assemblage consists of garnet, clinopyroxene, plagioclase, amphibole and secondary chlorite, albite and prehnite (Table 3). Texturally and compositionally, this rock subtype is an analogue of the subtype 2a, with the exception of rutile being part of the metamorphic paragenesis. Other differences are the extent of garnet retrograde decomposition and plagioclase alteration. Garnet crystalloblasts (~ 2 mm) are inter-mittently found completely obliterated (Fig. 28e), whereas plagioclase often records formation of 'neo-albite' and prehnite on its substrate.

#### 4.3.1.3. Garnet-diopside-hypersthene amphibolite

##### 4.3.1.3.1. *Porphyroblastic garnet-diopside-hypersthene amphibolite*

A porphyroblastic subtype of this rock variety has been recognised in samples X1 and U40 from the Vijaka locality. The metamorphic mineral paragenesis includes garnet, clinopyroxene, plagioclase, and amphibole as principal constituents, whereas rutile and magnetite are accessory phases (Table 3). A high match of this variety with the Grt-Di amphibolites of subtype 2b has been recognised due to their great textural, structural and compositional similarities. The main difference is due to the complex mode of orthopyroxene occurrence. Apart from the vermicular appearance of orthopyroxene in garnet kelyphitic rims, or in clinopyroxene reaction rims, orthopyroxene is found as part of the rock's matrix, as pinkish pleochroic and isometric crystalloblasts (Fig. 28g). Occasionally, orthopyroxene granoblasts include lobate and xenomorphic secondary amphiboles (Fig. 28h). Quite a similar occurrence was reported in the Brazilian amphibolites from the Curaçá Belt, São Francisco Craton. There, orthopyroxene granoblasts in the matrix were ascribed to metamorphic overgrowth at the expense of amphibole and probably they record the last temperature raise (D'el-Rey Silva et al. 2007). Another difference with respect to the Grt-Di amphibolites of the second subtype is related to the clinopyroxene crystalloblasts. They appear to be more frequent and comparably coarser (~1.5 mm), thus nicely defining the rock's relict cumulate (e.g. spinel pyroxenite) texture (Fig. 30c). Furthermore, the igneous nature of this rock variety is witnessed in the sharp contacts of contrasting mineral grain size. The sample X1 of this metamorphic rock's subtype possesses the earlier described phenomena of garnets, bearing the rutile needles of an apparent {111} crystallographic orientation.

##### 4.3.1.3.2. *Granoblastic garnet-diopside-hypersthene amphibolite*

This rock subtype is also characteristic for the metamorphic rocks from the Vijaka locality (sample V4). The metamorphic assemblage consists of amphibole, plagioclase, garnet

and orthopyroxene as well as minor clinopyroxene (Table 3). The rock texture is markedly granoblastic, defined by the prevailing isometric to rod-shaped polygonate amphibole grains (~ 0.5 mm). Other phases are mostly equidimensional, and fill the amphibole inner space. Amphibole is a green to dark-green pargasite exhibiting a distinct pleochroism. Commonly, the amphibole grains encompass small inclusions of clinopyroxene and plagioclase (Fig. 30d). The ubiquitous twinning is characteristic for plagioclase. However, certain rock domains witness its complete obliteration and formation of tiny aggregated albite. As in the previous subtype, orthopyroxene forms subhedral pinkish grains in the matrix and emerges in the garnet kelyphitic coronas around garnet. Garnet occurs only sporadically, and forms isometric medium to coarse grains (~0.2 mm) that may be highly altered. Clinopyroxene is rare and is mostly found within amphibole. Its Al<sub>2</sub>O<sub>3</sub> content (2.9 wt%) and its textural context do not necessarily classify it as an igneous relict.

#### 4.3.1.4. Diopside-amphibolite gneiss

This metamorphic rock variety has been recovered from the Žepče area (sample 10D). The metamorphic assemblage is confined to amphibole, clinopyroxene and altered plagioclase as major, and titanite, ilmenite, apatite and prehnite as accessory phases (Table 3). The rock's texture is transitional, nematoblastic to granoblastic, where changes in the relative abundances of amphibole and clinopyroxene define a conspicuous layering. This is seen as a successive alternation of amphibole- and clinopyroxene-rich bands, which form a clear shistosity (Fig. 28b). The polygonal, lobe-shaped amphibole of dark brownish colour and expressed pleochroism is the prevailing phase. It is characterised by elevated TiO<sub>2</sub> and Al<sub>2</sub>O<sub>3</sub> contents of 4.1 and 14.8 wt%, respectively. These compositional parameters are found to be typical for Ti-rich pargasites (kaersutitic variety) in high-grade metabasites from collision zones and subophiolitic metamorphic soles (e.g. Raase 1974). Occasionally, a secondary amphibole of an unstable xenomorphic mineral form is to be observed (Fig. 30e). Such Ti- and Al-poor, but Fe-rich amphibole is believed to appear on the account of primary kaersutitic pargasite and clinopyroxene due to the post-peak metamorphic instability. Clinopyroxene is a pale-green magmatic relict, apparently having no pleochroism. Apart from the layers it forms, one can encounter clinopyroxene within the rock's amphibole-rich portions, in epitaxial intergrowth. Although completely devastated by the secondary processes (prehnitisation and albitisation), plagioclase used to have clear xenomorphic shapes, concentrated within the leucocratic bands or lenses. Titanite is the common accessory phase, mostly found embedded in kaersutitic pargasite or it is a post-peak phase formed at the expense of ilmenite (Fig. 30f). The very high Ti-content of the bulk-rock has also been manifested in the high proportion of ilmenite, which occurs as lobate, anhedral medium-grained granoblasts (~ 0.2 mm).

#### 4.3.1.5. Plagioclase-garnet-diopside gneiss

This rock variety has also been recognised within the Žepče metamorphic terrain (sample Z1C). Its mineral assemblage consists of major clinopyroxene, plagioclase, garnet, orthopyroxene, ulvöspinel and minor ilmenite, as well as titanite. The rock's banded structure

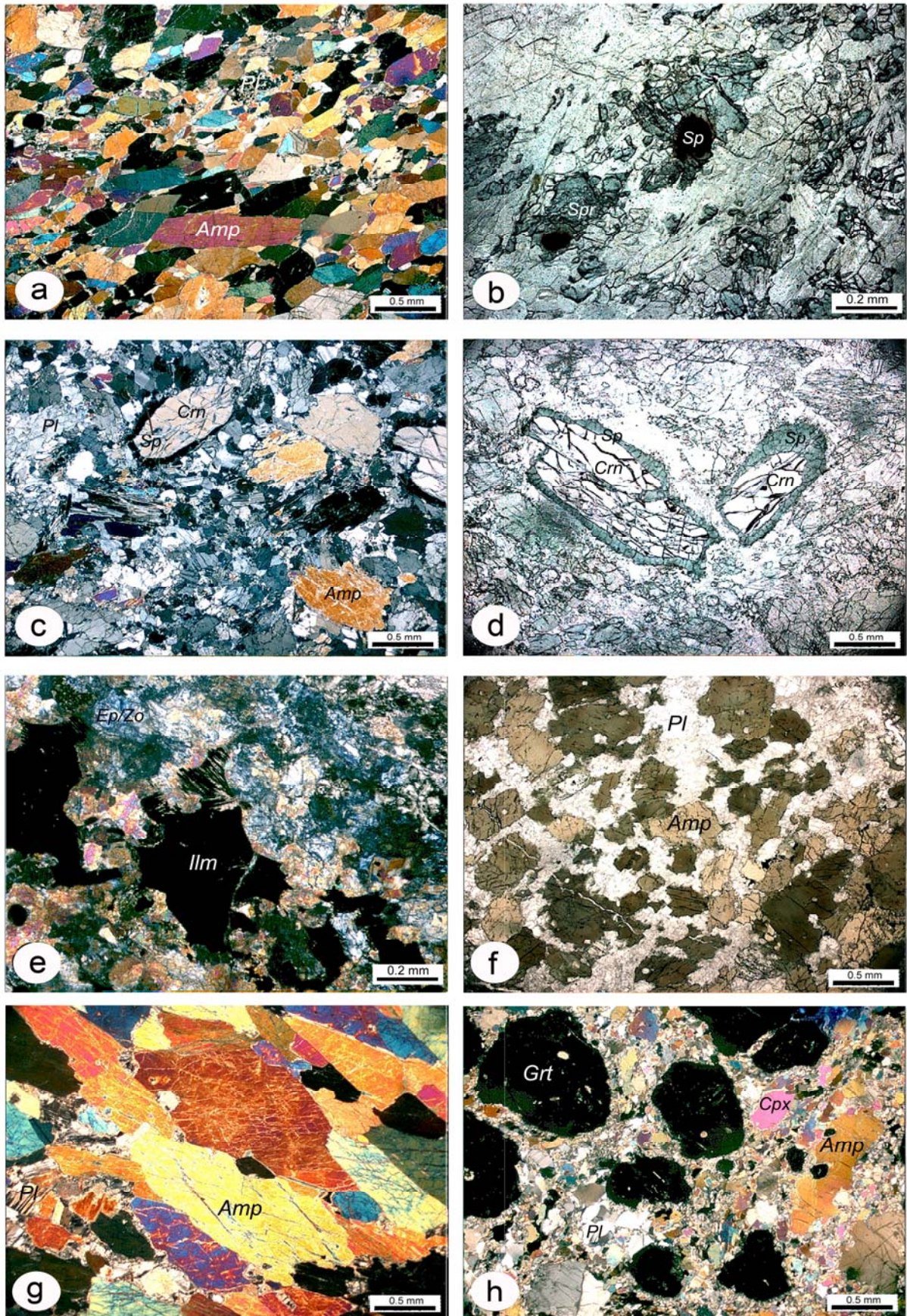


**Fig. 27a-h.** Selected microphotographs of analysed metamorphic rocks. For details see text (subchapter 4.3.1.); Amp = amphibole, Sp = spinel, Spr = sapphirine, Cpx = clinopyroxene, Pl = plagioclase, Grt = garnet, Crn = corundum



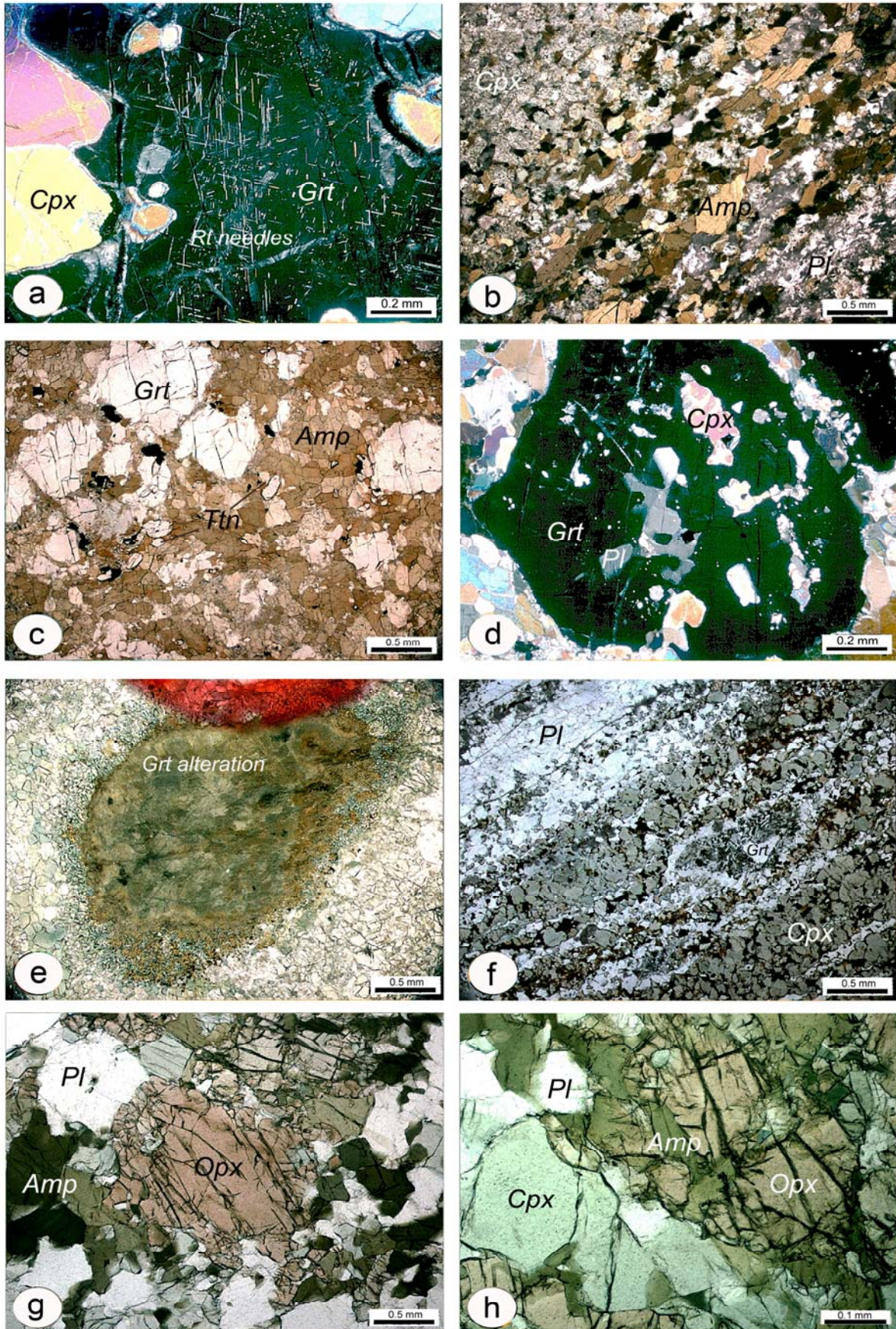


**Fig. 28a-h.** Selected microphotographs of analysed metamorphic rocks. For details see text (subchapter 4.3.1.); Amp = amphibole, Rt = rutil, Ttn = titanite, Cpx = clinopyroxene, Pl = plagioclase, Grt = garnet, Opx = orthopyroxene. Abbreviations after Kretz (1983).

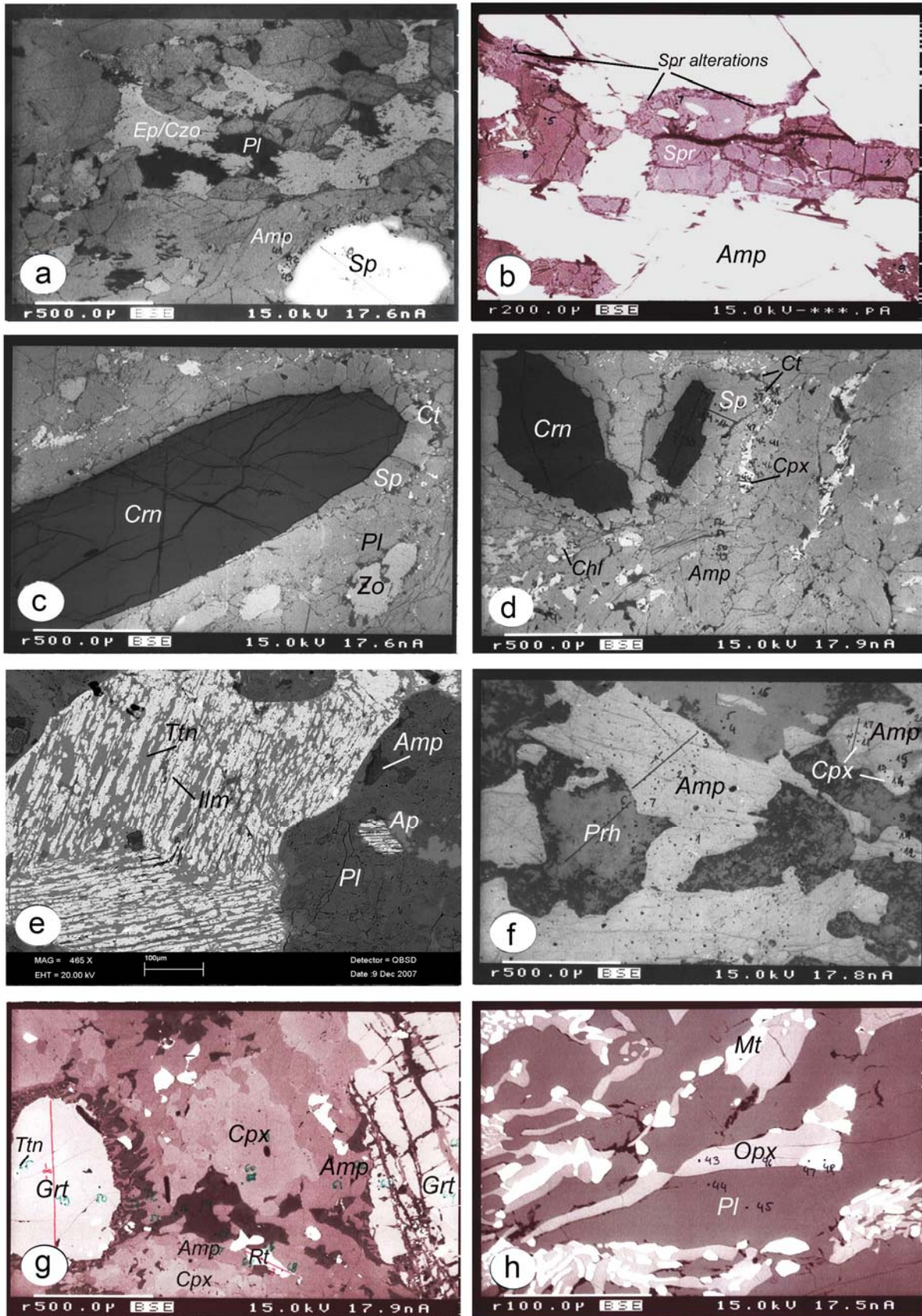


**Fig. 29a-h.** Selected BSE pictures of analysed metamorphic rocks. Description in text (subchapter 4.3.1). Numbers in microprobe BSE pictures refer to the respective mineral chemistry analyses (Appendix C , mineral chemistry); Ep/Czo = epidote/clinozoisite, Pl = plagioclase, Amp = amphibole, Sp = spinel, Spr = sapphirine, Crn = corundum, Ct = clintonite, Cpx = clinopyroxene, Chl = chlorite, Ttn = titanite, Ilm = ilmenite, Ap = apatite, Prh = prehnite, Grt = garnet, Rt = rutile, Mt = magnetite.

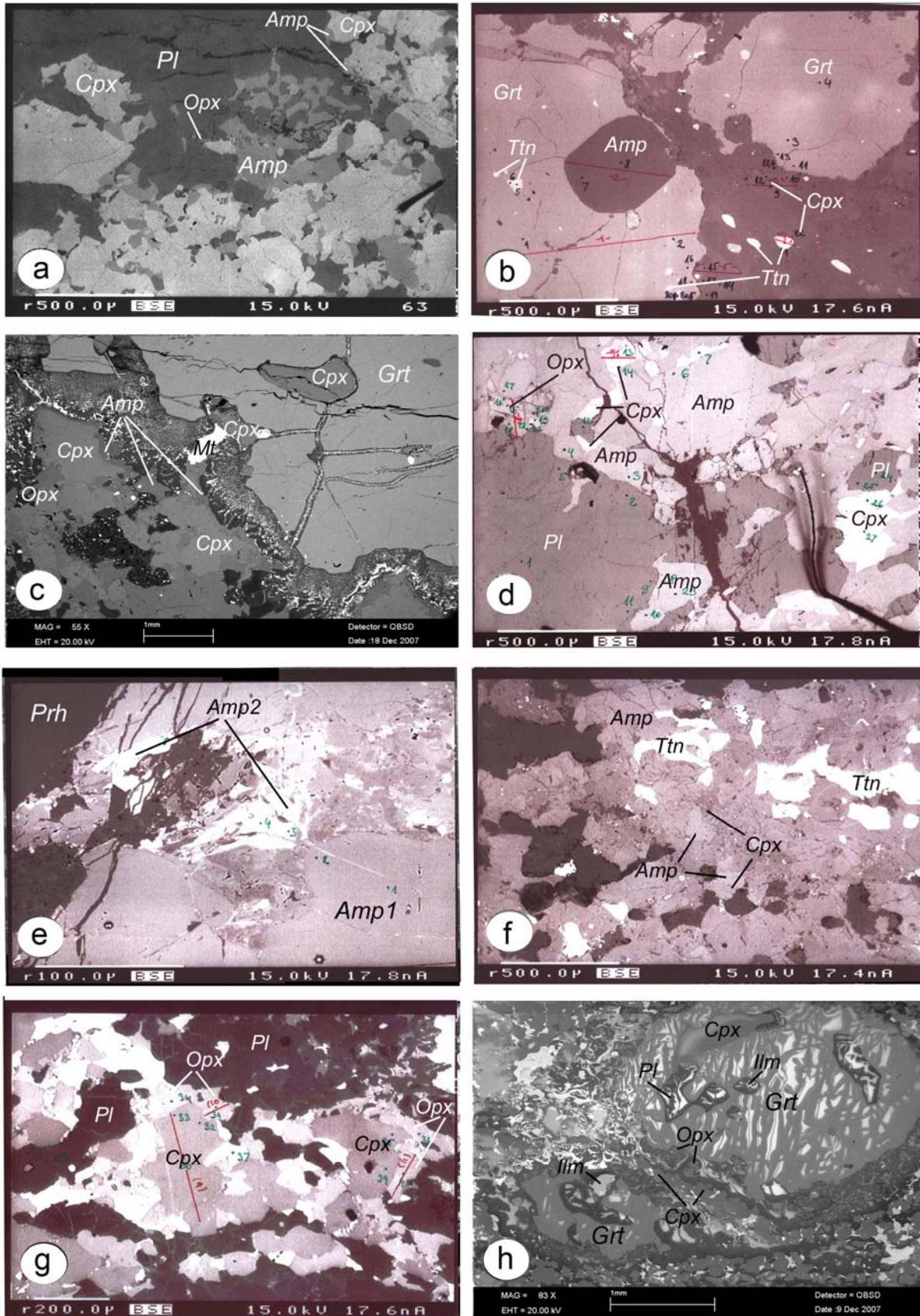


**Fig. 30a-h.** Selected BSE pictures of analysed metamorphic rocks. Description in text - subchapter 4.3.1. Numbers in microprobe BSE pictures refer to the respective mineral chemistry analyses (Appendix C , mineral chemistry); Pl = plagioclase, Amp = amphibole, Amp1 = first generation amphibole, Amp2 = second generation amphibole, Cpx = clinopyroxene, Opx = orthopyroxene, Ttn = titanite, Ilm = ilmenite, Grt = garnet, Mt = magnetite. Abbreviations after Kretz (1983).

is marked by a conspicuous alternation of dull-brownish layers of Cpx and apparently fade, lens-shaped, domains markedly composed of plagioclase (Fig. 28f). Prevailing clinopyroxene forms equidimensional polygonal blasts (~ 0.2 mm across) which define the rock's granoblastic texture. Cpx is an early formed, partly recrystallised magmatic phase found in alternation with plagioclase rich domains. The clinopyroxenes' distinct pale-green colour corroborates its salite chemistry. Pleochroism is weak or absent. An epitaxial orthopyroxene overgrow along the margins of clinopyroxene is commonly reported (Fig. 30g). Relatively small pinkish porphyroblasts or claw-shaped garnets do not exceed 1 mm across (Fig. 30h). They are constituents of the clinopyroxene-rich bands. The kelyitic coronas around garnet are 'embryonic' but ubiquitous. By the rule, garnet embeds or engulfs ilmenite, titanite, plagioclase, clinopyroxene and apatite. The dominant opaque phase in this metamorphic rock variety is xenomorphic or lobate, partly hydrated ulvöspinel, found in close but texturally disequibrated contact with clinopyroxene (Fig. 28). Due to the ulvöspinel texture and proportion in the system, it is believed that it had formed the pristine spinel phase, which upon oxidation may have yielded the Fe-rich ilmenite. Furthermore, the ilmenite was proven to be included or embayed by garnet (Fig. 30h), which, according to the reaction proposed by Sengupta et al. (1999), implicate that garnet grew at the expense of ilmenite (e.g. Fe-ilmenite + plagioclase ± quartz → ilmenite + garnet + oxygen). The plagioclase is of oligoclase composition and it appears as an anhedral, granular to rod-shaped crystalloblast (~ 0.5 mm) devoid of twinning. Pamić et al. (1973) already reported on this kind of metamorphic rock from the vicinity of Vareš. These authors explained it as a transitional metamorphic assemblage toward eclogites.

### 4.3.2. Mineral chemistry

#### 4.3.2.1. Amphibole

Amphibole in all analysed metamorphic rocks of the Krivaja-Konjuh ophiolite complex is, according to Leake et al. (1997), calcic and clusters through the broad compositional range from magnesio-hornblende, edenitic and pargasitic hornblende to pargasite, ferroan pargasite and magnesio-hastingsite (Fig. 30). A comprehensive dataset of amphibole chemistry, including cation structural distribution per formula unit, is provided in Appendix C (Tables I-1–I-14).

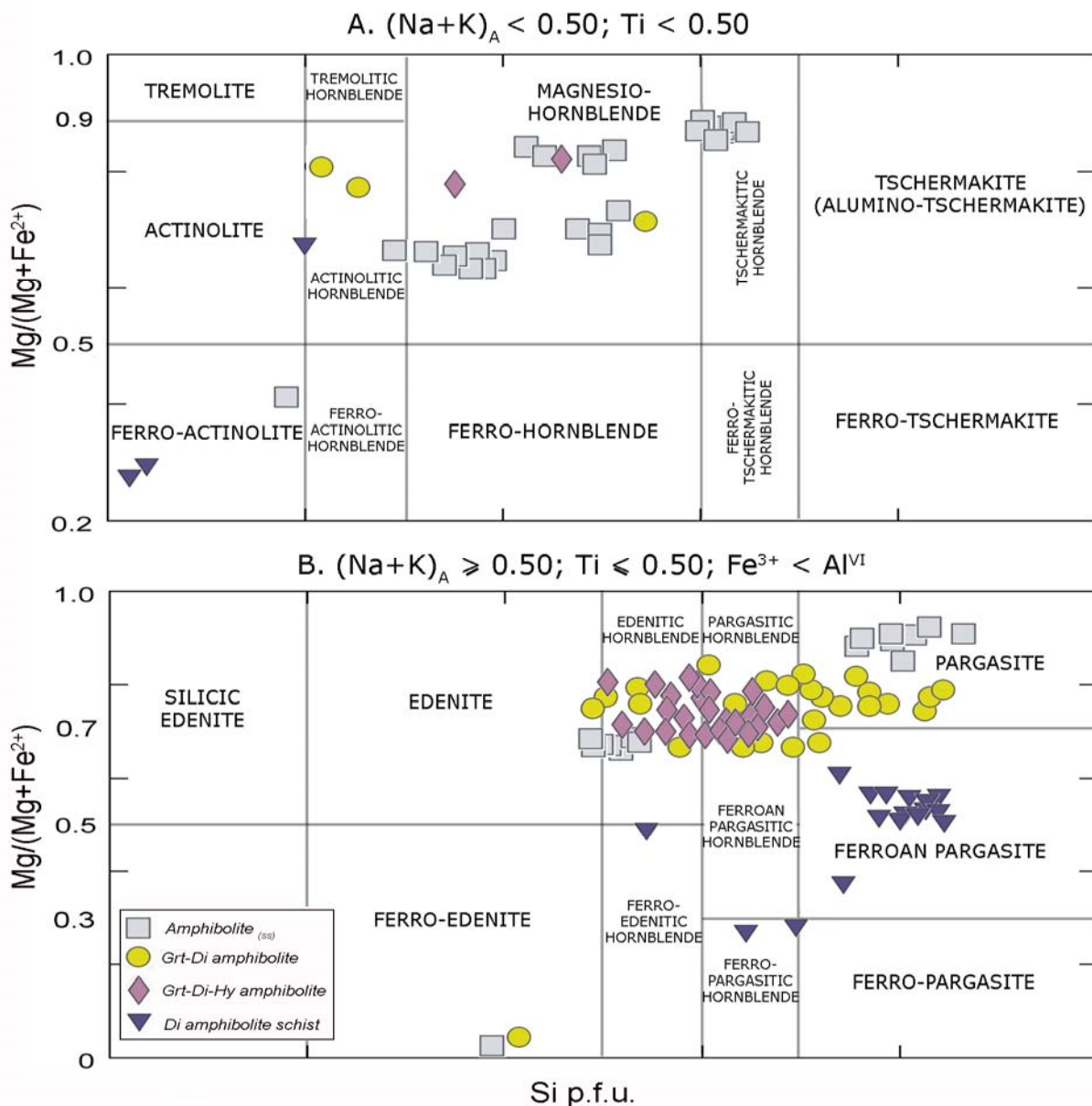


**Fig. 31.** Discrimination diagramme for classification and nomenclature of Calcium amphiboles (Leake et al. 1997). Samples from different metamorphic rock varieties in the KKOC.

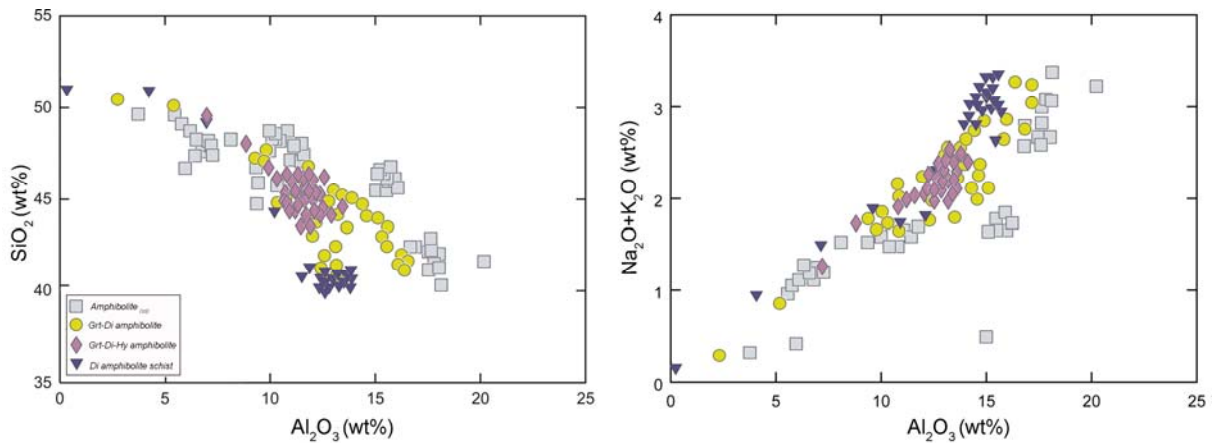


**Fig. 32.** Correlations of  $\text{SiO}_2$  vs  $\text{Al}_2\text{O}_3$  (left) and  $\text{Na}_2\text{O}+\text{K}_2\text{O}$  vs  $\text{Al}_2\text{O}_3$  (right) in amphiboles from different metamorphic rock varieties of the KKOC.

Within the amphibolite group of paragenesis, the amphibole is either magnesio-hornblende to tschermakitic hornblende or pargasite with minor actinolite, deciphering elevated metamorphic conditions. Magnesio-hornblende and edenitic hornblende are reported in samples U23, 11C, and R8 having no uniform composition, as it was the case with pargasite. According to Spear (1981), magnesio-hornblende and edenitic hornblende are stable at comparatively low pressures and temperatures, characteristic for an incipient segment of the amphibolite facies. In samples 11C and R8, secondary actinolitic amphibole is noticed, forming Di narrow margins especially in contact with altered plagioclase. The second group of paragenesis (Grt-Di amphibolite) comprises edenitic and pargasitic hornblende and pargasite with minor magnesio-hornblende and tremolitic hornblende. Pargasite and pargasitic hornblende are confined to samples DU5, U22, GR7 and MK2, whereas edenitic hornblende is characteristic for samples CC1 and V1. Occasionally, within the peculiar textural position of samples U22 and GR7, as well as V1, magnesio-hastingsite and actinolite have been reported. Increased  $\text{Fe}^{3+}$ -values (and decreased  $\text{Al}_{\text{tot}}$ ) in amphibole are linked to the oscillation and increase of  $f\text{O}_2$  (Spear 1981). Still, one must bear in mind that the amphibole discrimination based on its  $\text{Fe}^{3+}$  content must be taken with precaution due to the microprobe limitations measuring  $\text{Fe}^{3+}$  concentrations of analysed mineral phases. Apart from the amphibole crystalloblasts, all samples belonging to this paragenesis show two other modes of amphibole occurrence, the first forming radial symplectites in garnet kelyphitic coronas, or as epitaxial rims around clinopyroxene. The first type is featured by slightly elevated total iron abundances along with silica deficiency, being especially marked in sample GR7. The former shows no chemical differences compared to crystalloblasts, strongly suggesting that reported epitaxial margins were the first step of amphibole blastosis. The third group of paragenesis (Grt-Di-Hy amphibolite) embraces edenitic and pargasitic hornblende, though the fourth group of paragenesis (Di amphibolite gneisses) numbers ferroan pargasite along with minor ferro-pargasitic hornblende and ferro-actinolite. Compared to ferroan pargasite, the ferro-pargasitic hornblende is a retrograde phase, enriched in  $\text{FeO}_{\text{tot}}$  (~ 25 wt%) and impoverished in  $\text{MgO}$  (~ 4.7 wt%). Such an intermediate hornblende composition stands for incomplete retrograde reequilibrium (e.g. Carosi et al. 1997). An actinolite mineralization is sporadically reported along the pargasite margins or inner cracks.

Taking into account the calcic amphibole composition from different groups of paragenesis, one can elucidate that there is no systematic variation in their composition. Hence, the compositional changes in amphiboles reflect facies changes, along with decrease and increase of pressure and temperature during amphibole crystallisation.

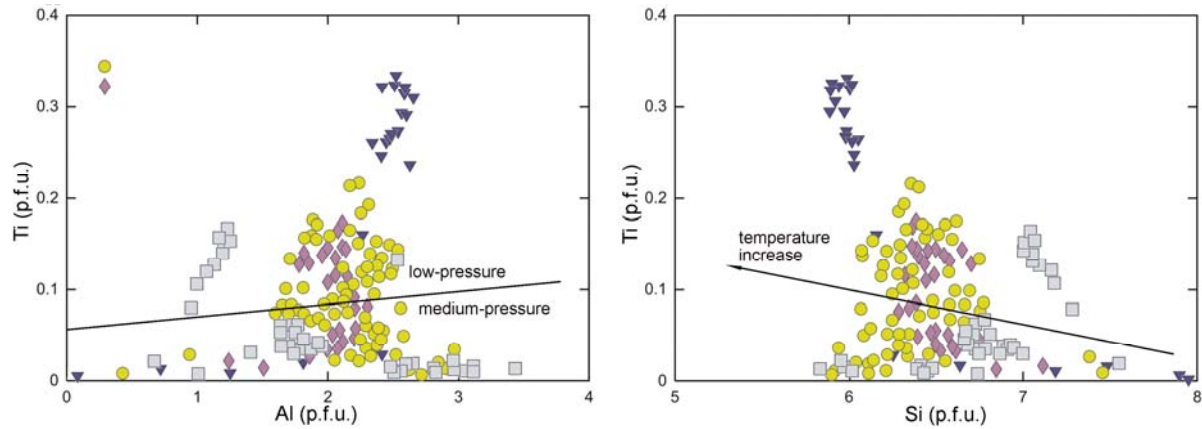


**Fig. 33.** Ti vs Al correlation in amphiboles from different metamorphic rock varieties of the KKOC illustrating changing pressure conditions (left); Ti vs Si correlation in amphiboles from the KKOC metamorphic rock varieties indicating highest temperatures for Di amphibolite gneisses. Both diagrammes are after Hynes (1982). For symbols see Fig. 32.

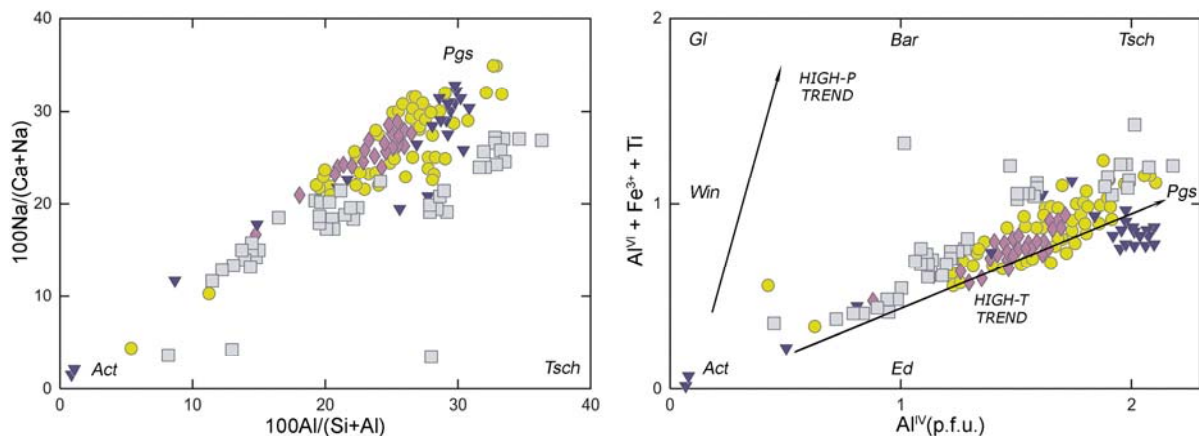


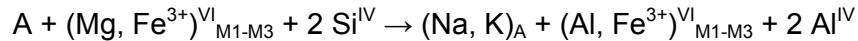
**Fig. 34.** Intercationic correlation for amphiboles from the different KKOC metamorphic rock varieties with main substitution trends indicated. For symbols see Fig.32.

The overall amphibole composition is marked by the following major element span:  $\text{SiO}_2$  (38.8-51.7 wt%),  $\text{TiO}_2$  (0.03-4.15 wt%),  $\text{Al}_2\text{O}_3$  (0.41-20.2 wt%),  $\text{FeO}_{\text{tot}}$  (4.1-27.4),  $\text{K}_2\text{O}$  (0.0-0.7 wt%),  $\text{MgO}$  (4.7-17.9 wt%), and  $\text{Mg\#}$  [ $100 \cdot \text{Mg}/(\text{Mg} + \text{Fe}^{2+})$ ] (28-100). In Fig. 32, the evidences of a strongly negative  $\text{SiO}_2$  vs  $\text{Al}_2\text{O}_3$  and a positive  $\text{Na}_2\text{O} + \text{K}_2\text{O}$  vs  $\text{Al}_2\text{O}_3$  correlation are shown, confirming almost linear increase of alumina and alkalis along with silica decrease in amphibole mineral chemistry during (mostly) prograde metamorphism. Fig. 33 shows a sharp increase of Ti (decrease), within the short Al interval (Si interval), regardless of the total alumina content or of bul-rock composition.

The peak-metamorphic ferroan pargasite of the diopside amphibolite gneiss is recorded as the Ti-richest amphibole variety. Additionally, a wide range of amphibole Ti abundances decipher low- to medium-pressures of crystallisation (Fig. 33), whereas higher Ti contents

generally indicate higher temperatures (Fig. 33, e.g. Raase 1974, Raase et al. 1986). The studied amphibole chemistry can be best depicted as complex solid solutions between independent end-member components: tremolite, tschermakite, pargasite and glaucophane.

Amphibole compositional oscillations in Krivaja-Konjuh metamorphites are essentially controlled by the pargasitic substitution vector (Fig. 34), which is defined by the reaction



(Grapes and Graham 1978). It implies a temperature-controlled metamorphism, whereby Al in tetrahedral coordination and Na in structural position A have been highly correlated. Relatively high  $\text{Al}^{\text{IV}}/\text{Al}^{\text{VI}}$  proportions in analysed amphiboles correspond to a moderate pressure increase. In retrograde assemblages, amphiboles correspond to actinolite composition having low-Al contents in both structural positions ( $\text{Al}^{\text{IV}} < 1$ ,  $\text{Al}^{\text{VI}} < 0.5$  p.f.u., Carosi et al. 1997). An increase of tschermakitic and pargasitic components over the hornblende component in amphibole crystalloblasts' profile analyses is manifested in total  $\text{Al}_2\text{O}_3$  content raise, going from the core toward the grain rim (Fig. 35.). Such a compositional trend defines the prograde metamorphism, featured by an increase of pressure and temperature conditions through the upper amphibolite and granulite facies. The described tendency is recognised, although not always clearly, in most of the analysed pargasites, ferroan pargasites and pargasitic hornblende. On the contrary, actinolite and various intermediate composition amphiboles mostly record the opposite trend, indicating a retrograde metamorphic event.

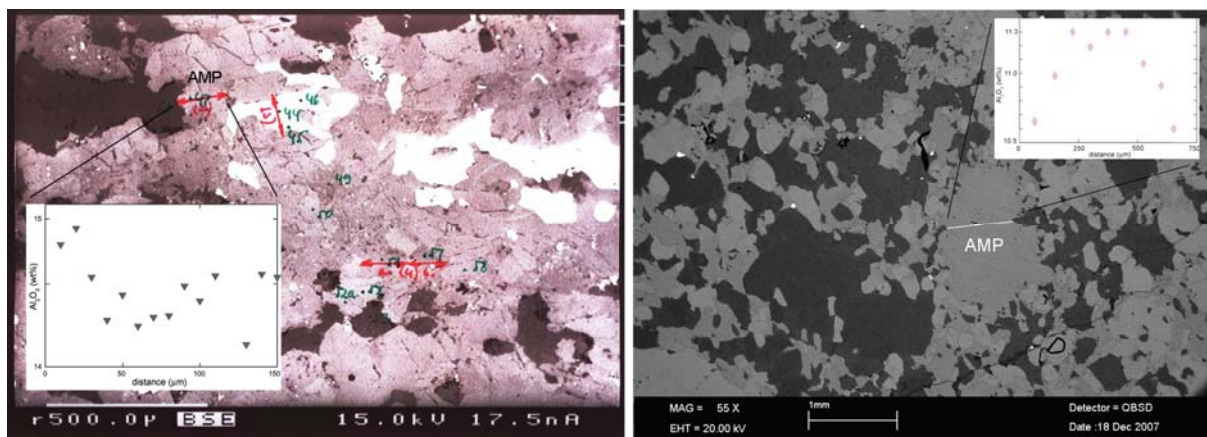


**Fig. 35.** Selected profiles for  $\text{Al}_2\text{O}_3$  made through the amphibole crystalloblasts from different KKOC metamorphic rock varieties.

#### 4.3.2.2. Garnet

The garnet composition of the analysed metamorphic rocks shows a broad compositional span within a range of  $\text{Py}_{22-56}\text{Alm}_{24-49}\text{Sp}_{00-05}\text{Gr}_{09-32}\text{And}_{00-10}$ . Its comprehensive mineral chemistry dataset, including proportions of the characteristic end-members, is provided in Appendix C (Tables J-1–J-6). The iron-rich garnet varieties in the PI-Grt-Di gneiss contain ~ 45 mol% of almandine component, whereas pyrope and grossular contents gradually increase in Grt-Di and Grt-Di-Hy amphibolites, reaching a maximum of 56 and 32 mol%, respectively (Fig. 35). The distinct Fe-Mg proportions in analysed samples are due to the bulk chemistry inconstancy.



A further division of the analysed garnets is performed on the base of different types of kelyphitic coronas observed around garnet grains (Fig. 36). Hence, garnets from gneisses, having *Opx-Pl* coronae possess the highest almandine abundances of the almandine component. The rest of the orthopyroxene containing corona paragenesis (*Opx+Pl+Mt+Py* and *Opx+Pl+Mt*) compositionally overlaps, holding lowest grossular and moderate pyrope as well as almandine concentrations. Garnet grains with Al-rich pargasite + plagioclase coronas are the richest in pyrope, whilst garnets having discrete 'cloudy' xonotlite-containing coronas of the same paragenesis report elevated grossular values. This may imply garnet growth at expense of hornblende and plagioclase (high grossularite values) as suggested by El-Naby et al. (2000). The small relict grains of pyrope (~95 mol%) recognised within the kelyphitic corona are found to be due to garnet alteration processes.

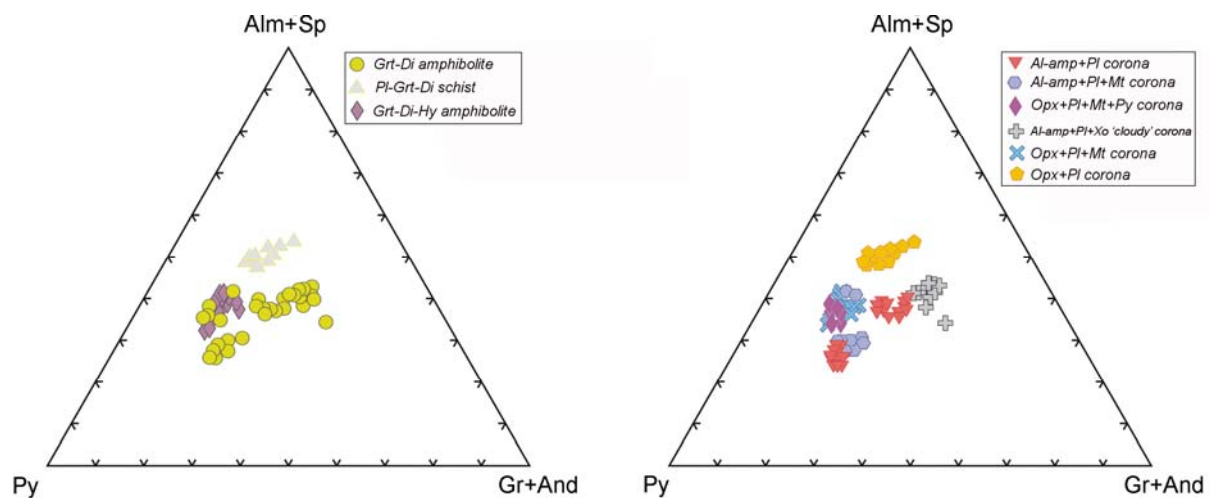


**Fig. 36** Garnet compositions in KKOC amphibolites in terms of almandine+spessartine (*Alm+Sp*), pyrope (*Py*), and grossular+andradite (*Gr+And*) molecular end-members. Discrimination is based on different source paragenesis (left) or different types of secondary coronas (right)

Evidences of garnet zoning, observed in grains originating from different metamorphic rock paragenesis, are given in Fig. 37a-d. Oscillations of grossular, almandine, spessartine and pyrope molar proportions have been tested. The spessartine zonation is apparently slightly concave in all depicted samples, reaching its maximum in the grain's core. Based on the distribution patterns of remaining components, the two following trends are recognised:

- the compositional zoning of garnet characterised by Fe-Mg substitution with gradual pyrope content increasing towards the rim of the grains, whereas almandine records opposite compositional trend, having higher values in the grain cores. Similar convex step-like trend is also depicted by grossular concentration pattern. Described trend is pertain to samples GR7 and Z1C (Fig. 37b,d)
- lack of garnet zoning reflecting a compositional equilibration (samples U22 and X1; Fig. 37a,c)

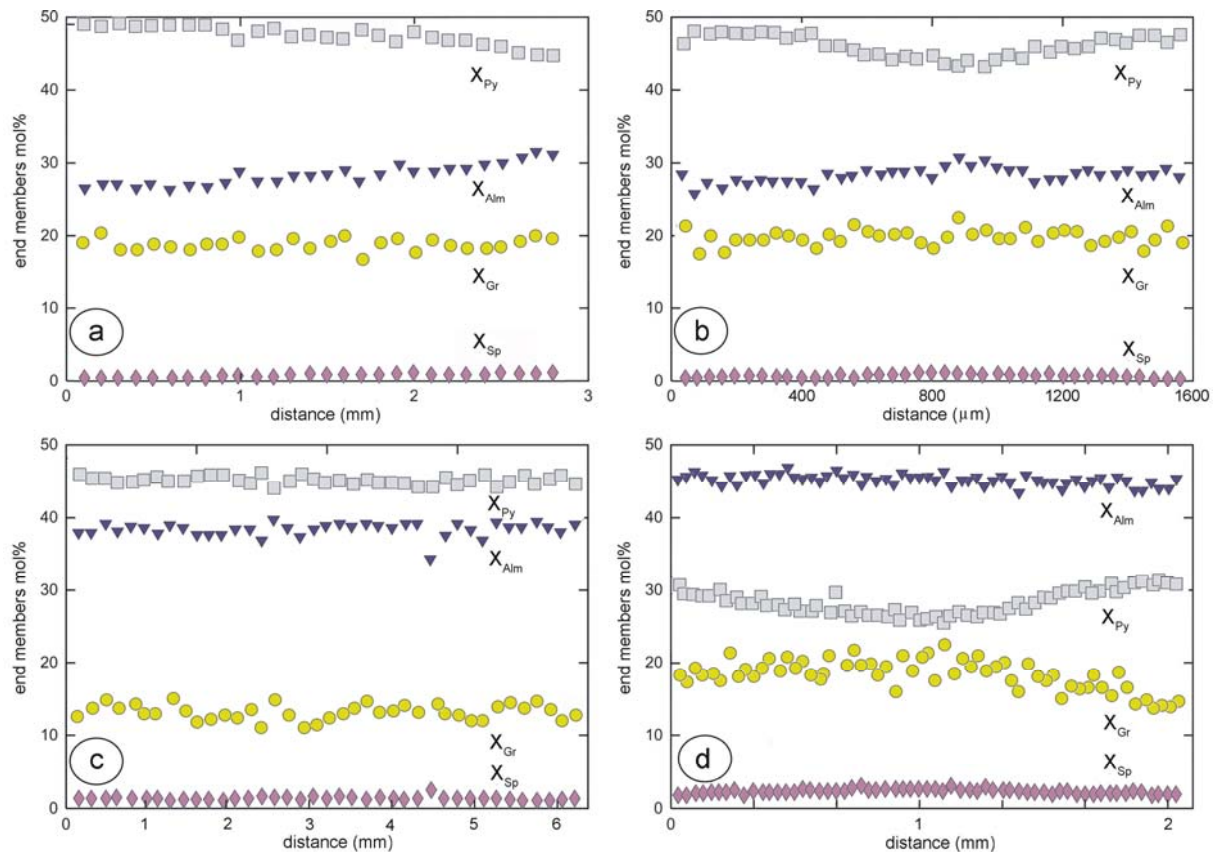


**Fig. 37a-d.** Representative zoning profiles of garnets recovered from the KKOC amphibolites with respect to variations in grossular, almandine, spessartine and pyrope molar proportions; (a) Sample U22: Grt-Di amphibolite (Al-amp+Pl corona), (b) Sample GR7: Grt-Di amphibolite (Al-amp+Pl+Mt+UnPh corona), (c) Sample X1: Grt-Di-Hy amphibolite (Opx+Pl+Mt corona), (d) Sample Z1C: Pl-Grt-Di gneiss (Opx+Pl+UnPh corona)

Former flat profile patterns, suggest phase equilibration and homogenisation by means of cation volume diffusion under the peak pressure-temperature conditions of metamorphism (e.g. Woodsworth 1977). The characteristic “U” shape of pyrope’s concentration patterns, accompanied by the opposite almandine pattern, clearly imply a prograde metamorphic event (e.g. Romano et al. 2006). On the other hand, the grossular and spessartine concave, and tending-to-be-concave compositional patterns, are a sign of retrogressive alterations.

#### 4.3.2.3. Plagioclase

The complete plagioclase mineral chemistry dataset, which includes albite, orthoclase and anorthite mineral proportions, is provided in Appendix C (Table K-1–K-10.). Plagioclase is a ubiquitous phase within the metamorphites of the Krivaja-Konjuh ophiolite complex. It occurs either as small anorthite-rich blasts, or as medium to coarse grained, less An-rich plagioclase. The former is thought to present the previous magmatic (gabbroic) structure. Plagioclase of the amphibolites is also An-rich (on average An<sub>81.3</sub>), which defines it as the most basic plagioclase variety (Fig. 38). An exception is sample R8, with plagioclase compositions within the oligoclase-labradorite range.

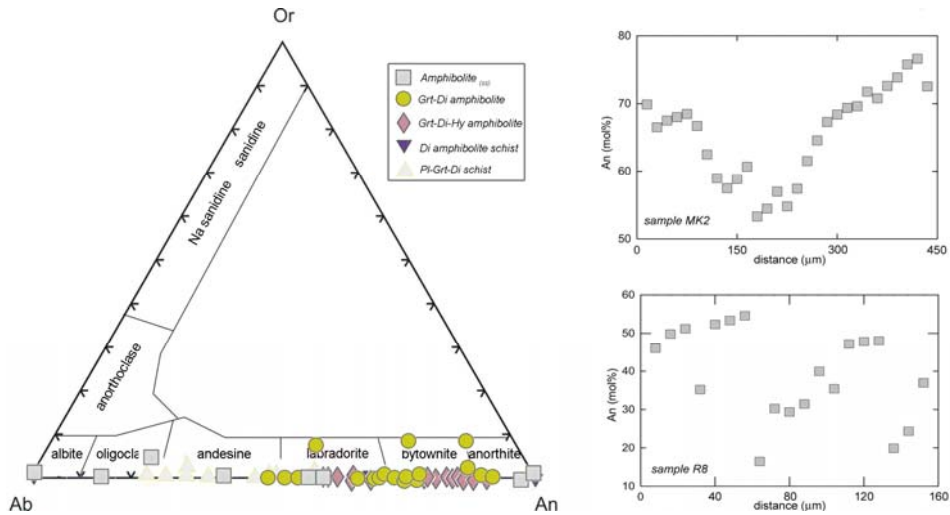


**Fig. 38.** *Ab-Or-An classification diagramme for feldspar from different metamorphic rock varieties (left, Deer et al. 1992); Line profiles of An mol% ( $100Ca/(Ca+Na+K)$ ) in plagioclase from the KKOC metamorphites (right). For more details, see text.*

Plagioclase analyses from Grt-Di amphibolites show uniform compositions corresponding mostly to labradorite and bytownite ( $An_{47-91}$ ) with an average of  $An_{69.9}$ . In samples GR7 and V1, plagioclase inclusions in garnet were also analysed, yielding lower anorthite proportions compared to the ‘outer’ matrix plagioclase ( $\sim 8$  mol% lower in An). Such a phenomenon confirms garnet growth at the expense of plagioclase, since mass balance in a closed system requires that, with ongoing plagioclase consumption, the remaining plagioclase becomes increasingly albitic (Spear et al. 1990). On the other hand, plagioclase inclusions in amphibole show no compositional difference compared to matrix constituents. Plagioclase originating from Grt-Di-Hy amphibolites is compositionally similar to the previous one ( $An_{58-90}$ ), with an average of  $An_{75.9}$ . Garnet-insulated plagioclase deciphers again a significant anorthite deficiency ( $\sim 10$  mol%). Plagioclase recovered from Di amphibolite gneiss is obliterated due to retrogression, whereas plagioclase from Pl-Grt-Di gneiss has andesine-oligoclase composition ( $An_{23-55}$ ), with an average of  $An_{36.7}$ . Taking into account all samples with developed orthopyroxene-plagioclase symplectites around garnet porphyroblasts, it is reported that in such cases plagioclase tends to be highly calcic ( $\sim 90\%$  An), likely having been formed through the breakdown of garnet at lower temperatures (Baldwin et al. 2003). Normally, the Or values in all analysed plagioclase grains are found to be  $< 1$  mol%, with an exception in samples R8 and CC1 reaching 4.4 and 7.2 mol%, respectively.

With respect to the alteration degree, plagioclase is reported to be: (1) completely altered to albite, or saussuritised containing minute inclusions of prehnite and clinozoisite, (2) affected by the incipient alteration processes recognised in its structure instability. In sample R8 a profile through the plagioclase grain is made recording pronounced oscillatory zoning of its anorthite content (Fig. 38). This kind of zoning is linked by some authors to the igneous origin of plagioclase, which may be preserved through high-grade metamorphism (e.g. Rutland et al. 1960). The remaining occurrence form of plagioclase (3) appears to be apparently intact (fresh) and mostly An-rich plagioclase minerals. It is generally homogenous within a single crystal, but occasionally shows a characteristic enrichment of An within the

grain rims, known as reverse plagioclase zoning (e.g. Cannon 1966). An illustrative profile is provided in Fig. 38, depicting a “U”-shape anorthite curve. Such a feature of the high-grade metabasites is common and usually explained by variations in *P-T* conditions during metamorphism.

Certain correlation trends between plagioclase and amphibole composition are recognised. The most basic plagioclase is reported in pargasite-bearing rocks (samples U29 and U30). As the plagioclase becomes more sodic, amphibole corresponds to edenitic and hornblende compositions (e.g. samples R8, U23 and CC1). However, this is not found to present a typical trend in analysed rocks since pargasite is found associated with less basic plagioclase as well (e.g. in samples GR7 and U40). Though, as it is suggested for amphibolite terrains (El-Naby et al. 2000), a tendency that bounds increased anorthite content in plagioclase to high temperature Al<sup>IV</sup>-rich pargasite amphibole is predicted.

#### 4.3.2.4. Clinopyroxene

Comprehensive microprobe analyses of clinopyroxene measured in the Krivaja-Konjuh metamorphic rocks are given in Appendix C (Table L-1–L-11.). The end-members of clinopyroxene were normalised on wollastonite (Wo), enstatite (En), and ferrosilite (Fs), with respect to different host metamorphic paragenesis and textural positions (Fig. 39). Analysed clinopyroxene has a composition in the range 44.8-55.9 wt% Wo, 23.7-44.8 wt% En, and 4.0-25.6 wt% Fs. The Al<sub>2</sub>O<sub>3</sub> content is highly variable and ranges from 0.51-11.30 wt%. The lower values are typical for matrix-structured clinopyroxene of sample 11C, most likely of metamorphic origin (0.51-1.95 wt% Al<sub>2</sub>O<sub>3</sub>), whereas Al<sub>2</sub>O<sub>3</sub> in the rest of analysed clinopyroxenes is significantly higher with an average value of 7.01 wt%. It suggests an igneous origin of clinopyroxene, already indicated by preserved magmatic rock textures and developed amphibole rims, replacing most of the clinopyroxene crystalloblasts (e.g. Önen and Hall 2000, Deer et al. 1992). Mg# values are recording a great span as well, ranging from 65.9-100.0. High-Mg# varieties are located in sample U29 (~ 98 Mg#), whereas clinopyroxene with low Mg# is recognised in sample Z1C (Mg# ≈ 70). Other significant elements range widely, with CaO from 18.89-25.62 wt% and Cr<sub>2</sub>O<sub>3</sub> from 0.00-0.93 wt%.

Most of the analysed clinopyroxenes are classified as salite (Fig. 38). Some of the Cpx from the Grt-Di amphibolites project into the field of diopside, whereas high-Wo clinopyroxene originating from the amphibolites is classified as aluminium diopside. Low-Mg# clinopyroxene from the Di amphibolite is transitional between salite and ferrosalite. Most clinopyroxenes from Pl-Grt-Di gneisses and Grt-Di-Hy amphibolites are augites. The textural position of analysed clinopyroxenes does not considerably affect their compositions (Fig. 39). Only clinopyroxene found as inclusion in garnet depicts slightly higher MgO and FeO, and lower CaO values. Both clinopyroxenes, relict igneous and metamorphic, show weak compositional zoning within grain margins depicting increasing Ca and decreasing Al towards the rim. This kind of zonation is imputed to retrograde alteration (e.g. Raase et al. 1986).

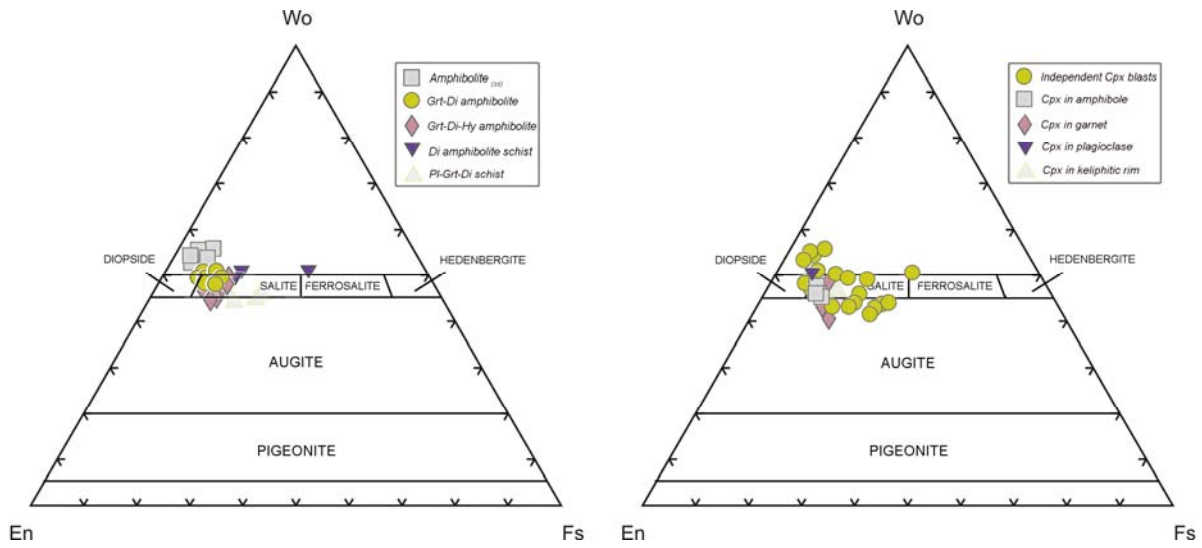


**Fig. 39.** Composition of clinopyroxene in different KKOC metamorphic rocks with respect to different host paragenesis (left), or textural position (right). Classification after Morimoto et al. (1989).

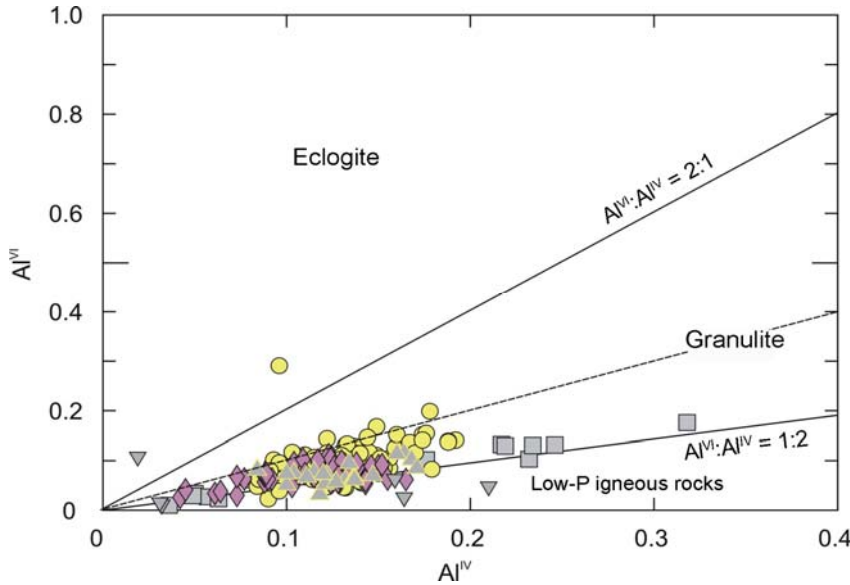


**Fig. 40.**  $Al^{VI}$  vs  $Al^{IV}$  diagramme for clinopyroxene from KKOC metamorphic rocks. Symbols as in Fig. 39.

The relative enrichment in Tschermaks component of analysed KKOC clinopyroxene, which is characteristic for granulite facies, can be assessed by usage of a  $Al^{VI}$  vs  $Al^{IV}$  diagramme (Fig. 40, Mukhopadhyay 1991). The diagramme suggests that igneous clinopyroxene experienced moderate metamorphic recrystallisation, having resulted in Al octahedral enrichment. The gradation trend toward eclogite facies clinopyroxene is not clearly established.

#### 4.3.2.5. Orthopyroxene

Microprobe analyses of orthopyroxene from the KKOC metamorphic rocks are provided in Appendix C (Tables M-1–M-3). Analysed orthopyroxene forms a solid solution between enstatite and ferrosilite plotting exclusively within the field of hypersthene (68.2-78.6 wt% En, Fig. 41). The Al and  $Fe^{3+}$  contents are normally low, with the highest  $Al_2O_3$  value of 6.08 wt% recorded in orthopyroxene originating from kelyphitic rims around garnet. Generally, Opx

from kelyphitic coronas possesses on average twice the Al content of Opx from other textural positions. The Mg# value of analysed orthopyroxene shows a narrower compositional span compared to clinopyroxene (70.8-81.5). Other important elements like Ca and Cr, are found within the range of 0.26-1.23 and 0.00-1.18 for CaO and Cr<sub>2</sub>O<sub>3</sub>, respectively.

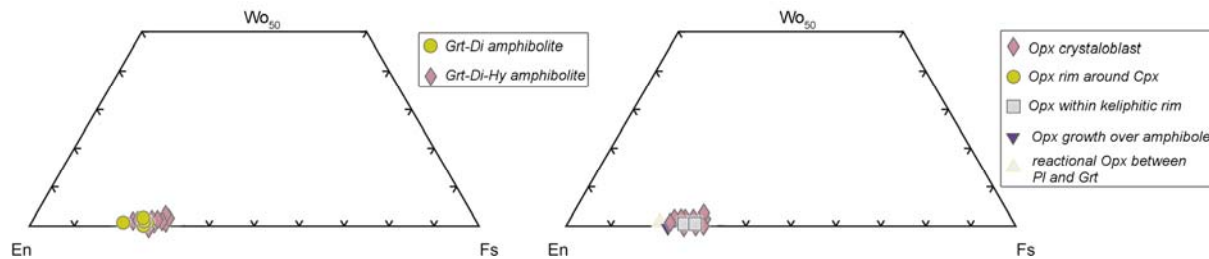


**Fig. 41.** Composition of orthopyroxene in different metamorphic rock varieties of the KKOC with respect to different host paragenesis (left), or textural position (right). Classification after Morimoto et al. (1989).

However, orthopyroxene from kelyphitic coronas around garnet is featured with the lowest CaO values (~ 0.3 wt%), and as already mentioned, the highest Al<sub>2</sub>O<sub>3</sub> abundances (~ 5.0 wt%). Prismatic orthopyroxenes, revealed mostly in Grt-Di-Hy amphibolite, do not depict clear compositional zoning, just a weak retrograde pattern already discussed in clinopyroxene.

#### 4.3.2.6. Other phases

Analyses of mineral chemistry with structural formulas of epidote-clinozoisite, prehnite, sapphirine, spinel, ulvöspinel, magnetite, ilmenite, titanite, corundum, clintonite, apatite and rutile are provided in Appendix C (Tables N-1–N-7).

*Epidote-clinozoisite* most usually occurs as epitaxial fine-grained pseudomorph after plagioclase (samples U30, U29, 11C) only rarely forming single grains (sample U30). It has the general formula  $\text{Ca}_{1.926-2.145}\text{Fe}^{3+}_{0.000-0.574}\text{Al}_{2.438-3.012}[\text{Si}_{2.938-3.052}\text{O}_4]_3(\text{OH})$ . The highest Fe<sup>3+</sup> values are reported in sample 11C (~ 0.5 a.p.f.u.).

*Prehnite* is found in samples 11C, R8, U23 and 10D. Similar to clinozoisite, the formation of prehnite depends on plagioclase decomposition. Its chemical composition is homogenous:  $\text{Ca}_{1.906-2.004}\text{Al}_{1.902-2.124}\text{Si}_{2.932-3.041}\text{O}_{10}(\text{OH})_2$ . Another Ca-Si hydrous phase is *xonotlite*, with the formula:  $\text{Ca}_{5.511-6.01}(\text{Si}_{5.71-5.97}\text{Al}_{0.03-0.34})\text{O}_{17}(\text{OH})_2$ . It emerges in sample DU5, forming cloudy aggregates of crystallites around porphyroblasts of garnet.

*Sapphirine* is encountered only in sample U30, having the composition  $(\text{Mg}_{3.129-3.241}\text{Al}_{4.291-4.396})(\text{Al}_{4.455-4.515}\text{Si}_{1.485-1.545})\text{O}_{20}$ .

*Spinel* is either an Al-rich variety, with a mineral chemistry best corresponding to pleonaste,  $(\text{Mg}_{0.551-0.751}\text{Fe}^{2+}_{0.240-0.423})(\text{Al}_{1.727-1.978}\text{Cr}_{0.004-0.239}\text{Fe}^{3+}_{0.002-0.036})\text{O}_4$ , or it is a Cr-rich igneous variety defined by the following formula:  $(\text{Mg}_{0.397-0.537}\text{Fe}^{2+}_{0.408-0.562})(\text{Al}_{0.910-1.193}\text{Cr}_{0.722-1.034}\text{Fe}^{3+}_{0.057-0.093})\text{O}_4$ . Pleonaste is recovered in sample U29 forming narrow rims around corundum, as well as in sample U30 where sapphirine develops on the account of spinel. In sample U29, Cr-rich varieties form characteristic euhedral to subhedral inclusions within the pargasite amphibole.

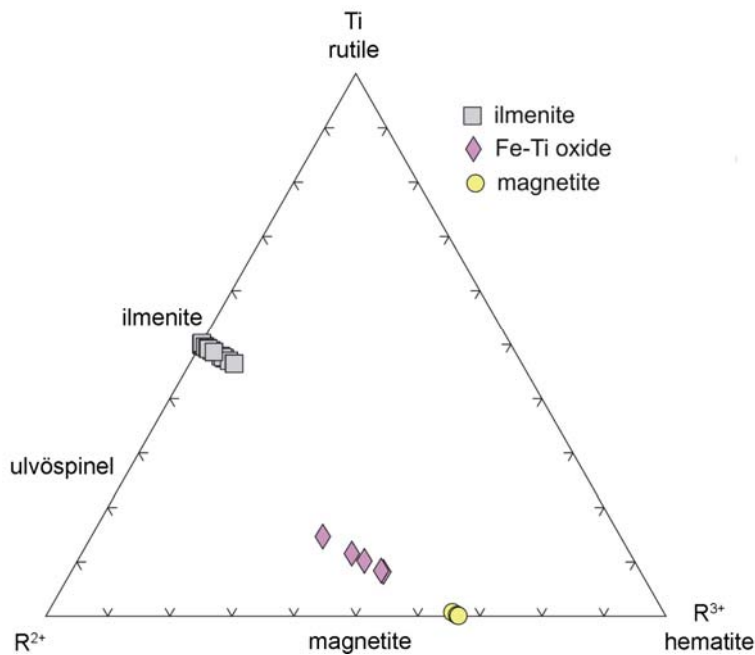


**Fig.42.** Discrimination of Fe-Ti oxides revealed from different KKOC metamorphic rocks in terms of Ti, R<sup>2+</sup>, R<sup>3+</sup> molar proportions. R<sup>2+</sup> represents Fe<sup>2+</sup>, Mn, Mg, Ca and Zn in spinel and ilmenite molecules, whereas in magnetite it stands only for Fe<sup>2+</sup>. R<sup>3+</sup> represents Al, Cr and Fe<sup>3+</sup>.

Fe-Ti oxides with compositions similar to those of ulvöspinel have been reported along with co-existing ilmenite in sample Z1C. They both lie on the ilmenite-magnetite junction in the related discrimination diagramme (Fig. 42). In sample 11C, ilmenite forms coarse grains featured by regular titanite exsolution lamellas, whereas in samples R8, CC1 and 10D, ilmenite is found as small euhedral, sometimes lobate blebs. The formula of ilmenite is  $\text{Fe}_{0.840-0.956}\text{Ti}_{0.928-1.003}\text{O}_3$ , and ulvöspinel has the composition  $(\text{Ti}_{0.244-0.440}\text{Fe}^{3+}_{1.061-1.354}\text{Al}_{0.052-0.154})\text{Fe}^{2+}_{1.201-1.413}\text{O}_4$ . On the other hand, the ulvöspinel mole percentage of magnetites, detected in samples U40 and V4, is low (Fig. 42). Magnetite occurrence is exclusively pertain to garnet kelfitic decomposition rims, and it is featured by high Fe content with only minor Al and Mg substitution,  $(\text{Fe}^{2+}_{0.967-0.988}\text{Mg}_{0.010-0.019})(\text{Fe}^{3+}_{1.861-1.963}\text{Al}_{0.021-0.110})\text{O}_4$ .

*Titanite* is a common mineral phase, mostly found in forms of blebs embedded by amphibole (samples 11C and 10D) or garnet (samples CC1, DU5, and Z1C) porphyroblasts. Occasionally, in Ti-rich metamorphic rocks, it is found intergrown with and forming at the expense of ilmenite (samples DU5 and 10D). The general titanite formula is  $\text{Ca}_{0.982-1.014}(\text{Ti}_{0.882-0.965}\text{Fe}^{3+}_{0.013-0.044}\text{Al}_{0.036-0.118})\text{SiO}_5$ , which implies equability of main element abundances in titanite formula, as well as low main substitution through the  $(\text{Al}, \text{Fe}^{3+}) + (\text{OH}^-, \text{F}^-) \leftrightarrow \text{Ti}^{4+} + \text{O}^{2-}$  mechanism (Higgins and Ribbe 1976). Such a low substitution degree, having resulted in a titanite formula stoichiometric purity, is known as a relative geothermometre and refers to elevated metamorphic conditions.

*Corundum* is reported in sample U29 where it is outlined as a subhedral rod-shaped porphyroblast always armoured by Al-spinel coronas. Mineral chemistry is uniform, having an Al<sub>2</sub>O<sub>3</sub> content between 99 and 100 wt%. FeO and Cr<sub>2</sub>O<sub>3</sub> abundances irregularly oscillate through the grain within the range of 0.07-0.25 wt% and 0.36-0.55 wt%, respectively. No amphibole and plagioclase inclusions have been reported as it was suggested in Operta

(2004), investigating corundum amphibolites from the southern portions of Krivaja-Konjuh ophiolite complex.

Appearance of *clintonite* is characteristic for the same sample, where it forms a discontinuous tiny outer rim around spinel coronas. Its chemical composition corresponds to  $\text{Ca}_{0.928-0.993}\text{Mg}_{1.923-2.016}\text{Al}_{5.416-5.686}\text{Si}_{2.203-2.469}\text{O}_{10}(\text{OH})_2$ .

*Rutile* emerges as small euhedral grains in sample CC1, whereas in samples U40 and MK2, it is reported to form peculiar needles in garnet porphyroblasts. First rutile occurrence is featured by a high  $\text{TiO}_2$  content ranging from 99.02-99.71 wt%, with the rest having very small concentrations of  $\text{Cr}_2\text{O}_3$  and FeO ranging from 0.12-0.26% and 0.24-0.61 wt%, respectively. Rutile needles are marked by slightly reduced  $\text{TiO}_2$  values ranging from 97.3-97.4 wt% and elevated MnO concentrations attaining the range of 1.08-1.31 wt%.





## 5. GEOCHEMISTRY OF KKOC ROCKS

### 5.1. Ultramafic rocks

#### 5.1.1. Peridotites

Whole-rock analyses of the Krivaja-Konjuh ultramafic rocks were performed on the same samples as the mineral analyses. In addition, three bulk-rock samples of plagioclase lherzolite from the Žepče region were analysed (yellow circles in the following diagrammes). Analyses were carried out on 4 samples of spinel lherzolite, 9 samples of plagioclase lherzolite, 2 samples of ultramafic cumulate and 2 samples of olivine websterite. The complete dataset is provided in Appendix D, Table X-1–X-2. The analyses were normalised on mean values of chondrite and primitive mantle for main and trace elements (including the rare earth elements) according to Taylor and McLennan (1985), Hofmann (1988), McDonough and Sun (1990, 1995).

In Fig. 43, variation diagrammes for a number of elements or element oxides versus MgO are displayed. For comparison, primitive mantle (PM) values from the literature are provided as shaded portions. In the peridotites, the majority of incompatible elements or their oxides (e.g. SiO<sub>2</sub>, TiO<sub>2</sub>, Al<sub>2</sub>O<sub>3</sub>, FeO, Na<sub>2</sub>O, Ba, Sr, Y, Yb) have somewhat lower abundances than PM, defining KKOC peridotites as relatively depleted mantle rocks. CaO, however, forms an exception. The compatible elements Cr, Ni and Sc are, however, not enriched and do not show consistent positive correlations with MgO. In the peridotites, most of the major elements show coherent covariation trends with respect to MgO, e.g. TiO<sub>2</sub>, Al<sub>2</sub>O<sub>3</sub>, CaO, Y, Yb, Zr and Sc show a negative correlation. Al<sub>2</sub>O<sub>3</sub> contents between 2.50 and 3.00 wt% are characteristic for some fertile orogenic massifs (e.g. Pyrenees, Bodinier et al. 2004; Lower Austria, Becker 1996). The analysed KKOC lherzolites do not show a negative correlation of Cr with MgO, which tends to be characteristic for many other Alpine peridotites and peridotite xenoliths from alkali basalts (e.g. Liang and Elthon 1990). Furthermore, a decrease of Sc with increasing MgO indicates melting within the spinel peridotite stability field, while a positive correlation of Sc with MgO would signalize melting in the garnet peridotite field (e.g. Liu et al. 2004). Al/Ti and Ca/Al ratios are somewhat higher than respective PM values. The measured ratios correspond very well to literature data of different CDOB peridotites (Al/Ti 21-50, Ca/Al 1.05-1.45; Lugović et al. 1991).

In summary, the covariation trends, as well as major and trace element abundances suggest a relatively fertile nature of the plagioclase and spinel lherzolites from the Krivaja-Konjuh ophiolite complex. Therefore it may well be that these peridotites were refertilised by metasomatic processes.

Invoking the rocks' modal mineralogy and phase chemistry (e.g. primary amphibole, plagioclase, pyroxene), the whole-rock compositions offer several possible lines of indication for refertilisation: (1) selective enrichment of LREE (La, Ce, Pr and Nd) in plagioclase lherzolites and La in spinel lherzolites (Gruau et al. 1998), (2) a selective enrichment in incompatible HFS elements and also in Th and U due to refertilisation after melt extraction (Niu and Hékinian 1997, Asimow 1999), and (3) pronounced negative SiO<sub>2</sub> and positive FeO covariation trends relative to MgO which are explained by olivine addition in the topmost mantle portions beneath mid-ocean ridges (Niu 1997, Niu 2004), (4) a higher Ca/Al ratio

than in PM, which might have been enhanced by selective precipitation of clinopyroxene at the expense of olivine or orthopyroxene (e.g. Fabriès et al. 1989). Comparing covariation trends for KKOC Iherzolites presented in Fig. 44a-c, as well as the normalised REE patterns with comprehensive models of the isobaric batch and near fractional melting of abyssal and ophiolite peridotites (Niu 2004, Bazylev et al. 2009), it is inferred that the batch melting model better deciphers the mantle history of the KKOC.

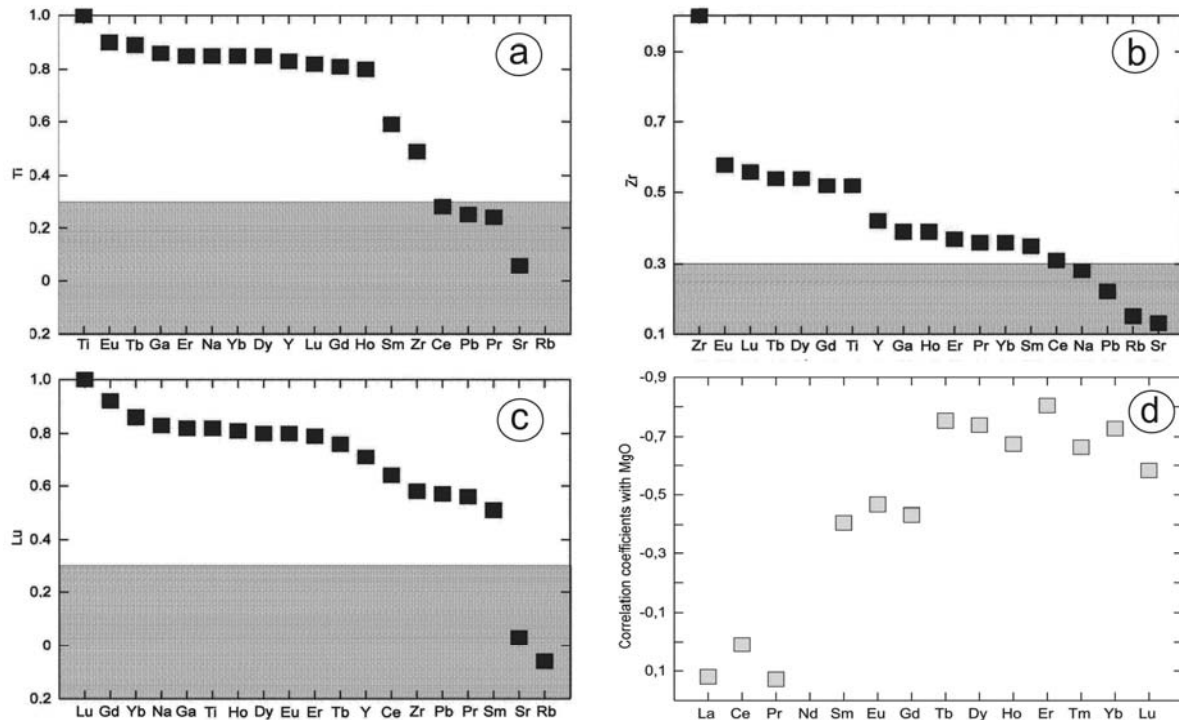


**Fig. 44a-c.** Correlation coefficients of relatively incompatible elements relative to those of Ti (a), Zr (b) and Lu (c). A higher correlation ( $R > 0.3$ ) suggests that the element is immobile during alterations and its behaviour is governed by magmatic processes. (d) Inverse correlations of REE with MgO suggest that MgO retained its initial mantle signatures.

LOI values of the KKOC Iherzolites (4.90-8.70 wt%) reflect the enhanced rock alteration during serpentinisation. Detected hydrous phases referred to alteration are serpentine, secondary amphibole, chlorite, pectolite and hibschite. These alterations caused a decrease of  $K_2O$  (below the detection limit of  $\sim 0.01$  wt%) and MgO (to  $\sim 35$  wt%) and partly a minor increase in  $Na_2O$ . Nowadays, it is generally estimated that due to serpentinisation and seafloor weathering, the moderately altered ultramafic rocks display a significant loss of MgO (e.g. Niu 2004). Therefore, the composition of the KKOC Iherzolites might have been severely affected by such processes. Furthermore, there is a widespread belief that serpentinisation in cumulate oceanic peridotites obliterates their magmatic signatures (e.g. Dick et al. 1984, Michael and Bonatti 1985). The following diagrammes, presented in Fig. 44a-c, were constructed in order to test this. They depict the correlation coefficients of highly immobile elements (Ti, Lu and Zr) with other incompatible elements. Except for the alkalis and Sr, the rest of the elements show a relatively high correlation ( $R > 0.3$ ), which suggests that the processes that led to the enrichments of the LREE or MREE (Sm, Eu, Gd) also led to

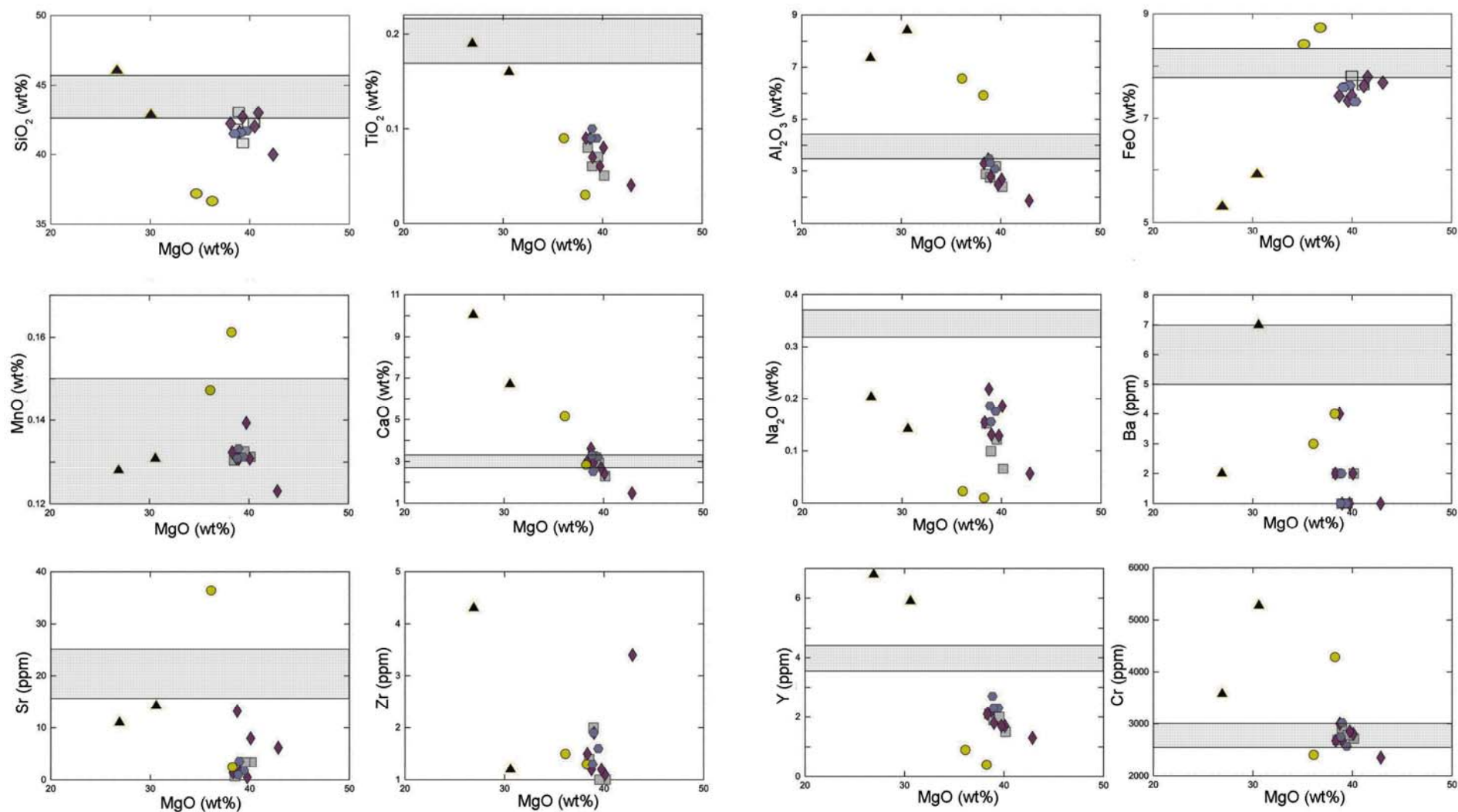


**Fig. 43.** Variation diagrammes of different KKOC ultramafic lithologies with respect to MgO, as well as Al/Ti and Ca/Al vs MgO diagrammes. Symbols:  $\square$  filled in grey = spinel lherzolite,  $\diamond$  filled in purple = plagioclase lherzolite,  $\circ$  filled in yellow = dunites,  $\blacktriangle$  = olivine websterite, blue hexagon = KKOC peridotites not analysed by EMPA. Shaded areas represent primitive mantle (PM) values (Taylor and McLennan 1985, McDonough and Sun 1995). Omissions are due to the y axis limitation (Zr, Ce, and Sm).

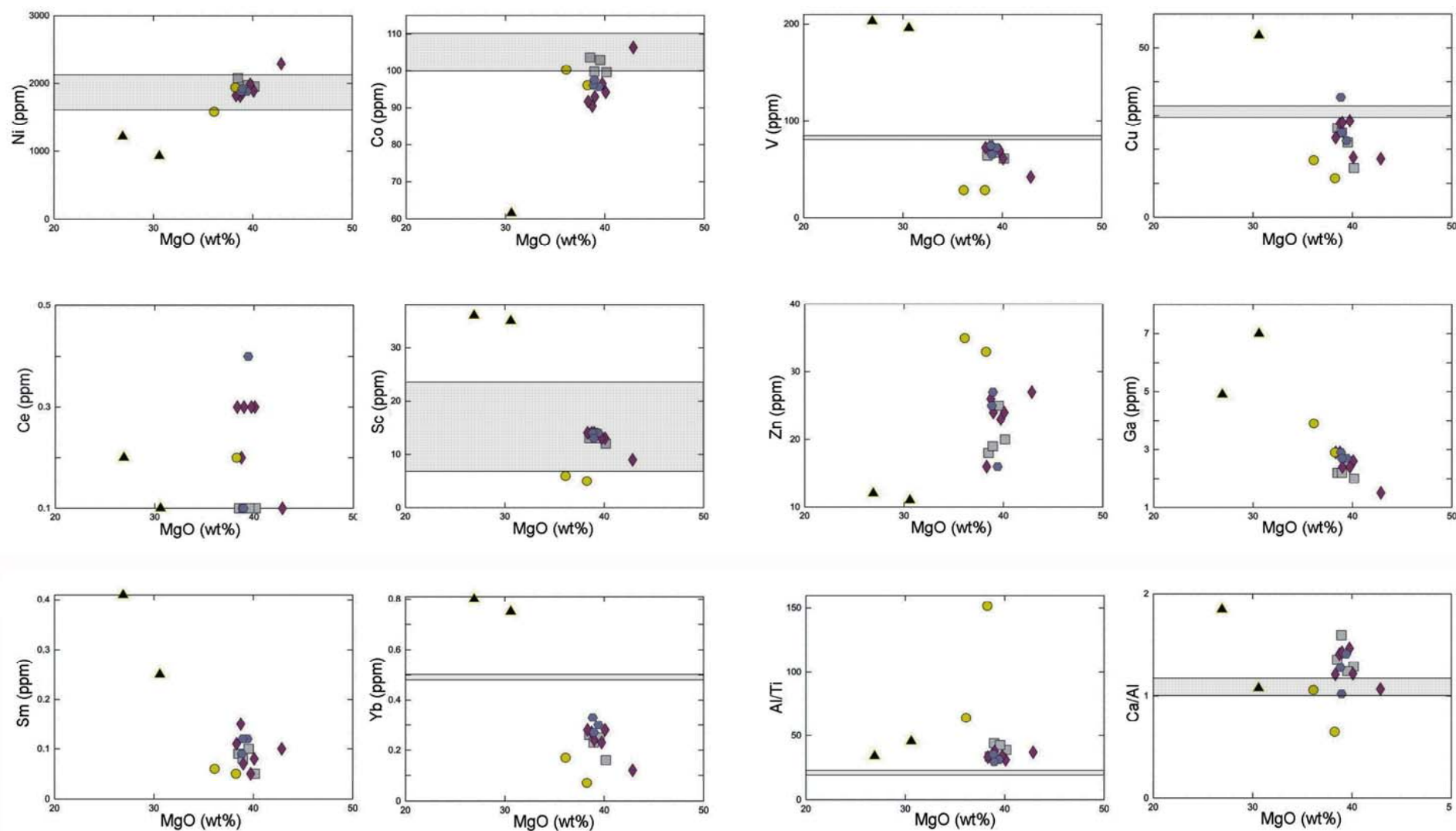


**Fig. 43.** (continued) Variation diagrams of different KKOC ultramafic lithologies with respect to MgO, as well as Al/Ti and Ca/Al vs MgO diagrams. Symbols:  $\square$  filled in grey = spinel lherzolite,  $\diamond$  filled in purple = plagioclase lherzolite,  $\circ$  filled in yellow = dunites,  $\blacktriangle$  = olivine websterite, blue hexagon = KKOC peridotites not analysed by EMPA. Shaded areas represent primitive mantle (PM) values (Taylor and McLennan 1985, McDonough and Sun 1995). Omissions are due to the y axis limitation (Zr, Ce, and Sm).

enrichments of the HREE and HFSE (e.g. Ti and Zr). Knowing that HFSE are essentially immobile during alteration or metamorphism, the presented rates imply that the pristine signatures remained intact during serpentinisation. Fig. 44d shows the correlation of MgO with a set of REE. Apart from the LREE, the MREE and especially the HREE display a significant correlation with MgO, thus suggesting that these elements fully track magmatic mantle signatures as defined by the highly incompatible elements. Even the HREE decreased during mantle melting, despite a possible mass loss of MgO due to serpentinisation and/or seafloor alteration. Therefore, the KKOC whole-rock chemistry data are still suitable for further petrogenetic considerations. As expected, only the alkalis and Sr are mainly governed by alterations caused by hydrous solutions (Fig. 44a,c). Elevated values of LREEs are, however, due to sub-solidus refertilisation.

Calculated CIPW normative mineral compositions of KKOC ultramafic rocks are given in Table X-1. One can notice that the analysed samples contain normative olivine and hypersthene. The presence of normative magnetite is an indicator of the advanced serpentinisation of olivine. The chemical classification of peridotites, based on their normative mineralogy calculated on a volatile-free basis (mode calculation after Lensch 1968) and plotted in the Ol-Opx-Cpx diagramme (not shown), defines the analysed KKOC ultramafic rocks as lherzolites (Streckeisen 1973).

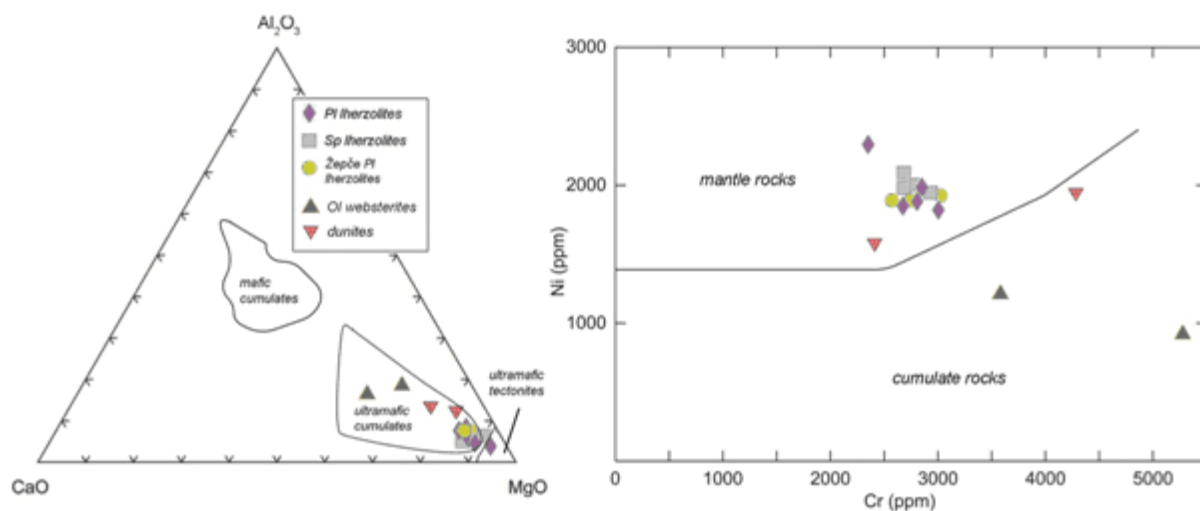


**Fig. 45.** Positions of the KKOC ultramafic rock samples in the MgO-CaO-Al<sub>2</sub>O<sub>3</sub> discrimination diagramme (Coleman 1977) (left); Positions of the KKOC ultramafic rocks in the Ni-Cr diagramme, discriminating mantle from cumulate rock series (Irvine and Findley 1972) (right). For symbols, see left image.

According to a discrimination diagramme proposed by Coleman (1977), the KKOC spinel and plagioclase lherzolites are characterised as ultramafic tectonites (Fig. 45). Although it is apparent that a part of the lherzolite samples is shifted to the field of ultramafic cumulates, one can explain this by effects of serpentinisation, which must have caused a decrease in MgO but an increase in CaO. The latter variation may also be attributed to sub-solidus events (e.g. formation of Cpx or Pl).

The olivine websterites plot into the field of ultramafic cumulates. Their origin, as it will be discussed later (see Chapter 5.1.2., Chapter 6.2.2.), is bound to mantle-derived ultramafic crystallisates, featured by regularly obscured cumulate textures. The other diagramme,

introduced by Irvine and Findley (1972), is used for distinguishing mantle from cumulate ultramafic rocks (Fig. 45). It takes into account the abundances of compatible Ni and Cr. Accordingly, all samples of spinel and plagioclase lherzolites are defined as mantle rocks, whereas the olivine websterites and ultramafic cumulates have a bulk-rock chemical composition of cumulate rocks. The ultramafite rock 'end-member' classification proposed by Piccardo (1995) characterises the spinel and plagioclase lherzolites of the Krivaja-Konjuh ophiolite complex as tectonite ultramafic rocks of the lherzolite-harzburgite type, derived from a moderately depleted mantle bounded to mid-ocean ridge magmatism.

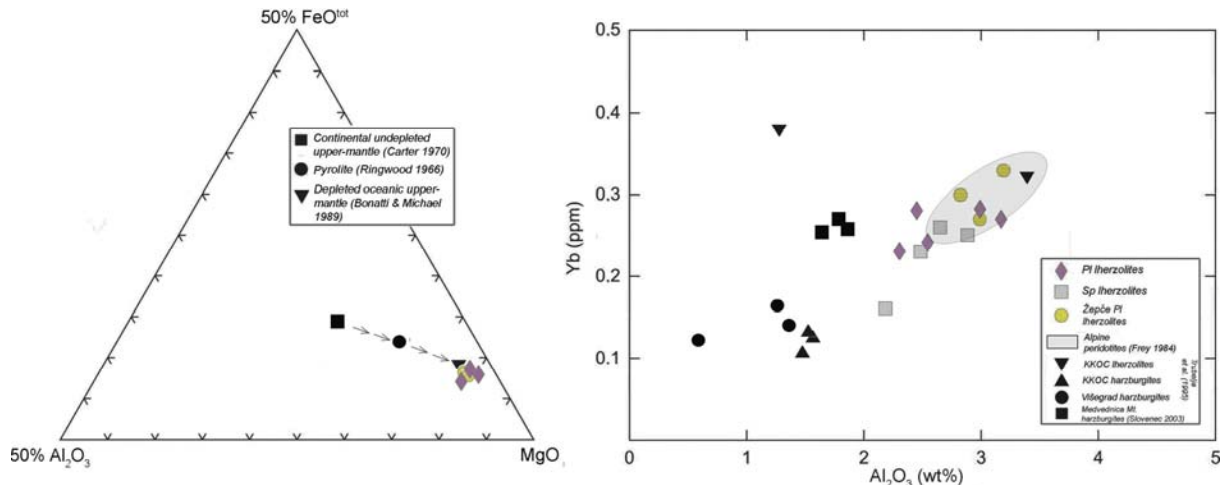


**Fig. 46.** Diagramme proposed by Bonatti and Michael (1989) displaying the relative abundances of Mg/Fe/Al which deciphers the major element composition of analysed KKOC lherzolites with respect to known fertile environments. Arrows point to an increasing degree of depletion (left); Positions of analysed KKOC lherzolites in the Yb-Al<sub>2</sub>O<sub>3</sub> diagramme with respect to literature data from the Alpine Tethyan realm and adjacent Dinaride ophiolite suite (right).

In Fig. 46, the chemical composition of KKOC lherzolites is given in the Al<sub>2</sub>O<sub>3</sub>-FeO-MgO space. Arrows indicate the mantle depletion sequence with a continental undepleted mantle as the starting point. According to the KKOC plagioclase and spinel lherzolites' major element compositions, one can infer their mild refractory nature, corresponding to the compositional range of fertile mid-oceanic ridge peridotite (Bonatti and Michael 1989). The nature of KKOC peridotites is further evaluated in the Yb-Al<sub>2</sub>O<sub>3</sub> diagramme (Frey 1984, Fig. 46), where the abundance of Al<sub>2</sub>O<sub>3</sub> is taken as a measure of depletion. Most of the tectonically emplaced and abyssal peridotites show a well-defined Yb-Al<sub>2</sub>O<sub>3</sub> correlation trend, with occasional exceptions of plagioclase-bearing peridotites, showing low Yb concentrations relative to Al<sub>2</sub>O<sub>3</sub> (Bodinier and Godard 2003). This is, however, not the case for the KKOC peridotites. Analysed lherzolites show a coherent Yb-Al<sub>2</sub>O<sub>3</sub> correlation and their values closely correspond to those of fertile Ligurian harzburgites and lherzolites. The values obtained for harzburgites derived from the Višegrad ophiolite complex (central and eastern CDOB, Trubelja et al. 1995), as well as from Medvednica Mt. peridotites (most western segment of VZ ophiolites, Slovenec 2003), suggest that these are typical high-grade residual rocks showing no similarities with the KKOC peridotites.

The geotectonic setting and the nature of Krivaja-Konjuh ophiolite spinel and plagioclase lherzolites can also be tested by means of an Al<sub>2</sub>O<sub>3</sub>-Mg# diagramme (Fig. 47). KKOC

Iherzolites have Mg# values of 89.2-89.8, which is characteristic for Alpine peridotites of the Tethyan collisional belts, including ophiolite areas of the CDOB and VZ (Coleman 1977). Hence, the diagramme is useful to test similarities within neighbouring peridotite areas, but also to compare them with other orogenic terrains in the world. One can notice that the analysed samples plot into the field of fertile Iherzolites, defined by Tethyan peridotites of the CDOB, Ligurides and Eastern Alps (Lugović et al. 1991, Majer 1993, Trubelja et al. 1995, Rampone et al. 1996, Koller et al. 1999 and Bazylev et al. 2009), fore-arc peridotites of the South-Sandwich island arc (Pearce et al. 2000), and Palaeozoic Uralian orogenic peridotites (Spadea et al. 2003). The match with the latest CDOB data, provided by Bazylev et al. (2009), is fully complete. The distinction from the field defined by harzburgites from the adjacent ophiolite terrains of the Vardar zone and Eastern Alps (Lugović 1986, Koller et al. 1999 and Slovenec 2003), as well as Oman and the South-Sandwich arc/fore-arc (Boudier and Juteau 2000, Pearce et al. 2000 and McInnes et al. 2001) is unequivocal.

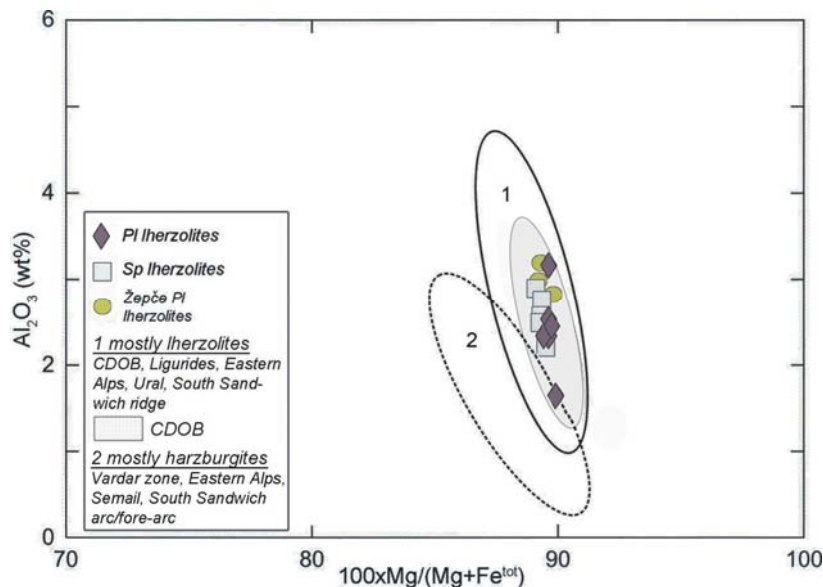


**Fig. 47.**  $Al_2O_3$ -Mg# discrimination diagramme for KKOC Iherzolites. Reference areas are: 1. mostly Iherzolites (Central Dinaric ophiolitic belt = CDOB, Ligurides, Eastern Alps, South-Sandwich islands arc, Ural; Bazylev et al. 2009, Trubelja et al. 1995, Lugović et al. 1991, Majer 1993, Rampone et al. 1996, Koller et al. 1999, Pearce et al. 2000, Spadea et al. 2003), 2. mostly harzburgites (Vardar zone, Semail, South-Sandwich islands & Guinea arc and fore-arc; Bazylev et al. 2009, Slovenec 2003, Lugović 1986, Koller et al. 1999, Boudier and Juteau 2000, Pearce et al. 2000, McInnes et al. 2001).

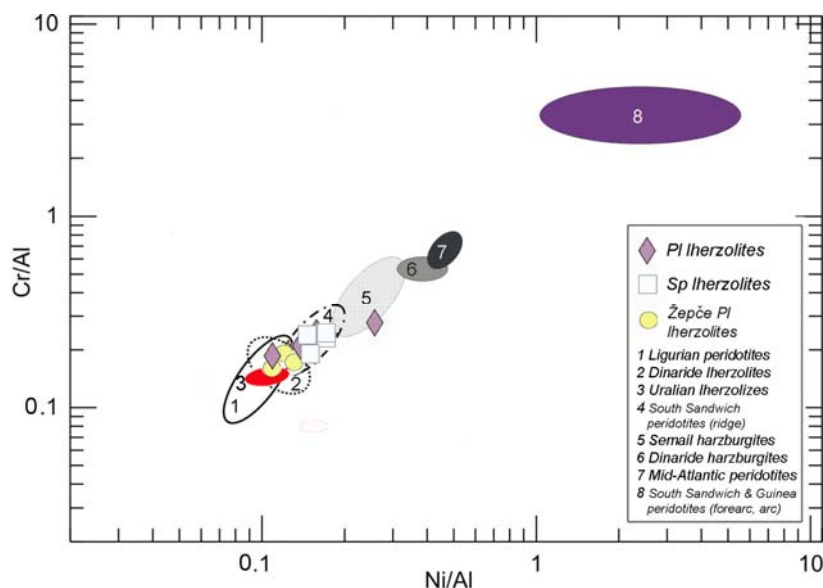


**Fig. 48.** Cr/Al-Ni/Al discrimination diagramme for KKOC Iherzolites. Reference areas are: Tethyan peridotites (Ligurides, Dinarides, Semail, Rampone et al. 1996, Slovenec 2003, Lugović 1986, Lugović et al. 1991, Majer 1993, Trubelja et al. 1995, Bazylev et al. 2003, Boudier and Juteau 2000), Late Palaeozoic Uralian Iherzolites (Spadea et al. 2003), Altered Miocene mid-Atlantic peridotites (Burgath et al. 1997) and Paleogene ridge and fore-arc peridotites (South-Sandwich islands, South Atlantic and Guinea, Pacific, Pearce et al. 2000, McInnes et al. 2001).



Average lherzolite abundances of compatible Cr and Ni (i.e. 2515 ppm Cr, 1949 ppm Ni) and a relatively high value of  $\text{Al}_2\text{O}_3$  result in moderate Cr/Al and Ni/Al ratios. Such Cr and Ni values are characteristic for Alpine peridotites, whereas the obtained Cr/Al and Ni/Al ratios are useful in estimating the depletion level of the peridotites (Liang and Elthon 1990, Roberts and Neary 1993). In Fig. 48, the KKOC peridotites clearly mark a fertile trend that ideally corresponds to the South-Sandwich lherzolite projections (Pearce et al. 2000). A high correlation degree of analysed rocks with the Dinaride and Liguride reference samples is reported as well (Rampone et al. 1996, Slovenec 2003, Lugović 1986, Lugović et al. 1991, Majer 1993, Trubelja et al. 1995, Bazylev 2003, Bazylev et al. 2009).

The following diagrammes (Figs. 49 and 50), which also discriminate the most plausible geotectonic position of peridotites, are based on the bulk-rock composition of (spinel) peridotites and the chromium number of primary spinel (Cr#). Generally, applied ratios show a good correlation trend. In Fig. 49, the correlation between the Cr# of bulk-rocks and that of their primary spinel is displayed. Plagioclase lherzolites together with cumulates and pyroxenites plot outside the correlation trend set by the spinel lherzolite samples. However, one sample of spinel lherzolite (U35) plots far off the correlation trend and lies within the field of plagioclase lherzolites, most probably due to the high degree of sub-solidus metasomatism. In plagioclase bearing rocks, the Cr# of spinel increases with the modal abundance of plagioclase (e.g. Bazylev et al. 2009). Still, two samples of the KKOC plagioclase lherzolites plot near the correlation trend, which indicates that the chemical composition of spinel may be only sporadically affected by the formation of plagioclase. The bulk-rock Cr# of plagioclase lherzolites fit the interval defined by the bulk-rock Cr# values of the spinel lherzolites. The ultramafic cumulates, however, show somewhat higher bulk-rock Cr# values (Table X-1–X-2).

One can notice that the compositions of spinel lherzolites from the Krivaja-Konjuh ophiolite complex, that are unaffected by sub-solidus refertilisation perfectly correspond to the analyses of other Dinaridic spinel peridotites as provided by Lugović et al. (1991) and Bazylev et al. (2009). This holds also true for the majority of analysed KKOC plagioclase lherzolites that plot within the field of Dinaridic plagioclase peridotites (Fig. 49). What needs to be pointed out is that the bulk-rock and spinel chemistry of KKOC fertile spinel lherzolites follow the residual trend of continuous melting of spinel peridotites as obtained for oceanic and alpine-type peridotites (Bazylev 2003, Niu 2004). In Fig. 49, whole-rock compositions of KKOC spinel and plagioclase lherzolites are compared with a possible mantle source by using  $\text{TiO}_2/\text{Al}_2\text{O}_3$  and  $\text{Al}_2\text{O}_3/\text{SiO}_2$  ratios. The possible mantle source of KKOC lherzolites closely corresponds to the estimated depleted mantle composition (DM), which passed through a certain degree of MORB extraction (e.g. Workman and Hart 2005). It is evident that the plagioclase lherzolites of the KKOC are compositionally similar to spinel lherzolites. This implies a residual nature of the plagioclase lherzolites prior to refertilisation and shows the relative insensibility of the applied ratios to sub-solidus alterations. In this diagramme, the KKOC plagioclase and spinel lherzolites do not form a clear residual trend of mantle rocks after partial melting (bold line). On the other hand, dunites and olivine websterites have much higher  $\text{Al}_2\text{O}_3$  and lower  $\text{TiO}_2$  values.

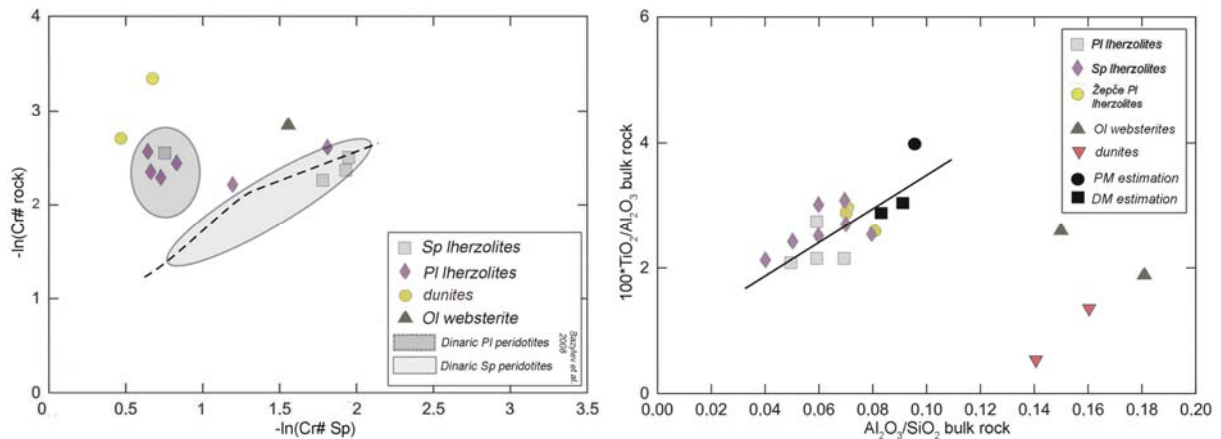


**Fig. 49.** Chromium numbers of bulk rocks and spinel in KKOC ultramafic rocks (left); Correlation of bulk-rock  $Al_2O_3/SiO_2$  and  $TiO_2/Al_2O_3$  ratios measured in samples of the KKOC ultramafic rocks (right). The composition of primitive mantle (PM) is taken from McDonough and Sun (1995), while the compositions of the depleted mantle (DM) are from Salters and Stracke (2004) and Workman and Hart (2005).

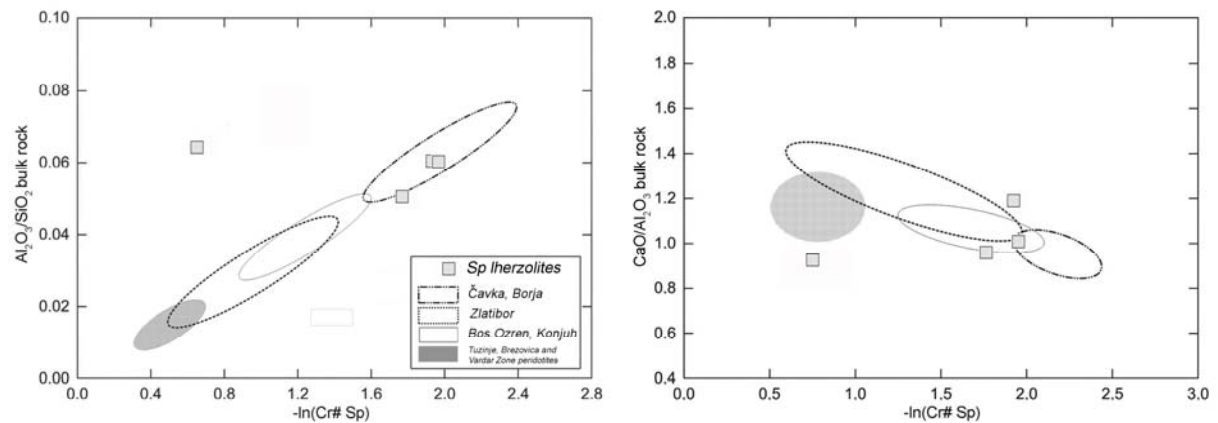
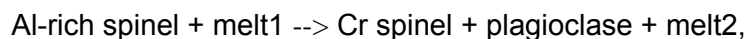


**Fig. 50.** Correlation of the  $Al_2O_3/SiO_2$  ratio in bulk-rock compositions of KKOC spinel lherzolites with the Cr# of spinels (left); Correlation of the  $CaO/Al_2O_3$  in bulk-rock compositions of KKOC lherzolites with Cr# of spinels (right). For symbols see left image. Values for the specified Dinaridic ophiolite complexes are from Bazylev et al. (2009).

Spinel peridotites unaffected by sub-solidus alterations show increasing  $Al_2O_3/SiO_2$  ratios with decreasing Cr# of their spinel. This relationship nicely reflects the melting extent of the original mantle source of the CDOB ophiolites (Fig. 50). Such a relationship does not hold for the plagioclase lherzolites, since plagioclase formation most probably follows the incongruent reaction:



resulting in an increased Cr# of spinel (e.g. Kaczmarek and Müntener 2008). It is to be inferred that the unaltered KKOC spinel lherzolites are at the point of melting, a trend set by the other large complexes of the Central Dinaric ophiolitic belt (CDOB) (Bazylev et al. 2009). One might question why acquired data from the KKOC correspond better to the provided compositional span of the Čavka and Borja complexes than to those of the Konjuh complex. Such discrepancies are however, expected, since the differences are within the normal range of a fertile ophiolite suite, such as the fertile spinel peridotites from Čavka and Borja, which are the western compositional equivalents of the KKOC peridotites (e.g. Lugović et al. 1991). The bulk-rock  $CaO/Al_2O_3$  ratio in less altered spinel peridotites also correlates well with the

Cr# of spinel. The negative correlation defines a melting trend in the CDOB ophiolites (Fig. 50). In fertile spinel lherzolites this ratio is found to be 0.8-0.9, whereas in refractory harzburgites it is higher, ranging from 1.0-1.3 (Bazylev et al. 2009). Analysed KKOC spinel lherzolites are similar to the reference data of the Borja, Bosanski Ozren, Čavka and Konjuh complexes, except the altered U35 sample, which has a much higher Cr# of spinel due to a partial loss of its Al content.

In Fig. 51, the concentrations of REE in KKOC lherzolites are displayed as chondrite-normalised values (according to McDonough and Sun 1995). One can see that the MREE and HREE contents, both in spinel and plagioclase lherzolites, are similar, gradually increasing from 0.5 to 1.1 x chondrites. Their slope is flat and moderately positive with average ratios of  $(\text{Sm/Yb})_N$  and  $(\text{Tb/Yb})_N$  being 0.42 and 0.84 respectively. On the other hand, the contents of LREE in spinel lherzolites (Fig. 51) are extremely depleted, typically having concentrations which were under the detection limit [ $(\text{Ce/Yb})_N = 0.09-0.16$ ]. Such  $(\text{REE})_N$  trends fit well the second group of chondrite-normalised REE patterns (ophiolitic lherzolites and cpx-harzburgites), as defined by Bodinier and Godard (2003). They are characterised by a highly LREE-depleted “N-MORB” pattern and lower LREE/MREE, MREE/HREE, and LREE/HREE ratios. The REE slopes increase monotonically with an extreme concentration jump in the Ce-Nd region ( $(\text{Ce/Nd})_N = 0.25$ ). The described trend is also reported from Cpx compositions (Rivalenti et al. 1996). The only difference with the aforementioned pattern is the unusually high La values spanning from 0.30-1.05 x chondrites, whereas normally they fit the 0.005-0.05 x chondrites range. Nevertheless, all the analysed La values in spinel lherzolites, except those in sample U35, are under the detection limit, which leaves the possibility that they actually fit the given range. Sample U35 is characterised by an unusual mineral paragenesis, containing an equilibrated primary amphibole. Invoking the metasomatic history of this sample, one can bound its extremely high La value to sub-solidus alterations. The metasomatic LREE enrichment in peridotites, especially of the highly incompatible and relatively mobile La, is typical for ophiolitic complexes and might be constrained to low-temperature alteration events (Frey 1984, Gruau et al. 1998). If we exclude La, the same REE distribution trends in spinel and plagioclase lherzolites are also reported from other CDOB ophiolitic complexes (Lugović et al. 1991).

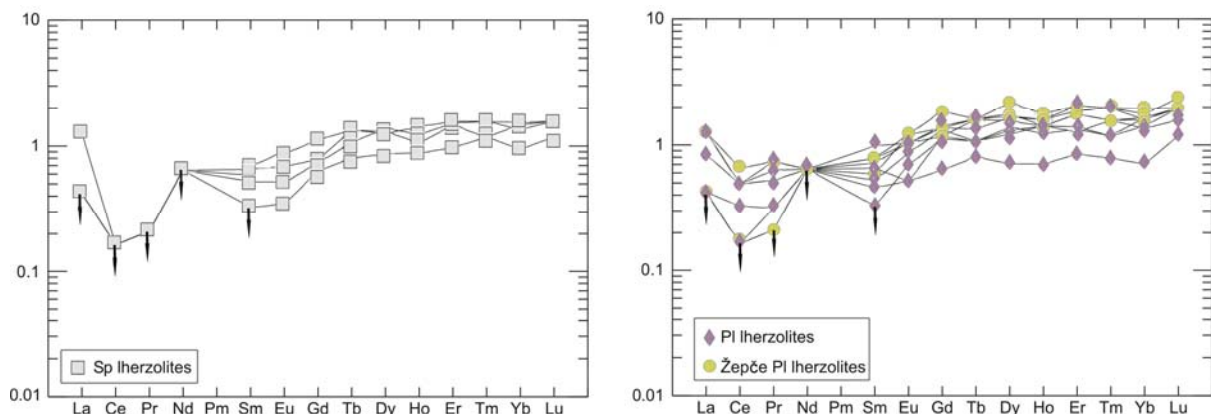


**Fig. 51.** Chondrite-normalised abundances of REEs in spinel lherzolites (left) and plagioclase lherzolites (right). Normalisation values after McDonough and Sun (1995). The arrows indicate measured concentrations of REE that are under the detection limit.

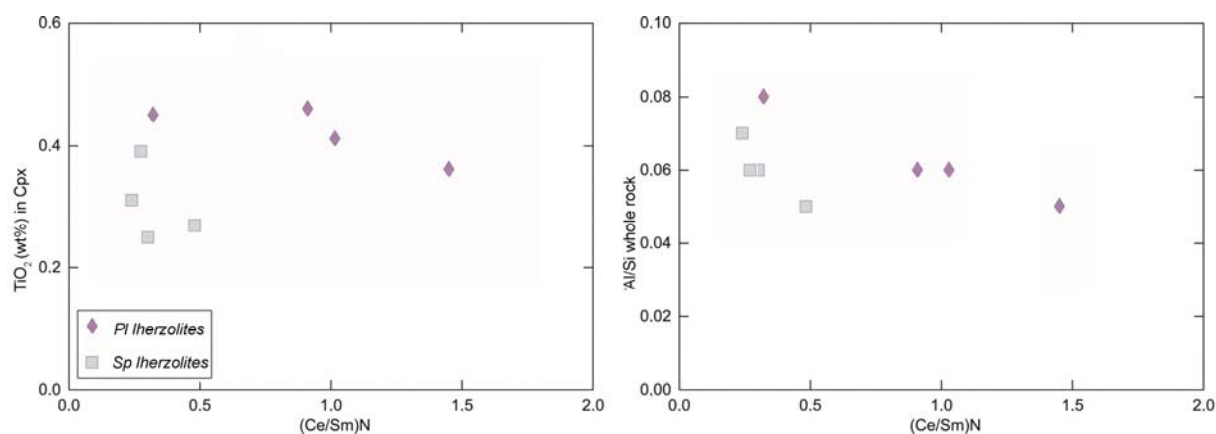


**Fig. 52.**  $\text{TiO}_2$  contents of Cpx vs  $(\text{Ce}/\text{Sm})_N$  of bulk-rocks (left);  $\text{Al}/\text{Si}$  ratio vs  $(\text{Ce}/\text{Sm})_N$  of whole-rock samples (right). Note the similar whole rock fertility of plagioclase and spinel lherzolites ( $\text{Al}/\text{Si}$ ) and their different Cpx  $\text{TiO}_2$  content due to sub-solidus reactions.

Plagioclase lherzolites from the KKOC display somewhat different REE distribution patterns (Fig. 51). Their LREE abundances (La, Ce and Pr) are progressively elevated, approaching the shape of the fourth group of “flat” or slightly sigmoid REE patterns (Bodinier and Godard 2003). Such a feature is characteristic for orogenic peridotite massifs, but it is also reported in those ophiolitic peridotites that underwent metasomatic changes (Prinzhofer and Allègre 1985), as well as in some mantle xenoliths (Song and Frey 1989). Additionally, observed REE trends in plagioclase lherzolites are marked by a negative correlation of LREE/MREE and HREE ratios versus HREE abundances (Dy-Yb). Elevated LREE abundances or slight enrichments of La ( $\pm$  Ce), relative to MREE, which caused the discussed flat REE patterns, are thought to be due to: (a) decreasing melting degrees under the oceanic ridge (Takazawa et al. 2003), (b) refertilisation by trapped or upwelling partial impregnation melts which freeze near-solidus (Cannat et al. 1990, Takahashi 2001, Barth et al. 2003 and Niu 2004) and (c) low-temperature metamorphic alterations induced by ground-water or meteoric water (Gruau et al. 1998).

In Fig. 52, one can notice that in KKOC plagioclase and spinel lherzolites, the LREE enrichment  $(\text{Ce}/\text{Sm})_N$  is not dependant on the overall rock fertility, since the  $\text{Al}/\text{Si}$  ratio is practically the same for both lherzolite varieties. However, in plagioclase lherzolites (and the metasomatised U35 spinel lherzolite), which contain Ti-rich clinopyroxene (A parametre being consensually set as a fertilisation indicator, e.g. Cannat et al. 1990), the LREE abundances are enhanced [ $(\text{Ce}/\text{Sm})_N \approx 1$ ]. Furthermore, low-temperature alterations involve fluids that are ultimately of seawater origin (e.g. sea-floor weathering, serpentinisation). But average seawater has REE levels up to six orders of magnitude lower than in peridotites (e.g. Elderfield and Greaves 1982), so seawater cannot be a reliable source for an excess of LREE in analysed plagioclase lherzolites (Niu 2004). Discussed lines of evidence advocate a refertilisation mechanism as the most probable process which may cause a selective and progressive enrichment of LREE. The strong depletion of LREE in spinel and pre-metasomatised plagioclase lherzolites of the KKOC most probably echoes a single event of melt extraction which probably occurred during adiabatic melting of upwelling asthenosphere. This is consistent with experimental and theoretical modelling, stating that only very small fractions of melt are needed to trigger the LREE segregation. So, the strong depletion of

LREE relative to HREE may be considered as proof for an incremental melt extraction, approaching the fractional melting model (Shaw 1970, Fig. 51).

Although the trace element patterns meet general standards set for fertile ophiolite peridotites (e.g. Bodinier and Godard 2003), and in spite of very low (undetectable) concentrations of certain highly incompatible elements, one is able to identify particularities pertaining to the discussed LREE enrichment. An abnormal Cs abundance in both plagioclase and spinel lherzolites (10-40 x primitive mantle) along with minor additions of other LILE to many other samples of both lherzolite types may indicate an incipient supra-subduction zone (SSZ) imprint, or just pronounce secondary alteration processes (Parkinson and Pearce 1998, Slovenec 2003). High Sr fluctuation and the frequent occurrence of positive anomalies of Sr especially in plagioclase lherzolites are attributed to the impregnating melts that were certainly enriched in highly incompatible elements and in volatiles, notably in water (e.g. Brenan et al. 1995). A strong enrichment in P and LREE (La and Ce) along with the sporadical occurrence of texturally equilibrated amphibole (sample U35) also indicates the presence of evolved residual melts. Finally, the Nb fractionation that is particularly significant in the U35 sample of spinel lherzolite might be attributed to minute amounts of rutile, which may easily precipitate from such evolved melts (Bodinier et al. 2004).

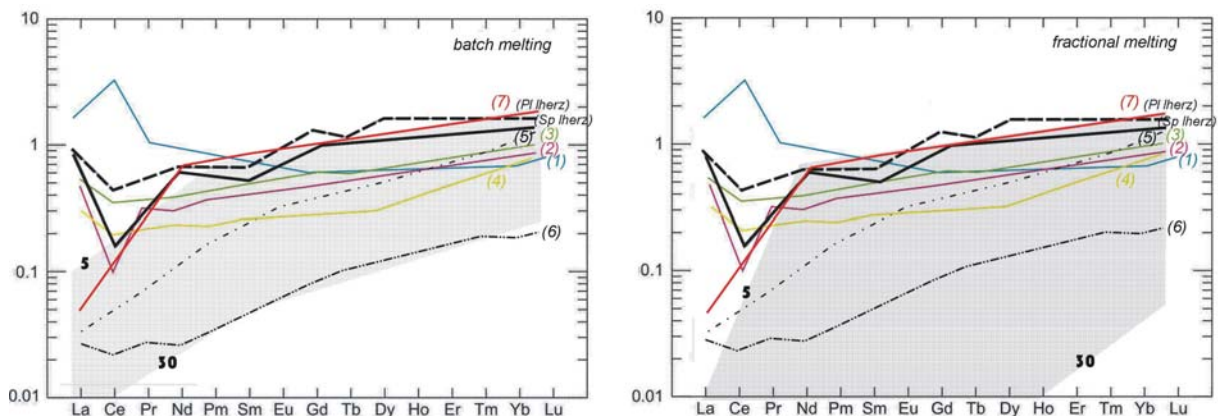


**Fig. 53.** Comparison of chondrite-normalised REE patterns of KKOC spinel and plagioclase lherzolites with several other world localities: (1) seawater altered peridotites of Islas Orcadas fracture zone (Kimball et al. 1985; Niu 2004), (2) Shaka fracture zone lherzolites and South-Sandwich fracture zone lherzolites (Pearce et al. 2000; Niu 2004), (3) Andrew Bain lherzolite (Peyve et al. 2007), (4) Medvednica Mt. SSZ harzburgites (west Vardar Zone, Slovenec 2003), (5) ophiolitic peridotites of Internal Ligurides (Rampone et al. 1996), (6) South-Sandwich fore-arc peridotites (Bodinier and Juteau 2000, Pearce et al. 2000, McInnes et al. 2001), and (7) CDOB fresh spinel and plagioclase lherzolites (Lugović et al. 1991). The shaded regions represent residues of 5-30% melting from a depleted mantle source according to the respective model. Normalisation values according to McDonough and Sun (1995).

In Fig. 53, chondrite-normalised REE abundances of analysed Krivaja-Konjuh lherzolites are presented in comparison to some of the world-known literature localities, which present different geotectonic peridotite settings (references in Fig. 53 captions). It is to be inferred that the plagioclase lherzolites show a high correlation with the abyssal Andrew Bain lherzolites (Indian Ocean), especially in the portion of the LREE enrichment, which underwent certain metasomatism (Peyve et al. 2007). However, the analysed rocks exhibit higher

fractionation degrees. Krivaja-Konjuh spinel lherzolites are in the concentration level, as expected, remarkably well correlated with other CDOB ophiolites (Lugović et al. 1991), but decipher some discrepancies in LILE abundances. Their LREE pattern corresponds better to fertile Shaka ophiolites and South-Sandwich abyssal fracture zone lherzolites, but on a slightly lower fractionation level (Pearce et al. 2000, Niu 2004).

Both in the compositional and intra-element relation sense, one can see clear differences when comparing the REE patterns of the KKOC rocks (Fig. 51) to: (a) South-Sandwich fore-arc peridotites (Boudier and Juteau 2000, Pearce et al. 2000, McInnes et al. 2001), (b) highly altered Islas Orcadas peridotites (Kimball et al. 1985, Niu 2004), and (c) refractory Ligurian ophiolites (Rampone et al. 2006). Some similarities, but with a huge compositional bias, are to be noticed with peridotites from the Medvednica Mt. ophiolite complex, which actually present a transitional peridotite type from depleted fore-arc harzburgites to fertile abyssal clinopyroxene harzburgites and lherzolites (Slovenec 2003).

The presented discussion clearly leads to the conclusion that analysed Krivaja-Konjuh peridotites are fertile ridge-related mantle rocks, which had experienced a higher (plagioclase lherzolite) or lower degree (spinel lherzolite) of sub-solidus alterations.

### 5.1.2. Olivine websterites and dunites

Whole-rock chemical analyses were performed on two olivine websterites and two dunites from the Krivaja-Konjuh complex. The complete data set is provided in Appendix D, Table X-1–X-2.

Pyroxenites are mantle rocks characterised by the predominance of modal pyroxene. In a broader sense, the term may even include lithologies rich in hornblende or phlogopite, or a different metamorphic sole paragenesis (Bodinier and Godard 2003). The mineralogical variation of mantle pyroxenites is due to the extensive range of their major-element compositions, as depicted in the  $\text{SiO}_2/\text{MgO}$  vs  $\text{Al}_2\text{O}_3$  diagramme (Fig. 54). The array of garnet (Grt)-free mantle pyroxenites stretches from ultramafic compositions adjacent to the field of mantle peridotites to Si- and Al-rich compositions of mafic intrusives and ridge basalts.

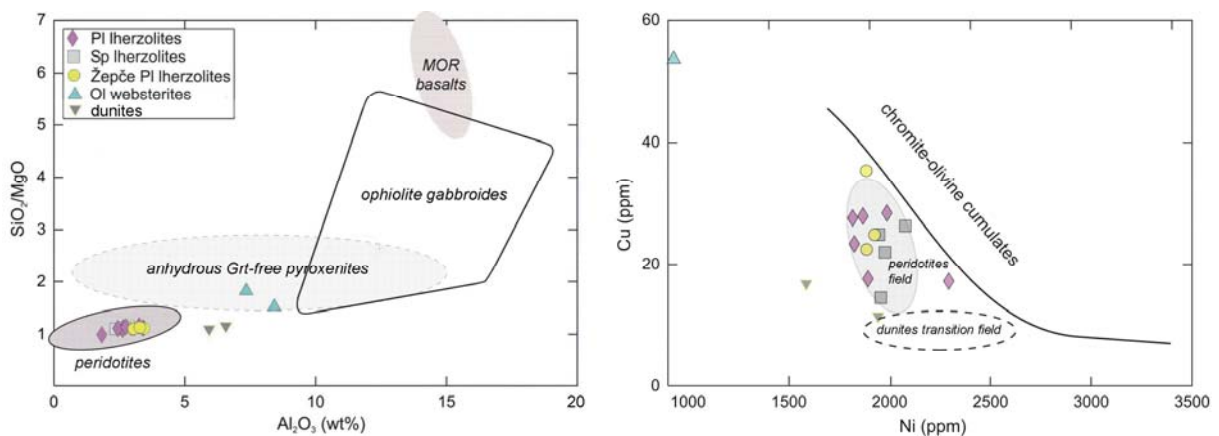


**Fig. 54.**  $\text{SiO}_2/\text{MgO}$  vs  $\text{Al}_2\text{O}_3$  diagram of representative rock lithologies originating from orogenic, ophiolitic and abyssal mantle portions with respect to the composition of analysed KKOC olivine websterites and dunites. Marked fields are according to Bodinier and Godard (2003) and references therein (left); The Cu vs. Ni diagramme depicting the composition of the KKOC ultramafic rocks by comparing peridotites and transition-zone dunites from Luobusa ophiolite (Zhou et al. 2005) (right).

The Krivaja-Konjuh olivine websterites plot into the field of anhydrous Grt-free pyroxenites, having a moderate  $\text{SiO}_2/\text{MgO}$  ratio ( $\sim 1.8$ ) and  $\text{Al}_2\text{O}_3$  contents below 10 wt%. These characteristics define them as low-alumina pyroxenites, approximating the Cr-diopside pyroxenite group, as defined by Shervais (1979). Compared to the average basalt composition (PetDB database), KKOC pyroxenites are strongly depleted in Si, Ti, Al, Fe, P and alkalis, enriched in Mg, whereas the Ca content is practically the same. The Mg# values ( $= 100 \times \text{Mg}/(\text{Mg}+\text{Fe}^{2+})$ ), 89.4 and 89.5, correspond well to those of the fertile spinel and plagioclase lherzolites, thus suggesting a low degree of differentiation of these rocks.

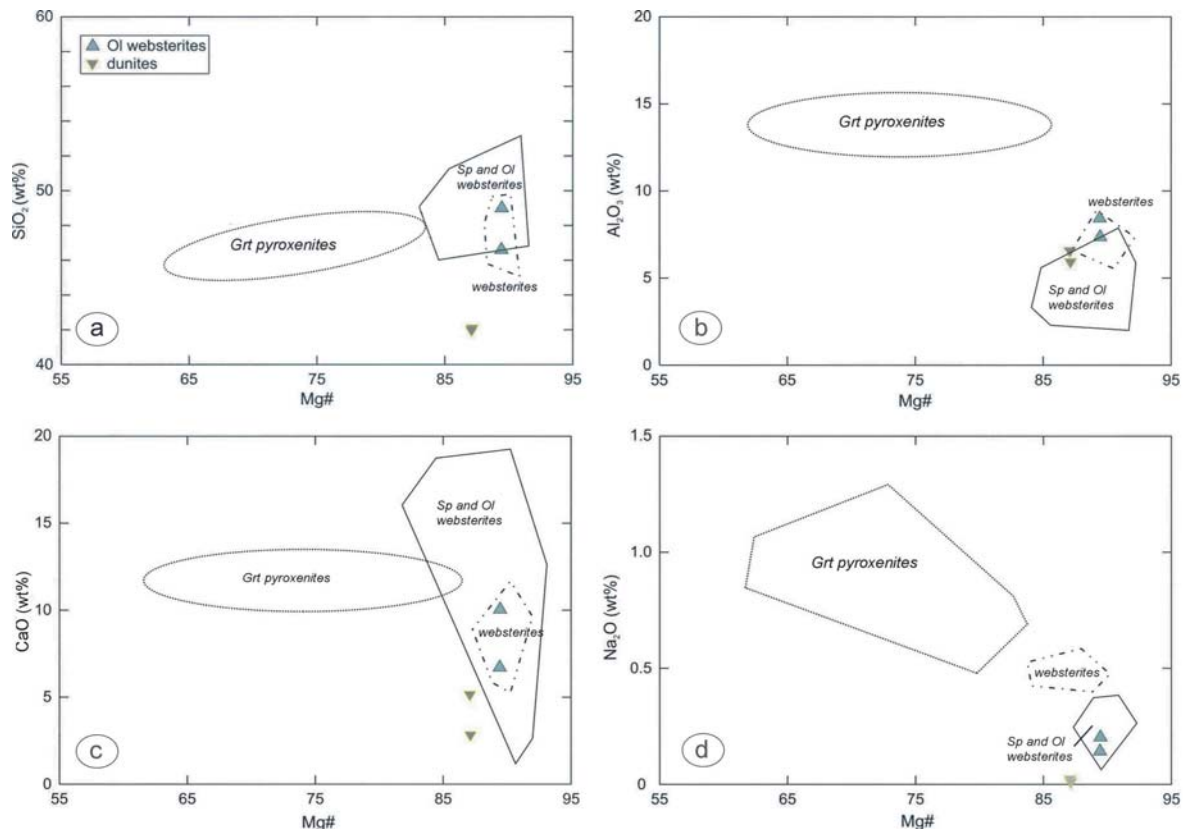


**Fig. 55a-d.** Variation diagrammes of  $\text{Na}_2\text{O}$ ,  $\text{CaO}$ ,  $\text{Al}_2\text{O}_3$  and  $\text{SiO}_2$  vs  $\text{Mg}\#$  ( $100 \times \text{Mg}/(\text{Mg}+\text{Fe}^{2+})$ ) for Krivaja-Konjuh olivine websterites and dunites. Compositional fields shown for comparison: Garnet pyroxenites (Pearson et al. 1993, Majer et al. 2003), spinel and olivine websterites (Oberger et al. 1995, Garido and Bodinier 1999), and websterites (Bodinier 1989).

As suggested by Garrido and Bodinier (1999), a strong depletion of  $\text{K}_2\text{O}$  and  $\text{P}_2\text{O}_5$  in comparison to average basalts argues against the possibility that the pyroxenites (olivine websterites) are actually frozen basaltic melts. Major element chemical variations and inter-element correlations are difficult to trace due to the small number of analysed samples. A set of variation diagrammes, i.e.  $\text{Na}_2\text{O}$ ,  $\text{CaO}$ ,  $\text{Al}_2\text{O}_3$  and  $\text{SiO}_2$  versus  $\text{Mg}\#$ , are provided in Fig. 55. The comparison with other mantle pyroxenite occurrences (e.g. Bosnia, Northern Italy, New Caledonia, and Thailand) shows that the KKOC olivine websterites are similar to Alpine layered websterites, likewise to those of the Lanzo ophiolite in Italy. A characteristic alumina deficiency ( $< 8$  wt%), very low contents of  $\text{TiO}_2$  (0.15-0.18 wt%), and high MgO (25.2-28.1 wt%), along with the constant  $\text{Mg}\#$  of  $\sim 89.5$  were also recognised in some of the back-arc ophiolite mantle sections (e.g. DeBari and Sleep 1991). Discrepancies in  $\text{SiO}_2$  and  $\text{CaO}$

contents (42.74 and 45.93, 6.15 and 9.41wt%, respectively) are in accordance with observed variations in their modal mineralogy.

The SiO<sub>2</sub> abundance of less than 45 wt% defines the analysed rocks as ultramafic, according to the Peccerillo and Taylor (1976) classification. The Al<sub>2</sub>O<sub>3</sub>-CaO-MgO diagramme (Fig. 45) of Coleman (1977) further classifies these rocks as ultramafic cumulates, whereas their AFM relations, as defined by Bread (1986), suggest an ophiolitic cumulate to an island-arc related mafic cumulate origin (not shown). A normative mineralogy (CIPW) classification, which is based on the rock's ol-opx-cpx proportion (Streckeisen 1973), defines these rocks as websterites and olivine orthopyroxenites (not shown).

Some of the trace element concentrations and their correlation with Mg# are provided in Fig. 56, along with the compositional fields of several pyroxenite varieties, which are shown for comparison. The olivine websterites are characterised by ~ 200 ppm V, ~ 35 ppm Sc and ~ 1000 ppm Ni, while the dunites have ~ 20 ppm V, ~ 5 ppm Sc and ~ 1700 ppm Ni. These differences are clearly related to the rocks' mineralogy. Portrayed trace element concentrations of the olivine websterites are nearly similar to those of olivine websterites from the Ronda ultramafic complex (Spain) as illustrated by Garrido and Bodinier (1999). In comparison with the average basalt composition (PetDB database, Chen and Lee 1996), the KKOC olivine websterites are enriched in Cr, Ni, and Co, they have a similar content of Cu and V, but are impoverished in Sr and Zr (not shown). A pronounced discrepancy in the Cr abundance between the two analysed samples (0.49 and 0.71 wt% Cr<sub>2</sub>O<sub>3</sub>) is in line with different proportions of Cr-enriched spinel. Likewise, the differences in the amount of Cu (176 vs 54 ppm) between the two samples (Table X-2) suggests the presence of sulphides in sample 1C. Compared to the KKOC Iherzolites, the analysed pyroxenites have higher contents of LILE, V, Sc, Cu and most of the REE, whereas they are depleted in Cr, Co, Ni and Zn. On average, eight times higher concentrations of Sr are reported in comparison to associated Iherzolites (Tables X-1 and X-2). This might reflect a seawater impact through ocean-floor metasomatism. Zr contents coincide with mantle abundances, both being considerably lower than those of average MORB melts. A reduced distribution coefficient ( $K_D$ ) for Zr of pyroxene in equilibrium with primitive mafic melts might have caused this (Downes 2007).

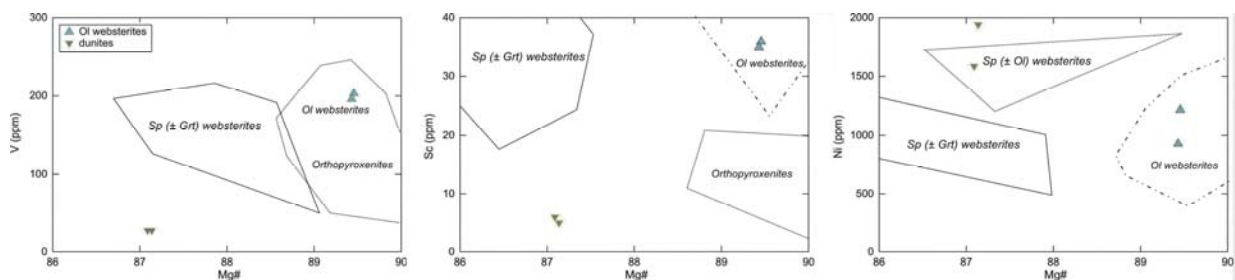


**Fig. 56.** Variation diagrammes of V, Sc, and Ni versus the Mg# for Krivaja-Konjuh olivine websterites and dunites. Compositional fields shown for comparison: Spinel (+Grt) pyroxenites (Majer et al. 2003, Garrido and Bodinier 1999), Olivine websterites and orthopyroxenites (Garrido and Bodinier 1999).

Chondrite-normalised REE patterns (normalisation after McDonough and Sun 1995) of KKOC olivine websterites show characteristics of a typical N-MORB moderately fractionated REE pattern (Fig. 57) with a relatively enriched HREE to MREE (3-4 x chondrites)



flat segment [ $(\text{Sm}/\text{Yb})_N = 0.57\text{--}0.79$ ] and a substantial LREE depletion ( $\text{Ce}_N < 0.2$  and  $(\text{Ce}/\text{Yb})_N = 0.03\text{--}0.06$ ). Such a depletion of LREE with regard to HREE, along with a lack of a Eu anomaly, is characteristic for non-intrusive, low-Al Cr-spinel clinopyroxenites, websterites, and orthopyroxenites (Garrido and Bodinier 1999, Bodinier and Godard 2003), and it is comparable to data provided by Frey (1984) on pyroxenites from various ophiolite bodies. Furthermore, such a LREE/HREE ratio suggests a depleted mantle source as parental to the olivine websterites. The LREE depletion is readily attributed to reflect the composition of pristine melts rather than being due to later equilibration with host LREE-depleted mantle lherzolites (Downes 2007). Compared with N-MORB, Krivaja-Konjuh olivine websterites possess markedly lower REE concentrations (LREE-HREE). The low abundances of MREE and HREE in the KKOC websterites are partly consistent with a MORB-picrite trace element composition, thus further advocating the unfractionated nature of parental melts (Elthon 1989). The olivine websterite REE patterns show a great similarity with the REE patterns of spatially associated plagioclase lherzolites of the Žepče displaced terrain (Fig. 51). Interestingly, similar REE patterns were found in pyroxenites from the Ronda massif in Spain (Gervilla and Remaidi 1993).

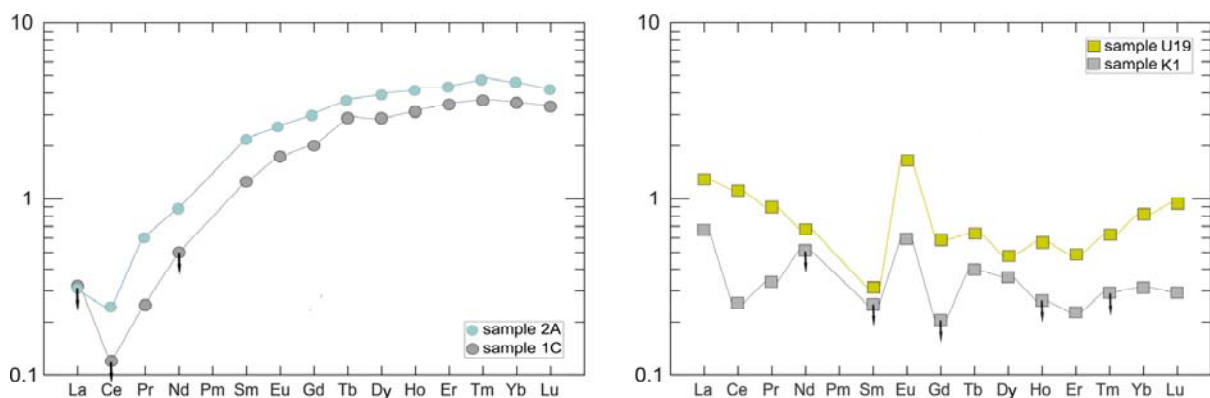


**Fig. 57.** Chondrite-normalised abundances of REE in KKOC olivine websterites (left) and dunites (right). Normalisation values are after McDonough and Sun (1995). The arrows indicate measured concentrations of REE that are under the detection limit.

Analogue to the olivine websterites, the dunites that are characterised by cumulate textures represent a minor lithological unit of the KKOC, being recognised only in the Duboštica and Karaula localities (Fig. 4). Chemical analyses of these rocks are given in Tables X-1–X-2. Relative to the olivine websterites, these rocks are characterised by lower  $\text{SiO}_2$ ,  $\text{Al}_2\text{O}_3$ ,  $\text{MgO}$ ,  $\text{Mg}\#$ ,  $\text{CaO}$ ,  $\text{Na}_2\text{O}$ , Sc, Cu, V, Y and most of the MREE and HREE. An increase is recorded in the concentrations of FeO and Zn, whereas the abundances of MnO,  $\text{P}_2\text{O}_5$ , Zr, Pb, Co, Ga, Tb and certain LREE (La and Nd) remain practically the same like in lherzolites. Since the dunites contain more serpentinised olivine than the olivine websterites, they show higher  $\text{H}_2\text{O}$  contents of ~10 wt%. The relatively high CaO content is due to formation of secondary Ca-rich phases within the olivine interstitial space (e.g. amphibole, prehnite, hydrogarnet, and chlorite). Unusually high  $\text{Al}_2\text{O}_3$  contents (~5.5 wt%; Tables X-1–X-2) are ascribed to the presence of modal plagioclase and a high proportion of Al-rich chromite (e.g. Zhou et al. 2001).

Due to the fact that the dunites are more Al-rich than the lherzolites and given the incompatible character of Al, it follows that the dunites cannot have originated by increased partial melting from the lherzolites. Moreover, the dunites have lower Mg# values than the lherzolites (Table X-1). Correlation diagrams of SiO<sub>2</sub>, Al<sub>2</sub>O<sub>3</sub>, CaO, Na<sub>2</sub>O and a suite of selected trace elements versus Mg# (Figs. 55 and 56) are not very informative, because of the limited number of dunite analyses.

Chondrite-normalised REE patterns of the Krivajah-Konjuh dunites are presented in Fig. 57 (normalisation after McDonough and Sun 1995), portraying a concave-upward, "U"-shaped pattern with a clear positive Eu anomaly. HREE concentrations range from 0.2-1.0 x chondrite, approximately the same as for the LREE, whereas the MREE form a depleted plateau with values in the range of 0.1-0.5 x chondrite (except Eu). This behaviour of REE is characteristic for transitional-zone dunites, formed by a pervasive melt impregnation on the host peridotite rocks (e.g. Zhou et al. 2005). An analogue REE trend has been reported for ophiolite peridotites of California (Trinity), being interpreted through the contamination by continental derived fluids (Gruau et al. 1998). So, the REE pattern of the Krivaja-Konjuh dunites clearly differs from the "N-MORB" trend observed in lherzolites, which tends to be LREE depleted with higher concentrations of MREE and HREE (Figs. 51 and 57).

## 5.2. Metamorphic sole

Comprehensive whole-rock chemical analyses of the Krivaja-Konjuh metamorphic rocks were performed on the same set of 16 samples used for petrographic and mineral chemistry researches. In addition, chemical data on two samples (YU145, YU137) were included in the investigation. These additional samples were recovered from Vijaka and the central KKOC domain (vicinity of Careva Ćuprija) during prior field works. The complete data set of bulk-rock chemical analyses is listed in Appendix D, Tables Y-1–Y-2.

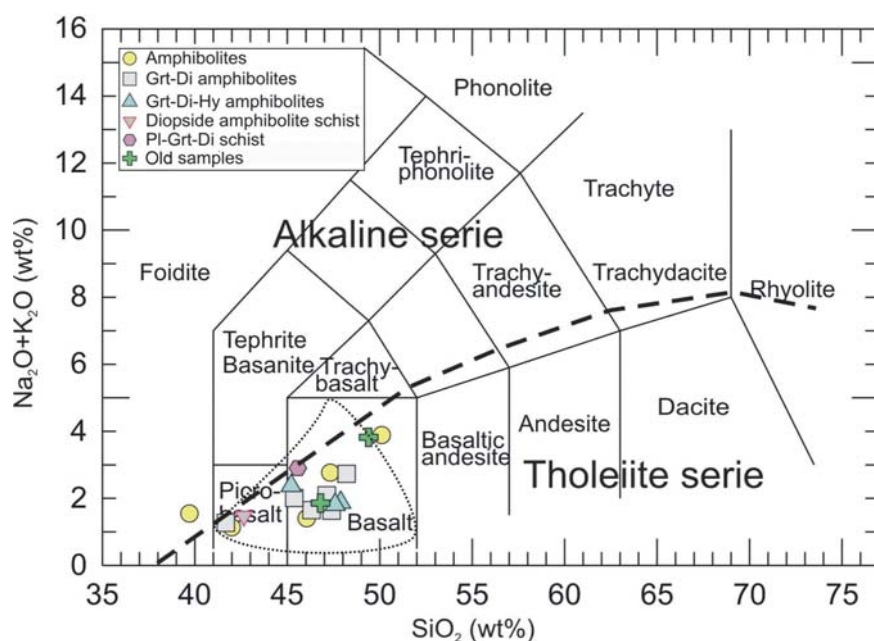


**Fig. 58.** SiO<sub>2</sub> vs (Na<sub>2</sub>O+K<sub>2</sub>O) diagramme used for the classification of volcanic rocks and their magmatic affinities. After Le Maitre et al. (2002). The dashed line separating alkaline from tholeiite series is from Irvine and Baragar (1971). Dotted line defines the projection area of the Krivajah-Konjuh mafic rocks (cumulate gabbros and dolerites or diabases; after Pamić et al. 1977, Trubelja et al. 1995, Babajić 2009).

Major element compositions are typical for ultramafic to mafic igneous rocks, with SiO<sub>2</sub> in the range from 39.7 to 50.1 wt%, MgO from 8.4 to 20.0 wt% and Al<sub>2</sub>O<sub>3</sub> from 12.6 to 27.5 wt% (Table Y-1). However, some of the samples (e.g. U29, 10D) have Al<sub>2</sub>O<sub>3</sub> contents that are either too high or too low for mafic igneous rocks. Likewise, an MgO content of 20.0 wt% (sample U30) and a CaO content of 19.3 wt% (sample 10D) are also beyond the respective ranges of normal igneous rocks. Mg# values of primary mantle melts [ $Mg\# = 100 \times MgO / (MgO + 0.9FeO_{tot})$ ] should be around 70. Therefore, analyses with Mg# > 70 are most probably metacumulates (e.g. U30, U29, U23, YU145; Table Y-1).

In the TAS diagramme (Le Maitre et al. 2002) the analyses of the mafic metamorphic rocks fall into the fields of basalt and picobasalt, characterised by (extremely) low contents of Na<sub>2</sub>O+K<sub>2</sub>O (Fig. 58). With the exception of sample 10D, all analyses show (very) low contents of incompatible elements and in particular of potassium (Tables Y-1–Y-2). Although it is well known that the alkalis and some chemically related elements (e.g. Ba and Sr) may be highly mobile during low-temperature alterations (e.g. Staudigel et al. 1981), the analyses of the mafic rocks at first glance suggest a tholeiitic affinity of their precursor rocks. This seems to be corroborated by their HFSE contents (e.g. Fig. 59, Nb/Y vs Zr/(P<sub>2</sub>O<sub>5</sub>\*10000, Floyd and Winchester 1975). However, SiO<sub>2</sub> contents of most samples are significantly lower than those of MORB (~ 47-51 wt%) and consequently, most samples have CIPW normative ne, which is not observed in modern MORB. We conclude, that many of the analysed mafic metamorphic rocks must have cumulate protoliths, which questions the rock nomenclature yielded by employment of the TAS classification scheme.

In a diagramme of TiO<sub>2</sub> vs Mg# (Fig. 59), one can notice that the Krivaja-Konjuh metamorphic rocks form three distinct clusters. Keeping in mind that the metamorphism of amphibolite rocks is a process essentially inferred as isochemical (e.g. Vernon and Clarke 2008), plausible protoliths of analysed rocks are thus defined as low to high titanium basalts with Mg# values reaching 70, above which they are assumed to have a cumulate origin. Cumulates often retain relict magmatic cumulate gabbro textures, as it is reported for analysed amphibolites (sample U23) and garnet-diopside-hypersthene amphibolites (samples X1 and U40) (see Chapter 4.3.1.). Partly, their ultramafic affinity is corroborated by low abundances of SiO<sub>2</sub> (39.7-48.2 wt%) and TiO<sub>2</sub> (0.06-0.55 wt%), and comparatively higher MgO (9.3-20.0 wt%). Sample Z1C characterised as high Ti basalt, also records the lowest MgO and highest FeO values, and it is virtually devoid of modal amphibole. Similarly, samples discriminated as low Ti basalts show relatively low abundances of MgO (< 9 wt%), but relatively high FeO contents (> 8 wt%). Besides preserved relict textures, cumulates are featured by an elevated MgO content (over 10 wt%), and comparatively lower SiO<sub>2</sub> and FeO (average 45 and 6 wt%, respectively). Their amphibole is defined as pargasite to pargasitic hornblende (Chapter 4.3.2.1.). Comparing discussed MgO and TiO<sub>2</sub> contents of the Krivaja-Konjuh metamorphites to those of well-documented gabbro and basalt localities from the neighbouring Alpine ophiolite complexes and from oceanic environments, one states high correspondence of the vast majority of analysed rocks and ophiolitic cumulate gabbros from the Alpine, Corsican and Ligurian regions (e.g. Bertrand et al. 1987, Serri and Saitta 1980, Beccaluva et al. 1977). Conversely, the low-Ti basalts (samples Z1C, YU137, 10D and R8) depict similarities with basalts originated from modern oceanic fracture zones (e.g. Juan de Fuca, Langmuir and Bender 1984).

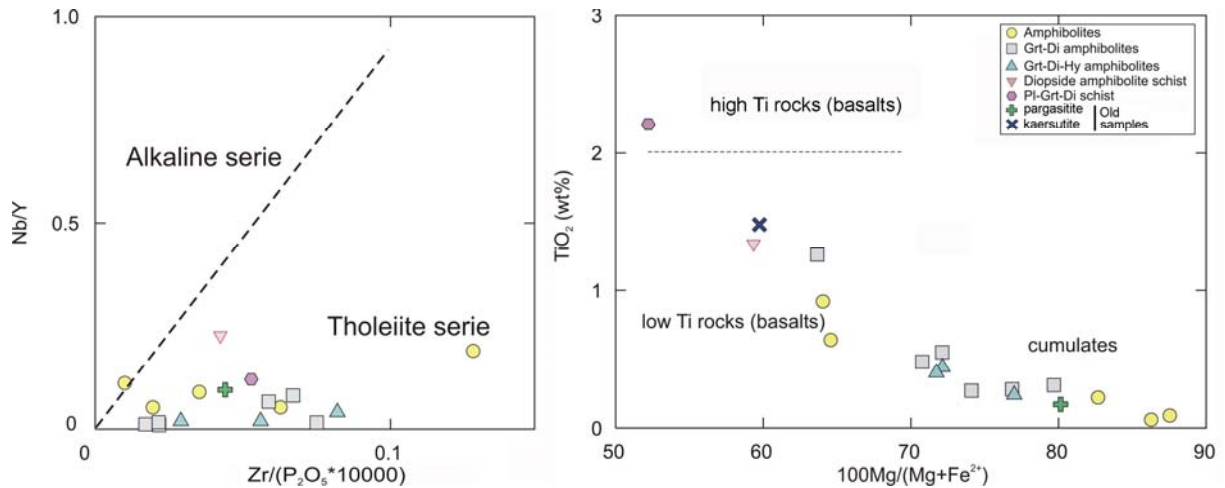


**Fig. 59.**  $Zr/(P_2O_5 \cdot 10000)$  versus  $Nb/Y$  discrimination diagramme depicting tholeiitic affinity of analysed rocks (after Floyd and Winchester 1975) (left);  $Mg$ -number versus  $TiO_2$  diagramme showing differences between the high- and low-Ti basalts (2 wt%  $TiO_2$  limit), along with the position of assumed ultramafic and mafic cumulates (diagramme from Gómez-Pugnaire et al. 2003) (right).

The concentrations of trace elements in the analysed rocks are also controlled by the geochemical affinity of the protolith. Thus, the high-Mg# metamorphic rocks regarded as former cumulates show moderate to high concentrations of compatible elements (e.g. 35 to 269 ppm Ni, 30.4 to 53.7 ppm Co and 41 to 257 ppm V). On the other hand, the concentrations of incompatible elements such as Zr (1 – 20 ppm, Y (1.8 – 11.1 ppm) or Ba (2 – 26 ppm) are significantly lower with respect to possible basaltic protoliths which would have 25 – 100 ppm Zr, 18 – 46 ppm Y and 15 – 200 ppm Ba. The diabbases of Krivaja-Konjuh, for example, have average values of 77 ppm Zr, 12 ppm Y and 32 ppm Ba (Trubelja et al. 1995, Babajić 2009).

Particularly high concentrations of incompatible trace elements, along with moderate Ni and Co values for the KKOC mafic metamorphic rocks may suggest a pronounced fractionation of their parental melts. This can be further tested by looking at the variation of selected major and trace elements with Zr as fractionation index (Fig. 60). Although most elements show no clear correlation pattern with the fractionation index, a rough increase in Sm,  $P_2O_5$ ,  $TiO_2$  and  $SiO_2$ , and decrease in Mg# and  $Al_2O_3$  with increasing Zr is obvious. In particular, it is inferred that P and Ti show the most pronounced positive correlations with Zr. This leads to the conclusion that Ti-rich phases (e.g. ilmenite, rutile, Ti-rich amphibole) must have fractionated in the more evolved melts (e.g. Gómez-Pugnaire et al. 2003). It is important to remark that the metamorphic rocks, previously shown to have originated from mafic and ultramafic cumulates (Zr 1 – 20 ppm), are not featured by the disambiguated correlation trends established for metamorphic rocks having Zr contents above 20 ppm. The exception is inferred for some REE (Eu),  $TiO_2$  and Mg#, possessing obscured positive, namely negative correlations.

The proposed discrimination of the KKOC metamorphic rocks, based on their major and trace element geochemistry, is best elucidated from the chondrite-normalised REE patterns (Fig. 61, normalisation after McDonough and Sun 1995). Four groups of metamorphic rocks

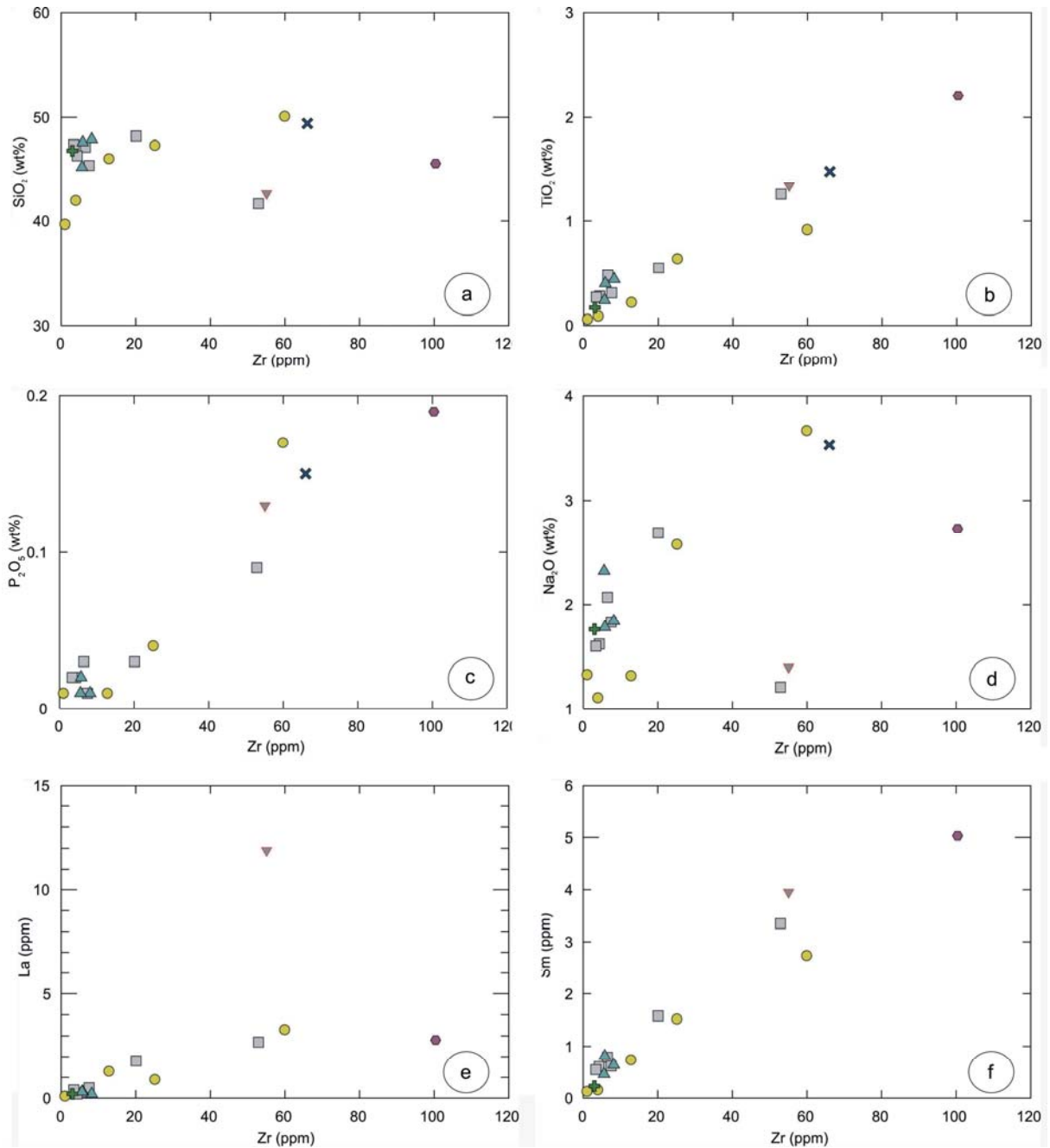


**Fig. 60a-f.** Selected major and trace element variation plots for Krivaja-Konjuh metamorphic rocks with Zr used as differentiation index. See text for discussion. Symbols as in Fig. 59.

can be distinguished. The first rock group (Group 1 hereafter) is the most numerous. It comprises samples from all defined petrographic groups, except gneisses (U29, U30, GR7, MK2, V1, U22, X1, U40, and V4). The lowest total REE abundances are displayed by members of this group, having a very narrow compositional span, ranging from 0.3–2.0 for the LREE to 1-8 x chondrite values for the HREE. Their similar, almost parallel and mutually overlapping REE patterns are characteristic for rocks sharing a common origin. Most of the rocks exhibit slightly LREE depleted patterns [(La/Yb)<sub>N</sub> = 0.12-0.47], occasionally being flat [sample U30 with (La/Yb)<sub>N</sub> = 1.12]. Samples U29 and U30 slightly deviate from the rest of the group in terms of bulk REE concentrations and partly also in LREE depletion. Some but

not all of these samples show a relative impoverishment of Ce which may be caused by sea-floor alterations.  $Ce^{4+}$  may be transported away by seawater under oxidising conditions. All samples of this group decipher flat HREE plots [ $(Tb/Yb)_N = 0.79-1.47$ ] and substantial positive Eu anomalies ( $Eu/Eu^* = 1.29-3.02$ ). This implies plagioclase accumulation in the early stage of magma evolution, preferably accompanied by pyroxene for samples having more Yb than La (majority of samples), and eventually olivine for samples having the same proportion of Yb and La (sample U30). This geochemical consideration is consistent with the previous discussion, characterising these samples to have had an ultramafic to mafic cumulate origin based on their high Mg-number (above 70), lower concentrations in all incompatible elements, and partly preserved cumulate gabbroic textures.

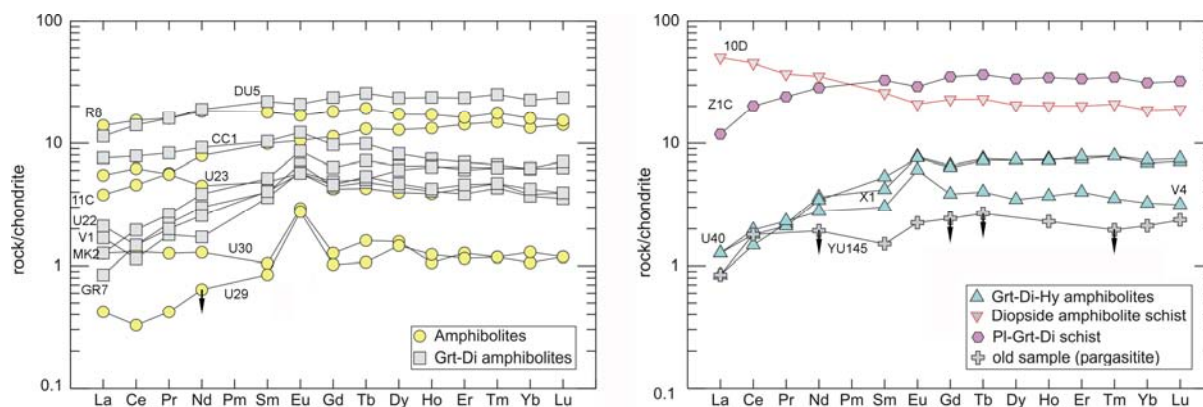


**Fig. 61.** Chondrite-normalised abundances of REEs in the KKOC metamorphites: normal amphibolites and garnet-diopside amphibolites (left); Garnet-diopside-hypersthene amphibolites, diopside amphibolite gneisses, plagioclase-garnet-diopside gneisses and old samples (right). Normalisation values are after McDonough and Sun (1995). The arrows indicate measured concentrations of REE that are under the detection limit.

The second group of metamorphic rocks (Group 2 hereafter) comprises samples DU5, R8, Z1C and 11C. Their REE patterns are also featured by parallel trends, attaining relatively higher concentration levels, up to 20 x chondrite. The LREE depletion is, in comparison with Group 1, more pronounced [ $(La/Yb)_N = 0.27-0.82$ ], and all samples show a weak negative Eu anomaly ( $Eu/Eu^* = 0.86-0.97$ ). This is characteristic for an early incorporation of  $Eu^{2+}$  in a plagioclase crystal structure, leading to its impoverishment in evolved magmas. Thus, a fractional crystallisation is inferred as the main mechanism governing the generation of this group. The fractionated REE patterns of samples from this group are consistent with derivation through relatively low degrees of partial melting. Samples DU5 and Z1C, being the most fractionated, also possess the most pronounced negative Eu anomaly and the lowest Mg# values. This geochemical characterisation bounds the discussed group to the N-MORB geotectonic setting. Furthermore, this fully corresponds to the fact that all analysed samples belonging to this group have already been suggested, based on their main elements geochemistry, to correspond to low and high Ti metabasalts (metadolerites). Since rocks from this group decipher moderate LREE depletion, their derivation from a slightly depleted source is hypothesised, whereas the flat normalised heavy REE patterns indicate the absence of residual garnet within the mantle source (e.g. Wood et al. 1979).

The third group of samples (Group 3 hereafter) consists of samples CC1 and U23. They depict relatively flat REE patterns  $[(La/Yb)_N = 1.16-1.35]$ , featured by a moderately developed positive Eu anomaly ( $Eu/Eu^* = 1.21-1.23$ ). Bulk REE concentration values are on the 5 – 8 x chondrite levels. The rocks of this group are considered to be genetically linked to group 1 metamorphites, having practically identical chemical characteristics, the same level of HREE, but a less developed Eu anomaly and being markedly LREE enriched. The explanation of these differences might be linked to an enriched mantle source and a lower level of crystal accumulation.

The fourth group of metamorphics (Group 4 hereafter) consists only of sample 10D. Its main chemistry, REE fractionation index, and minor negative Eu anomaly ( $Eu/Eu^* = 0.84$ ) highly correspond to those of rocks belonging to Group 2. Significant LREE enrichment makes the difference  $[(La/Yb)_N = 0.84]$ . This discrepancy is best explained by a different provenance of this sample, which suits transitional to evolved MORB patterns (Sun and McDonough 1989, Saunders 1984).

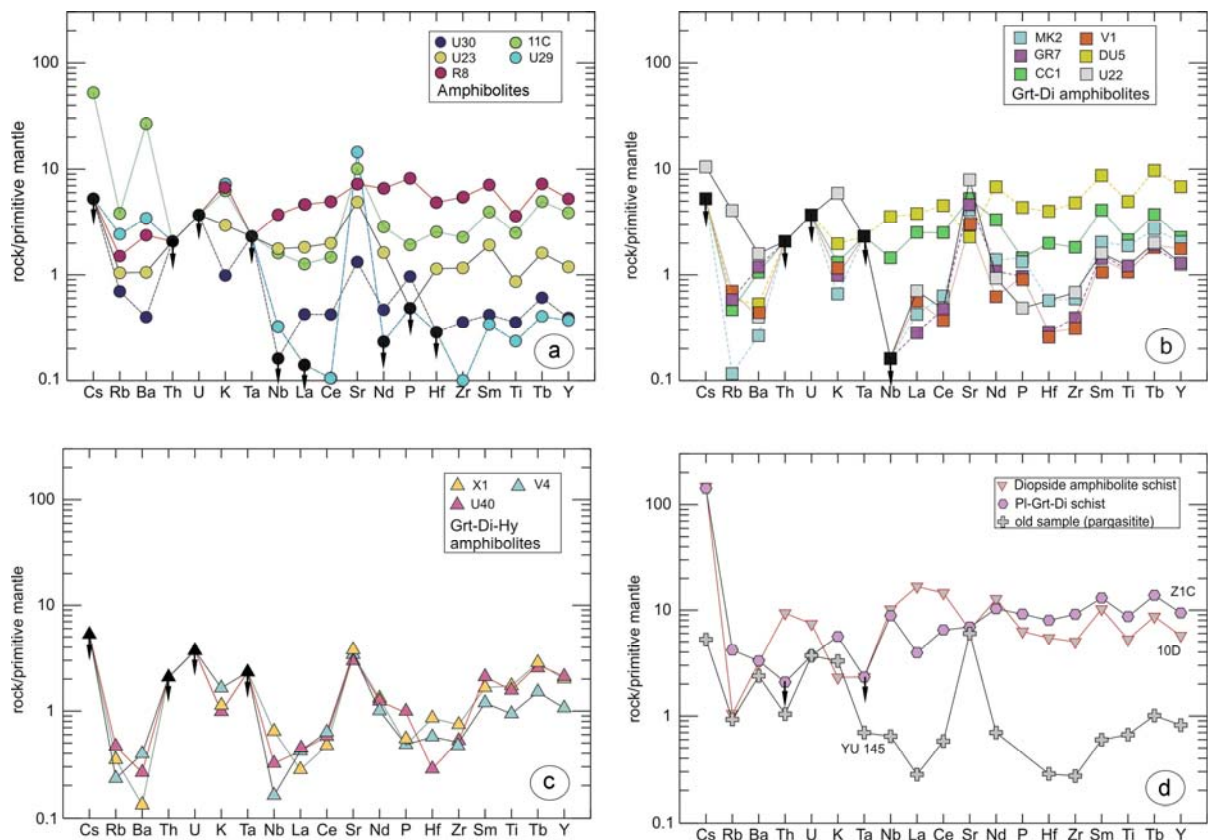


**Fig. 62a-d.** Primitive mantle-normalised abundances of trace elements in the KKOC metamorphic rocks: (a) amphibolites, (b) garnet-diopside amphibolites, (c) garnet-diopside-hypersthene amphibolites, (d) gneisses and old samples. Normalisation values after Hofmann (1988). Arrows indicate measured concentrations of trace elements that are under the detection limit.

Comparing the REE patterns of metamorphic rocks from the KKOC with the most recent literature data of the mafic intrusives and extrusives from the same complex (Babajić 2009), several lines of conclusion can be made that will be briefly discussed in here (for further discussion, the reader is referred to Chapter 6.3.1). The rocks belonging to Group 1, being

interpreted as metacumulates, show excellent correspondence with gabbros, gabbro-norites to amphibole gabbro-norites originated mainly from Kamenica and Duboštica (Krivaja domain), as well as the Muška Voda and Karaula (Konjuh domain) localities. Samples U30 and U29, displaying discrepancies in comparison to other members of the group, in terms of the bulk REE composition and LREE enrichment, are reported to correlate best with troctolites of the Kamenica and Maoča localities of the Krivaja domain, along with those of the Karaula locality at SE Konjuh. Apart from troctolites, the REE distribution patterns of these two samples correspond well to those of mafic dykes of the Muška Voda locality. Members of Group 2, featured by an unambiguous MORB affiliation, nicely correlate with dolerites, diabases and pillow basalts (spilites) of the Ribnica area (Konjuh domain). Some compositional affinity can be drawn with few gabbro samples from the Kamenica and Duboštica areas. Still, the gabbro cumulate nature is traced in a weak positive Eu and Sr anomaly. The REE geochemical signatures of metamorphic Group 3 cannot be recognised in the available REE patterns of the Krivaja-Konjuh mafic extrusives and intrusives. Sample 10D, which solely forms the metamorphic Group 4, depicts certain similarities with the sample of diorite from Duboštica. They are both featured with highly fractionated REE patterns, having an extremely LREE enrichment.

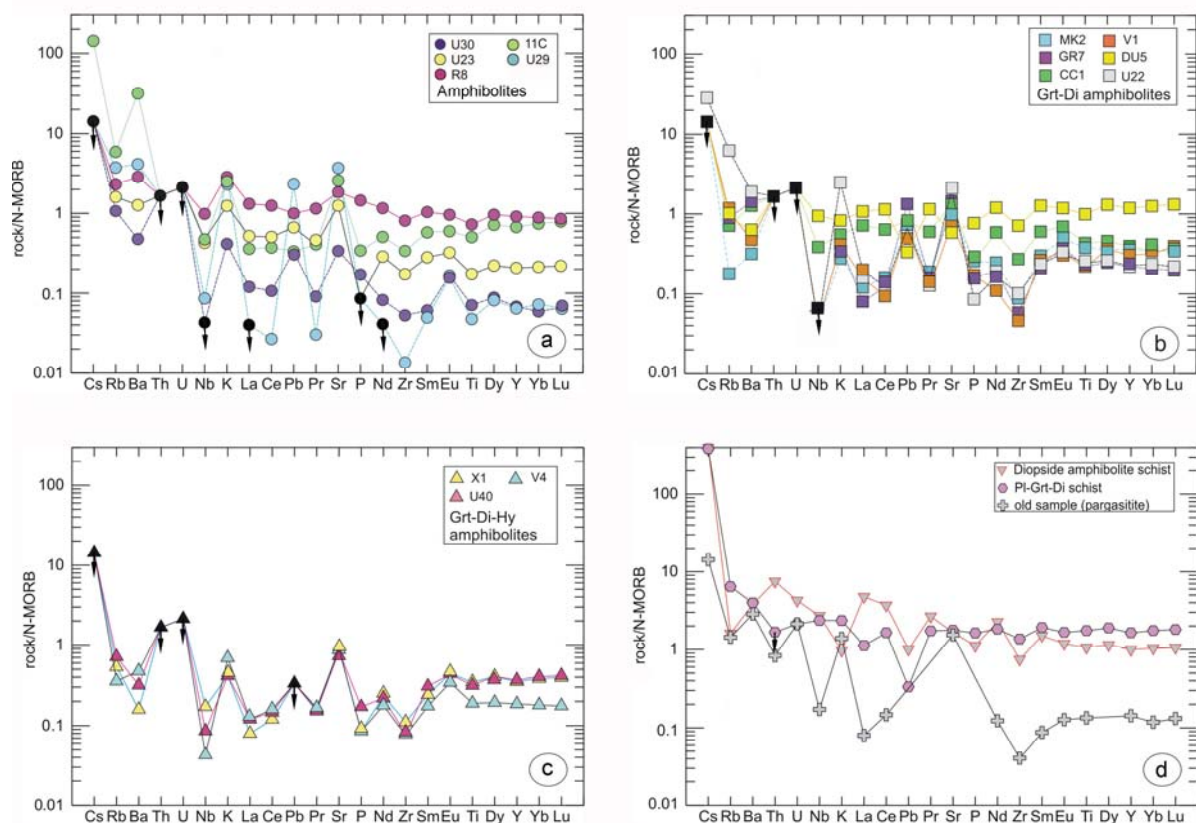


**Fig. 63a-d.** N-MORB-normalised abundances of trace elements in the KKOC metamorphic rocks: (a) amphibolites, (b) garnet-diopside amphibolites, (c) garnet-diopside-hypersthene amphibolites, (d) and gneisses with old samples. Normalisation values are after Hofmann (1988). Arrows indicate measured concentrations of trace elements that are under the detection limit.



Figs. 62 and 63 depict the behaviour of trace elements in the analysed metamorphic rocks with respect to the concentrations in primitive mantle and N-MORB. Both normalisation standards were employed for the sake of the presentation clarity, due to relatively large number of analysed samples. All groups of metamorphic rocks decipher roughly similar trace element patterns, featured by apparent MORB characteristics. However, most of the analysed trace element distribution patterns are affected by the process of crystal accumulation, along with influences characteristic for SSZ environments. The patterns of Group 1, defined to have had a cumulate protolith, show no or low enrichment in LILE, except a moderately positive K anomaly in the N-MORB normalised diagrams. Th and U abundances were under the detection limit. In general, most of the element values are below the N-MORB standard and substantially correspond to primitive mantle values. Highly incompatible elements are depleted, especially in samples U29 and U30, set to possess troctolite's geochemical signatures. Therefore, they are featured by the highest Sr and Eu positive anomalies ( $Sr/Sr^* = 116$ ). The Sr and Eu anomalies are well correlated, since they are consistent with the accumulation of plagioclase. Moreover, due to the Cr high compatibility in olivine, these samples record 10 x higher concentrations of Cr compared to other analysed metamorphic rocks (0.26 and 0.72 wt%  $Cr_2O_3$  respectively). Other members of this group are also coupled with the Sr positive anomaly. Clear Ti and Zr negative anomalies, that are attributed to an early fractionation of Ti-rich phases (ilmenite, rutile, magnetite) are moreover characteristic for all rocks of the group. Zirconium deficiency may be linked to the strong preference that ilmenite show toward this element during a crystal/melt or crystal/fluid partitioning (e.g. Green 1994). The distinct positive Pb anomaly, along with the slightly negative Nb and Hf anomaly, coupled with generally lower Nb/Y ratios are interpreted as echoes of the hypothesised SSZ geotectonic regime, which might have influenced a formation of cumulate protoliths in a BARB geotectonic environment. Oscillations in the trace element patterns between samples U29 and U30, compared to the rest of the group are due to different modal contents of plagioclase, pyroxene and olivine in the original protoliths (metatroctolites versus metagabbronorites).

A study of the trace element geochemistry of Group 2 metamorphic rocks confirmed the same geotectonic provenance, as their clear N-NORB rare-earth elements' distribution had already suggested. Total trace element abundances roughly correspond to MORB values, exceeding the primitive mantle up to 10 times. Occasionally, they show a weak Ti and Zr negative anomaly, but no clear parameters pertain to the oceanic crust involvement. Trace element normalisation patterns of this metamorphic rock group decipher a slight LILE enrichment that may connote an enriched mantle source. Still, one needs to stay reserved, since alkali and REEs are quite mobile, and their enrichment might have had an origin in secondary processes. Members of Group 3 and Group 4 show trace element geochemical characteristics compatible to those of Group 1 and Group 2, respectively.

It is inferred that the trace-element distribution in analysed metamorphics fully correlates to the REE and main elements' geochemical behaviour. Additionally, differences and characteristics of various metamorphic groups are more accentuated in the trace element spider diagrams. Origin of magmatic precursors of Group 1 are best explained in terms of a silicate mineral accumulation (plagioclase, pyroxene with minor olivine and ilmenite

or Ti-magnetite) in different modal abundances, yielding the shallow ocean-crust gabbroic rocks. Most probably, these rocks experienced a minor SSZ influx, documented in related geochemical parameters, which most ideally place them in a hypothetical back-arc basin environment (see Chapter 6.3.1.). The rocks of Group 2 possess no such influences. They are highly fractionated, up to the MORB level, and clearly correspond to the MORB geotectonic setting. A recent comprehensive research on the differences of cumulate gabbros and N-MORB within the oceanic crust (Hart et al. 1999) showed that the average upper 500 m gabbro section is somewhat lower than the average N-MORB in trace elements such as Ba (30 %), Nb (50 %), U (40 %), and heavy REE (Yb and Lu, 30 %), but somewhat enriched in others, such as La (23 %), Ce (24 %), Pb (23 %), and Sr (40 %). This is found valid, employed to the differences between the KKOC Group 1 and 2, which are supposed to represent an oceanic crust relating gabbroic and basaltic rocks, respectively.



## 6. DISCUSSION

### 6.1. Geothermobarometry

#### 6.1.1. Introduction

Differences in the occupancy of a certain crystal site depend upon the crystallochemical properties of the respective position, as well as the chemical properties of the elements involved. The first stands for the site coordination number and the nature of surrounding atoms, whereas the second denotes the atomic valence, charge and radius. Independent variables like pressure ( $P$ ), temperature ( $T$ ) and bulk-rock chemistry ( $X$ ) influence the paragenesis and chemical compositions of coexisting phases. The partitioning of elements among phases in equilibrium, which tends to be strongly dependent on external variables ( $P$  and  $T$ ) and less on the mineral chemistry itself, have been calibrated and used as thermobarometric tools in petrology. Hence, reactions based on the exchange of elements having similar ionic radii and oxygen coordination values, are normally characterised by large entropy changes ( $\Delta S$ ) and low volume changes ( $\Delta V$ ) (The 'Clausius-Clapeyron law', for details see Carswell and Harley 1990). Those kinds of exchanges are employed as potential geothermometers. On the other hand, the exchange of elements having diverse ionic radii and different crystal site occupancies causes significant volume adjustments ( $\Delta V$ ) of the coexisting phases. This makes the specified reactions suitable in geobarometric calculations.

Generally, it is to be concluded that thermobarometers used in geology are based on the chemical analyses of coexisting phases, which are found in the state of heterogeneous equilibrium. The thermodynamic background of calibrations used for the  $P$ - $T$  estimations will be shortly addressed here. As mentioned, the relationship between pressure, temperature and mineral composition counts for the main thermodynamic dependency, defining the employed set of thermobarometers. In other words, the experimentally determined inter-ionic exchange equilibrium is a function of those parameters. A fundamental thermodynamic expression describing equilibrium is presented in:

$$\Delta\mu = \Delta G^\circ + RT \ln K. \quad (1)$$

This equation states that the overall chemical potential, which in equilibrium equals zero, is the sum of changes in Gibbs free energy and an expression, resulting in multiplying the equilibrium constant ( $K$ ), temperature ( $T$ ) and gas constant ( $R$ ). Gibbs free energy is defined by pressure and temperature. The changes in entropy ( $\Delta S$ ), enthalpy ( $\Delta H$ ), volume ( $\Delta V$ ) and heat capacity ( $\Delta C_p$ ) of the system are accounted influencing the same. In natural minerals, besides  $P$  and  $T$ , Gibbs free energy is determined by the element distribution in crystal lattice, which in thermodynamics is expressed through the activity-composition relationships. For the reaction between solids, it is assumed that the heat capacity and volumes of minerals are not influenced by changes in  $P$  and  $T$  (Vernon and Clarke 2008). Bearing in mind those simplifications and the fact that the free energy of reaction in equilibrium states zero, Gibbs free energy of reaction may be expressed as:

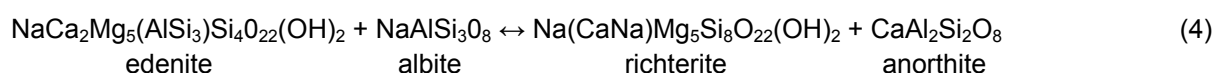
$$\Delta G^\circ = 0 = \Delta H - T \Delta S + (P - 1) \Delta V + RT \ln K. \quad (2)$$

The equilibrium constant ( $K$ ) for pure phases equals 1, leading  $\ln K$  to equal zero. However, for transfers between phases having a substantial solid solution,  $K$  serves as an input variable in the thermobarometric calculation, as it is discussed later on. By rearranging the equation (2),  $K$  is expressed as:

$$\ln K = -(\Delta H - T \Delta S + (P - 1) \Delta V) / RT. \quad (3)$$

This clearly differentiates the thermodynamic data, constant for a given reaction (right side of the equation), from  $K$ , normally expressed by the activity ratios of elements involved (left side). Activity values are best obtained through the formula recalculation of the microprobe acquired data. A simple linear relationship between  $P$  and  $T$  is apparent in a hypothetical state of equilibrium.

For example, a widely known geothermometer of Holland and Blundy (1994), used on coexisting amphibole and plagioclase, is based on the following reaction:



The constant of ideal mixing equilibrium ( $K$ ) of this reaction is expressed through the activity ( $a$ ) ratio of products and reactants equalling:

$$K^{\text{ed-rich}} = 0.423[(a(\text{Na}^{\text{M4}})a(\text{Si}^{\text{T1}}))/(a(\text{Ca}^{\text{M4}})a(\text{Al}^{\text{T1}}))]^{\text{Amp}}[a(\text{Ca})/a(\text{Na})]^{\text{Pl}}. \quad (5)$$

Activity ( $a_j$ ) of a certain component  $j$  is normally expressed as the product of the related mole proportion ( $X_j$ ) and activity coefficient ( $\gamma_j$ ) ( $a_j = x_j \cdot \gamma_j$ ). In an ideal basic system, the values of the activity and mole proportion are equal. However, in multi-component natural systems this is not the case, due to the non-ideal behaviour of the components involved. In order to determine the real activity values under such circumstances, one needs to utilise the appropriate solubility model (functional relation between the activity and mole proportion of the element involved). Thus, in such cases, either the experimentally derived data or those being obtained by the compositional correction of measured values have been availed.

Expressions found in the superscripts of elements stand for the structural position of the related element within the crystal. Referring to the relation presented in equation (3), authors have provided a thermometer, calibrated against an extensive dataset of natural and synthetic amphiboles, which also acknowledges a non-ideal mixing in amphibole and plagioclase. Simplified, it can be written as:

$$T = [78.44 + Y_{\text{ab-an}} - 33.6a(\text{Na}^{\text{M4}}) - (66.8 - 2.92P)a(\text{Al}^{\text{M2}}) + 78.5a(\text{Al}^{\text{T1}}) + 9.4a(\text{Na}^{\text{A}})] / [0.0721 - R \ln K^{\text{ed-rich}}] \quad (6)$$

(Note:  $Y_{\text{ab-an}}$  is 3 kJ for  $a(\text{Na})^{\text{PL}} > 0.5$ , otherwise it is  $12(2a(\text{Na})^{\text{PL}} - 1) + 3$  kJ)

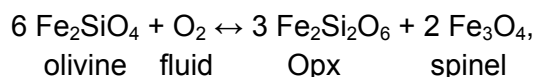
When applying the experimentally calibrated thermometers to natural mineral assemblages, it is often necessary to extrapolate the relatively narrowest part of the calibrated  $P$ - $T$ - $X$  dependences. This may lead to uncertainties. So, to secure a reliable extrapolation from the simple model experiments to complex natural systems, one needs to perform a set of thermodynamic modelling. Further uncertainties in  $P$ - $T$  condition estimations are often linked to the microprobe data analyses (e.g.  $\text{Fe}^{3+}/\text{Fe}^{2+}$  distribution).

*P-T* calculations yielding conditions of equilibration and formation of the KKOC metamorphic rocks were performed by usage of *PT Calc-1 Peridotite* and *PT Calc-2 Granulite* software developed by Friedhelm Henjes-Kunst and Hans-Peter Meyer from the Institute of Geosciences, Ruprecht-Karls University of Heidelberg. The calculation software designed by Dale et al. (2000), and those of Holland and Blundy (1994) (*Hbl-PI*) have been additionally consulted for the calculation of metamorphic *P-T* equilibration values, whereas PTEXL3 software was employed for the revealing of the mantle assemblages' equilibration conditions (developed by Thomas Köhler and Andrei Girnīs, downloaded from the webpage of the Johann-Wolfgang-Goethe University of Frankfurt - Gerhard Brey personal pages).

Besides pressure and temperature, oxygen fugacity ( $fO_2$ ) or redox-state is a third variable known to govern metamorphic processes. It defines the oxidation state of Earth's interior, having an important impact on mantle dynamics (i.e. magma genesis, metasomatism, chemical differentiation, mantle-core equilibria and a number of geophysical properties of the mantle; Woodland and Koch 2003, Ballhaus et al. 1991 and references therein). Furthermore,  $fO_2$  oversees speciation of volatiles, which may influence the mantle melting regime. For example,  $CH_4$ -enriched fluids, having originated in deeper mantle portions, readily interact with more oxidising peridotites, triggering water formation that instantaneously affects the solidus of mantle rocks, initiating partial melting (Taylor and Green 1988).

A comprehensive study of Woodland and Koch (2003) on 49 ultramafic xenoliths from South Africa and Lesotho has shown a systematic, non-monotonic, decrease in  $fO_2$  with depth, hence corroborating mantle heterogeneity. Based on olivine-orthopyroxene-spinel equilibria, one can summarise the behaviour of  $fO_2$  through the lithosphere as follows (Ballhaus et al. 1991): The MOR-type fertile peridotites show moderately reduced oxygen fugacity around -2 log units, relative to the fayalite-magnetite-quartz (FMQ) buffer. Depleted abyssal peridotites and mid-ocean ridge basalts (N-MORB) are slightly oxidised, plotting around FMQ - 1. Peridotites impregnated by oxidising melt/fluid are featured by  $fO_2$  values ranging from 0 to +1 log units relative to the FMQ buffer. Finally, SSZ affiliated peridotites and arc-related magmas are the most oxidised, varying around FMQ + 2. Bearing all this in mind, a conclusion may be drawn, pointing to  $fO_2$  as a useful tool in assessment of various mantle processes.

In four-phase spinel lherzolite assemblages, the oxygen barometer is normally based on experimental calibration of spinel-olivine-orthopyroxene Fe-Mg exchange (e.g. Ballhaus et al. 1991). The reaction that depicts Ol-Opx-Sp thermodynamic equilibrium is defined as:



with the following compounds used as buffers: Fe-FeO (IW), WC-WO<sub>2</sub>-C, Ni-NiO (NNO), and Fe<sub>2</sub>O<sub>4</sub>-Fe<sub>2</sub>O<sub>3</sub> (MH). In the present study, the ferric iron content of spinel was not analysed directly. It was calculated assuming the stoichiometric spinel composition in the form  $R^{2+}R^{3+}_2O_4$ . The obtained results were inadequate having yielded unreliable  $fO_2$  estimations.

## 6.1.2. Peridotites

Determination of the  $P$ - $T$  equilibration conditions of the analysed ultramafic rocks is based upon at least two mineral reactions operating in the sample concerned. The first reaction serves as a thermometer and the second as a barometer. Several applicable geothermobarometers were utilised in order to constrain equilibration values. Following these calculations, the acquired results are presented in Table 4, depicting equilibration values of the Krivaja-Konjuh ultramafic varieties (spinel and plagioclase lherzolites, and olivine websterites).

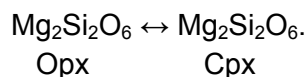
It is important to remark that in samples having no disequilibrium characteristics (e.g. zoning, exsolution and breakdown occurrence), there are no confinements in combining the applicable geothermobarometers. Conversely, in samples that are un-equilibrated, one needs to be cautious when choosing the adequate thermometer-barometer pair. For instance, the diffusion rate of Al in pyroxene is extremely slow in comparison with elements of high diffusivities (Fe, Mg, and Ca). Under such conditions the combination of the Al-in-Opx barometer and a 2-pyroxene thermometer would yield values of the last equilibration that are not real (e.g. Garašić 1994). However, the total number of thermometer-barometer combinations is reduced with regard to the analysed rocks since a barometer of Köhler and Brey (1990) is the sole applicable to garnet-free peridotitic assemblages.

### 6.1.2.1. Geothermometers

Over the years, numerous calibrations have been introduced as geothermo-meters, estimating the equilibrium temperatures of mineral parageneses in spinel peridotites. Four of the most widely accepted geothermometers were applied to the analysed KKOC ultramafic rocks. These are: (a) the 2-pyroxene thermometer (Wells 1977), (b) the Ca-in-orthopyroxene thermometer (Brey and Köhler 1990), (c) the spinel-orthopyroxene-olivine thermometer (Witt-Eickschen and Seck 1991), and (d) the spinel-olivine thermometer (Fabriès 1979). The values of pressure estimated by the usage of Köhler and Brey (1990) geobarometer were used as input pressures needed for the calculation of equilibrium temperatures using a respective thermo-meter.

#### 1. Wells (1977)

The *Wells* thermometer is based on the long known (e.g. Boyd 1973, Wood and Banno 1973) temperature dependent exchange of the enstatite component between coexisting ortho- and clinopyroxene:



Assuming that  $\Delta V$  and  $\Delta C_p$  of the above reaction equal zero, Wells (1977) provided an optimum expression for the reaction equilibrium coefficient:

$$\ln K = -7341/T + 3.355.$$

Further recasting of the expression for  $K$  yielded the following thermometric formula:

$$T = 7341 / (3.355 + 2.44X(\text{Fe})^{\text{Opx}} - \ln K),$$

with

$$X(\text{Fe})^{\text{Opx}} = \text{Fe}^{2+} / (\text{Fe}^{2+} + \text{Mg}).$$

The presented thermometer is consistent with the experimental data over a range from 785 to 1500 °C, which makes it suitable for the application in mantle rocks and high-grade granulites. One needs to pay attention to Fe and Al amounts in orthopyroxene, since they are reported to significantly reduce the activity of the  $\text{Mg}_2\text{Si}_2\text{O}_6$  component. The range from 0 to 1 would be optimal for  $X(\text{Fe})^{\text{Opx}}$ , whereas the alumina content should not exceed 12 wt%. Observed uncertainties for experimentally aluminous enstatite and diopside solid solutions are found within the range of 70 °C.

### 2. Brey and Köhler (1990)

This thermometer is primarily designed to constrain the transfer of enstatite between coexisting ortho- and clinopyroxene. Additionally, the authors have provided thermometers based solely on the amount of Ca in Opx, and on the partitioning equilibrium of Na between Opx and Cpx. All thermometers were calibrated on experimental samples of four phase's peridotites.

The two-pyroxene thermometric expression has been formulated as:

$$T = [23664 + (24.9 + 126.3X(\text{Fe})^{\text{Cpx}})P] / [13.38 + (\ln K)^2 + 11.593X(\text{Fe})^{\text{Opx}}].$$

The thermometer based on the Ca content in orthopyroxene is expressed as:

$$T = (6425 + 26.4P) / (-\ln X(\text{Ca})^{\text{Opx}} + 1.843),$$

while the other thermometer taking into account the partition of Na equals:

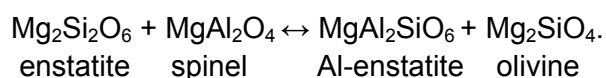
$$T = (35000 + 61.5P) / (\ln(X(\text{Na})^{\text{Opx}}/X(\text{Na})^{\text{Cpx}}) + 19.8).$$

Presented equations are based on the assumption that Ca is restricted to the M2 site of pyroxene and that  $(\text{Mg}^{\text{M1}})_{\text{Cpx}}/(\text{Mg}^{\text{M1}})_{\text{Opx}}$  should equal 1. Moreover, the Al values need to be identical under certain  $P$ - $T$  conditions. All thermometers were shown to possess an analytical error ranging from 20 to 50 °C.

By using these calibrations, one needs to take the temperature estimations with caution because the Ca content in orthopyroxene is supposed to have been influenced by the subsolidus mantle metasomatism (see Chapters 6.2.1.1. and 4.2.2.2.).

### 3. Witt-Eickschen and Seck (1991)

Experiments performed on spinel peridotites have shown that the Al content in orthopyroxene, which is found in an equilibrium state with olivine (forsterite) and spinel, is primarily temperature dependent, whereas pressure is a subordinate factor. The Tschermak component solubility in orthopyroxene is defined through the following reaction:



In natural systems, the alumina solubility is not just a function of temperature. It also depends on the other chemical components present in the system concerned. Thus, Sachtleben and Seck (1981) found that the molar proportion of Al in orthopyroxene is



conditioned by the Cr-number of coexisting spinel. Witt-Eickschen and Seck (1991) proposed an improved version of the former empirical geothermometer, derived from the evaluation of solubilities of Ca and Al in orthopyroxene. Using a least square regression, they expressed the equilibrium constant as:

$$\ln K = \ln[(X^{2}(\text{Mg})^{\text{Ol}} X(\text{Al})^{\text{Opx}})]/[X^{2}(\text{Al})^{\text{Sp}} X(\text{Mg})^{\text{Sp}} X(\text{Mg})^{\text{Opx}}],$$

Referring to the values from the thermometer of Brey and Köhler (1990) for  $X(\text{Al})^{\text{Opx}}$  and  $X(\text{Ca})^{\text{Opx}}$ , the authors provided the following temperature equation:

$$T = 2248.25 + 991.58 \ln K + 153.32 \ln^2 K + 539.95 Y(\text{Cr})^{\text{Sp}} - 2005.54 Y^2(\text{Cr})^{\text{Sp}},$$

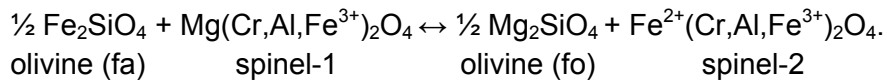
with

$$Y(\text{Cr})^{\text{Sp}} = \text{Cr}/(\text{Cr} + \text{Al}).$$

This thermometer is reported to operate under the confidence range of about  $\pm 20$  °C.

#### 4. Fabriès (1979)

The basis of this thermometer is the exchange of Fe and Mg between coexisting spinel and olivine through the following reaction:



Apart from the temperature, this reaction equilibrium is reported to depend on molecular proportions of cations that occupy the spinel octahedral sites (Cr, Al and  $\text{Fe}^{3+}$ ). Numerous calibrations have been based upon this exchange, with those of Fabriès (1979) being the most commonly accepted. He defined the reaction equilibrium as:

$$\ln K = \ln(X(\text{Mg})^{\text{Ol}} X(\text{Fe})^{\text{Sp}} / X(\text{Fe})^{\text{Ol}} X(\text{Mg})^{\text{Sp}}),$$

with the temperature expressed as:

$$T = (4250 Y(\text{Cr})^{\text{Sp}} + 1343) / (\ln K + 1.825 Y(\text{Cr})^{\text{Sp}} + 0.571),$$

and

$$Y(\text{Cr})^{\text{Sp}} = \text{Cr}/(\text{Cr} + \text{Al} + \text{Fe}^{3+}).$$

This geothermometer is quite suitable for estimating the last equilibration stages (deformation and/or recrystallisation) under low temperatures, when the steady thermal state is almost reached. Moreover, it is reported to be appropriate when olivine has a composition near to  $\text{Fo}_{90}$ , and spinel contains limited amounts of  $\text{Fe}^{3+}$  (usually under 0.05 a.p.f.u.) The KKOC spinel and plagioclase lherzolites possess  $> 0.05$  and  $0.05 - 0.07$  a.p.f.u. of ferric iron, respectively. The analytical uncertainty of this calibration yields  $\pm 50$  °C.

#### **6.1.2.2. Geobarometer**

In garnet-devoid spinel and plagioclase peridotites of the Krivaja-Konjuh ophiolite complex, the Ca-in-olivine/clinopyroxene barometer of Köhler and Brey (1990) was employed. It operates on the basis of the Ca exchange between olivine and clinopyroxene, generally understood as a function of pressure, but the model is also temperature sensitive.

Thermometric data estimated by presented thermometers were used as input temperatures. Calculated pressure estimations of each analysed sample are summarised in Table 4.

The calibration of Köhler and Brey (1990) yielded the following pressure expressions with respect to the non-linear solubility of Ca in olivine at around 1100 °C:

$$P = (-T \ln D_{Ca} - 11982 + 3.61 T) / 56.2 \text{ for } T \geq (1275.25 + 2.827 P),$$

and

$$P = (-T \ln D_{Ca} - 5792 - 1.25 T) / 42.5 \text{ for } T \leq (1275.25 + 2.827 P),$$

where

$$D_{Ca} = X(Ca)^{Ol} / X(Ca)^{Cpx}.$$

Suggested uncertainties for this geobarometer are estimated at around  $\pm 0.17$  GPa, although the error may widen at higher temperatures.

This geobarometer yielded unreliable results for plagioclase lherzolites due to the fact that their  $X(Ca)^{Ol}/X(Ca)^{Cpx}$  ratios were compromised during subsolidus mantle impregnations. Furthermore, the pressure estimations for spinel lherzolites obtained via Ca-in-Opx input temperatures might have also been compromised due to the same reason (for details see Chapter 6.2.1.1.).

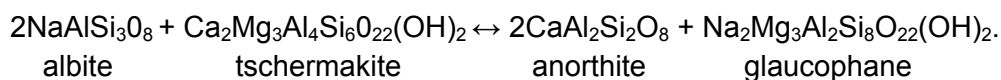
### 6.1.3. Metamorphic rocks

In order to estimate the  $P$ - $T$  conditions of the formation of metamorphic rocks from the Krivaja-Konjuh ophiolite complex, two different approaches have been engaged. Firstly, a set of different classical exchange geothermobarometers is used in order to cover a huge span of parageneses encountered in analysed metamorphic rocks. Calculations were performed for peak metamorphic assemblages, as well as for retrograde parageneses (kelyphitic coronas of garnets or secondary amphibole assemblages). Secondly, the metamorphic  $P$ - $T$  space has been defined through appropriate reaction curves calibrated in a basaltic system (NCFMASH and CFMASH). Results of described techniques used for the  $P$ - $T$  estimates are discussed in Chapter 6.3.2.2. In this chapter, one can find short descriptions and main exchange reactions of applied geothermobarometers. Some of them, used in the  $P$ - $T$  modelling of mantle rocks, are presented in Chapter 6.1.2. A table, listing all applied techniques and obtained results, is provided at the end of the present chapter (Table 5).

#### 6.1.3.1. Geothermometers

##### 1. Spear (1980)

This thermometer operates on the equilibrium between coexisting *plagioclase* and *amphibole*. The exchange reaction, calibrated using data from natural amphibolites, is defined as:



The equilibrium constant is expressed as:

$$K = [(X(\text{Na}^{\text{M4}})/X(\text{Ca}^{\text{M4}}))^{\text{AMP}} [X(\text{Ca})/X(\text{Na})]^{\text{PL}}]$$

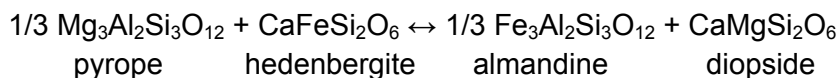
Information on temperature is being extrapolated from the empirical equilibrium model, based on the above-mentioned calibration. The diagramme is defined by values of  $\ln(X(\text{Ca}^{\text{M4}})/X(\text{Na}^{\text{M4}}))$  in amphibole and  $\ln(X(\text{Ca})/X(\text{Na}))$  in plagioclase. The implementation of this thermometer may be jeopardised by uncertainties in the calculation of amphibole formulas, especially concerning the allocation of Na at the M4 structural position and the composition of neighbouring phases. Suggested errors are within the range of  $\pm 50$  °C.

### 2. Holland and Blundy (1994)

The principles of the thermometer proposed by Holland and Blundy (1994) were already provided as an example of reaction equilibrium thermodynamics [equations (4), (5), and (6)]. Essentially, it is based on the  $\text{NaSiCa}^{-1}\text{Al}^{-1}$  exchange vector between amphibole and plagioclase. The authors noted that this thermometer, based on reaction (4), is most useful at high temperatures, where An-rich plagioclase predominates and the silica activity is low. In low-temperature metamorphic rocks like greenschists, having practically solely albitic plagioclase, this thermometer is not to be used. Uncertainties of the thermometer are  $\sim 35$ – $40$  °C, largely depending on amphibole chemistry, but primarily on  $\text{Fe}^{2+}/\text{Fe}^{3+}$  distribution.

### 3. Krogh (1988)

The thermometer of Krogh (1988) uses partitioning effects of  $\text{Fe}^{2+}$  and Mg between garnet and clinopyroxene, according to the reaction:



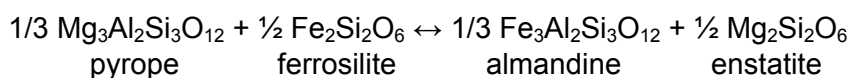
The  $P$ - $T$  dependence of the equilibrium constant ( $K$ ) for this reaction has been experimentally calibrated by Krogh (1988) and some other authors (e.g. Ellis and Green 1979, Powell 1985). Accordingly, Krogh (1988) offered an expression based on the curvilinear relationship between the  $\ln K$  and Ca activity in garnet ( $a(\text{Ca})^{\text{Grt}}$ ), yielding the temperature:

$$T = ((-6173(a(\text{Ca})^{\text{Grt}})^2 + 6173(a(\text{Ca})^{\text{Grt}}) + 1879 + 10P) / ((\ln K + 1.392) - 273))$$

Estimated errors are within the range of 30 to 50 °C. One needs to be aware of several possible circumstances hampering the suitability of thermometer: (1) in low Ca garnets, the relationship of  $\ln K$  and  $X(\text{Ca})^{\text{GRT}}$  is not clearly established (e.g. Grt peridotites), (2) stoichiometry of clinopyroxene with regard to  $\text{Fe}^{2+}/\text{Fe}^{3+}$  distribution and/or intergrowths of low silica phases, such as amphibole, jeopardise the calculation, and (3) significant variations of the jadeite component within the pyroxene formula is not included in this calibration.

### 4. Harley (1984)

The thermometer proposed by Harley (1984) is based on the  $\text{Fe}^{2+}$ –Mg partitioning equilibrium between coexisting garnet and orthopyroxene. The exchange reaction describing the distribution is defined as:



The geothermometer is given by the following equation:

$$T = [(3.740 + 1.4 X(\text{Ca})^{\text{Grt}} + 22.86 P) / (R \ln K + 1.96)] - 273$$

with partition coefficient ( $K$ ) being defined as:

$$K = (\text{Fe/Mg})^{\text{Grt}} / (\text{Fe/Mg})^{\text{Opx}}$$

and

$$X(\text{Ca})^{\text{Grt}} = (\text{Ca}/(\text{Ca}+\text{Mg}+\text{Fe}))^{\text{Grt}}$$

The thermometer is highly applicable to granulites and garnet peridotites. At lower temperatures, its precision becomes limited by analytical uncertainties. The following possibilities are needed to be taken into account, in order to use the thermometer successfully: (1) minor impurities in garnet, not considered in calibration (e.g. Mn, Cr<sup>3+</sup> and Fe<sup>3+</sup>) may significantly affect  $K$ , (2) the Fe<sup>2+</sup>/Fe<sup>3+</sup> distribution is of great importance, since even a small reduction of  $K$ , having resulted from inadequate iron distribution, influences the estimated temperatures (uncertainties of 20 to 100 °C).

### 5. Lee and Ganguly (1988)

This thermometer also operates on the Fe<sup>2+</sup>-Mg fractionation between coexisting garnet and orthopyroxene. The exchange reaction describing this process is the same like in the case of Harley's thermometer. The exchange mechanism is arbitrary taken as isobaric, due to the small  $\Delta V$  changes, allowing the coefficient of equilibrium to be expressed in a simpler way:

$$\ln K = 2269 (\pm 142) / T - 0.96$$

Respecting uncertainties induced by the mineral chemistry particularities discussed previously (Harley's thermometer) and assuming that the coefficient of equilibrium is independent of the Fe/Mg ratio, the following geothermobarometric expression recasted from the  $K$  equation was suggested:

$$T = [1971 + 11.91 P + 1/R(\Delta W_{\text{Ca}}X_{\text{Ca}} + \Delta W_{\text{Mn}}X_{\text{Mn}})]^{\text{Grt}} / (\ln K + 0.96),$$

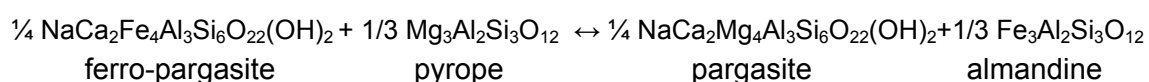
with

$$\Delta W_{\text{Ca}} \sim \Delta W_{\text{Mn}} \sim 3000 (\pm 500) \text{ cal/mol of cation for } X_{\text{Ca}} \text{ and } X_{\text{Mn}} < 30 \text{ in garnet.}$$

The authors suggested that uncertainties in the mixing property and the analytical data will cause an average error ranging from 30 to 50 °C when estimating the equilibration temperature of most of the natural mineral parageneses (granulites, garnet peridotites), at least above 1000 °C.

### 6. Graham and Powell (1984)

The thermometer introduced by the above authors is established on the FeMg<sup>-1</sup> exchange between garnet and amphibole, and the exchange reaction may be represented as:



It is calibrated against the garnet-clinopyroxene geothermometer of Ellis and Green (1979), using data on coexisting garnet, amphibole, and clinopyroxene in amphibolite- and granulite-facies assemblages. By using the robust regression approach, the authors suggested the following form of the thermometer:

$$T = (2880 + 3280 X(\text{Ca})^{\text{Grt}}) / (\ln K + 2.426) - 273,$$

where

$$K = (\text{Fe}/\text{Mg})^{\text{Grt}} / (\text{Fe}/\text{Mg})^{\text{Amp}}$$

and

$$X(\text{Ca})^{\text{Grt}} = [\text{Ca}/(\text{Ca}+\text{Mg}+\text{Fe})]^{\text{Grt}}$$

The described thermometer is usually recommended for metamorphic conditions up to 850 °C and at low oxygen activity with Mn-poor garnet [ $X(\text{Mn})^{\text{Grt}} < 0.1$ ].

### 7. Krogh Ravna (2000)

The thermometer of Krogh Ravna (2000) also follows the  $\text{FeMg}^{-1}$  exchange between garnet and amphibole, being calibrated on natural samples from basaltic and intermediate rocks having coexisting garnet–clinopyroxene–hornblende assemblages. The partition coefficient ( $K$ ) between amphibole and garnet is a function of  $P$ ,  $T$  and compositional parameters of garnet [ $X(\text{Ca})^{\text{Grt}}$  and  $X(\text{Mn})^{\text{Grt}}$ ]. By recasting the relations yielding  $K$ , Krogh Ravna (2000) provided the following geothermometric expression:

$$T = [1504 + 1784(X(\text{Ca})^{\text{Grt}} + X(\text{Mn})^{\text{Grt}})] / (\ln K + 0.720) - 273,$$

where

$$K = (\text{Fe}^{2+}/\text{Mg})^{\text{Grt}} / (\text{Fe}^{2+}/\text{Mg})^{\text{Amp}}$$

and

$$X(\text{Ca})^{\text{Grt}} = [\text{Ca}/(\text{Ca}+\text{Mg}+\text{Fe}^{2+}+\text{Mn})]^{\text{Grt}},$$

$$X(\text{Mn})^{\text{Grt}} = [\text{Mn}/(\text{Ca}+\text{Mg}+\text{Fe}^{2+}+\text{Mn})]^{\text{Grt}}.$$

The presented thermometer found its application in the study of various metamorphic rocks, notably garnet amphibolites and hornblende-bearing pelitic rocks. This thermometer represents an upgrade of previously calibrated garnet-amphibole thermometers, like that of Graham and Powell (1984). As expected, minor difficulties in the application of this mechanism are encountered due to the complex  $\text{Fe}^{2+}$  and Mg distribution over several structural positions of amphibole, and uncertainties with the ferric–ferrous iron ratio determination in this mineral group. The average error was reported range from 20 to 50 °C.

### 8. Owen and Greenough (1991)

The partition of Fe and Mg between sapphirine and spinel may serve as a geothermometer and it functions according to the following reaction:



The partition coefficient is defined as:

$$K = [X(\text{Fe})^{\text{Sp}}/X(\text{Mg})^{\text{Sp}}] / [X(\text{Fe})^{\text{Sa}}/X(\text{Mg})^{\text{Sa}}].$$

Equilibration temperatures are based upon an empirical sapphirine-spinel Mg-Fe exchange, and calibrated data from the literature resulted with the expression:

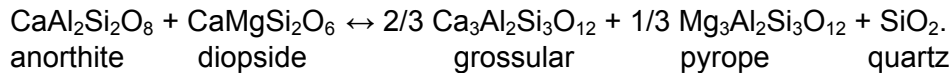
$$T = [800 + (228 \ln K)] - 273.$$

Uncertainties are considered to be around  $\pm 100$  °C, largely depending on the phase chemistry, especially on the  $\text{Fe}^{3+}$  allocation. Redistribution of Mg and Fe during cooling may also influence the results of this geothermometer.

### 6.1.3.2. Geobarometers

#### 1. Newton and Perkins (1982)

This barometer, which is based on the exchange of  $\text{Fe}^{2+}$  and Mg between garnet, clinopyroxene and plagioclase, is expressed by the continuous reaction:



The equilibrium coefficient ( $K$ ) of this reaction is defined as:

$$K = [X^2(\text{Ca})X^2(\text{Mg})]^{\text{Grt}}/[X(\text{Ca})^{\text{Pl}}X(\text{CaMg})^{\text{Cpx}}],$$

and the recasted barometric formula, featured by an uncertainty  $\pm 0.16$  GPa, is expressed as:

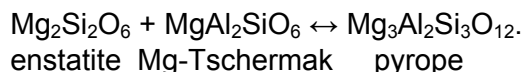
$$P = 675 + 17.179T + 3.5962 T \ln K.$$

The analytical error ( $\pm 0.16$  GPa) is due to non-ideal behaviour in the solid solution of silica phases, although at elevated temperature, an equi-partitioning of  $\text{Fe}^{2+}$  and Mg in garnet is assumed. However, there is no clear agreement on the behaviour of the Ca and Mn components. This barometric equation was further reformulated by Eckert et al. (1991), deriving the following expression:

$$P = 2.60 + 0.0171 \cdot T + 0.003596 \cdot T \ln K.$$

#### 2. Harley and Green (1982) and Nickel and Green (1985)

The barometer of Harley and Green (1982) is based on the garnet-orthopyroxene equilibrium. The germane reaction that buffers the orthopyroxene alumina content with coexisting garnet is expressed as:



This reaction induces a large change of volume ( $\Delta V$ ), thus being an adequate geobarometric tool. By calibrating such a process, the authors offered an equation quite useful as a geobarometer in granulite terrains or garnet peridotites:

$$P = 1/\Delta V [(R \ln K - 2.93)T + 5.650 + 5.157(1 - X(\text{Al})^{\text{Opx}}(1 - 2X(\text{Al})^{\text{Opx}}) X(\text{Fe})^{\text{Opx}}) - 6.300[X(\text{Ca})^{\text{Grt}} X(\text{Fe})^{\text{grt}} + X^2(\text{Ca})^{\text{Grt}}],$$

with

$$K = [X(\text{Al})^{\text{Opx}}(1 - X(\text{Al})^{\text{Opx}}) / (1 - X^3(\text{Ca})^{\text{Grt}})],$$

and

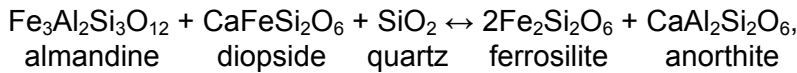
$$\Delta V = -[183.3 + 178.98(X(\text{Al})^{\text{Opx}}(1 - X(\text{Al})^{\text{Opx}}))].$$

Uncertainties of the barometer are within  $\pm 0.1$  GPa. When employed, one may experience serious difficulties in situations of the elevated activity of Fe and Mn in both phases, or a high Cr-content in garnet. In addition, some problems may induce a low alumina content of pyroxene, or uncertainties with the temperature estimation.

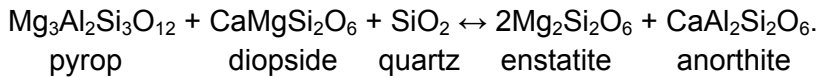
Nickel and Green (1985) offered a barometer, analogue to this one and based on the same reaction, depicting the garnet-orthopyroxene equilibrium. The new mechanism was calibrated somewhat differently, taking into account the Cr-content of garnet as well.

### 3. Paria et al. (1988)

This barometer is based on the following reactions, characteristic for the granulite facies assemblage:



and



Paria et al. (1988) provided the barometric expressions for both end-members, Fe and Mg, as follows:

$$P(\text{Fe}) = 32.097T - 26385 - 22.79(T - 848 - T \ln(T/848)) - (3.655 + 0.0138T)((T-848)^2/T) - 3.123T \ln K_{\text{Fe}}$$

$$P(\text{Mg}) = 9.270T - 4006 - 0.9305(T - 848 - T \ln(T/848)) - (1.1963 - 6.0128 \cdot 10^{-3}T)((T-848)^2/T) - 3.489T \ln K_{\text{Mg}},$$

with

$$K_{\text{Fe}} = (X(\text{Ca}^{\text{Pl}})(X^2(\text{Fe}^{\text{Cpx}})) / (X(\text{Fe}^{\text{Grt}})X(\text{Fe})^{\text{Opx}}),$$

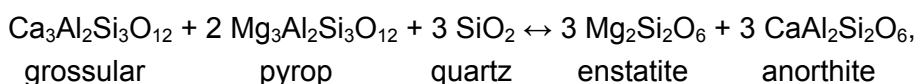
and

$$K_{\text{Mg}} = (X(\text{Ca}^{\text{Pl}})(X^2(\text{Mg}^{\text{Opx}})) / (X(\text{Mg}^{\text{Grt}})X(\text{Mg})^{\text{Cpx}}).$$

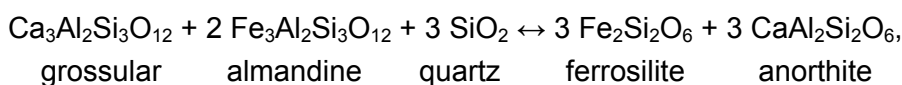
Pressure values obtained through the Fe end-member equilibrium are reported to be more accurate than those from the Mg-end member reaction. The commonly known non-ideal mixing of silicates, especially garnet, is recognised as a major cause of discrepancies between the two. Uncertainties, experienced by the usage of this barometre are known to fit the range of 0.0004 to 1.5 GPa and 0.0004 to 0.06 for the Fe and Mg end-members, respectively.

### 4. Perkins and Chipera (1985)

Based on the equilibrium between garnet, orthopyroxene and plagioclase, the above authors have calibrated the following reactions:



and



yielding precise barometric equations of the following forms:

$$P(\text{Mg}) = 6.1346 - 0.3471 \ln K_{\text{Mg}} + 0.0136T - 0.000997T \ln K_{\text{Mg}}$$

$$P(\text{Fe}) = 0.0630 - 0.3482 \ln K_{\text{Fe}} + 0.0143T - 0.000997T \ln K_{\text{Fe}},$$

with

$$K_{\text{Mg}} = [X^3(\text{En})(X^3(\text{An}))] / [X(\text{Grs})X^2(\text{Py})],$$

and

$$K_{\text{Fe}} = [X^3(\text{Fs})(X^3(\text{An}))] / [X(\text{Grs})X^2(\text{Alm})]$$

Small uncertainties in temperature estimates ( $\pm 50$  °C) influence the Mg-reaction up to  $\pm 0.05$  GPa, and the Fe-reaction up to 0.1 GPa. Normally, the suggested garnet-orthopyroxene-plagioclase-quartz barometry yields an accurate and precise pressure to within 0.1 GPa.

### 5. Plyusnina (1982)

The base of this geothermobarometer is the dependence of the alumina content in Ca-amphibole and coexisting plagioclase on  $P$ - $T$  conditions of their crystallisation. The calibrated reaction is defined as:



The author has provided a diagramme, having used values of the An-content in plagioclase and the Al-content in Ca-amphibole. Isobars are noted according to the variation of the Al-content in amphibole in dependence of both  $P$  and  $T$ , whereas isotherms are a function of the An-content in plagioclase. The standard error of this geothermobarometer is based upon the analytical uncertainty in the compositions of plagioclase and amphibole, and it is usually  $\pm 0.1$  GPa and  $\pm 10$ - $15$  °C. The presented mechanism is very useful for analyses of metamorphic conditions of metabasites, especially for those assemblages containing zoisite or epidote. One needs to be aware that the application of this Pl-Hbl geothermobarometer is limited to calcic and sub-calcic amphiboles, containing more than 1.5 Ca atoms per formula unit.





**Table 4.** Thermobarometric data for the KKOC lherzolites, dunites and olivine websterites. For analytical uncertainties, please consult the brief description of the respective method provided in text above

Sample	02	Z2	Z4	U35	GR2	GR12	M2	U4
Rock type	Sp Lh	Sp Lh	Sp Lh	Sp Lh	Pl Lh	Pl Lh	Pl Lh	Pl Lh
<b>GEO THERMOMETRES (in °C):</b>								
<u>2-pyroxene thermometer</u>								
1. WELLS (1977)	921	938	1043	920	945	932	948	917
<u>Ca-in-OPX thermometer</u>								
1. BREY and KÖHLER (1990)	1000	1045	1009	992	1033	1090	975	1021
<u>Spinel-OPX-olivine thermometer</u>								
1. WITT-EICKSCHEN AND SECK (1991)	n.a.	n.a.	809	723	910	n.a.	1028	751
<u>Spinel-olivine thermometer</u>								
1. FABRIÈS (1979)	662	621	637	550	596	587	625	597
<b>GEOBAROMETRE (in GPa):</b>								
<u>Ca-in-olivine/CPX barometer</u>								
1. KÖHLER AND BREY (1990)								
a) T (Wells 1977)	1.73	2.18	2.01	2.20	n.a.	n.a.	n.a.	n.a.
b) T (Brey and Köhler 1990)	2.75(?)	3.06(?)	3.20(?)	3.15(?)	n.a.	n.a.	n.a.	n.a.
c) T (Witt-Eickschen and Seck)	n.a.	n.a.	n.a.	n.a.	n.a.	n.a.	n.a.	n.a.

Sp Lh = spinel lherzolite. Pl Lh = plagioclase lherzolite. n.a. = not applicable. ? = not reliable results. Discrepancies obtained by the geobarometer of Köhler and Brey (1990) are due to the input temperature differences (see text for details)

**Table 4.** (continued) Thermobarometric data for the KKOC lherzolites, dunites and olivine websterites. For analytical uncertainties, please consult the brief description of the respective method provided in text above

Sample	4A	R7	K1	U19	2A	1C
Rock type	Pl Lh	Sp Lh	Dun	Dun	Ol web	Ol web
<b>GEO THERMOMETERS (in °C):</b>						
<u>2-pyroxene thermometer</u>						
1. WELLS (1977)	891	1038	n.a.	n.a.	903	912
<u>Ca-in-OPX thermometer</u>						
1. BREY and KÖHLER (1990)	986	932	n.a.	n.a.	1112	1092
<u>Spinel-OPX-olivine thermometer</u>						
1. WITT-EICKSCHEN AND SECK (1991)	1056	n.a.	n.a.	n.a.	n.a.	782
<u>Spinel-olivine thermometer</u>						
1. FABRIÈS (1979)	626	627	682	594	n.a.	624
<b>GEOBAROMETER (in GPa):</b>						
<u>Ca-in-olivine/CPX barometer</u>						
1. KÖHLER AND BREY (1990)						
a) T (Wells 1977)	n.a.	n.a.	n.a.	n.a.	2.38	2.21
b) T (Brey and Köhler 1990)	n.a.	n.a.	n.a.	n.a.	n.a.	n.a.
c) T (Witt-Eickschen and Seck)	n.a.	n.a.	n.a.	n.a.	n.a.	1.12

Pl Lh = plagioclase lherzolite. Ol web = olivine websterite, Dun = dunite. n.a. = not applicable. Discrepancies obtained by geobarometer of Köhler and Brey (1990) are due to the input temperature differences (see text for details)

**Table 5.** Thermometric data for the KKOC metamorphic rocks. For analytical uncertainties, please consult the brief description of the respective method provided in text above

Sample Rock type	U30 Amp	U29* Amp	11C Amp	R8 Amp	U23 Amp	CC1 G-D A	MK2 G-D A	GR7 G-D A
<b>GEOTHERMOMETERS (in °C):</b>								
<u>AMPH-PLAGIOCLASE</u>								
1. SPEAR (1980)	n.a.	n.a.	n.a.	550-730	750-800	725-750	750-800	>800
2. HOLLAND and BLUNDY (1994)	n.a.	n.a.	n.a.	675-770	780-820	750-820	850-920	940-997
<u>PAIR GRT-CPX</u>								
1. KROGH (1988)	n.a.	n.a.	n.a.	n.a.	n.a.	943-962	869-908	870-1019
<u>PAIR GRT-OPX</u>								
1. HARLEY (1984)	n.a.	n.a.	n.a.	n.a.	n.a.	n.a.	780-790	1100-1149
2. LEE and GANGULY (1988)	n.a.	n.a.	n.a.	n.a.	n.a.	n.a.	810-833	1170-1184
<u>PAIR GRT-AMPH</u>								
1. GRAHAM and POWELL (1984)	n.a.	n.a.	n.a.	n.a.	n.a.	816-827	n.a.	926
2. KROGH RAVNA (2000)	n.a.	n.a.	n.a.	n.a.	n.a.	802-840	n.a.	911
<u>TWO PYROXENES</u>								
1. WELLS (1977)	n.a.	n.a.	n.a.	n.a.	n.a.	n.a.	860-880	n.a.
2. BREY and KÖHLER (1990)	n.a.	n.a.	n.a.	n.a.	n.a.	n.a.	825-832	n.a.
<u>SAPPHIRINE-SPINEL</u>								
1. OWEN and GREENOUGH (1991)	880	n.a.	n.a.	n.a.	n.a.	n.a.	n.a.	n.a.

Amp=amphibolite. G-D A=Grt-Di amphibolite. n.a. = not applicable. \* = Sample U29 is unsuitable for any conventional geothermometric method due to its peculiar mineralogical assemblage. For details, see Chapter 6.3.2.2.

**Table 5.** (continued) Barometric data for the KKOC metamorphic rocks. For analytical uncertainties, please consult the brief description of the respective method provided in text above.

Sample	U30	U29	11C	R8	U23	CC1	MK2	GR7
Rock type	Amp	Amp	Amp	Amp	Amp	G-D A	G-D A	G-D A
<b>GEOBAROMETERS (in GPa):</b>								
<u>Al in AMPH</u>								
1. SCHMIDT (1992)	0.92-0.96	1.02-1.33	0.49-0.55	0.21-0.27	0.53-0.61	0.59-0.82	0.50-0.69	0.80-0.87
<u>CONTACT GRT-CPX-PL</u>								
1. NEWTON and PARKINS (1982)	n.a.	n.a.	n.a.	n.a.	n.a.	1.32-1.37	1.36-1.38	1.36-1.40
<u>PAIR GRT-OPX</u>								
1. HARLEY and GREEN (1982)	n.a.	n.a.	n.a.	n.a.	n.a.	n.a.	1.15-1.25	1.24-1.25
2. NICKEL and GREEN (1985)	n.a.	n.a.	n.a.	n.a.	n.a.	n.a.	1.10-1.26	1.29-1.30
<u>CONTACT OPX-CPX-GRT-PL</u>								
1. PARIA et al. (1988)	n.a.	n.a.	n.a.	n.a.	n.a.	n.a.	1.05-1.11	n.a.
<u>CONTACT OPX-GRT-PL</u>								
1. PERKINS and CHIPERA (1985)	n.a.	n.a.	n.a.	n.a.	n.a.	n.a.	1.11-1.13	1.26-1.31
<b>GEOOTHERMOBAROMETRES (in °C, GPa):</b>								
<u>PAIR AMPH-PL</u>								
1. PLYUSNINA (1982)	n.a.	n.a.	n.a.	530-650	n.a.	≥ 650	n.a.	n.a.
				0.25-0.55		≥ 0.4		

Amp=amphibolite. G-D A=Grt-Di amphibolite. n.a. = not applicable.

**Table 5.** (continued) Thermometric data for the KKOC metamorphic rocks. For analytical uncertainties, please consult the brief description of the respective method provided in text above.

Sample	V1	DU5	U22	X1	U40	V4	10D	Z1C
Rock type	G-D A	G-D A	G-D A	G-D-H	G-D-H	G-D-H	D-A-S	PGDS
<b>GEOTHERMOMETERS (in °C):</b>								
<u>PAIR AMPH-PL</u>								
1. SPEAR (1980)	> 750	n.a.	> 750	> 750	> 750	> 750	n.a.	n.a.
2. HOLLAND and BLUNDY (1994)	820-950	n.a.	820-865	810-840	835-967	847-880	n.a.	n.a.
<u>PAIR GRT-CPX</u>								
1. KROGH (1988)	814-977	507-533	1028	859-886	868-892	843-879	n.a.	726-1023
<u>PAIR GRT-OPX</u>								
1. HARLEY (1984)	855	n.a.	n.a.	714-868	854	780-822	n.a.	705
2. LEE and GANGULY (1988)	895	n.a.	n.a.	749-911	891	798-862	n.a.	732
<u>PAIR GRT-AMPH</u>								
1. GRAHAM and POWELL (1984)	n.a.	834-966	944	771	n.a.	800-821	n.a.	n.a.
2. KROGH RAVNA (2000)	n.a.	801-840	922	740	n.a.	787-802	n.a.	n.a.
<u>TWO PYROXENES</u>								
1. WELLS (1977)	907-920	n.a.	n.a.	833-859	947-958	890-910	n.a.	844-890
2. BREY and KÖHLER (1990)	828-847	n.a.	n.a.	713-777	856-889	821-880	n.a.	729-812

G-D A = Grt-Di amphibolite. G-D-H = Grt-Di-Hy amphibolite. D-A-S = Di amphibolite gneiss. PGDS = Pl-Grt-Di gneiss. n.a. = not applicable.

**Table 5.** (continued) Barometric data for the KKOC metamorphic rocks. For analytical uncertainties, please consult the brief description of the respective method provided in text above.

Sample Rock type	V1 G-D A	DU5 G-D A	U22 G-D A	X1 G-D-H	U40 G-D-H	V4 G-D-H	10D D-A-S	Z1C PGDS
<b>GEOBAROMETERS (in GPa):</b>								
<u>Al in AMPH</u>								
1. SCHMIDT (1992)	0.52-0.76	n.a.	0.81-1.11	0.68-0.73	0.71-0.72	0.69-0.73	0.84-0.89*	n.a.
<u>CONTACT GRT-CPX-PL</u>								
1. NEWTON and PARKINS (1982)	0.94-1.11	n.a.	unreal	0.85-1.10	1.04-1.11	0.84-1.05	n.a.	1.10-1.20
<u>PAIR GRT-OPX</u>								
1. HARLEY and GREEN (1982)	1.08-1.17	n.a.	n.a.	0.67-0.74	0.70-0.82	0.68-0.75	n.a.	1.40-1.59
2. NICKEL and GREEN (1985)	unreal	n.a.	n.a.	unreal	0.94-0.11	0.85-0.93	n.a.	unreal
<u>CONTACT OPX-CPX-GRT-PL</u>								
1. PARIJA et al. (1988)	1.01-1.10	n.a.	n.a.	0.90-1.01	n.a.	0.95-1.02	n.a.	1.40-1.60
<u>CONTACT OPX-GRT-PL</u>								
1. PERKINS and CHIPERA (1985)	1.10	n.a.	n.a.	0.95-1.04	1.01-1.03	0.98-0.99	n.a.	1.25-1.35
<b>GEO THERMOBAROMETERS (in °C, GPa):</b>								
<u>PAIR AMPH-PL</u>								
1. PLYUSNINA (1982)	n.a.	n.a.	n.a.	n.a.	n.a.	n.a.	n.a.	n.a.

G-D A=Grt-Di amphibolite. G-D-H=Grt-Di-Hy amphibolite. D-A-S=Di amphibolite gneiss. PGDS=Pl-Grt-Di gneiss. n.a. = not applicable.

\* = Pressure values for the post-peak Fe-enriched hornblende (analyses 3) are estimated to 0.26 GPa

## 6.2. Petrogenesis of peridotitic rocks

### 6.2.1. Mantle peridotites

#### 6.2.1.1. Composition and equilibration of KKOC upper mantle

The Krivaja-Konjuh ultramafic domain is predominantly composed of mantle peridotites, having the characteristic lherzolite composition (Ol, Opx, Cpx, Sp,  $\pm$ Pl). Most of the analysed samples are characterised by a porphyroclastic texture and a foliated structure, marked by elongated pyroxene grains embedded in a medium to fine-grained olivine matrix, which underwent a certain degree of serpentinisation (e.g. Đorđević and Pamić 1972; Figs. 9 and 11g, see Chapter 4.2.1.). Within the suite of the KKOC lherzolitic lithologies, one can distinguish two main varieties based on their modal mineralogy, mineral phase and bulk-rock chemistry, and textural characteristics. First variety is spinel lherzolite, whereas the second one is plagioclase lherzolite. Plagioclase lherzolite occupies the eastern portion of the Krivaja-Konjuh ophiolitic complex, roughly constrained to the area of the Krivaja ultramafic segment, whilst spinel lherzolite has been encountered within the Konjuh ultramafic domain, eastwards from the river Krivaja and the present position of the main metamorphic mass (Figs. 3 and 4). Differences between the two will be summarised in the following paragraph, since they are referred to be essential for the complete understanding of the peridotite equilibration processes and mantle dynamics as whole.

According to the classification of Mercier and Nicolas (1975) and Basu (1977), plagioclase lherzolites depict transitional protogranular to porphyroclastic textures and plagioclase as a usual constituent of their modal mineralogy. On the other hand, spinel lherzolites are devoid of plagioclase, but occasionally comprise primary pargasitic amphibole. Their texture is reported as typical mantle porphyroclastic, implying that these rocks experienced a comparatively higher degree of mantle deformations (see Chapters 4.2.1.1. and 4.2.1.2.). *Olivine* from both plagioclase and spinel lherzolite is chemically homogenous (Fo ~ 90), showing no zonation (see Chapter 4.2.2.1.). Such homogeneity indicates that a large portion of the upper mantle, up to several hundred square kilometres in size, has been affected by partial melting and subsequently equilibrated under the constant pressure regime (e.g. Arai 1994). The NiO abundances of both varieties fit the range from 0.32 to 0.46 wt%, defining the analysed rocks in the Fo-NiO space as mantle ultramafic rocks (Fig. 12). However, in plagioclase lherzolites, a discrete olivine mineralization is detected, depicting a low NiO content ranging from 0.33 to 0.35 wt%. Such a peculiar mineralization is interpreted to be due to low crystallisation degrees of impregnation melts that coexisted with the host peridotite (e.g. Niu 2004, Takahashi 2001). There are no significant differences between *orthopyroxene* from plagioclase and spinel lherzolite (see Chapter 4.2.2.2.). Still higher Al<sub>2</sub>O<sub>3</sub> values are recovered in *orthopyroxene* from spinel lherzolite compared to those from plagioclase lherzolite. This trend is consistent with the transition from the spinel to plagioclase peridotite stability field (e.g. Borghini et al. 2007), but possibly also due to the late interactions with percolating melts (e.g. Rampone et al. 1997). The first possibility is taken as a more liable scenario, since *orthopyroxene* from plagioclase lherzolites also possesses elevated Ti and Ca abundances (e.g. Cannat et al. 1990). The *clinopyroxene* chemistry delivers even higher inconsistency with respect to the Al<sub>2</sub>O<sub>3</sub> contents of spinel and



plagioclase lherzolites (see Chapter 4.2.2.3.). Thus, clinopyroxene originated from spinel lherzolite records almost double the  $\text{Al}_2\text{O}_3$  content than its counterpart from plagioclase lherzolite (Fig. 16). Furthermore, clinopyroxene from spinel lherzolite shows a positive correlation of  $\text{SiO}_2$  and a negative of  $\text{Na}_2\text{O}$  and  $\text{Al}_2\text{O}_3$  with respect to Mg# (Fig. 17). Such a trend is however not reported in case of clinopyroxene from plagioclase lherzolite, corroborating their metasomatic record. The Ti content of clinopyroxene from plagioclase lherzolites further argues in favour of such a metasomatic trend, being significantly elevated in comparison to clinopyroxene from spinel lherzolite (Figs. 17d, 18). The  $\text{Al}^{\text{VI}}/\text{Al}^{\text{IV}}$  ratio of clinopyroxene in spinel lherzolite doubles that of clinopyroxene in plagioclase lherzolite (Fig. 18), thus inferring deeper equilibration pressure of spinel lherzolites. The analogue trend is reported for the distribution of Na, where a higher Na content in clinopyroxene from spinel lherzolites is known to be typical for an early oceanic rifting environment (Nicholls et al. 1981). Zonation in the ortho- and clinopyroxene porphyroclasts is relatively uniform, no matter of their host paragenesis (Figs. 15, 16). The most obvious discrepancy between spinel and plagioclase lherzolites is their spinel composition. In spinel lherzolites, spinel has Cr# values between 7 and 50, whereas in plagioclase lherzolites, spinel is more brownish, with a composition of chromium picotite (Cr# 30-50) (Fig. 21).

Differences in the KKOC lherzolite types are recorded in their bulk-rock chemical composition as well. With regard to the main elements' distribution, there is no difference between the lherzolite types. However, due to the impregnation, plagioclase lherzolites possess elevated LREE (La, Ce and Pr) concentrations, whereas spinel lherzolites are higher in La values (see Chapter 5.1.1.).

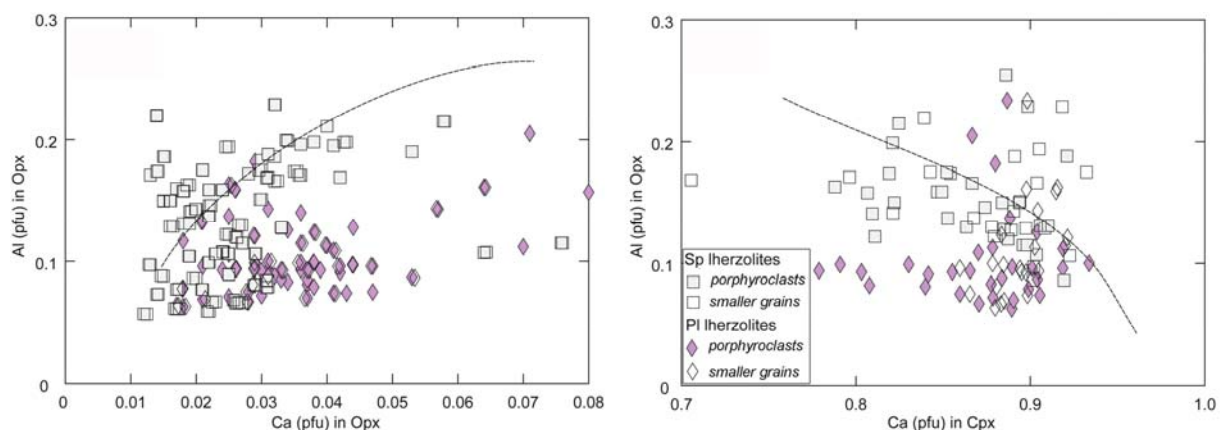


**Fig. 64.** Al vs Ca in orthopyroxene (left) and Al in Opx vs Ca in Cpx in KKOC lherzolites (right). Dashed curves represent the theoretical equilibrium between the Al amount in orthopyroxene and Ca in clinopyroxene (after Cabanes and Mercier 1988).

The geothermometry of KKOC lherzolites indicates consistent comparative discrepancies between the values obtained by the two-pyroxene, Ca-in-Opx and spinel-Opx-olivine thermometers (Wells 1977, Brey and Köhler 1990, Witt-Eickschen and Seck 1991) with respect to those of the spinel-olivine thermometer (Fabriès 1979) (see Table 4). The first three thermometers yielded temperatures ranging from 809 to 1012 °C (T1), whilst the spinel-olivine calibration resulted within the range of 550 to 682 °C (T2). For both, spinel and

plagioclase lherzolites, the differences between T1 and T2 values is found to be in the range of  $200 \pm 20$  °C. Such differences are to be expected, since the geothermometer of Fabriès (1979), based on the Fe-Mg exchange between olivine and spinel, is well-known to be sensitive to later thermal events. This makes the thermometer suitable for estimating the last 'equilibration' stages during cooling of the peridotites. Furthermore, these differences are taken to imply a relatively fast and continuous cooling of the 'mantle column' during its ascent under the spreading MOR environment (Dick and Bullen 1984, Bazylev and Silantyev 2000).

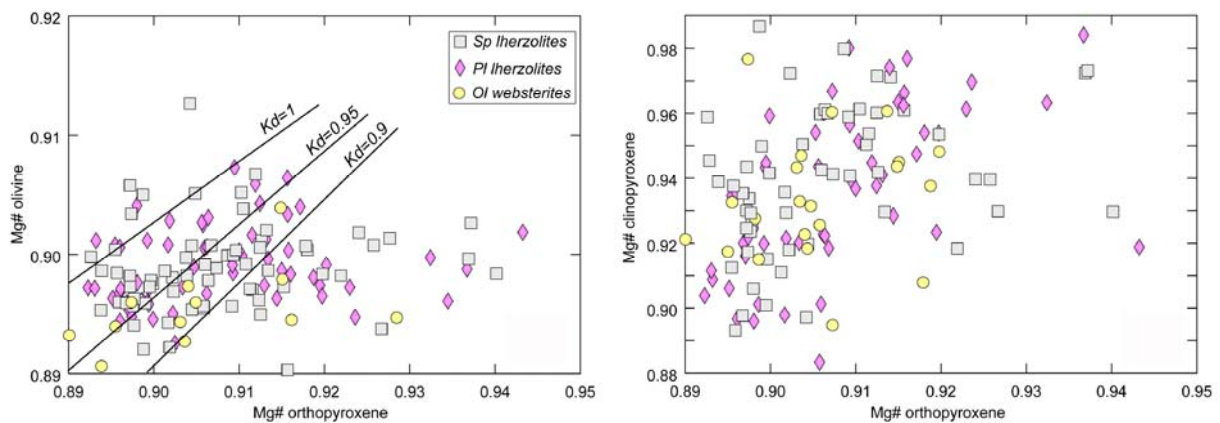


**Fig. 65.** Mg# in Opx vs Mg# in olivine (left) and Mg# in Opx vs Mg# in clinopyroxene (right) in KKOC lherzolites. Solid lines represent the theoretical isothermal equilibrium for the exchange reaction with different Fe/Mg distribution coefficients between olivine and orthopyroxene (after Aldanmaz et al. 2009).

Within the analysed lherzolites, the observed temperature gap (T2 - T1) has also been recorded in their textural characteristics. Recrystallisation and equilibration occurred in the lower temperature range (T2) and are reflected in the formation of numerous strain-free mosaic neoblasts of pyroxene and olivine. On the other hand, textural characteristics are due to the main deformational stage that took place in the higher temperature range (T1). These deformations produced ortho- and clinopyroxene porphyroclasts, kink bands, exsolution lamellae and chadacryst inclusions (see Chapter 4.2.1.). It needs to be noted that the upper limit of the T1 equilibration range (1012 °C) might be slightly overestimated, being preferably somewhat lower (ca 50-100 °C). The highest values of equilibration temperatures were acquired by the Ca-in-Opx thermometry. The Ca content in orthopyroxene is readily affected by late metasomatic processes (see Chapter 4.2.2. and Chapter 6.2.1.2.). This can easily be observed in Fig. 64, where Ca in pyroxene from plagioclase and partly spinel lherzolite is being shifted away from the theoretical equilibrium curves. Still, the Fe-Mg distribution between olivine and orthopyroxene, along with the inter-pyroxene equilibrium, has not been compromised by subsolidus reactions, as seen in Fig. 65, reflecting a complete chemical equilibrium between the phases.

The range of equilibration pressures in analysed spinel and plagioclase lherzolites is defined by their parageneses, mineral phase chemistry and textural characteristics, as well as the values of estimated temperatures. For temperatures T1 (809-1012 °C), the oceanic and rift-ridge geotherms yield the equilibration pressure ranging from 1.2 to 2.0 GPa (ca. 40-65 km depth). This means that the concerned mantle portion first experienced a certain

degree of partial melting, being subsequently equilibrated in the spinel peridotite stability field. The final equilibration level, which recorded the temperature span T2 (550-682 °C), and the neoblast formation occurred under pressures below 1.0 GPa. This process is normally initiated along the kink-band boundaries, causing the development of a small-scaled mosaic texture with grain boundaries converging at 120 ° triple points. In garnet-devoid spinel and plagioclase peridotites, the only useful barometer is based on the equilibrium of coexisting olivine/clinopyroxene pairs (Köhler and Brey 1990). However, in KKOC peridotites, due to the late metasomatism and uncertainties in the measured Ca content of olivine, this calibration resulted with anomalously high values of pressure. Still, the provided pressure constraints can be discussed in terms of the pyroxene chemistry, especially because its Al<sub>2</sub>O<sub>3</sub> and CaO contents are known to be sensitive to equilibrium conditions (e.g. Benoit 1987). The large orthopyroxene grains have the highest values of Al<sub>2</sub>O<sub>3</sub> and are free of clinopyroxene segregations, whereas orthopyroxene grains featured by spinel blebs and Cpx exsolution lamellae are comparatively impoverished in Al<sub>2</sub>O<sub>3</sub>. The lowest Al<sub>2</sub>O<sub>3</sub> values are observed in small orthopyroxene neoblasts (see Chapter 4.2.2.2., Fig. 13). Since all orthopyroxene grains unaffected by the late metasomatism form a distinct compositional trend with respect to the Al-Ca equilibrium curve, the above-mentioned differences in the Opx alumina content indicate discrepancies in rock equilibration conditions (Fig. 64). Hence, the first mentioned orthopyroxene group of coarse exsolution-free grains presents the deepest equilibrated rocks. As the mantle deformation proceeds, equilibrium temperatures decrease, recording the lowest values in recrystallised neoblasts (T2 temperatures,  $P < 1.0$  GPa). Furthermore, relatively high CaO values and Al<sub>2</sub>O<sub>3</sub>/Cr<sub>2</sub>O<sub>3</sub> ratios in all orthopyroxene porphyroclasts are typical to high-temperature dry systems, lacking a significant pressure oscillation (e.g. Werner and Pilot 1997). These constrain Cpx exsolution lamellae and spinel segregation in Opx porphyroclasts to have occurred in the deeper lithospheric portions. The correlation trend of main oxides (Na<sub>2</sub>O, Al<sub>2</sub>O<sub>3</sub> and SiO<sub>2</sub>) vs Mg# in clinopyroxene from spinel lherzolites is very clear, whereas for clinopyroxene from plagioclase lherzolites such a trend is somewhat less pronounced (Fig. 17a-c). According to Grégoire et al. (2005) and Smith (2000), garnet peridotites do not display any correlation. Therefore, these characteristics strongly suggest that KKOC lherzolites are mantle peridotites, equilibrated in the spinel-peridotite stability field. The span of Al<sup>VI</sup>/Al<sup>IV</sup> values of clinopyroxene from spinel lherzolite (0.05-1.60) is generally twice as high as that of clinopyroxene from plagioclase lherzolites or olivine websterites (0.05-0.80) (Fig. 18). Apart from impregnation, this also suggests deeper equilibration of spinel lherzolite compared to plagioclase lherzolite and pyroxenite, which were partially re-equilibrated at shallower subsolidus levels.

The zoning patterns of principal phases in KKOC lherzolites call upon the processes of cooling and partial subsolidus re-equilibration, induced by the decreasing pressure and temperature conditions and/or metasomatic processes. In orthopyroxene, there is a clear tendency in the FeO distribution toward higher abundances in grain rims, whereas conversely, the Al<sub>2</sub>O<sub>3</sub> content is found elevated within the core (Fig. 15). CaO and Cr<sub>2</sub>O<sub>3</sub> show no regular distribution through the grains. The Al<sub>2</sub>O<sub>3</sub> and partly also CaO decrease in orthopyroxene margins are mainly attributed to the loss of its Ca-Tschermak component with the fall of pressure and temperature. In clinopyroxene from plagioclase lherzolites, the rims

are enriched in MgO and impoverished in CaO contents (Fig. 19). FeO behaves similarly to MgO, whereas Al<sub>2</sub>O<sub>3</sub> records a completely unpredictable pattern. Like in orthopyroxene, the CaO loss in clinopyroxene margins is explained by the decreased solubility of the Ca-Tschermak component at lower equilibration conditions. On the other hand, the increase of MgO in Cpx rims is interpreted through reactions with late interstitial fluids, under increased oxygen fugacity (e.g. Hewins 1974). For clinopyroxene from spinel lherzolite no significant grain zonation is reported with respect to CaO and MgO/FeO. Al<sub>2</sub>O<sub>3</sub> abundances oscillate through the grain. The plagioclase zonation trend is defined by the oscillatory saw-tooth zoning of the An component, along with its enrichment at grain margins (Fig. 24). Such a W-shaped Ca-Na zoning pattern invokes to the upper-mantle melt impregnation that, according to Takahashi (2001), occurred at shallower lithospheric levels when the adiabatically ascending mantle portion passed the solidus.

Based on presented lines of evidence, the following equilibration path of KKOC lherzolites is to be concluded. Analysed rocks present the mantle column that experienced relatively fast and continuous adiabatic ascent under the spreading MOR environment. Assuming an average adiabatic gradient of 0.4 °C/km and a temperature of 1365 °C at 100 km below the ocean ridge (Hamlyn and Bonatti 1980), the estimated KKOC lherzolite equilibration depth (40-65 km) is found above the experimentally determined garnet-spinel peridotite inversion at depth (55-80 km). The main stage of equilibration reported for the coarse-grained and porphyroclastic plagioclase and spinel lherzolites (809-1012 °C, 1.2 to 2.0 GPa, Table 4) happened shortly after partial melting (~ 7.7 %) and melt segregation followed by the mantle thermal relaxation and cooling of the rock residue and the remaining melt fraction. Further ascent of the KKOC mantle portion passed the dry solidus and led to subsolidus re-equilibration and mineralogical changes (e.g. mineral zonation, strain-free neoblasts formation) under temperatures reported by the olivine-spinel thermometry (550-682 °C, < 1.0 GPa). Peculiarities in the mineral chemistry of pyroxene, olivine and spinel, along with the presence of plagioclase and amphibole in some of the KKOC lherzolites strongly appeal to the subsolidus melt impregnation of those mantle regions during the final stage of the rocks' equilibration (see Chapters 4.2.2. and 6.2.1.2.). Taking into account the above discussion, one can suggest that the final steady state of phases in analysed rocks was reached below 30 km depth, prior to their exhumation and emplacement to the southern continental margin as part of an ophiolite sequence (see Chapter 6.2.1.3.).

#### 6.2.1.2. Nature of upper mantle dynamics

This subchapter provides an overview on the compositional characteristics and the equilibration path of the KKOC mantle domain. In that sense, the significant episodes that are explanatory to the heterogeneity and chemical dynamics of the analysed mantle portion are just being shortly addressed. Therefore, the following points will be discussed: (a) nature and regime of the upper mantle partial melting, (b) spreading character of an ocean ridge, and (c) modality of subsolidus metasomatism and the origin of plagioclase.

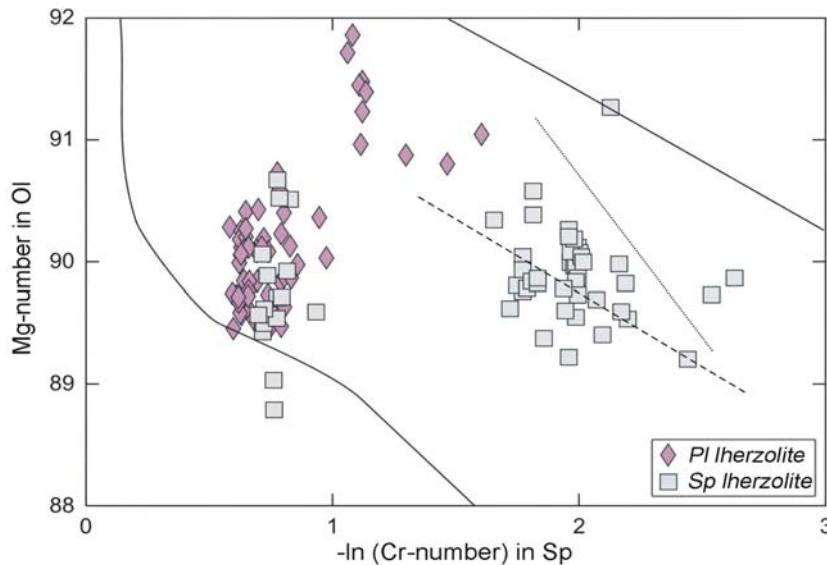


**Fig. 66.** Olivine-spinel relationship in KKOC mantle period-tites, depicting changes in the mineral chemistry during partial melting. The solid lines stand for the olivine-spinel mantle array (Arai 1987). Dashed line indicates a trend of N-MORB spinel peridotite mineral composition (Bazylev 2003). Dotted line points to a trend of subcontinental spinel peridotite mineral compositions (Bazylev 2003).

The Krivaja-Konjuh Iherzolites show characteristics of fertile solid residues having resulted from low to moderate degrees of MORB partial melting. As it is suggested in the equilibration model presented earlier, melting might have started along the garnet-spinel peridotite transition, being completely equilibrated under spinel-facies conditions (809-1012 °C, 1.2 to 2.0 GPa, Table 4). The geochemical parameters corroborating mantle fertility include: (a) low Mg# of olivine, (b) moderate values of Mg# and broad ranges of the  $\text{Al}_2\text{O}_3$  content in pyroxene, (c) low to moderate Cr# of spinel, and (d) bulk-rock chemistry, recording slight depletion in  $\text{Al}_2\text{O}_3$ , CaO,  $\text{Na}_2\text{O}$ , FeO and REEs, along with a weak enrichment in compatible Ni and Co (see Chapters 4.2.2. and 5.1.1.). The range of Fo values of olivine in both spinel and plagioclase Iherzolite is quite narrow (88.79-91.86 and 89.16-90.73, respectively), suggesting a rather fertile nature of the entire KKOC mantle portion. A similar conclusion is derived from high  $\text{Al}_2\text{O}_3$  values in orthopyroxene (up to 6.21 wt%), whereas with an average Mg# of clinopyroxene being around 91, the KKOC mantle rocks are inferred to be less depleted in comparison to fertile abyssal peridotites (e.g. Garrett transform fault, North Atlantic peridotites, Michael and Bonatti 1985, Cannat et al. 1990). The chromium content of spinel is known to be very informative with respect to the processes of partial melting as well as late impregnation metasomatism. The Cr# from spinel Iherzolites normally fits the range of 8 to 20, and thus defines the analysed rocks as fertile mantle residues of abyssal or Alpine peridotite affinity (Fig. 21). Due to metasomatism, the Cr# of spinel in plagioclase Iherzolites is normally > 30, which hampers its usage in petrogenetic considerations.

Mantle fertility can also be evaluated from whole-rock chemical data. A mild refractory nature of KKOC peridotites is clearly seen from their  $\text{Al}_2\text{O}_3$ -MgO-FeO systematics, which completely overlap with those of fertile MOR abyssal peridotites (Fig. 46). The same line of fertility witnesses the well-defined Y- $\text{Al}_2\text{O}_3$  trend, which closely corresponds to the trend of fertile Ligurian peridotites (Fig. 46). A low depletion level is further elucidated from the Mg# vs  $\text{Al}_2\text{O}_3$  and Cr/Al vs Ni/Al ratios (Fig. 47-48). Both fertile trends are nicely defined, thus

bounding the KKOC mantle rocks to the occurrences of other fertile peridotites known from the literature (e.g. the South-Sandwich lherzolites, Pearce et al. 2000).

Relatively low melting degrees of the KKOC mantle domain, inferred from the peridotite mineral and whole-rock chemistry, have also been tested with respect to the trend of continuous melting of spinel peridotites originated from the fertile ocean and/or Alpine-type peridotites. A relationship of the Cr# in spinel vs the Mg# in olivine is known to define an olivine-spinel mantle array, whose changing composition may nicely depict a melting trend of peridotite (Arai 1987). In Fig. 66, the dashed line indicates a depletion trend of spinel peridotites affiliated to the MOR setting. Spinel peridotites recovered from xenoliths and orogenic massifs (subcontinental mantle) show a faster increase in the olivine Mg# as the Cr# of spinel increases (dotted line in same diagramme, Bazylev 2003). One can notice that KKOC spinel lherzolites, having a pre-metasomatic spinel chemistry, are clearly plotted along the sub-oceanic (MOR) melting trend. These results are consistent with the data from the neighbouring ophiolitic complexes of Ozren and Borja (Fig. 4, Bazylev et al. 2009). Due to the metasomatism and sensitivity of the spinel chemistry, such a melting trend cannot be suggested for plagioclase lherzolites. However, if one compares the  $Al_2O_3/SiO_2$  vs  $TiO_2/Al_2O_3$  correlation in KKOC mantle rocks with respect to primitive and depleted mantle estimations (Fig. 49, PM, DM respectively), it is evident that the plagioclase and spinel lherzolites whole-rock chemistry follows the same depletion trend, roughly corresponding to DM, and subsequently experiencing a low degree of MOR melting. It is important to remark that although metasomatism has seriously affected the mineral chemistry of spinel, it has not considerably influenced the bulk-rock major element chemistry, or values of the Mg# of spinel and pyroxene. Therefore, a pre-metasomatic residual nature of plagioclase lherzolites is suggested. The conclusion on the melting regime drawn for the spinel lherzolites are, as well, equally applicable to plagioclase lherzolites.

In order to constrain the degree of partial melting experienced by the KKOC fertile mantle rocks, the equation of Hellebrand et al. (2001) has been employed, having yielded an average melting degree of ~ 7.7 % for spinel lherzolites. This result is indicative with respect to the behaviour of the REEs in KKOC mantle rocks during the processes of partial melting. Both melting models, batch and fractional, have been presented in Fig. 53. A proposed melting degree of ~ 7.7 % based on the spinel chemistry and REE normalisation values in KKOC peridotites are in good agreement with the batch model of partial melting, with an estimated degree of melting being around 5 %. Based on the spinel Cr# and calculated melting degree, it is also possible to assess the variations in crustal thickness and its dependence on a spreading rate. Taking the melt production rate and depth of melting onset (~ 70 km) as constant values, the simple expression of Hellebrand et al. (2002) yielded the KKOC oceanic crust thickness to be around 5.4 km. According to the modelling of Reid and Jackson (1981), such a crustal thickness would imply the predicted ridge spreading rate of 32 mm/year. This spreading velocity defines a KKOC spreading system as slow-rated (< 55 mm/year). Slow spreading ridges are generally characterised by large wide rift valleys (often > 10 km) and a coarse terrain at the ridge crest that can have a relief of up to 1 km (Fig. 67). Melting is proposed to be low and vary along the spreading centres of such slow spreading ridges (e.g. Whitehead et al. 1984). Bearing this in mind, the fertility of the KKOC

mantle rocks is best explained through low melting degrees along slow spreading middle ocean ridges, like nowadays existent in the Northern Atlantic or the Indian Ocean.

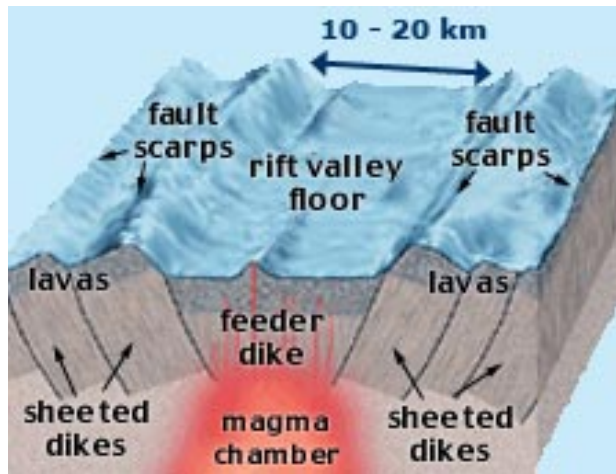


**Fig. 67.** Model of a slow spreading mid ocean ridge. Picture was taken from [www.divediscover.whoi.edu](http://www.divediscover.whoi.edu).

There are numerous lines of evidence suggesting the existence of processes of late metasomatism or melt refertilisation that affected the large portion of the KKOC mantle rock, resulting in the formation of plagioclase and amphibole. Metasomatism also causes peculiar geochemical changes in the mineral chemistry, as well as in the trace element bulk rock chemistry. Such features were mentioned in previous chapters (4 and 5), and here they will be further discussed. According to the proposed ascent model of the KKOC mantle column (see Chapter 6.2.1.1.) and the fact that the plagioclase formation is not an omnipresent occurrence within the suite of KKOC mantle rocks, it is believed that analysed rocks had cooled to subsolidus temperatures prior to entering the stability field of plagioclase peridotites. Thus, a sub-solidus partial equilibration and mantle impregnation of the KKOC mantle domain most probably occurred at temperatures and pressures (T<sub>2</sub>) that closely correspond to depths of the spinel-plagioclase peridotite transition.

The mineral chemistry of *olivine* does not display significant differences between spinel and plagioclase lherzolites. However, a discrete olivine mineralization is detected in plagioclase lherzolites, depicting a low NiO content, ranging from 0.33 to 0.35 wt%. Such values are bound to low degrees of crystallisation from partial melts, which impregnated and/or coexisted with the host peridotite (e.g. Niu 2004, Takahashi 2001). In *orthopyroxene* from plagioclase lherzolites, late metasomatism is seen in elevated TiO<sub>2</sub> and reduced Al<sub>2</sub>O<sub>3</sub> contents (Figs. 13-14). The same behaviour of TiO<sub>2</sub> and Al<sub>2</sub>O<sub>3</sub> is also reported in *clinopyroxene* from plagioclase lherzolites. *Spinel* from plagioclase lherzolites has, in comparison to those from spinel lherzolites, a higher Cr# value and TiO<sub>2</sub> content, which implies that such a spinel crystallised from, or was influenced by an impregnation fluid (see Chapter 4.2.2.4.). It is known that Al is readily removed from the spinel crystal lattice during metasomatism or alteration, whereas Cr and Fe<sup>3+</sup> are added into the structure (e.g. Barnes and Röder 2001). The *plagioclase* mineral chemistry also offers an evidence of upper mantle melt metasomatism. Namely, oscillatory Na-Ca saw-zoning, observed in the KKOC plagioclase grains is a new trend reported for mantle rocks, and denotes incipient partial melting and melt migration processes in the upper mantle (Fig. 24, Takahashi 2001). The

REE distribution pattern in plagioclase lherzolites provides undisputable evidence calling for late-metasomatic alterations (Fig. 51). Thus, LREE abundances (La, Ce and Pr) are progressively elevated, approaching the shape of the REE normalisation curves to “flat”, slightly sigmoid type, having the same ratio of LREE, MREE and HREE. Such a feature is known to be characteristic for orogenic peridotite massifs, but in this case, it is referred to ophiolite peridotites, which underwent a degree of metasomatic changes through an interaction of the depleted mantle and LREE enriched melt (e.g. Prinzhofer and Allègre 1985). In Fig. 68, the variation trend of certain REEs with the melt depletion index of  $Al_2O_3$  has been provided, depicting the shift of metasomatically affected plagioclase lherzolites from the trend of partial melting. Furthermore, it is evident that the elements of a higher degree of incompatibility are more affected by metasomatic processes ( $D_{Sm} > D_{Yb}$ ).

It can be summarised that the plagioclase-bearing peridotites are related to melt impregnation processes, whereas the plagioclase formation itself is explained through the crystallisation from such metasomatic fluids. Presented geochemical evidences argue against the formation of plagioclase via the simple spinel- to plagioclase peridotite facies transition. Moreover, such a plagioclase-facies recrystallisation is usually recorded by plagioclase and olivine rims around Al-rich spinel, which was not reported in the KKOC mantle rocks.

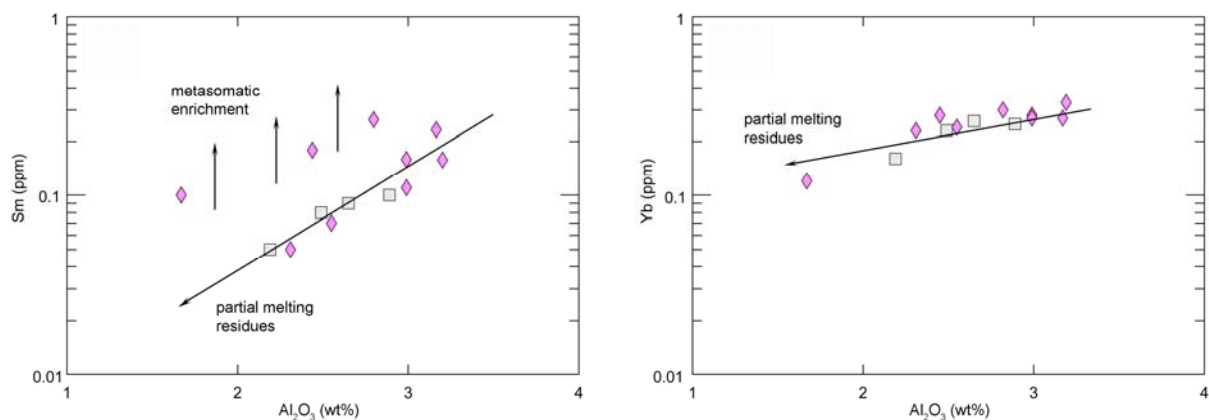


**Fig. 68.** Variations of Sm (left) and Yb (right) with the melt depletion index of  $Al_2O_3$  for the KKOC lherzolites. Trend of the partial melting depletion taken from Aldanmaz et al. (2009).

### 6.2.1.3. KKOC geotectonic setting and regional implications

The compositional variations in the KKOC mantle rocks' mineral and whole-rock chemistry were shown to prove their distinct equilibration history, along with the differences in melting regimes and impregnation metasomatism (see Chapters 6.2.1.1. and 6.2.1.2.). Further on, the presented geochemical data indicates that the Krivaja-Konjuh mantle rocks are fertile residues, mainly formed in an ocean-ridge tectonic environment, which laterally evolved into the SSZ-type of geotectonic setting.



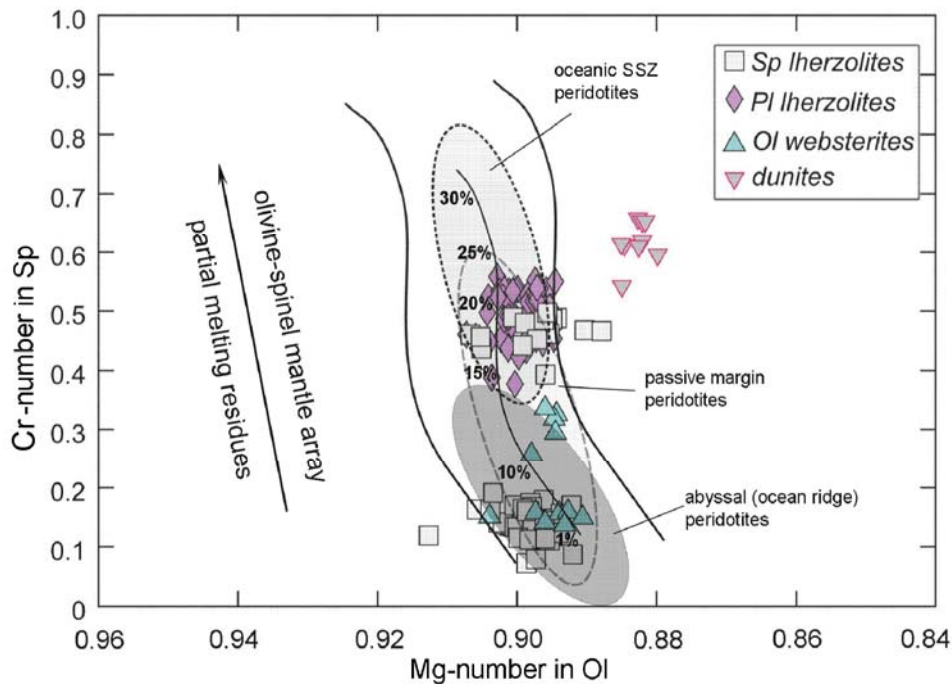


**Fig. 69.** Mg# in olivine vs Cr# in spinel for KKOC ultramafic rocks. The approximate fields for abyssal (ocean-ridge) peridotites, oceanic arc peridotites and passive continental margin peridotites are according to Dick and Bullen (1984) and Pearce et al. (2000), respectively. The olivine-spinel mantle array and melting trend are from Arai (1987).

The majority of analysed KKOC mantle rocks were produced in a geotectonic setting marked by a ridge-type melting regime. Numerous evidences, presented in the previous chapter, defined those rocks as residual, moderately depleted, lherzolites. Such a fertile geochemical pattern clearly points to normal and shallow MOR processes, resulting in up to 10% of partial melting of the MORB source. Moreover, the origin of olivine websterites, which are associated with the analysed lherzolites, is bound to deeper portions of an ocean-ridge setting. There, a higher degree of partial melting affected an already depleted MORB mantle source (see Chapter 6.2.2.). It is important to keep in mind that the KKOC mantle residues are compositionally complementary to the whole-rock REE geochemistry of associated metamorphic rocks (see Sm/Yb vs La/Yb for metamorphites, Fig. 77), as well as those of mafic extrusives exposed at the KKOC northern margins (Babajić 2009). Certain geochemical focal points, recognised as essential in the illustration of the MOR geotectonic setting of KKOC mantle rocks are being summarised and presented here. Bearing in mind the sensitiveness of the composition of spinel to different melting regimes, one can notice that in the Cr# in spinel vs Mg# in olivine diagramme (Fig. 69), the metasomatism-free fertile residues having a spinel lherzolite mineralogy are plotted in the lower portion of the diagramme, being defined in the field of abyssal (ocean-ridge) peridotites. The experimentally determined degree of partial melting of such rocks, set under 10 %, fully corresponds to the calculated values of melting for KKOC peridotites (~ 7.7 %, see Chapter 6.2.1.2.). Sodium content of clinopyroxene in peridotites is known as an empirical parameter, important for a better discrimination of geotectonic settings of analysed host peridotites.

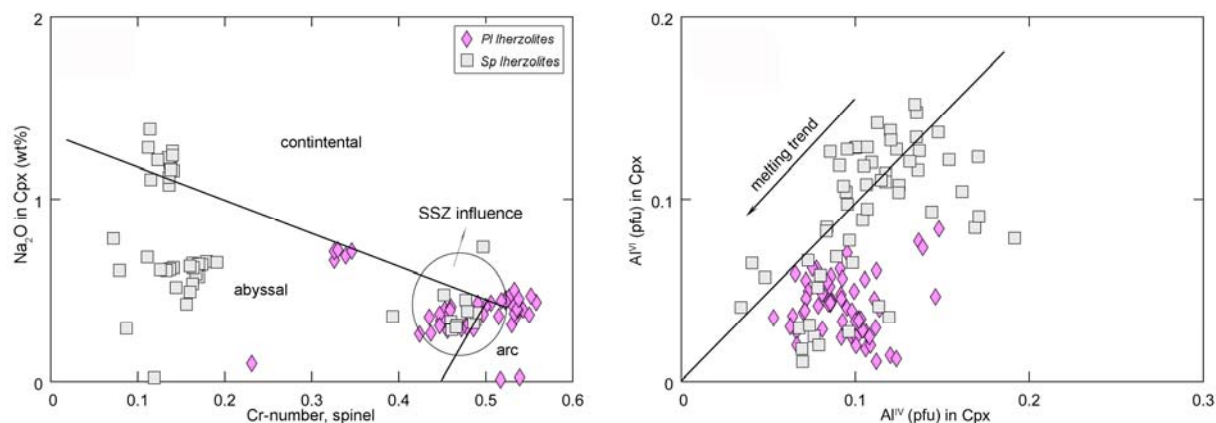


**Fig. 70.** Correlation between the  $\text{Na}_2\text{O}$  content in Cpx vs Cr# in spinel (left) and  $\text{Al}^{\text{IV}}$  and  $\text{Al}^{\text{VI}}$  in clinopyroxene (right) in the KKOC mantle rocks. The discrimination line between continental and abyssal peridotites is after Arai (1992).

The distribution coefficient of Na between melt and clinopyroxene or among solid peridotite phases is pressure and temperature sensitive, causing Na enrichment in clinopyroxene during high-pressure (subcontinental) partial melting. Conversely, Na is found impoverished in the solid phase, during low-pressure (oceanic) melting (e.g. Kornprobst et al. 1981). In Fig. 70, one can see that the vast majority of KKOC mantle rocks, including the plagioclase lherzolites, is of oceanic type, having a  $\text{Na}_2\text{O}$  content below 0.5 wt%. It is interesting to remark how the Na content in clinopyroxene roughly decreases as the Cr# of spinel increases. Such a relationship is characteristic for the normal MOR settings, not being reported in peridotites from the anomalous MOR segments, where the Na content of clinopyroxene does not demonstrate any regular decline in the most depleted mantle domains (e.g. Bonatti et al. 1992).

At this point, it is necessary to refer to the geochemical features, which might be consistent with an influence of the SSZ geotectonic setting. Such peculiar characteristics have been recognised in sample U35, recovered from the eastern slope of Konjuh Mt, where the primary paragenesis comprises pargasitic amphibole and Cr-rich spinel (Fig. 10h). Nowadays, an occurrence of small amphibole grains, especially along olivine-orthopyroxene-clinopyroxene triple junctions, is widely accepted to indicate a mantle fluxing by subduction fluids or melts (e.g. Grégoire et al. 2005). This highly corresponds to erstwhile geochemical parameters, especially the Cr# of spinel. A careful study of the relationship between Mg# in Ol and Cr# in Sp (Fig. 69) reveals that a part of the KKOC spinel lherzolites (sample U35, plagioclase lherzolites excluded) possess an elevated Cr# of spinel (~ 0.4 to 0.5) for constant values of Mg# in olivine. According to Dick and Bullen (1984), those peridotites are classified as oceanic SSZ peridotites, which underwent 13 to 25 % of partial melting. Moreover, a somewhat increased Na content of clinopyroxene with respect to the related spinel composition (Fig. 70) has been considered as indicative of a SSZ setting of the concerned peridotite (sample U35). Finally, the whole-rock trace element study has shown certain dissimilarities of sample U35 with the rest of KKOC spinel lherzolites. Thus, the respective sample depicts the highest REE normalisation values and an elevated La content (Fig. 51). Lanthanum enrichment is typical for the ophiolite complexes being affected by refertilisation processes (e.g. Gruau et al. 1998). Furthermore, sample U35 is characterized

by elevated P and Nb values. Phosphorus is bound to the subduction influx and it is readily hosted in the texturally equilibrated pargasitic amphibole, whereas the Nb fractionation may be linked to a minute Nb-rutile mineralization, which easily precipitates from subduction-released fluids or melts. It is important to mention that not far from the U35 sampling location, the depleted harzburgites and dunites were recovered (e.g. Lugović et al. 2006), whilst along the whole KKOC associated volcanites and metamorphites of known protoliths, indicate a transition between the two ophiolite types, a slow-spreading MOR and SSZ type (Babajić et al. 2009). The offered discussion on the partial SSZ imprint of the most eastern segment of the Krivaja-Konjuh ophiolite segment gave rise to the following conclusions. A supra-subduction geotectonic regime required by the motion change of the Tethyan oceanic plates, from divergent to convergent, with ongoing subduction processes operating in the vicinity of the KKOC mantle domain. An interaction of such mantle-wedge peridotites with fluids and melts released from the subducted plate caused an extensive melting of the (probably already depleted) MORB source. As well, the interaction processes resulted in the described enrichment of source lherzolite in more incompatible elements (e.g. REE). The lateral evolution of the clear MOR-type to the SSZ-type of the geotectonic setting within the scope of the Krivaja-Konjuh ophiolite suite, suggests a localised influence of hydrous melting, leaving large areas of a pristine MORB source unaffected. A similar composite development of contrasting geotectonic regimes has been reported elsewhere within the suite of Mediterranean ophiolites (e.g. Albania, Turkey and Greece, Robertson et al. 2009, Koepke et al. 2002).

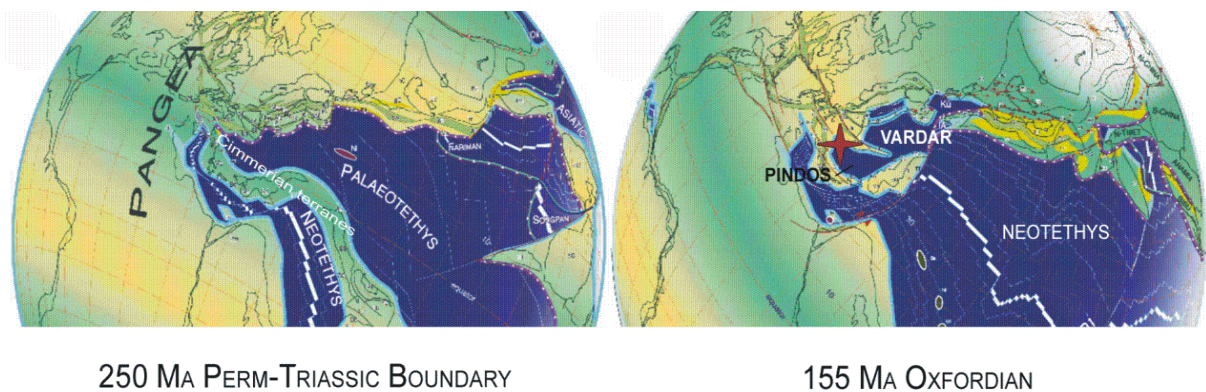


**Fig. 71.** Paleotectonic and paleogeographic reconstruction of the Tethyan development; Permian-Triassic boundary (250 Ma) (left) and Oxfordian (Late Jurassic, 155 Ma) (right). The red cross indicates the approximate position of the KKOC within the Dinaridic part of the Pindos ocean. Reconstruction after Stampfli and Borel (2004).

The SSZ geochemical imprint of the eastern KKOC mantle domain referred above should not be brought in connection with the formation of plagioclase-bearing lherzolites that compose much of the western Krivaja segment of the KKOC. As it was discussed in detail in the previous chapter, the processes of plagioclase formation are strictly bound to a subsolidus metasomatism of the shallow lithospheric mantle. This area is, according to the modelling of Niu (2004), also known as a thermal boundary layer (TBL). Considerable KKOC mantle heterogeneities, reflected in the existence of two peridotite mineralogies (spinel and

plagioclase Iherzolites), are characteristic for the MOR-type lithosphere generation coupled by an extensive interaction between the MORB source and percolating melts or fluids.

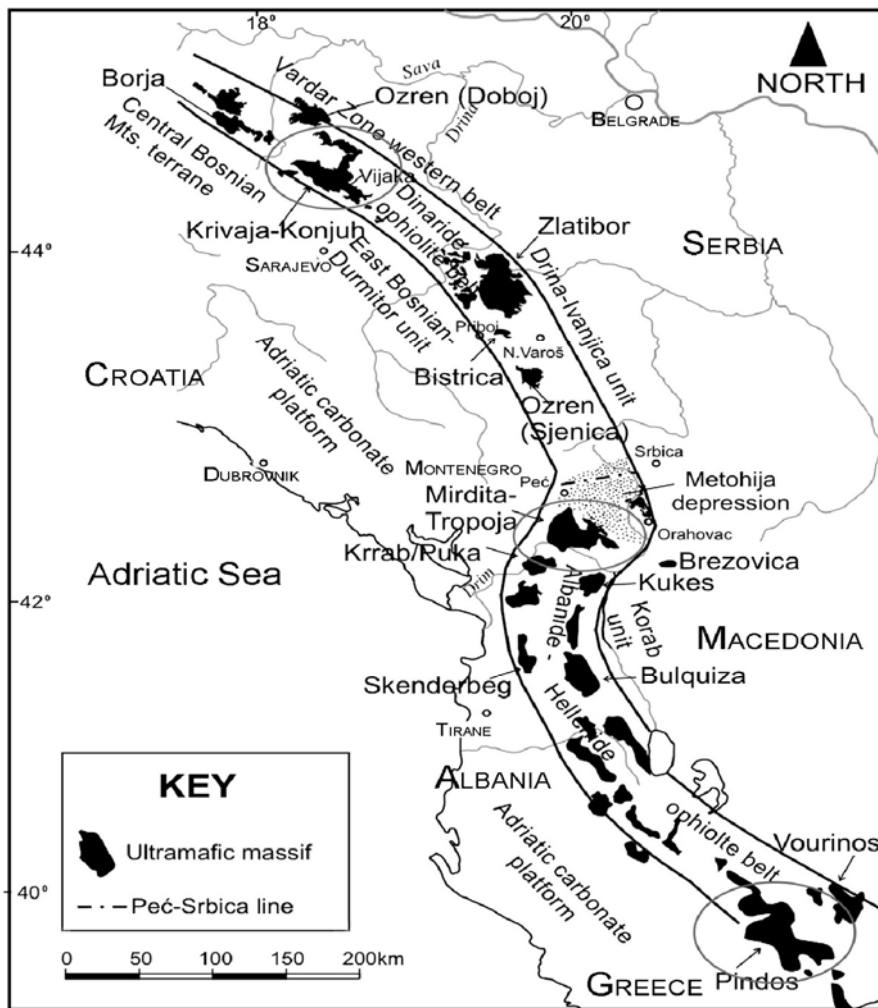


**Fig. 72.** Main ophiolitic complexes of the CDOB in Bosnia-Herzegovina and Serbia, the Mirdita zone in northern Albania and the Pindos zone in Greece. These ophiolitic complexes form the remnants of the Tethyan Pindos Ocean. Ophiolitic units of the Vardar belt are omitted. Modified after Robertson et al. 2009.

In order to have a complete understanding of the genesis and development of the Krivaja-Konjuh Ophiolite Complex, geodynamic modelling in the geological time and context is required. In the late Permian, a decomposition of Pangea took place, initiating an opening of the Neotethyan Ocean coupled by the detachment of the Cimmerian terranes and their subsequent northwards motion (Fig. 71). The most western parts of the Cimmerian terranes were composed of various microplates (Apulia, Adria, Ionian and western-Crete) (Stampfli and Borel 2004). In the following 40 Ma, the Neotethyan oceanic domain replaced the Palaeozoic Palaeotethyan Ocean, leading to the opening of many back-arc type oceans along the northern Palaeotethys suture zone (i.e. Maliac, Pindos and Vardar). Due to their Triassic to Jurassic age, those oceanic zones are often referred as part of the peri-Gondwanian Neotethyan Ocean, although, according to Garfunkel (2004) and Stampfli and Borel (2004), they were not in direct geological nor geographical connection. A middle Permian siliciclastic unit, ~ 1000 m thick, is found exposed at the locality of Mrzle Vodice in NW Croatia. It comprises deep-sea sediments, including black cherts, dated to be of Pennsylvanian and early-mid Permian age, as well as conodonts of the Carboniferous age.

According to Aljinović and Kozur (2003), this represents a fragment of a Eurasian fore-arc basin that collided with Adria, when Palaeotethys closed in middle Permian time, prior to the opening of marginal back-arc basins along the northern Palaeothetyan suture (i.e. Dinaric Tethys or Pindos).

Bearing in mind the KKOC petrological and geochemical characteristics, especially concerning the metamorphic sole formation and composite nature of peridotites, having both MOR-like and SSZ-like parts, striking similarities between the KKOC and ophiolitic masses of the rest of the CDOB (Bosnia, Serbia, Bazylev et al. 2009, Lugović et al. 1991), the western Mirdita (Albania, Nicolas et al. 1999), Pindos (Greece, Robertson 2002) and Crete (Greece, Koepke et al. 2002) are to be drawn. This allows one to constrain the Bosnian CDOB oceanic realm, and its sigmoidal SE prolongation in Albanides and Hellenides to present remnants of the Pindos Ocean seafloor (Fig. 72). Having this in mind, the position of the KKOC within the Late Jurassic Tethyan development was marked in red (Fig. 71), pointing to the most westwards branch of the Pindos oceanic basin.

### **6.2.2. Pyroxenites, dunites, and chromitites**

The Krivaja-Konjuh olivine websterites are reported to crop out at the Žepče locality along the canyon of river Ograjna, where minor pyroxenite lenses (up to 20 cm wide) are found, associated with dominant fresh plagioclase lherzolites. The contact between these lithologies is sharp and non-diffuse, and both rocks share common textural characteristics which correspond to the emplacement and/or post-emplacement period. Such a transition pattern between two rock-types may serve as the first indication of infiltration of pyroxenite nascent fluids and an ensuing joint geological evolution. The Žepče ultramafic domain represents the most western and detached segment of the Krivaja-Konjuh ophiolitic complex, being tectonically displaced from the main peridotite mass in Palaeogene (Pamić et al. 1977, see Chapter 3.3, Fig. 4).

The pyroxenite mineral paragenesis is mainly composed of big euhedral grains of both pyroxenes, which defines a recondite cumulate texture, largely obscured by extensive plastic mantle deformation. The porphyroclasts' inner space is filled by small to medium-grained mosaic olivine, and rarely by spinel. Occasionally, plagioclase is formed around coarser spinel grains, where it is found completely altered. Rarely one can notice embryonic agglomeration of hydrous garnet, grown alongside pyroxene planes, together with sporadic chlorite occurrences. Both phases are ascribed to later subsolidus processes. For more details on the Krivaja-Konjuh petrography the reader is referred to Chapter 4.2.1.6., Table 2, Figs. 10h, 11d, 11e.

Pyroxenite mineral chemistry shows a great similarity to those of plagioclase and spinel lherzolites. Only an elevated Ti content of clinopyroxene in one sample makes a difference and it is prescribed to small quantities of trapped melt (see Chapter 4.2.2.3., Fig. 18). Major element chemistry reveals that in comparison with an average basalt composition (PetDB database), the analysed pyroxenites are depleted in Si, Ti, Al, Fe, P and alkalis, while they possess more Mg and the same amount of Ca. The Mg# value fits the peridotite range (89.4 and 89.5). Such correspondence is taken in favour of a pyroxene and host peridotite cogenetic evolution in terms of the common mantle processes. A set of correlation diagrammes between certain major and trace elements vs Mg# value (Figs. 55 and 56,

Chapter 5.1.2.) yields a high resemblance of the analysed pyroxenites and western Alpine layered websterites, alike those of the Lanzo ophiolite in Italy or the Ronda massif in Spain. The mechanism established as the most liable for the formation of Alpine pyroxenites is defined as segregation of partial melts from the associated host peridotites (e.g. Voshage et al. 1988, Bodinier et al. 1986a, b). Both the chondrite-normalised REE patterns, and the trace element spider diagrammes of the Krivaja-Konjuh pyroxenites, are comparable to those of neighbouring lherzolites (see Chapter 5.1.2.), revealing significantly higher concentration levels (especially HREE).

The origin of pyroxenite is still highly debatable, supporting a broad range of hypotheses that are occasionally mutually complementary. According to Bodinier and Godard (2003) and Downes (2007), the following processes were recognised as most liable explaining the genesis of mantle pyroxenites: (1) high-pressure (cumulus) crystal precipitation, (2) recrystallisation of subducted oceanic crust, and (3) metasomatic replacement of peridotites. The first process comprises in-situ precipitation and dissolution of pyroxene within host peridotites (e.g. Chen et al. 2001), as well as crystal precipitation (accumulation) from silicate magmas passing through the lithosphere. The former process is advocated as the mechanism yielding pyroxenites recovered from Alpine ophiolites and recent ocean-ridge domains (e.g. Shervais 1979, Frey 1980, Dantas et al. 2007). Recrystallisation of the subducted crust is a complex mechanism. It may encompass a partial incorporation of subducted slab into the lithosphere due to the mantle convection (e.g. Pamić 1977a, Allegre and Turcotte 1986, Gjata et al. 1992), but pyroxenites may also result either from melts originated from subducted oceanic crust (e.g. Pearson et al. 1993), or represent residuum from such subduction-related melting (e.g. Blichert-Toft et al. 1999). The last process of metasomatic replacement is often referred to the formation of pyroxenites in the entrapped supra-subduction mantle wedges. Either a metasomatism took place during an incipient evolutionary phase of intra-oceanic subduction (e.g. Garrido and Bodinier 1999), or mantle pyroxenites were affected by impregnation fluids after the ophiolite emplacement (e.g. Lenoir et al. 2001). In both cases, the pyroxenites record diverse isotopic compositions with respect to the host peridotites, and mostly depict a positive Eu anomaly. Taking into account presented models of mantle dynamics, which yielded ophiolite pyroxenites, but also the structural and textural relationship of pyroxenites and host peridotites, one can further classify them as (Bodinier and Godard 2003): (a) dikes and veins, (b) replacive pyroxenites, and (c) deformed pyroxenites. Dikes and veins are presented with a variety of (ultra)mafic lithologies, which crystallised in magma conduits from deep-seated parental melts. Such melts are not related to host peridotites, occasionally having a boninitic origin (e.g. Oberger et al. 1995). Pyroxenites that emerge as swarms or elongated lenses in harzburgites and dunites are featured by a virtual lack of deformation. They belong to the group of replacive pyroxenites. Their origin is interpreted through the replacement of peridotite by invasive melts (e.g. Kelemen et al. 1995). Like dunites or clinopyroxene-rich peridotites, they possess a convex-upward REE pattern. Deformed pyroxenites decipher characteristic plastic deformations, indicative for neighbouring mantle peridotites. Furthermore, their geochemical characteristics are analogue to those of peridotites. These pyroxenites are believed to have formed through several different processes, such as partial melt segregation, melting of pre-existing garnet pyroxenites, or through re-crystallisation and/or metasomatism of crustal

material (e.g. Lenoir et al. 2001, Obata and Niida 2002). Based on the geochemical data presented in the introductory paragraph, and on relevant textural indications, the Krivaja-Konjuh olivine websterites roughly correspond to the last group of deformed pyroxenites. Still, all liable hypotheses will be tested, and further discussion will provide lines of evidence to define a plausible evolutionary model confined by the scheme of this classification.

The appearance of pyroxenite lenses within the Krivaja-Konjuh ophiolite is not an isolated occurrence in the Dinarides, nor is it in the neighbouring ophiolitic terrains. The following authors reported on pyroxenite rocks throughout the CDOB (Fig. 3), as for instance in the following ophiolitic complexes: Skatavica (Pamić 1985), Borja (Pamić and Majer 1973), Bosanski Ozren (Trubelja and Pamić 1965), and Zlatibor-Varda (Popević and Pamić 1973, Milovanović 1988). Most of the mentioned works treat metamorphic rocks, only sporadically providing petrological descriptions of pyroxenite occurrences. Moreover, in early Yugoslavian literature, metamorphic sole rocks were often considered as pyroxenites. A comprehensive geochemical study of garnet pyroxenites from the Solila locality in the Borja complex (Fig. 3; ~ 10 km from the pyroxenite occurrence analysed in this study) is provided by Majer et al. (2003). These rocks show no similarity with the Krivaja-Konjuh pyroxenites, since they are virtually devoid of orthopyroxene, and garnet often emerges as coarse porphyroblast or – clast having kelyphitic coronas. Additionally, the whole-rock chemistry of these rocks corresponds well to Al-rich mafic rocks. The authors advocate that mantle-derived melts yielded the Solila pyroxenites via high-pressure crystal segregation. Their microtextural characteristics, along with the conspicuous mineral chemistry of garnet and amphibole, might have suggested different pyroxenite genesis (i.e. metamorphic origin). Garnet pyroxenites are also known from breccias, which have originated from the Mirdita ophiolite pile at Derveni, Albania (Gjata et al. 1992). The Albanian ophiolite terrains are quite similar to those of the Dinarides and both share a partial joint development within a single oceanic realm (e.g. Robertson et al. 2009). The Derveni pyroxenites are high-temperature and –pressure rocks (ca. 1200 °C, 1.5 GPa), containing garnet, spinel and both pyroxenes, whereas their mantle porphyroclastic texture shows high similarity to those of the Krivaja-Konjuh pyroxenites. The authors have proposed that the hydrothermally altered ocean-floor gabbroic rocks were entrained in the subduction cycle by the ocean contraction leading to re-crystallisation of the oceanic crust at an asthenospheric level with subsequent formation of garnet pyroxenites. Thereafter, the whole ophiolite suite was uplifted by obduction. This genetic consideration is excluded as plausible for the Krivaja-Konjuh pyroxenites due to their pronounced ultramafic chemical provenience (see later discussion), but is highly indicative for the understanding of metamorphic rocks associated to the Mediterranean ophiolites (see Chapter 6.3.2.).

The Krivaja-Konjuh pyroxenites are suggested to have formed under high pressures at deeper asthenospheric levels. It is notably invoked by the lack of primary plagioclase, and high total Al<sub>2</sub>O<sub>3</sub> in clinopyroxene (ca. 4–7 wt%) and orthopyroxene (ca. 2–5 wt%). Furthermore, the extensive plastic deformations, which include grain-size reduction at the boundaries of larger pyroxene grains, introduced the development of a fine- to medium-grained mosaic texture with well-developed 120° triple junctions. These tend to be diagnostic of the textural equilibrium and static recovery at high temperatures above 1000 °C (Mercier and Nicolas 1975). In one of the analysed samples, of spinel breaks down,

which leads to the appearance of plagioclase coronas, presently being completely altered (Fig. 11e). Such subsolidus equilibration usually occurs at ca 0.7 GPa and 1000-1250 °C, roughly corresponding to the plagioclase-spinel transition zone (Gasparik 1984).

The petrogenetic mechanisms invoked to have operated during the formation of garnet pyroxenites in Bosnia and Albania (Majer et al. 2003 and Gjata et al. 1992 respectively) are crystallisation from mafic melts, in-situ segregation and oceanic crust recrystallisation. These processes tend to be unsuitable in the case of the Krivaja-Konjuh pyroxenites. The whole-rock chemistry of the analysed rocks is defined by higher MgO (ca. 25-28 wt%) than is reported in any mafic melts (Downes 2007). Besides, the analysed pyroxenites have much lower TiO<sub>2</sub> and Al<sub>2</sub>O<sub>3</sub> contents than basaltic (MORB) melts, which make it very hard to believe that they represent the reworked oceanic crust.

Mg# values of pyroxene and olivine are around 90 (see Chapter 4.2.2.), and this is not encountered even in the most primitive basaltic melts. On the other hand, such Mg# tend to be consistent with those reported in primitive mafic cumulates from ocean-ridge domains (e.g. Dantas et al. 2007). In the CaO/Al<sub>2</sub>O<sub>3</sub> and Ni vs MgO diagrams (Fig. 73), pyroxenites of Krivaja-Konjuh greatly match with data of the western Alpine pyroxenites, as it was pointed out before (see Chapter 5.1.2.), while, at the same time, they lie away from the area of the oceanic crust. A closer inspection of the diagram reveals that pyroxenite projections are found close to the peridotite-MORB melting trend, but also they coincide with the clinopyroxene-orthopyroxene junction. Although, there are a small number of samples concerned, this suggests that the stress-induced small-scale pyroxene enrichment might have played a role in the formation of the Krivaja-Konjuh pyroxenites.

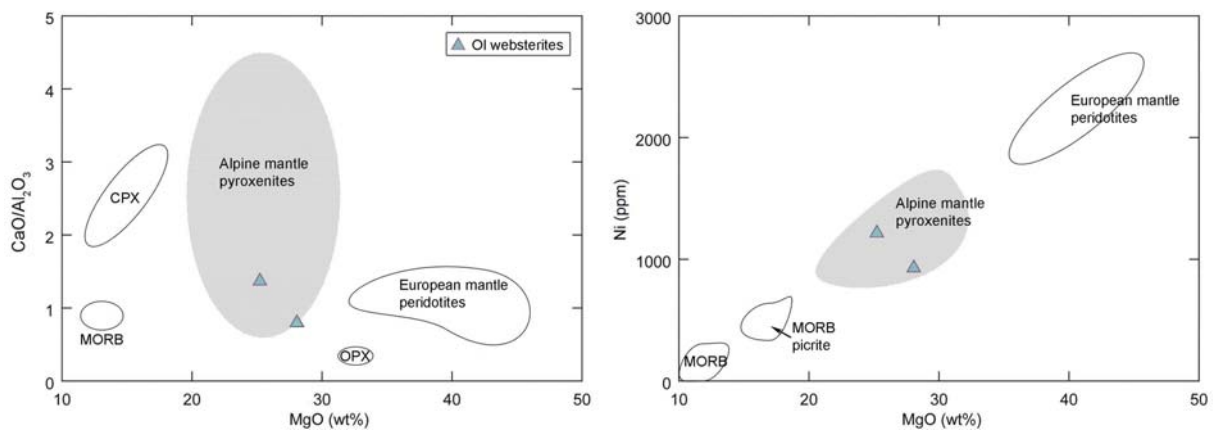


**Fig. 73.** CaO/Al<sub>2</sub>O<sub>3</sub> and Ni versus MgO diagrammes for the Krivaja-Konjuh mantle pyroxenites (olivine websterites). Comparison with similar rocks reported from the western Alpine ophiolites as well as with medium composition of clinopyroxene, orthopyroxene, average MORB, MORB picrite and European mantle peridotites. Data from: Alpine pyroxenites (Bodinier 1988, Garrido and Bodinier 1999, Downes 2007), MORB and MORB picrite (Sun and McDonough 1989, Elthon 1989), European mantle peridotites (Downes 2001). CPX and OPX = phase mineral compositions in pyroxenites (same authors as for Alpine pyroxenite whole-rock chemistry).

The final evidences opposing the origin of these pyroxenites from mafic melts or reworked oceanic crust are offered in the REE and trace element geochemistry. Their absolute concentrations are far below MORB or oceanic crust estimates (Chapter 5.1.2.).



Furthermore, the primitive mantle normalised trace-element diagramme (see Chapter 5.1.2.; Fig. 57) depicts unclear negative anomalies in certain HFSE (e.g. Hf) and a highly pronounced variation in LILE enrichment. Such a trace-element distribution is not expected in mafic melts (Downes 2007). A lack of any Eu anomaly corroborates the absence of plagioclase within the pyroxenite primary mineralogy. At present, one can exclude a formation of the analysed pyroxenite rocks through metasomatic enrichment as part of subduction-related processes, since such rocks display significant LREE enrichment ("bell"-shape REE pattern, i.e. reported in Cabo Ortegal massif in NW Spain, Santos et al. 2002).

In spite of the relatively small number of analysed samples of the Krivaja-Konjuh pyroxenites, clear geochemical evidences stated above, unambiguously imply a different genetic history than proposed for similar rocks from the region. Their REE pattern is markedly LREE depleted, having lower absolute concentrations than any mafic melt, but approaching the concentrations and pattern-shape of the analysed Krivaja-Konjuh lherzolites (see Chapter 5.1.1.). Hence, it is suggested that the analysed pyroxenites are cumulates, crystallised from primitive large-degree partial melts. The cumulate origin was tested with regard to the main and trace element pyroxenite geochemistry (MgO-CaO-Al<sub>2</sub>O<sub>3</sub> and Cr-Ni diagrammes of Coleman (1977) and Irvine and Findley (1972) respectively; see Chapter 5.1.1.), where both suggested discrimination criteria unambiguously define them as ultramafic cumulates. The parental pristine melts are further characterised by high values of Mg# in olivine and in clinopyroxene crystallites (see Chapter 4.2.2.), which is reported as characteristic for primitive cumulates of MOR areas. Moreover, the high Al content of both pyroxenes is indicative for the crystallisation of high-pressure cumulates, since at lower pressure plagioclase would have emerged as primary phase. The MREE/HREE content of analysed rocks converges into those of MORB picrite, but with reduced LREE concentrations. It gives rise to the deduction that parental melts of the Krivaja-Konjuh pyroxenites represent extensive melt fractions (~ 10 % mantle source melting), produced from peridotites that have already undergone a low degree of partial melting. The theory of deep-seated cumulate crystallisation which explains the analysed pyroxenites, is further recognised in the characteristic coarse-grained cumulate texture of analysed rocks (Chapter 4.2.1.6.) featured by high-temperature low-stress plastic deformations, suggesting that the crystallisation and equilibration of pyroxenites occurred whilst the host rocks were still hot and ductile (Dantas et al. 2004).

The presented discussion leads to the conclusion that the Krivaja-Konjuh pyroxenites are deeply originated ultramafic cumulates, crystallised at high pressures and temperatures, through high-degree partial melting of an already depleted MORB mantle source. It is suggested that crystallisation took place in thermal conduits, located under the ocean ridge system, where significant cooling of conductive melt takes place. The fact that clinopyroxene found in the analysed rocks has the same (elevated) Ti and Na contents as the host plagioclase lherzolites (see Chapter 4.2.2.3.; Fig.18), is believed to indicate that both rocks experienced a common impregnation history which is bound to the late-stage of ocean-ridge development (see Chapter 6.2.1.3.). Reconciling this and clear mantle textural features possessed by both lithologies, the formation of the analysed pyroxenites is constrained to an incipient phase of the MOR evolution of the Krivaja-Konjuh oceanic domain, which took place

in early Jurassic. These pyroxenite occurrences are an important factor, proving pronounced sub-continental dynamics, especially knowing that the pyroxenite domains, due to their comparably lower melting values, are more prone to generate various mafic melts (e.g. Tuff et al. 2005). The mafic rocks are reported as abundant within the Krivaja-Konjuh ultramafic terrain, showing a wide range of lithologies (e.g. Babajić 2009). In order to ascertain the proposed petrogenesis of the Krivaja-Konjuh pyroxenites and to shed light on the role of small-scale pyroxene enrichment, it is essential to extend the number of analysed pyroxenites in future works, and besides the detailed geochemical analyses, to pursue a comprehensive isotopic study as well.

Dunites are recovered from two opposite points of the Krivaja-Konjuh ophiolite complex, at sites Duboštica and Karaula. Both occurrences depict similar cumulate textures and modal mineralogy, which contains major olivine (~ 90 vol.%) and some minor clinopyroxene, spinel, altered plagioclase, along with the secondary phases like amphibole, chlorite, hydrogarnet, and prehnite (see Chapter 4.2.1.7., Table 2, Fig. 10b). Major element geochemistry defines these rocks as depleted in SiO<sub>2</sub>, MgO, and Na<sub>2</sub>O, and slightly enriched in Al<sub>2</sub>O<sub>3</sub>, FeO and water, compared to the surrounding lherzolites. The REE pattern possesses a concave-upward "U"-shaped form with a clear positive Eu anomaly, whereas the primitive-mantle normalised spider-diagramme of trace elements deciphers only a slight variance in comparison to those from plagioclase and spinel lherzolites (see Chapter 5.1.2., Table X-1–X-2). Again, it is important to stress that a small lens of podiform refractory chromite is associated to the Duboštica dunite body (see Chapter 4.2.1.8., e.g. Sunarić-Pamić and Olujić 1968, Popević 1971). On the other hand, a second dunite sample is taken from the Karaula area of SE Konjuh (Fig. 4), which is featured by mantle peridotites, having a strong positive Eu anomaly along with the "U"-shaped REE pattern at a normalised concentration level, typical for metasomatised peridotites (Lugović et al. 2006). Moreover, the nearby locality of Muška Voda is dominated by spinel lherzolites marked by the growth of metasomatic amphibole, and the occurrence of a high chromian spinel (Cr# ~ 50) (see Chapters 4.2.1.2. and 4.2.2.4., Fig. 73).

In literature, the origin of dunites and other refractory ultramafic rocks has often been ascribed to the high-degrees of partial melting of the undepleted (or moderately depleted) mantle sequence (e.g. Johnson and Dick 1992). In order to produce orthopyroxene free dunites, like the analysed ones, more than 60% of melting of MORB-source mantle would be needed (Kostopoulos 1991). Since the values of mantle melting established for neighbouring peridotites do not exceed 10%, it is unlikely to expect that even the multi-stage process of mantle segregation could yield such, spatially limited, melting record (see Chapter 6.2.1.2.). Even if it were possible, the impoverishment of REE and other incompatible elements would be apparent. The analysed dunites are, on the contrary, REE enriched, which together with the fact that dunite Mg-number is actually lower than in peridotites, rule out the hypothesis of simple mantle melting as a liable explanation of dunite formation.

As a possible answer to the question of dunite origin by invasive melt percolation was first advocated by Dick (1977) and Berger and Vannier (1984). They pointed out that dunites found in contact with lherzolites are characterised by a comparatively lower Mg# value as well as lower Fo content of olivine. The same trend is reported in the Krivaja-Konjuh

dunites (see Chapter 4.2.2.1.). It is known that basaltic melts during their ascend into shallower mantle portions tend to become orthopyroxene undersaturated, due to their instability at lower pressures (Stolper 1980). Thereupon, such melts being out of equilibrium with peridotites, completely dissolve orthopyroxene and change the clinopyroxene content of affected mantle rocks (e.g. Kelemen 1990, Kelemen et al. 1992, Remaidi 1993, Oberger et al. 1995). This process is known as 'orthopyroxene incongruent melting' resulting in the precipitation of olivine and the formation of silica-enriched melts (orthopyroxene = olivine + SiO<sub>2</sub> rich melt). Besides these modal mineralogy changes, the impregnated rocks are also enriched in incompatible elements, which is best reflected in the high LREE or accentuated bulk rock and interstitial clinopyroxene Ti content (see Chapter 4.2.2.3.). Furthermore, the Mg# of infiltrated rocks along with the Fo content of its olivine remains unchanged or even becomes lower. Since in the Krivaja-Konjuh dunites values of both parametres have been indeed attenuated, one can, based on the Kelemen (1990) modelling, conclude that a quantity of extracted magma from the percolated lherzolite is smaller in comparison to the initial amount of entering fluid. This phenomenon commonly occurs in situations when affected peridotite is (much) colder than the invasive fluid (Oberger et al. 1995), thus inciting partial crystallisation of the melt in form of hydrous phases, like amphibole or hydrogarnet (see Chapters 4.2.1.7. and 4.2.2.6.). The presented line of evidence implies the formation of the Krivaja-Konjuh dunites at relatively shallow and cold lithospheric levels (the uppermost part of the dunite transitional zone). Tectonic settings favourable for the generation of hydrous, highly magnesian pervasive fluids of basaltic (boninitic) composition are the supra-subduction zones where released volatiles promote formation of melt, capable to infiltrate the large volume of peridotites.

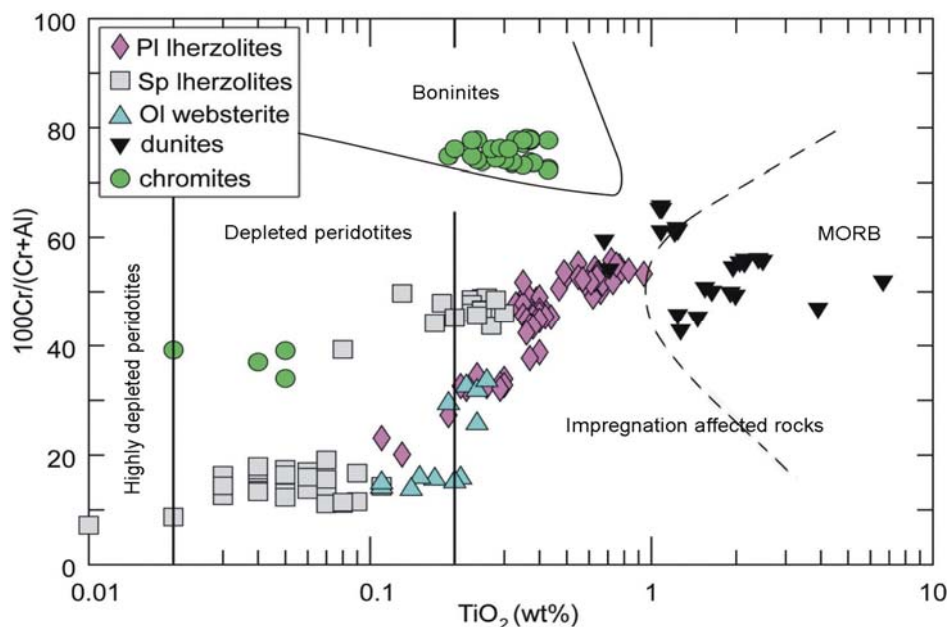


**Fig. 74.** Cr-number versus TiO<sub>2</sub> (wt%) values of chromium spinel. The diagram depicts the entire ultramafic rock suite of the Krivaja-Konjuh ophiolite complex

Not only the geochemical signatures of the dunites witness a melt-rock interaction. It is also recognised in spinel microtextural characteristics. In lherzolites, spinel commonly occurs in form of small amoeboid or skeletal grains, often having different holly-leaf lobated shapes (see Fig. 11b), whereas in dunites spinel grows and coalesces as coarser, massive euhedral

grains (see Fig. 11e). Nicolas and Prinzhofer (1983) have reported this morphological change as accustomed in transitional zones of several ophiolite massifs, and Bussod and Christie (1991) have experimentally shown the same transition in mantle lherzolites affected by capillary silicate melt.

In order to extend the discussion on the genesis of the Krivaja-Konjuh dunites, I further refer to its incompatible element content, whereby high abundances argue against the MORB-mantle melting model as the exclusive model for the formation of the analysed dunites. High LREE/MREE ratios strongly corroborate it. In the recent literature, such REE proportioning is explained by melt-rock interaction, as Takazawa et al. (2003) suggested for the Oman ophiolites, which are marked by a pronounced REE “U”-shape pattern. This REE behaviour defines refractory dunites and harzburgites, and it is believed to reflect the rock’s partial melting, accompanied by fluid impregnation processes (e.g. Suhr et al. 1998). The chromitite body associated with the dunite occurrence at the Duboštica locality is characterised by an elevated Cr proportion in spinel ( $Cr\# \approx 80$ , Fig. 74). Such values point to subduction-related melts, most probably boninitic, as parental to this mineralization (see Chapter 4.2.2.4., Fig. 74). Boninitic melts are known to possess a “U”-shaped REE normalisation pattern (Zhou et al. 1996), thus being positioned as crucial for the formation of the Duboštica chromites as well as dunites, since both parageneses share the same REE geochemical signatures (see Chapter 5.1.2.). Distinct positive Eu anomalies reported in the analysed dunites, but also in depleted harzburgites of SE Konjuh (Lugović et al. 2006), are consistent with a late-stage mantle metasomatism, which gave rise to small amounts of plagioclase, prone to host Eu in its crystal structure. The relationship of Cu and Ni in dunites is, as proposed by Zhou et al. (2005), very informative for the identification of the percolating melt type. In mantle rocks, Cu is hosted in chalcopyrite, and since the invasive boninitic melts are known as sulphur undersaturated, they readily dissolve sulphides, thus removing Cu from the system. Along with this process, Ni as a compatible element is progressively enriched. This is nicely depicted in Fig. 54, where the Krivaja-Konjuh dunites presented in the Cu-Ni space, are shifted away from the peridotite field, mainly due to Cu depletion and in lesser extent to the enrichment of Ni (e.g. Lorand et al. 1993, Keays 1995). The influence of boninitic melts can be further traced in the  $Al_2O_3$  content of chromitite interstitial clinopyroxenes, being half of those in neighbouring lherzolites (~ 1.3 wt%).

The massive dunite occurrences coupled with chromitite pods are characteristic for the crust-mantle border zone, better known as the transition zone. This dunite-dominated unit is used to be known as the deepest part of the magmatic sequence, and its ultramafic content was interpreted as cumulate originated (Coleman 1977). On the other hand, starting with Dick (1977), Nicolas et al. (1980) and others, a theory of the dunite residual origin coupled with melt impregnation processes, has commenced to be advocated as favourable. Indeed, the Krivaja-Konjuh dunites recovered from both localities are featured by a cumulate texture (see Chapter 4.2.1.7.), where olivine and spinel tend to be cumulus phases, whereas in the intercumulus interstices, one can notice altered plagioclase, clinopyroxene, and secondary phases, like amphibole, hydrogarnet and chlorite. This may indicate that the analysed rocks actually represent the uppermost part of the transitional zone formed by crystal fractionation from the crustal magma chamber. However, due to the set of presented

geochemical, mineralogical and textural evidences, it is more likely that this process was followed by a sizable melt-rock metasomatism. Initially, the chromitites segregated from the invading (boninitic) melt, which subsequently percolated neighbouring rocks, producing dunites and harzburgites. Highly metasomatized harzburgites are not reported to be associated with the dunite occurrence of Duboštica. They are reported in the vicinity of Karaula, the second sampling spot of Krivaja-Konjuh dunites (Lugović et al. 2006). If this model holds true, it is expected that the future work on Duboštica ultramafics will also confirm the presence of impregnated harzburgites as the third member of the rock suite, formed from or in interaction with invasive melts.

A model that summarises the formation of the Krivaja-Konjuh dunites and chromites fits the geotectonic frame provided for the genesis of predominant tectonite peridotites (see Chapters 6.2.1.1. and 6.2.1.3.). Thus, only facts pertaining to the dunite and chromite formation will here be underlined. In the Oxfordian, when the initial shortening of the Dinaride oceanic segment took place (~ 157 Ma) (Lanphere et al. 1975), the previously formed MORB (or back-arc related?) Neo-Tethyan lithosphere started to contract. Within the Krivaja-Konjuh oceanic domain, this process invoked the incipient low-angle thrusting as the Krivaja lithospheric segment has overridden the Konjuh lower-plate, thus enabling the analysed metamorphic sequence to form (see Chapter 6.3.). Further thrusting led to an extensive metasomatism of the trapped Krivaja mantle wedge by fluids released from the submerged lower-plate. Alongside, in the metasomatized wedge, the hydrous basaltic (boninitic) melts were produced. On their way to the surface, through tectonic predisposed areas, they reached a colder domain of crust-mantle transition, where the mantle flow changes from vertical to horizontal as suggested by Zhou et al. (2005). The invading melts reacted with peridotite rocks, which was explained earlier, triggered the chromitite segregation and the subsequent dunite envelope formation of the Duboštica locality. For dunite recovered from the Karaula locality, an analogue scenario is predicted. The Konjuh segment is less metasomatized compared to the Krivaja counterpart, but its SE part was also subject to serious metasomatism. It is recognised in form of the Karaula dunite, amphibole-bearing lherzolites, along with IAT and "U"-shaped REE harzburgites and boninitic dykes. Most probably the Konjuh lithospheric domain has been affected by a similar type of metasomatism, initiated from the hypothetical submerged ocean domain placed somewhere eastwards. The roots of such a domain were completely consumed as the ocean shortened, or were not preserved during late Tithonian ophiolite obduction over the Adriatic platform. Within the Konjuh transition zone, the boninitic melt rock interaction was not comprehensive enough to trigger the chromitite segregation, or the chromitite pods are comparably smaller and being not detected yet.

The chromitite extraction itself, characteristic for the formation of the Duboštica chromite body, follows a model proposed by Zhou et al. (1996) and Kelemen et al. (1990). Due to the pyroxene removal from the peridotite rocks affected by the invasive fluids, the silica content of melt increases, as it was discussed above. Thus, melt becomes more boninitic, which is reflected in its lower Mg/Si ratio, whereas the Mg/Si and Al/Si ratios of the new-formed dunite increase (Fig. 75). The dunites' Al content tends to keep the same

values as in peridotites, whereas the variable Al/Ca ratio is due to various serpentinisation degrees causing Ca depletion (Fig. 75).

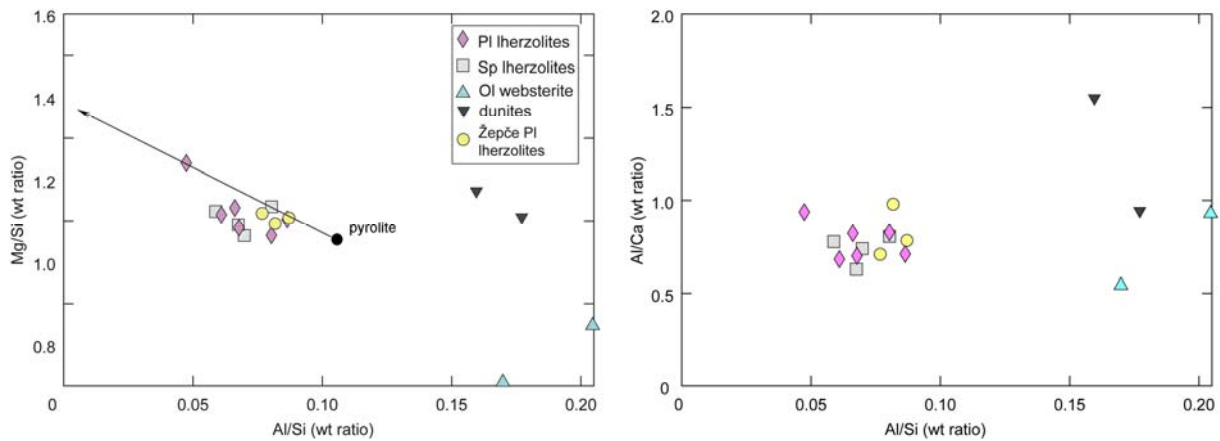


**Fig. 75.** Al/Si versus Mg/Si (left) and Al/Ca (right) of ultramafic rocks of the Krivaja-Konjuh ophiolite complex. Mantle ratios are: Al/Si = 0.1; Al/Ca = 0.95; and Mg/Si = 1.09 (after Jagoutz et al. 1979, Zhou et al. 2001).

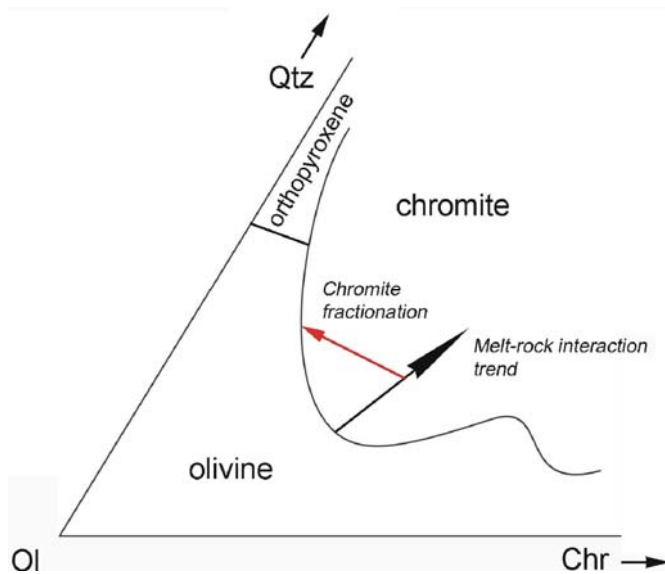


**Fig. 76.** Simplified scheme after Zhou et al. (1996) depicting the olivine-quartz-chromite system and its phase relations (Irvine 1977). Black arrow deciphers how primitive (boninitic) magma changes through the host-rock interaction entering chromite stability field thus precipitating monomineralic chromite. Red arrow indicates return of the crystallising liquid toward olivine-chromitite cotectic as chromite mineralization advances.

Such a Si-enriched, and Ca-impoverished boninitic melt, having only a small Cr content, is actually able to generate monomineralic chromitite pods or layers. One explains it through an approximation of the chromitite parental melts by the olivine-quartz-chromite system of Irvine (1977) (Fig. 76). The primitive magma reacts with host rocks, thus entering the chromite stability field. The chromitite precipitates for some period, changing the composition of liquid toward the olivine-chromitite cotectic. In case the new primitive magma is being introduced to the system, further chromitite crystallisation is sustained. Otherwise, the dunite envelopes and depleted harzburgites that are often associated are formed.

## 6.3. Petrogenesis of metamorphic rocks

### 6.3.1. Protolith and its original geotectonic setting

The Krivaja-Konjuh ophiolite complex (KKOC), being composed of two major individual peridotite blocks, is featured by an elongated domain of metamorphic rocks, which is placed along the blocks' junction zone. The northern parts of the domain are formed from small, dismembered patches of metamorphic rocks, whereas the main metamorphic portion is found along the southern rims of the KKOC, constituting the large Duboštica and Vijaka amphibolite zones. A variety of metamorphic paragenesis, textures and structures have been recognised within this metamorphic terrain. Textures are characterised either as crystalloblastic, defined by the grano- to nematoblastic amphibole and clinopyroxene, or porphyroblastic, in case of the garnet porphyroblasts' presence. The rock structures are more often than not parallel, showing an alternation of 'white' and 'black' rock segments. Rarely, in the northern and central parts of this domain, one encounters rocks having massive (homogeneous) metamorphic structures. Besides complex textural and structural characteristics of analysed rocks, they depict rich and mutually different modal mineral paragenesis, thus reflecting discrepancies in the protolith geochemistry, as well as different conditions of metamorphism. Based on the classification criteria proposed by Yardley (1989), which include rock's texture, structure, modal mineralogy, and foreseen precursor, the following metamorphic varieties were assigned as: (1) granoblastic amphibolite, (2) porphyroblastic garnet-diopside amphibolite, (3) garnet-diopside-hypersthene amphibolite, (4) diopside-amphibole gneiss and plagioclase-garnet-diopside gneiss. The first three rock varieties are further divided, according to minor mineralogical particularities. This classification of the KKOC metamorphic rocks is however not territorial, meaning that the provided groups are not exclusive metamorphic lithologies in certain areas. Still, it needs to be noted that rocks devoid of garnet are more characteristic for the northern and central portions of the Krivaja-Konjuh metamorphic terrain (e.g. areas of Manastir, Žepče, Maoča). Reader interested in more details on the petrography of these rocks is referred to Chapter 4.3.1.

In Chapter 5.2., the bulk chemistry of metamorphic rocks was discussed, yielding a detailed classification of analysed rocks with respect to their major, trace, and rare-Earth elements' content. Furthermore, several lines of conclusions were made on the nature of the possible protolith. Due to the fact that metamorphism, including the upper segment of amphibolite and granulite facies is taken as an isochemical process (e.g. Vernon and Clarke 2008), it was inferred that two-thirds of the analysed metamorphic rocks bear geochemical signatures of ultramafic to mafic cumulate gabbroic rocks (Groups 1 and 3), whereas the rest corresponds to the more evolved basalts of the tholeiitic affinity (Groups 2 and 4). The potential precursors of analysed metamorphic rocks are thus unambiguously defined to be of magmatic origin. Moreover, in case of metacumulates, their REE patterns implied a SSZ overprint over the clear MORB trend of its normalisation curves, whilst in case of metabasalts the overprint misses.

In this Chapter, attention will be placed on the further determination and clarification of igneous processes that took place at the original geotectonic setting of the protoliths. It will be done by conducting detailed analyses of trace and REE geochemistry of metamorphics,

and using the standard set of discrimination diagrammes. The hypothetical precursors of cumulate origin do not represent original basaltic melts. Therefore, most of the following discussion is focused on the petrogenesis of rocks having characteristics of fractionated magmas.

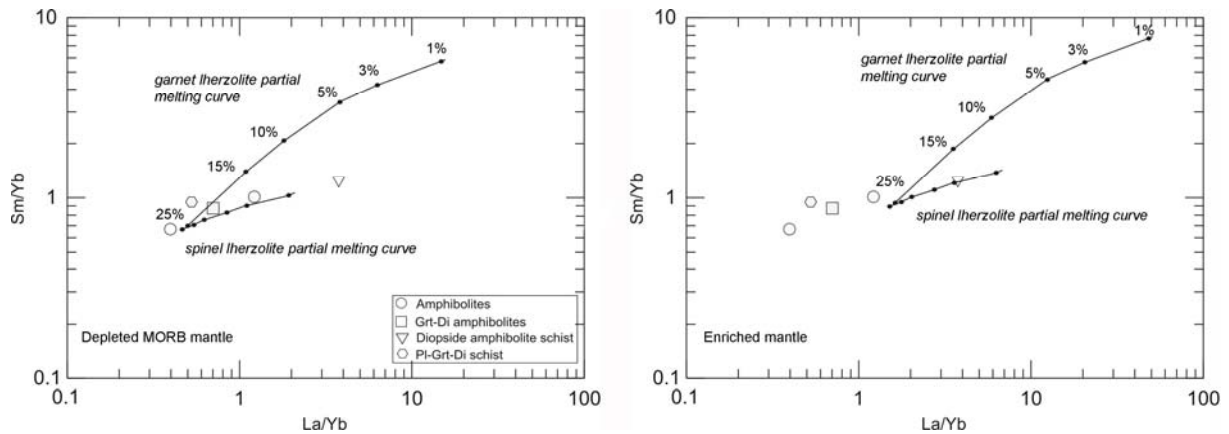


**Fig. 77.** Variation diagrammes of La/Yb versus Sm/Yb (according to Chan et al. 2008) for the KKOC metamorphic rocks having tholeiitic basalt affinities. Non-modal, batch melting curves for spinel and garnet lherzolites are indicated (Grt lherzolite is 59.8% Ol, 21.1% Opx, 7.6% Cpx, 11.5% Grt that melts in the proportions 5% Ol, 20% Opx, 30% Cpx, 45% Grt; Sp lherzolite is 57.8% Ol, 27.0% Opx, 11.9% Cpx, 3.3% Sp that melts in the proportions 10% Ol, 27% Opx, 50% Cpx, 13% Sp; Thirlwall et al. 1994).

The distinct trace element ratios La/Sm and Zr/Nb show moderate ranges of 0.56 – 3.01 and 8.75 – 26.04, respectively, for those metamorphic rocks having basaltic signatures. If we exclude sample 10D from the concerned group, both element ratios get significantly narrower, ranging from 0.59 to 1.20 and 18.25 to 26.04, respectively. Such a small-scale variation could be due to melt generation through fractional crystallisation. However, according to Sun and McDonough (1989), La/Sm and Zr/Nb variations are known as relatively insensitive to magmatic differentiation. Hence, the explanation of differences in incompatible trace element contents, especially for sample 10D, is rather attributed to partial melting processes of the mantle. In order to decipher the characteristics of the mantle source region, which yielded the parental mafic precursors, a simple modelling proposed by Chan et al. (2008) has been performed and presented in Fig. 77. There, non-modal, batch melting is hypothesised with the distribution coefficients of McKenzie and O’Nions (1991), whereas depleted and primitive (enriched) mantle compositions are calculated according to Workman and Hart (2005) and Sun and McDonough (1989), respectively. In the Sm/Yb versus La/Yb space, melting curves are provided for garnet and spinel lherzolites for the two main mantle compositions: depleted MORB mantle (left), and primitive mantle (right). It is well observed that the KKOC basaltic rocks, precursors of analysed metamorphites, fully match with the melting curve of depleted spinel lherzolite (Fig. 77), advocating up to 10 % of partial melting. This result, suggesting a mantle source devoid of garnet, is consistent with already presented narrow La/Sm and Zr/Nb variations. It is important to notice that in case of the primitive mantle source, any variable degrees of partial melting, neither of spinel nor of garnet lherzolites, could have generated the analysed rocks. A following conclusion can be delivered, stating that the formation of magmas occurred within the spinel peridotite stability field of depleted mantle source, thus maximally reaching depths of 70 to 90 km.



Experiments of Takahashi and Kushiro (1983) indicated that the SiO<sub>2</sub> content of mantle partial melts is strongly dependent on the pressure in the range of 1 to 3 GPa. Later Sakuyama et al. (2009) have conducted research on peridotites ranging from fertile to depleted, in terms of their chemical and mineralogical compositions, at variable degrees of melting and *P-T* conditions, and confirmed that the different values of silica in nascent primitive melts strongly suggest to their segregation from mantle at different depths. They estimated that primitive melts having a SiO<sub>2</sub> content from 49.87 to 50.10 (high SiO<sub>2</sub>), 47.11 to 48.88 (medium SiO<sub>2</sub>) and < 47.22 wt% (low SiO<sub>2</sub>) have been formed in the following pressure ranges of 1.4 to 2.1, 1.9 to 2.7, and > 3.0 to 2.6 GPa, respectively. The water content of the melt is set to be less than 2.5 wt%. Furthermore, SiO<sub>2</sub> content oscillations, taken to reflect changes in melting pressures, are coupled by the distinct Na<sub>2</sub>O distribution. The partition coefficient of Na<sub>2</sub>O between clinopyroxene and melt increases with increasing pressure (e.g. Johnson 1998), thus leading to the lowest Na<sub>2</sub>O concentrations in the low-SiO<sub>2</sub> melts, formed under the highest pressures. The Krivaja-Konjuh metabasites show a large SiO<sub>2</sub> compositional span, ranging from 41.67 to 50.10 wt%. The average water concentration does not exceed 1.69 wt%. It is quite indicative that the Na<sub>2</sub>O amounts show a nearly perfect positive correlation with silica ( $r^2 = 0.956$ ). Combining these parameters with the above-mentioned experimental modelling, it is inferred that the melts that yielded the Krivaja-Konjuh metabasalts segregated from different portions of depleted mantle under pressures ranging from ca 1.0 to 3.0 GPa. Amongst them, distinct magmas parental to Maoča (samples R8 and YU137) and Žepče (samples 11C and Z1C) metabasites show geochemical signatures of fractional crystallisation. More on the mechanism of mantle melting is elucidated using a set of trace element ratios presented in Fig. 78 (Ce/Yb vs Ce, Ce/Zr vs Zr, Ce/Yb vs Sm and Y/Nb vs Zr/Nb). The positive slope of metabasalts shown in the Ce/Yb versus Ce diagramme (Fig. 78a) is generally attributed to the variable degrees of mantle melting, since as already stated, fractional crystallisation cannot result in a variation of trace element ratios in such extent. Due to the large intra-sample discrepancies in those ratios, a heterogeneous mantle source is envisaged, melted at different pressure conditions. Mantle melting is nicely depicted in the Ce/Yb versus Sm diagramme (Fig. 78c), where the dashed line represents the trend of hypothetical melting that would have operated under low-pressure fractional crystallisation from the evolved MORB-like asthenospheric melts (Gómez-Pugnaire et al. 2003). A similar trend is perceived in the Ce/Zr versus Zr diagramme (Fig. 78b), where the real values could have been affected by the early fractionation of Zr (see Chapter 5.2.). Finally, in the diagramme Y/Nb versus Zr/Nb (Fig. 78d), the partial melting regime in the mantle is best displayed with the indicated trend maintaining its positive slope. Three potential melting events (Me1-Me3) recording different pressure conditions, have been suggested as parental to analysed metabasalts.

More information on the character of the original geotectonic setting of protoliths of the KKOC metamorphic rocks is obtained through usage of incompatible trace-element ternary discrimination diagrammes. Pearce and Cann (1973) were amongst the first to show that the geotectonic provenience of different basalts can be discriminated based on their geochemical characteristics, primarily regarding to their trace-elements content. In the Zr-Ti-Y diagramme of the same authors (Fig. 79), some of the analysed rocks are discriminated as

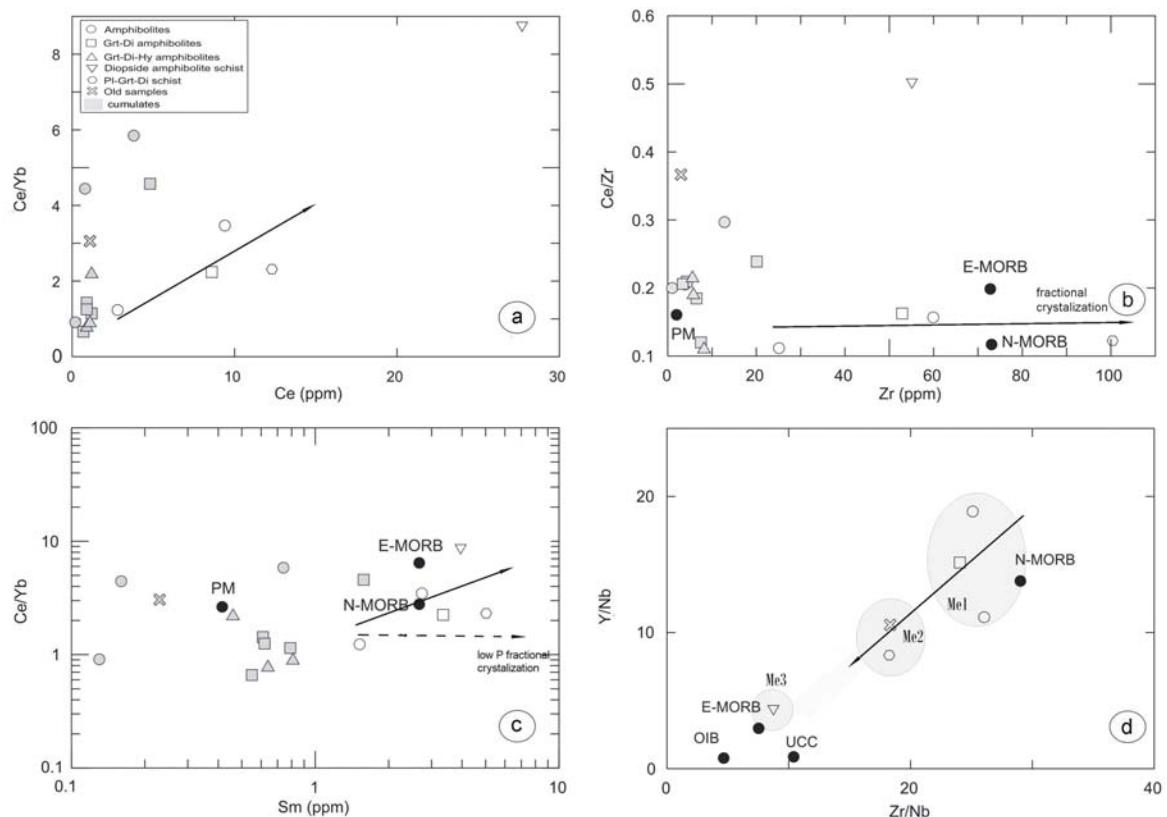


**Fig. 78a-d.** Ce/Yb vs Ce (a), Ce/Zr vs Zr (b), Ce/Yb vs Sm (c), and Y/Nb vs Zr/Nb (d) for the KKOC metamorphites. Arrows show trends and, where indicated, trends of fractional crystallisation. N-MORB and E-MORB stand for normal- and transitional-type Mid Ocean Ridge Basalts, PM (Primitive Mantle), OIB (Ocean Islands Basalts), and UCC (Upper Continental Crust), according to Sun and McDonough (1989). Symbols in grey indicate samples of cumulative origin. Me1-Me3 is for envisaged melting events of mantle source.

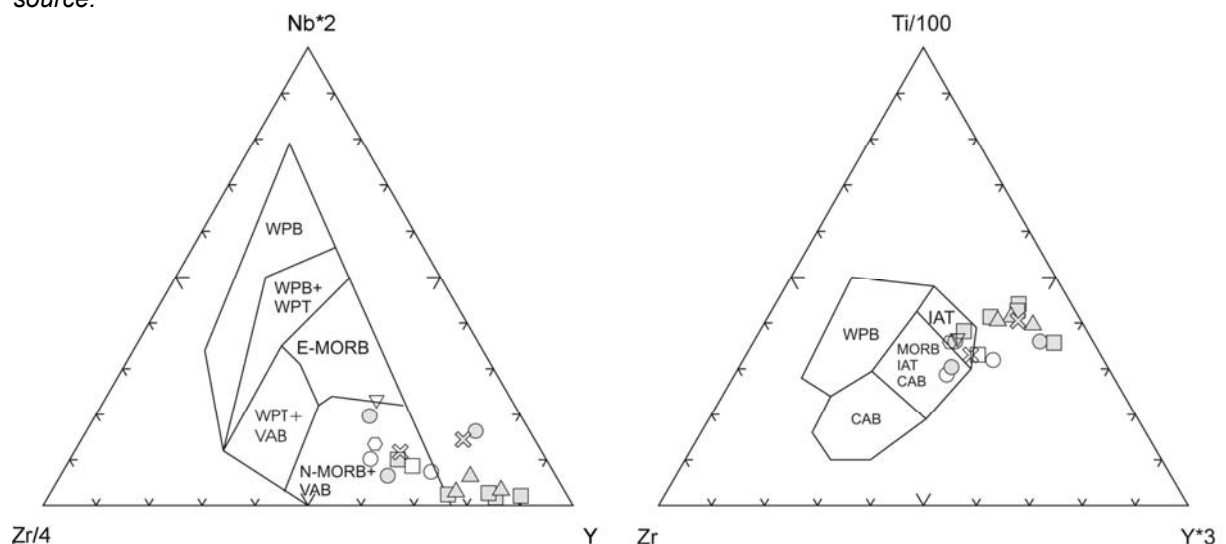


**Fig. 79.** Zr-Nb-Y discrimination diagramme of Meschede (1986) (left) and Ti-Zr-Y diagramme of Pearce and Cann (1973) (right) for the KKOC metamorphites. WPB = Within Plate Basalts, WPT = Within Plate Tholeiites, VAB = Volcanic Arc Basalts, IAT = Island Arc Tholeiites, CAB = Continental Arc Basalts. Other abbreviations and symbols as in Fig. 78.

IAT to transitional MORB-IAT-CAB. A large portion of samples is found outside the discrimination area, partly due to the fractionation of Ti and Zr, and a cumulative nature of the rocks concerned. On the

other hand, in the Zr-Nb-Y diagramme of Meschede (1986) (Fig. 79), all metabasites are found within the transitional N-MORB-VAB field, whereas metacumulates plot outside the projection. In the Th-Zr-Nb diagramme of Wood (1980), metabasalts are defined as N- and E-MORBs, and metacumulates bear arc signatures (here CAB). However, the results of this discrimination should be slightly corrected toward the Zr peak, due to the Zr fractionation and concentrations of Th that were under the detection limit. The ternary diagramme based on the normalised values of Ce-Sr-Sm (Ikeda 1990) presented in Fig. 80, depicts only samples of metabasalts because of the significant Sr accumulation in cumulates (see Chapter 5.2.). Analysed rocks are N-MORBs, except sample 10D which is featured by pronounced concentrations of some trace elements (especially LILE), fitting the E-MORB field. The diagramme of V vs Ti (Shervais 1982) clearly confirms a MORB affiliation of the analysed metabasalts (Fig. 81).

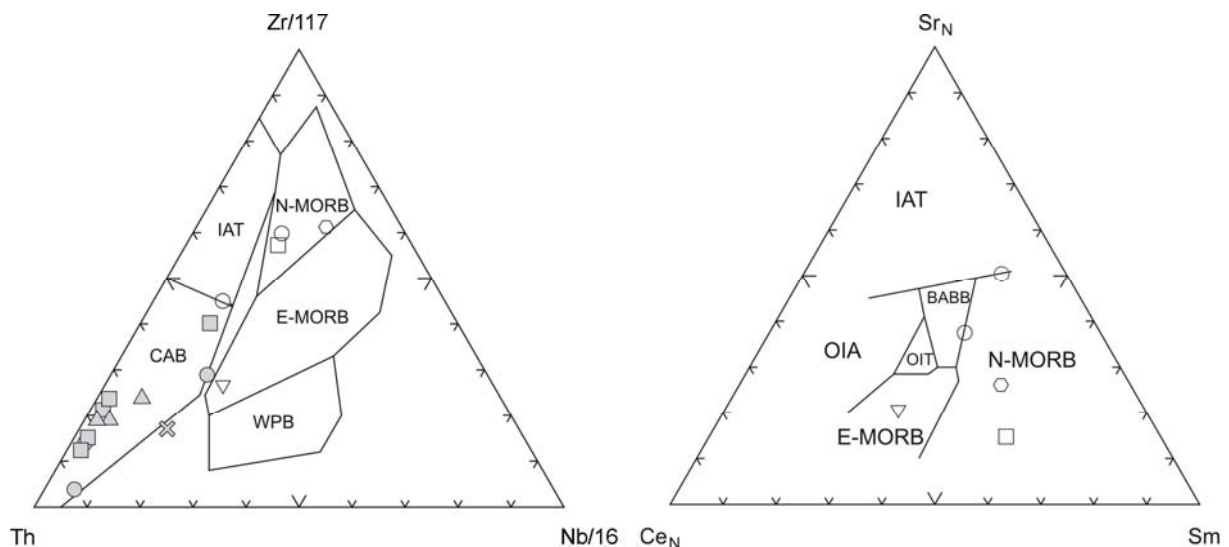


**Fig. 80.** Th-Zr-Nb discrimination diagramme of Wood (1980) (left) and  $Ce_N$ - $Sr_N$ - $Sm_N$  diagramme of Ikeda (1990) (right) for the KKOC metamorphites and metabasalts respectively. OIA = Ocean Island Alkalis. Other abbreviations and symbols as in Fig. 78.

Cumulate samples were not excluded, showing here an IAT affiliation geochemistry. Two more common discrimination diagrammes were employed, based on the incompatible trace element ratios of Zr/Y and Ti/Y (Figs. 81 and 82), both diagrammes ascertain a MORB setting of the analysed metabasalts. The Cr versus Y plot of Pearce (1982) and Pearce and Parkinson (1993) depicts KKOC metabasalts stretching within the entire MORB field. This fact combined with a lack of trend, which could be taken as a fractionation pattern, points to the variable degrees of partial melting under different depths, as it was discussed earlier. This diagramme does not distinguish MORB and WPB, but clearly defines the analysed rocks as non-arc (VAB) related. Metacumulates are characterised by an elevated compatible Cr content reflecting their primitive chemistry.

The above-mentioned discussion on the geotectonic setting yields a clear conclusion that the analysed metabasalts, which correspond to Group 2, are of N-MORB origin. Sample 10D, which solely forms Group 4, is characterised as E-MORB due to its comparably higher

Ce, Nb, and Th concentrations, coupled with higher Ce/Yb and Ce/Zr, as well as lower Y/Nb ratios. Indicated geochemical features clearly call for an enriched source that, apart from the hypothesised E-MORB environment, can be recognised either in OIB plumes or it is an outcome of crustal involvement (e.g. subcontinental lithosphere origin).

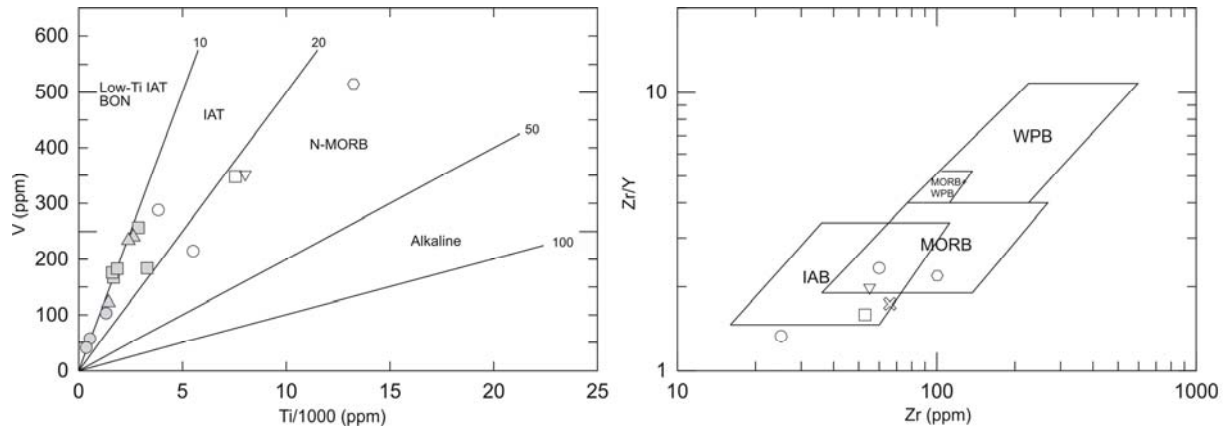


**Fig. 81.** V vs Ti variation diagramme of Shervais (1982) (left) and Zr/Y vs Zr diagramme of Pearce and Norry (1979) (right) for the KKOC metamorphites and metabasalts respectively. Abbreviations and symbols as in Fig. 78.

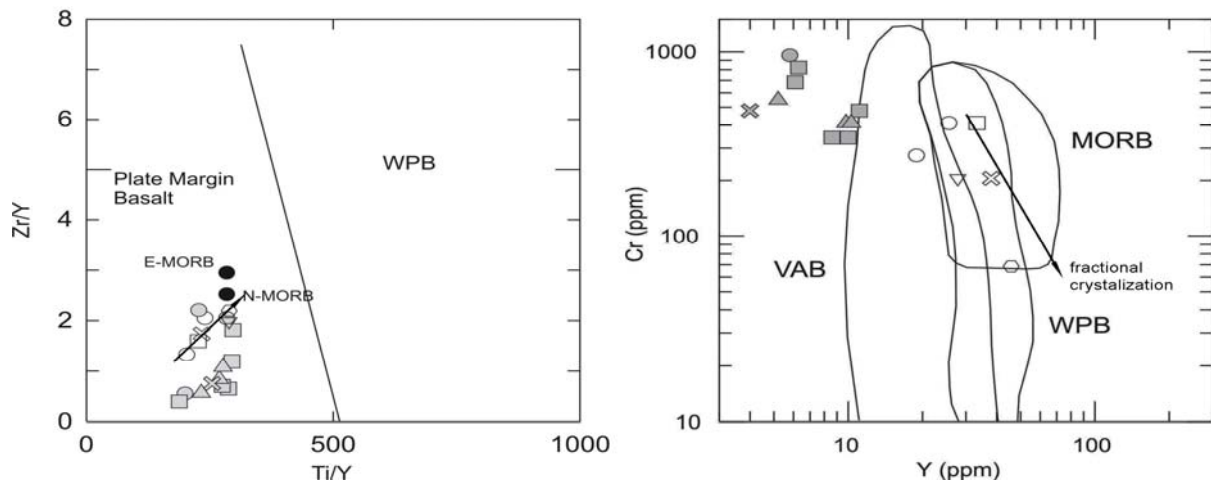


**Fig. 82.** Zr/Y vs Ti/Y diagramme of Pearce and Gale (1977) (left) and Cr vs Y diagramme of Pearce (1982) and Pearce and Parkinson (1993) (right) for the KKOC metamorphites. Abbreviations and symbols as in Fig. 78.

The presented MORB affiliation of metabasalts (Groups 2 and 4), along with the SSZ geochemical signatures recognised in metacumulates (Groups 1 and 3) had already been inferred in the discussion on the REE and trace element distribution in metamorphic rocks (see Chapter 5.2.). Here, in Fig. 83, the REE normalisation plots of four metamorphic groups have been schematised and presented in comparison with those of different mafic intrusives and extrusives, thoroughly sampled over the area of the Krivaja-Konjuh ophiolite complex (Babajić 2009). In this way, it is possible to conclude more regarding the plausible protolith, and to test results of their geotectonic discrimination. Rocks of Group 1 are considered as metacumulates due to their primitive major chemistry parameters (e.g. Mg# > 70), lack of

fractionation trends, and pronounced Eu and Sr positive anomalies characteristic for an early-stage plagioclase accumulation followed by clinopyroxene and olivine. These rocks possess a general MORB affinity, coupled with evidences, which are compatible with chemical affinities influenced by the arc-related chemistry (see Chapter 5.2.). According to Fig. 83b, they correspond well to the mafic intrusives (gabbros, gabbronorites to amphibole gabbronorites) of Kamenica and Duboštica (Krivaja domain), as well as the Muška Voda and Karaula (Konjuh domain) localities. Great variation in their major chemistry (Table Y-1–Y-2) indicates that crystal accumulation in the ocean ridge environment occurred at different depths. Samples U30 and U29, displaying discrepancies in comparison to other members of the group, in terms of the bulk REE composition and LREE enrichment, are reported to correlate best with troctolites of the Kamenica and Maoča localities of the Krivaja domain, along with those of the Karaula locality at SE Konjuh (Fig. 83a). Apart from troctolites, the REE distribution patterns of these two samples correspond well to those of mafic dykes of the Muška Voda locality (Fig. 83d).

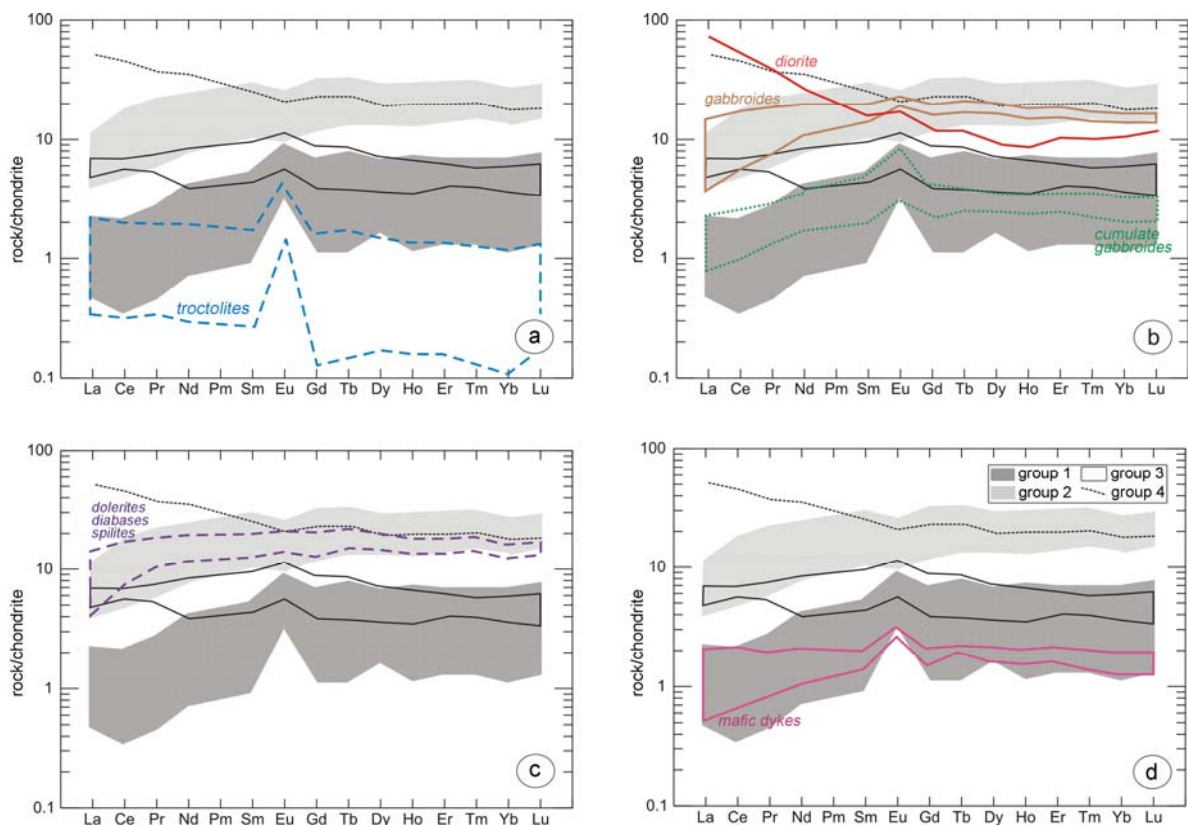


**Fig. 83.** Comparison of the chondrite-normalised REE patterns of the four groups of KKOC metamorphic rocks with normalisation patterns of KKOC mafic intrusives and extrusives (Babajić 2009). Mafic rocks marked with lines of different colour. Normalisation values according to McDonough and Sun (1995).

The Cr values, which are 5 to 10 times higher in these samples, strongly advocate troctolites as more probable magmatic precursors. Taking into account all these facts, one infers that the most suitable environment for the formation of cumulates would be a back-arc spreading basin (BARB). Members of Group 2 have been featured by a clear MORB setting, as strongly suggested in numerous discrimination diagrammes. A large portion of the

depleted heterogeneous mantle source is envisaged to have experienced up to 10 % batch melting under pressures ranging from ca. 1 to 3 GPa. Their magmatic precursor is recognised in mafic extrusives (dolerites, diabases and pillow basalts) of the Ribnica area (Konjuh domain) (Fig. 83c). Sample 10D (Group 4) depicts certain similarities with the sample of diorite from Duboštica (Fig. 83b). They are both featured with highly fractionated REE patterns and comparatively higher incompatible trace element concentrations, characteristic for an enriched mantle source.

### 6.3.2. Conditions and model of metamorphism

#### 6.3.2.1. Metamorphic evolution recorded in petrographic characteristics

Petrographic characteristics of the analysed Krivaja-Konjuh metamorphic rocks are highly informative on the question of the course of their metamorphic evolution. An appropriate interpretation of rock's textural features thus witnesses its importance, especially taking into account that in high-temperature metamorphites of granulite facies, the diffusion rates are rapid and most often the prograde metamorphic history is poorly preserved. Textures and structures of analysed rocks were discussed in detail in Chapter 4.3.1. Here they will be interpreted in the context of rock's genesis track.

The majority of samples are characterized by a paragenesis comprising coarse, low-energy idiomorphs of amphibole along with isometric and euheedral medium-sized plagioclase. Part of the parageneses also comprises porphyroblasts of garnet, igneous clinopyroxene and, in one sample, corundum (Fig. 84a; Fig. 27h). The described grains' morphologies are vastly indicative for a gabbro type of protolith. Such a conclusion is correlated with geochemical considerations, which define most of these rocks as meta-gabbros, meta-gabbronorites and meta-troctolites (see Chapter 6.3.1). On the other hand, samples defined as gneisses (10D and Z1C), are marked by fine-grained granoblasts of amphibole and clinopyroxene, accompanied by rounded or tabular plagioclase aligned to the rock's fabric (Fig. 84b; Fig. 28f). Such a textural context calls for diabase or dolerite as plausible precursors, as it had been suggested by the rocks' geochemistry which bounds the analysed gneisses to mafic extrusives of the Konjuh area (locality of Ribnica, see Chapter 6.3.1).

In the study of Hacker and Mosenfelder (1996), dimensions of minerals in a metamorphic sole assemblage were recognised as one of the indicators determining the distance from the thrust peridotite upper-plate. Accordingly, the majority of meta-gabbroids, having an average amphibole coarser than 200  $\mu\text{m}$  are found within 130 m of the peridotite. Samples U30 and U29, virtually featured by coarse amphibole crystalloblasts devoid of subgrain development, probably represent the 40 m upper-top section of the metamorphic column. The fact that these rocks experienced the strongest heat influx is further recognised in the highest  $\text{Al}_2\text{O}_3$  and  $\text{K}_2\text{O}$  content of their pargasitic amphibole, attaining  $\sim 17$  wt% and  $\sim 0.69$  wt%, respectively, and in characteristic tapered mechanical twinning of highly basic plagioclase. The bulk-rock silica deficiency, alumina enrichment traced by the formation of Al-phases such as corundum or sapphirine, and conservation of calcite blebs in amphibole

idioblasts imply that part of the sedimentary cover might have also been affected by metamorphism (see Chapter 5.2.).

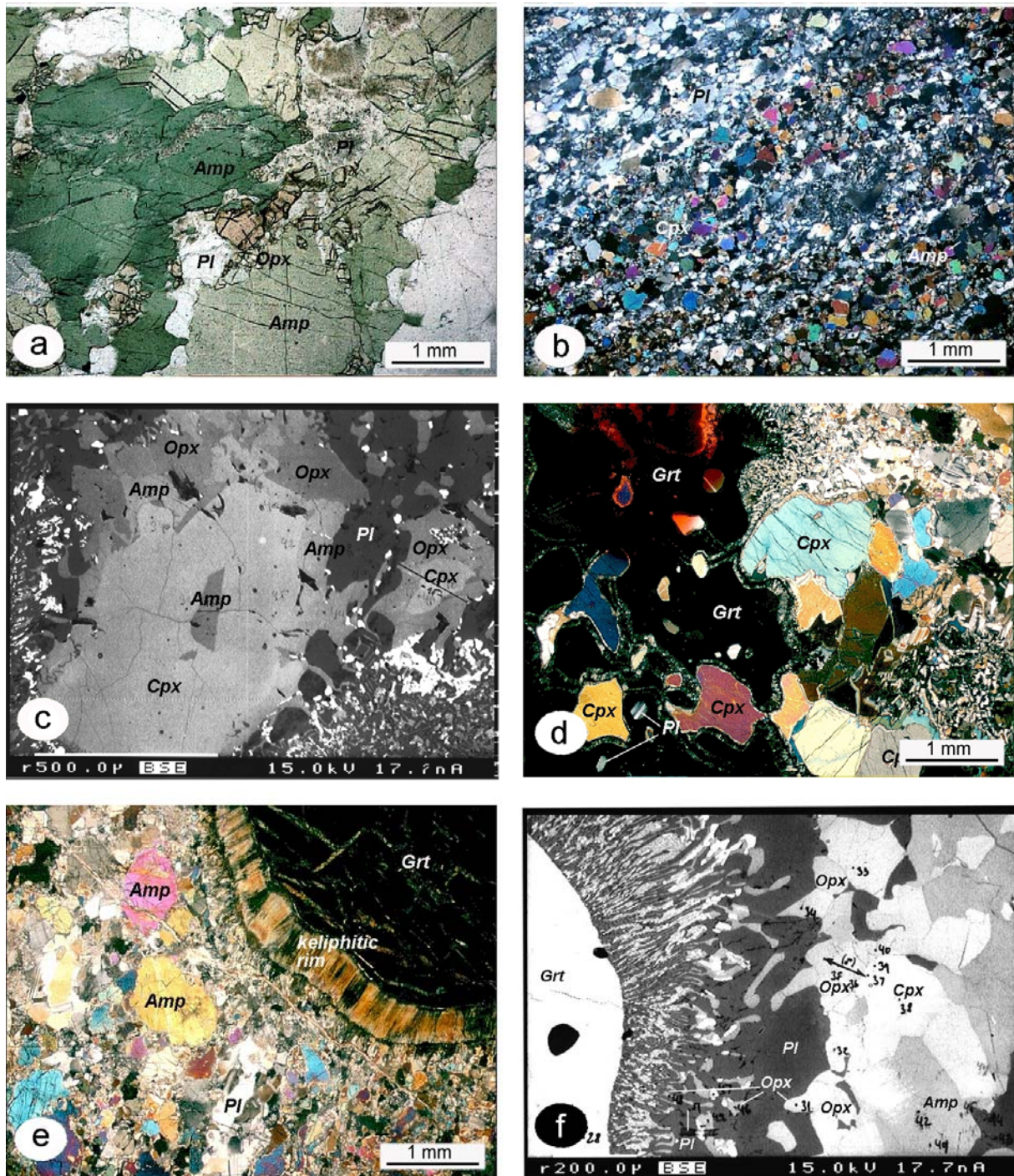


**Fig. 84a-f.** Selected microphotographs and BSE pictures of analysed KKOC metamorphic rocks showing different microtextural characteristics (see text). Numbers in BSE pictures indicate respective microprobe analyses available in the appendix. Pl = plagioclase, Amp = amphibole, Grt = garnet, Opx = orthopyroxene, Cpx = clinopyroxene. Abbreviations after Kretz (1983).

An intimate contact with the upper-plate peridotite can be recognised in Cr-spinel inclusions in crystalloblasts of amphibole (sample U29, see Chapter 4.3.1.). Their Cr# values and TiO<sub>2</sub> contents suggest an igneous origin, most probably being derived from the upper-plate serpentinised lherzolites. High-temperature textures, like those of samples U30 and

U29 are in other meta-gabbroids overprinted by deformation, porphyroblast formation and matrix recrystallisation. Thus, in those samples, dominant phases become garnet and clinopyroxene. Finally, fine-grained meta-extrusives are placed away from the thrust-plane, experiencing a different metamorphic history, mainly controlled by pressure.

Garnet grains are reported to have rounded subhedral morphologies, with the diameter occasionally reaching several millimetres. More often than not, garnet shows a characteristic sieve texture, embedding clinopyroxene, amphibole, titanite, plagioclase and minor phases and suggesting that it might have grown on their account. However, due to the lack of clear textural context, it is not unlikely that garnet and its inclusions belong to the same metamorphic paragenesis, with the late having grown at a much slower rate than garnet that engulfs them (Fig. 84d; Figs. 30c, 30h.). It is indicative that porphyroblasts of garnet mostly occur as isometric, well shaped and rounded, neither helicoidal nor elongated blasts, being devoid of curved inclusion trails. This suggests that garnet growth was post-kinematic with respect to the main deformational event or events, enabling garnet to 'capture' re-crystallised matrix phases. A weak chemical zoning in coarse porphyroblasts is expected, calling for the rapid intracrystalline diffusion of main elements and subsequent system homogenisation under peak metamorphic conditions. Still, a partial prograde nature of analysed garnet grains has been identified in an indistinct concave zoning of pyrope component (see Chapter 4.3.2.2.). The consequences of decompression and cooling in rocks that contain porphyroblasts of garnet are the formation of garnet reaction coronas or kelyphitic rims. Though they comprise a variety of secondary assemblages (amphibole, albite, xonotlite, orthopyroxene, magnetite), it is clear that they are formed through the retrograde reaction of garnet with silica saturated oxidising fluids having caused the garnet decompression breakdown and formation of vermicular and radial symplectites (e.g. Prakash et al. 2007; Figs. 84e, 84f, 29g, 29h). Peak grain-size is normally coarser than the scale of retrograde diffusion, being rarely reported that garnet was completely obliterated by regression (Fig. 28e).

Similar to garnet, the coarse blasts of amphibole are characterised by weak zoning, with  $Al_2O_3$  content rising from the core towards the rim (see Chapter 4.3.2.1.). Such a trend, often reported in analysed pargasites, ferroan pargasites and pargasitic hornblende, is characteristic for the prograde amphibolites. On the contrary, actinolite and various intermediate composition amphiboles, mostly record the opposite trend, indicating a retrograde metamorphic event.

A clear sign of a prograde metamorphism in weakly to moderately deformed rocks, like the KKOC meta-gabbroids, is partial pseudomorphism (Guidotti and Johnson 2002). This is delineated in crystallographically controlled replacement of igneous clinopyroxene with amphibole and in lesser extent orthopyroxene (Figs. 84c, 30a, 30c). As it is shown in Fig. 84c, replacing amphibole and orthopyroxene may advance from grain boundaries, but it is equally possible that they project from inwards through the crystal fractures. Often, amphibole completely replaces clinopyroxene, whilst it is not a usual occurrence in the case of orthopyroxene. The appearance of orthopyroxene is bounded to extreme metamorphic conditions of the granulite facies. The same metamorphic environment is essential for the formation of rutile needles in garnet via garnet {110} microparting and the formation of



microscale partial melts that reacted with the host mineral, leaving behind the TiO<sub>2</sub> mineralization (Hwang et al. 2007; Fig. 28a).

The greenschist metamorphic overprint is found to affect the entire metamorphic column, being manifested differently in the respective part of the column depending on the mineral assemblage. Thus, beside the garnet kelyphitic rims, this process influenced basic plagioclase, being replaced by albite, epidote, pumpellyite and prehnite symplectites. Aluminous amphibole tends to become impoverished in Ti and Al and richer in Fe, whereas ilmenite and ulvöspinel are being transformed to titanite (Figs. 29a, 29e, 29f, 30e). Massive prehnite veins traversing sample 10D (Fig. 30e) are not linked to regression, since the late-stage brittle deformations are believed to mark the ophiolite obduction and exhumation-cooling processes (Guilmette et al. 2008).

Compiling the germane textural and microtextural characteristics of the analysed KKOC metamorphites, the following facts are to be consulted when interpreting the course of metamorphic history. The uppermost segment of the metamorphic column is a rock consisting of coarse amphibole idiomorphs and basic plagioclase laths. Due to the reasons discussed at the beginning, an influx of sediment material during metamorphism is hypothesised. Dissociating from the thrust-plane, most of the analysed metamorphic textures experienced post-peak deformations, having yielded an overall grain-size reduction, recrystallisation, and a subsequent garnet porphyroblast formation. A retrograde greenschist imprint engaged the entire column, leading to the formation of a variety of hydrous phases. Even though, prograde microtextural features are preserved with the best example being an epitaxial overgrowth of amphibole and orthopyroxene at the expense of relict clinopyroxene.

#### 6.3.2.2. Mineral assemblages and *P-T* conditions of metamorphism

Results of a geothermobarometric study of the KKOC metamorphic rocks (Table 5, see Chapter 6.1.3.) will be discussed in this chapter, taking into account different metamorphic paragenesis that are indicative for certain *P-T* conditions. In order to decipher the KKOC metamorphic history, it was essential to identify the phase reactions that had yielded domains where particular diagnostic assemblages dominate. With respect to the petrographic classification of KKOC metamorphites, determined metamorphic sequences are presented in Fig. 85. It is important to remark that the peak-metamorphic *P-T* conditions of granulite facies are often reset by diffusion, in case of exchange geothermometers, whereas the net transfer reactions, which record geobarometric information, tend to be less sensitive to such a phenomenon. In literature, this problem is known as the 'granulite uncertainty principle' (e.g. Harley and Green 1982), mostly addressing Precambrian granulite terranes that experienced slow cooling (O'Brian and Rötzler 2003). The KKOC metamorphites are believed to have formed by a rapid *HT-HP* metamorphic overprint, induced by thickening of the upper-plate magmatic arc and subsequent quick obduction of the entire ophiolite domain. Therefore, such a rapid metamorphism and fast cooling had probably maintained the peak-metamorphic mineral chemistry uncompromised.

Generally, it is considered that under elevated *P-T* conditions *amphibole* records the following chemical changes. Titanium content progressively increases, which is reflected in

modification of its colour from light green to dark-olive green or brown. Total octahedral and tetrahedral Al increases, along with the Na and Fe/Mg ratio, whereas the amounts of Si and Mg decrease (Spear 1981). Apart from pressure and temperature, the bulk rock chemistry, oxygen fugacity and SiO<sub>2</sub> activity further influence the amphibole composition. *Garnet* is a common mineral in metamorphic rocks, showing a broad *P-T* stability span, which makes changes in garnet mineral chemistry a reliable marker of evolution of a certain metamorphic system. Hence, the zoning in garnet is of particular interest, being well pronounced under conditions not exceeding 650 °C, whereas in high-grade metamorphic rocks, garnet is usually chemically homogenous. Mineral chemistry of *plagioclase* is sensitive to the oscillation of metamorphic conditions, with respect to mean Na and Ca, as well as the tetrahedral Al and Si distribution. Like in garnets, zoning is also common in metamorphic plagioclase. Prograde metamorphism is featured by Na enrichments along grain rims, whereas during regression those domains are found enriched in Ca. Small plagioclase blasts are often reported to be of anorthite composition, which is linked to the retrograde net transfer of garnet, epidote, and/or carbonate. In *clinopyroxene*, the tetrahedral and octahedral abundances of Al increase with metamorphic grade, favouring the tetrahedral coordination under extreme *P-T* conditions. The alumina content of clinopyroxene is usually expressed as the Tschermak component. Metamorphic *orthopyroxene* is hypersthene or bronzite featured by the oscillatory amount of Al. The alumina content is controlled by the rock chemistry and mineral assemblage, rather than by metamorphic conditions (Tribaudino and Talarico 1992). In the lower amphibolite facies, *titanite* is the usual Ti phase, whereas in the upper amphibolite and granulite facies it is found embedded by amphibole, or it is transformed into ilmenite. Liou et al. (1985) reported that the disappearance of titanite is bounded to the redistribution of Ca into other silicates, like plagioclase. Due to the high modal proportion of Fe-Ti minerals in high-grade metamorphites, the Ti content of amphibole significantly decreases. Minerals belonging to the group of *epidote/clinozoisite* tend to be stable under medium pressures, but with temperature increase, they vacate the metamorphic system (550-600 °C, Liou et al. 1985). In this study, the appearance of minerals from the epidote/clinozoisite group makes a clear sign of retrograde dissolution of plagioclase.

Main mineral phases present in the KKOC petrographic variety *amphibolite* are amphibole and plagioclase with minor epidote/clinozoisite, corundum, sapphirine, titanite, ilmenite, apatite, clinopyroxene, Al pumpellyite, and calcite. The range of substitution in amphibole (magnesian-hornblende to pargasite) offers the first indication of the large *P-T* span that these rocks experienced. Absence of garnet and rutile advocates metamorphism under medium to low pressures. However, samples U30 and U29 are estimated to have formed under the *P-T* conditions of 0.90-1.30 GPa and ~ 880 °C. Due to the high anorthite content in plagioclase, it was impossible to recover the temperature information based on the amphibole-plagioclase exchange geothermometers (Spear 1980, Holland and Blundy 1994). For that reason, the sapphirine-spinel geothermometer was employed to reveal the temperature data for sample U30 (Owen and Greenough 1991). Presence of sapphirine and corundum in related samples corroborates their high *P* and *T* nature. Naturally, the appearance of these minerals is greatly controlled by the bulk-rock silica deficiency, as well as alumina enrichment (Tables Y-1–Y-2).

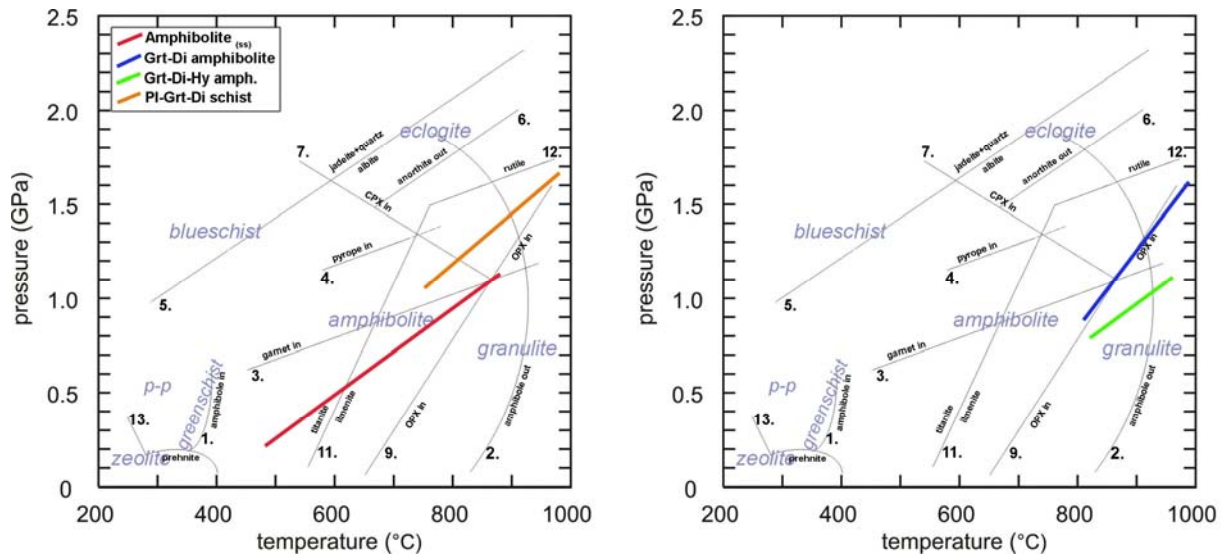


**Fig. 85.** The *P-T* diagramme for thermobarometry of the KKOC metamorphic rocks (after Guilmette et al. 2008). Offered thermobarometric results are based on data presented in Table 5., Chapter 6.1.3. List of employed geothermobarometres is overviewed in Chapter 6.1.3. Left picture presents data for amphibolites and PI-Grt-Di gneisses. Right picture presents data of Grt-Di and Grt-Di-Hy amphibolites. Reaction curves: (1), (2), and (3) from Ernst and Liu (1988); (4), (5), and (6) from Green and Ringwood (1967); (7), (8), and (9) from Mukhopadhyay and Bose (1994); (11) and (12) from Liu et al. (1996); (13) from Frey et al. (1991).

In silica-unsaturated systems the appearance of sapphirine denotes a progressive silification, with a minimum pressure of 0.7 GPa and temperature of 650 °C (Williams 1984, Gnos and Kurz 1994). Operta et al. (2003) had reported a corundum occurrence in pargasitic amphibolites of the Vijaka locality, formed at temperatures between 620 and 830 °C and pressures of 0.6 to 1.0 GPa. Al-spinel and clintonite forming necklace-rims around corundum formed under changing conditions, i.e. having required a higher water activity and moderate *P-T* conditions (Nitch et al. 1985, Liati 1988). The rest of the samples belonging to this petrographic variety are characterised by lower equilibration pressures and temperatures ranging from 0.21 to 0.61 GPa and 550 to 820 °C, respectively (Spear 1980, Holland and Blundy 1994). Amphibole in those samples is Al-poor magnesio-hornblende. The patches of clinopyroxene are of metamorphic origin, implying that these rocks have apparently attained the amphibolite-granulite facies transition at ~650°C and ~0.8 GPa (Spear 1981, El-Naby et al. 2000). Furthermore, according to the modelling of Ernst and Liu (1998), clinopyroxene should be stable above around 700 °C in metabasite systems at a pressure of 0.8 to 1.0 GPa. Formation of clinozoisite and pumpellyite is characteristic for the sub-solidus retrogressive changes, most clearly seen in ilmenite replacement by titanite (~ 600 °C, sample 11C). Such a reaction is facilitated by hydration that followed a breakdown of the upper-amphibolite or granulite-facies assemblage (e.g. Ilnicki 2002, Liu 1996).

Mineral assemblages of the *garnet-diopside amphibolite* group dominantly comprise garnet, amphibole, plagioclase, and clinopyroxene with minor titanite, ilmenite, rutile, calcite, orthopyroxene, magnetite, chlorite, and xonotlite. This paragenesis is usually taken as diagnostic for the high-pressure Opx-free garnet-clinopyroxene granulite subfacies, which is taken as transitional between the intermediate orthopyroxene-plagioclase granulite subfacies

and eclogite facies (Mukhopadhyay and Bose 1994, Pattison 2003). Referring to textural features of those rocks, addressed in the previous chapter (e.g. garnet coronas, poikilitic garnet and relict clinopyroxene porphyroblasts), a multi stage metamorphic history of this petrographic variety is hypothesised. Firstly, the initial magmatic assemblage comprising clinopyroxene and plagioclase was metamorphosed at high-pressure granulite facies conditions, having experienced garnet formation (reaction curves 3 and 4 clinopyroxene and plagioclase recrystallisation (clinopyroxene accommodates more octahedral Al, see Chapter 4.3.2.4.), and epitaxial substitution of clinopyroxene by edenitic to pargasitic amphibole. An incipient isothermal decompression of these rocks is manifested by the appearance of orthopyroxene and plagioclase symplectites, forming kelyphite coronas of garnet or emerging as the outer-rim crystal necklaces around garnet (see Chapter 6.3.2.1.). The discrete orthopyroxene rims developed over clinopyroxene porphyroblasts are bound to the same metamorphic stage (reaction curves 8 and 9 in Fig. 85). The occurrence of ilmenite intergrowing with titanite is frequently reported. Such a textural context leads to the conclusion that this decompression stage was coupled by hydration or oxidation via the ilmenite reaction with clinopyroxene and amphibole respectively (Harlov et al. 2006). Reaction curves 3, 4 and 12 define the entrance of garnet and rutile into the system. The presence of these minerals in MORB-derived metamorphic rocks indicates minimum pressures of 1.0 to 1.2 GPa, regardless of the temperature (Ernst and Liu 1998). The occurrence of clinopyroxene without orthopyroxene under such pressure should connote peak values of temperature between 750 and 800 °C (Guilmette et al. 2008). The geothermobarometric calculations based on the amphibole-plagioclase equilibrium yielded temperatures ranging from 725 to 925 °C (Holland and Blundy 1994). The Fe-Mg exchange geothermometers between garnet and clinopyroxene, as well as between garnet and amphibole support these values, having provided a temperature span from 802 to 1028 °C (Krogh 1988, Graham and Powell 1984, Krogh Ravná 2000). An isothermal character of metamorphic evolution reported in these rocks is corroborated by data procured by the usage of orthopyroxene-based geothermometers (780-1100 °C, Harley 1984, Lee and Ganguly 1988, Wells 1977, Brey and Köhler 1990). Geobarometric data based on the Grt-Cpx-Pl equilibrium are consistent and range between 0.94 and 1.40 GPa (calibration of Newton and Parkins 1982), whereas the exchange geobarometers, which include clinopyroxene, yielded slightly lower pressures, varying from 0.90 to 1.30 GPa (Harley and Green 1982, Nickel and Green 1985, Paria et al. 1988, Perkins and Chipera 1985).

The third petrographic variety is *garnet-diopside-hypersthene amphibolite*. The main mineral assemblage is composed of garnet, clinopyroxene, plagioclase, amphibole and orthopyroxene, whilst the minor phases are rutile and magnetite. The metamorphic history of this rock variety is analogue to the previous one, with a difference in length of the last metamorphic stage characterised by a drop of pressure and subsequent orthopyroxene formation. Moderate *P*, and high *T* conditions lasted long enough to initiate the growth of coarse orthopyroxene. Medium-sized orthopyroxene porphyroblasts usually embed inclusions of amphibole, recording the last temperature raise of the system (D'el-Rey Silva et al. 2007). As one might have expected, differences between the peak (Opx-free) and medium-P post peak (Opx present) metamorphic conditions are more pronounced, recording an average 0.15 to 0.20 GPa difference between the two (Table 5., see Chapter 6.1.3).

The *diopside-amphibole gneiss* is characterised by the main mineral assemblage composed of amphibole, clinopyroxene and altered plagioclase, whereas minor phases are titanite, ilmenite, apatite and prehnite. This paragenesis implies elevated to moderate temperature conditions, pointing to the lack of garnet as an intriguing occurrence. Due to the plagioclase obliteration and aforementioned absence of garnet, it was impossible to acquire any temperature information. Therefore, this rock variety was not depicted in Fig. 85. Occasionally, Ti and Al-poor, Fe-enriched secondary amphibole is reported to grow on the account of Ti-pargasite and clinopyroxene due to the post-peak metamorphic instability (0.26 GPa pressure).

The last petrographic variety is the *plagioclase-garnet-diopside gneiss*, composed of major clinopyroxene, plagioclase, garnet, ulvöspinel, and minor ilmenite, as well as titanite. Apart the schistose texture and amphibole absence, this variety shows a certain degree of resemblance to the Grt-Di amphibolites. The Fe-Mg exchange geothermometry yielded spans of 726-1023 and 729-890 °C for the garnet-clinopyroxene pair and two pyroxenes, respectively (Krogh 1988, Wells 1977, Brey and Köhler 1990). The geobarometric data for this variety are reported to be comparably the highest, ranging from 1.10 to 1.60 GPa in pressure (Newton and Perkins 1982, Harley and Green 1982, Paria et al. 1988, Perkins and Chipera 1985). Such high pressures, lack of amphibole, and almandine-rich garnet may present an indication of transitional eclogite-facies conditions. A similar metamorphic rock had been found by Pamić et al. (1973) in the vicinity of the Vareš locality. The authors named this a 'transitional eclogite'. As previously reported, the orthopyroxene encirclement of clinopyroxene in form of tight border zones suggests an isothermal cooling that operated over a short time. The rock is unusually rich in TiO<sub>2</sub> (~2.21 wt%), having resulted in an ubiquitous ulvöspinel formation, which upon oxidation yielded Fe-rich ilmenite. Furthermore, ilmenite was proved to be included or embayed by garnet, which, according to the reaction proposed by Sengupta et al. (1999), implicates the garnet growth at the expense of ilmenite at ≥ 650 °C (Fe-ilmenite + plagioclase ± quartz → ilmenite + garnet + oxygen).

#### 6.3.2.3. *P-T-t* path of metamorphism

Based on previously discussed geothermobarometric calculations and textural characteristics, hypothetical *P-T-t* paths or trajectories were constructed for four out of five petrographic varieties of the KKOC metamorphic rocks. The remaining one is omitted due to lack of thermobarometric data (*diopside amphibolites*). The first thoughts on the metamorphic evolution of analysed rocks were presented in Chapter 6.3.2.2., here presenting its extension and further discussion.

The *amphibolites* are marked by the characteristic amphibole + plagioclase assemblage which, depending on the rock sub-variety, include a set of other phases like corundum, sapphirine and others. Peak values of pressure and temperature are estimated to be at ~ 1.1 GPa and ~ 850 °C (trajectory *a* in Fig. 86). As amphibole changes its composition, by transforming to magnesio-hornblende and/or actinolitic to edenitic hornblende, pressures and temperatures slowly abate. Those rocks follow a cooler metamorphic path. The incomplete retrograde assemblage indicating lower facies overprint of the high-grade metabasalts is usually recognised by the presence of typical greenschist metamorphic phases (e.g. Önen

and Hall 2000). Hence, the occurrence of actinolite, ferroan pargasite, titanite, albite and epidote, are consistent with the final re-equilibration at pressure and temperature values of 0.2 GPa and 500 °C, respectively. The respective  $P$ - $T$ - $t$  path would have a clockwise loop behaviour.

The second petrographic variety, *garnet-diopside amphibolites*, consists of clinopyroxene, plagioclase, garnet and amphibole with minor titanite, ilmenite, rutile, calcite, orthopyroxene, and other phases. Although the  $P$ - $T$  determination of peak metamorphic conditions experienced a certain inconsistency due to the post-peak re-crystallisation, it is elucidated that these amphibolites encountered a two stage metamorphic history. Initially, the plagioclase-clinopyroxene magmatic assemblages underwent a high-pressure granulite metamorphism at 1.1-1.3 GPa and 850-1100 °C (trajectory *b* in Fig. 86). Afterwards, medium-pressure conditions were imposed, coupled by a slight thermal-relaxation heating and orthopyroxene formation (~ 1 GPa, up to 1200 °C). The suggested scenario is enforced by the presence of copious coronal textures of garnet, and clinopyroxene linked to this decompression. The most liable tectonic environment, parental to these rocks, would assume an ocean thrusting and subsequent intraoceanic subduction, since the metamorphism clearly operated at mantle pressures (up to about 40 km).

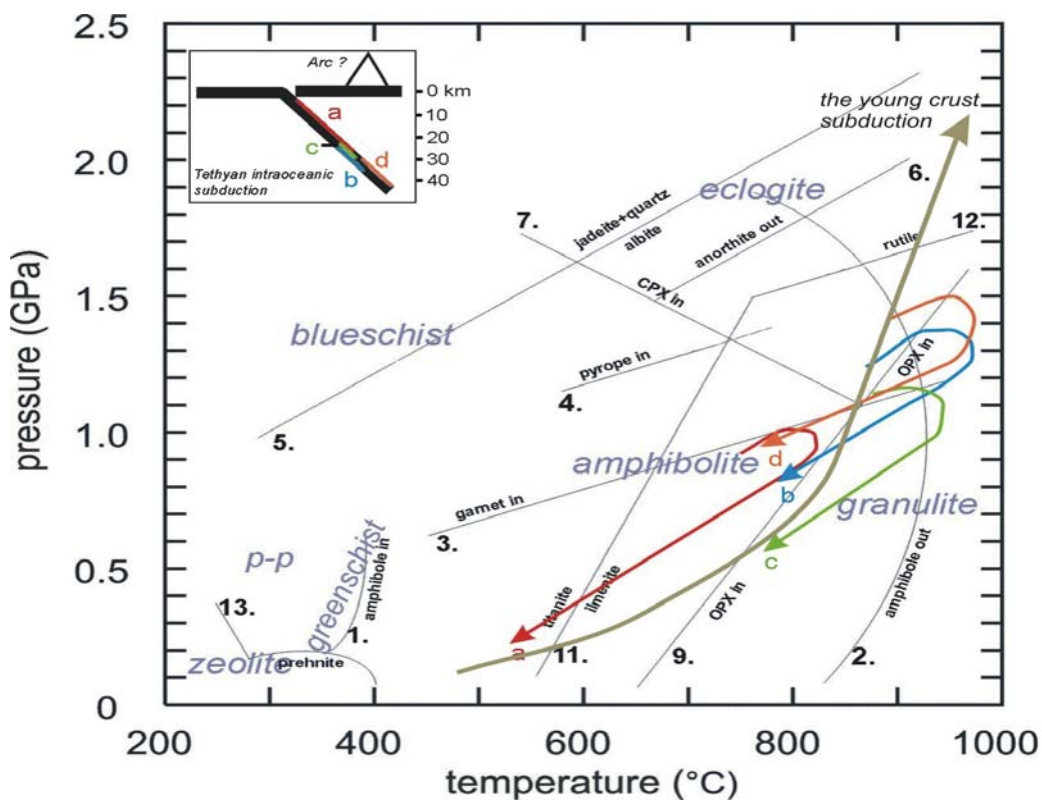


**Fig.86.** Hypothetical  $P$ - $T$ - $t$  paths for the four petrographic varieties of the KKOC meta-morphics (different colours): a) Amphibolites, b) Grt-Di amphibolites, c) Grt-Di-Hy amphibolites, and d) Pl-Grt-Di gneisses). The drawing in upper left corner depicts nascent subduction-related domains of the particular rock varieties. The  $P$ - $T$ - $t$  path of young oceanic lithosphere is from Peacock et al. (1994).

Rocks belonging to the next petrographic variety, *garnet-diopside-hypersthene amphibolites*, possess a more pronounced two-stage metamorphic evolution (trajectory *c* in Fig. 86). This is particularly well observed in their textural characteristics, defined by the orthopyroxene blastosis and pronounced garnet coronal decomposition. Peak conditions are

at ~ 1 GPa and ~ 850 °C, followed by a pressure drop of ~ 0.2 GPa. Both HP petrographic varieties show signs of retrograde alterations like for instance, titanite formation or plagioclase decomposition. However, low  $P$  and  $T$  values were not obtained, thus suggesting that these rocks experienced a short-lived HP main metamorphic event, which was followed by a medium pressure overprint, finally resulting with a rapid exhumation. Described alterations, including the vein precipitation of prehnite, are ascribed to sub-solidus processes related to the ophiolite emplacement. Like in the case of the *amphibolite* samples, for Grt-Di and Grt-Di-Hy amphibolites, a clockwise loop  $P$ - $T$ - $t$  path is suggested.

The samples of *plagioclase-garnet-diopside gneiss* are featured by extreme pressure conditions attaining 1.6 GPa, whereas peak temperatures oscillate between 750 and 1050 °C (trajectory  $d$  in Fig. 86). The peculiar rock texture (orthopyroxene rims around clinopyroxene) implies a two-step decompression metamorphic evolution, although clear thermobarometric evidences is missing. Based on the pressure information, granoblastic textural characteristics, garnet composition, and the lack of amphibole, the transitional eclogite facies conditions and a clockwise  $P$ - $T$ - $t$  path are inferred.

It is very informative to notice that all suggested KKOC  $P$ - $T$ - $t$  trajectories are partly compatible with the trajectory modelled by Peacock et al. (1994), depicting a metamorphic path of the young, slow-subducting ocean crust under the hot mantle at a constant shear. This path is typical for most of the dynamothermal soles reaching their peak-metamorphic conditions (e.g. Guilmette et al. 2008, Önen and Hall 2000). The Krivaja-Konjuh metamorphites also followed this path until the peak metamorphic conditions were attained. The overall space contraction of Jurassic Tethyan realm prevented further HP burial, having caused the medium pressure-high temperature metamorphic overprint, and initiated the buoyancy-driven exhumation of analysed metamorphites.

Compiling the textural and geothermobarometric data presented here, one can speculate about the positions of particular domains of the subducted ocean crust that were metamorphosed, having yielded a related variety of KKOC metamorphites. Thus, the Pl-Grt-Di gneiss presents the deepest part of the subducted slab (~ 30-42 km), followed by the Grt-Di and Grt-Di-Hy amphibolites (~ 24-35 and ~ 24-30 km respectively). The shallowest domains of the metamorphosed crust belong to amphibolites, approximating from 4 to 30 km depths. A simple drawing depicting a hypothetical architecture of the subducted crust metamorphism is provided as annexe of Fig. 86 (upper-left corner).

#### 6.3.2.4. Geodynamic significance of metamorphism

The thermobarometric data estimated for the KKOC metamorphic rocks, along with their mineral assemblages are highly consistent with those of many dismembered dynamothermal soles, pointing to the genetically related metamorphites of neighbouring Tethyan ophiolites in Albania (Mirdita zone), Serbia (Brezovica) and Greece (Pindos and Othrys zone) (e.g. Gjata et al. 1992, Carosi et al. 1997, Karamata 1968, Pomonis et al. 2002, Gartzos et al. 2009).

Field textural evidence, radiometric data, as well as comprehensive petrogenetic researches presented in this study, but also in Operta 2004, Operta et al. 2003, Pamić et al. 1977, suggest that the Krivaja-Konjuh metamorphic rocks, along with prevailing ultramafic

rocks, make a single entity. It leads to the conclusion that both domains experienced a common Mesozoic history, characteristic for the entire CDOB (Central Dinaride Ophiolitic Belt). A dismembered dynamothermal metamorphic sole origin, where heat is derived from the hot overlying mantle peridotites, is thus inferred as the most liable. Values of high pressure attained at metamorphic peak-conditions (up to about 1.6 GPa) put forward the idea of an oceanic crustal thrust or subduction plane (up to about 40 km depth) as nascent to the KKOC metamorphites. The model presented in Fig. 87a is proposed as an explanation for the metamorphic rock genesis, notwithstanding the geodynamic schemes of the Krivaja-Konjuh oceanic domain that question the existence of a single subduction plane of the western Pindos ocean (Dinaric segment, see Chapter 6.2.1.1.).

Accordingly, the processes of an intraoceanic near-ridge thrusting have commenced in the Oxfordian leading to a local overthrusting of the oceanic crustal succession (lower plate Krivaja). The driving forces for the oceanic shortening, causing the north-dipping intraoceanic thrusting are the large-scale Jurassic-Cretaceous compression induced by the northward moving of Africa (Cavazza et al. 2004). High pressures in the sole rocks are thus explained by the transport along the subduction zone to a depth of about 40 km, and subsequent two-step decompression by exhumation. Young subducted mafic rocks were metamorphosed up to the granulite, and possibly transitional eclogite-granulite facies, due to the crustal thickening pressure increase (arc formation?), and the high temperature released from the hot hanging wall of the subduction zone. Metamorphic assemblages were scrapped off from the downgoing plate, being accreted to the upper one, facilitated by the continuing subduction, which has been uplifting the entire pile. According to Naby et al. (2000), the proposed mechanism can best explain the rapid exhumations and further cooling without significant retrograde alterations.

Metamorphic  $P$ - $T$ - $t$  paths have shown that the consumed crust was a ridge proximal as suggested by a high correlation with the modelled  $P$ - $T$ - $t$  path of the young oceanic lithosphere (Peacock et al. 1994, see Chapter 6.3.2.3.). This is consistent with results of the protolith study, suggesting that metamorphosed rocks partly have geochemical signatures characteristic for MORB (see Chapter 6.3.1.). The rest of the analysed rocks are characterized by SSZ signatures. Keeping in mind the proposed model and SSZ imprint, one suggests an aborted fore-arc spreading centre in the upper plate (Konjuh) as parental to these rocks. Alternatively, they might be of arc origin (Fig. 87a). Regardless to the exact origin, they ended up in a subduction zone in form of bulldozed olistoliths captured as *mélange* in the trench. In the case of a non-single thrust plane (see Chapter 6.2.1.1.), the SSZ imprint should be linked to another subduction front placed westwards.



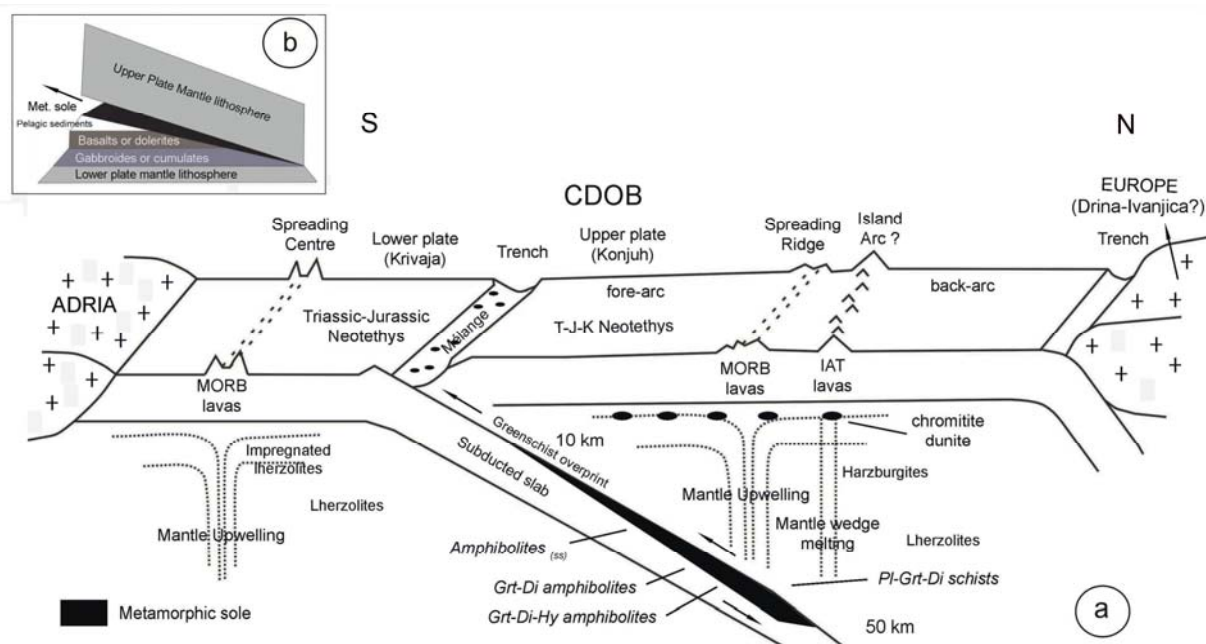


**Fig. 87a-b.** Reconstruction of the hypothetical geodynamic model by which the Krivaja-Konjuh metamorphic rocks (dynamothermal soles) were generated via an intraoceanic thrusting of the young oceanic lithosphere. (a) Initial shortening of the Dinaride segment of Tethys in Oxfordian, leading to the near-ridge upper-plate overthrusting; (b) architecture of late Jurassic sole formation with metamorphites being scrapped off from the downgoing plate and accreted to the upper plate. Thereupon, both units are placed on the lower-plate oceanic sequence, shortly prior the final ophiolite emplacement.

Thermobarometric data, reconstructed  $P$ - $T$ - $t$  paths, mineral parageneses, as well as textural characteristics of analysed metamorphites, all being discussed in previous sub-chapters, are quite coherent, indicating that each of the petrographic rock varieties experienced particular metamorphic conditions. Hence, the amphibolites are inferred to present the shallowest segment of the thrust plane, being in direct contact with a hanging wall. Furthermore, this variety solely depicts a clear gradation in retrograde metamorphism from the upper segment of amphibolite facies toward the greenschist facies metamorphism. At deeper mantle levels, dissociating from the thrust plane, garnet-diopside and garnet-diopside-hypersthene amphibolites were formed, featured by an overall grain-size reduction, clinopyroxene re-crystallisation, and garnet porphyroblasts formation. Both varieties have passed a two-step cooling, followed by a rapid exhumation. Firstly, due to the pressure drop and a subsequent short thermal increase, orthopyroxene emerged, whereas garnet depicted a set of coronal textures. Afterwards, the course of metamorphism proceeded rapidly, exhumating accreted metamorphites upwards. The plagioclase-garnet-diopside gneisses experienced a similar two-step exhumation history. However, estimated pressures attaining at about 1.6 GPa and a characteristic mineral assemblage suggest that these rocks might have experienced the transitional eclogite-granulite peak metamorphism at a depth of about 40 km.

The pronounced compression resulted in the structuration of exhumed rocks at the lower-plate level (Fig. 87b), before being obducted in form of dismembered ophiolitic mélangé at the margins of the Adriatic carbonate platform in late Jurassic. Those processes finally shaped the whole complex, introducing a strong isoclinal faulting (Pamić et al. 1977).

## 7. CONCLUSIONS

This doctoral study enrolled an extensive petrological and geochemical research of the ultramafic and metamorphic segment of the Krivaja-Konjuh Ophiolitic Complex (NE Bosnia and Herzegovina) yielding the following conclusions:

- The KKOC, comprising dismembered peridotite blocks and minor metamorphites, pyroxenites, dunites, gabbroides and chromitites, forms an allochthonous Jurassic magmatic-sedimentary ophiolite, which is characteristic for most of the CDOB ophiolites.
- Peridotites are composed of olivine, orthopyroxene, clinopyroxene, spinel and occasionally plagioclase and amphibole. Most of the samples are characterized by a mantle porphyroclastic texture.
- Most of the KKOC peridotites are fertile MOR lherzolites, which according to the list of differences in modal mineralogy, along with the phase and bulk-rock chemistry have been divided in: (a) spinel lherzolites and (b) plagioclase lherzolites.
- The main equilibration took place under temperatures and pressure that correspond to 809 to 1012 °C and 1.2 to 2.0 GPa (ca 40-65 km depth), respectively.
- Final subsolidus reequilibration occurred at temperatures under 550 to 682 °C and pressures < 1.0 GPa.
- The chemical composition of spinel in conjunction with REE normalisation trends constrain the average batch melting degree of the KKOC mantle portion to ~ 7.7 %, which points to an oceanic crust thickness of about 5.4 km coupled by an average ridge spreading-rate of 32 mm/year.
- The most eastern part of KKOC is reported to have geochemical parameters (primary amphibole, Cr-spinel etc.) characteristic for a SSZ-type of geotectonic setting.
- Plagioclase growths are linked to subsolidus equilibration and melt metasomatism of lithospheric mantle in the MOR-type geotectonic setting.
- Pyroxenites crop out only sporadically in close association with dominant plagioclase lherzolites.
- The mineral paragenesis of pyroxenites comprises big euhedral grains of ortho- and clinopyroxene, which define a recondite cumulate texture. The intercumulus space is occupied by small to medium-grained mosaic olivine and rarely spinel.
- Petrological and geochemical evidence suggests that KKOC pyroxenites formed at high pressures and temperatures, suggesting a relatively deep origin of ultramafic cumulates. The crystallisation took place in thermal conduits, located under the ocean ridge system, where significant cooling of conductive melt occurs.
- Dunites possess typical cumulate texture, containing major olivine (~ 90 vol.%) and some minor olivine and spinel.
- Dunite geochemistry reveals its refractory nature that underwent an extensive melting in a SSZ-type of geotectonic setting, also influenced by boninitic fluid impregnation processes.

- In close association with dunites, the chromitite emerges, characterised by high Cr content of spinel ( $Cr\# \approx 80$ ).
- It was inferred that KKOC dunites and associated chromitites actually represent the uppermost part of the transitional zone (crust-mantle transition), formed by crystal fractionation from a hypothetical crustal magma chamber. This process was followed by an intensive melt-rock metasomatism. Initially, the chromitites segregated from the invading (boninitic) melt, which subsequently percolated into neighbouring rocks, producing dunites.
- Metamorphic units of KKOC are reported to form an elongated domain between the two main peridotite masses (Krivaja and Konjuh), having the main metamorphic portion in the south, near the villages Duboštica and Vijaka.
- Textures of the metamorphic rocks are either crystalloblastic or porphyroblastic. The rock structures are more often than not parallel, showing an alternation of 'white' and 'black' rock segments.
- Several rock varieties have been recognised within the KKOC metamorphites. Those are: (1) *granoblastic amphibolite*, (2) *Grt-Di amphibolite*, (3) *Grt-Di-Hy amphibolite*, (4) *diopside amphibolite gneiss*, and (5) *Pl-Grt-Di gneiss*.
- Major and trace element geochemistry, as well as petrographic data show that  $\sim 2/3$  of the KKOC metamorphites bear geochemical signatures of mafic to ultramafic gabbroic rocks (SSZ-type setting), whereas the rest corresponds to more evolved basalts of tholeiitic affinity (MOR-type setting).
- Geothermobarometric calculations, based on the chemistry of different coexisting minerals, yielded ranges of temperature and pressures for the different KKOC petrographic varieties:  $\sim 880$  °C and 0.90-1.30 GPa for granoblastic amphibolites, 802-1028 °C and 0.94-1.40 GPa for Grt-Di amphibolites, 0.84-0.89 GPa for Di amphibolites and 729-890 °C and 1.10-1.60 GPa for Pl-Grt-Di gneisses.
- Hypothetical clockwise *P-T-t* paths or trajectories were constructed, suggesting that the Pl-Grt-Di schists present the deepest part of the subducted slab ( $\sim 30$ -42 km), followed by the Grt-Di and Grt-Di-Hy amphibolites ( $\sim 24$ -35 and  $\sim 24$ -30 km respectively). The shallowest domains of the metamorphosed oceanic crust are represented by the granoblastic amphibolites, generated at depths of 4 to 30 km.
- The generation of the KKOC commenced in the Late Triassic by opening of the Pindos ocean and subsequent Late Triassic to Early Jurassic spreading of the Dinaridic Ocean through the detachment of the Drina-Ivanjica microplate from the Adriatic microplate.
- The extensional processes might have lasted for some 30 to 40 Ma, when in the Early to Middle Jurassic (Bajorcian-Taorcian period), due to the continuous northward movement of Africa, an intra-oceanic NE-dipping subduction took place, indicating the overall space shortening.
- Strong petrological and geochemical evidence implies the proximity of Dinaric intra-oceanic subduction zone and KKOC mantle domain. Furthermore, in order to reconcile the features of two contrasting geotectonic settings (MOR and SSZ) displayed by almost

all KKOC lithological units, one suggests that a subducted slab must have been placed under the Krivaja-Konjuh mantle domain.

- The metamorphic sole is also related to such a defined inter-oceanic subduction and underplating of the cold oceanic crust under the hot mantle wedge. Part of the oceanic crust is found deeply subducted, having recorded the highest metamorphic grades.
- During the Late Jurassic to Early Cretaceous transition period, the subduction trench collided with the Adriatic microplate, and the KKOC among other CDOB ultramafic complexes was thrust southwestwards on the Adriatic carbonate platform.
- Throughout the emplacement, the eastern KKOC mantle portion most probably was tectonically exhumed along the ancient subduction channels, causing an erosion of the overlying plagioclase-containing lithospheric mantle (impregnation zone). This resulted in the present-day exposure of spinel lherzolites of the Konjuh domain at the same altitude with the plagioclase lherzolites of the western Krivaja segment, whereas the metamorphic soles are found situated in-between the two.



## 8. REFERENCES

- Abouin J, Blanchet R, Cadet JP, Celet P, Charvet J, Chorowicz J, Cousin J, Rampnoux J (1970) Essai sur la géologie des Dinarides. *Bull. Soc. Géol. France* 12: 1060-1093
- Aldanmaz E, Schmidt MW, Gourgaud A, Meisel T (2009) Mid-ocean ridge and supra-subduction geochemical signatures in spinel-peridotites from the Neotethyan ophiolites in SW Turkey: Implications for upper mantle melting processes. *Lithos* 113: 691-708
- Aljinović D, Kozur H (2003) Resedimented Carboniferous and Lower Permian radiolarians in Roadian (Middle Permian) deep-water clastic complex of Gorski Kotar region (Croatia). In: Vlahović E (Ed.), 22<sup>nd</sup> International Association of Sedimentologists, Meeting of Sedimentology, Opatija, Croatia. *Abstract Book* vol. 4
- Allegre CJ, Turcotte DL (1986) Implications of a two-component marble-cake mantle. *Nature* 323: 123-127
- Arai S (1987) An estimation of the least depleted spinel peridotite on the basis of olivine-spinel mantle array. *N. Jb. Miner. Mh.* 8: 347-354
- Arai S (1992) Chemistry of chromian spinel in volcanic rocks as a potential guide to magma chemistry. *Mineral. Mag.* 56: 173-184
- Arai S (1994) Characterization of spinel peridotites by olivine-spinel compositional relationships: Review and Interpretation. *Chem. Geol.* 113: 191-204
- Arai S, Okamura H, Kadoshima K, Ninomya C, Suzuki K (2007) Chromian spinel chemistry in ultramafic-mafic plutonic rocks as a discriminato of tectonic settings. *Eur. J. Mineral.* 19: 617-622
- Asimow PD (1999) A model that reconciles major- and trace- element data from abyssal peridotites. *Earth Planet. Sci. Lett.* 169: 303-319
- Augé T (1983) Etude Minéralogique et Pétrographique des Roches Basiques et Ultrabasiques du Complexe Ophiolitique du Nord Oman. *Docum. BRGM* 65: 263 p
- Babajić E (2009) Petrološko-geohemijska obilježja mafitnih stijena Krivajsko-konjuškog ofiolitnog kompleksa. *PhD thesis. Univ. Tuzla (Bosnia and Herzegovina)*, 163 p
- Bailey SW (1988) Chlorites: Structures and Crystal Chemistry.- In: Bailey SW (ed.): Hydrous Phyllosilicates. *Rev. Miner. Soc. America* 13: 347-403
- Baldwin JA, Bowring SA, Williams ML (2003) Petrological and geochronological constraints on high pressure, high temperature metamorphism in the Snowbird tectonic zone, Canada. *J. metam. Geol.* 21: 81-98
- Ballhaus C, Berry RF, Green DH (1991) High pressure experimental calibration of the olivine-orthopyroxene-spinel oxygen geobarometer: implications for the oxidation state of the upper mantle. *Contrib. Min. Petrol.* 107: 27-40
- Barnes SJ, Röder PL (2001) The Range of Spinel Compositions in Terrestrial Mafic and Ultramafic Rocks. *J. Petrol.* 42: 2279-2302
- Barth MG, Mason PRD, Davies GR, Dijkstra AH, Drury M (2003) Geochemistry of the Othris Ophiolite, Greece: Evidence for Refertilization? *J. Petrol.* 44: 1759-1785
- Basu AR (1977) Textures, microstructures and deformation of ultramafic xenoliths from San Quintin, Baja California. *Tectonophysics* 42: 213-246
- Bazylev BA (2003) Petrology and geochemistry of oceanic and alpine-type spinel peridotites in relation to the problem of the mantle matter evolution. *PhD thesis, Vernadsky Institute (Moscow)* 213 p
- Bazylev BA, Karamata S, Zakariadze GS (2003) Petrology and evolution of the Brezovica ultramafic massif, Serbia. In: Dilek Y, Robinson PT (eds.) Ophiolites in Earth History *Geol. Soc. London* 18: 91-108

- Bazylev BA, Popević A, Karamata S, Kononkova NN, Simakin SG, Olujić J, Vujnović L, Memović E (2009) Mantle peridotites from the Dinaridic ophiolite belt and the Vardar zone western belt, central Balkan. *Lithos* 108: 37–71
- Bazylev BA, Sylantiev SA (2000) Geodynamic interpretation of the subsolidus recrystallization of mantle spinel peridotites: Ophiolites and xenoliths. *Petrology* 8: 311-331
- Beccaluva L, Ohnenstetter D, Ohnenstetter M, Venturelli G (1977) Trace element geochemistry of Corsican ophiolites. *Contrib. Min. Petrol.* 64: 11-31
- Becker H (1996) Geochemistry of garnet peridotite massifs from lower Austria and the composition of deep lithosphere beneath Paleozoic convergent plate margin. *Chem. Geol.* 134: 49-65
- Benoit V (1987) Etat d'équilibre de péridotites du manteau supérieur : application au plateau du Colorado. *PhD Thesis, IPG Paris et Université Paris VII*
- Berger E, Vannier M (1984) Les dunites en enclave dans les basaltes alcalins des îles océaniques: Approche pétrologique. *Bull. Minéral.* 107: 649-663
- Bertrand J, Dietrich V, Nievergelt P, Vuagnat M (1987) Comparative major and trace element geochemistry of gabbroic and volcanic rock sequences, Mont Genève Ophiolite, Western Alps. *Schw. Min. Petr. Mitt.* 67: 147-169
- Blichert-Toft J, Albarede F, Kornprobst J (1999) Lu-Hf isotope systematics of garnet pyroxenites from Beni Bousera, Morocco: implication for basalt origin. *Science* 283: 1303-1306
- Bodinier JL (1988) Geochemistry and petrogenesis of the Lanzo peridotite body, western Alps. *Tectonophysics* 149: 67-88
- Bodinier JL (1989) Distribution des terres rares dans les massifs lherzolitiques de Lanzo et de l'Ariège. *PhD thesis, Univ. of Montpellier* 89 p
- Bodinier JL, Guiraud M, Dupuy C, Dostal J (1986a) Geochemistry of basic dykes in the Lanzo Massif (Western Alps): petrogenetic and geodynamic implications. *Tectonophysics* 128: 77-95
- Bodinier JL, Guiraud M, Fabriès J, Dostal J, Dupuy C (1986b) Petrogenesis of layered pyroxenites from the Lherz, Freychinède and Prades ultramafic bodies (Ariège, French Pyrénées). *Geochim. Cosmochim. Acta* 51: 279-290
- Bodinier JL, Godard M (2003) Orogenic, Ophiolitic, and Abyssal Peridotites. *In: The mantle and Core* (ed. Carlson RW) Vol.2. (eds. Holland HD, Turekian KK) Treatise on Geochemistry. *Elsevier-Pergamon, Oxford* 103-171
- Bodinier JL, Menzies MA, Shimizu N, Frey FA, McPherson E (2004) Silicate, hydrous and carbonate metasomatism at Lherz, France: contemporaneous derivatives of silicate melt-harzburgite reaction. *J. Petrol.* 45: 299-320
- Bonatti E, Michael P (1989) Mantle peridotites from continental rifts to ocean basins to subduction zones. *Earth Planet. Sci. Lett.* 91: 297-311
- Bonatti E, Peyve A, Kepezhinskas P, Kurentsova N, Seyler M, Skolotnev S, Udintsev G (1992) Upper mantle heterogeneity below the Mid-Atlantic Ridge, 0°-15°N. *J. Geophys. Res.* 97:4461-4476
- Borghini G, Fumagalli P, Rampone E (2007) Experimental and natural constraints on the spinel-plagioclase subsolidus transition in mantle peridotites. *Geoph. Res. Abstrac.* 9: 07687
- Boudier F, Nicolas A (1985) Harzburgite and lherzolite subtypes in ophiolitic and oceanic environments. *Earth Planet. Sci. Lett.* 76:84-92
- Boudier F, Juteau T (2000) The ophiolite of Oman and United Arab Emirates. *Marine Geoph. Res.* 21: 145-146

- Boyd FR (1973) A pyroxene geotherm. *Geochim. Cosmochim. Acta* 37: 2533-2544
- Boyd FR, Pokhilenko NP, Pearson DG, Mertzman SA, Sobolev NV, Finger LW (1997) Composition of the Siberian cratonic mantle: evidence from Udachnaya peridotite xenoliths. *Contrib. Mineral. Petrol.* 128: 228-246
- Bread JS (1986) Characteristic mineralogy of arc-related cumulate gabbros: implications for the tectonic setting of gabbroic plutons and for andesite genesis. *Geology* 14: 848-851
- Brenan J-M, Shaw HF, Ryerson FJ (1995) Experimental evidence for the origin of lead enrichment in convergent margin magma. *Nature* 378:54-56
- Brey GP, Köhler T (1990) Geothermobarometry in Four-phase Lherzolites II. New Thermobarometers, and Practical Assessment of Existing Thermobarometers. *J. Petrol.* 31:1353-1378
- Bucher K, Frey M (1994) Petrogenesis of Metamorphic Rocks. *Springer* Berlin
- Burgath KP, Marchig V, Mussallam K (1997) 29. Data report: Mineralogic, structural, and chemical variability of mantle sections from Holes 920B and 920D. *In: Karson JA, Cannat M, Miller DJ, Elthon D (eds.) Proc. ODP. Sci. Results College Station, Texas* 153
- Bussod GY, Christie JM (1991): Textural development and melt topology in spinel lherzolite experimentally deformed at hypersolidus conditions. *J. Petrol. Spec. Issue* 17-39
- Cabanes N, Mercier JCC (1988) Insight into the upper mantle beneath an active extensional zone: the spinel-peridotite xenoliths from San Quintin (Baja, California, Mexico). *Contrib. Mineral. Petrol.* 100: 374-382
- Cannat M, Bideau D, Hébert R (1990) Plastic deformation and magmatic impregnation in serpentinized ultramafic rocks from the Garrett transform fault (East Pacific Rise). *Earth Planet. Sci. Lett.* 101: 216-232
- Cannon RT (1966) Plagioclase zoning and twinning in relation to the metamorphic history of some amphibolites and granulites. *Am. J. Sci.* 264: 526-542
- Carosi R, Cortesogno L, Gaggero L, Marroni M (1997) Geological and petrological features of the metamorphic sole from the Mirdita Nappe, Northern Albania. *Ophioliti* 21: 21-40
- Carswell DA, Harley SM (1990) Mineral barometry and thermometry. *In: Carswell DA (ed.) Eclogite facies rocks*, 93-110, Blackie, Glasgow
- Cavazza W, Roure F, Ziegler PA (2004) The Mediterranean Area and the Surrounding Regions: Active Processes, Remnants of Former Tethyan Oceans and Related Thrust Belts.- *In: Cavazza W, Roure F, Spakman W, Stampfli G, Ziegler PA (eds.) The TRANSMED Atlas. 32<sup>th</sup> Int. Geol. Congress, Florence*
- Çelik ÖF, Delaloye MF (2006) Characteristics of ophiolite-related metamorphic rocks in the Beyşehir ophiolitic mélange (Central Taurides, Turkey), deduced from whole rock and mineral chemistry. *J. Asian Earth Sci.* 26: 461-476
- Chan GHN, Malpas J, Xenophontos C, Lo CH (2008) Magmatism associated with Gondwanaland rifting and Neo-Tethyan oceanic basin development: evidence from the Mamonia Complex, SW Cyprus *J. Geol. Soc.* 165: 699-709
- Chen JC and Lee KL (1996) Geochemistry of Miocene basaltic rocks recovered by the Ocean Drilling Program from the Japan Sea. *J. South East Asian Earth Sci.* 13: 29-38
- Chen S, O'Reilly SY, Zhou X, Griffin WL, Zhang G, Sun M, Feng J, Zhang M (2001) Thermal and Petrological structure of the lithosphere beneath Hannuoba, Sino-Korea craton, China: evidence from xenoliths. *Lithos* 56: 267-301
- Coleman RG (1977) Ophiolites. *Springer-Verlag Berlin* 229 p
- Cvetković V, Downes H, Prelević D, Lazarov M, Resimić-Šarić K (2007) Geodynamic significance of ultramafic xenoliths from Eastern Serbia: Relics of sub-arc continental mantle. *J. Geodynam.* 43: 504-527



- Dale J, Holland T, Powell R (2000) Hornblende-garnet-plagioclase thermobarometry: a natural assemblage calibration of the thermodynamics of hornblende. *Contrib. Miner. Petrol.* 140: 353-362
- Dantas C, Ceuleneer G, Gregoire M, Pythin M, Freyrier R, Warren J, Dick HJB (2007) Pyroxenites from the Southwest Indian Ridge, 9-16°E: Cumulates from Incremental Melt Fractions Produced at the Top of a Cold Melting Regime. *J. Petrol.* 48: 647- 660
- DeBari SM, Sleep NH (1991) High-Mg, low-Al bulk composition of the Talkeetna island arc, Alaska: implications for primary magmas and the nature of the arc crust. *Geol. Soc. Am. Bull.* 103: 37-47
- Deer WA, Howie RA, Zussman J (1992) An introduction to rock-forming minerals. 2<sup>nd</sup> edition. *Pearson Educ. Ltd. Harlow* 696 p
- D'el-Rey Silva LJH, Dantas EL, Guimarães Teixeira JB, Laux JH, da Glória da Silva M (2007) U–Pb and Sm–Nd geochronology of amphibolites from the Curaçá Belt, São Francisco Craton, Brazil: Tectonic implications. *Gondwana Res.* 12: 454-467
- Dessai AG, Dessai A, Markwick A, Vaselli O, Downes H (2004) Granulite and pyroxenite xenoliths from the Deccan Trap: insight into the nature and composition of the lower lithosphere beneath cratonic India. *Lithos* 78: 263-290
- Dick HJB (1977) Partial melting in the Josephine peridotite: 1. The effect on mineral composition and its consequences for geobarometry and geothermometry. *Am. J. Sci.* 277: 801-832
- Dick HJB, Fisher RL, Bryan WB (1984) Mineralogical variability of the uppermost mantle along mid-ocean ridges. *Earth Planet. Sci. Lett.* 69: 88-106
- Dick HJB, Bullen T (1984) Chromian spinel as a petrogenetic indicator in abyssal and alpine-type peridotites and spatially associated lavas. *Contrib. Min. Petrol.* 86: 54-76
- Dick HJB (1989) Abyssal peridotites, very slow spreading ridges and ocean ridge magmatism. *In: Sonders AD, Norry MJ (eds.) Magmatism in the ocean basins. Geol. Soc. London Spec. Publ.* 42: 71-105
- Dick HJB, Natland JH (1996) Late stage melt evolution and transport in the shallow mantle beneath the East Pacific Rise: Deep Sea Drilling Project. *Initial Reports* 147: 103-134
- Dilek Y, Flower MFJ (2003) Arc-trench rollback a forearc accretion: 2. A model template for ophiolites in Albania, Cyprus, and Oman *In: Ophiolites in earth history (eds. Dilek Y, Robinson PT) Geol. Soc. London Spec. Publ.* 218: 43-69
- Dilek Y, Shallo M, Furnes H (2008) Geochemistry of the Jurassic Mirdita Ophiolite (Albania) and the MORB to SSZ evolution of a marginal basin oceanic crust. *Lithos* 100: 174-209
- Dimitrijević MD, Dimitrijević MN (1973) Olistostrome mélange in the Yugoslavian Dinarides and Late Mesozoic plate tectonics. *J. Geol.* 81: 328-340
- Đorđević D, Pamić J (1972) Petroloski izvjestaj za osnovnu geolosku kartu, list Vlasenica, 1:100000. *Fond struc. dok. Instituta geol. istr. Sarajevo*
- Đorđević P (1958) Bazični eruptivi okoline Vareša (Bosna). *Zbornik radova RGF-a (Belgrade)* 5: 39-44
- Downes H (2007) Origin and significance of spinel and garnet pyroxenites in the shallow lithospheric mantle: Ultramafic massifs in orogenic belts in Western Europe and NW Africa. *Lithos* 99: 1-24
- Džepina D (1970) Rezultati mineraloško-petroloških ispitivanja regionalno metamorfisanih bazičnih stijena južnog dijela planine Borje u Bosni. *Gl. prirod. muz. Belgrade* 25/A: 129-144
- Eckert JO, Newton RC, Kleppa OJ (1991) The  $\Delta H$  of reaction and recalibration of garnet-clinopyroxene-plagioclase-quartz geobarometers in the CMAS system by solution calorimetry. *Amer. Mineral.* 76:148-160

- Elderfield H, Greaves MJ (1982) The rare earth elements in seawater. *Nature* 296: 214-218
- Ellis DJ, Green DH (1979) An experimental study on the effect of Ca upon garnet-clinopyroxene Fe-Mg exchange equilibria. *Contrib. Miner. Petrol.* 71:13-22
- El-Naby HA, Frisch W, Hegner E (2000) Evolution of the Pan-African Wadi Haimur metamorphic sole, Eastern Desert, Egypt. *J. metam. Geol.* 18: 639-651
- Elthon D (1989) Pressure of origin of primary mid-ocean ridge basalts. *In: Sounders AD, Norry MJ (Eds.) Magmatism in Ocean Basins. Geol. Soc. Spec. Publ.* 42: 125-136
- Erlank AJ, Waters FG, Hawkesworth CJ, Haggerty SE, Allsopp HL, Rickard RS, Menzies M (1987) Evidence for mantle metasomatism in peridotites noduls from the Kimberley pipes, South Africa. *In: Menzies M, Hawkesworth CJ (eds.) Mantle Metasomatism. Acad. Press London* 221-309
- Ernewein M, Pflumio C, Whitechurch H (1988) The death of an accretion zone as evidenced by the magmatic history of the Semail ophiolite (Oman). *Tectonophysics* 151: 247-274
- Ernst WG, Liu J (1998) Experimental phase-equilibrium study of Al-and Ti-contents of calcic amphibole in MORB; a semiquantitative thermobarometer. *Amer. Mineral.* 83: 952-969
- Fabriès J, Bodinier JL, Dupuy C, Lorand JP, Benkerrou C (1989) Evidence for modal metasomatism in the orogenic spinel lherzolite body from Caussou (North-eastern Pyrénées, France). *J. Petrol.* 30: 199-229
- Fabriès J (1979) Spinel-olivine geothermometry in peridotites from ultramafic complexes. *Contrib. Mineral. Petrol.* 69: 329-336
- Finger F, Cooke R, Janoušek V, Konzett J, Pin C, Roberts MP, Tropper P (2003) Petrogenesis of the south Bohemian granulites: The importance of crystal-melt relationships. *J. Czech Geol. Soc.* 48: 44-45
- Flower MFJ, Dilek Y (2003) Arc-trench rollback a forearc accretion: 1. A collision-induced mantle flow model for Tethyan ophiolites. *In: Ophiolites in earth history (eds. Dilek Y, Robinson PT) Geol. Soc. London Spec. Publ.* 218: 21-41
- Floyd PA, Winchester JA (1975) Magma type and tectonic setting discrimination using immobile elements *Earth Planet. Sci. Lett.* 27: 211-218
- Frey FA (1980) The origin of pyroxenites and garnet pyroxenites from Salt Lake Crater, Oahu, Hawaii: trace element evidence. *Am. J. Sci.* 280: 427-449
- Frey FA (1984) Rare earth element abundances in upper mantle rocks. *In: Henderson, P. (ed.) Rare Earth Element Geochemistry. Elsevier* 153-203
- Frey M, DeCapitani D, Liou JG (1991) A new petrogenetic grid for low-grade metabasites. *J. metam. Geol.* 9: 497-509
- Garašić V (1994) Mantelxenolithe als Dokumente der thermischen Entwicklung des Erdmantels unter den Chyulu Hills, Kenia. *PhD thesis, Univ. Heidelberg*, 220 p.
- Garfunkel Z (2004) Origin of the Eastern Mediterranean basin: a re-evaluation. *Tectonophysics* 391: 11-34
- Garrido CJ, Bodinier JL (1999) Diversity of mafic rocks in the Ronda peridotite: evidence for pervasive melt-rock reaction during heating of sub-continental lithosphere by upwelling asthenosphere. *J. Petrol.* 40: 729-754
- Gartzos E, Dietrich VJ, Migiros G, Serelis K, Lymperopoulou Th (2009) The origin of amphibolite from metamorphic soles beneath the ultramafic ophiolites in Evia and Lesvos (Greece) and their geotectonic implication. *Lithos* 108: 224-242
- Gasparik T (1984) Two-pyroxene thermobarometry with new experimental data in the system CaO-MgO-Al<sub>2</sub>O<sub>3</sub>-SiO<sub>2</sub>. *Contrib. Min. Petrol.* 87: 87-97
- Gervilla F, Remaïdi M (1993) Field trip to the Ronda ultramafic massif: an example of asthenosphere-lithosphere interaction? *Ophioliti* 18: 21-35

- Girardeau J, Francheteau J (1993) Plagioclase-wehrlites and peridotites on the East Pacific Rise (Hess Deep) and the Mid-Atlantic Ridge (DSDP Site 339) evidence for magma percolation in the oceanic upper mantle. *Earth Planet. Sci. Lett.* 115: 137-149
- Gjata K, Kornprobst J, Kodra A, Briot D, Pineau F (1992) Subduction chaude à l'aplomb d'une dorsal? Exemple des enclaves de pyroxénite à grenat de la brèche serpentiniteuse de Derveni (Albanie). *Bull. Soc. géol. France* 163: 469-476
- Gnos E, Peters TJ (1993) K-Ar ages of the metamorphic sole of the Semail ophiolite: Implications for ophiolite cooling history. *Contrib. Mineral. Petrol.* 113: 325-332
- Gnos E, Kurz D (1994) Sapphirine-quartz and sapphirine-corundum assemblages in metamorphic rocks associated with the Semail Ophiolite (United Arab Emirates). *Contrib. Mineral. Petrol.* 116: 398-410
- Gómez-Pugnaire MT, Azor A, Fernández-Soler JM, López Sánchez-Vizcaino V (2003) the amphibolites from the Ossa-Morena/Central Iberian Variscian suture (Southwestern Iberian Massif): geochemistry and tectonic interpretation *Lithos* 932: 1-20
- Graham CM, Powell R (1984) A garnet-hornblende geothermometer; calibration, testing, and application to the Pelona Schist, Southern California. *J. metam. Geol.* 2: 13-31
- Grapes RH, Graham CM (1978) The actinolite – hornblende series in metabasites and so called miscibility gap. A review. *Lithos* 11: 85 – 97
- Green DH (1994) Experimental studies of trace-element partitioning applicable to igneous petrogenesis—Sedona 16 years later. *Chem. Geol.* 117: 1-36
- Green DH, Ringwood AE (1967) the genesis of basaltic magmas. *Contrib. Mineral. Petrol.* 15: 103-190
- Grégoire M, Tinguely C, Bell DR, le Roex AP (2005) Spinel lherzolite xenoliths from the Premier kimberlite (Kaapvaal craton, South Africa): Nature and evolution of the shallow upper mantle beneath the Bushveld complex. *Lithos* 84: 185-205
- Gruau G, Bernard-Griffiths J, Lécuyer C (1998) The origin of U-shaped rare earth patterns in ophiolite peridotites: Assessing the role of secondary alteration and melt/rock reaction. *Geochim. Cosmochim. Acta* 62: 3545-3560
- Gueguen Y, Nicolas A (1980) Deformation of mantle rocks. *Ann. Rev. Earth Planet. Sci.* 8: 119-144
- Guidotti CV, Johnson SE (2002) Pseudomorphs and associated microstructures of western Maine, USA. *J. Struct. Geol.* 24: 1139-1156
- Guilmette C, Hébert R, Dupuis C, Wang CS, Li Z (2005) Metamorphic history of highly foliated amphibolites from the ophiolitic mélange beneath the Yarlung Zangbo Ophiolites, Xigaze area, Tibet. *J. metam. Geol.* 3: 231-243
- Guilmette C, Hébert R, Dupuis C, Wang CS, Li Z (2008) Metamorphic history and geodynamic significance of high-grade metabasites from the ophiolitic mélange beneath the Yarlung Zangbo ophiolites, Xigaze area, Tibet. *J. Asian Earth Sci* 32: 423-437
- Hacker BR, Mosenfelder JL (1996) Metamorphism and deformation along the emplacement thrust of the Semail ophiolite, Oman *Earth Planet. Sci. Lett.* 144: 435-451
- Halamić J, Goričan Š (1995) Triassic radiolarites from Mts. Kalnik and Medvednica (northwestern Croatia). *Geol. Croat.* 48: 129-146
- Hamlyn PR, Bonatti E (1980) Petrology of mantle-derived ultramafics from the Owen fracture zone, Northwest Indian Ocean: Implications for the nature of the oceanic upper mantle. *Earth Planet. Sci. Lett.* 48: 65-79
- Harley SL (1984) An experimental study of the partitioning of Fe and Mg between garnet and orthopyroxene. *Contrib. Min. Petrol.* 86:359-373
- Harley SL, Green DH (1982) Garnet-orthopyroxene barometry for granulites and peridotites. *Nature* 300:697-701

- Harlov D, Tropper P, Seifert W, Nijland T, Förster H-J (2006) Formation of Al-rich titanite (CaTiSiO<sub>4</sub>O–CaAlSiO<sub>4</sub>OH) reaction rims on ilmenite in metamorphic rocks as a function of  $f_{H_2O}$  and  $f_{O_2}$ . *Lithos* 88: 72-84
- Hart RS, Blusztajn J, Dick HJB, Meyer PS, Muehlenbach K (1999) The fingerprint of seawater circulation in a 500-meter section of ocean crust gabbros. *Geochim. Cosmochim. Acta* 63: 4059–4080
- Hébert R, Laurent R (1989) Mineral chemistry of ultramafic and mafic plutonic rocks of the Appalachian ophiolites, Québec, Canada. *Chem. Geol.* 77: 265-285
- Hellebrand E, Snow JE, Dick HJB, Hofmann AW (2001) Coupled major and trace elements as indicators of the extent of melting in mid-ocean-ridge peridotites. *Nature* 410: 677-681
- Hellebrand E, Snow JE, Mühe R (2002) Mantle melting beneath Gakkel Ridge (Arctic Ocean): abyssal peridotite spinel compositions. *Chem. Geol.* 182: 227-235
- Herak M (1986) A new concept of the geotectonics of the Dinarides. *Acta Geol. (Zagreb)* 16: 1-42
- Hewins RH (1974) Pyroxene crystallization trends and contrasting augite zoning in the Sudbury Nickel Irruptive. *Amer. Mineral.* 59: 120-126
- Hey MH (1954) A new review of the chlorites. *Mineral. Mag.* 224: 277-292
- Hofmann WA (1988) Chemical differentiation of the Earth: the relationship between mantle, continental crust and oceanic crust. *Earth. Planet. Sci. Lett.* 90: 297-314
- Holland T, Blundy J (1994) Non-ideal interactions in calcic amphiboles and their bearing on amphibole-plagioclase thermometry. *Contrib. Min. Petrol.* 116:433-447
- Higgins JB, Ribbe PH (1976) The crystal chemistry and space groups of natural and syntetic titanites. *Amer. Mineral.* 61: 878-888
- Hrvatović H (2006) Geological guide through Bosnia and Herzegovina. *Geol. Surv. Bosnia and Herzegovina*, 172 p
- Hynes A (1982) A comparison of amphiboles from medium and low-pressure metabasites. *Contrib. Min. Petrol.* 81: 119-125
- Hwang SL, Yui TF, Chu HT, Shen P, Schertel HP, Zhang RY, Liou JG (2007) On the origin of oriented rutile needles in garnet from UHP eclogites. *J. metam. Geol.* 25: 349-362
- Ikeda Y (1990) Ce<sub>N</sub>/Sr<sub>N</sub>/Sm<sub>N</sub>: A trace element discriminant for basaltic rocks from different tectonomagmatic environments. *N. Jb. Miner. Mh. Jg.* 4: 145-158
- Ilnicki S (2002) Amphibolites and metabasites from the Izera block, West Sudetes. *Mineral. Soc. Poland. Spec. Papers* 20: 262-269
- Irvine TN (1977) Origin of chromite layers in the Muskox intrusion and other stratiform intrusions: A new interpretation. *Geology* 5: 273-277
- Irvine TN, Findlay TC (1972) Alpine-type peridotite with particular reference to the Bay of Islands Complex. In: The ancient oceanic lithosphere. *Publ. Earth Physics Branch (Ottawa, Canada)* 97-128
- Irvine TN, Baragar WRA (1971) A guide to chemical classification of common volcanic rocks. *Can. J. Earth Sci.* 8: 523-548
- Ishii T, Robinson PT, Mackawa H, Fiske R (1992) Petrological studies of peridotites from diapiric serpentine seamounts in the Izu-Ogasawara-Mariana forearc. In: Fryer P, Pearce JA, Stokking LB et al. (eds.). *Proceed. Ocean Drill. Prog.* 125: 445-485
- Jagoutz E, Palme H, Baddenhausen H, Blum K, Cendales M, Dreibus G, Spettel B, Lorenz V, Wanke H (1979) The abundances of major, minor and trace elements in the earth's mantle as derived from primitive ultramafic nodules. *Proc. Lunar Planet. Sci. Con 10th* 2031-2050

- Johnson KTM, Dick HJB (1992) Open system melting and temporal and spatial variation of peridotite and basalts at the Atlantis II Fracture Zone. *J. Geoph. Res.* 97: 9219-9241
- Johnson K (1998) Experimental determination of partition coefficients for rare earth and high-field-strength elements between clinopyroxene, garnet, and basaltic melt at high pressures. *Contrib. Mineral. Petrol.* 133: 60-68
- Jovanović R (1957) Pregled razvoja mezozoika i neki novi podaci za stratigrafiju NR BiH. // *Kong. Geol. Jugoslav. Sarajevo* 38-63
- Juteau T, Berger E, Cannat M. (1990) Serpentinized, residual mantle peridotites from the M.A.R. Median Valley, ODP hole 670A (21°10'N, 45°02'W, Leg 109): primary mineralogy and geothermometry. *Proceed. Ocean Drill. Prog.* 106/109 (eds) Detrick R, Honnorez J, Brian WB, Juteau T *College Station, TX* 27-45
- Karamata S, Pamić J (1960) Gabrovi, dijabazi i spiliti područja Tribije (Vareš). *Simp. probl. alps. inicij. magmat., Sarajevo* 3: 1-15
- Karamata S (1968) Zonality in contact metamorphic rocks around the ultramafic mass of Brezovica (Serbia, Yugoslavia). *Proceed. 13<sup>th</sup> Int. Geol. Cong. Prague* 1: 197-207
- Karamata S, Sladić-Trifunović M, Cvetković V, Milovanović D, Šarić K, Olujić J, Vujnović L (2005) The western belt of the Vardar Zone with special emphasises to the ophiolites of Podkozarje - The youngest ophiolitic rocks of the Balkan Peninsula. *Bull. Acad. Sci. Art. Serbe* 43: 85-96
- Kaczmarek MA, Müntener O (2008) Juxtaposition of Melt Impregnation and High-Temperature Shear Zones in the Upper Mantle; Field and Petrological Constraints from the Lanzo Peridotite (Northern Italy). *J. Petrol.* 49: 2187-2220
- Keays RR (1995) The role of komatitic and picritic magmatism and S-saturation in the formation of the ore deposits. *Lithos* 34: 1-18
- Kelemen PB (1990) Reaction between ultramafic rock and fractionating basaltic magma I. Phase relations, the origin of calc-alkaline magma series, and the formation of discordant dunite. *J. Petrol.* 31: 51-98
- Kelemen PB, Dick HJB, Quick JE (1992) Production of harzburgite by pervasive melt-rock reaction in the upper mantle. *Nature* 358: 635-641
- Kelemen PB, Shimizu N, Salters VJM (1995) Extraction of mid-ocean-ridge basalt from the upwelling mantle by focused flow of melting dunite channels. *Nature* 375: 747-753
- Kimball KL, Spear FS, Dick HJB (1985) High temperature alteration of Abyssal ultramafics from the Islas Orcadas Fracture Zone, South Atlantic. *Contrib. Min. Petrol.* 91: 307-320
- Kišpać M (1897) Kristalinsko kamenje serpetinske zone u Bosni. *Rad JAZU (Zagreb)* 133: 95-231
- Kišpać M (1902) Mineraloške biljke iz Bosne. *Rad JAZU (Zagreb)* 151: 50-63
- Köhler TP, Brey GP (1990): Calcium exchange between olivine and clinopyroxene calibrated as a geothermobarometer for natural peridotites from 2 to 60 kb with applications. *Geochim. Cosmochim. Acta* 54: 2375-2388.
- Koepke J, Seidel E, Kreuzer H (2002) Ophiolites on the Southern Aegean islands Crete, Karpathos and Rhodes: composition, geochronology and position within the ophiolite belts of the Eastern Mediterranean. *Lithos* 65: 183-203
- Koller F, Melcher F, Meisel T, Puhl J, Bertle R (1999) The composition of mesozoic peridotite tectonites of the Eastern Alps. *Ophioliti* 24: 118-119
- Korikovski SP, Popević A, Kurdyukov EB, Karamata S (1996) Prograde contact metamorphism around the Ozren ultramafic massif, Serbia. *In: Knežević V, Kristić B (Eds) Terr. Serbia (Belgrade)* 253-258.

- Kornprobst J, Ohnenstetter D, Ohnenstetter M (1981) Na and Cr contents in clinopyroxenes from peridotites: a possible discriminant between "Sub-continental" and "Sub-oceanic" mantle. *Earth Planet. Sci. Lett.* 53: 241-254
- Kostopoulos DK (1991) Melting of the shallow upper mantle: a new perspective. *J. Petrol.* 32: 671-699
- Kretz R (1983) Symbols for rock-forming minerals. *Amer. Mineral.* 68: 277-279
- Krogh EJ (1988) The garnet-clinopyroxene Fe-Mg geothermometer - a reinterpretation of existing experimental data. *Contrib. Miner. Petrol.* 99: 44-48
- Krogh Ravn E (2000) Distribution of Fe<sup>2+</sup> and Mg between coexisting garnet and hornblende in synthetic and natural systems: an empirical calibration of the garnet-hornblende Fe-Mg geothermobarometer. *Lithos* 53:265-277
- Langmuir CH, Bender JF (1984) The geochemistry of oceanic basalts in the vicinity of transform faults: observations and implications. *Earth Planet. Sci. Lett.* 69: 107-127
- Lanphere M, Coleman RC, Karamata S, Pamić J (1975) Age of amphibolites associated with alpine peridotites in the Central Dinaride Ophiolite Belt, Yugoslavia. *Earth Planet. Sci. Lett.* 26: 271-276
- Leake BE *et al.* (1997) Nomenclature of amphiboles, Report of the Subcommittee on Amphiboles of the International Mineralogical Association, Commission on New Minerals and Mineral names. *Eur. J. Mineral.* 9: 623-651
- Leblanc M, Dupuy C, Merlet C (1984) Nickel content of olivine as a discriminatory factor between tectonite and cumulate peridotite in ophiolites. *Sci. Geol. Bull.* 37: 131-135
- Lee HY, Ganguly J (1988) Equilibrium compositions of coexisting garnet and orthopyroxene: Experimental determinations in the system FeO-MgO-Al<sub>2</sub>O<sub>3</sub>-SiO<sub>2</sub>, and applications *J. Petrol.* 29:93-113
- Lehmann J (1983) Diffusion between olivine and spinel: application to geothermometry. *Earth Planet. Sci. Lett.* 64: 123-138
- Le Maitre RW, Streckeisen A, Zanettin B, Le Bas MJ, Bonin B, Bateman P, Bellieni G, Dudek A, Efremova S, Keller J, Lamere J, Sabine PA, Schmid R, Sorensen H, Woolley AR (2002) Igneous Rocks: A Classification and Glossary of Terms, Recommendations of the International Union of Geological Sciences, Subcommittee of the Systematics of Igneous Rocks. *Cambridge: Cambridge University Press* 236 p
- Lenoir X, Garrido CJ, Bodinier JL, Dautria JM, Gervilla F (2001) The recrystallization front from the Ronda peridotite: evidence for melting and thermal erosion of sub-continental lithospheric mantle beneath the Alboran Basin. *J. Petrol.* 42: 141-158
- Lensch (1968) Der normative Mineralbestand von Mafiten. *Neues Jahrb. Monatsch.* 306-320
- Liang Y, Elthon D (1990) Evidence from chromium abundances in mantle rocks for extraction of picrite and komatiite melts. *Nature* 343: 551-553
- Liati A (1988) Amphibolitized eclogites in the Rhodope-Crystalline Complex, near Xanthi (N. Greece). *N. Jahrb. Mineral. Monatsh.* 1: 1-8
- Lippard SJ, Shelton AW, Gass IG (eds) (1986) The Ophiolite of Northern Oman. *Geol. Soc. Mem. (London)* 11: 178 p
- Liou JG, Maruyama S, Cho M (1985) Phase-equilibria and mineral parageneses of metabasites in low-grade metamorphism. *Mineral. Mag.* 49: 321-333
- Liu J, Bohlen SR, Ernst WG (1996) Stability of hydrous phases in subducting oceanic crust. *Earth Planet. Sci. Lett.* 143: 161-171
- Liu F, Xu Z, Liou JG, Song B (2004) SHRIMP U-Pb ages of ultrahigh pressure and retrograde metamorphism of gneisses, south-western Sulu terrane, eastern China. *J metam. Geol.* 22: 315-326

- Lorand JP, Keays RR, Bodinier JL (1993) Copper and noble metal enrichments across the lithosphere-asthenosphere boundary of the mantle diapirs: evidence from the Lanzo Iherzolite massif. *J. Petrol.* 34: 1110-1140
- Lugović B (1986) Gabro-peridotitska asocijacija stijena sjeverozapadnog oboda ofiolitnog masiva Maljena. *PhD thesis, Univ. Zagreb (Croatia)* 207 p.
- Lugović B, Altherr R, Raczek I, Hofmann AW, Majer V (1991) Geochemistry of peridotites and mafic igneous rocks from the Central Dinaridic Belt, Yugoslavia. *Contrib. Mineral. Petrol.* 106: 201-216
- Lugović B, Šegvić B, Babajić E, Trubelja F (2006) Evidence of short-living intraoceanic subduction in the Central Dinarides, Konjuh ophiolite complex (Bosnia-Herzegovina) - Mesozoic ophiolite belts of northern part of the Balkan Peninsula. *In: Resimić-Šarić K (ed.). Proceedings Uni Belgrade, Fac. Min. Geol.* 72-75
- Lugović B, Slovenec D, Halamić J, Altherr R (2007) Petrology, geochemistry and tectonic significance of Mesozoic ultramafic rocks from the Zagorje-Mid-Transdanubian Zone in Croatia. *Geol. Carpath.* 58: 511-530
- Majer V, Jurković I (1963) Bilješka o nalazu hrom-spinela kod Čelinca u Bosni. *Geol. vjes. (Zagreb)* 15: 337-338
- Majer V, Kreuzer J, Harre W, Seidel E, Altherr R, Okrusch M (1979) Petrology and geochronology of metamorphic rocks from Banija, Yugoslavia. *Inter. Ophiol. Symp. Abstracts (Nicosia)* 46-47
- Majer V (1993) Ofiolitni kompleks Banije s Pokupljem u Hrvatskoj i Pasireva u Bosni. *Acta Geol. (Zagreb)* 23: 39-84
- Majer V, Ackerman D, Vrkljan M (2003) Garnet pyroxenites and hornblendites associated with Iherzolites of Solila region in Borje mountain, central Dinaride ophiolite belt, Bosnia. Petrography and petrology. *Rad HAZU (Zagreb)* 27: 17-56
- Maksimović Z, Majer V (1981) Accessory spinels of two main zones of Alpine ultramafic rocks in Yugoslavia. *Bull. Acad. Sci. Arts Serbe* 21: 13-26
- Maksimović Z, Kolomejceva-Jovanović L (1987) Sastav koegzistirajućih minerala peridotita Jugoslavije i problemi geotermometrije i geobarometrije ultramafitskih zona. *Glas. Acad. Sci. Arts Serbe* 345: 21-52
- Meinhold G, Anders B, Kostopoulos D, Reischmann T (2008) Rutile chemistry and thermometry as provenience indicator: An example from Chios island, Greece *Sedim. Geol.* 203: 98-111
- Meschede M (1986) A method of discriminating between different types of mid-ocean basalts and continental tholeiites with the Nb-Zr-Y diagram. *Chem. Geol.* 56: 207-218
- McDonough WF, Sun SS (1990) Composition of the Earth's primitive mantle. *In: Lipin BR. and McKay GA (eds.): Geochemistry and mineralogy of REE. Rev. Miner.* 21: 99-145
- McDonough WF, Sun SS (1995) The composition of the Earth. *Chem. Geol.* 120: 223-253
- McInnes BIA, Gregoire M, Binns RA, Herzig PM, Hannington MD (2001) Hydrous metasomatism of oceanic sub-arc mantle, Lihir, Papua New Guinea: petrology and geochemistry of fluid-metasomatised mantle wedge xenoliths. *Earth Planet. Sci. Lett.* 188: 169-183
- McKenzie D, O'Nions RK (1991) Partial melt distribution from inversion of rare earth element concentrations. *J. Petrol.* 32: 1021-1091
- Mercier JCC, Nicolas A (1975) Textures and fabrics of Upper-mantle peridotites as illustrated by xenoliths from basalts. *J. Petrol.* 16: 454-487.
- Michael PJ, Bonatti E (1985) Peridotite composition from the North Atlantic: regional and tectonic variations and implications for partial melting. *Earth. Planet. Sci. Lett.* 73: 91-104

- Milovanović D (1988) Garnet-pyroxene amphibolites near Bistrica, southern part of Zlatibor ultramafic massif. *Vesnik Geoz. (Belgrade)* 44: 197-213
- Mikes T, Christ D, Petri R, Dunkl I, Frei D, Báldi-Beke M, Reitner J, Wemmer K, Hrvatović H, von Eynatten H (2008) Provenance of the Bosnian Flysch. *Swiss J. Geosci.* 101: S31–S54
- Miyashiro A (1975) Classification, characteristics, and origin of ophiolites *J. Geol.* 83: 249-281
- Moore E, Kellogg LH, Dilek Y (2000) Tethyan ophiolites, mantle convection, and tectonic 'historical contingency': resolution of the 'ophiolite conundrum'. *In: Ophiolites and oceanic crust: New insights from field studies and the Ocean Drilling Program* (eds. Dilek Y, Moore EM, Elthon D, Nicolas A). *Geol. Soc. Am.* 349: 3-12
- Morimoto N *et al.* (1989) Nomenclature of pyroxenes. *Can. Mineral.* 27: 143-156
- Morishita T, Arai SA (2001) Petrogenesis of Corundum-Bearing Mafic Rock in the Horoman Peridotite Complex, Japan. *J. Petrol.* 42: 1279-1299
- Mukhopadhyay B (1991) Garnet–clinopyroxene geobarometry. The problems, prospects and an approximate solution with some applications. *Amer. Mineral.* 76: 512-529
- Mukhopadhyay B, Bose MK (1994) Transitional granulite-eclogite facies metamorphism of basic supracrustal rocks in a shear zone complex in the Precambrian shield of south India. *Miner. Mag.* 58: 87-118
- Newton RC, Perkins D (1982) Thermodynamic calibration of geobarometers based on the assemblages garnet-plagioclase-orthopyroxene (clinopyroxene)-quartz. *Amer. Mineral.* 67: 203-222
- Nicholls IA, Ferguson J, Jones H, Marks GP, Mutter JC (1981) Ultramafic blocks from the ocean floor southwest from Australia. *Earth Planet. Sci. Lett.* 56: 362-374
- Nickel KG, Green DH (1985) Empirical geothermobarometry for garnet peridotites and implications for the nature of the lithosphere, kimberlites and diamonds. *Earth Planet. Sci. Lett.* 73:158-170
- Nicolas A, Bouchez JL, Boudier F, Mercier JC (1971) Textures, structures and fabrics due to solid state flow in some European lherzolites. *Tectonophysics* 12:55-86
- Nicolas A, Boudier F, Bouchez JL (1980) Interpretation of peridotite structures from ophiolitic and oceanic environments. *Am. J. Sci.* 280: 192-210
- Nicolas A, Boudier F, Meshi A (1999) Slow spreading accretion and mantle denudation in the Mirdita ophiolite (Albania). *J. Geophys. Res.* 104: 15155-15167
- Nicolas A, Boudier F (2003) Where ophiolites come from and what do they tell us *Geol. Soc. Am. Spec. Pap. (Boulder, USA)* 373
- Nicolas A, Prinzhofer A (1983) Cumulative or residual origin for the transition zones in ophiolites, structural evidence. *J. Petrol.* 24: 188-206
- Niida K (1997) 12, Mineralogy of Mark peridotites: replacement through magma channeling examined from Hole 920D, Mark area *In: Karson JA, Cannat M, Miller DJ and Elthon D* (eds.) *Proc. Ocean Dril. Prog.* 153
- Nitsch KH, Storre B, Thein K (1985) Die Bildung von Spinel in Al-haltigen dolomitischen Marmoren. *Fortschr. Min.* 63: Beiheft 1
- Niu Y (1997) Mantle melting and melt extraction processes beneath ocean ridges: evidence from abyssal peridotites. *J. Petrol.* 38: 1047-1074
- Niu Y, Hékinian R (1997) Basaltic liquids and harzburgitic residues in the Garrett transform: a case study at fast spreading-ridges. *Earth Planet. Sci. Lett.* 146: 243-258
- Niu Y (2004) Bulk-rock major and trace element compositions of abyssal peridotites: Implications for mantle melting, melt extraction and post-melting processes beneath mid-ocean ridges. *J. Petrol.* 45: 2423-2458



- Obata M, Niida K (2002) Summary and Synthesis. In *Forth International Workshop on orogenic Iherzolites and mantle processes field guide*. Samani, Hokkaido, 63-64
- Oberger B, Lorand JP, Girardeau J, Mercier JCC, Pitragool S (1995) Petrogenesis of ultramafic rocks and associated chromitites in the Nan Uttaradit ophiolite, Northern Thailand. *Lithos* 35: 153-182
- O'Brien PJ, Rötzler J (2003) High-pressure granulites: formation, recovery of peak conditions and implications for tectonics. *J. metam. Geol.* 21: 3-20
- Önen AP, Hall R (2000) Sub-ophiolite metamorphic rocks from NW Anatolia, Turkey. *J. metam. Geol.* 18: 483-495
- Operta M, Pamić J, Balen D, Tropper P (2003) Corundum-bearing amphibolites from the metamorphic basement of the Krivaja-Konjuh ultramafic massif (Central Dinaride Ophiolite Belt, Bosnia). *Min. Petrol.* 77: 287-295
- Operta M (2004) Mineraloške i petrografske karakteristike amfibolita iz okolice Vareša. *PhD thesis. Univ. Tuzla (Bosnia and Herzegovina)*, 243 p
- Ozawa K, Takahashi N (1995) P-T history of a mantle diapir: the Horoman peridotite complex, Hokkaido, northern Japan. *Contrib. Min. Petrol.* 120: 223-248
- Owen JV, Greenough JD (1991) An empirical sapphirine-spinel Mg-Fe exchange thermometer and its application to high grade xenoliths in the Popes Harbour dyke, Nova Scotia, Canada. *Lithos* 26: 317-332
- Pamić J (1968) Petrološki izvještaj za tumač lista Zavidovići. *Fond struč. dok. Instit. geol. istra. Sarajevo*
- Pamić J (1970) Petrološki izvještaj za tumač lista Vareš, 1:200000. *Fond struč. dok. Instit. geol. istra. Sarajevo*
- Pamić J (1974) Alpine-type gabbros within the Krivaja-Konjuh massifs in the ophiolite zone of the Dinarides, Yugoslavia. *Tschermak's Min. Petr. Mitt.* 21: 261-279
- Pamić J (1978) Krivajsko-konjuški kompleks In: Goelogija Bosne i Hercegovine (eds. Čičić S and Pamić J) *Institut za geologiju (Sarajevo)* 99-135
- Pamić J (1983) Consideration on the boundary between Iherzolite and harzburgite subprovinces in the Dinarides and northern Hellenides. *Ofioliti* 8: 153-164
- Pamić J, Antić R (1964) Anklave peridotitskih stijena u gabroidnom kompleksu Gostovičke rijeke kod Zavidovića (Bosna). *Geol. glas. (Sarajevo)* 9: 5-14
- Pamić J, Desmons J (1989) A complete ophiolite sequence in Ržav area of Zlatibor and Varda ultramafic massifs, the Central Dinaride Ophiolite Belt. *Ofioliti* 14: 13-32
- Pamić J, Keppeler I (1971) Korunski amfiboliti na južnom obodu Krivajsko-Konjuškog ultramafitskog masiva. *Geol. anali Balk. poluost. (Belgrade)* 35: 399-408
- Pamić J, Majer V (1974) Eklogiti i amfiboliti Crnog potoka na južnom obodu ultramafitskog masiva planine Borje u Bosni. *Geol. glas. (Sarajevo)* 17: 119-133
- Pamić J, Sunarić-Pamić O, Olujić J, Antić R (1977) Petrografija i petrologija krivajsko-konjuškog ofiolitskog kompleksa i njegove osnovne geološke karakteristike. *Acta geol. (Zagreb)* 9: 59-135
- Pamić J (1977a) Variation in geochemistry and geobarometry of peridotite intrusions in the Dinaride Central Ophiolite Zone, Yugoslavia. *Amer. Mineral.* 62: 874-886
- Pamić J, Majer V (1973) Eclogites and amphibolites from Crni Potok on the southern border of the Borja ultramafic massif in Bosnia (Yugoslavia). *Geol. glasnik (Sarajevo)* 17: 119-131
- Pamić J, Šćavničar S, Međimorec S (1973) Mineral assemblages of amphibolites associated with Alpine-Type Ultramafics in the Dinaride Ophiolite Zone (Yugoslavia). *J. Petrol.* 14: 133-157

- Pamić J (1985) Ofiolitski kompleks Ljubića, Čavke i Snjegotinje u sjevernoj Bosni. *Geol. Mazedon. (Štip)* 2/1: 147-171
- Pamić J, Tomljenović B (1998) Basic geological data on the Croatian part of the Mid-Transdanubian Zone as exemplified by Mt. Medvednica located along the Zagreb-Zemlin Fault Zone. *Acta Geol. Hung.* 41: 389-400.
- Pamić J, Tomljenović B, Balen D (2002) Geodynamic and petrogenetic evolution of Alpine ophiolites from the central and NW Dinarides: An overview. *Lithos* 65: 113-142
- Pamić J, Gušić I, Jelaska V (1998a) Geodynamic evolution of the central Dinarides. *Tectonophysics* 297: 251-268
- Paria P, Bhattacharya A, Sen SK (1988) The reaction garnet + clinopyroxene + quartz = 2 orthopyroxene + anorthite: A potential geobarometers for granulites. *Contrib. Miner. Petrol.* 99:126-133
- Parkinson IJ, Pearce JA (1998) Peridotites from the Izu-Bonin-Mariana forearc (ODP Leg 125): evidence for mantle melting and melt-mantle interaction in a supra-subduction zone setting. *J. Petrol.* 39: 1577-1618
- Paterson SR, Vernon RH, Tobisch OT (1989) A review of criteria for the identification of magmatic and tectonic foliations in granitoids. *J. Structural Geol.* 11: 349-363
- Pattison DRM (2003) Petrogenetic significance of orthopyroxene-free garnet + clinopyroxene + plagioclase ± quartz-bearing metabasites with respect to the amphibolite and granulite facies. *J. metam. Geol.* 21: 21-34
- Pattison DRM, Newton RC (1989) Reverse experimental calibration of the garnet-clinopyroxene Fe-Mg exchange thermometer. *Contrib. Miner. Petrol.* 101: 87-103
- Peacock SM, Rushmer T, Thompson AB (1994) Partial melting of subducting oceanic crust. *Earth Planet. Sci. Lett.* 121: 227-244
- Pearce JA, Cann JR (1973) Tectonic setting of basic volcanic rocks determined using trace element analysis. *Earth Planet. Sci. Lett.* 19: 290-300
- Pearce JA, Gale GH (1977) Identification of ore-deposition environment from trace-element geochemistry of associated igneous host rocks. *Geol. Soc. London Spec. Publ.* 7: 14-24
- Pearce JA, Norry ML (1979) Petrogenetic implications of Ti, Zr, Y, and Nb variations in volcanic rocks. *Contrib. Mineral. Petrol.* 69: 33-47
- Pearce JA (1980) Geochemical evidence for the genesis and eruptive setting of lavas from Tethyan ophiolites. In: Panayiotou A (ed.), *Ophiolites: Proc. Int. Simp., Cyprus, 1979, Cyprus geol. survey dept.* 261-272
- Pearce JA (1982) Trace element characteristics of lavas from destructive plate margins. In: Thorpe RS (ed.), *Andesites: Orogenic andesites and related rocks.* Wiley, New York 525-548
- Pearce JA, Parkinson IJ (1993) Trace element model for the mantle melting: application to the volcanic arc petrogenesis. In: Prichard HM, Alabaster T, Harris N, Band Neary CR (eds.) *Magmatic Processes and plate tectonics.* *Geol. Soc. Spec. Publ.* 76: 373-404
- Pearce JA, Barker PF, Edwards SJ, Parkinson IJ, Leat PT (2000) Geochemistry and tectonic significance of peridotites from the South Sandwich arc-basin, South Atlantic. *Contrib. Mineral. Petrol.* 139: 36-53
- Pearson DG, Davies GR, Nixon PH (1993) Geochemical constraints on the petrogenesis of diamond facies pyroxenites from the Beni Bousera peridotite massif, North Morocco. *J. Petrol.* 34: 125-172
- Peccerillo A, Taylor R (1976) Geochemistry of Eocene calc-alkaline volcanic rocks from the Alban Hills (Roman comagmatic region) as inferred from trace element geochemistry. *Contrib. Mineral. Petrol.* 58: 63-81

- Peck DC, Keays RR (1990) Geology, geochemistry and origin of platinum-group nt-chromitite occurrences in the Heazlewood River complex, Tasmania. *Econ. Geol.* 85: 765-793
- Perkins D, Chipera SJ (1985) Garnet-orthopyroxene-plagioclase-quartz barometry: refinement and application to the English River subprovince and the Minnesota River valley. *Contrib. Miner. Petrol.* 89:69-80
- Peters T (1968) Distribution of Mg, Fe, Ca and Al in coexisting olivine, orthopyroxene and clinopyroxene in the total serpentinite (Davos, Switzerland) and in the Apline metamorphosed Malenco serpentinite (N. Italy). *Contrib. Mineral. Petrol.* 18: 65-75
- Petković K (1961) Tektonska karta FNR Jugoslavije. *Glas SANU (Belgrade)* 149: 129-139
- Peyve AA and 21 other authors (2006) Investigation of the Andrew Bain Transform Fault Zone (African-Antarctic Region). *Doklady Earth Sci. (Moscow)* 416: 991-994
- Piccardo GV (1995) Plate Tectonics. The first Twenty-Five Years. *Proc. VIII Summer Sch. Earth Planet. Sci. (Siena)* 267-296
- Plyusnina LP (1982) Geothermometry and geobarometry of plagioclase-hornblende bearing assemblages. *Contrib. Miner. Petrol.* 80: 140-146
- Pomonis P, Tsikouras B, Hatzipanagiotou K (2002) Origin, evolution and radiometric dating of sub-ophiolitic metamorphic rocks from the Koziakas ophiolite (W. Thessaly, Greece). *N. Jb. Miner. Abh.* 177: 255-276
- Popević A (1971) The mode of occurrence and chemical properties of the chromites of southern Zlatibor and their correlation with the chromites from Duboštica, Troglav, Trnava, Koriš-Mušutište and Brezovica. *Uni Belgrade, Trans. Fac Min Geol Met* 14: 41-48
- Popević A, Pamić J (1973) Korund-amfibolitski škriljci u amfibolitima Bistrice na južnom obodu Zlatiborskog ultramafitskog masiva. *Gl. prir. muz. (Belgrade)* A28, 31-39
- Popević A, Korikovskiy SP, Karamata S (1993) Garnet clinopyroxenite from Bistrica, southern Zlatibor, Serbia. *Bull. Geol. Soc. Greece XXVIII.* 2: 93-103
- Pouchou JL, Pichoir F (1984) A new model for quantitative analyses. I. Application to the analysis of homogeneous samples. *La Recherche Aérospatiale (Chatillon-sous-Bagneux)* 3: 13-38
- Pouchou JL, Pichoir F (1985) "PAP" (f-r-Z) correction procedure for improved quantitative microanalysis. In: Armstrong JT (ed) *Microbeam Anal. San Franc.Press* 104-106
- Powell R (1985) Regression diagnostics and robust regression in geothermometer / geobarometer calibration: the garnet-clinopyroxene geothermometer revisited. *J. metam. Geol.* 3: 327-342
- Powell R, Holland TJB (1994) Optimal geothermometry and geobarometry. *Amer. Mineral.* 79: 120-133
- Prakash D, Arima M, Mohan A (2007) Ultrahigh-temperature mafic granulites from Panrimalai, south India: Constraints from phase equilibria and thermobarometry. *J. Asian Earth Sci.* 29: 41-61
- Prinzhofer A, Allègre CJ (1985) Residual peridotites and mechanisms of partial melting. *Earth Planet. Sci. Lett.* 74: 251-265
- Raase P (1974) Al and Ti contents of hornblende, indicators pressure and temperature of regional metamorphism. *Contrib. Min. Petrol.* 45: 231-236
- Raase P, Raith M, Ackermann D, Lal RK (1986) Progressive metamorphism of mafic rocks from greenschist to granulite facies in the Dharwar Craton of South India. *J. Geol.* 94: 261-281
- Rampone E, Hofmann AW, Piccardo GB, Vanucci R, Bottazzi P, Ottolini L (1996) Trace element and isotope geochemistry of depleted peridotites from an N-MORB type type ophiolite (Internal Ligurides, N. Italy) *Contrib. Min. Petrol.* 123: 61-76

- Rampone E, Piccardo GB, Vannucci R, Bottazzi P (1997) Chemistry and origin of trapped melts in ophiolitic peridotites. *Geochim. Cosmochim. Acta* 61: 4557-4569
- Rampnoux JP (1970) Regard sur les Dinarides internes Yougoslaves (Serbie méridionale et Monténégro oriental): Stratigraphie, évolution, paléogéographie et magmatique. *Bull. Soc. Géol. France* 7: 948-966
- Reid I, Jackson R (1981) Oceanic spreading rate and crustal thickness. *Mer. Geophys. Res.* 5: 165-172
- Remaïdi M (1993) Étude pétrologique et géochimique d'une association péridotites réfractaires-pyroxénites dans le massif de Ronda (Espagne) - Implications pour les mécanismes de circulation des magmas dans le manteau supérieur. *PhD thesis, Univ. Montpellier (France)* 386 p
- Ristić P, Mudrinić C (1965) Raspodjela mikroelemenata u J I JZ dijelu planine Konjuh sa posebnim osvrtom na nikl. *Arhiv za tehnolog. (Tuzla)* 3/1: 1-7
- Rivalenti G, Vannucci R, Rampone E, Mazzucchelli M, Piccardo GB, Piccirillo EM, Bottazzi P, Ottolini L (1996) Peridotite clinopyroxene chemistry reflects mantle processes rather than continental versus oceanic settings. *Earth Planet. Sci. Lett.* 139: 423-437
- Roberts S, Neary C (1993) Petrogenesis of ophiolitic chromitite. *In: Prichard HM, Alabaster T, Hariss NWB and Neary CR (eds.) Magmatic processes and plate tectonics. Geol. Soc. London Spec. Publ.* 76: 257-272
- Rutland RWR, Holmes M, Jones MA (1960) Granites of the Glomfjord area, northern Norway: *Internat. Geol. Cong. 21<sup>st</sup>, Copenhagen* 19: 43-53
- Robertson S (1999) BGS Rock Classification Scheme, Volume 2, Classification of metamorphic rocks. *Brit. Geol. Sur. Res. Report* RR 99-02
- Robertson AHR (2002) Overview of the genesis and emplacement of Mesozoic ophiolites in the Eastern Mediterranean Tethyan region. *Lithos* 65: 1-67
- Robertson AHR, Karamata S, Šarić, K (2009) Overview of ophiolites and related units in the Late Palaeozoic-Early Cenozoic magmatic and tectonic development of Tethys in the northern part of the Balkan region. *Lithos* 109: 1-36
- Roeder PL, Campbell IH, Jamieson HE (1979) Re-evaluation of the olivine-spinel geothermometer. *Contrib. Mineral. Petrol.* 68: 325-334
- Roksandić MN (1971) Geotektonski položaj i oblik velikih peridotitskih masiva Dinarida u svetlosti geofizičkih podataka. *Ves. Zav. Geol. istr. (Belgrade)* C. 12/13: 139-147
- Rollinson H (2007) Early Earth Systems A Geochemical Approach. *Black. Publ. Oxford* 285 p
- Romano SS, Brix MR, Dörr W, Fiala J, Krenn E, Zulauf G (2006) The Carboniferous to Jurassic evolution of the pre-Alpine basement of Crete: constraints from U-Pb and U-(Th)-Pb dating of orthogneiss, fission-track dating of zircon, structural and petrological data. *In: Robertson AHF, Mountrakis D (eds.) Tectonic development of the Eastern Mediterranean region. Geol. Soc. London Spec. Publ.* 260: 34-52
- Sabzehei M (2002) Rodingitization of Iranian basic rocks: A new interpretation. *J. Sci. (IR of Iran)* 13: 155-160
- Sachtleben T, Seck HA (1981) Chemical control of Al solubility in orthopyroxene and its implication on pyroxene geothermometry. *Contrib. Mineral. Petrol.* 78: 157-165
- Sack RO (1982) Spinel as petrogenetic indicators; activity-composition relations at low-pressure. *Contrib. Mineral. Petrol.* 79: 169-186
- Sakuyama T, Ozawa K, Sumino H, Nagao K (2009) Progressive melt extraction from upwelling mantle constrained by the Kita-Matsuura basalts in NW Kyushu, SW Japan. *J. Petrol.* 50: 725-779
- Salters V, Stracke A (2004) Composition of the depleted mantle. *Geochem. Geophys. Geosys.*: 5 doi:10.1029/2003GC000587

- Santos JF, Schärer U, Gil Ibarguchi JI, Grardeau J (2003) Genesis of pyroxenite-ridge peridotite at Cabo Ortegal (NW Spain): geochemical and Pb-Sr-Nd isotop data. *J. Petrol.* 43: 17-43
- Saunders AD (1984) The rare earth element characteristics of igneous rocks from the ocean basins. *In: Henderson P (ed). Rare Earth Element Geochemistry. Elsevier, Amsterdam* 205-236
- Schmidt MW (1992) Amphibole composition in tonalite as a function of pressure: An experimental calibration of the Al-in-hornblende barometer. *Contrib. Miner. Petrol.* 110: 304-310
- Šegvić B, Lugović B, Ignjatić S (2006) Petrochemical and geotectonic characteristics of amphibolites from the Zagorje-Mid-Transdanubian shear Zone (Mt. Kalnik, Croatia) *In: Velić I, Vlahović I, Biondić R (eds). Third Croatian Geological Congress. Croat. Geol. Sur. (Zagreb)* 143-144
- Sengupta P, Sen J, Dasgupta S, Raith M, Bhui UK, Ehl J (1999) Ultra-high Temperature Metamorphism of Metapelitic Granulites from Kondapalle, Eastern Ghats Belt: Implications for the Indo-Antarctic Correlation. *J. Petrol.* 40: 1068-1087
- Serri G, Saitta M (1980) Fractionation trends of the gabbroic complexes from high-Ti and low-Ti ophiolites and the crust of major oceanic basins: a comparison *Ophioliti* 5: 241-264
- Shaw DM (1970) Trace element fractionation during anatexis. *Geochim. Cosmochim. Acta.* 34: 237-243
- Shervais JW (1979) Ultramafic and mafic layers in the alpine-type Iherzolites massif at Balmuccia NW Italy. *Mem. Sci. Geol. (Padova)* 33: 135-145
- Shervais JW (1982) Ti-V plots and the petrogenesis of modern and ophiolitic lavas. *Earth Planet. Sci. Lett.* 59: 101-118
- Shervais JW (2001) Birth, death, and resurrection: the life cycle of suprasubduction zone ophiolites. *Geochem. Geophys. Geosys. (G3)* 2: 2000GC000080
- Sijarić G, Šibenik-Studen M (1989) The mineralogical characteristics of the serpentines from Bosnia. *Glasnik Zemaljskog muzeja BiH (Sarajevo)* 28: 65-89
- Slovenec Da (2003) Petrologija i geokemija ofiolitnih stijena Medvednice. *PhD thesis, Univ. Zagreb (Croatia)* 180 p
- Smith D (2000) Insights into the evolution of the uppermost continental mantle from xenolith localities on and near the Colorado Plateau and regional comparisons. *J. Geoph. Res.* 105 (B7): 16769-16781
- Song Y, Frey FA (1989) Geochemistry of peridotite xenoliths in basalts from Hannuoba, Eastern China: Implications for subcontinental mantle heterogeneity. *Geochim. Cosmochim. Acta.* 53: 97-113
- Spadea P, Zanetti A, Vannucci R (2003) Mineral chemistry of ultramafic massifs in the Southern Uralides orogenic belt (Russia) and the petrogenesis of the lower Palaeozoic ophiolites of the Uralian ocean. *In: Dilek Y, Robinson PT (eds.) Ophiolites in Earth History. Geol. Soc. London Spec. Publ.* 218: 567-596
- Spear FS (1980) NaSi ↔ CaAl exchange equilibrium between plagioclase and amphibole. An empirical model. *Contrib. Miner. Petrol.* 72: 33-41
- Spear FS (1981) An experimental study of hornblende stability and compositional variability in amphibolite. *Am. J. Sci.* 281: 697-734
- Spear FS, Kohn MJ, Florence FP, Menard T (1990) A model for garnet and plagioclase growth in pelitic schists: implications for thermobarometry and P-T path determinations. *J. Metam. Geol.* 8: 683-696

- Stampfli MG, Mosar J, Faure P, Pillevuit A, Vannay JC (2000) Permo-Mesozoic evolution of the western Tethys realm: The Neotethys Est mediterranean Basin connection *In: Ziegler P, Cawazza W, Robertson AHF, Crasquin-Soleau S (eds.) Peri-Tethys Memoir Mem. Mus. Hist. Nat., Paris* 6: 51-108
- Stampfli MG, Borel GD (2004) The TRANSMED Transects in Space and Time: Constraints on the Paleotectonic Evolution of the Mediterranean Domain.- *In: Cavazza W, Roure F, Spakman W, Stampfli MG, Ziegler PA (eds.) The TRANSMED Atlas. 32<sup>th</sup> Int. Geol. Congress, Florence*
- Staudigel H, Hart SR, Richardson SH (1981) Alteration of the oceanic crust: process and timing. *Earth Planet. Sci. Lett.* 52: 311-327
- Stolper EM (1980) A phase diagram for mid-ocean ridge basalts: Preliminary results and implications for petrogenesis. *Contrib. Mineral. Petrol.* 74: 13-27
- Stormer JC Jr. (1973) Calcium zoning in olivine and its relationship to silica activity and pressure. *Geochim. Cosmochim. Acta* 37: 1815-1821
- Streckeisen A (1973) Classification and Nomenclature of Plutonic Rocks. *N. Jb. Miner. Abh. H.* 4: 149-164
- Suhr G, Seck HA., Shimizu N, Günther D, Jenner G (1998). Infiltration of refractory melts into the lowermost oceanic crust: evidence from dunite- and gabbro-hosted clinopyroxenes in the Bay of Islands Ophiolite. *Contrib. Min. Petrol.* 131: 136-154
- Sun SS, McDonough WF (1989) Chemical and isotopic systematics of oceanic basalts: implication for mantle composition and processes. *In: Saunders AD, Norry MJ (Eds.) Magmatism in Ocean Basins. Geol. Soc. Sp. Pub.* 42: 313-345
- Sunarić-Pamić O, Olujić J (1968) Osnovne geološke karakteristike ležišta hromita Duboštica. *Geol. glas. (Sarajevo)* 12: 261-271
- Takahashi E, Kushiro I (1983) Melting of a dry peridotite at high pressures and basalt magma genesis. *Amer. Mineral.* 68: 859-879
- Takahashi N (2001) Origin of Plagioclase Lherzolite from the Naikanbetsu Peridotite Complex, Hokkaido, Northern Japan: Implications for Incipient Melt Migration and Segregation in the Partially Molten Upper Mantle. *J. Petrol.* 42: 39-54
- Takazawa E, Okayasu T, Satoh X, Keiichi X (2003) Geochemistry and origin of the basal lherzolites from the northern Oman ophiolite (northern Fizh block). *Geochim. Geophys. Geosys. (G3)* 4: 2000GC000080
- Taylor WR, McLennan SM (1985) The continental crust: its composition and evolution. *Black. Publ. Oxford* 312 p
- Taylor WR, Green DH (1988) Measurement of reduced peridotite-C-O-H solidus and implications for redox melting of the mantle. *Nature* 332: 349-352
- Thirlwall MF, Upton BGJ, Jenkins C (1994) Interaction between continental lithosphere and the Iceland Plume — Sr–Nd–Pb isotope geochemistry of Tertiary basalts, NE Greenland. *J. Petrol.* 35: 839-879
- Tribaudino M, Talarico F (1992) Orthopyroxenes from granulite rocks of the Wilson Terrane (Victoria Land, Antarctica): crystal chemistry and cooling history. *Eur. J. Mineral.* 4: 453-463
- Trubelja F (1961) Magmatske stijene jugoistočnog dijela planine Konjuh (Bosna). *Geol. glas. (Sarajevo)* 5: 241-262
- Trubelja F, Pamić J (1965) Petrološka studija planine Ozren. *Acta Geol (Zagreb)* 4: 265-314
- Trubelja F, Šibenik-Studen M, Sijarić G (1974) Pukotinski minerali u bazičnim magmatskim stijenama u Bosni i Hercegovini, 8. *Jugosl. geol. kongr. (Bled, Slovenia)*
- Trubelja F, Marchig V, Burgath KP, Vujović Z (1995) Origin of Jurassic Tethyan ophiolites in Bosnia: A geochemical approach to tectonic setting. *Geol. Croat.* 48: 49-66

- Tuff J, Takahashi E, Gibson SA (2005) Experimental constraints of the role of garnet pyroxenite in the genesis of high-Fe mantle plume derived melts. *J. Petrol.* 46: 2023-2058
- Ustaszewski K, Schmid SM, Lugović B, Schuster R, Caron M, Rettenmund C., Kounov A (2006) Does the Sava-zone represent a remnant of the Vardar ocean and when did it close?- structure, geochemistry and the age of Kozara ophiolites (northern Bosnia-Herzegovina). *In: Mesozoic ophiolite belts of the northern part of Balkan Peninsula. Proc. Intern. Sym. Fac. Mining Geol. Univ. Belgrade (Serbia)* 136-138
- Vernon RG, Clarke GL (2008) Principles of Metamorphic Petrology. *Cambridge Univ. Press New York*
- Voshage H, Sinigoi S, Mazzucelli M, Demarchi G, Rivalenti G, Hofmann A (1988) Isotopic constraints on the origin of ultramafic and mafic dikes in the Balamuccia peridotite (Ivrea zone). *Contrib. Mineral. Petrol.* 100: 261-267
- Wager IR, Brown GM (1968) Layered igneous rocks. *Oliver & Boyd (Edinb. & London)* 588 p
- Wells PRA (1977) Pyroxene thermometry in simple and complex systems. *Contrib. Miner. Petrol.* 62:129-139
- Werner CD, Pilot J (1997) 26. Data report: Geochemistry and mineral chemistry of ultramafic rocks from the Kane area (Mark) in Karson JA, Cannat M, Miller DJ, Elthon D (eds.) *Proc. ODP. Sci. Results, College Station, Texas* 153
- Williams R (1984) Field relations and chemistry of sapphirine bearing rocks from the Rønesund area. Fiskeneset, Western Greenland. *Can. Mineral.* 22: 417-421
- Workman RK, Hart SR (2005) Major and trace element composition of the Depleted MORB mantle (DMM). *Earth Planet. Sci. Lett.* 231: 53-72
- Whitehead JA, Dick HJB, Schouten H (1984) A mechanism for magmatic accretion under spreading ridges. *Nature* 312: 146-148
- Witt-Eickschen G, Seck HA (1991) Solubility of Ca and Al in orthopyroxene from spinel peridotite: An improved version of an empirical geothermometer. *Contrib. Mineral. Petrol.* 106: 431-439
- Wood BJ, Banno S (1973) Garnet-orthopyroxene and orthopyroxene-clinopyroxene relationships in simple and complex systems. *Contrib. Mineral. Petrol.* 42: 109-124
- Woodland AB, Koch M (2003) Variation in oxygen fugacity with depth in the upper mantle beneath the Kaapvaal craton, Southern Africa. *Earth Planet. Sci. Lett.* 214: 295-310
- Woodsworth (1977) Homogenization of zoned garnets from pelitic schists. *Can. Miner.* 15: 230-242
- Wood DA, Joron JL, Treuil M, Norry M, Tarney J (1979) Elemental and Sr isotope variations in basic lavas from Iceland and the surrounding ocean floor; the nature of mantle source inhomogeneities. *Contrib. Mineral. Petrol.* 70: 319-339
- Wood DA (1980) The application of a Th-Hf-Ta diagram to problems of tectonomagmatic classification and to establishing the nature of crustal contamination of basaltic lavas of the British Tertiary volcanic province. *Earth Planet. Sci. Lett.* 50: 11-30
- Yardley BWD (1989) An Introduction to Metamorphic Petrology. *Longman, Harlow*
- Zanetti A, D'Antonio M, Spadea P, Raffone N, Vannucci R, Brugeir R (2006) Petrogenesis of mantle peridotites from the Izu-Bonin-Mariana (IBM) forearc. *Ophioliti* 31: 189-206
- Zhou MF, Robinson PT, Malpas J, Li Z (1996) Podiform Chromitites in the Luobusa Ophiolite (Southern Tibet): Implications for Melt-Rock Interaction and Chromite Segregation in the Upper Mantle. *J. Petrol.* 37: 3-21
- Zhou MF, Malpas J, Robinson PT, Sun M, Li JW (2001) Crystallization of podiform chromitites from silicate magmas and the formation of nodular textures. *Res. Geol.* 51: 1-6

Zhou MF, Robinson PT, Malpas J, Edwards SJ, Qi L (2005) REE and PGE Geochemical Constraints on the Formation of Dunites in the Luobusa Ophiolite, Southern Tibet. *J. Petrol.* 46: 615-639





## APPENDIX

### A. Materials

Samples for this thesis were gathered in three cycles. The first sampling took place in September 2006 and the second one in June 2007. Small quantities of old samples collected decades ago were also at my disposal. The dataset covered 110 thin-sections of ultramafic and mafic rocks. For an extensive further analytical treatment of mineral phase chemistry, a set of 36 samples was selected. They tended to be the most representative with respect to lithology and the best preserved ones. Bulk-rock chemical analyses were performed on practically the same set of 34 samples.

Thin-sections for optical analyses were produced at the Faculty of Mining, Geology and Petroleum Engineering of University of Zagreb and partly at the Croatian Geological Institute in Zagreb, Croatia. Additional thin-sections needed for microprobe and SEM measurements were done at the Institute of Geosciences of the Ruprecht-Karls University of Heidelberg, Germany. The whole-rock chemical analyses required ca. 40 g of pulverized rock sample. Alteration crusts with secondary phases were manually removed from the split rocks. Before analysis, the rock powders were dried at 110 °C for approximately 45 min. Some 20 g of each sample amount were used for XRF, while the rest went for ICP-MS.

Table 6 offers a complete list of analytically treated rock samples. For every one of them, the following parameters are indicated: (a) locality of sampling, (b) analytical methods performed, (c) rock mineral composition and (d) rock determination. Detailed rock mineralogy, petrographic features, phase chemistry and whole-rock chemical composition are introduced and fully described in Chapter 4.



## B. Analytical techniques

Methods of optical microscopy. The rock-chips were attenuated and pasted to a sheet glass. The cover slip glass capped the sample. As a binder, a Canadian balsam made by 'Kemika' was used. Optical characteristics of balsam were used as an internal standard. The standard thickness of 0.02-0.03 mm was attained by fine sample polishing.

The research was performed in orthoscopic light, using standard microscopic equipment. The magnification ranged from 5x to 100x.

Igneous rock nomenclature is in accordance with the IUGS subcommittee's recommendation for the classification and nomenclature of plutonic rocks (Streckeisen 1973). The metamorphic rocks were classified with respect to the BGS Rock Classification Scheme for metamorphic rocks (Robertson 1999).

The microscoping work including microphotographing was performed at the Faculty of Mining, Geology and Petroleum Engineering of the University of Zagreb using a Leica microscope equipped with a digital camera.

Mineral phase analyses. Analyses of mineral phases was completed by using an electron microprobe (EPMA) of Cameca. A scanning electron microscope (SEM) equipped with an energy dispersive spectrometer (EDS) and a secondary ion mass spectrometer (SIMS) were also utilised. The SEM was used in order to obtain back-scattered electron (BSE) photos, necessary for further work with the EPMA. The employed device was a Leo 440 SEM model placed at the Institute of Geosciences of the Ruprecht-Karls University of Heidelberg. It is fully computer-controlled, fitted with an integrated Oxford instruments SEM/WDS system. Also, it includes a secondary electron detector and a 4-quadrant solid-state backscattered electron detector. The instrument has a magnification range from 10x to 500000x, with beam voltage spanning from 300 to 40000 V. The samples were examined under a vacuum of average  $1.29 \cdot 10^{-4}$  mbar pressure. Before the examinations in SEM, all the samples were coated with carbon.

Major elements and some minor elements were determined by using a CAMECA SX51 model equipped with 5 wavelength dispersive spectrometers. The operating parameters were 15 kV accelerating voltage, 20 nA beam current,  $\sim 1 \mu\text{m}$  beam size and mostly 10 s counting time. Natural minerals, oxides (corundum, spinel, hematite and rutile) and silicates (albite, orthoclase, anorthite and wollastonite) were used for calibration (see Table 7 for microprobe operative details). The measurements' error is better than 1 % relative. Measurements were performed at the Institute of Geosciences of the Ruprecht-Karls University of Heidelberg.

Phase chemical analyses were carried out by in-situ (spot) measuring method. At least two analyses per mineral grain were done. Typically, the rim and core of the grain were investigated, in order to determine phase chemical homogeneity. The grains suspected to have been chemically heterogeneous, were measured by the method of linear profiles. Hence, one acquires clear image upon the intensity and mode of alteration of mineral chemistry. The results of measurements are given in weight percentage. Raw data for all analyses were corrected for matrix effects with the PAP algorithm (Pouchou & Pichoir 1984; Pouchou & Pichoir 1985) implemented by CAMECA. Formula calculations were done using a software package, designed by Dr. H-P. Meyer (Institute of Geosciences of the Ruprecht-Karls University of Heidelberg).

Whole-rock chemical analyses. The X-ray fluorescence (XRF) and inductively coupled plasma-mass spectrometry (ICP-MS) were employed. Major element contents are expressed in weight percentage of the oxides, whereas that of microelements is expressed in ppm (weight). The rock beads, obtained by lithiumtetraborate fusion of rock-powder, were used in order to determine the main elements content. For microelements, beads produced by the pastel rock-powder pressing were applied. Repeated analyses of different aliquots of a sample indicated a relative standard deviation ( $100 \cdot SD/X$ ) of  $\pm 5\%$ . The accuracy of the analyses with respect to international standard DNC-1/A for macro elements fits the range of  $\pm 8\%$ . A set of international standards of magmatic and metamorphic rocks was utilised for the instrument calibration. The XRF measurements were carried out at the Mineralogical Institute of the University of Heidelberg.

ICP-MS measurements tested the microelements content obtained by XRF. Additionally, set of following microelements was revealed: Cs, U, Ta, Hf and all REE.

**Table 6.** List of analysed samples with indication of: (a) sampling locality, (b) mineral paragenesis, (c) type of the rock, and (d) analytical methods performed

SAMPLE NAME	SAMPL. LOCALITY	MIN. PARAGENESIS	ROCK TYPE	ANALYTICAL METHODS
<b><u>ULTRAMAFIC MAGMATIC ROCKS</u></b>				
GR2	Stipanovići	Ol, Opx, Cpx, Pl, Sp, and Srp	Plagioclase Iherzolite	EMPA, SEM, XRF, ICP-MS
GR12	Gostovića Rijeka	Ol, Opx, Cpx, Pl, Sp, and Srp	Plagioclase Iherzolite	EMPA, SEM, XRF, ICP-MS
U4	Manastir	Ol, Opx, Cpx, Pl, Sp, and Srp	Plagioclase Iherzolite	EMPA, SEM, XRF, ICP-MS
M2	Manastir	Ol, Opx, Cpx, Pl, Sp, and Srp	Plagioclase Iherzolite	EMPA, SEM, XRF, ICP-MS
R7	Maoče	Ol, Opx, Cpx, Sp, and Srp	Spinel Iherzolite	EMPA, SEM, XRF, ICP-MS
K1	Karaula	Ol, Sp, and Srp	Dunite	EMPA, SEM, XRF, ICP-MS
D5	Dunoštica North	Ol, Opx, Cpx, Pl, Sp, and Srp	Plagioclase Iherzolite	EMPA, SEM, XRF, ICP-MS
197 U19	Duboštica	Ol, Sp, Cpx, Srp, Chl, and h-Grt	Dunite	EMPA, SEM, XRF, ICP-MS
D16	Duboštica	n.a.	Chromitite	EMPA
D17	Duboštica	n.a.	Chromitite	EMPA
D18	Duboštica	n.a.	Chromitite	EMPA
1B	Žepče	n.a.	Chromitite	XRF
1C	Žepče	Ol, Sp, Opx, Cpx, Chl, Srp, Amp	Olivine websterite	EMPA, SEM, XRF, ICP-MS
2A	Žepče	Cpx, Opx, Ol, Srp, and h-Grt	Olivine websterite	EMPA, SEM, XRF, ICP-MS
4A	Žepče	Ol, Opx, Cpx, Pl, Srp, Sp, Pec, and Chl	Spinel Iherzolite	EMPA, SEM, XRF, ICP-MS
O2	Olovo	Ol, Sp, Opx, Cpx, and Srp	Spinel Iherzolite	EMPA, SEM, XRF, ICP-MS
U35	Muška Voda	Ol, Sp, Opx, Srp, Chl, and Amp	Spinel Iherzolite	EMPA, SEM, XRF, ICP-MS
Z2	Zlaća	Ol, Sp, Opx, Cpx, and Srp	Spinel Iherzolite	EMPA, SEM, XRF, ICP-MS
Z4	Zlaća	Ol, Sp, Cpx, Opx, Srp, Chl, and Amp	Spinel Iherzolite	EMPA, SEM, XRF, ICP-MS

n.a. = not available, h-Grt = hydro Garnet (hybschite). EMPA = Electronic Microprobe Analyses, SEM = Scanning Electron Microscope, XRF = X-Ray Fluorescence, ICP-MS = Inductively Coupled Plasma-Mass Spectrometry. Mineral abbreviation after Kretz (1983), extended by Bucher and Frey (1994).

**Table 6 (continued).** List of analysed samples with indication of: (a) sampling locality, (b) mineral paragenesis, (c) type of the rock, and (d) analytical methods performed

SAMPLE NAME	SAMPL. LOCALITY	MIN. PARAGENESIS	ROCK TYPE	ANALYTICAL METHODS
<b><u>METAMORPHIC ROCKS</u></b>				
GR7	Stipanovići	Amp, Pl, Grt, Cpx, Mt, and Opx	Grt-Di amphibolite	EMPA, SEM, XRF, ICP-MS
MK2	Krivaja	Amp, Pl, Grt, Cpx, Mt, and Opx	Grt-Di amphibolite	EMPA, SEM, XRF, ICP-MS
U29	Krivaja-Vozuća	Amp, Pl, Crn, Czo, Cpx, Ct, Pmp, Cc, Cpx, and Sp	Granoblastic amphibolite	EMPA, SEM, XRF, ICP-MS
U30	Krivaja-Vozuća	Amp, Pl, Czo, Spr, and Sp	Granoblastic amphibolite	EMPA, SEM, XRF, ICP-MS
R8	Maoče	Amp, Pl, Tit, Ap, Ilm, and Chl	Granoblastic amphibolite	EMPA, SEM, XRF, ICP-MS
CC1	Careva Čuprija	Amp, Grt, Pl, Cpx, Ttn, Rt, Cc, and Ilm	Grt-Di amphibolite	EMPA, SEM, XRF, ICP-MS
198 V1	Vijaka Stream	Amp, Pl, Cpx, Opx, Mt, and Grt	Grt-Di amphibolite	EMPA, SEM, XRF, ICP-MS
U40	Vijaka Stream	Amp, Cpx, Opx, Grt, Pl, Mt, and Rt	Grt-Di-Hy amphibolite	EMPA, SEM, XRF, ICP-MS
V4	Vijaka South	Grt, Cpx, Pl, Amp, Opx, and Mt	Grt-Di-Hy amphibolite	EMPA, SEM, XRF, ICP-MS
X1	Vijaka South	Amp, Cpx, Opx, Grt, Pl, and Rt	Grt-Di-Hy amphibolite	EMPA, SEM, XRF, ICP-MS
U23	Duboštica	Amp, Pl, Tit, Ap, Ilm, Prh, and Chl	Granoblastic amphibolite	EMPA, SEM, XRF, ICP-MS
DU5	Duboštica	Grt, Amp, Pl, Cpx, Ttn, and Xo	Grt-Di amphibolite	EMPA, SEM, XRF, ICP-MS
U22	Duboštica North	Grt, Amp, Pl, Cpx, and Chl	Grt-Di amphibolite	EMPA, SEM, XRF, ICP-MS
10D	Žepče	Amp, Cpx, Pl, Ttn, Ilm, Ap, and Prh	Di amphibolite gneiss	EMPA, SEM, XRF, ICP-MS
11C	Žepče	Amp, Pl, Ep, Prh, Ilm, Cpx, Ttn, Ap, Pmp, and Chl	Granoblastic amphibolite	EMPA, SEM, XRF, ICP-MS
Z1C	Žepče	Grt, Cpx, Pl, Sp, Opx, Ttn, and Ilm	Pl-Grt-Di gneiss	EMPA, SEM, XRF, ICP-MS

n.a. = not available. EMPA = Electronic Microprobe Analyses, SEM = Scanning Electron Microscope, XRF = X-Ray Fluorescence, ICP-MS = Inductively Coupled Plasma-Mass Spectrometry. Mineral abbreviation after Kretz (1983), extended by Bucher and Frey (1994).

**Table 7.** Analytical setups and parametres used during electron probe microanalysis

Atomic number	Element	Spectral line	Standard	Crystal	Counting time (s)	Concentration in standard
14	Si	<i>K<math>\alpha</math></i>	Wollastonite	TAP	10	24.08 % Si
22	Ti	<i>K<math>\alpha</math></i>	TiO <sub>2</sub>	PET	10	59.95 % Ti
13	Al	<i>K<math>\alpha</math></i>	Al <sub>2</sub> O <sub>3</sub>	TAP	10	52.93 % Al
38	Sr	<i>L<math>\alpha</math></i>	Celestine	PET	20	47.70 % Sr
24	Cr	<i>K<math>\alpha</math></i>	Cr <sub>2</sub> O <sub>3</sub>	PET	10	68.42 % Cr
26	Fe	<i>K<math>\alpha</math></i>	Fe <sub>2</sub> O <sub>3</sub>	LiF	10	69.94 % Fe
28	Ni	<i>K<math>\alpha</math></i>	NiO	LiF	30	78.58 % Ni
30	Zn	<i>K<math>\alpha</math></i>	Gahnite	LiF	30	34.14 % Zn
25	Mn	<i>K<math>\alpha</math></i>	Rhodonite	LiF	10	33.68 % Mn
12	Mg	<i>K<math>\alpha</math></i>	Periclase	TAP	10	60.31 % Mg
20	Ca	<i>K<math>\alpha</math></i>	Wollastonite	PET	10	34.12 % Ca
			Anorthite (for Fs)	PET	10	34.12 % Ca
56	Ba	<i>L<math>\alpha</math></i>	Barite	LiF	20	58.84 % Ba
11	Na	<i>K<math>\alpha</math></i>	Albite	TAP	10	8.71 % Na
19	K	<i>K<math>\alpha</math></i>	Orthoclase	PET	10	12.18 % K





## APPENDIX C. Mineral chemistry

### Ultramafic rocks

#### Olivine

Table A-1. Microprobe analyses and formulae of olivines from different ultramafic lithologies of the Krivaja-Konjuh ophiolite complex

Rock type	Plagioclase Iherzolite																	
Sample-Nr.	r2-3	gr2-4	gr2-6	gr2-9	gr2-11	gr2-27	gr2-29	gr2-32	gr2-33	gr2-44	gr2-45	gr2-46	gr2-54	gr2-54	gr12-6	gr12-7	gr12-9	gr12-10
Remark	r	c		r	r	r	r	r	c	r	r	c	c	r	c	r		c
SiO <sub>2</sub>	40.81	40.82	41.07	41.05	40.68	41.05	41.15	40.99	40.92	40.92	40.81	41.05	40.95	40.69	40.82	41.29	40.74	40.84
TiO <sub>2</sub>	0.01	0.03	0.01	0.00	0.01	0.00	0.01	0.03	0.00	0.00	0.03	0.00	0.00	0.00	0.01	0.00	0.01	0.00
Al <sub>2</sub> O <sub>3</sub>	0.01	0.01	0.02	0.00	0.01	0.02	0.00	0.01	0.00	0.00	0.01	0.00	0.00	0.00	0.00	0.00	0.00	0.00
Cr <sub>2</sub> O <sub>3</sub>	0.04	0.00	0.14	0.03	0.00	0.03	0.08	0.00	0.00	0.01	0.02	0.01	0.00	0.01	0.00	0.00	0.02	0.01
FeO	9.59	10.10	9.65	10.05	10.13	10.03	9.25	10.04	10.14	10.02	10.07	10.00	10.25	10.22	9.82	9.51	9.49	9.73
MnO	0.14	0.09	0.09	0.21	0.09	0.10	0.09	0.19	0.15	0.09	0.17	0.11	0.19	0.15	0.16	0.14	0.11	0.10
NiO	0.40	0.42	0.36	0.42	0.39	0.40	0.41	0.40	0.41	0.46	0.39	0.42	0.44	0.47	0.40	0.43	0.39	0.41
MgO	48.73	48.77	49.37	48.63	48.81	48.48	48.91	48.41	48.63	49.04	48.86	48.94	48.72	48.73	49.52	49.56	49.28	49.59
CaO	0.03	0.01	0.02	0.03	0.03	0.00	0.03	0.01	0.02	0.01	0.01	0.02	0.02	0.01	0.01	0.02	0.02	0.02
Na <sub>2</sub> O	0.01	0.01	0.00	0.00	0.00	0.00	0.01	0.01	0.00	0.00	0.00	0.00	0.00	0.01	0.00	0.00	0.01	0.00
K <sub>2</sub> O	0.00	0.00	0.01	0.00	0.00	0.01	0.00	0.00	0.02	0.00	0.02	0.00	0.00	0.00	0.00	0.00	0.00	0.01
Total	99.77	100.26	100.74	100.41	100.14	100.11	99.94	100.10	100.28	100.55	100.39	100.56	100.59	100.29	100.74	100.94	100.06	100.71
Si	1.002	1.000	0.999	1.004	0.998	1.006	1.007	1.005	1.002	0.999	0.999	1.002	1.001	0.998	0.995	1.002	0.998	0.995
Ti	0.000	0.000	0.000	0.000	0.000	0.000	0.000	0.000	0.000	0.000	0.000	0.000	0.000	0.000	0.000	0.000	0.000	0.000
Al	0.000	0.000	0.000	0.000	0.000	0.000	0.000	0.000	0.000	0.000	0.000	0.000	0.000	0.000	0.000	0.000	0.000	0.000
Cr	0.001	0.000	0.003	0.001	0.000	0.001	0.002	0.000	0.000	0.000	0.000	0.000	0.000	0.000	0.000	0.000	0.000	0.000
Fe <sup>2+</sup>	0.197	0.207	0.196	0.205	0.208	0.206	0.189	0.206	0.208	0.205	0.206	0.204	0.210	0.210	0.200	0.193	0.194	0.198
Mn	0.003	0.002	0.002	0.004	0.002	0.002	0.002	0.004	0.003	0.002	0.004	0.002	0.004	0.003	0.003	0.003	0.002	0.002
Ni	0.008	0.008	0.007	0.008	0.008	0.008	0.008	0.008	0.008	0.009	0.008	0.008	0.009	0.009	0.008	0.008	0.008	0.008
Mg	1.784	1.781	1.790	1.773	1.785	1.771	1.784	1.770	1.776	1.785	1.782	1.781	1.775	1.782	1.799	1.792	1.799	1.801
Ca	0.001	0.000	0.001	0.001	0.001	0.000	0.001	0.000	0.000	0.000	0.000	0.001	0.001	0.000	0.000	0.000	0.001	0.000
Na	0.001	0.001	0.000	0.000	0.000	0.000	0.001	0.000	0.000	0.000	0.000	0.000	0.000	0.001	0.000	0.000	0.001	0.000
K	0.000	0.000	0.000	0.000	0.000	0.000	0.000	0.000	0.001	0.000	0.001	0.000	0.000	0.000	0.000	0.000	0.000	0.000
Fo	90.10	89.60	90.12	89.63	89.64	89.63	90.45	89.66	89.55	89.77	89.62	89.71	89.42	89.54	90.05	90.33	90.35	90.17

Formulae of olivine calculated on the basis of 4 oxygens and all Fe as FeO. c = grain core. r = grain rim.

**Table A-2.** Microprobe analyses and formulae of olivines from different ultramafic lithologies of the Krivaja-Konjuh ophiolite complex

Rock type	Plagioclase Iherzolite																	
Sample-Nr.	gr12-11	gr12-12	gr12-15	gr12-16	gr12-26	gr12-27	gr12-37	gr12-38	gr12-39	gr12-45	gr12-46	gr12-50	m2-3	m2-6	m2-8	m2-9	m2-10	m2-14
Remark	r	r	r	r	c	r	r	c	o.sp.	c	r	r		r	r	r	c	
SiO <sub>2</sub>	40.72	41.06	41.03	40.80	40.96	40.67	40.94	41.19	40.91	41.15	41.01	41.08	40.47	40.47	40.53	40.64	40.45	40.45
TiO <sub>2</sub>	0.00	0.00	0.01	0.00	0.00	0.01	0.00	0.01	0.03	0.01	0.02	0.03	0.01	0.01	0.02	0.02	0.03	0.02
Al <sub>2</sub> O <sub>3</sub>	0.00	0.00	0.00	0.00	0.00	0.00	0.02	0.01	0.01	0.01	0.01	0.01	0.01	0.01	0.01	0.02	0.01	0.01
Cr <sub>2</sub> O <sub>3</sub>	0.00	0.00	0.09	0.01	0.00	0.01	0.04	0.00	0.04	0.07	0.05	0.00	0.02	0.02	0.08	0.07	0.01	0.04
FeO	10.05	9.95	9.64	9.93	9.57	9.92	9.43	9.59	9.69	9.69	9.37	10.09	9.44	9.49	9.02	9.32	9.52	9.93
MnO	0.14	0.10	0.17	0.15	0.18	0.11	0.20	0.14	0.14	0.11	0.11	0.15	0.18	0.15	0.15	0.12	0.09	0.10
NiO	0.35	0.41	0.40	0.38	0.35	0.39	0.45	0.40	0.40	0.36	0.39	0.32	0.44	0.44	0.44	0.38	0.43	0.45
MgO	49.31	49.37	49.67	49.27	49.17	49.20	49.58	49.51	49.42	49.55	49.77	49.43	48.90	48.93	49.49	49.36	48.50	48.64
CaO	0.03	0.01	0.00	0.02	0.02	0.02	0.00	0.01	0.01	0.02	0.03	0.02	0.01	0.03	0.01	0.03	0.01	0.01
Na <sub>2</sub> O	0.01	0.00	0.01	0.00	0.00	0.00	0.00	0.00	0.00	0.00	0.00	0.01	0.00	0.00	0.00	0.00	0.00	0.00
K <sub>2</sub> O	0.00	0.01	0.02	0.01	0.02	0.02	0.01	0.02	0.00	0.00	0.01	0.01	0.01	0.00	0.00	0.00	0.00	0.00
Total	100.60	100.92	101.03	100.57	100.28	100.34	100.67	100.90	100.65	100.97	100.77	101.15	99.47	99.55	99.74	99.95	99.03	99.63
Si	0.994	0.999	0.996	0.996	1.001	0.995	0.997	1.000	0.997	0.999	0.997	0.997	0.997	0.997	0.995	0.996	1.001	0.997
Ti	0.000	0.000	0.000	0.000	0.000	0.000	0.000	0.000	0.001	0.000	0.000	0.001	0.000	0.000	0.000	0.000	0.001	0.000
Al	0.000	0.000	0.000	0.000	0.000	0.000	0.000	0.000	0.000	0.000	0.000	0.000	0.000	0.000	0.000	0.000	0.000	0.000
Cr	0.000	0.000	0.002	0.000	0.000	0.000	0.001	0.000	0.001	0.001	0.001	0.000	0.000	0.000	0.002	0.001	0.000	0.001
Fe <sup>2+</sup>	0.205	0.202	0.196	0.203	0.196	0.203	0.192	0.195	0.197	0.197	0.190	0.205	0.195	0.195	0.185	0.191	0.197	0.205
Mn	0.003	0.002	0.003	0.003	0.004	0.002	0.004	0.003	0.003	0.002	0.002	0.003	0.004	0.003	0.003	0.003	0.003	0.002
Ni	0.007	0.008	0.008	0.007	0.007	0.008	0.009	0.008	0.008	0.007	0.008	0.006	0.009	0.009	0.009	0.008	0.008	0.009
Mg	1.795	1.790	1.798	1.793	1.791	1.795	1.799	1.792	1.795	1.793	1.803	1.789	1.797	1.797	1.810	1.803	1.789	1.788
Ca	0.001	0.000	0.000	0.000	0.001	0.000	0.000	0.000	0.000	0.001	0.001	0.000	0.000	0.001	0.000	0.001	0.000	0.000
Na	0.000	0.000	0.001	0.000	0.000	0.000	0.000	0.000	0.000	0.000	0.000	0.000	0.000	0.000	0.000	0.000	0.000	0.000
K	0.000	0.000	0.001	0.000	0.001	0.001	0.000	0.001	0.000	0.000	0.000	0.000	0.000	0.000	0.000	0.000	0.000	0.000
Fo	89.72	89.86	90.23	89.85	90.27	89.82	90.45	90.27	90.12	90.14	90.41	89.77	90.24	90.26	90.73	90.45	90.17	89.75

Formulae of olivine calculated on the basis of 4 oxygens and all Fe as FeO. c = grain core. r = grain rim.. o.sp. = olivine encircling spinel

**Table A-3.** Microprobe analyses and formulae of olivines from different ultramafic lithologies of the Krivaja-Konjuh ophiolite complex

Rock type	Plagioclase Iherzolite																	
Sample-Nr.	m2-16	m2-17	m2-19	m2-28	m2-29	m2-38	m2-39	m2-47	m2-48	m2-49	u4-13	u4-14	u4-15	u4-20	u4-22	u4-28	u4-29	u4-38
Remark	c	r		c	r	c.opx	r.opx	r	r	c	c	c	r		e.sp			
SiO <sub>2</sub>	40.31	40.16	40.44	40.75	40.87	40.95	41.22	40.99	40.90	40.72	40.81	40.48	40.61	40.53	40.73	40.31	40.31	39.57
TiO <sub>2</sub>	0.01	0.01	0.00	0.00	0.00	0.00	0.00	0.01	0.01	0.01	0.02	0.01	0.00	0.01	0.00	0.01	0.00	0.00
Al <sub>2</sub> O <sub>3</sub>	0.01	0.01	0.00	0.01	0.00	0.00	0.02	0.01	0.01	0.00	0.01	0.00	0.00	0.00	0.00	0.00	0.00	0.03
Cr <sub>2</sub> O <sub>3</sub>	0.00	0.00	0.03	0.00	0.02	0.05	0.05	0.10	0.11	0.03	0.01	0.03	0.00	0.08	0.11	0.00	0.02	0.02
FeO	9.83	10.11	9.60	10.10	9.75	10.01	10.22	9.65	9.66	9.97	10.39	10.14	10.06	9.23	9.52	10.01	9.87	10.09
MnO	0.15	0.20	0.19	0.17	0.13	0.13	0.20	0.11	0.16	0.14	0.17	0.19	0.18	0.10	0.09	0.13	0.12	0.14
NiO	0.42	0.44	0.44	0.44	0.43	0.36	0.39	0.35	0.40	0.40	0.35	0.40	0.36	0.43	0.41	0.35	0.35	0.35
MgO	48.34	48.22	49.11	48.88	48.74	48.78	48.88	48.95	49.44	48.91	49.55	49.29	49.30	49.84	50.26	49.62	49.15	48.93
CaO	0.03	0.03	0.01	0.01	0.01	0.02	0.02	0.01	0.01	0.01	0.03	0.03	0.02	0.01	0.00	0.04	0.02	0.03
Na <sub>2</sub> O	0.00	0.00	0.00	0.02	0.00	0.00	0.00	0.00	0.00	0.00	0.00	0.01	0.00	0.00	0.00	0.00	0.01	0.00
K <sub>2</sub> O	0.00	0.00	0.00	0.01	0.00	0.00	0.01	0.00	0.00	0.01	0.00	0.00	0.00	0.00	0.00	0.00	0.01	0.00
Total	99.09	99.16	99.84	100.38	99.94	100.31	101.01	100.19	100.70	100.20	101.33	100.58	100.54	100.23	101.12	100.47	99.87	99.16
Si	0.999	0.996	0.994	0.998	1.003	1.002	1.003	1.002	0.996	0.998	0.991	0.990	0.993	0.991	0.988	0.987	0.992	0.983
Ti	0.000	0.000	0.000	0.000	0.000	0.000	0.000	0.000	0.000	0.000	0.000	0.000	0.000	0.000	0.000	0.000	0.000	0.000
Al	0.000	0.000	0.000	0.000	0.000	0.000	0.001	0.000	0.000	0.000	0.000	0.000	0.000	0.000	0.000	0.000	0.000	0.001
Cr	0.000	0.000	0.001	0.000	0.000	0.001	0.001	0.002	0.002	0.001	0.000	0.001	0.000	0.002	0.002	0.000	0.000	0.000
Fe <sup>2+</sup>	0.204	0.210	0.197	0.207	0.200	0.205	0.208	0.197	0.197	0.204	0.211	0.208	0.206	0.189	0.193	0.205	0.203	0.210
Mn	0.003	0.004	0.004	0.004	0.003	0.003	0.004	0.002	0.003	0.003	0.003	0.004	0.004	0.002	0.002	0.003	0.003	0.003
Ni	0.008	0.009	0.009	0.009	0.008	0.007	0.008	0.007	0.008	0.008	0.007	0.008	0.007	0.009	0.008	0.007	0.007	0.007
Mg	1.786	1.783	1.800	1.784	1.783	1.779	1.772	1.785	1.795	1.787	1.794	1.798	1.797	1.816	1.818	1.811	1.802	1.812
Ca	0.001	0.001	0.000	0.000	0.000	0.000	0.001	0.000	0.000	0.000	0.001	0.001	0.001	0.000	0.000	0.001	0.001	0.001
Na	0.000	0.000	0.000	0.001	0.000	0.000	0.000	0.000	0.000	0.000	0.000	0.001	0.000	0.000	0.000	0.000	0.001	0.000
K	0.000	0.000	0.000	0.000	0.000	0.000	0.000	0.000	0.000	0.000	0.000	0.000	0.000	0.000	0.000	0.000	0.000	0.000
Fo	89.84	89.52	90.13	89.61	89.95	89.74	89.53	90.06	90.13	89.75	89.52	89.66	89.73	90.65	90.47	89.84	89.95	89.66

Formulae of olivine calculated on the basis of 4 oxygens and all Fe as FeO. c = grain core, r = grain rim., c.opx/r.opx = chadacrysts in opx, e.sp. = embayment in spinel

**Table A-4.** Microprobe analyses and formulae of olivines from different ultramafic lithologies of the Krivaja-Konjuh ophiolite complex

Rock type	Plagioclase Iherzolite																	
Sample-Nr.	u4-46b	u4-48	u4-49	u4-53	u4-53b	u4-55d	u4-63	u4-66	u4-70	u4-75	u4-82	u4-83	d5-4	d5-6	d5-7	d5-8	d5-23	d5-24
Remark				r	c	r					c	r			c	r	r	c
SiO <sub>2</sub>	40.70	40.41	40.76	40.84	40.82	40.57	40.37	40.16	41.02	40.49	40.13	40.34	40.68	40.49	40.60	40.25	40.48	40.65
TiO <sub>2</sub>	0.01	0.00	0.01	0.02	0.00	0.01	0.00	0.00	0.00	0.00	0.00	0.01	0.02	0.00	0.05	0.00	0.02	0.01
Al <sub>2</sub> O <sub>3</sub>	0.00	0.00	0.00	0.01	0.03	0.00	0.00	0.00	0.00	0.00	0.00	0.01	0.01	0.00	0.02	0.00	0.02	0.02
Cr <sub>2</sub> O <sub>3</sub>	0.04	0.03	0.00	0.09	0.03	0.05	0.06	0.06	0.05	0.26	0.05	0.00	0.04	0.03	0.04	0.00	0.00	0.03
FeO	9.76	9.94	9.84	9.82	9.83	9.49	9.80	9.91	9.63	9.19	10.04	9.98	9.66	9.40	9.98	9.90	10.29	9.98
MnO	0.20	0.20	0.12	0.14	0.17	0.21	0.14	0.18	0.10	0.15	0.12	0.13	0.13	0.04	0.12	0.15	0.17	0.13
NiO	0.37	0.36	0.36	0.40	0.41	0.36	0.36	0.40	0.37	0.36	0.37	0.41	0.42	0.40	0.44	0.41	0.44	0.42
MgO	50.00	49.47	49.56	49.73	49.44	49.74	49.66	49.45	49.49	49.94	49.28	49.35	49.10	48.91	48.62	48.47	48.94	48.79
CaO	0.02	0.01	0.04	0.02	0.01	0.01	0.03	0.04	0.02	0.03	0.02	0.01	0.02	0.02	0.03	0.02	0.01	0.03
Na <sub>2</sub> O	0.00	0.01	0.00	0.00	0.00	0.00	0.00	0.00	0.00	0.00	0.00	0.00	0.00	0.00	0.00	0.00	0.00	0.00
K <sub>2</sub> O	0.02	0.00	0.02	0.00	0.00	0.00	0.00	0.00	0.00	0.00	0.00	0.01	0.00	0.00	0.01	0.02	0.00	0.00
Total	101.11	100.41	100.71	101.08	100.74	100.44	100.41	100.20	100.67	100.42	100.02	100.26	100.08	99.29	99.90	99.22	100.37	100.06
Si	0.989	0.989	0.994	0.992	0.995	0.991	0.988	0.986	0.999	0.988	0.987	0.989	0.997	0.999	0.998	0.997	0.993	0.998
Ti	0.000	0.000	0.000	0.000	0.000	0.000	0.000	0.000	0.000	0.000	0.000	0.000	0.000	0.000	0.001	0.000	0.000	0.000
Al	0.000	0.000	0.000	0.000	0.001	0.000	0.000	0.000	0.000	0.000	0.000	0.000	0.000	0.000	0.001	0.000	0.001	0.001
Cr	0.001	0.000	0.000	0.002	0.001	0.001	0.001	0.001	0.001	0.005	0.001	0.000	0.001	0.001	0.001	0.000	0.000	0.001
Fe <sup>2+</sup>	0.198	0.204	0.201	0.199	0.200	0.194	0.200	0.203	0.196	0.188	0.207	0.205	0.198	0.194	0.205	0.205	0.211	0.205
Mn	0.004	0.004	0.002	0.003	0.003	0.004	0.003	0.004	0.002	0.003	0.003	0.003	0.003	0.001	0.003	0.003	0.004	0.003
Ni	0.007	0.007	0.007	0.008	0.008	0.007	0.007	0.008	0.007	0.007	0.007	0.008	0.008	0.008	0.009	0.008	0.009	0.008
Mg	1.811	1.805	1.801	1.801	1.796	1.811	1.811	1.810	1.796	1.817	1.807	1.804	1.794	1.798	1.782	1.789	1.789	1.785
Ca	0.001	0.000	0.001	0.001	0.000	0.000	0.001	0.001	0.001	0.001	0.001	0.000	0.001	0.001	0.001	0.001	0.000	0.001
Na	0.000	0.000	0.000	0.000	0.000	0.000	0.000	0.000	0.000	0.000	0.000	0.000	0.000	0.000	0.000	0.000	0.000	0.000
K	0.001	0.000	0.001	0.000	0.000	0.000	0.000	0.000	0.000	0.000	0.000	0.000	0.000	0.000	0.000	0.001	0.000	0.000
Fo	90.14	89.95	90.03	90.06	90.04	90.36	90.03	89.96	90.22	90.63	89.76	89.84	90.16	90.34	89.77	89.76	89.54	89.76

Formulae of olivine calculated on the basis of 4 oxygens and all Fe as FeO. c = grain core, r = grain rim.

**Table A-5.** Microprobe analyses and formulae of olivines from different ultramafic lithologies of the Krivaja-Konjuh ophiolite complex

Rock type	Plagioclase Iherzolite – Spinel Iherzolite																	
Sample-Nr.	d5-27b	d5-29	d5-31	d5-32	d5-33	d5-44	d5-45	o2-4	o2-11	o2-12	o2-17	o2-18	o2-25	o2-30	o2-31	o2-33	o2-43	o2-44
Remark				c	r	c	r	s.cpx	c	r				c	r		c	r
SiO <sub>2</sub>	40.51	40.89	40.46	40.48	40.55	40.10	40.22	40.63	40.56	40.85	40.54	40.59	40.67	40.88	40.35	40.74	40.78	40.61
TiO <sub>2</sub>	0.00	0.01	0.01	0.03	0.00	0.00	0.00	0.00	0.00	0.00	0.02	0.03	0.01	0.00	0.03	0.01	0.02	0.00
Al <sub>2</sub> O <sub>3</sub>	0.02	0.01	0.00	0.00	0.01	0.01	0.01	0.02	0.03	0.01	0.00	0.00	0.00	0.01	0.01	0.00	0.01	0.02
Cr <sub>2</sub> O <sub>3</sub>	0.10	0.39	0.06	0.02	0.00	0.03	0.01	0.03	0.00	0.03	0.00	0.00	0.02	0.02	0.00	0.03	0.02	0.00
FeO	9.81	9.43	9.63	10.39	9.95	10.13	10.49	9.77	9.80	9.68	9.54	9.85	9.69	9.94	9.66	9.56	9.96	9.55
MnO	0.15	0.21	0.14	0.15	0.10	0.14	0.13	0.16	0.14	0.11	0.06	0.12	0.13	0.12	0.15	0.15	0.20	0.10
NiO	0.38	0.37	0.39	0.40	0.45	0.40	0.43	0.43	0.46	0.46	0.37	0.41	0.38	0.39	0.38	0.41	0.43	0.37
MgO	49.04	49.31	49.00	48.41	48.40	48.15	48.41	49.27	49.28	49.53	49.61	49.61	49.34	49.46	49.20	49.25	49.39	49.35
CaO	0.03	0.02	0.02	0.01	0.01	0.03	0.02	0.02	0.01	0.03	0.03	0.01	0.02	0.01	0.02	0.01	0.00	0.01
Na <sub>2</sub> O	0.00	0.00	0.00	0.00	0.00	0.00	0.01	0.01	0.00	0.03	0.00	0.02	0.00	0.01	0.00	0.00	0.02	0.00
K <sub>2</sub> O	0.02	0.01	0.00	0.02	0.00	0.00	0.01	0.01	0.00	0.00	0.00	0.00	0.01	0.00	0.01	0.01	0.01	0.00
Total	100.06	100.63	99.72	99.90	99.46	98.99	99.73	100.35	100.28	100.72	100.17	100.65	100.25	100.84	99.80	100.17	100.82	100.02
Si	0.994	0.996	0.996	0.997	1.001	0.996	0.994	0.994	0.993	0.995	0.992	0.991	0.995	0.995	0.992	0.997	0.994	0.995
Ti	0.000	0.000	0.000	0.001	0.000	0.000	0.000	0.000	0.000	0.000	0.000	0.001	0.000	0.000	0.001	0.000	0.000	0.000
Al	0.000	0.000	0.000	0.000	0.000	0.000	0.000	0.000	0.001	0.000	0.000	0.000	0.000	0.000	0.000	0.000	0.000	0.001
Cr	0.002	0.007	0.001	0.000	0.000	0.001	0.000	0.001	0.000	0.001	0.000	0.000	0.000	0.000	0.000	0.001	0.000	0.000
Fe <sup>2+</sup>	0.201	0.192	0.198	0.214	0.205	0.211	0.217	0.200	0.201	0.197	0.195	0.201	0.198	0.202	0.199	0.196	0.203	0.196
Mn	0.003	0.004	0.003	0.003	0.002	0.003	0.003	0.003	0.003	0.002	0.001	0.003	0.003	0.002	0.003	0.003	0.004	0.002
Ni	0.008	0.007	0.008	0.008	0.009	0.008	0.009	0.008	0.009	0.009	0.007	0.008	0.007	0.008	0.007	0.008	0.008	0.007
Mg	1.795	1.791	1.797	1.778	1.781	1.784	1.783	1.797	1.799	1.799	1.810	1.805	1.800	1.795	1.804	1.797	1.795	1.803
Ca	0.001	0.000	0.001	0.000	0.000	0.001	0.000	0.001	0.000	0.001	0.001	0.000	0.000	0.000	0.001	0.000	0.000	0.000
Na	0.000	0.000	0.000	0.000	0.000	0.000	0.000	0.001	0.000	0.001	0.000	0.001	0.000	0.001	0.000	0.000	0.001	0.000
K	0.001	0.000	0.000	0.001	0.000	0.000	0.000	0.000	0.000	0.000	0.000	0.000	0.000	0.000	0.000	0.000	0.000	0.000
Fo	89.93	90.34	90.11	89.36	89.76	89.45	89.23	90.06	90.02	90.14	90.32	90.03	90.15	89.94	90.18	90.28	89.85	90.26

Formulae of olivine calculated on the basis of 4 oxygens and all Fe as FeO. c = grain core, r = grain rim. s.cpx = chadacrysts in cpx

**Table A-6.** Microprobe analyses and formulae of olivines from different ultramafic lithologies of the Krivaja-Konjuh ophiolite complex

Rock type	Spinel lherzolite																	
Sample-Nr.	o2-47	o2-52	o2-55	z2-7	z2-8	z2-9	z2-10	z2-11	z2-18	z2-19	z2-20	z2-23	z2-42	z2-54	z2-56	z4-4	z4-5	z4-7
Remark				r	r	c	r	c	r	r	c			r.cpx	c.cpx			r
SiO <sub>2</sub>	41.02	41.00	40.88	41.07	41.50	41.07	41.10	41.09	41.07	41.06	40.97	40.56	40.99	41.16	41.10	40.66	40.47	40.66
TiO <sub>2</sub>	0.00	0.02	0.03	0.00	0.00	0.00	0.00	0.00	0.02	0.00	0.00	0.04	0.00	0.00	0.00	0.00	0.02	0.00
Al <sub>2</sub> O <sub>3</sub>	0.01	0.00	0.00	0.00	0.01	0.01	0.00	0.00	0.00	0.00	0.01	0.02	0.00	0.01	0.02	0.00	0.00	0.01
Cr <sub>2</sub> O <sub>3</sub>	0.02	0.11	0.03	0.03	0.02	0.04	0.00	0.00	0.12	0.15	0.05	0.02	0.00	0.00	0.02	0.03	0.11	0.12
FeO	9.72	9.72	9.73	9.70	9.70	10.12	9.90	9.88	9.17	9.40	9.33	9.72	10.54	9.82	9.78	9.85	10.13	10.05
MnO	0.17	0.10	0.16	0.09	0.17	0.19	0.15	0.17	0.12	0.18	0.12	0.15	0.16	0.12	0.17	0.17	0.09	0.15
NiO	0.37	0.43	0.40	0.34	0.39	0.37	0.40	0.36	0.42	0.47	0.40		0.35	0.40	0.44	0.40	0.39	0.40
MgO	49.30	49.82	49.50	47.68	49.18	48.99	48.94	48.71	49.46	49.55	48.96	48.70	48.92	48.69	48.90	48.76	48.68	49.23
CaO	0.02	0.01	0.01	0.04	0.03	0.02	0.03	0.02	0.03	0.01	0.00	0.04	0.00	0.03	0.01	0.01	0.00	0.01
Na <sub>2</sub> O	0.00	0.00	0.00	0.02	0.01	0.02	0.00	0.00	0.00	0.00	0.02	0.02	0.00	0.00	0.00	0.01	0.03	0.03
K <sub>2</sub> O	0.00	0.02	0.00	0.01	0.01	0.01	0.01	0.00	0.01	0.00	0.00	0.00	0.02	0.02	0.01	0.00	0.02	0.02
Total	100.63	101.23	100.75	98.98	101.00	100.84	100.53	100.23	100.42	100.81	99.86	99.26	100.98	100.25	100.43	99.87	99.94	100.67
Si	1.000	0.994	0.996	1.015	1.006	1.000	1.003	1.005	1.001	0.998	1.004	1.001	0.999	1.006	1.003	0.999	0.996	0.993
Ti	0.000	0.000	0.001	0.000	0.000	0.000	0.000	0.000	0.000	0.000	0.000	0.001	0.000	0.000	0.000	0.000	0.000	0.000
Al	0.000	0.000	0.000	0.000	0.000	0.000	0.000	0.000	0.000	0.000	0.000	0.001	0.000	0.000	0.001	0.000	0.000	0.000
Cr	0.000	0.002	0.001	0.001	0.000	0.001	0.000	0.000	0.002	0.003	0.001	0.000	0.000	0.000	0.000	0.001	0.002	0.002
Fe <sup>2+</sup>	0.198	0.197	0.198	0.201	0.197	0.206	0.202	0.202	0.187	0.191	0.191	0.200	0.215	0.201	0.200	0.202	0.208	0.205
Mn	0.004	0.002	0.003	0.002	0.003	0.004	0.003	0.004	0.002	0.004	0.003	0.003	0.003	0.002	0.003	0.003	0.002	0.003
Ni	0.007	0.008	0.008	0.007	0.008	0.007	0.008	0.007	0.008	0.009	0.008	0.000	0.007	0.008	0.009	0.008	0.008	0.008
Mg	1.791	1.800	1.797	1.757	1.778	1.779	1.780	1.776	1.796	1.796	1.788	1.791	1.777	1.775	1.780	1.786	1.786	1.792
Ca	0.000	0.000	0.000	0.001	0.001	0.001	0.001	0.000	0.001	0.000	0.000	0.001	0.000	0.001	0.000	0.000	0.000	0.000
Na	0.000	0.000	0.000	0.001	0.000	0.001	0.000	0.000	0.000	0.000	0.001	0.001	0.000	0.000	0.000	0.001	0.001	0.002
K	0.000	0.001	0.000	0.000	0.000	0.000	0.000	0.000	0.000	0.000	0.000	0.000	0.001	0.001	0.000	0.000	0.001	0.001
Fo	90.04	90.12	90.14	89.85	90.03	89.65	89.86	89.83	90.62	90.45	90.36	89.94	89.26	89.83	89.94	89.86	89.53	89.74

Formulae of olivine calculated on the basis of 4 oxygens and all Fe as FeO. c = grain core, r = grain rim, c.cpx/r.cpx = chadacrysts in cpx

**Table A-7.** Microprobe analyses and formulae of olivines from different ultramafic lithologies of the Krivaja-Konjuh ophiolite complex

Rock type	Spinel lherzolite																		
Sample-Nr.	z4-9	z4-15	z4-23	z4-24	z4-33	z4-34	z4-47	z4-52	z4-53	u35-1	u35-3	u35-8b	u35-17b	u35-18	u35-20	u35-20b	u35-26	u35-34	
Remark	r	r	c	r	c	r	o.sp.	r	c	r				c	c				r
SiO <sub>2</sub>	40.78	40.71	40.50	40.64	40.82	40.42	41.10	40.82	40.72	40.50	40.48	40.85	40.53	40.57	39.42	40.01	40.39	40.20	
TiO <sub>2</sub>	0.01	0.03	0.00	0.01	0.00	0.01	0.01	0.01	0.00	0.01	0.00	0.01	0.00	0.00	0.00	0.00	0.00	0.00	
Al <sub>2</sub> O <sub>3</sub>	0.00	0.01	0.02	0.01	0.01	0.00	0.01	0.02	0.00	0.00	0.02	0.05	0.01	0.00	0.01	0.00	0.01	0.01	
Cr <sub>2</sub> O <sub>3</sub>	0.01	0.00	0.00	0.01	0.00	0.02	0.11	0.02	0.00	0.01	0.02	0.00	0.03	0.03	0.06	0.47	0.06	0.03	
FeO	9.75	10.06	9.91	10.31	9.89	10.15	9.22	9.58	9.89	10.31	10.23	10.05	9.72	10.22	10.16	9.92	10.02	10.81	
MnO	0.21	0.11	0.16	0.12	0.19	0.15	0.12	0.16	0.11	0.13	0.15	0.18	0.19	0.17	0.16	0.10	0.17	0.13	
NiO	0.39	0.40	0.41	0.38	0.41	0.39	0.43	0.36	0.37	0.40	0.41	0.38	0.41	0.41	0.45	0.40	0.39	0.32	
MgO	49.18	49.11	48.84	48.65	49.20	48.88	49.25	48.78	49.00	48.92	48.91	49.11	49.40	49.23	48.76	49.46	48.98	49.20	
CaO	0.00	0.01	0.00	0.01	0.00	0.00	0.01	0.00	0.01	0.02	0.00	0.02	0.01	0.01	0.04	0.04	0.03	0.03	
Na <sub>2</sub> O	0.00	0.00	0.00	0.00	0.02	0.02	0.01	0.01	0.00	0.00	0.01	0.01	0.01	0.00	0.01	0.01	0.00	0.01	
K <sub>2</sub> O	0.02	0.02	0.00	0.00	0.02	0.01	0.01	0.01	0.00	0.00	0.00	0.01	0.01	0.01	0.00	0.00	0.00	0.00	
Total	100.34	100.47	99.83	100.14	100.57	100.04	100.26	99.76	100.11	100.29	100.21	100.65	100.31	100.65	99.07	100.41	100.05	100.73	
Si	0.997	0.996	0.996	0.998	0.997	0.994	1.003	1.003	0.998	0.994	0.994	0.997	0.992	0.992	0.981	0.982	0.993	0.985	
Ti	0.000	0.001	0.000	0.000	0.000	0.000	0.000	0.000	0.000	0.000	0.000	0.000	0.000	0.000	0.000	0.000	0.000	0.000	
Al	0.000	0.000	0.000	0.000	0.000	0.000	0.000	0.000	0.000	0.000	0.001	0.001	0.000	0.000	0.000	0.000	0.000	0.000	
Cr	0.000	0.000	0.000	0.000	0.000	0.000	0.002	0.000	0.000	0.000	0.000	0.000	0.001	0.001	0.001	0.009	0.001	0.001	
Fe <sup>2+</sup>	0.199	0.206	0.204	0.212	0.202	0.209	0.188	0.197	0.203	0.212	0.210	0.205	0.199	0.209	0.211	0.204	0.206	0.221	
Mn	0.004	0.002	0.003	0.002	0.004	0.003	0.003	0.003	0.002	0.003	0.003	0.004	0.004	0.003	0.003	0.002	0.004	0.003	
Ni	0.008	0.008	0.008	0.008	0.008	0.008	0.008	0.007	0.007	0.008	0.008	0.007	0.008	0.008	0.009	0.008	0.008	0.006	
Mg	1.793	1.790	1.791	1.781	1.791	1.792	1.791	1.786	1.791	1.789	1.790	1.787	1.803	1.794	1.810	1.809	1.795	1.797	
Ca	0.000	0.000	0.000	0.000	0.000	0.000	0.000	0.000	0.000	0.000	0.000	0.000	0.000	0.000	0.001	0.001	0.001	0.001	
Na	0.000	0.000	0.000	0.000	0.001	0.001	0.001	0.000	0.000	0.000	0.000	0.000	0.001	0.000	0.001	0.000	0.000	0.000	
K	0.000	0.001	0.000	0.000	0.001	0.000	0.000	0.000	0.000	0.000	0.000	0.000	0.000	0.000	0.000	0.000	0.000	0.000	
Fo	90.03	89.74	89.85	89.42	89.94	89.65	90.52	90.14	89.85	89.44	89.52	89.76	90.15	89.63	89.57	89.96	89.75	89.03	

Formulae of olivine calculated on the basis of 4 oxygens and all Fe as FeO. c = grain core, r = grain rim, o.sp. = chadocryst in spinel



**Table A-8.** Microprobe analyses and formulae of olivines from different ultramafic lithologies of the Krivaja-Konjuh ophiolite complex

Rock type	Spinel lherzolite																	
Sample-Nr.	u35-34b	u35-40	u35-41	u35-42	u35-68	u35-69	u35-70	u35-75	4a-4	4a-5	4a-7	4a-9	4a-10	4a-26	4a-27	4a-33	4a-35	4a-36
Remark	c	r	r		c	r						r	c	c	r		r	c
SiO <sub>2</sub>	40.36	40.78	40.84	40.72	40.86	40.80	40.89	40.41	41.03	41.28	41.37	41.00	41.10	40.97	41.10	40.82	40.72	40.63
TiO <sub>2</sub>	0.00	0.01	0.00	0.03	0.00	0.00	0.01	0.02	0.00	0.00	0.00	0.00	0.00	0.01	0.03	0.00	0.02	0.01
Al <sub>2</sub> O <sub>3</sub>	0.01	0.01	0.01	0.02	0.01	0.00	0.01	0.00	0.01	0.01	0.01	0.00	0.02	0.00	0.00	0.00	0.00	0.0 <sub>1</sub>
Cr <sub>2</sub> O <sub>3</sub>	0.00	0.30	0.09	0.42	0.31	0.07	0.04	0.10	0.02	0.18	0.19	0.03	0.03	0.00	0.02	0.03	0.04	0.00
FeO	10.98	9.31	9.92	9.18	9.33	10.24	10.03	9.77	8.35	8.01	8.17	8.61	8.36	9.02	8.93	8.80	8.88	8.37
MnO	0.19	0.14	0.18	0.15	0.12	0.20	0.16	0.21	0.39	0.39	0.37	0.39	0.40	0.37	0.37	0.00	0.00	0.00
NiO	0.39	0.41	0.45	0.42	0.38	0.37	0.39	0.35										
MgO	48.78	49.81	49.64	50.05	49.99	49.56	49.14	49.53	50.30	50.69	50.76	50.26	50.11	49.96	49.88	50.17	50.13	49.89
CaO	0.02	0.02	0.02	0.01	0.01	0.02	0.02	0.00	0.01	0.02	0.00	0.01	0.01	0.03	0.00	0.01	0.03	0.02
Na <sub>2</sub> O	0.00	0.01	0.00	0.00	0.00	0.00	0.02	0.02	0.00	0.00	0.00	0.00	0.00	0.02	0.03	0.00	0.01	0.00
K <sub>2</sub> O	0.00	0.01	0.00	0.00	0.01	0.02	0.03	0.00	0.00	0.00	0.01	0.00	0.01	0.00	0.01	0.01	0.00	0.01
Total	100.73	100.80	101.15	100.99	101.03	101.26	100.71	100.41	101.04	101.46	101.79	101.24	100.96	101.37	101.33	100.81	100.79	99.86
Si	0.990	0.992	0.992	0.988	0.991	0.991	0.997	0.989	0.998	0.998	0.998	0.997	1.001	0.997	1.000	0.997	0.995	0.999
Ti	0.000	0.000	0.000	0.000	0.000	0.000	0.000	0.000	0.000	0.000	0.000	0.000	0.000	0.000	0.001	0.000	0.000	0.000
Al	0.000	0.000	0.000	0.000	0.000	0.000	0.000	0.000	0.000	0.000	0.000	0.000	0.001	0.000	0.000	0.000	0.000	0.000
Cr	0.000	0.006	0.002	0.008	0.006	0.001	0.001	0.002	0.000	0.004	0.004	0.001	0.001	0.000	0.000	0.001	0.001	0.000
Fe <sup>2+</sup>	0.225	0.189	0.202	0.186	0.189	0.208	0.205	0.200	0.170	0.162	0.165	0.175	0.170	0.184	0.182	0.180	0.181	0.172
Mn	0.004	0.003	0.004	0.003	0.002	0.004	0.003	0.004	0.008	0.008	0.008	0.008	0.008	0.008	0.008	0.000	0.000	0.000
Ni	0.008	0.008	0.009	0.008	0.007	0.007	0.008	0.007										
Mg	1.783	1.806	1.798	1.811	1.808	1.795	1.787	1.807	1.824	1.827	1.825	1.822	1.819	1.813	1.809	1.826	1.826	1.828
Ca	0.000	0.001	0.001	0.000	0.000	0.000	0.000	0.000	0.000	0.000	0.000	0.000	0.000	0.001	0.000	0.000	0.001	0.000
Na	0.000	0.000	0.000	0.000	0.000	0.000	0.001	0.001	0.000	0.000	0.000	0.000	0.000	0.001	0.001	0.000	0.000	0.000
K	0.000	0.000	0.000	0.000	0.000	0.000	0.001	0.000	0.000	0.000	0.000	0.000	0.000	0.000	0.000	0.000	0.000	0.000
Fo	88.83	90.45	89.92	90.75	90.56	89.63	89.75	90.07	91.54	91.95	91.76	91.27	91.44	90.88	90.93	91.05	91.06	91.47

Formulae of olivine calculated on the basis of 4 oxygens and all Fe as FeO. c = grain core, r = grain rim.

**Table A-9.** Microprobe analyses and formulae of olivines from different ultramafic lithologies of the Krivaja-Konjuh ophiolite complex

Rock type	Spinel Iherzolite – Olivine websterite																	
Sample-Nr.	4a-37	4a-46	1c-2	1c-4	1c-7	1c-14	1c-15	1c-19	1c-20	1c-25	1c-28	1c-31	1c-36	1c-50	1c-53	1c-55	1c-56	2a-1
Remark			r	c	r	c	r	c	r						r	c	c	r
SiO <sub>2</sub>	40.85	41.30	41.57	39.72	39.74	40.56	41.82	39.90	40.74	40.77	40.52	40.70	40.50	41.22	40.85	40.96	41.96	40.71
TiO <sub>2</sub>	0.01	0.04	0.03	0.00	0.00	0.02	0.00	0.01	0.00	0.01	0.02	0.04	0.02	0.01	0.00	0.01	0.01	0.00
Al <sub>2</sub> O <sub>3</sub>	0.01	0.02	0.09	0.01	0.02	0.00	0.01	0.00	0.00	0.01	0.01	0.01	0.00	0.02	0.01	0.01	0.04	0.02
Cr <sub>2</sub> O <sub>3</sub>	0.03	0.04	0.05	0.00	0.01	0.00	0.00	0.00	0.00	0.02	0.01	0.00	0.03	0.28	0.09	0.04	0.00	0.00
FeO	8.42	8.53	9.88	10.04	10.43	10.33	8.93	10.58	10.17	10.70	10.47	10.30	10.32	10.12	10.74	10.54	10.40	10.41
MnO	0.00	0.00	0.11	0.21	0.20	0.23	0.11	0.27	0.16	0.20	0.18	0.16	0.18	0.15	0.15	0.14	0.13	0.18
NiO			0.48	0.46	0.42	0.46	0.44	0.46	0.45	0.42	0.44	0.47	0.43	0.41	0.43	0.37	0.41	
MgO	50.07	50.14	48.77	49.25	49.31	49.02	47.11	49.35	49.13	48.86	49.12	49.10	49.08	48.88	48.46	48.50	48.75	48.80
CaO	0.00	0.01	0.00	0.03	0.01	0.02	0.06	0.01	0.01	0.01	0.02	0.01	0.03	0.02	0.02	0.00	0.02	0.05
Na <sub>2</sub> O	0.00	0.00	0.00	0.00	0.01	0.00	0.00	0.00	0.00	0.01	0.00	0.01	0.02	0.00	0.01	0.00	0.02	0.00
K <sub>2</sub> O	0.00	0.01	0.01	0.01	0.00	0.01	0.03	0.00	0.01	0.00	0.00	0.00	0.02	0.00	0.00	0.01	0.00	0.00
Total	100.32	101.02	100.99	99.73	100.13	100.66	98.52	100.58	100.67	101.01	100.78	100.81	100.62	101.10	100.75	100.59	101.75	100.17
Si	1.000	1.003	1.009	0.982	0.980	0.992	1.033	0.980	0.995	0.995	0.991	0.994	0.991	1.002	0.999	1.002	1.012	0.998
Ti	0.000	0.001	0.001	0.000	0.000	0.000	0.000	0.000	0.000	0.000	0.000	0.001	0.000	0.000	0.000	0.000	0.000	0.000
Al	0.000	0.000	0.002	0.000	0.000	0.000	0.000	0.000	0.000	0.000	0.000	0.000	0.000	0.000	0.000	0.000	0.001	0.000
Cr	0.001	0.001	0.001	0.000	0.000	0.000	0.000	0.000	0.000	0.000	0.000	0.000	0.001	0.005	0.002	0.001	0.000	0.000
Fe <sup>2+</sup>	0.172	0.173	0.201	0.208	0.215	0.211	0.184	0.217	0.208	0.218	0.214	0.210	0.211	0.206	0.220	0.216	0.210	0.214
Mn	0.000	0.000	0.002	0.004	0.004	0.005	0.002	0.006	0.003	0.004	0.004	0.003	0.004	0.003	0.003	0.003	0.003	0.004
Ni			0.009	0.009	0.008	0.009	0.009	0.009	0.009	0.008	0.009	0.009	0.008	0.008	0.008	0.007	0.008	
Mg	1.827	1.816	1.764	1.814	1.812	1.788	1.735	1.807	1.789	1.778	1.791	1.787	1.791	1.771	1.767	1.768	1.753	1.784
Ca	0.000	0.000	0.000	0.001	0.000	0.001	0.002	0.000	0.000	0.000	0.000	0.000	0.001	0.001	0.001	0.000	0.000	0.001
Na	0.000	0.000	0.000	0.000	0.001	0.000	0.000	0.000	0.000	0.001	0.000	0.001	0.001	0.000	0.001	0.000	0.001	0.000
K	0.000	0.000	0.000	0.000	0.000	0.000	0.001	0.000	0.000	0.000	0.000	0.000	0.001	0.000	0.000	0.000	0.000	0.000
Fo	91.44	91.32	89.84	89.72	89.45	89.46	90.47	89.35	89.63	89.19	89.38	89.56	89.54	89.65	88.96	89.13	89.34	89.36

Formulae of olivine calculated on the basis of 4 oxygens and all Fe as FeO. c = grain core, r = grain rim.

**Table A-10.** Microprobe analyses and formulae of olivines from different ultramafic lithologies of the Krivaja-Konjuh ophiolite complex

Rock type	Olivine websterite – Dunite																	
Sample-Nr.	2a-2	2a-3	2a-4	2a-5	2a-6	u19-3	u19-4	u19-5	u19-15	u19-17	u19-19	u19-20	u19-27	u19-29	u19-31	u19-32	u19-33	u19-36
Remark	c	c	r	c	r		r	c			c	r				c	r	
SiO <sub>2</sub>	40.57	40.51	40.70	41.21	40.79	40.47	40.93	40.71	40.24	40.43	39.65	39.86	40.38	39.90	40.24	40.22	40.27	40.43
TiO <sub>2</sub>	0.01	0.02	0.00	0.00	0.03	0.00	0.00	0.01	0.03	0.05	0.05	0.06	0.03	0.00	0.02	0.03	0.06	0.01
Al <sub>2</sub> O <sub>3</sub>	0.00	0.00	0.01	0.00	0.00	0.02	0.01	0.03	0.02	0.03	0.01	0.02	0.00	0.01	0.01	0.00	0.02	0.01
Cr <sub>2</sub> O <sub>3</sub>	0.04	0.00	0.03	0.00	0.02	0.00	0.04	0.02	0.01	0.04	0.02	0.00	0.01	0.04	0.05	0.05	0.00	0.03
FeO	9.80	10.57	10.32	10.50	10.62	11.72	11.69	11.86	10.68	10.94	12.10	11.39	12.15	11.77	11.46	11.71	11.66	11.60
MnO	0.19	0.15	0.20	0.17	0.13	0.23	0.28	0.16	0.24	0.18	0.18	0.17	0.12	0.15	0.14	0.21	0.20	0.23
NiO																		
MgO	48.63	48.98	49.17	49.16	48.85	47.75	47.91	47.41	48.58	48.38	47.31	47.20	47.88	47.77	47.79	48.07	47.65	48.13
CaO	0.03	0.02	0.04	0.02	0.02	0.03	0.09	0.11	0.03	0.03	0.12	0.10	0.05	0.02	0.05	0.07	0.04	0.08
Na <sub>2</sub> O	0.00	0.01	0.00	0.00	0.02	0.00	0.03	0.00	0.00	0.01	0.00	0.01	0.00	0.02	0.00	0.02	0.01	0.00
K <sub>2</sub> O	0.02	0.01	0.00	0.01	0.02	0.00	0.02	0.01	0.00	0.01	0.02	0.01	0.01	0.00	0.02	0.00	0.01	0.00
Total	99.28	100.26	100.49	101.07	100.49	100.22	101.00	100.30	99.85	100.09	99.46	98.81	100.62	99.67	99.78	100.38	99.91	100.53
Si	1.001	0.994	0.995	1.001	0.998	0.998	1.001	1.003	0.993	0.995	0.989	0.997	0.994	0.991	0.996	0.991	0.996	0.994
Ti	0.000	0.000	0.000	0.000	0.001	0.000	0.000	0.000	0.001	0.001	0.001	0.001	0.001	0.000	0.000	0.001	0.001	0.000
Al	0.000	0.000	0.000	0.000	0.000	0.001	0.000	0.001	0.001	0.001	0.000	0.001	0.000	0.000	0.000	0.000	0.001	0.000
Cr	0.001	0.000	0.001	0.000	0.000	0.000	0.001	0.000	0.000	0.001	0.000	0.000	0.000	0.001	0.001	0.001	0.000	0.001
Fe <sup>2+</sup>	0.202	0.217	0.211	0.213	0.217	0.242	0.239	0.244	0.220	0.225	0.252	0.238	0.250	0.244	0.237	0.241	0.241	0.239
Mn	0.004	0.003	0.004	0.003	0.003	0.005	0.006	0.003	0.005	0.004	0.004	0.004	0.003	0.003	0.003	0.004	0.004	0.005
Ni																		
Mg	1.789	1.791	1.792	1.780	1.781	1.755	1.747	1.741	1.786	1.775	1.759	1.759	1.757	1.768	1.763	1.766	1.757	1.764
Ca	0.001	0.001	0.001	0.000	0.000	0.001	0.002	0.003	0.001	0.001	0.003	0.003	0.001	0.001	0.001	0.002	0.001	0.002
Na	0.000	0.000	0.000	0.000	0.001	0.000	0.002	0.000	0.000	0.000	0.000	0.000	0.000	0.001	0.000	0.001	0.000	0.000
K	0.001	0.000	0.000	0.000	0.001	0.000	0.001	0.000	0.000	0.000	0.001	0.000	0.000	0.000	0.001	0.000	0.000	0.000
Fo	89.84	89.23	89.55	89.33	89.12	87.93	88.05	87.72	89.04	88.74	87.53	88.15	87.54	87.97	88.14	88.05	87.96	88.12

Formulae of olivine calculated on the basis of 4 oxygens and all Fe as FeO. c = grain core, r = grain rim.

**Table A-11.** Microprobe analyses and formulae of olivines from different ultramafic lithologies of the Krivaja-Konjuh ophiolite complex

Rock type	Dunite																	
Sample-Nr.	u19-38	u19-40	u19-41	u19-42	k1-3	k1-4	k1-5	k1-7	k1-8	k1-12	k1-13	k1-14	k1-15	k1-16	k1-17	k1-20	k1-24	k1-25
Remark			c	r	r	r	c	r	c			c	r	c	r		r	c
SiO <sub>2</sub>	40.11	40.62	40.47	40.49	39.96	40.44	40.37	40.04	40.34	39.89	40.08	40.15	40.43	40.12	40.33	39.97	40.23	40.43
TiO <sub>2</sub>	0.00	0.01	0.03	0.02	0.00	0.03	0.00	0.00	0.01	0.01	0.01	0.02	0.00	0.01	0.00	0.02	0.02	0.02
Al <sub>2</sub> O <sub>3</sub>	0.01	0.03	0.02	0.02	0.02	0.01	0.03	0.02	0.03	0.03	0.03	0.03	0.02	0.01	0.02	0.02	0.02	0.01
Cr <sub>2</sub> O <sub>3</sub>	0.00	0.02	0.00	0.00	0.00	0.02	0.02	0.01	0.03	0.07	0.02	0.02	0.04	0.00	0.04	0.02	0.11	0.07
FeO	11.45	11.21	11.85	11.91	11.54	11.08	11.27	10.99	11.20	11.01	11.18	11.29	11.38	11.21	10.98	11.03	10.69	11.44
MnO	0.15	0.23	0.31	0.22	0.15	0.17	0.15	0.22	0.22	0.12	0.19	0.24	0.20	0.28	0.19	0.21	0.20	0.22
NiO					0.38	0.35	0.38	0.35	0.38	0.33	0.35	0.35	0.38	0.36	0.39	0.37	0.45	0.36
MgO	48.26	48.21	47.79	47.31	47.42	47.83	47.29	47.26	47.22	47.56	47.18	47.37	47.57	47.47	47.72	47.29	47.55	47.78
CaO	0.05	0.07	0.09	0.09	0.11	0.15	0.19	0.12	0.13	0.11	0.12	0.17	0.18	0.17	0.13	0.11	0.16	0.15
Na <sub>2</sub> O	0.01	0.01	0.00	0.02	0.01	0.00	0.00	0.01	0.00	0.00	0.01	0.00	0.00	0.00	0.02	0.02	0.03	0.00
K <sub>2</sub> O	0.00	0.00	0.00	0.02	0.00	0.01	0.00	0.00	0.00	0.01	0.00	0.00	0.00	0.00	0.01	0.00	0.01	0.00
Total	100.03	100.41	100.55	100.07	99.59	100.07	99.71	99.02	99.56	99.13	99.16	99.64	100.19	99.64	99.83	99.05	99.47	100.47
Si	0.991	0.998	0.996	1.001	0.994	0.998	1.001	0.999	1.001	0.994	0.999	0.997	0.998	0.996	0.998	0.997	0.998	0.996
Ti	0.000	0.000	0.000	0.000	0.000	0.001	0.000	0.000	0.000	0.000	0.000	0.000	0.000	0.000	0.000	0.000	0.000	0.000
Al	0.000	0.001	0.001	0.000	0.000	0.000	0.001	0.001	0.001	0.001	0.001	0.001	0.000	0.000	0.001	0.001	0.001	0.000
Cr	0.000	0.000	0.000	0.000	0.000	0.000	0.000	0.000	0.001	0.001	0.000	0.000	0.001	0.000	0.001	0.000	0.002	0.001
Fe <sup>2+</sup>	0.236	0.230	0.244	0.246	0.240	0.229	0.234	0.229	0.232	0.229	0.233	0.234	0.235	0.233	0.227	0.230	0.222	0.236
Mn	0.003	0.005	0.006	0.005	0.003	0.003	0.003	0.005	0.005	0.003	0.004	0.005	0.004	0.006	0.004	0.005	0.004	0.005
Ni	0.000	0.000	0.000	0.000	0.008	0.007	0.008	0.007	0.008	0.007	0.007	0.007	0.007	0.007	0.008	0.007	0.009	0.007
Mg	1.777	1.765	1.754	1.743	1.758	1.759	1.747	1.757	1.747	1.767	1.753	1.753	1.751	1.757	1.760	1.759	1.759	1.754
Ca	0.001	0.002	0.002	0.002	0.003	0.004	0.005	0.003	0.003	0.003	0.003	0.005	0.005	0.004	0.004	0.003	0.004	0.004
Na	0.000	0.000	0.000	0.001	0.000	0.000	0.000	0.001	0.000	0.000	0.001	0.000	0.000	0.000	0.001	0.001	0.001	0.000
K	0.000	0.000	0.000	0.001	0.000	0.000	0.000	0.000	0.000	0.000	0.000	0.000	0.000	0.000	0.000	0.000	0.000	0.000
Fo	88.33	88.54	87.82	87.64	88.07	88.56	88.23	88.56	88.38	88.56	88.38	88.24	88.27	88.35	88.68	88.44	88.87	88.24

Formulae of olivine calculated on the basis of 4 oxygens and all Fe as FeO. c = grain core, r = grain rim.

**Table A-12.** Microprobe analyses and formulae of olivines from different ultramafic lithologies of the Krivaja-Konjuh ophiolite complex

Rock type	Dunite – Mylonitized spinel lherzolite																	
Sample-Nr.	k1-27	k1-28	k1-29	r7-8	r7-19	r7-24	r7-25	r7-26	r7-27	r7-29	r7-34	r7-38	r7-40	r7-45	r7-46	r7-58	r7-59	r7-61
Remark	r	c	r			r	c						c	r				r
SiO <sub>2</sub>	40.35	40.24	40.28	40.58	40.82	40.19	40.66	40.29	40.70	42.43	40.54	40.66	40.90	39.78	39.89	41.03	41.32	40.90
TiO <sub>2</sub>	0.00	0.01	0.00	0.02	0.02	0.00	0.02	0.01	0.02	0.00	0.00	0.02	0.01	0.00	0.00	0.00	0.00	0.00
Al <sub>2</sub> O <sub>3</sub>	0.01	0.01	0.01	0.00	0.00	0.00	0.01	0.01	0.00	0.04	0.44	0.00	0.00	0.00	0.01	0.03	0.06	0.00
Cr <sub>2</sub> O <sub>3</sub>	0.17	0.09	0.10	0.00	0.00	0.03	0.00	0.02	0.03	0.07	0.08	0.03	0.03	0.00	0.00	0.02	0.05	0.02
FeO	10.86	11.20	11.16	9.66	10.02	10.07	9.77	10.49	10.13	8.13	9.89	10.02	10.14	9.83	10.07	9.99	9.72	9.94
MnO	0.20	0.21	0.19	0.12	0.14	0.13	0.13	0.18	0.16	0.12	0.13	0.14	0.13	0.15	0.12	0.14	0.20	0.14
NiO	0.37	0.39	0.34	0.37	0.46	0.41	0.42	0.37	0.39	0.38	0.40	0.48	0.46	0.41	0.35	0.43	0.46	0.41
MgO	48.04	47.69	47.86	48.64	48.27	48.61	48.61	48.63	48.61	47.67	48.48	48.40	48.01	48.65	48.62	48.44	48.26	48.06
CaO	0.15	0.17	0.13	0.01	0.01	0.01	0.02	0.02	0.03	0.05	0.09	0.02	0.03	0.01	0.01	0.08	0.09	0.02
Na <sub>2</sub> O	0.01	0.01	0.01	0.02	0.00	0.00	0.02	0.00	0.00	0.04	0.00	0.00	0.00	0.00	0.00	0.00	0.01	0.01
K <sub>2</sub> O	0.01	0.00	0.01	0.00	0.01	0.00	0.01	0.00	0.00	0.00	0.00	0.01	0.01	0.02	0.01	0.02	0.00	0.00
Total	100.17	100.00	100.10	99.42	99.74	99.45	99.67	100.02	100.07	98.92	100.03	99.76	99.74	98.84	99.07	100.18	100.17	99.51
Si	0.995	0.995	0.995	1.001	1.005	0.994	1.001	0.992	1.000	1.039	0.995	1.001	1.007	0.990	0.990	1.005	1.011	1.008
Ti	0.000	0.000	0.000	0.000	0.000	0.000	0.000	0.000	0.000	0.000	0.000	0.000	0.000	0.000	0.000	0.000	0.000	0.000
Al	0.000	0.000	0.000	0.000	0.000	0.000	0.000	0.000	0.000	0.001	0.013	0.000	0.000	0.000	0.000	0.001	0.002	0.000
Cr	0.003	0.002	0.002	0.000	0.000	0.001	0.000	0.000	0.001	0.001	0.001	0.001	0.001	0.000	0.000	0.000	0.001	0.000
Fe <sup>2+</sup>	0.224	0.232	0.230	0.199	0.206	0.208	0.201	0.216	0.208	0.167	0.203	0.206	0.209	0.204	0.209	0.205	0.199	0.205
Mn	0.004	0.004	0.004	0.003	0.003	0.003	0.003	0.004	0.003	0.003	0.003	0.003	0.003	0.003	0.003	0.003	0.004	0.003
Ni	0.007	0.008	0.007	0.007	0.009	0.008	0.008	0.007	0.008	0.007	0.008	0.009	0.009	0.008	0.007	0.008	0.009	0.008
Mg	1.765	1.758	1.762	1.788	1.771	1.792	1.784	1.786	1.779	1.740	1.773	1.777	1.762	1.804	1.800	1.769	1.760	1.766
Ca	0.004	0.004	0.004	0.000	0.000	0.000	0.000	0.000	0.001	0.001	0.002	0.001	0.001	0.000	0.000	0.002	0.002	0.000
Na	0.000	0.000	0.001	0.001	0.000	0.000	0.001	0.000	0.000	0.002	0.000	0.000	0.000	0.000	0.000	0.000	0.000	0.001
K	0.000	0.000	0.000	0.000	0.000	0.000	0.000	0.000	0.000	0.000	0.000	0.000	0.000	0.001	0.000	0.001	0.000	0.000
Fo	88.74	88.42	88.44	90.05	89.65	89.63	89.96	89.22	89.55	91.36	89.73	89.67	89.45	89.89	89.64	89.65	89.87	89.65

Formulae of olivine calculated on the basis of 4 oxygens and all Fe as FeO. c = grain core, r = grain rim.

**Table A-13.** Microprobe analyses and formulae of olivines from different ultramafic lithologies of the Krivaja-Konjuh ophiolite complex

Rock type	Mylonitized spinel lherzolite - Chromitite							
Sample-Nr.	r7-62	r7-63	r7-64	d17-3	d17-4	d17-5	d17-6	d17-7
Remark	c	r	c					
SiO <sub>2</sub>	40.58	40.84	40.55	40.32	40.63	40.88	40.75	40.69
TiO <sub>2</sub>	0.02	0.01	0.00	0.01	0.02	0.01	0.00	0.00
Al <sub>2</sub> O <sub>3</sub>	0.00	0.00	0.00	0.00	0.00	0.01	0.00	0.00
Cr <sub>2</sub> O <sub>3</sub>	0.03	0.01	0.00	0.00	0.02	0.01	0.00	0.00
FeO	10.07	9.93	9.93	8.30	8.27	7.95	8.01	7.64
MnO	0.13	0.14	0.17	0.09	0.06	0.08	0.10	0.09
NiO	0.39	0.48	0.45	0.57	0.51	0.53	0.52	0.55
MgO	48.35	48.50	48.01	50.15	50.62	50.40	50.31	50.94
CaO	0.02	0.02	0.03	0.01	0.03	0.02	0.00	0.00
Na <sub>2</sub> O	0.00	0.00	0.00	0.01	0.03	0.00	0.00	0.00
K <sub>2</sub> O	0.01	0.00	0.00	0.00	0.00	0.00	0.02	0.00
Total	99.59	99.93	99.14	99.45	100.20	99.90	99.72	99.92
Si	1.001	1.003	1.004	0.990	0.990	0.996	0.996	0.991
Ti	0.000	0.000	0.000	0.000	0.000	0.000	0.000	0.000
Al	0.000	0.000	0.000	0.000	0.000	0.000	0.000	0.000
Cr	0.001	0.000	0.000	0.000	0.000	0.000	0.000	0.000
Fe <sup>2+</sup>	0.208	0.204	0.206	0.170	0.169	0.162	0.164	0.156
Mn	0.003	0.003	0.003	0.002	0.001	0.002	0.002	0.002
Ni	0.008	0.009	0.009	0.011	0.010	0.010	0.010	0.011
Mg	1.778	1.776	1.773	1.836	1.838	1.831	1.832	1.849
Ca	0.000	0.000	0.001	0.000	0.001	0.000	0.000	0.000
Na	0.000	0.000	0.000	0.001	0.001	0.000	0.000	0.000
K	0.000	0.000	0.000	0.000	0.000	0.000	0.001	0.000
Fo	89.54	89.76	89.63	91.57	91.62	91.94	91.86	92.22

Formulae of olivine calculated on the basis of 4 oxygens and all Fe as FeO. c = grain core, r = grain rim.

Orthopyroxene

**Table B-1.** Microprobe analyses and formulae of orthopyroxene porphyroclasts from different ultramafic lithologies of the Krivaja-Konjuh ophiolite complex

Rock type	Plagioclase Iherzolite																	
Sample-Nr.	gr2-19	gr2-21	gr2-24	gr2-34	gr2-35	gr2-48	gr2-49	m2-4	m2-11	m2-24	m2-33	m2-34	m2-35	m2-36	m2-37	m2-40	u4-31	u4-32
Remark	r	r	r	r	c	r	c	r	c	r	r	r	r	r	r	c	r	c
SiO <sub>2</sub>	56.44	56.67	56.55	56.37	56.26	57.16	56.33	54.08	53.40	56.49	56.56	56.47	52.47	53.11	55.95	55.13	55.93	53.26
TiO <sub>2</sub>	0.15	0.16	0.25	0.21	0.20	0.16	0.20	0.15	0.11	0.14	0.15	0.14	0.30	0.24	0.16	0.14	0.11	0.14
Al <sub>2</sub> O <sub>3</sub>	2.05	1.77	2.00	2.02	2.23	1.75	1.94	3.01	2.70	2.30	2.17	2.61	2.96	2.87	2.88	3.13	2.32	2.29
Cr <sub>2</sub> O <sub>3</sub>	0.56	0.51	0.58	0.67	0.70	0.46	0.72	0.62	0.84	0.51	0.43	0.57	0.34	0.89	0.74	0.97	0.62	0.62
Fe <sub>2</sub> O <sub>3</sub>	0.13	0.00	0.00	0.00	0.00	0.00	0.00	0.55	3.57	0.00	0.00	0.00	0.62	0.22	0.00	0.63	1.64	3.21
FeO	6.74	6.62	6.75	7.12	6.89	7.19	6.81	7.00	3.47	6.92	6.78	6.67	6.10	6.64	6.88	6.29	5.53	3.92
MnO	0.19	0.11	0.21	0.18	0.12	0.16	0.09	0.25	0.22	0.13	0.21	0.18	0.13	0.08	0.17	0.15	0.19	0.14
MgO	33.32	33.19	33.00	33.09	33.00	33.67	32.90	31.45	32.37	33.23	33.27	33.41	32.80	31.12	33.23	32.57	33.82	32.57
CaO	0.92	0.81	1.01	0.81	1.14	0.69	1.02	0.88	1.87	0.83	0.87	0.67	0.97	0.72	0.49	1.19	0.71	1.22
Na <sub>2</sub> O	0.02	0.03	0.02	0.02	0.02	0.02	0.00	0.06	0.04	0.00	0.02	0.02	0.01	0.01	0.01	0.01	0.01	0.02
K <sub>2</sub> O	0.01	0.01	0.00	0.00	0.00	0.02	0.00	0.02	0.00	0.00	0.01	0.00	0.00	0.00	0.01	0.00	0.00	0.01
Total	100.53	99.87	100.37	100.49	100.55	101.27	100.00	98.07	98.58	100.54	100.47	100.74	99.68	100.19	100.52	100.21	100.88	97.40
Si	1.946	1.962	1.952	1.947	1.941	1.956	1.952	1.920	1.883	1.946	1.949	1.939	1.915	1.927	1.928	1.911	1.921	1.897
Ti	0.004	0.004	0.007	0.005	0.005	0.004	0.005	0.004	0.003	0.003	0.004	0.004	0.008	0.006	0.004	0.004	0.003	0.004
Al	0.083	0.072	0.081	0.082	0.091	0.071	0.079	0.126	0.112	0.093	0.088	0.106	0.127	0.123	0.117	0.128	0.094	0.096
Cr	0.015	0.014	0.016	0.018	0.019	0.013	0.020	0.017	0.023	0.014	0.012	0.016	0.030	0.025	0.020	0.027	0.017	0.018
Fe <sup>3+</sup>	0.003	0.000	0.000	0.000	0.000	0.000	0.000	0.015	0.095	0.000	0.000	0.000	0.017	0.006	0.000	0.016	0.042	0.086
Fe <sup>2+</sup>	0.194	0.192	0.195	0.206	0.199	0.206	0.197	0.208	0.102	0.199	0.195	0.192	0.064	0.180	0.198	0.182	0.159	0.117
Mn	0.005	0.003	0.006	0.005	0.003	0.005	0.003	0.007	0.007	0.004	0.006	0.005	0.004	0.002	0.005	0.004	0.006	0.004
Mg	1.713	1.713	1.698	1.703	1.697	1.718	1.700	1.664	1.702	1.706	1.709	1.710	1.714	1.726	1.707	1.683	1.732	1.730
Ca	0.034	0.030	0.037	0.030	0.042	0.025	0.038	0.034	0.070	0.031	0.032	0.025	0.038	0.034	0.018	0.044	0.026	0.047
Na	0.001	0.002	0.001	0.001	0.001	0.001	0.000	0.004	0.002	0.000	0.002	0.001	0.002	0.001	0.001	0.000	0.001	0.001
K	0.001	0.000	0.000	0.000	0.000	0.001	0.000	0.001	0.000	0.000	0.000	0.000	0.000	0.000	0.000	0.000	0.000	0.001
Wo	1.71	1.52	1.91	1.55	2.28	1.34	1.97	1.76	3.63	1.67	1.79	1.34	1.37	1.59	0.94	2.37	1.39	2.45
En	87.8	88.4	87.7	87.6	87.4	87.9	87.7	86.3	86.1	88.0	88.0	88.5	88.2	87.8	88.5	87.2	88.1	87.2
Fs	10.4	10.1	10.4	10.8	10.4	10.8	10.3	11.9	10.3	10.5	10.4	10.2	10.5	10.7	10.5	10.5	10.5	10.4

Formulae of orthopyroxene calculated on the basis of 6 oxygens. c = grain core. r = grain rim.

**Table B-2.** Microprobe analyses and formulae of orthopyroxene porphyroclasts from different ultramafic lithologies of the Krivaja-Konjuh ophiolite complex

Rock type	Plagioclase Iherzolite																	
Sample-Nr.	u4-34	u4-36	u4-37	u4-42	u4-43	u4-45	u4-55c	u4-57	u4-67c	u4-76	u4-77	u4-79	d5-12	d5-37	d5-11	d5-38	d5-41	d5-43
Remark	r			r	c	r	r	r	r	c	c	r	c	c	r	r	r	r
SiO <sub>2</sub>	56.79	56.50	56.06	55.67	56.01	55.75	55.68	55.50	55.67	55.11	55.18	55.07	55.57	55.45	56.38	55.31	55.82	55.83
TiO <sub>2</sub>	0.11	0.11	0.14	0.14	0.16	0.14	0.16	0.15	0.14	0.12	0.13	0.14	0.20	0.22	0.21	0.20	0.15	0.23
Al <sub>2</sub> O <sub>3</sub>	1.56	1.92	2.10	1.83	2.30	2.26	2.28	2.43	2.46	2.27	2.26	2.07	2.15	2.10	1.71	1.80	1.80	1.63
Cr <sub>2</sub> O <sub>3</sub>	0.39	0.52	0.53	0.51	0.63	0.66	0.63	0.65	0.74	0.61	0.59	0.65	0.70	0.58	0.54	0.57	0.53	0.35
Fe <sub>2</sub> O <sub>3</sub>	1.15	1.21	1.42	2.37	1.00	1.43	1.36	1.66	1.35	1.76	1.38	2.07	0.65	0.71	0.00	0.62	0.84	0.48
FeO	5.74	5.80	5.57	4.40	5.90	5.68	5.49	5.48	5.31	5.08	5.64	4.98	6.06	6.03	6.60	6.04	6.11	6.41
MnO	0.14	0.23	0.23	0.10	0.19	0.08	0.19	0.10	0.17	0.16	0.17	0.09	0.21	0.15	0.14	0.14	0.17	0.20
MgO	34.41	34.20	33.63	34.02	33.46	33.62	33.45	33.45	33.66	33.32	33.32	33.48	32.61	32.69	33.15	32.79	33.11	33.27
CaO	0.50	0.49	1.01	1.16	0.98	0.80	1.01	0.96	0.85	1.05	0.64	0.87	1.61	1.43	0.98	1.24	1.11	0.74
Na <sub>2</sub> O	0.01	0.01	0.02	0.01	0.02	0.01	0.03	0.01	0.02	0.00	0.01	0.01	0.03	0.05	0.01	0.02	0.03	0.01
K <sub>2</sub> O	0.03	0.01	0.00	0.00	0.02	0.00	0.00	0.01	0.01	0.00	0.02	0.02	0.01	0.00	0.00	0.00	0.01	0.01
Total	100.84	100.98	100.71	100.20	100.67	100.43	100.28	100.40	100.37	99.48	99.34	99.45	99.79	99.41	99.72	98.72	99.67	99.15
Si	1.947	1.936	1.929	1.922	1.929	1.923	1.924	1.917	1.920	1.919	1.924	1.919	1.934	1.935	1.957	1.942	1.942	1.950
Ti	0.003	0.003	0.004	0.004	0.004	0.004	0.004	0.004	0.004	0.003	0.003	0.004	0.005	0.006	0.005	0.005	0.004	0.006
Al	0.063	0.078	0.085	0.074	0.093	0.092	0.093	0.099	0.100	0.093	0.093	0.085	0.088	0.087	0.070	0.075	0.074	0.067
Cr	0.011	0.014	0.014	0.014	0.017	0.018	0.017	0.018	0.020	0.017	0.016	0.018	0.019	0.016	0.015	0.016	0.015	0.010
Fe <sup>3+</sup>	0.030	0.031	0.037	0.061	0.026	0.037	0.035	0.043	0.035	0.046	0.036	0.054	0.017	0.019	0.000	0.016	0.022	0.013
Fe <sup>2+</sup>	0.165	0.166	0.160	0.127	0.170	0.164	0.159	0.158	0.153	0.148	0.164	0.145	0.176	0.176	0.192	0.177	0.178	0.187
Mn	0.004	0.007	0.007	0.003	0.005	0.002	0.005	0.003	0.005	0.005	0.005	0.003	0.006	0.004	0.004	0.004	0.005	0.006
Mg	1.758	1.747	1.725	1.751	1.718	1.729	1.723	1.722	1.730	1.730	1.732	1.739	1.692	1.701	1.715	1.716	1.717	1.732
Ca	0.018	0.018	0.037	0.043	0.036	0.030	0.037	0.036	0.031	0.039	0.024	0.033	0.060	0.053	0.037	0.047	0.041	0.028
Na	0.001	0.000	0.002	0.001	0.001	0.001	0.002	0.000	0.002	0.000	0.001	0.000	0.002	0.003	0.001	0.001	0.002	0.001
K	0.001	0.000	0.000	0.000	0.001	0.000	0.000	0.000	0.000	0.000	0.001	0.001	0.000	0.000	0.000	0.000	0.000	0.001
Wo	0.91	0.95	1.93	2.25	1.82	1.56	1.93	1.88	1.64	2.06	1.23	1.78	3.15	2.73	1.97	2.43	2.17	1.44
En	89.0	88.7	87.7	88.2	87.9	88.1	87.9	87.8	88.5	87.9	88.3	88.1	86.7	87.1	88.1	87.5	87.5	88.1
Fs	10.0	10.4	10.4	9.6	10.3	10.4	10.2	10.4	9.9	10.1	10.5	10.2	10.2	10.2	10.0	10.1	10.4	10.5

Formulae of orthopyroxene calculated on the basis of 6 oxygens. c = grain core. r = grain rim.



**Table B-3.** Microprobe analyses and formulae of orthopyroxene porphyroclasts from different ultramafic lithologies of the Krivaja-Konjuh ophiolite complex

Rock type	Spinel lherzolite																	
Sample-Nr.	o2-10	o2-54	o2-5	o2-6	o2-8	o2-53	o2-2	z2-24	z2-26	z2-29	z2-31	z2-39	z2-45	z2-47	z4-17	z4-26	z4-38	z4-40
Remark	c	c	r	r	r	in(cpx)	r	r		c	r	c		c	r	r	r	c
SiO <sub>2</sub>	52.48	54.56	54.39	54.52	54.42	54.81	54.96	54.66	55.48	55.85	54.62	55.21	54.71	54.73	54.95	54.75	54.61	54.55
TiO <sub>2</sub>	0.06	0.13	0.09	0.05	0.06	0.12	0.11	0.08	0.12	0.07	0.11	0.08	0.08	0.08	0.11	0.08	0.07	0.04
Al <sub>2</sub> O <sub>3</sub>	4.49	4.79	4.48	4.12	3.65	4.27	4.27	3.90	4.25	3.89	4.84	4.30	4.82	4.87	4.67	4.31	4.74	5.18
Cr <sub>2</sub> O <sub>3</sub>	0.53	0.58	0.53	0.50	0.39	0.50	0.54	0.49	0.58	0.44	0.61	0.65	0.70	0.70	0.50	0.53	0.64	0.68
Fe <sub>2</sub> O <sub>3</sub>	3.96	0.45	1.04	1.27	1.97	0.80	0.00	0.95	0.00	0.00	0.00	0.00	0.34	0.00	0.00	1.13	0.00	0.26
FeO	3.85	6.06	5.52	4.71	4.89	5.89	6.19	5.79	6.65	6.55	6.47	6.56	6.26	6.57	6.19	5.85	6.45	5.98
MnO	0.10	0.06	0.18	0.17	0.12	0.17	0.11	0.15	0.19	0.05	0.18	0.15	0.07	0.13	0.16	0.19	0.17	0.09
MgO	32.26	32.15	32.65	32.94	33.38	32.63	33.04	33.01	32.63	33.01	31.96	32.31	32.37	32.14	32.08	32.92	32.38	32.29
CaO	0.84	1.12	0.82	1.14	0.40	0.96	0.38	0.47	0.76	0.49	1.15	0.80	0.97	1.02	1.43	0.57	0.66	1.07
Na <sub>2</sub> O	0.06	0.10	0.04	0.04	0.02	0.04	0.02	0.00	0.00	0.00	0.03	0.00	0.05	0.03	0.05	0.02	0.00	0.06
K <sub>2</sub> O	0.00	0.01	0.00	0.00	0.00	0.00	0.00	0.01	0.00	0.00	0.01	0.01	0.00	0.00	0.00	0.00	0.00	0.00
Total	98.62	100.00	99.73	99.46	99.29	100.20	99.61	99.51	100.66	100.35	99.97	100.05	100.36	100.26	100.14	100.33	99.71	100.20
Si	1.848	1.889	1.887	1.892	1.893	1.894	1.904	1.899	1.907	1.921	1.893	1.909	1.888	1.891	1.899	1.889	1.894	1.883
Ti	0.002	0.003	0.002	0.001	0.001	0.003	0.003	0.002	0.003	0.002	0.003	0.002	0.002	0.002	0.003	0.002	0.002	0.001
Al	0.186	0.195	0.183	0.169	0.150	0.174	0.174	0.160	0.172	0.158	0.198	0.175	0.196	0.198	0.190	0.175	0.194	0.211
Cr	0.015	0.016	0.014	0.014	0.011	0.014	0.015	0.013	0.016	0.012	0.017	0.018	0.019	0.019	0.014	0.014	0.017	0.018
Fe <sup>3+</sup>	0.105	0.012	0.027	0.033	0.051	0.021	0.000	0.025	0.000	0.000	0.000	0.000	0.009	0.000	0.000	0.029	0.000	0.007
Fe <sup>2+</sup>	0.113	0.175	0.160	0.137	0.142	0.170	0.179	0.168	0.191	0.188	0.188	0.190	0.181	0.190	0.179	0.169	0.187	0.173
Mn	0.003	0.002	0.005	0.005	0.004	0.005	0.003	0.004	0.005	0.002	0.005	0.004	0.002	0.004	0.005	0.006	0.005	0.002
Mg	1.693	1.659	1.688	1.704	1.731	1.681	1.706	1.710	1.672	1.692	1.651	1.666	1.665	1.656	1.653	1.694	1.674	1.662
Ca	0.032	0.041	0.030	0.042	0.015	0.035	0.014	0.017	0.028	0.018	0.043	0.030	0.036	0.038	0.053	0.021	0.025	0.040
Na	0.004	0.007	0.003	0.003	0.001	0.003	0.002	0.000	0.000	0.000	0.002	0.000	0.003	0.002	0.003	0.001	0.000	0.004
K	0.000	0.001	0.000	0.000	0.000	0.000	0.000	0.000	0.000	0.000	0.000	0.000	0.000	0.000	0.000	0.000	0.000	0.000
Wo	1.61	2.25	1.64	2.23	0.86	1.94	0.77	0.93	1.57	1.08	2.34	1.66	1.98	2.03	2.87	1.19	1.34	2.16
En	87.0	87.8	88.3	88.7	89.1	87.9	89.7	88.8	88.2	89.1	87.5	88.2	88.0	87.8	87.5	88.3	88.5	88.2
Fs	11.4	10.0	10.1	9.1	10.2	10.3	9.6	10.2	10.4	10.0	10.2	10.3	10.1	10.3	9.7	10.6	10.2	9.7

Formulae of orthopyroxene calculated on the basis of 6 oxygens. c = grain core, r = grain rim, in(cpx) = opx lamella in cpx

**Table B-4.** Microprobe analyses and formulae of orthopyroxene porphyroclasts from different ultramafic lithologies of the Krivaja-Konjuh ophiolite complex

Rock type	Spinel lherzolite – Olivine websterite																	
Sample-Nr.	u35-11	u35-12	u35-8	u35-9	4a-18	4a-19	4a-21	4a-23	4a-30	4a-31	4a-39	4a-40	1c-26	1c-30	1c-33	1c-40	1c-42	1c-27
Remark			r	c	c	r	r	r	c	r	r	c	r	r	r	r	r	c
SiO <sub>2</sub>	54.95	55.22	55.24	55.40	54.45	56.80	55.51	54.46	53.77	55.40	55.26	54.77	55.67	55.97	55.97	54.88	55.02	54.96
TiO <sub>2</sub>	0.14	0.15	0.17	0.14	0.16	0.12	0.13	0.18	0.17	0.14	0.15	0.11	0.22	0.21	0.19	0.16	0.13	0.24
Al <sub>2</sub> O <sub>3</sub>	2.62	2.59	2.18	2.61	5.04	2.38	3.40	4.50	5.80	3.46	3.51	4.00	2.99	2.88	2.83	3.99	3.51	3.87
Cr <sub>2</sub> O <sub>3</sub>	0.86	0.83	0.65	0.80	0.77	0.46	0.74	0.83	0.95	0.75	0.69	0.87	0.58	0.48	0.46	0.56	0.55	0.59
Fe <sub>2</sub> O <sub>3</sub>	1.31	1.41	1.35	1.69	0.34	0.52	1.05	1.80	2.44	0.83	0.65	1.11	0.55	0.15	0.35	2.07	0.89	1.79
FeO	5.68	5.52	5.69	5.49	5.81	6.23	5.34	4.89	3.55	5.48	5.59	5.42	6.28	6.88	6.35	5.39	6.14	5.25
MnO	0.13	0.16	0.17	0.24	0.10	0.11	0.17	0.16	0.16	0.12	0.13	0.11	0.15	0.20	0.26	0.22	0.21	0.15
MgO	33.16	33.44	33.33	33.44	31.73	34.20	33.60	33.15	30.81	33.36	33.29	33.14	33.19	33.10	33.19	32.49	32.31	32.18
CaO	0.65	0.62	0.67	0.67	1.91	0.57	0.69	0.80	4.23	0.97	0.85	0.69	0.78	0.72	0.99	1.75	1.53	2.18
Na <sub>2</sub> O	0.02	0.01	0.01	0.02	0.07	0.00	0.02	0.03	0.09	0.01	0.02	0.02	0.02	0.02	0.02	0.00	0.00	0.07
K <sub>2</sub> O	0.00	0.01	0.01	0.03	0.00	0.00	0.03	0.00	0.00	0.00	0.00	0.00	0.02	0.00	0.00	0.00	0.00	0.02
Total	99.51	99.94	99.45	100.52	100.38	101.39	100.67	100.78	101.97	100.52	100.13	100.23	100.45	100.62	100.60	101.50	100.28	101.29
Si	1.914	1.914	1.925	1.912	1.881	1.936	1.906	1.871	1.837	1.906	1.907	1.891	1.920	1.928	1.927	1.881	1.906	1.887
Ti	0.004	0.004	0.004	0.004	0.004	0.003	0.003	0.005	0.004	0.004	0.004	0.003	0.006	0.005	0.005	0.004	0.003	0.006
Al	0.108	0.106	0.089	0.106	0.205	0.096	0.137	0.182	0.234	0.140	0.143	0.163	0.121	0.117	0.115	0.161	0.143	0.157
Cr	0.024	0.023	0.018	0.022	0.021	0.012	0.020	0.022	0.026	0.020	0.019	0.024	0.016	0.013	0.013	0.015	0.015	0.016
Fe <sup>3+</sup>	0.034	0.037	0.035	0.044	0.009	0.013	0.027	0.047	0.063	0.022	0.017	0.029	0.014	0.004	0.009	0.053	0.023	0.046
Fe <sup>2+</sup>	0.165	0.160	0.166	0.158	0.168	0.178	0.153	0.140	0.101	0.158	0.161	0.157	0.181	0.198	0.183	0.154	0.178	0.151
Mn	0.004	0.005	0.005	0.007	0.003	0.003	0.005	0.005	0.005	0.004	0.004	0.003	0.004	0.006	0.008	0.006	0.006	0.004
Mg	1.722	1.728	1.731	1.720	1.634	1.738	1.720	1.697	1.570	1.711	1.713	1.705	1.706	1.700	1.704	1.660	1.668	1.647
Ca	0.024	0.023	0.025	0.025	0.071	0.021	0.025	0.029	0.155	0.036	0.031	0.025	0.029	0.027	0.036	0.064	0.057	0.080
Na	0.001	0.001	0.001	0.001	0.005	0.000	0.002	0.002	0.006	0.001	0.001	0.002	0.002	0.002	0.001	0.000	0.000	0.005
K	0.000	0.000	0.000	0.001	0.000	0.000	0.001	0.000	0.000	0.000	0.000	0.000	0.001	0.000	0.000	0.000	0.000	0.001
Wo	1.25	1.22	1.37	1.34	3.77	1.13	1.38	1.53	1.27	1.88	1.67	1.35	1.58	1.49	1.94	3.39	2.94	4.29
En	88.3	88.5	88.2	88.0	86.7	89.0	89.1	88.5	82.9	88.7	88.9	88.9	88.2	87.9	87.8	85.6	86.3	85.4
Fs	10.4	10.3	10.5	10.7	9.5	9.9	9.6	10.0	8.9	9.5	9.4	9.8	10.3	10.8	10.3	11.1	10.7	10.4

Formulae of orthopyroxene calculated on the basis of 6 oxygens. c = grain core, r = grain rim.

**Table B-5.** Microprobe analyses and formulae of orthopyroxene porphyroclasts from different ultramafic lithologies of the Krivaja-Konjuh ophiolite complex

Rock type	Olivine websterite – Mylonitized spinel lherzolite																
Sample-Nr.	1c-45	2a-10	2a-11	2a-14	2a-15	2a-16	2a-19	2a-21	2a-23	2a-40	2a-41	2a-9a	r7-1	r7-2	r7-20	r7-47	r7-48
Remark	c	c	r	r	c	r	in(cpx)	r	r	c	r	r	c	r	c	c	r
SiO <sub>2</sub>	53.94	53.35	55.26	55.61	55.38	56.00	56.31	55.54	55.17	56.29	56.37	54.45	54.40	54.07	56.51	54.22	55.32
TiO <sub>2</sub>	0.13	0.15	0.24	0.16	0.12	0.18	0.12	0.15	0.21	0.16	0.11	0.16	0.10	0.16	0.09	0.11	0.07
Al <sub>2</sub> O <sub>3</sub>	5.40	6.21	3.55	3.01	3.72	3.21	2.57	3.14	2.96	2.62	1.96	3.98	5.36	5.56	3.24	4.52	4.22
Cr <sub>2</sub> O <sub>3</sub>	0.54	0.51	0.59	0.54	0.50	0.48	0.41	0.45	0.48	0.51	0.39	0.60	0.56	0.49	0.27	0.42	0.45
Fe <sub>2</sub> O <sub>3</sub>	1.07	0.45	0.00	0.69	0.74	0.00	0.36	0.91	1.39	0.00	1.44	1.64	0.00	0.00	0.00	0.65	0.06
FeO	6.03	6.09	6.80	6.26	6.13	6.90	6.72	6.21	5.98	6.63	5.39	5.12	6.71	6.67	7.02	6.15	6.62
MnO	0.13	0.12	0.09	0.19	0.18	0.19	0.20	0.13	0.18	0.20	0.17	0.12	0.16	0.21	0.16	0.10	0.17
MgO	32.16	30.15	30.86	33.22	33.06	32.98	33.45	33.08	32.78	33.34	34.19	32.93	31.69	31.09	33.15	32.55	33.05
CaO	0.73	2.66	1.04	0.67	0.81	0.72	0.69	0.90	1.07	0.79	0.73	0.91	0.37	0.86	0.50	0.41	0.35
Na <sub>2</sub> O	0.04	0.12	0.08	0.02	0.01	0.01	0.00	0.02	0.04	0.03	0.01	0.03	0.00	0.05	0.02	0.03	0.01
CaO	0.00	0.00	0.00	0.00	0.00	0.00	0.00	0.01	0.01	0.00	0.01	0.00	0.01	0.01	0.01	0.01	0.01
Total	100.17	99.81	98.51	100.36	100.65	100.67	100.83	100.52	100.26	100.57	100.78	99.93	99.35	99.17	100.97	99.17	100.32
Si	1.866	1.860	1.941	1.919	1.906	1.927	1.935	1.915	1.911	1.937	1.934	1.886	1.893	1.888	1.936	1.891	1.906
Ti	0.003	0.004	0.006	0.004	0.003	0.005	0.003	0.004	0.005	0.004	0.003	0.004	0.003	0.004	0.002	0.003	0.002
Al	0.220	0.255	0.147	0.122	0.151	0.130	0.104	0.128	0.121	0.106	0.079	0.163	0.220	0.229	0.131	0.186	0.171
Cr	0.015	0.014	0.016	0.015	0.014	0.013	0.011	0.012	0.013	0.014	0.011	0.016	0.015	0.013	0.007	0.012	0.012
Fe <sup>3+</sup>	0.028	0.012	0.000	0.018	0.019	0.000	0.009	0.024	0.036	0.000	0.037	0.043	0.000	0.000	0.000	0.017	0.002
Fe <sup>2+</sup>	0.174	0.178	0.200	0.181	0.176	0.198	0.193	0.179	0.173	0.191	0.155	0.148	0.195	0.195	0.201	0.179	0.191
Mn	0.004	0.004	0.003	0.006	0.005	0.006	0.006	0.004	0.005	0.006	0.005	0.003	0.005	0.006	0.005	0.003	0.005
Mg	1.659	1.567	1.616	1.709	1.696	1.692	1.713	1.700	1.692	1.711	1.749	1.701	1.643	1.618	1.693	1.692	1.698
Ca	0.027	0.099	0.039	0.025	0.030	0.027	0.025	0.033	0.040	0.029	0.027	0.034	0.014	0.032	0.018	0.015	0.013
Na	0.003	0.008	0.006	0.001	0.001	0.001	0.000	0.001	0.002	0.002	0.000	0.002	0.000	0.003	0.001	0.002	0.000
K	0.000	0.000	0.000	0.000	0.000	0.000	0.000	0.000	0.001	0.000	0.001	0.000	0.000	0.000	0.001	0.000	0.001
Wo	1.44	5.37	2.18	1.33	1.56	1.48	1.33	1.76	2.08	1.53	1.45	1.76	0.88	1.73	1.07	0.89	0.74
En	87.7	84.3	87.0	88.2	88.0	88.0	88.0	87.7	86.9	88.3	88.7	88.2	88.5	87.4	88.3	88.8	89.0
Fs	10.9	10.4	10.9	10.5	10.4	10.6	10.7	10.6	11.0	10.2	10.0	10.1	10.8	10.9	10.7	10.4	10.3

Formulae of orthopyroxene calculated on the basis of 6 oxygens. c = grain core, r = grain rim, in(cpx) = opx lamella in cpx.

**Table C-1.** Microprobe analyses and formulae of small deformed orthopyroxene and orthopyroxene in mosaic aggregates from different ultramafic lithologies of the Krivaja-Konjuh ophiolite complex

Rock type	Plagioclase Iherzolite																	
Sample-Nr.	gr2-7	gr2-8	gr2-12	gr2-15	gr2-16	gr2-18	gr12-4	gr12-5	gr12-18	gr12-19	gr12-23	gr12-24	m2-13	m2-20	m2-25	m2-26	m2-34	u4-16
Remark	r	c	r	r	r	c			r	c	c	r	r	c	c	r	r	r
SiO <sub>2</sub>	56.26	56.31	56.57	56.78	56.51	56.39	56.58	56.56	56.49	56.37	55.51	55.89	55.35	54.61	55.76	56.03	56.47	55.27
TiO <sub>2</sub>	0.19	0.16	0.21	0.16	0.07	0.14	0.21	0.22	0.22	0.20	0.23	0.17	0.15	0.12	0.18	0.17	0.14	0.12
Al <sub>2</sub> O <sub>3</sub>	1.92	2.00	1.82	1.89	1.69	2.08	1.76	1.85	1.62	2.05	2.31	2.21	2.45	3.02	2.81	2.42	2.61	2.32
Cr <sub>2</sub> O <sub>3</sub>	0.73	0.56	0.64	0.63	0.71	0.71	0.65	0.60	0.49	0.58	0.59	0.50	0.61	0.74	0.74	0.59	0.57	0.56
Fe <sub>2</sub> O <sub>3</sub>	0.87	0.11	0.00	0.00	0.00	0.00	1.08	0.57	0.38	0.00	1.97	1.19	0.88	1.40	0.63	0.00	0.00	2.16
FeO	6.22	6.77	7.09	6.67	6.27	6.51	5.98	6.54	6.28	6.48	5.21	5.93	5.86	5.57	6.28	6.66	6.67	4.95
MnO	0.10	0.21	0.15	0.20	0.14	0.21	0.25	0.12	0.14	0.11	0.13	0.19	0.19	0.17	0.17	0.14	0.18	0.15
MgO	33.58	32.99	33.25	33.18	33.61	32.58	34.05	33.71	33.89	33.35	33.40	33.37	33.03	32.57	32.95	32.91	33.41	33.56
CaO	0.92	1.21	0.89	0.96	0.55	0.88	0.65	0.75	0.70	1.09	1.23	1.05	0.98	1.23	1.16	0.91	0.67	0.92
Na <sub>2</sub> O	0.02	0.03	0.02	0.02	0.00	0.00	0.01	0.02	0.00	0.00	0.03	0.00	0.03	0.00	0.03	0.01	0.02	0.02
K <sub>2</sub> O	0.00	0.00	0.01	0.00	0.00	0.01	0.01	0.01	0.00	0.00	0.00	0.01	0.00	0.01	0.01	0.00	0.00	0.00
Total	100.80	100.34	100.65	100.47	99.54	99.52	101.22	100.93	100.21	100.21	100.61	100.50	99.54	99.44	100.72	99.84	100.74	100.02
Si	1.943	1.955	1.953	1.965	1.966	1.967	1.945	1.943	1.957	1.955	1.913	1.937	1.938	1.918	1.925	1.943	1.946	1.918
Ti	0.001	0.003	0.012	0.005	0.003	0.006	0.018	0.015	0.018	0.019	0.015	0.004	0.001	0.004	0.005	0.003	0.006	0.004
Al	0.083	0.085	0.077	0.085	0.078	0.095	0.078	0.073	0.077	0.089	0.095	0.098	0.104	0.126	0.118	0.106	0.116	0.096
Cr	0.025	0.026	0.024	0.026	0.024	0.025	0.026	0.024	0.013	0.026	0.023	0.014	0.026	0.023	0.025	0.026	0.023	0.026
Fe <sup>3+</sup>	0.024	0.003	0.003	0.005	0.002	0.004	0.035	0.013	0.012	0.003	0.052	0.034	0.023	0.041	0.022	0.002	0.001	0.064
Fe <sup>2+</sup>	0.184	0.206	0.203	0.197	0.183	0.198	0.174	0.198	0.184	0.194	0.157	0.173	0.177	0.167	0.187	0.196	0.195	0.144
Mn	0.002	0.014	0.005	0.015	0.007	0.017	0.016	0.006	0.005	0.008	0.008	0.014	0.016	0.003	0.014	0.004	0.016	0.008
Mg	1.725	1.706	1.716	1.706	1.746	1.696	1.748	1.734	1.747	1.724	1.724	1.725	1.714	1.694	1.697	1.706	1.717	1.737
Ca	0.033	0.045	0.035	0.047	0.028	0.035	0.026	0.037	0.035	0.045	0.057	0.046	0.043	0.057	0.046	0.037	0.024	0.036
Na	0.004	0.004	0.003	0.004	0.009	0.008	0.007	0.006	0.003	0.008	0.008	0.004	0.007	0.004	0.005	0.004	0.006	0.004
K	0.006	0.004	0.005	0.005	0.006	0.004	0.007	0.004	0.005	0.007	0.003	0.008	0.003	0.006	0.004	0.005	0.007	0.006
Wo	1.72	2.30	1.68	1.83	1.04	1.70	1.22	1.40	1.32	2.07	2.31	1.97	1.88	2.37	2.21	1.75	1.28	1.72
En	87.86	87.21	87.61	87.95	89.39	88.10	88.31	88.08	88.74	88.16	87.26	87.45	87.90	87.12	87.34	88.05	88.52	87.93
Fs	10.42	10.49	10.70	10.22	9.57	10.20	10.47	10.52	9.94	9.77	10.43	10.58	10.22	10.51	10.45	10.21	10.19	10.35

Formulae of orthopyroxene calculated on the basis of 6 oxygens. c = grain core, r = grain rim.

**Table C-2.** Microprobe analyses and formulae of small deformed orthopyroxene and orthopyroxene in mosaic aggregates from different ultramafic lithologies of the Krivaja-Konjuh ophiolite complex

Rock type	Plagioclase Iherzolite – Spinel Iherzolite																	
Sample-Nr.	u4-17	u4-18	u4-19	u4-21	u4-58	u4-59	u4-60	u4-62	u4-67d	u4-68	u4-69	u4-72	u4-86	d5-27	d5-17	d5-19	d5-21	o2-27
Remark	c	r	c	c	c	r			r	c				r	r	r	r	
SiO <sub>2</sub>	55.52	55.63	55.56	56.37	55.83	55.81	55.98	56.20	55.47	55.98	55.83	56.23	56.00	55.96	55.79	55.36	53.45	53.33
TiO <sub>2</sub>	0.14	0.11	0.15	0.11	0.18	0.16	0.15	0.14	0.17	0.15	0.15	0.14	0.18	0.23	0.29	0.24	0.24	0.07
Al <sub>2</sub> O <sub>3</sub>	2.46	2.35	2.49	1.50	2.67	2.39	2.32	2.17	2.79	2.45	2.43	2.41	2.59	1.92	2.24	2.33	2.95	3.95
Cr <sub>2</sub> O <sub>3</sub>	0.62	0.60	0.63	0.52	0.73	0.68	0.76	0.66	0.75	0.62	0.65	0.56	0.61	0.59	0.63	0.58	0.56	0.40
Fe <sub>2</sub> O <sub>3</sub>	1.73	1.97	0.91	1.23	0.32	1.12	1.67	1.24	1.10	0.99	1.38	1.25	1.44	0.02	0.30	0.48	1.98	3.66
FeO	5.19	5.01	5.70	5.49	6.21	5.76	5.54	5.75	5.92	5.91	5.73	6.12	5.72	6.84	6.55	6.73	5.67	3.91
MnO	0.16	0.18	0.16	0.17	0.13	0.15	0.21	0.17	0.14	0.19	0.23	0.19	0.15	0.19	0.15	0.11	0.18	0.22
MgO	33.34	33.70	33.10	34.08	33.09	33.27	33.75	33.84	33.12	33.43	33.60	33.59	33.80	33.06	33.02	32.57	31.86	32.61
CaO	1.21	0.98	1.28	0.84	1.12	1.19	0.78	0.84	1.08	1.03	0.79	0.82	0.75	0.90	1.06	1.11	1.01	1.01
Na <sub>2</sub> O	0.04	0.01	0.01	0.01	0.03	0.03	0.03	0.00	0.00	0.01	0.01	0.03	0.01	0.00	0.01	0.02	0.04	0.04
K <sub>2</sub> O	0.01	0.01	0.00	0.00	0.00	0.00	0.01	0.00	0.00	0.01	0.00	0.00	0.00	0.00	0.01	0.00	0.01	0.02
Total	100.40	100.55	99.99	100.31	100.32	100.56	101.21	101.00	100.53	100.76	100.79	101.32	101.24	99.70	100.04	99.52	97.94	99.24
Si	1.925	1.925	1.933	1.945	1.936	1.929	1.925	1.935	1.916	1.935	1.927	1.934	1.927	1.959	1.935	1.938	1.906	1.874
Ti	0.003	0.005	0.005	0.006	0.007	0.008	0.006	0.004	0.007	0.006	0.008	0.005	0.006	0.018	0.016	0.017	0.015	0.007
Al	0.106	0.102	0.106	0.063	0.116	0.107	0.098	0.098	0.118	0.108	0.105	0.106	0.105	0.086	0.097	0.105	0.124	0.164
Cr	0.023	0.023	0.023	0.016	0.025	0.025	0.029	0.029	0.027	0.027	0.024	0.020	0.024	0.024	0.028	0.027	0.026	0.015
Fe <sup>3+</sup>	0.044	0.054	0.025	0.038	0.014	0.037	0.047	0.038	0.036	0.036	0.048	0.039	0.047	0.006	0.014	0.015	0.057	0.109
Fe <sup>2+</sup>	0.156	0.145	0.176	0.167	0.186	0.178	0.165	0.167	0.175	0.174	0.165	0.188	0.168	0.207	0.197	0.209	0.178	0.117
Mn	0.005	0.013	0.007	0.016	0.007	0.009	0.016	0.005	0.006	0.015	0.014	0.017	0.009	0.019	0.005	0.007	0.015	0.014
Mg	1.723	1.736	1.713	1.753	1.708	1.718	1.727	1.737	1.708	1.718	1.729	1.715	1.725	1.718	1.7164	1.694	1.696	1.708
Ca	0.044	0.046	0.055	0.037	0.049	0.047	0.039	0.039	0.047	0.047	0.035	0.036	0.034	0.037	0.046	0.048	0.047	0.047
Na	0.005	0.005	0.006	0.006	0.007	0.006	0.008	0.008	0.005	0.005	0.004	0.007	0.005	0.006	0.007	0.007	0.008	0.006
K	0.003	0.004	0.007	0.005	0.006	0.004	0.005	0.007	0.006	0.007	0.003	0.008	0.007	0.004	0.008	0.005	0.009	0.005
Wo	2.28	1.84	2.43	1.56	2.14	2.25	1.47	1.58	2.04	1.94	1.48	1.53	1.41	1.71	2.03	2.14	1.96	1.94
En	87.55	87.95	87.64	88.57	87.97	87.55	87.93	88.14	87.50	87.76	87.95	87.60	88.11	87.79	87.61	86.98	86.43	86.95
Fs	10.17	10.20	9.92	9.86	9.90	10.20	10.61	10.28	10.46	10.30	10.57	10.87	10.48	10.50	10.36	10.88	11.61	11.11

Formulae of orthopyroxene calculated on the basis of 6 oxygens. c = grain core, r = grain rim.

**Table C-3.** Microprobe analyses and formulae of small deformed orthopyroxene and orthopyroxene in mosaic aggregates from different ultramafic lithologies of the Krivaja-Konjuh ophiolite complex

Rock type	Spinel lherzolite																	
Sample-Nr.	o2-49	o2-16	o2-15	o2-29	o2-37	o2-38	o2-41	o2-51	o2-42	z2-55	z2-48	z2-32	z2-34	z2-36	z2-40	z2-40b	z2-41	z2-49
Remark		c	r	r	r	r	r	r	in(cpx)		c	r	r	r	r	r	r	r
SiO <sub>2</sub>	54.39	54.49	53.87	54.57	54.39	54.07	55.41	54.07	54.81	55.61	55.68	55.93	54.81	54.43	55.45	55.26	55.57	55.47
TiO <sub>2</sub>	0.10	0.14	0.15	0.09	0.10	0.07	0.14	0.12	0.09	0.08	0.13	0.03	0.25	0.08	0.07	0.07	0.05	0.04
Al <sub>2</sub> O <sub>3</sub>	4.50	5.05	5.27	4.12	3.87	3.97	3.61	4.88	3.89	3.99	3.82	3.37	3.15	4.60	4.05	4.36	4.10	4.14
Cr <sub>2</sub> O <sub>3</sub>	0.41	0.52	0.57	0.43	0.41	0.51	0.47	0.50	0.49	0.48	0.54	0.48	0.62	0.62	0.52	0.50	0.44	0.55
Fe <sub>2</sub> O <sub>3</sub>	1.10	0.00	1.29	1.10	1.42	2.27	1.32	1.13	1.05	0.00	0.00	0.00	0.00	0.90	0.00	0.01	0.00	0.00
FeO	5.58	6.01	4.98	5.53	5.26	4.61	5.36	5.61	5.54	6.81	6.48	6.41	6.58	6.01	6.71	6.96	6.85	6.58
MnO	0.18	0.08	0.13	0.12	0.12	0.21	0.13	0.11	0.17	0.15	0.20	0.11	0.04	0.09	0.17	0.10	0.12	0.15
MgO	32.67	31.65	32.02	32.67	33.02	33.15	33.58	32.41	33.04	32.74	32.59	33.05	32.76	32.50	32.67	32.52	32.60	32.39
CaO	0.77	1.54	1.56	1.02	0.59	0.50	0.61	0.91	0.65	0.76	1.18	0.59	0.78	0.84	0.64	0.81	0.88	0.83
Na <sub>2</sub> O	0.02	0.09	0.08	0.03	0.03	0.03	0.05	0.02	0.04	0.03	0.02	0.02	0.08	0.01	0.00	0.02	0.02	0.01
K <sub>2</sub> O	0.01	0.01	0.00	0.00	0.00	0.01	0.00	0.00	0.00	0.00	0.01	0.00	0.01	0.00	0.00	0.00	0.01	0.00
Total	99.74	99.58	99.91	99.68	99.21	99.39	100.68	99.76	99.76	100.66	100.66	100.00	98.57	100.08	100.28	100.60	100.65	100.15
Si	1.894	1.895	1.876	1.894	1.897	1.882	1.907	1.887	1.905	1.917	1.928	1.935	1.925	1.883	1.913	1.905	1.915	1.923
Ti	0.005	0.007	0.008	0.005	0.006	0.003	0.005	0.006	0.003	0.006	0.005	0.009	0.016	0.003	0.004	0.004	0.003	0.003
Al	0.183	0.219	0.227	0.178	0.164	0.164	0.154	0.205	0.164	0.165	0.154	0.148	0.228	0.194	0.165	0.183	0.172	0.174
Cr	0.012	0.017	0.025	0.014	0.016	0.015	0.013	0.014	0.016	0.014	0.013	0.017	0.025	0.025	0.016	0.016	0.015	0.016
Fe <sup>3+</sup>	0.035	0.005	0.036	0.037	0.045	0.068	0.034	0.032	0.037	0.003	0.003	0.006	0.004	0.026	0.007	0.007	0.006	0.005
Fe <sup>2+</sup>	0.166	0.174	0.144	0.166	0.154	0.137	0.155	0.163	0.168	0.202	0.192	0.192	0.183	0.177	0.198	0.206	0.207	0.194
Mn	0.017	0.005	0.007	0.008	0.003	0.015	0.006	0.005	0.015	0.003	0.012	0.003	0.005	0.009	0.004	0.004	0.007	0.008
Mg	1.698	1.649	1.654	1.696	1.717	1.724	1.724	1.688	1.714	1.684	1.676	1.704	1.618	1.688	1.682	1.672	1.674	1.677
Ca	0.036	0.068	0.067	0.044	0.025	0.028	0.023	0.037	0.023	0.035	0.045	0.025	0.037	0.037	0.023	0.033	0.035	0.036
Na	0.004	0.017	0.014	0.006	0.003	0.007	0.002	0.006	0.002	0.006	0.004	0.006	0.006	0.005	0.004	0.004	0.006	0.005
K	0.003	0.006	0.007	0.007	0.004	0.006	0.003	0.005	0.004	0.007	0.003	0.007	0.005	0.004	0.006	0.004	0.007	0.004
Wo	1.49	3.05	3.05	1.97	1.14	0.96	1.15	1.77	1.25	1.48	2.27	1.15	1.49	1.63	1.25	1.57	1.70	1.63
En	88.28	87.51	87.35	87.99	88.82	88.73	88.92	87.97	88.72	88.02	87.64	89.00	88.11	87.89	88.33	87.74	87.76	88.10
Fs	10.23	9.44	9.60	10.04	10.04	10.31	9.93	10.26	10.03	10.50	10.08	9.85	10.39	10.48	10.42	10.69	10.53	10.27

Formulae of orthopyroxene calculated on the basis of 6 oxygens. c = grain core, r = grain rim, in(cpx) = opx lamella in cpx.

**Table C-4.** Microprobe analyses and formulae of small deformed orthopyroxene and orthopyroxene in mosaic aggregates from different ultramafic lithologies of the Krivaja-Konjuh ophiolite complex

Rock type	Spinel Iherzolite																	
Sample-Nr.	z2-52	z4-41	z4-8	z4-20	z4-44	z4-3	z4-11b	z4-19	z4-14	z4-13	u35-27	u35-13	u35-32	u35-64b	u35-66	u35-72	u35-31	u35-13b
Remark	r	r		r	r	r		r	r	r	r	r	r	r	r	r	c	c
SiO <sub>2</sub>	54.39	54.49	53.87	54.57	54.39	54.07	55.41	54.07	54.81	55.61	55.68	55.93	54.81	54.43	55.45	55.26	55.57	55.47
TiO <sub>2</sub>	0.10	0.14	0.15	0.09	0.10	0.07	0.14	0.12	0.09	0.08	0.13	0.03	0.05	0.08	0.07	0.07	0.05	0.04
Al <sub>2</sub> O <sub>3</sub>	4.50	5.05	5.27	4.12	3.87	3.97	3.61	4.88	3.89	3.99	3.82	3.37	4.15	4.60	4.05	4.36	4.10	4.14
Cr <sub>2</sub> O <sub>3</sub>	0.41	0.52	0.57	0.43	0.41	0.51	0.47	0.50	0.49	0.48	0.54	0.48	0.62	0.62	0.52	0.50	0.44	0.55
Fe <sub>2</sub> O <sub>3</sub>	1.10	0.00	1.29	1.10	1.42	2.27	1.32	1.13	1.05	0.00	0.00	0.00	0.00	0.90	0.00	0.01	0.00	0.00
FeO	5.58	6.01	4.98	5.53	5.26	4.61	5.36	5.61	5.54	6.81	6.48	6.41	6.58	6.01	6.71	6.96	6.85	6.58
MnO	0.18	0.08	0.13	0.12	0.12	0.21	0.13	0.11	0.17	0.15	0.20	0.11	0.04	0.09	0.17	0.10	0.12	0.15
MgO	32.67	31.65	32.02	32.67	33.02	33.15	33.58	32.41	33.04	32.74	32.59	33.05	32.76	32.50	32.67	32.52	32.60	32.39
CaO	0.77	1.54	1.56	1.02	0.59	0.50	0.61	0.91	0.65	0.76	1.18	0.59	1.78	0.84	0.64	0.81	0.88	0.83
Na <sub>2</sub> O	0.02	0.09	0.08	0.03	0.03	0.03	0.05	0.02	0.04	0.03	0.02	0.02	0.58	0.01	0.00	0.02	0.02	0.01
K <sub>2</sub> O	0.01	0.01	0.00	0.00	0.00	0.01	0.00	0.00	0.00	0.00	0.01	0.00	0.01	0.00	0.00	0.00	0.01	0.00
Total	99.74	99.58	99.91	99.68	99.21	99.39	100.68	99.76	99.76	100.66	100.66	100.00	98.57	100.08	100.28	100.60	100.65	100.15
Si	1.894	1.897	1.873	1.893	1.897	1.888	1.906	1.884	1.903	1.915	1.924	1.934	1.926	1.884	1.913	1.903	1.916	1.926
Ti	0.005	0.006	0.007	0.004	0.005	0.008	0.005	0.005	0.004	0.008	0.005	0.009	0.015	0.006	0.004	0.006	0.006	0.005
Al	0.186	0.215	0.226	0.175	0.166	0.167	0.153	0.207	0.165	0.166	0.157	0.144	0.226	0.199	0.166	0.187	0.177	0.177
Cr	0.014	0.013	0.025	0.017	0.015	0.016	0.014	0.018	0.016	0.013	0.018	0.018	0.024	0.026	0.017	0.018	0.014	0.012
Fe <sup>3+</sup>	0.033	0.004	0.034	0.036	0.044	0.064	0.035	0.036	0.037	0.004	0.009	0.007	0.008	0.025	0.008	0.006	0.003	0.003
Fe <sup>2+</sup>	0.166	0.177	0.144	0.165	0.153	0.133	0.156	0.163	0.1685	0.209	0.194	0.196	0.186	0.173	0.195	0.205	0.202	0.195
Mn	0.017	0.006	0.003	0.004	0.004	0.012	0.007	0.004	0.013	0.007	0.013	0.005	0.004	0.008	0.003	0.003	0.006	0.007
Mg	1.694	1.643	1.654	1.693	1.716	1.723	1.7284	1.685	1.715	1.684	1.675	1.702	1.513	1.683	1.682	1.675	1.677	1.673
Ca	0.033	0.066	0.065	0.045	0.024	0.024	0.025	0.034	0.026	0.036	0.044	0.023	0.022	0.034	0.023	0.038	0.034	0.034
Na	0.004	0.015	0.016	0.004	0.003	0.005	0.004	0.003	0.008	0.008	0.006	0.005	0.004	0.006	0.006	0.006	0.003	0.007
K	0.005	0.004	0.007	0.006	0.004	0.006	0.003	0.002	0.007	0.009	0.003	0.006	0.005	0.007	0.007	0.004	0.004	0.006
Wo	1.49	3.05	3.05	1.97	1.14	0.96	1.15	1.77	1.25	1.48	2.27	1.15	1.49	1.63	1.25	1.57	1.70	1.63
En	88.28	87.51	87.35	87.99	88.82	88.73	88.92	87.97	88.72	88.02	87.64	89.00	88.11	87.89	88.33	87.74	87.76	88.10
Fs	10.23	9.44	9.60	10.04	10.04	10.31	9.93	10.26	10.03	10.50	10.08	9.85	9.39	10.48	10.42	10.69	10.53	10.27

Formulae of orthopyroxene calculated on the basis of 6 oxygens. c = grain core, r = grain rim.

**Table C-5.** Microprobe analyses and formulae of small deformed orthopyroxene and orthopyroxene in mosaic aggregates from different ultramafic lithologies of the Krivaja-Konjuh ophiolite complex

Rock type	Spinel Iherzolite – Olivine websterite																	
Sample-Nr.	u35-63	u35-74	u35-5	u35-17c	u35-45	u35-48	u35-49	u35-50	u35-52	u35-55	u35-59	u35-59b	u35-61	u35-72b	1c-3	1c-44	1c-49	1c-51
Remark	c	c													r	r	r	r
SiO <sub>2</sub>	56.44	56.38	56.26	57.03	54.31	56.72	56.98	56.30	56.11	54.64	57.50	57.37	57.04	56.86	54.51	55.57	55.55	56.61
TiO <sub>2</sub>	0.07	0.15	0.10	0.07	0.07	0.11	0.07	0.15	0.15	0.13	0.08	0.09	0.07	0.07	0.19	0.13	0.15	0.12
Al <sub>2</sub> O <sub>3</sub>	1.51	1.64	1.50	1.21	3.07	1.72	1.58	2.00	1.84	2.24	1.34	1.25	1.55	1.36	3.91	3.28	3.29	2.08
Cr <sub>2</sub> O <sub>3</sub>	0.39	0.40	0.27	0.25	0.48	0.51	0.34	0.45	0.41	0.38	0.27	0.21	0.29	0.34	0.60	0.53	0.65	0.40
Fe <sub>2</sub> O <sub>3</sub>	1.15	1.24	1.31	1.16	0.41	0.84	1.09	0.99	1.04	1.94	0.75	0.91	0.98	0.65	1.75	0.87	0.44	0.13
FeO	5.96	5.85	5.97	6.09	7.08	6.47	6.23	6.10	6.12	5.86	6.34	6.22	6.39	6.44	5.46	6.73	6.92	7.32
MnO	0.11	0.09	0.16	0.14	0.16	0.16	0.18	0.14	0.18	0.28	0.16	0.22	0.10	0.21	0.18	0.17	0.13	0.20
MgO	34.14	33.99	34.00	34.39	31.83	33.93	34.22	33.76	33.64	32.56	34.61	34.53	34.27	34.02	32.99	32.99	32.70	33.28
CaO	0.45	0.72	0.47	0.48	0.60	0.58	0.47	0.78	0.75	0.88	0.47	0.47	0.48	0.55	0.70	0.56	0.86	0.69
Na <sub>2</sub> O	0.01	0.02	0.00	0.01	0.03	0.00	0.03	0.01	0.00	0.03	0.00	0.02	0.02	0.00	0.00	0.03	0.02	0.01
K <sub>2</sub> O	0.00	0.01	0.01	0.02	0.04	0.01	0.01	0.00	0.00	0.01	0.00	0.00	0.00	0.01	0.00	0.00	0.00	0.01
Total	100.23	100.47	100.03	100.84	98.08	101.06	101.20	100.67	100.24	98.94	101.52	101.29	101.19	100.51	100.28	100.87	100.71	100.86
Si	1.956	1.947	1.953	1.964	1.924	1.953	1.951	1.944	1.948	1.923	1.969	1.960	1.955	1.964	1.886	1.915	1.923	1.953
Ti	0.005	0.006	0.006	0.008	0.007	0.009	0.004	0.003	0.007	0.006	0.005	0.009	0.007	0.005	0.017	0.007	0.007	0.006
Al	0.063	0.074	0.063	0.056	0.138	0.072	0.067	0.082	0.08	0.094	0.057	0.058	0.064	0.060	0.168	0.139	0.139	0.085
Cr	0.016	0.019	0.015	0.012	0.014	0.015	0.019	0.013	0.016	0.017	0.016	0.016	0.016	0.019	0.025	0.016	0.025	0.017
Fe <sup>3+</sup>	0.037	0.037	0.038	0.033	0.016	0.028	0.035	0.035	0.038	0.059	0.023	0.024	0.039	0.028	0.056	0.024	0.018	0.009
Fe <sup>2+</sup>	0.174	0.174	0.174	0.175	0.217	0.192	0.183	0.189	0.184	0.177	0.185	0.189	0.187	0.196	0.168	0.198	0.203	0.216
Mn	0.002	0.008	0.003	0.008	0.004	0.004	0.017	0.008	0.012	0.012	0.003	0.018	0.006	0.013	0.019	0.004	0.004	0.014
Mg	1.765	1.757	1.756	1.765	1.685	1.738	1.756	1.736	1.739	1.714	1.768	1.764	1.755	1.755	1.707	1.699	1.688	1.719
Ca	0.027	0.034	0.028	0.023	0.026	0.027	0.023	0.033	0.038	0.039	0.026	0.026	0.024	0.027	0.036	0.024	0.036	0.038
Na	0.005	0.006	0.003	0.004	0.004	0.006	0.009	0.008	0.004	0.007	0.003	0.008	0.008	0.009	0.004	0.007	0.005	0.006
K	0.003	0.007	0.002	0.006	0.005	0.003	0.004	0.004	0.006	0.005	0.006	0.003	0.005	0.007	0.008	0.006	0.004	0.004
Wo	0.84	1.34	0.88	0.89	1.17	1.09	0.88	1.46	1.40	1.69	0.86	0.87	0.89	1.02	1.34	1.07	1.65	1.31
En	88.78	88.37	88.46	88.60	87.14	88.14	88.42	88.10	87.97	86.54	88.80	88.67	88.43	88.42	87.89	87.50	87.21	87.43
Fs	10.37	10.29	10.66	10.51	11.69	10.77	10.71	10.44	10.63	11.78	10.34	10.46	10.68	10.55	10.77	11.43	11.14	11.27

Formulae of orthopyroxene calculated on the basis of 6 oxygens. c = grain core, r = grain rim.



**Table C-6.** Microprobe analyses and formulae of small deformed orthopyroxene and orthopyroxene in mosaic aggregates from different ultramafic lithologies of the Krivaja-Konjuh ophiolite complex

Rock type	Olivine websterite – Spinel lherzolite																	
Sample-Nr.	1c-1	2a-14	2a-25	2a-29	2a-34	2a-35	2a-10	2a-24	2a-30	r7-3	r7-4	r7-6	r7-10	r7-13	r7-16	r7-18	r7-33	r7-56
Remark	c	r	r	r	r	r	c	c	c	r	c							
SiO <sub>2</sub>	53.02	55.61	55.63	55.98	55.63	55.68	53.35	55.94	55.59	55.49	55.63	56.33	56.41	56.89	56.66	56.57	55.79	56.94
TiO <sub>2</sub>	0.19	0.16	0.14	0.15	0.15	0.16	0.15	0.14	0.17	0.11	0.10	0.06	0.06	0.07	0.05	0.04	0.08	0.04
Al <sub>2</sub> O <sub>3</sub>	5.24	3.01	2.88	2.96	2.65	2.81	6.21	2.86	2.84	3.44	3.48	2.93	2.11	1.90	1.80	2.17	3.01	1.77
Cr <sub>2</sub> O <sub>3</sub>	0.58	0.54	0.51	0.44	0.43	0.49	0.51	0.53	0.53	0.23	0.22	0.24	0.13	0.30	0.14	0.16	0.29	0.24
Fe <sub>2</sub> O <sub>3</sub>	2.36	0.69	1.31	0.89	1.95	1.12	0.45	1.78	1.58	0.00	0.00	0.00	0.00	0.00	0.00	0.00	0.36	0.00
FeO	4.31	6.26	5.56	6.35	5.26	6.02	6.09	5.59	5.16	6.61	6.49	6.76	6.89	6.74	6.87	6.87	6.72	6.93
MnO	0.18	0.19	0.15	0.15	0.17	0.21	0.12	0.15	0.19	0.11	0.13	0.18	0.15	0.15	0.21	0.18	0.19	0.22
MgO	31.35	33.22	33.02	33.34	33.03	33.03	30.15	33.80	32.89	32.49	32.35	33.10	33.28	33.19	33.64	33.50	33.09	33.35
CaO	2.29	0.67	1.44	0.71	1.75	1.10	2.66	0.74	2.06	0.52	0.53	0.43	0.42	0.47	0.38	0.40	0.54	0.44
Na <sub>2</sub> O	0.05	0.02	0.05	0.03	0.02	0.04	0.12	0.02	0.00	0.04	0.04	0.02	0.01	0.00	0.02	0.02	0.04	0.02
K <sub>2</sub> O	0.01	0.00	0.01	0.03	0.00	0.00	0.00	0.00	0.00	0.00	0.01	0.00	0.01	0.00	0.03	0.00	0.00	0.01
Total	99.58	100.36	100.68	101.02	101.04	100.66	99.81	101.53	101.00	99.05	98.99	100.05	99.48	99.71	99.79	99.90	100.11	99.95
Si	1.855	1.924	1.923	1.924	1.915	1.925	1.867	1.919	1.917	1.937	1.947	1.94	1.96	1.978	1.968	1.966	1.936	1.973
Ti	0.003	0.006	0.007	0.004	0.007	0.000	0.008	0.008	0.004	0.004	0.004	0.008	0.004	0.007	0.005	0.003	0.008	0.004
Al	0.226	0.128	0.125	0.129	0.119	0.119	0.265	0.114	0.126	0.140	0.148	0.127	0.096	0.085	0.077	0.093	0.127	0.078
Cr	0.027	0.017	0.018	0.018	0.017	0.018	0.016	0.016	0.018	0.019	0.019	0.016	0.006	0.013	0.005	0.004	0.014	0.017
Fe <sup>3+</sup>	0.065	0.023	0.036	0.026	0.055	0.037	0.013	0.059	0.049	0.008	0.007	0.003	0.005	0.002	0.006	0.005	0.012	0.006
Fe <sup>2+</sup>	0.134	0.187	0.164	0.188	0.156	0.173	0.187	0.167	0.155	0.197	0.198	0.206	0.203	0.205	0.203	0.200	0.193	0.203
Mn	0.013	0.016	0.008	0.004	0.003	0.014	0.006	0.004	0.014	0.005	0.006	0.014	0.004	0.004	0.016	0.019	0.017	0.012
Mg	1.634	1.715	1.694	1.718	1.698	1.705	1.575	1.729	1.697	1.699	1.686	1.708	1.726	1.718	1.748	1.738	1.715	1.723
Ca	0.097	0.024	0.059	0.036	0.064	0.049	0.108	0.038	0.089	0.028	0.027	0.026	0.027	0.027	0.015	0.017	0.023	0.028
Na	0.005	0.007	0.005	0.006	0.009	0.007	0.015	0.006	0.007	0.006	0.006	0.005	0.008	0.005	0.004	0.004	0.002	0.006
K	0.003	0.005	0.006	0.008	0.004	0.003	0.008	0.004	0.005	0.003	0.004	0.004	0.005	0.003	0.003	0.003	0.003	0.005
Wo	4.49	1.27	2.72	1.35	3.28	2.09	5.34	1.39	3.88	1.01	1.05	0.82	0.80	0.90	0.73	0.75	1.03	0.84
En	85.40	88.19	87.09	87.85	86.20	87.19	84.28	87.91	86.17	88.69	88.74	88.74	88.67	88.75	88.79	88.76	88.15	88.52
Fs	10.11	10.54	10.19	10.80	10.52	10.72	10.38	10.70	9.96	10.30	10.20	10.44	10.53	10.35	10.48	10.49	10.82	10.64

Formulae of orthopyroxene calculated on the basis of 6 oxygens. c = grain core, r = grain rim.

*Clinopyroxene*

**Table D-1.** Microprobe analyses and formulae of clinopyroxene porphyroclasts from different ultramafic lithologies of the Krivaja-Konjuh ophiolite complex

Rock type	Plagioclase Iherzolite																	
Sample-Nr.	gr2-13	gr2-14	gr2-17	gr2-30	gr2-31	gr2-50	gr2-20	gr2-22	gr2-23	gr2-51	gr12-22	gr12-20	gr12-21	gr12-25	gr12-34	gr12-33	m2-41	m2-31
Remark	c	r	r	r	c	c	r	r	r	r	c	r	r	r	c	r	c	r
SiO <sub>2</sub>	52.41	52.33	52.56	52.88	52.42	53.10	52.67	53.34	52.48	53.41	52.13	52.16	52.49	52.76	52.17	52.92	52.60	53.55
TiO <sub>2</sub>	0.49	0.47	0.54	0.41	0.38	0.44	0.46	0.39	0.46	0.42	0.45	0.44	0.52	0.41	0.44	0.49	0.29	0.24
Al <sub>2</sub> O <sub>3</sub>	3.57	3.32	3.17	3.22	3.47	3.27	3.26	2.19	3.34	2.83	3.11	2.85	3.05	2.72	3.17	2.31	3.49	2.05
Cr <sub>2</sub> O <sub>3</sub>	1.42	1.29	1.32	1.19	1.27	1.20	1.23	0.94	1.29	1.00	1.27	1.08	1.17	1.11	1.05	0.86	1.20	0.83
Fe <sub>2</sub> O <sub>3</sub>	0.00	1.81	0.47	0.18	0.44	0.00	0.59	0.58	0.00	0.44	1.69	0.00	0.46	1.71	0.00	0.26	1.00	0.36
FeO	3.15	1.47	2.72	3.37	2.65	3.56	2.37	1.79	2.69	3.20	1.67	3.38	2.49	1.39	4.08	2.63	1.83	1.94
MnO	0.09	0.05	0.07	0.05	0.05	0.22	0.15	0.08	0.10	0.05	0.13	0.06	0.02	0.06	0.13	0.10	0.12	0.09
MgO	16.09	17.08	17.49	17.77	17.10	18.19	16.32	16.71	16.49	18.50	18.32	16.65	16.83	17.08	17.31	16.88	16.53	16.89
CaO	22.49	22.72	21.63	20.82	21.58	19.69	23.16	24.04	22.48	20.52	20.64	20.89	22.28	22.96	19.71	22.55	23.35	23.58
Na <sub>2</sub> O	0.44	0.41	0.36	0.39	0.46	0.31	0.45	0.36	0.43	0.36	0.39	0.41	0.47	0.46	0.37	0.43	0.39	0.41
K <sub>2</sub> O	0.00	0.01	0.00	0.00	0.02	0.00	0.00	0.00	0.00	0.02	0.01	0.00	0.00	0.00	0.02	0.01	0.00	0.00
Total	100.13	100.94	100.33	100.28	99.84	99.98	100.65	100.42	99.76	100.75	99.81	97.92	99.78	100.65	98.43	99.43	100.82	99.94
Si	1.909	1.888	1.905	1.915	1.907	1.922	1.908	1.934	1.914	1.921	1.894	1.934	1.914	1.908	1.925	1.936	1.901	1.947
Ti	0.013	0.013	0.015	0.011	0.011	0.012	0.012	0.011	0.013	0.011	0.012	0.012	0.014	0.011	0.012	0.014	0.008	0.007
Al	0.153	0.141	0.135	0.137	0.149	0.140	0.139	0.093	0.144	0.120	0.133	0.125	0.131	0.116	0.138	0.100	0.149	0.088
Cr	0.041	0.037	0.038	0.034	0.036	0.034	0.035	0.027	0.037	0.028	0.037	0.032	0.034	0.032	0.031	0.025	0.034	0.024
Fe <sup>3+</sup>	0.000	0.049	0.013	0.005	0.012	0.000	0.016	0.016	0.000	0.012	0.046	0.000	0.013	0.047	0.000	0.007	0.027	0.010
Fe <sup>2+</sup>	0.096	0.044	0.082	0.102	0.081	0.108	0.072	0.054	0.082	0.096	0.051	0.105	0.076	0.042	0.126	0.080	0.055	0.059
Mn	0.003	0.001	0.002	0.002	0.002	0.007	0.005	0.003	0.003	0.002	0.004	0.002	0.001	0.002	0.004	0.003	0.004	0.003
Mg	0.874	0.919	0.945	0.959	0.927	0.982	0.881	0.903	0.897	0.992	0.992	0.921	0.915	0.921	0.952	0.921	0.891	0.916
Ca	0.878	0.879	0.840	0.808	0.842	0.764	0.899	0.934	0.878	0.791	0.803	0.830	0.870	0.890	0.779	0.884	0.904	0.919
Na	0.031	0.029	0.025	0.028	0.033	0.022	0.032	0.025	0.030	0.025	0.028	0.030	0.033	0.033	0.027	0.030	0.028	0.029
K	0.000	0.000	0.000	0.000	0.001	0.000	0.000	0.000	0.000	0.001	0.000	0.000	0.000	0.000	0.001	0.000	0.000	0.000
Wo	47.4	46.4	44.6	43.1	45.2	41.1	48.0	48.9	47.2	41.8	42.4	44.7	46.4	46.8	41.9	46.6	48.1	48.2
En	47.2	48.6	50.2	51.1	49.8	52.8	47.1	47.3	48.2	52.4	52.3	49.6	48.8	48.4	51.2	48.6	47.4	48.0
Fs	5.31	5.04	5.26	5.82	5.14	6.26	4.97	3.83	4.65	5.87	5.33	5.75	4.82	4.75	7.02	4.84	4.66	3.83

Formulae of clinopyroxene calculated on the basis of 6 oxygens. c = grain core, r = grain rim.

**Table D-2.** Microprobe analyses and formulae of clinopyroxene porphyroclasts from different ultramafic lithologies of the Krivaja-Konjuh ophiolite complex

Rock type	Plagioclase Iherzolite – Spinel Iherzolite																	
Sample-Nr.	m2-32	u4-46	u4-56	u4-85	4a-14	4a-13	4a-20	4a-22	4a-24	d5-15	d5-16	d5-18	d5-39	d5-40	d5-48	o2-1	o2-3	o2-7
Remark	r				c	r	r	r	r	c	r	r	r	r	c	c	r	r
SiO <sub>2</sub>	52.92	52.28	51.99	53.49	51.00	52.44	52.53	51.34	51.34	51.35	51.45	51.85	52.52	51.54	51.94	51.31	51.19	51.38
TiO <sub>2</sub>	0.29	0.33	0.33	0.32	0.43	0.48	0.38	0.48	0.51	0.63	0.59	0.61	0.41	0.39	0.44	0.30	0.37	0.33
Al <sub>2</sub> O <sub>3</sub>	3.02	3.19	3.17	2.54	4.50	3.87	3.80	4.99	4.97	3.59	3.16	2.78	2.54	3.06	2.97	6.69	6.48	5.84
Cr <sub>2</sub> O <sub>3</sub>	0.94	1.03	1.18	0.84	1.08	0.98	1.10	1.37	1.22	1.33	1.02	0.99	1.06	1.19	1.13	1.03	0.96	0.91
Fe <sub>2</sub> O <sub>3</sub>	0.86	1.47	1.11	0.49	3.10	0.72	1.76	1.62	1.95	1.01	1.38	1.62	0.29	2.15	0.66	1.97	2.23	1.24
FeO	2.08	1.82	1.62	2.38	0.00	1.39	0.92	1.11	0.75	1.95	1.72	1.34	2.47	1.25	2.51	0.79	0.78	1.42
MnO	0.17	0.10	0.05	0.10	0.20	0.02	0.14	0.05	0.09	0.08	0.17	0.01	0.07	0.15	0.04	0.11	0.10	0.08
MgO	17.57	17.44	16.40	17.30	16.80	16.18	16.46	15.91	15.94	15.84	16.40	17.64	16.42	16.93	16.80	15.51	15.87	15.22
CaO	22.05	22.25	23.44	23.01	22.26	23.16	22.99	22.63	22.83	22.94	22.54	21.90	23.01	22.14	21.75	21.26	21.34	21.64
Na <sub>2</sub> O	0.37	0.28	0.33	0.31	0.66	0.69	0.71	0.71	0.72	0.50	0.44	0.36	0.41	0.44	0.45	1.26	1.08	1.16
K <sub>2</sub> O	0.00	0.00	0.00	0.01	0.00	0.01	0.00	0.00	0.00	0.00	0.00	0.00	0.00	0.01	0.01	0.00	0.01	0.01
Total	100.27	100.18	99.63	100.77	100.01	99.93	100.78	100.22	100.32	99.24	98.87	99.11	99.17	99.23	98.70	100.22	100.42	99.22
Si	1.915	1.898	1.902	1.930	1.854	1.905	1.894	1.864	1.861	1.889	1.897	1.900	1.929	1.892	1.914	1.852	1.846	1.876
Ti	0.008	0.009	0.009	0.009	0.012	0.013	0.010	0.013	0.014	0.017	0.016	0.017	0.011	0.011	0.012	0.008	0.010	0.009
Al	0.129	0.136	0.137	0.108	0.193	0.166	0.161	0.213	0.212	0.156	0.137	0.120	0.110	0.132	0.129	0.285	0.276	0.251
Cr	0.027	0.030	0.034	0.024	0.031	0.028	0.031	0.039	0.035	0.039	0.030	0.029	0.031	0.034	0.033	0.029	0.027	0.026
Fe <sup>3+</sup>	0.023	0.040	0.031	0.013	0.085	0.020	0.048	0.044	0.053	0.028	0.038	0.045	0.008	0.059	0.018	0.054	0.061	0.034
Fe <sup>2+</sup>	0.063	0.055	0.050	0.072	0.000	0.042	0.028	0.034	0.023	0.060	0.053	0.041	0.076	0.038	0.077	0.024	0.024	0.043
Mn	0.005	0.003	0.001	0.003	0.006	0.001	0.004	0.002	0.003	0.003	0.005	0.000	0.002	0.005	0.001	0.003	0.003	0.003
Mg	0.948	0.944	0.894	0.930	0.910	0.876	0.885	0.861	0.862	0.869	0.901	0.963	0.899	0.927	0.923	0.835	0.853	0.829
Ca	0.855	0.865	0.919	0.889	0.867	0.901	0.888	0.880	0.887	0.904	0.890	0.860	0.905	0.871	0.859	0.822	0.825	0.847
Na	0.026	0.020	0.024	0.021	0.047	0.048	0.050	0.050	0.051	0.036	0.032	0.026	0.029	0.031	0.032	0.088	0.075	0.082
K	0.000	0.000	0.000	0.000	0.000	0.001	0.000	0.000	0.000	0.000	0.000	0.000	0.000	0.000	0.001	0.000	0.000	0.000
Wo	45.1	45.4	48.5	46.6	46.4	49.0	47.9	48.3	48.5	48.5	47.2	45.0	47.9	45.8	45.7	47.3	46.7	48.2
En	50.0	49.5	47.2	48.8	48.7	47.6	47.8	47.3	47.2	46.6	47.7	50.5	47.6	48.8	49.1	48.0	48.3	47.2
Fs	4.82	5.23	4.35	4.63	4.94	3.45	4.36	4.43	4.34	4.95	5.16	4.53	4.55	5.46	5.23	4.64	4.96	4.56

Formulae of clinopyroxene calculated on the basis of 6 oxygens. c = grain core, r = grain rim.

**Table D-3.** Microprobe analyses and formulae of clinopyroxene porphyroclasts from different ultramafic lithologies of the Krivaja-Konjuh ophiolite complex

Rock type	Spinel lherzolite																	
Sample-Nr.	o2-9	o2-32	o2-34	o2-35	o2-36	o2-39	o2-40	z2-12	z2-13	z2-21	z2-22	z2-25	z2-27	z2-33	z2-35	z2-37	z2-50	z2-51
Remark	r		c	r	r	r	r	r	c	c	r	r	r	r	r	r	r	r
SiO <sub>2</sub>	51.86	50.86	50.83	52.09	51.92	51.62	51.27	51.62	51.60	52.54	52.03	53.22	52.79	52.32	51.62	52.15	51.72	52.38
TiO <sub>2</sub>	0.36	0.67	0.33	0.36	0.39	0.35	0.30	0.15	0.24	0.24	0.28	0.21	0.33	0.31	0.32	0.23	0.25	0.28
Al <sub>2</sub> O <sub>3</sub>	5.94	5.51	6.54	5.31	5.35	6.01	6.15	5.16	5.89	4.65	5.32	3.25	4.71	5.03	5.44	4.71	5.25	5.37
Cr <sub>2</sub> O <sub>3</sub>	0.94	0.64	0.98	0.72	0.86	0.96	0.95	0.86	1.00	0.97	0.99	0.67	0.84	0.86	1.06	0.80	0.94	1.01
Fe <sub>2</sub> O <sub>3</sub>	0.32	2.41	0.97	0.69	0.82	0.84	1.77	0.00	0.00	0.00	0.39	1.09	0.00	0.08	0.49	0.78	0.54	0.00
FeO	2.48	0.57	1.67	2.11	1.76	1.71	1.38	2.75	2.82	2.51	2.10	1.21	2.52	2.13	2.08	1.73	2.20	3.30
MnO	0.03	0.10	0.08	0.12	0.09	0.05	0.06	0.12	0.14	0.11	0.09	0.07	0.06	0.12	0.07	0.08	0.05	0.10
MgO	15.92	15.43	15.14	15.59	15.34	14.94	15.83	16.63	15.25	15.72	15.66	16.87	15.69	15.75	15.42	15.85	15.59	16.22
CaO	20.21	22.36	20.89	20.96	21.89	21.77	20.72	20.62	22.12	22.78	22.89	23.38	22.90	23.06	23.02	23.09	22.39	20.55
Na <sub>2</sub> O	1.20	1.00	1.20	1.23	1.12	1.24	1.16	0.59	0.66	0.64	0.65	0.54	0.65	0.64	0.62	0.62	0.73	0.61
K <sub>2</sub> O	0.00	0.00	0.00	0.01	0.00	0.00	0.00	0.00	0.00	0.00	0.01	0.01	0.00	0.00	0.00	0.01	0.00	0.01
Total	99.25	99.54	98.63	99.18	99.53	99.50	99.59	98.49	99.73	100.14	100.39	100.52	100.49	100.29	100.14	100.04	99.64	99.83
Si	1.887	1.856	1.865	1.900	1.891	1.880	1.863	1.895	1.879	1.905	1.883	1.920	1.907	1.894	1.875	1.893	1.885	1.899
Ti	0.010	0.018	0.009	0.010	0.011	0.010	0.008	0.004	0.007	0.007	0.007	0.006	0.009	0.008	0.009	0.006	0.007	0.008
Al	0.255	0.237	0.283	0.228	0.230	0.258	0.263	0.223	0.253	0.199	0.227	0.138	0.201	0.215	0.233	0.201	0.225	0.230
Cr	0.027	0.018	0.028	0.021	0.025	0.028	0.027	0.025	0.029	0.028	0.028	0.019	0.024	0.025	0.031	0.023	0.027	0.029
Fe <sup>3+</sup>	0.009	0.066	0.027	0.019	0.022	0.023	0.049	0.000	0.000	0.000	0.011	0.030	0.000	0.002	0.013	0.021	0.015	0.000
Fe <sup>2+</sup>	0.075	0.017	0.051	0.064	0.054	0.052	0.042	0.084	0.086	0.076	0.064	0.037	0.076	0.065	0.063	0.052	0.067	0.100
Mn	0.001	0.003	0.002	0.004	0.003	0.002	0.002	0.004	0.004	0.003	0.003	0.002	0.002	0.004	0.002	0.002	0.001	0.003
Mg	0.864	0.839	0.828	0.848	0.832	0.811	0.857	0.910	0.828	0.850	0.845	0.907	0.845	0.849	0.835	0.858	0.847	0.876
Ca	0.788	0.874	0.821	0.819	0.854	0.849	0.807	0.811	0.863	0.885	0.887	0.904	0.886	0.894	0.896	0.898	0.874	0.798
Na	0.085	0.070	0.086	0.087	0.079	0.087	0.082	0.042	0.046	0.045	0.045	0.037	0.046	0.045	0.044	0.044	0.051	0.043
K	0.000	0.000	0.000	0.001	0.000	0.000	0.000	0.000	0.000	0.000	0.001	0.001	0.000	0.000	0.000	0.000	0.000	0.000
Wo	45.4	48.6	47.5	46.7	48.4	48.9	45.9	44.8	48.5	48.8	49.0	48.1	49.0	49.3	49.5	49.0	48.4	44.9
En	49.7	46.6	47.9	48.3	47.2	46.7	48.8	50.3	46.5	46.9	46.7	48.3	46.7	46.8	46.1	46.8	46.9	49.3
Fs	4.92	4.82	4.66	4.94	4.52	4.46	5.24	4.97	5.15	4.34	4.38	3.63	4.36	3.96	4.35	4.28	4.65	5.85

Formulae of clinopyroxene calculated on the basis of 6 oxygens. c = grain core, r = grain rim.

**Table D-4.** Microprobe analyses and formulae of clinopyroxene porphyroclasts from different ultramafic lithologies of the Krivaja-Konjuh ophiolite complex

Rock type	Spinel lherzolite – Olivine websterite																	
Sample-Nr.	z4-36	z4-37	z4-42	z4-55	z4-54	u35-22	u35-21	u35-30	u35-51	u35-53	r7-11	r7-12	r7-49	r7-50	1c-38	1c-39	1c-41	1c-43
Remark	r	c	r	c	r	c	r			c	r	c	r	r	r	r	r	r
SiO <sub>2</sub>	51.81	50.10	51.51	50.66	52.25	44.81	53.22	52.20	52.97	52.96	52.40	53.70	51.48	50.83	51.61	51.04	51.37	51.64
TiO <sub>2</sub>	0.22	0.22	0.23	0.25	0.16	0.22	0.26	0.25	0.26	0.31	0.34	0.26	0.47	0.47	0.47	0.44	0.41	0.39
Al <sub>2</sub> O <sub>3</sub>	5.93	6.83	6.04	6.21	6.62	6.14	2.04	2.87	2.36	2.31	4.92	2.45	6.70	6.23	4.74	5.58	5.12	4.93
Cr <sub>2</sub> O <sub>3</sub>	0.95	1.18	1.02	1.01	0.98	6.61	0.78	0.78	0.87	0.88	0.63	0.28	0.94	0.86	0.89	0.86	0.87	0.85
Fe <sub>2</sub> O <sub>3</sub>	0.22	1.68	2.99	2.12	2.70	7.08	1.34	2.05	1.29	1.64	0.32	0.00	0.99	0.49	1.29	1.45	1.80	2.88
FeO	3.21	1.11	0.11	0.80	1.23	0.00	1.25	0.91	1.48	1.27	2.24	2.21	1.77	2.25	1.70	1.66	1.57	0.73
MnO	0.05	0.10	0.09	0.06	0.14	0.07	0.08	0.07	0.14	0.05	0.07	0.08	0.06	0.12	0.05	0.09	0.16	0.12
MgO	18.43	14.88	17.91	15.78	17.22	16.34	17.28	17.47	17.12	17.10	15.21	16.27	14.37	14.84	15.85	15.55	15.70	17.13
CaO	18.55	22.97	21.25	22.62	21.07	19.36	23.65	22.62	23.35	23.42	21.79	23.56	21.95	22.05	23.22	23.01	23.20	22.49
Na <sub>2</sub> O	0.49	0.62	0.53	0.61	0.49	0.28	0.31	0.32	0.33	0.38	1.22	0.59	1.38	0.89	0.50	0.53	0.51	0.41
K <sub>2</sub> O	0.00	0.03	0.00	0.00	0.00	0.01	0.00	0.02	0.00	0.02	0.00	0.00	0.00	0.00	0.02	0.00	0.00	0.00
Total	99.86	99.72	101.67	100.11	100.09	100.93	100.22	99.57	100.18	100.33	99.12	99.40	100.12	99.02	100.35	100.21	100.71	101.55
Si	1.869	1.829	1.831	1.839	1.808	1.659	1.931	1.904	1.924	1.921	1.914	1.959	1.866	1.865	1.873	1.855	1.860	1.849
Ti	0.006	0.006	0.006	0.007	0.004	0.006	0.007	0.007	0.007	0.008	0.009	0.007	0.013	0.013	0.013	0.012	0.011	0.010
Al	0.252	0.294	0.253	0.266	0.290	0.268	0.087	0.123	0.101	0.099	0.212	0.105	0.286	0.269	0.203	0.239	0.218	0.208
Cr	0.027	0.034	0.029	0.029	0.021	0.193	0.022	0.022	0.025	0.025	0.018	0.008	0.027	0.025	0.026	0.025	0.025	0.024
Fe <sup>3+</sup>	0.006	0.046	0.080	0.058	0.036	0.197	0.037	0.056	0.035	0.045	0.009	0.000	0.027	0.013	0.035	0.040	0.049	0.077
Fe <sup>2+</sup>	0.097	0.034	0.003	0.024	0.056	0.000	0.038	0.028	0.045	0.038	0.069	0.067	0.054	0.069	0.052	0.050	0.048	0.022
Mn	0.002	0.003	0.003	0.002	0.004	0.002	0.002	0.002	0.004	0.002	0.002	0.002	0.002	0.004	0.001	0.003	0.005	0.004
Mg	0.991	0.810	0.949	0.853	0.953	0.902	0.935	0.950	0.927	0.925	0.828	0.885	0.776	0.812	0.858	0.843	0.848	0.914
Ca	0.717	0.899	0.809	0.879	0.873	0.768	0.919	0.884	0.908	0.910	0.853	0.921	0.852	0.867	0.903	0.896	0.900	0.863
Na	0.034	0.044	0.036	0.043	0.033	0.020	0.022	0.023	0.023	0.026	0.086	0.042	0.097	0.063	0.035	0.037	0.036	0.028
K	0.000	0.001	0.000	0.000	0.000	0.001	0.000	0.001	0.000	0.001	0.000	0.000	0.000	0.000	0.001	0.000	0.000	0.000
Wo	39.6	50.1	43.9	48.4	48.8	41.1	47.6	46.0	47.3	47.4	48.4	49.1	49.8	49.1	48.8	48.9	48.7	45.9
En	54.7	45.2	51.5	47.0	47.8	48.2	48.4	49.5	48.3	48.2	47.1	47.2	45.4	46.0	46.4	46.0	45.8	48.6
Fs	5.84	4.66	4.78	4.63	5.39	10.75	4.00	4.55	4.43	4.40	4.58	3.70	4.84	4.97	4.89	5.13	5.57	5.57

Formulae of clinopyroxene calculated on the basis of 6 oxygens. c = grain core, r = grain rim.

**Table D-5.** Microprobe analyses and formulae of clinopyroxene porphyroclasts from different ultramafic lithologies of the Krivaja-Konjuh ophiolite complex

Rock type	Olivine websterite – Dunite																	
Sample-Nr.	1c-43	1c-46	2a-5	2a-6	2a-7	2a-8	2a-9	2a-13	2a-17	2a-18	2a-20	2a-22	2a-31	2a-32	2a-36	2a-33	u19-45	u19-44
Remark	r	c	r	c	c	r	r	r	r	c	r	r	r	c	r	r	c	r
SiO <sub>2</sub>	51.64	50.31	52.16	51.88	51.14	51.08	52.77	51.95	52.16	52.09	52.41	52.51	51.81	51.64	52.30	52.15	53.62	49.42
TiO <sub>2</sub>	0.39	0.33	0.40	0.39	0.44	0.48	0.41	0.41	0.47	0.55	0.45	0.38	0.42	0.45	0.38	0.35	0.09	2.05
Al <sub>2</sub> O <sub>3</sub>	4.93	7.16	3.70	5.16	5.77	5.32	3.92	3.51	4.12	4.86	3.88	3.97	4.22	6.27	3.81	4.19	1.45	4.75
Cr <sub>2</sub> O <sub>3</sub>	0.85	0.72	0.93	0.80	0.84	0.78	0.88	0.94	0.69	0.66	0.70	0.61	0.82	0.57	0.88	0.79	0.22	1.13
Fe <sub>2</sub> O <sub>3</sub>	2.88	1.10	0.39	0.26	1.65	1.23	1.67	1.84	0.72	0.61	0.37	0.00	1.07	0.57	0.92	0.63	1.80	2.46
FeO	0.73	2.24	2.61	2.60	1.54	2.09	1.28	1.22	2.08	2.42	3.03	3.80	1.91	2.45	2.27	2.29	1.01	1.48
MnO	0.12	0.12	0.09	0.10	0.12	0.10	0.07	0.12	0.11	0.08	0.12	0.13	0.13	0.10	0.11	0.10	0.12	0.09
MgO	17.13	15.01	16.26	15.74	15.78	15.93	17.35	16.69	16.18	15.85	16.77	18.12	16.12	15.45	16.28	15.95	16.98	15.50
CaO	22.49	22.77	22.25	22.54	22.86	21.89	22.46	22.62	23.04	22.82	21.62	18.13	22.79	22.90	22.74	22.93	24.26	22.43
Na <sub>2</sub> O	0.41	0.47	0.55	0.59	0.54	0.62	0.52	0.52	0.49	0.59	0.50	0.43	0.50	0.58	0.50	0.53	0.37	0.65
K <sub>2</sub> O	0.00	0.00	0.00	0.00	0.00	0.00	0.01	0.01	0.00	0.02	0.00	0.00	0.00	0.01	0.01	0.02	0.00	0.00
Total	101.55	100.23	99.34	100.08	100.67	99.53	101.34	99.83	100.05	100.53	99.85	98.07	99.78	100.97	100.19	99.91	99.91	99.97
Si	1.849	1.829	1.910	1.885	1.849	1.866	1.889	1.893	1.896	1.885	1.907	1.928	1.889	1.860	1.901	1.899	1.952	1.813
Ti	0.010	0.009	0.011	0.011	0.012	0.013	0.011	0.011	0.013	0.015	0.012	0.010	0.011	0.012	0.010	0.010	0.002	0.057
Al	0.208	0.307	0.160	0.221	0.246	0.229	0.166	0.151	0.177	0.207	0.166	0.172	0.181	0.266	0.163	0.180	0.062	0.206
Cr	0.024	0.021	0.027	0.023	0.024	0.022	0.025	0.027	0.020	0.019	0.020	0.018	0.024	0.016	0.025	0.023	0.006	0.033
Fe <sup>3+</sup>	0.077	0.030	0.011	0.007	0.045	0.034	0.045	0.051	0.020	0.017	0.010	0.000	0.029	0.015	0.025	0.017	0.049	0.068
Fe <sup>2+</sup>	0.022	0.068	0.080	0.079	0.047	0.064	0.038	0.037	0.063	0.073	0.092	0.117	0.058	0.074	0.069	0.070	0.031	0.045
Mn	0.004	0.004	0.003	0.003	0.004	0.003	0.002	0.004	0.003	0.003	0.004	0.004	0.004	0.003	0.003	0.003	0.004	0.003
Mg	0.914	0.813	0.887	0.852	0.851	0.868	0.926	0.907	0.877	0.855	0.910	0.991	0.876	0.829	0.882	0.866	0.922	0.848
Ca	0.863	0.887	0.873	0.877	0.886	0.857	0.862	0.883	0.897	0.885	0.843	0.713	0.891	0.884	0.886	0.895	0.946	0.882
Na	0.028	0.033	0.039	0.042	0.038	0.044	0.036	0.037	0.034	0.041	0.035	0.031	0.036	0.040	0.035	0.037	0.026	0.046
K	0.000	0.000	0.000	0.000	0.000	0.000	0.000	0.000	0.000	0.001	0.000	0.000	0.000	0.000	0.000	0.001	0.000	0.000
Wo	45.9	49.2	47.1	48.2	48.4	46.9	46.0	46.9	48.2	48.3	45.3	39.1	47.9	49.0	47.5	48.3	48.5	47.8
En	48.6	45.1	47.9	46.9	46.4	47.5	49.4	48.2	47.1	46.7	48.9	54.3	47.2	45.9	47.3	46.8	47.2	45.9
Fs	5.54	5.76	5.09	4.93	5.26	5.58	4.66	4.93	4.68	5.06	5.77	6.64	4.99	5.14	5.28	4.99	4.30	6.36

Formulae of clinopyroxene calculated on the basis of 6 oxygens. c = grain core, r = grain rim.

**Table E-1.** Microprobe analyses and formulae of small-grain and exsolved clinopyroxene from different ultramafic lithologies of the Krivaja-Konjuh ophiolite complex

Rock type	Plagioclase Iherzolite																	
Sample-Nr.	gr2-38	gr2-39	gr12-28	gr12-29	m2-44	m2-45	m2-35	m2-36	u4-35	u4-25	u4-26	u4-27	u4-40	u4-44	u4-78b	u4-80	u4-30	u4-33
Remark	r	in(opx)	c	r	r(sp)	r(sp)	r	r		c	c	r		in(opx)		c	in(opx)	in(opx)
SiO <sub>2</sub>	52.87	52.80	52.52	52.46	52.73	52.63	52.47	53.11	51.66	50.99	52.21	52.82	52.10	52.15	51.70	51.26	52.64	52.86
TiO <sub>2</sub>	0.48	0.47	0.46	0.47	0.36	0.34	0.30	0.24	0.36	0.60	0.33	0.20	0.32	0.32	0.36	0.31	0.40	0.25
Al <sub>2</sub> O <sub>3</sub>	2.96	3.01	2.70	2.54	2.99	3.03	2.96	2.87	2.86	5.42	2.91	1.46	3.60	3.09	2.87	2.96	2.88	2.00
Cr <sub>2</sub> O <sub>3</sub>	1.07	1.12	0.99	0.94	1.24	1.37	1.04	0.89	0.91	1.36	0.94	0.40	1.24	1.05	1.04	1.17	0.97	0.56
Fe <sub>2</sub> O <sub>3</sub>	0.00	0.12	0.14	1.01	0.32	0.18	0.62	0.22	2.84	1.79	1.22	2.73	1.80	1.81	2.31	2.30	1.79	1.27
FeO	3.04	2.91	2.51	1.83	2.65	2.56	2.10	2.64	0.29	0.96	1.92	0.00	1.43	1.23	0.71	0.48	1.14	1.18
MnO	0.09	0.12	0.10	0.03	0.00	0.12	0.13	0.08	0.10	0.03	0.09	0.06	0.07	0.06	0.16	0.04	0.04	0.05
MgO	16.45	16.25	16.50	17.12	16.80	16.93	16.80	17.12	17.52	15.63	17.19	19.81	16.61	17.08	16.68	16.66	16.82	17.35
CaO	22.48	23.18	22.76	22.57	22.98	22.68	22.97	22.72	22.61	22.61	22.50	22.32	23.14	23.07	23.33	23.14	23.80	23.48
Na <sub>2</sub> O	0.34	0.40	0.43	0.40	0.29	0.29	0.31	0.30	0.33	0.79	0.26	0.24	0.39	0.29	0.34	0.37	0.35	0.26
K <sub>2</sub> O	0.00	0.00	0.01	0.00	0.00	0.00	0.00	0.00	0.00	0.01	0.00	0.00	0.01	0.00	0.03	0.00	0.01	0.00
Total	99.77	100.38	99.12	99.38	100.34	100.10	99.68	100.19	99.48	100.18	99.58	100.04	100.70	100.14	99.52	98.69	100.82	99.25
Si	1.928	1.919	1.928	1.919	1.914	1.914	1.915	1.927	1.888	1.852	1.907	1.911	1.886	1.896	1.894	1.891	1.902	1.934
Ti	0.013	0.013	0.013	0.013	0.010	0.009	0.008	0.006	0.010	0.016	0.009	0.006	0.009	0.009	0.010	0.009	0.011	0.007
Al	0.127	0.129	0.117	0.110	0.128	0.130	0.127	0.123	0.123	0.232	0.125	0.062	0.153	0.132	0.124	0.128	0.122	0.086
Cr	0.031	0.032	0.029	0.027	0.036	0.039	0.030	0.025	0.026	0.039	0.027	0.011	0.035	0.030	0.030	0.034	0.028	0.016
Fe <sup>3+</sup>	0.000	0.003	0.004	0.028	0.009	0.005	0.017	0.006	0.078	0.049	0.034	0.074	0.049	0.050	0.064	0.064	0.049	0.035
Fe <sup>2+</sup>	0.093	0.088	0.077	0.056	0.080	0.078	0.064	0.080	0.009	0.029	0.059	0.000	0.043	0.037	0.022	0.015	0.034	0.036
Mn	0.003	0.004	0.003	0.001	0.000	0.004	0.004	0.002	0.003	0.001	0.003	0.002	0.002	0.002	0.005	0.001	0.001	0.002
Mg	0.894	0.880	0.903	0.934	0.909	0.918	0.914	0.926	0.954	0.846	0.936	1.069	0.897	0.926	0.911	0.916	0.906	0.946
Ca	0.878	0.903	0.895	0.885	0.894	0.884	0.898	0.883	0.885	0.880	0.881	0.865	0.898	0.898	0.916	0.915	0.921	0.920
Na	0.024	0.028	0.031	0.028	0.020	0.020	0.022	0.021	0.023	0.055	0.019	0.017	0.027	0.021	0.024	0.026	0.025	0.018
K	0.000	0.000	0.000	0.000	0.000	0.000	0.000	0.000	0.000	0.001	0.000	0.000	0.000	0.000	0.001	0.000	0.000	0.000
Wo	47.0	48.1	47.6	46.5	47.3	46.8	47.3	46.5	45.9	48.7	46.1	43.0	47.5	47.0	47.8	47.9	48.2	47.5
En	47.9	46.9	48.0	49.1	48.0	48.6	48.2	48.8	49.5	46.9	49.0	53.2	47.5	48.4	47.5	47.9	47.4	48.8
Fs	5.13	5.14	4.53	4.54	4.78	4.65	4.58	4.74	4.78	4.49	5.03	3.88	5.08	4.67	4.73	4.28	4.49	3.84

Formulae of clinopyroxene calculated on the basis of 6 oxygens. c = grain core, r = grain rim, in(opx) = cpx lamella in opx or cpx inclusion in opx, r(sp) = rim around spinel.

**Table E-2.** Microprobe analyses and formulae of small-grain and exsolved clinopyroxene from different ultramafic lithologies of the Krivaja-Konjuh ophiolite complex

Rock type	Plagioclase Iherzolite – Spinel Iherzolite																	
Sample-Nr.	u4-67a	u4-67b	d5-34	d5-35	z2-4	z2-28	z2-46	z4-18	z4-21	z4-22	z4-49	z4-50	u35-4	u35-10	u35-10b	u35-58	u35-58b	r7-5
Remark	r	c	c	r	in(opx)	in(opx)	r	r	c	r	c		r	in(opx)	in(opx)	c	r	
SiO <sub>2</sub>	52.19	52.25	51.63	51.36	52.52	51.92	51.88	52.18	53.88	51.98	50.35	51.18	52.73	51.76	51.33	52.99	53.19	52.45
TiO <sub>2</sub>	0.34	0.30	0.51	0.43	0.23	0.40	0.34	0.36	0.32	0.28	0.25	0.31	0.32	0.46	0.45	0.37	0.18	0.34
Al <sub>2</sub> O <sub>3</sub>	2.91	3.19	3.07	3.11	4.53	5.42	5.37	3.81	2.46	5.49	6.11	5.87	2.25	3.60	3.58	2.44	1.88	4.50
Cr <sub>2</sub> O <sub>3</sub>	1.02	1.13	1.13	1.23	0.74	0.80	1.05	0.55	0.32	0.98	0.95	0.87	0.80	1.45	1.52	0.83	0.67	0.47
Fe <sub>2</sub> O <sub>3</sub>	1.86	0.78	1.38	2.84	0.89	0.00	0.99	1.25	0.00	0.00	2.90	0.77	0.80	1.41	1.72	0.95	1.89	1.62
FeO	1.07	1.99	1.73	0.63	1.82	2.69	1.60	1.17	2.26	2.57	0.40	1.74	2.08	1.53	1.25	1.89	0.94	1.20
MnO	0.10	0.09	0.11	0.03	0.07	0.07	0.09	0.06	0.05	0.06	0.13	0.10	0.08	0.11	0.08	0.06	0.08	0.13
MgO	17.15	16.56	16.20	17.40	16.39	15.71	15.53	16.16	16.75	16.20	16.65	15.47	16.93	16.35	16.31	16.93	17.73	15.70
CaO	23.03	23.11	22.95	21.92	22.73	22.60	22.96	23.63	23.66	21.05	21.56	22.82	22.97	22.89	22.86	23.25	23.20	22.30
Na <sub>2</sub> O	0.31	0.33	0.44	0.44	0.59	0.57	0.76	0.52	0.42	0.63	0.56	0.61	0.34	0.47	0.45	0.38	0.30	1.11
K <sub>2</sub> O	0.01	0.00	0.02	0.01	0.01	0.00	0.02	0.01	0.01	0.00	0.00	0.00	0.00	0.00	0.01	0.00	0.02	0.00
Total	99.98	99.73	99.16	99.40	100.51	100.18	100.58	99.69	100.12	99.23	99.86	99.74	99.29	100.04	99.55	100.09	100.07	99.81
Si	1.899	1.908	1.900	1.880	1.896	1.883	1.875	1.902	1.952	1.893	1.829	1.864	1.932	1.887	1.881	1.926	1.930	1.904
Ti	0.009	0.008	0.014	0.012	0.006	0.011	0.009	0.010	0.009	0.008	0.007	0.008	0.009	0.013	0.012	0.010	0.005	0.009
Al	0.125	0.137	0.133	0.134	0.193	0.232	0.229	0.164	0.105	0.236	0.262	0.252	0.097	0.155	0.155	0.104	0.080	0.193
Cr	0.029	0.033	0.033	0.035	0.021	0.023	0.030	0.016	0.009	0.028	0.027	0.025	0.023	0.042	0.044	0.024	0.019	0.013
Fe <sup>3+</sup>	0.051	0.021	0.038	0.078	0.024	0.000	0.027	0.034	0.000	0.000	0.079	0.021	0.022	0.039	0.047	0.026	0.052	0.044
Fe <sup>2+</sup>	0.032	0.061	0.053	0.019	0.055	0.081	0.048	0.036	0.068	0.078	0.012	0.053	0.064	0.047	0.038	0.057	0.028	0.037
Mn	0.003	0.003	0.003	0.001	0.002	0.002	0.003	0.002	0.002	0.002	0.004	0.003	0.003	0.003	0.003	0.002	0.003	0.004
Mg	0.931	0.901	0.888	0.949	0.882	0.849	0.836	0.878	0.905	0.880	0.901	0.840	0.925	0.889	0.891	0.917	0.959	0.850
Ca	0.898	0.904	0.905	0.860	0.879	0.878	0.889	0.923	0.918	0.821	0.839	0.890	0.902	0.894	0.897	0.906	0.902	0.868
Na	0.022	0.024	0.031	0.031	0.041	0.040	0.053	0.036	0.030	0.045	0.040	0.043	0.024	0.033	0.032	0.027	0.021	0.078
K	0.000	0.000	0.001	0.000	0.001	0.000	0.001	0.000	0.000	0.000	0.000	0.000	0.000	0.000	0.000	0.000	0.001	0.000
Wo	46.9	47.8	47.9	45.1	47.7	48.5	49.3	49.3	48.5	46.1	45.7	49.3	47.1	47.8	47.8	47.5	46.4	48.1
En	48.6	47.7	47.1	49.8	47.9	46.9	46.4	46.9	47.8	49.4	49.1	46.5	48.3	47.5	47.5	48.1	49.3	47.2
Fs	4.54	4.56	5.03	5.25	4.43	4.66	4.34	3.87	3.74	4.52	5.24	4.37	4.64	4.72	4.74	4.57	4.35	4.72

Formulae of clinopyroxene calculated on the basis of 6 oxygens. c = grain core, r = grain rim, in(opx) = cpx lamella in opx or cpx inclusion in opx.



**Table E-3.** Microprobe analyses and formulae of small-grain and exsolved clinopyroxene from different ultramafic lithologies of the Krivaja-Konjuh ophiolite complex

Rock type	Spinel lherzolite – Dunite – Chromitite																
Sample-Nr.	r7-7	r7-9	r7-14	r7-15	r7-17	r7-57	r7-43	r7-44	1c-34c	1c-34	u19-22	u19-23	d18-03	d18-04	d18-05	d18-14	d18-15
Remark							c	r	c	r	r	c					
SiO <sub>2</sub>	52.91	53.00	52.54	52.00	51.71	52.75	52.63	52.58	52.17	52.16	50.24	49.72	54.16	54.37	53.94	54.23	54.18
TiO <sub>2</sub>	0.40	0.28	0.41	0.08	0.29	0.35	0.47	0.39	0.93	0.88	1.57	1.72	0.06	0.08	0.09	0.10	0.06
Al <sub>2</sub> O <sub>3</sub>	3.94	3.04	3.86	4.73	4.20	3.69	5.22	4.90	3.56	3.74	4.40	4.49	1.31	1.44	1.61	1.22	1.22
Cr <sub>2</sub> O <sub>3</sub>	0.43	0.43	0.37	0.38	0.62	0.56	0.60	0.50	0.67	0.48	0.99	1.06	1.06	1.15	0.97	1.11	1.12
Fe <sub>2</sub> O <sub>3</sub>	0.62	0.89	0.85	3.30	3.08	1.05	0.56	0.73	1.46	0.71	1.52	2.41	1.99	0.72	2.34	0.89	0.62
FeO	2.03	1.56	1.83	0.00	0.00	1.73	2.23	1.83	1.71	2.09	2.00	1.56	0.63	1.91	0.07	1.24	1.31
MnO	0.08	0.07	0.08	0.15	0.11	0.10	0.03	0.07	0.11	0.31	0.03	0.06	0.10	0.05	0.07	0.07	0.05
MgO	16.08	16.61	15.72	28.26	21.43	16.18	15.32	15.38	16.44	16.19	15.34	15.61	17.39	17.30	17.31	17.26	17.01
CaO	22.96	24.00	23.13	19.80	21.17	23.32	21.73	22.20	23.13	23.47	22.79	22.42	22.96	22.61	23.39	22.84	23.28
Na <sub>2</sub> O	0.74	0.36	0.78	0.29	0.68	0.61	1.28	1.18	0.53	0.39	0.62	0.61	0.78	0.71	0.78	0.77	0.72
K <sub>2</sub> O	0.01	0.00	0.00	0.00	0.00	0.00	0.00	0.00	0.01	0.00	0.01	0.00	0.02	0.01	0.00	0.02	0.00
Total	100.20	100.22	99.56	108.99	103.29	100.34	100.07	99.75	100.71	100.43	99.52	99.64	100.45	100.36	100.58	99.73	99.57
Si	1.916	1.922	1.917	1.729	1.816	1.911	1.905	1.909	1.888	1.893	1.848	1.828	1.956	1.966	1.945	1.970	1.973
Ti	0.011	0.008	0.011	0.002	0.008	0.010	0.013	0.011	0.025	0.024	0.043	0.047	0.001	0.002	0.002	0.003	0.002
Al	0.168	0.130	0.166	0.185	0.174	0.158	0.223	0.210	0.152	0.160	0.191	0.194	0.056	0.062	0.069	0.052	0.053
Cr	0.012	0.012	0.011	0.010	0.017	0.016	0.017	0.014	0.019	0.014	0.029	0.031	0.030	0.033	0.028	0.032	0.032
Fe <sup>3+</sup>	0.017	0.024	0.023	0.083	0.081	0.028	0.015	0.020	0.040	0.019	0.042	0.067	0.054	0.020	0.063	0.024	0.017
Fe <sup>2+</sup>	0.062	0.047	0.056	0.000	0.000	0.052	0.067	0.055	0.052	0.063	0.062	0.048	0.019	0.058	0.002	0.038	0.040
Mn	0.002	0.002	0.002	0.004	0.003	0.003	0.001	0.002	0.003	0.010	0.001	0.002	0.003	0.002	0.002	0.002	0.002
Mg	0.868	0.898	0.855	1.401	1.122	0.874	0.826	0.832	0.887	0.876	0.841	0.856	0.936	0.932	0.931	0.935	0.924
Ca	0.891	0.932	0.904	0.706	0.796	0.905	0.843	0.864	0.897	0.913	0.898	0.883	0.888	0.876	0.904	0.889	0.908
Na	0.052	0.025	0.055	0.019	0.046	0.043	0.090	0.083	0.037	0.028	0.044	0.043	0.054	0.050	0.054	0.054	0.051
K	0.000	0.000	0.000	0.000	0.000	0.000	0.000	0.000	0.000	0.000	0.001	0.000	0.001	0.000	0.000	0.001	0.000
Wo	48.4	49.0	49.1	32.2	39.8	48.6	48.1	48.7	47.7	48.5	48.7	47.6	46.7	46.4	47.5	47.1	48.0
En	47.2	47.2	46.5	63.9	56.0	46.9	47.2	46.9	47.2	46.6	45.6	46.1	49.3	49.4	48.9	49.5	48.9
Fs	4.43	3.96	4.42	4.07	4.24	4.57	4.89	4.44	5.15	4.97	5.78	6.39	4.03	4.26	3.68	3.40	3.14

Formulae of clinopyroxene calculated on the basis of 6 oxygens. c = grain core, r = grain rim.

Spinel

Table F-1. Microprobe analyses and formulae of spinels from different ultramafic lithologies of the Krivaja-Konjuh ophiolite complex

Rock type	Plagioclase Iherzolite																	
Sample-Nr.	gr2-1	gr2-2	gr2-5	gr2-10	gr2-25	gr2-26	gr2-28	gr2-41	gr2-42	gr2-43	gr12-1	gr12-2	gr12-3	gr12-8	gr12-13	gr12-14	gr12-17	gr12-31
Remark	c	r	r	r	c	r	r	c	r	r	c	r	r		c	r	r	c
TiO <sub>2</sub>	0.62	0.64	0.63	0.50	0.62	0.58	0.60	0.65	0.47	0.63	0.69	0.72	0.64	0.66	0.55	0.55	0.49	0.64
Al <sub>2</sub> O <sub>3</sub>	22.66	22.53	22.44	22.28	22.84	23.47	23.14	22.55	24.06	22.01	21.83	20.43	22.06	23.57	20.58	21.85	21.03	24.16
Cr <sub>2</sub> O <sub>3</sub>	38.75	38.33	38.21	37.50	38.67	37.15	37.80	38.73	36.70	38.96	37.76	38.41	37.57	35.19	37.80	36.34	36.26	35.95
Fe <sub>2</sub> O <sub>3</sub>																		
FeO	25.61	26.20	26.44	26.78	25.80	26.38	25.75	25.42	24.56	26.31	26.73	27.72	26.89	26.86	29.89	29.20	29.06	24.75
MnO	0.17	0.10	0.24	0.23	0.31	0.19	0.13	0.22	0.16	0.22	0.21	0.17	0.28	0.17	0.20	0.27	0.18	0.15
ZnO	0.33	0.27	0.31	0.32	0.30	0.26	0.25	0.26	0.27	0.23	0.38	0.26	0.29	0.23	0.40	0.37	0.42	0.30
MgO	10.04	9.87	9.95	9.58	9.91	10.00	9.81	9.73	10.12	9.61	10.42	10.01	10.49	10.69	9.08	9.52	9.16	11.30
CaO	0.01	0.01	0.01	0.01	0.03	0.03	0.04	0.00	0.01	0.01	0.00	0.00	0.00	0.01	0.01	0.02	0.00	0.00
Total	98.19	97.96	98.24	97.19	98.49	98.06	97.53	97.56	96.35	97.97	98.02	97.71	98.22	97.37	98.51	98.12	96.60	97.24
Ti	0.030	0.031	0.030	0.024	0.030	0.028	0.029	0.031	0.023	0.030	0.033	0.035	0.031	0.032	0.026	0.027	0.024	0.030
Al	1.270	1.268	1.259	1.265	1.277	1.313	1.304	1.275	1.362	1.243	1.226	1.160	1.234	1.319	1.167	1.232	1.209	1.345
Cr	1.458	1.447	1.438	1.429	1.451	1.394	1.429	1.468	1.394	1.476	1.422	1.463	1.411	1.320	1.437	1.375	1.398	1.342
Fe <sup>3+</sup>	0.227	0.240	0.258	0.270	0.228	0.252	0.224	0.210	0.211	0.235	0.303	0.325	0.309	0.314	0.356	0.353	0.357	0.267
Fe <sup>2+</sup>	0.528	0.538	0.530	0.539	0.531	0.530	0.537	0.540	0.517	0.546	0.508	0.528	0.506	0.502	0.564	0.544	0.553	0.474
Mn	0.005	0.003	0.006	0.006	0.008	0.005	0.004	0.006	0.004	0.006	0.006	0.005	0.007	0.005	0.006	0.007	0.005	0.004
Zn	0.008	0.006	0.007	0.008	0.007	0.006	0.006	0.006	0.006	0.005	0.009	0.006	0.007	0.005	0.009	0.009	0.010	0.007
Mg	0.475	0.468	0.471	0.459	0.468	0.472	0.466	0.464	0.483	0.458	0.493	0.479	0.495	0.504	0.434	0.453	0.444	0.531
Ca	0.000	0.000	0.000	0.000	0.001	0.001	0.001	0.000	0.000	0.000	0.000	0.000	0.000	0.000	0.000	0.001	0.000	0.000
Cr#	53.4	53.3	53.3	53.0	53.2	51.5	52.3	53.5	50.6	54.3	53.7	55.8	53.3	50.0	55.2	52.7	53.6	49.9
Mg#	47.4	46.5	47.0	45.9	46.8	47.1	46.5	46.2	48.3	45.6	49.3	47.6	49.5	50.1	43.5	45.4	44.6	52.8
Fe <sup>3+</sup> #	7.73	8.51	8.78	9.14	7.78	8.56	7.64	7.18	7.15	8.08	10.3	11.0	10.5	10.6	12.0	11.9	12.0	9.05

Total iron as FeO. Fe<sup>3+</sup> calculations on the basis of spinel stoichiometry; Mg#=100Mg/(Mg+Fe), Cr#=100Cr/(Cr+Al), Fe<sup>3+</sup>#=100Fe<sup>3+</sup>/(Fe<sup>3+</sup>+Cr+Al); c = grain core, r = grain rim.

**Table F-2.** Microprobe analyses and formulae of spinels from different ultramafic lithologies of the Krivaja-Konjuh ophiolite complex

Rock type	Plagioclase Iherzolite																	
Sample-Nr.	gr12-32	gr12-40	gr12-41	gr12-42	gr12-43	gr12-44	m2-1	m2-2	m2-5	m2-7	m2-12	m2-15	m2-18	m2-42	m2-43	m2-46	u4-12	u4-47
Remark	r		r	c	r	r	c	r	r	r	r	c	r	c	r	r		
TiO <sub>2</sub>	0.62	0.67	0.40	0.63	0.64	0.61	0.38	0.39	0.38	0.36	0.33	0.35	0.35	0.41	0.40	0.40	0.44	0.40
Al <sub>2</sub> O <sub>3</sub>	24.65	23.16	30.99	22.87	22.65	23.49	28.62	26.43	28.02	25.53	26.79	26.90	24.40	27.47	26.39	28.10	29.17	29.47
Cr <sub>2</sub> O <sub>3</sub>	35.42	36.72	29.25	37.39	37.61	37.41	35.39	37.32	35.55	37.60	36.40	36.77	39.01	36.64	37.83	36.49	36.06	37.22
Fe <sub>2</sub> O <sub>3</sub>																		
FeO	24.89	26.16	23.01	25.50	25.50	26.01	22.31	32.00	21.91	22.74	23.04	22.88	23.81	22.54	22.95	22.19	22.29	21.51
MnO	0.13	0.08	0.12	0.12	0.21	0.19	0.16	0.14	0.19	0.14	0.16	0.27	0.12	0.24	0.12	0.21	0.16	0.06
ZnO	0.24	0.25	0.29	0.26	0.26	0.24	0.25	0.18	0.24	0.25	0.28	0.27	0.22	0.28	0.22	0.25	0.30	0.21
MgO	11.22	10.94	12.98	10.66	10.61	10.76	12.29	11.51	12.03	11.19	11.32	11.16	10.59	11.65	11.38	11.66	11.74	12.04
CaO	0.05	0.00	0.01	0.00	0.00	0.02	0.02	0.00	0.00	0.00	0.01	0.00	0.00	0.00	0.06	0.02	0.02	0.02
Total	97.21	97.98	97.06	97.43	97.48	98.73	99.42	107.96	98.32	97.80	98.32	98.59	98.52	99.23	99.35	99.32	100.18	100.92
Ti	0.029	0.032	0.018	0.030	0.031	0.028	0.009	0.008	0.009	0.008	0.008	0.008	0.008	0.009	0.009	0.009	0.010	0.009
Al	1.370	1.289	1.662	1.283	1.272	1.299	1.019	0.889	1.011	0.939	0.976	0.978	0.900	0.988	0.954	1.008	1.034	1.036
Cr	1.321	1.371	1.053	1.408	1.417	1.388	0.845	0.842	0.860	0.928	0.889	0.897	0.966	0.884	0.917	0.878	0.858	0.877
Fe <sup>3+</sup>	0.265	0.291	0.258	0.263	0.264	0.270	0.119	0.252	0.111	0.115	0.120	0.109	0.118	0.109	0.110	0.096	0.088	0.069
Fe <sup>2+</sup>	0.478	0.494	0.412	0.501	0.501	0.501	0.445	0.512	0.450	0.478	0.475	0.482	0.505	0.467	0.479	0.469	0.472	0.467
Mn	0.003	0.002	0.003	0.003	0.006	0.005	0.004	0.003	0.005	0.004	0.004	0.007	0.003	0.006	0.003	0.005	0.004	0.002
Zn	0.006	0.006	0.007	0.006	0.006	0.006	0.006	0.004	0.005	0.006	0.006	0.006	0.005	0.006	0.005	0.006	0.007	0.005
Mg	0.526	0.513	0.587	0.505	0.503	0.502	0.553	0.490	0.549	0.521	0.522	0.513	0.494	0.530	0.520	0.529	0.526	0.535
Ca	0.002	0.000	0.000	0.000	0.000	0.001	0.001	0.000	0.000	0.000	0.000	0.000	0.000	0.000	0.002	0.001	0.001	0.000
Cr#	49.1	51.5	38.8	52.3	52.7	51.7	45.3	48.6	46.0	49.7	47.7	47.8	51.7	47.2	49.0	46.6	45.3	45.9
Mg#	52.4	50.9	58.8	50.2	50.1	50.1	55.4	48.9	55.0	52.1	52.3	51.6	49.4	53.2	52.1	53.0	52.7	53.4
Fe <sup>3+</sup> #	9.04	9.92	8.74	8.95	9.06	9.17	6.02	12.7	5.65	5.83	6.04	5.56	5.97	5.53	5.67	4.83	4.59	3.57

Total iron as FeO. Fe<sup>3+</sup> calculations on the basis of spinel stoichiometry; Mg#=100Mg/(Mg+Fe), Cr#=100Cr/(Cr+Al), Fe<sup>3+</sup>#=100Fe<sup>3+</sup>/(Fe<sup>3+</sup>+Cr+Al); c = grain core, r = grain rim.

**Table F-3.** Microprobe analyses and formulae of spinels from different ultramafic lithologies of the Krivaja-Konjuh ophiolite complex

Rock type	Plagioclase lherzolite																	
Sample-Nr.	u4-50	u4-54	u4-55b	u4-71	u4-24	u4-70b	u4-70c	u4-23	u4-25	u4-61	4a-1	4a-2	4a-6	4a-8	4a-11	4a-12	4a-29	4a-32
Remark					c	c	r	r	r		r	c	r	r	r	c		
TiO <sub>2</sub>	0.38	0.35	0.36	0.42	0.39	0.40	0.37	0.38	0.36	0.37	0.22	0.26	0.30	0.24	0.21	0.29	0.11	0.19
Al <sub>2</sub> O <sub>3</sub>	29.19	29.66	30.27	29.67	30.09	30.04	30.75	30.93	31.62	35.04	38.84	38.46	37.62	36.87	38.43	38.16	43.34	42.42
Cr <sub>2</sub> O <sub>3</sub>	36.19	36.99	36.59	36.73	36.26	36.23	35.53	35.51	34.66	31.58	27.37	27.72	28.76	29.10	27.77	27.99	19.45	23.75
Fe <sub>2</sub> O <sub>3</sub>																		
FeO	23.56	22.45	21.87	23.05	22.02	23.15	21.96	21.58	21.55	21.98	17.95	17.66	17.59	19.07	17.91	18.14	19.19	17.10
MnO	0.13	0.14	0.18	0.11	0.08	0.22	0.13	0.15	0.14	0.06	0.06	0.15	0.11	0.09	0.12	0.13	0.09	0.11
ZnO	0.31	0.32	0.25	0.31	0.27	0.29	0.31	0.23	0.25	0.37	0.31	0.20	0.27	0.23	0.27	0.19	0.00	0.00
MgO	10.61	11.43	11.74	11.12	11.35	11.28	11.46	11.59	11.81	12.49	14.87	14.78	14.72	14.28	14.64	14.69	15.07	15.39
CaO	0.01	0.01	0.00	0.01	0.01	0.01	0.00	0.02	0.02	0.02	0.01	0.05	0.02	0.00	0.00	0.00	0.00	0.02
Total	100.38	101.34	101.25	101.43	100.47	101.62	100.50	100.38	100.40	101.92	99.62	99.28	99.38	99.88	99.35	99.59	97.25	98.98
Ti	0.009	0.008	0.008	0.009	0.009	0.009	0.008	0.009	0.008	0.008	0.009	0.011	0.013	0.010	0.009	0.013	0.005	0.008
Al	1.041	1.042	1.060	1.044	1.063	1.052	1.083	1.089	1.108	1.193	1.961	1.951	1.914	1.878	1.950	1.934	2.186	2.117
Cr	0.866	0.872	0.859	0.867	0.860	0.851	0.839	0.839	0.815	0.721	0.927	0.943	0.981	0.994	0.945	0.952	0.658	0.795
Fe <sup>3+</sup>	0.076	0.071	0.065	0.071	0.059	0.078	0.061	0.056	0.061	0.070	0.098	0.089	0.086	0.112	0.091	0.095	0.148	0.075
Fe <sup>2+</sup>	0.520	0.489	0.478	0.504	0.493	0.497	0.488	0.483	0.475	0.461	0.364	0.364	0.366	0.385	0.369	0.371	0.359	0.354
Mn	0.003	0.003	0.004	0.003	0.002	0.006	0.003	0.004	0.003	0.001	0.001	0.004	0.003	0.002	0.003	0.003	0.002	0.003
Zn	0.007	0.007	0.005	0.007	0.006	0.006	0.007	0.005	0.005	0.008	0.007	0.004	0.006	0.005	0.006	0.004	0.000	0.000
Mg	0.478	0.508	0.520	0.495	0.507	0.500	0.510	0.516	0.523	0.538	0.633	0.632	0.631	0.613	0.627	0.628	0.641	0.647
Ca	0.000	0.000	0.000	0.000	0.000	0.000	0.000	0.001	0.001	0.001	0.000	0.002	0.001	0.000	0.000	0.000	0.000	0.001
Cr#	45.4	45.6	44.8	45.4	44.7	44.7	43.7	43.5	42.4	37.7	32.1	32.6	33.9	34.6	32.6	33.0	23.1	27.3
Mg#	47.9	51.0	52.1	49.5	50.7	50.1	51.1	51.6	52.4	53.9	63.5	63.4	63.3	61.5	62.9	62.8	64.1	64.7
Fe <sup>3+</sup> #	3.83	3.67	3.39	3.64	3.06	4.08	3.13	2.88	3.13	3.56	3.33	3.08	2.93	3.89	3.14	3.28	4.90	2.56

Total iron as FeO. Fe<sup>3+</sup> calculations on the basis of spinel stoichiometry; Mg#=100Mg/(Mg+Fe), Cr#=100Cr/(Cr+Al), Fe<sup>3+</sup>#=100Fe<sup>3+</sup>/(Fe<sup>3+</sup>+Cr+Al); c = grain core, r = grain rim.

**Table F-4.** Microprobe analyses and formulae of spinels from different ultramafic lithologies of the Krivaja-Konjuh ophiolite complex

Rock type	Plagioclase Iherzolite – Spinel Iherzolite																	
Sample-Nr.	4a-38	4a-42	4a-43	d5-1	d5-2	d5-5	d5-25	d5-26	d5-28	d5-30	o2-13	o2-14	o2-20	o2-21	o2-22	o2-23	o2-26	o2-28
Remark		r	c	c	r	r	c	r	r	r	c	r	r	r	c	r	r	r
TiO <sub>2</sub>	0.13	0.30	0.29	0.77	0.94	0.57	0.78	0.73	0.75	0.83	0.07	0.05	0.04	0.07	0.03	0.05	0.05	0.07
Al <sub>2</sub> O <sub>3</sub>	48.15	38.17	38.38	21.81	22.73	23.72	22.50	23.68	21.74	21.90	54.33	54.40	54.59	53.89	54.57	54.57	54.78	54.45
Cr <sub>2</sub> O <sub>3</sub>	18.05	27.82	27.09	39.31	38.62	38.77	39.01	37.94	39.58	38.19	13.17	12.98	12.85	13.14	12.94	12.66	12.90	13.18
Fe <sub>2</sub> O <sub>3</sub>																		
FeO	15.35	17.49	17.58	25.61	25.19	24.42	25.09	25.53	26.09	26.66	11.88	11.32	11.42	11.16	11.83	11.80	11.98	11.52
MnO	0.04	0.11	0.20	0.18	0.11	0.17	0.16	0.18	0.22	0.16	0.08	0.08	0.05	0.08	0.10	0.06	0.13	0.11
ZnO	0.00	0.00	0.00	0.22	0.18	0.18	0.27	0.22	0.26	0.21	0.13	0.19	0.27	0.16	0.17	0.14	0.26	0.15
MgO	16.49	15.05	14.86	10.15	10.56	10.76	10.34	10.64	9.95	9.94	19.38	19.20	19.51	19.33	19.46	19.43	19.29	19.58
CaO	0.01	0.09	0.01	0.02	0.03	0.01	0.00	0.00	0.00	0.02	0.01	0.00	0.00	0.00	0.00	0.01	0.00	0.00
Total	98.21	99.03	98.40	98.07	98.36	98.59	98.16	98.92	98.59	97.90	99.04	98.22	98.74	97.82	99.11	98.72	99.39	99.07
Ti	0.005	0.013	0.013	0.037	0.044	0.027	0.037	0.035	0.036	0.040	0.001	0.001	0.001	0.001	0.001	0.001	0.001	0.001
Al	2.352	1.938	1.959	1.227	1.268	1.313	1.260	1.309	1.220	1.235	1.693	1.707	1.702	1.697	1.697	1.702	1.701	1.694
Cr	0.592	0.948	0.928	1.484	1.445	1.440	1.466	1.406	1.490	1.445	0.275	0.273	0.269	0.277	0.270	0.265	0.269	0.275
Fe <sup>3+</sup>	0.049	0.095	0.094	0.234	0.221	0.206	0.218	0.233	0.236	0.260	0.030	0.018	0.028	0.023	0.032	0.031	0.029	0.029
Fe <sup>2+</sup>	0.322	0.357	0.362	0.526	0.517	0.502	0.520	0.512	0.535	0.538	0.233	0.233	0.225	0.227	0.229	0.230	0.235	0.226
Mn	0.001	0.003	0.005	0.005	0.003	0.004	0.004	0.005	0.006	0.004	0.002	0.002	0.001	0.002	0.002	0.001	0.003	0.002
Zn	0.000	0.000	0.000	0.005	0.004	0.004	0.006	0.005	0.006	0.005	0.003	0.004	0.005	0.003	0.003	0.003	0.005	0.003
Mg	0.679	0.645	0.639	0.482	0.497	0.503	0.488	0.496	0.471	0.473	0.764	0.762	0.769	0.770	0.765	0.767	0.758	0.770
Ca	0.000	0.003	0.000	0.001	0.001	0.000	0.000	0.000	0.000	0.001	0.000	0.000	0.000	0.000	0.000	0.000	0.000	0.000
Cr#	20.1	32.8	32.1	54.7	53.3	52.3	53.8	51.8	55.0	53.9	14.0	13.8	13.6	14.1	13.7	13.5	13.6	14.0
Mg#	67.8	64.4	63.9	47.8	49.0	50.0	48.4	49.2	46.8	46.8	76.6	76.5	77.4	77.3	76.9	76.9	76.3	77.3
Fe <sup>3+</sup> #	1.64	3.26	3.22	7.93	7.56	7.08	7.43	7.95	8.07	8.98	1.53	0.99	1.43	1.15	1.69	1.66	1.43	1.48

Total iron as FeO. Fe<sup>3+</sup> calculations on the basis of spinel stoichiometry; Mg#=100Mg/(Mg+Fe), Cr#=100Cr/(Cr+Al), Fe<sup>3+</sup>#=100Fe<sup>3+</sup>/(Fe<sup>3+</sup>+Cr+Al); c = grain core, r = grain rim.

**Table F-5.** Microprobe analyses and formulae of spinels from different ultramafic lithologies of the Krivaja-Konjuh ophiolite complex

Rock type	Spinel lherzolite																	
Sample-Nr.	o2-45	o2-46	o2-48	o2-50	z2-2	z2-3	z2-5	z2-6	z2-15	z2-16	z2-17	z2-30	z2-38	z2-43	z2-44	z4-1	z4-2	z4-6
Remark	c	r	r	r	c	r	c	r	c	r	r	in(opx)	r	r	c	c	r	r
TiO <sub>2</sub>	0.04	0.05	0.06	0.05	0.04	0.04	0.04	0.05	0.09	0.03	0.05	0.07	0.06	0.04	0.05	0.06	0.06	0.04
Al <sub>2</sub> O <sub>3</sub>	53.59	54.14	53.72	54.01	50.45	50.28	48.03	47.68	51.36	51.56	51.37	50.19	50.46	52.46	51.23	52.74	54.10	54.51
Cr <sub>2</sub> O <sub>3</sub>	12.79	12.80	13.18	12.46	15.41	15.35	15.58	15.02	15.35	15.02	14.88	17.63	15.37	12.88	14.95	14.95	12.84	12.76
Fe <sub>2</sub> O <sub>3</sub>																		
FeO	12.47	12.92	12.90	12.10	14.81	14.59	17.71	18.27	13.18	13.84	14.15	11.77	16.43	14.85	13.20	13.39	14.39	13.71
MnO	0.04	0.02	0.08	0.07	0.12	0.12	0.15	0.03	0.11	0.07	0.09	0.14	0.04	0.12	0.00	0.18	0.06	0.09
ZnO	0.25	0.20	0.24	0.27	0.24	0.30	0.51	0.55	0.24	0.16	0.25	0.17	0.30	0.28	0.26	0.21	0.19	0.23
MgO	19.10	19.00	18.80	19.27	17.55	17.29	16.50	16.10	18.17	17.79	17.26	18.77	15.61	17.32	18.41	18.33	17.91	18.00
CaO	0.00	0.00	0.01	0.01	0.07	0.14	0.03	0.02	0.00	0.00	0.01	0.00	0.02	0.02	0.01	0.00	0.00	0.00
Total	98.28	99.14	98.97	98.24	98.69	98.10	98.54	97.71	98.49	98.48	98.07	98.74	98.29	97.97	98.10	99.86	99.55	99.33
Ti	0.001	0.001	0.001	0.001	0.002	0.002	0.002	0.002	0.004	0.001	0.002	0.003	0.002	0.002	0.002	0.001	0.001	0.001
Al	1.685	1.690	1.683	1.695	2.420	2.427	2.339	2.345	2.451	2.465	2.473	2.394	2.456	2.516	2.450	1.652	1.695	1.707
Cr	0.270	0.268	0.277	0.262	0.496	0.497	0.509	0.496	0.491	0.482	0.480	0.564	0.502	0.414	0.479	0.314	0.270	0.268
Fe <sup>3+</sup>	0.043	0.040	0.037	0.041	0.082	0.074	0.149	0.157	0.052	0.051	0.044	0.038	0.038	0.068	0.068	0.031	0.033	0.024
Fe <sup>2+</sup>	0.235	0.246	0.249	0.229	0.281	0.284	0.308	0.321	0.263	0.279	0.293	0.240	0.353	0.292	0.253	0.267	0.286	0.281
Mn	0.001	0.000	0.002	0.002	0.003	0.003	0.003	0.001	0.003	0.002	0.002	0.003	0.001	0.003	0.000	0.004	0.001	0.002
Zn	0.005	0.004	0.005	0.005	0.005	0.006	0.010	0.011	0.005	0.003	0.005	0.003	0.006	0.006	0.005	0.004	0.004	0.005
Mg	0.760	0.750	0.745	0.765	0.710	0.704	0.678	0.668	0.731	0.717	0.700	0.755	0.641	0.700	0.742	0.726	0.710	0.713
Ca	0.000	0.000	0.000	0.000	0.002	0.004	0.001	0.001	0.000	0.000	0.000	0.000	0.001	0.000	0.000	0.000	0.000	0.000
Cr#	13.8	13.7	14.1	13.4	17.0	17.0	17.9	17.4	16.7	16.3	16.3	19.1	17.0	14.1	16.4	16.0	13.7	13.6
Mg#	76.4	75.3	74.9	77.0	71.6	71.3	68.7	67.6	73.5	72.0	70.5	75.9	64.5	70.6	74.5	73.2	71.2	71.7
Fe <sup>3+</sup> #	2.23	2.06	1.99	2.05	2.77	2.54	5.08	5.26	1.74	1.78	1.59	1.34	1.35	2.39	2.36	1.65	1.73	1.29

Total iron as FeO. Fe<sup>3+</sup> calculations on the basis of spinel stoichiometry; Mg#=100Mg/(Mg+Fe), Cr#=100Cr/(Cr+Al), Fe<sup>3+</sup>#=100Fe<sup>3+</sup>/(Fe<sup>3+</sup>+Cr+Al); c = grain core, r = grain rim, in(opx) = inclusion in opx

**Table F-6.** Microprobe analyses and formulae of spinels from different ultramafic lithologies of the Krivaja-Konjuh ophiolite complex

Rock type	Spinel lherzolite																	
Sample-Nr.	z4-10	z4-12	z4-16	z4-45	z4-46	u35-7a	u35-7b	u35-14	u35-16	u35-24	u35-25	u35-28	u35-43	u35-44	u35-46	u35-47	u35-62	u35-67
Remark	r	r	c	c	r	r	c	r	c	r	c				c	r		
TiO <sub>2</sub>	0.04	0.03	0.03	0.07	0.06	0.25	0.23	0.30	0.26	0.23	0.23	0.18	0.20	0.25	0.25	0.27	0.17	0.30
Al <sub>2</sub> O <sub>3</sub>	54.28	55.23	54.04	52.86	52.37	25.75	26.10	28.09	26.37	26.30	26.71	26.93	28.33	27.65	27.86	29.67	28.87	27.91
Cr <sub>2</sub> O <sub>3</sub>	12.44	11.92	13.61	14.55	14.86	36.61	36.85	35.67	37.66	35.82	34.05	36.97	34.88	36.15	36.23	34.29	34.09	35.40
Fe <sub>2</sub> O <sub>3</sub>																		
FeO	13.62	12.64	12.70	13.81	13.76	27.54	26.61	25.51	25.25	27.41	26.68	25.16	25.01	25.65	25.13	24.66	26.67	25.99
MnO	0.05	0.08	0.07	0.13	0.13	0.21	0.26	0.22	0.15	0.17	0.21	0.17	0.21	0.15	0.17	0.10	0.17	0.21
ZnO	0.12	0.23	0.16	0.19	0.17	0.39	0.41	0.13	0.24	0.23	0.23	0.36	0.34	0.34	0.35	0.28	0.47	0.32
MgO	18.24	18.68	18.64	18.41	18.14	8.99	8.89	10.19	9.83	9.12	9.73	9.50	10.07	9.96	10.02	10.57	9.75	9.65
CaO	0.00	0.00	0.00	0.00	0.01	0.01	0.01	0.01	0.04	0.06	0.16	0.11	0.03	0.03	0.01	0.02	0.05	0.02
Total	98.78	98.82	99.23	100.01	99.51	99.76	99.36	100.12	99.80	99.34	98.00	99.38	99.05	100.17	100.01	99.87	100.22	99.80
Ti	0.001	0.001	0.000	0.001	0.001	0.006	0.005	0.007	0.006	0.005	0.005	0.004	0.005	0.006	0.006	0.006	0.004	0.007
Al	1.705	1.725	1.690	1.653	1.648	0.944	0.960	1.010	0.959	0.965	0.985	0.983	1.027	0.997	1.005	1.060	1.037	1.010
Cr	0.262	0.250	0.285	0.305	0.314	0.901	0.909	0.860	0.919	0.882	0.842	0.906	0.849	0.875	0.877	0.822	0.821	0.860
Fe <sup>3+</sup>	0.031	0.024	0.023	0.040	0.035	0.143	0.119	0.116	0.109	0.143	0.162	0.103	0.115	0.117	0.107	0.106	0.135	0.116
Fe <sup>2+</sup>	0.273	0.256	0.258	0.267	0.272	0.574	0.575	0.535	0.543	0.570	0.535	0.549	0.529	0.539	0.536	0.519	0.545	0.551
Mn	0.001	0.002	0.001	0.003	0.003	0.006	0.007	0.006	0.004	0.004	0.006	0.005	0.005	0.004	0.004	0.003	0.004	0.006
Zn	0.002	0.004	0.003	0.004	0.003	0.009	0.009	0.003	0.005	0.005	0.005	0.008	0.008	0.008	0.008	0.006	0.010	0.007
Mg	0.725	0.738	0.737	0.728	0.722	0.417	0.414	0.463	0.452	0.423	0.454	0.439	0.462	0.454	0.457	0.478	0.443	0.442
Ca	0.000	0.000	0.000	0.000	0.000	0.000	0.000	0.000	0.001	0.002	0.005	0.004	0.001	0.001	0.000	0.001	0.002	0.001
Cr#	13.3	12.6	14.4	15.6	16.0	48.8	48.6	46.0	48.9	47.7	46.1	47.9	45.2	46.7	46.6	43.7	44.2	46.0
Mg#	72.7	74.2	74.0	73.2	72.6	42.1	41.8	46.4	45.5	42.6	45.9	44.4	46.6	45.7	46.0	47.9	44.8	44.5
Fe <sup>3+</sup> #	1.54	1.28	1.24	2.05	1.88	7.20	6.05	5.87	5.53	7.27	8.26	5.24	5.89	5.96	5.45	5.38	6.85	5.89

Total iron as FeO. Fe<sup>3+</sup> calculations on the basis of spinel stoichiometry; Mg#=100Mg/(Mg+Fe), Cr#=100Cr/(Cr+Al), Fe<sup>3+</sup>#=100Fe<sup>3+</sup>/(Fe<sup>3+</sup>+Cr+Al); c = grain core, r = grain rim.

**Table F-7.** Microprobe analyses and formulae of spinels from different ultramafic lithologies of the Krivaja-Konjuh ophiolite complex

Rock type	Spinel Iherzolite – Olivine websterite																	
Sample-Nr.	u35-71	u35-73	r7-39	r7-51	r7-54	r7-27b	r7-21	r7-41	r7-22	r7-28	r7-42	r7-36	r7-32	r7-31	1c-35	1c-13	1c-23	1c-47
Remark							c	c	r	r	r		c	r		c	c	c
TiO <sub>2</sub>	0.24	0.28	0.09	0.13	0.08	0.01	0.02	0.07	0.00	0.00	0.11	0.05	0.08	0.08	0.24	0.21	0.17	0.22
Al <sub>2</sub> O <sub>3</sub>	28.10	26.51	55.65	25.11	25.18	59.02	57.77	55.72	47.07	58.43	53.03	54.97	55.71	55.43	43.57	51.64	52.10	37.06
Cr <sub>2</sub> O <sub>3</sub>	35.06	37.23	10.74	36.94	24.30	6.85	8.17	10.42	9.49	7.47	13.18	11.45	10.47	10.64	22.49	14.45	14.35	26.70
Fe <sub>2</sub> O <sub>3</sub>																		
FeO	25.86	25.73	12.97	24.00	15.56	13.00	13.35	13.22	13.71	13.25	13.53	13.50	12.78	12.93	15.73	13.83	13.66	21.27
MnO	0.21	0.20	0.02	0.09	0.16	0.04	0.13	0.07	0.16	0.12	0.12	0.08	0.03	0.07	0.20	0.12	0.04	0.19
ZnO	0.35	0.27	0.19	0.32	0.15	0.16	0.19	0.18	0.26	0.29	0.10	0.24	0.22	0.18	0.10	0.11	0.09	0.46
MgO	9.97	9.87	19.22	10.08	6.17	19.52	19.22	19.36	21.96	19.47	18.55	19.10	19.20	19.20	17.12	18.57	19.09	13.26
CaO	0.04	0.00	0.03	0.62	14.56	0.01	0.00	0.00	0.03	0.00	0.07	0.04	0.02	0.02	0.02	0.03	0.01	0.01
Total	99.83	100.09	98.90	97.27	86.15	98.63	98.84	99.04	92.70	99.04	98.68	99.43	98.49	98.54	99.46	98.93	99.50	99.15
Ti	0.006	0.007	0.002	0.003	0.002	0.000	0.000	0.001	0.000	0.000	0.002	0.001	0.002	0.001	0.005	0.004	0.003	0.005
Al	1.014	0.961	1.729	0.935	1.023	1.813	1.782	1.727	1.547	1.793	1.671	1.706	1.736	1.728	1.423	1.632	1.632	1.272
Cr	0.849	0.906	0.224	0.923	0.662	0.141	0.169	0.217	0.209	0.154	0.278	0.238	0.219	0.222	0.493	0.306	0.302	0.615
Fe <sup>3+</sup>	0.126	0.120	0.044	0.136	0.310	0.046	0.048	0.053	0.243	0.053	0.047	0.054	0.043	0.047	0.074	0.054	0.059	0.103
Fe <sup>2+</sup>	0.536	0.542	0.242	0.498	0.138	0.237	0.244	0.237	0.077	0.236	0.256	0.243	0.240	0.239	0.291	0.256	0.244	0.415
Mn	0.005	0.005	0.000	0.002	0.005	0.001	0.003	0.002	0.004	0.003	0.003	0.002	0.001	0.002	0.005	0.003	0.001	0.005
Zn	0.008	0.006	0.004	0.007	0.004	0.003	0.004	0.003	0.005	0.005	0.002	0.005	0.004	0.003	0.002	0.002	0.002	0.010
Mg	0.455	0.453	0.755	0.475	0.317	0.758	0.750	0.759	0.913	0.756	0.739	0.750	0.756	0.757	0.707	0.742	0.757	0.576
Ca	0.001	0.000	0.001	0.021	0.538	0.000	0.000	0.000	0.001	0.000	0.002	0.001	0.000	0.001	0.001	0.001	0.000	0.000
Cr#	45.6	48.5	11.5	49.7	39.3	7.2	8.7	11.1	11.9	7.9	14.3	12.3	11.2	11.4	25.7	15.8	15.6	32.6
Mg#	45.9	45.5	75.8	48.8	69.6	76.2	75.5	76.2	92.3	76.2	74.3	75.5	75.9	76.0	70.9	74.3	75.6	58.1
Fe <sup>3+</sup> #	6.34	6.02	2.26	6.88	15.65	2.39	2.46	2.74	12.27	2.69	2.36	2.74	2.18	2.49	3.76	2.79	3.06	5.24

Total iron as FeO. Fe<sup>3+</sup> calculations on the basis of spinel stoichiometry; Mg#=100Mg/(Mg+Fe), Cr#=100Cr/(Cr+Al), Fe<sup>3+</sup>#=100Fe<sup>3+</sup>/(Fe<sup>3+</sup>+Cr+Al); c = grain core, r = grain rim.



**Table F-8.** Microprobe analyses and formulae of spinels from different ultramafic lithologies of the Krivaja-Konjuh ophiolite complex

Rock type	Olivine websterite – Dunite																	
Sample-Nr.	1c-11	1c-16	1c-24	1c-29	1c-32	1c-48	1c-52	1c-54	u19-1	u19-2	u19-7	u19-8	u19-13	u19-14	u19-18	u19-24	u19-25	u19-28
Remark	r	r	r	r	r	r	r	r	r	c	r	c	c	r	r	c	r	r
TiO <sub>2</sub>	0.20	0.15	0.11	0.11	0.14	0.24	0.19	0.26	2.40	2.49	6.66	1.55	1.91	1.64	1.99	1.46	1.27	1.24
Al <sub>2</sub> O <sub>3</sub>	52.02	49.54	53.66	53.12	53.56	37.62	39.59	36.41	18.37	18.36	20.56	21.47	20.44	21.33	21.32	26.12	27.93	26.79
Cr <sub>2</sub> O <sub>3</sub>	13.79	14.00	13.12	13.82	12.67	26.13	24.60	27.42	35.01	34.56	33.22	32.99	30.31	31.88	31.06	32.26	31.24	33.70
Fe <sub>2</sub> O <sub>3</sub>																		
FeO	13.31	13.70	12.88	12.83	13.53	20.47	20.16	21.46	32.59	32.58	30.64	30.43	32.29	31.90	31.06	27.08	24.77	25.32
MnO	0.03	0.10	0.10	0.09	0.07	0.25	0.20	0.19	0.17	0.20	0.36	0.16	0.22	0.28	0.11	0.24	0.20	0.19
ZnO	0.11	0.18	0.18	0.11	0.12	0.42	0.40	0.45	0.00	0.00	0.00	0.00	0.00	0.00	0.00	0.00	0.00	0.00
MgO	18.76	18.02	19.51	18.87	19.36	13.41	13.67	12.72	8.76	8.99	10.30	10.19	9.20	9.23	9.54	11.90	12.25	12.18
CaO	0.01	0.26	0.01	0.06	0.00	0.00	0.00	0.01	0.00	0.01	0.02	0.04	0.00	0.02	0.04	0.02	0.01	0.08
Total	98.22	95.95	99.58	99.00	99.44	98.54	98.79	98.92	97.30	97.19	101.76	96.84	94.36	96.27	95.11	99.08	97.66	99.50
Ti	0.004	0.003	0.002	0.002	0.003	0.005	0.004	0.006	0.059	0.061	0.155	0.038	0.048	0.040	0.049	0.034	0.029	0.028
Al	1.648	1.616	1.667	1.667	1.668	1.294	1.347	1.260	0.709	0.708	0.751	0.813	0.799	0.817	0.824	0.942	1.011	0.959
Cr	0.293	0.306	0.273	0.291	0.265	0.603	0.561	0.636	0.906	0.894	0.814	0.838	0.795	0.820	0.805	0.781	0.758	0.810
Fe <sup>3+</sup>	0.051	0.071	0.055	0.038	0.062	0.093	0.084	0.092	0.266	0.275	0.125	0.274	0.310	0.283	0.273	0.210	0.173	0.174
Fe <sup>2+</sup>	0.249	0.246	0.229	0.248	0.237	0.407	0.403	0.434	0.627	0.617	0.669	0.544	0.586	0.584	0.578	0.484	0.463	0.469
Mn	0.001	0.002	0.002	0.002	0.001	0.006	0.005	0.005	0.005	0.006	0.009	0.004	0.006	0.008	0.003	0.006	0.005	0.005
Zn	0.002	0.004	0.004	0.002	0.002	0.009	0.008	0.010	0.000	0.000	0.000	0.000	0.000	0.000	0.000	0.000	0.000	0.000
Mg	0.752	0.743	0.767	0.749	0.762	0.583	0.588	0.557	0.428	0.439	0.476	0.488	0.455	0.447	0.466	0.543	0.561	0.552
Ca	0.000	0.008	0.000	0.002	0.000	0.000	0.000	0.000	0.000	0.000	0.001	0.001	0.000	0.001	0.001	0.001	0.000	0.003
Cr#	15.1	15.9	14.1	14.9	13.7	31.8	29.4	33.6	56.1	55.8	52.0	50.8	49.9	50.1	49.4	45.3	42.9	45.8
Mg#	75.1	75.1	77.0	75.1	76.3	58.9	59.4	56.2	40.6	41.6	41.6	47.3	43.7	43.4	44.6	52.9	54.8	54.1
Fe <sup>3+</sup> #	2.55	3.63	2.78	1.96	3.14	4.78	4.26	4.74	14.1	14.6	7.45	14.2	16.3	14.7	14.4	10.9	8.94	9.07

Total iron as FeO. Fe<sup>3+</sup> calculations on the basis of spinel stoichiometry; Mg#=100Mg/(Mg+Fe), Cr#=100Cr/(Cr+Al), Fe<sup>3+</sup>#=100Fe<sup>3+</sup>/(Fe<sup>3+</sup>+Cr+Al); c = grain core, r = grain rim.

**Table F-9.** Microprobe analyses and formulae of spinels from different ultramafic lithologies of the Krivaja-Konjuh ophiolite complex

Rock type	Dunite – Chromitites																	
Sample-Nr. Remark	u19-30 r	u19-34 c	u19-35 r	u19-37 r	u19-39 r	k1-1 c	k1-2 r	k1-9 c	k1-10 r	k1-11 r	k1-19 r	k1-22 c	k1-23 r	k1-26 r	d16-1a	d16-1b	d16-2a	d16-2b
TiO <sub>2</sub>	3.91	2.06	2.15	2.14	1.95	0.68	0.71	1.23	1.08	1.21	1.24	1.08	1.07	1.09	0.35	0.43	0.37	0.36
Al <sub>2</sub> O <sub>3</sub>	22.92	19.19	19.14	19.16	19.75	19.88	22.73	18.61	18.79	18.48	18.49	16.17	16.25	16.28	10.89	10.77	10.45	10.30
Cr <sub>2</sub> O <sub>3</sub>	30.34	35.75	36.25	35.51	35.44	43.49	40.17	44.79	44.20	43.05	43.85	46.44	45.50	45.59	54.70	55.78	55.20	54.62
Fe <sub>2</sub> O <sub>3</sub>																		
FeO	29.12	31.65	30.86	31.15	30.48	22.68	23.24	22.06	23.31	25.57	24.25	24.83	27.27	27.35	23.17	22.43	22.96	22.92
MnO	0.30	0.27	0.32	0.30	0.21	0.15	0.29	0.16	0.18	0.25	0.22	0.22	0.23	0.26	0.14	0.01	0.13	0.00
ZnO	0.00	0.00	0.00	0.00	0.14	0.13	0.08	0.16	0.08	0.08	0.17	0.14	0.17	0.00	0.29	0.00	0.27	0.00
MgO	9.85	9.28	9.54	9.43	9.41	11.83	12.07	11.95	11.01	9.49	10.42	10.00	8.23	8.27	9.79	9.77	9.53	9.43
CaO	0.04	0.00	0.00	0.00	0.01	0.01	0.03	0.00	0.00	0.01	0.02	0.00	0.00	0.01	0.00	0.01	0.00	0.00
Total	96.48	98.21	98.26	97.70	97.25	98.86	99.36	98.86	98.73	98.13	98.56	98.90	98.68	99.02	99.04	99.48	98.64	97.88
Ti	0.095	0.050	0.052	0.052	0.048	0.016	0.017	0.029	0.026	0.030	0.030	0.026	0.026	0.027	0.009	0.011	0.009	0.009
Al	0.869	0.730	0.727	0.731	0.755	0.739	0.830	0.695	0.706	0.706	0.699	0.618	0.629	0.628	0.426	0.420	0.412	0.409
Cr	0.771	0.912	0.923	0.909	0.909	1.084	0.984	1.122	1.114	1.103	1.113	1.190	1.182	1.180	1.435	1.459	1.459	1.456
Fe <sup>3+</sup>	0.170	0.258	0.246	0.255	0.241	0.145	0.154	0.125	0.128	0.131	0.128	0.140	0.136	0.137	0.122	0.100	0.111	0.117
Fe <sup>2+</sup>	0.613	0.596	0.585	0.588	0.586	0.453	0.448	0.459	0.494	0.562	0.523	0.533	0.613	0.612	0.521	0.521	0.531	0.529
Mn	0.008	0.007	0.009	0.008	0.006	0.004	0.007	0.004	0.005	0.007	0.006	0.006	0.006	0.007	0.004	0.000	0.004	0.000
Zn	0.000	0.000	0.000	0.000	0.000	0.003	0.003	0.002	0.004	0.002	0.002	0.004	0.003	0.004	0.000	0.007	0.000	0.007
Mg	0.472	0.446	0.458	0.455	0.455	0.556	0.557	0.564	0.523	0.459	0.498	0.483	0.403	0.404	0.484	0.482	0.475	0.474
Ca	0.001	0.000	0.000	0.000	0.000	0.000	0.001	0.000	0.000	0.000	0.001	0.000	0.000	0.000	0.000	0.000	0.000	0.000
Cr#	47.0	55.5	56.0	55.4	54.6	59.5	54.2	61.8	61.2	61.0	61.4	65.8	65.3	65.3	77.1	77.7	78.0	78.1
Mg#	43.5	42.8	43.9	43.6	43.7	55.1	55.4	55.1	51.5	44.9	48.8	47.5	39.7	39.8	48.2	48.1	47.2	47.2
Fe <sup>3+</sup> #	9.45	13.6	13.0	13.5	12.6	7.44	7.86	6.44	6.67	6.85	6.68	7.23	7.08	7.15	6.29	5.06	5.64	5.98

Total iron as FeO. Fe<sup>3+</sup> calculations on the basis of spinel stoichiometry; Mg#=100Mg/(Mg+Fe), Cr#=100Cr/(Cr+Al), Fe<sup>3+</sup>#=100Fe<sup>3+</sup>/(Fe<sup>3+</sup>+Cr+Al); c = grain core, r = grain rim.

**Table F-10.** Microprobe analyses and formulae of spinels from different ultramafic lithologies of the Krivaja-Konjuh ophiolite complex

Rock type	Chromitite																	
Sample-Nr.	d16-6a	d16-6b	d16-7a	d16-7b	d16-9a	d16-9b	d16-10a	d16-10b	d16-13a	d16-13b	d16-19a	d16-19b	d16-20a	d16-20b	d17-1ad17-1b	d17-2a	d17-2b	
Remark																		
TiO <sub>2</sub>	0.37	0.33	0.37	0.35	0.43	0.43	0.37	0.38	0.32	0.35	0.05	0.02	0.05	0.04	0.32	0.30	0.27	0.30
Al <sub>2</sub> O <sub>3</sub>	10.47	10.40	10.39	10.45	13.05	13.30	12.67	12.80	12.73	12.80	32.98	32.68	35.77	32.94	12.32	12.42	11.47	11.55
Cr <sub>2</sub> O <sub>3</sub>	54.17	54.32	54.23	54.20	51.47	51.63	53.12	53.19	52.71	52.18	31.58	31.41	27.43	28.88	51.73	52.82	53.05	53.29
Fe <sub>2</sub> O <sub>3</sub>																		
FeO	23.22	23.86	24.01	23.95	23.78	23.75	23.29	22.97	23.65	23.51	20.97	21.16	22.44	25.17	24.88	24.22	24.81	25.07
MnO	0.01	0.04	0.00	0.07	0.00	0.11	0.06	0.11	0.04	0.14	0.12	0.11	0.20	0.16	0.10	0.03	0.09	0.16
ZnO	0.22	0.00	0.21	0.00	0.25	0.00	0.23	0.00	0.20	0.00	0.33	0.00	0.40	0.00	0.13	0.19	0.00	0.00
MgO	9.58	9.48	9.41	9.48	9.95	10.21	9.83	9.84	10.10	10.08	13.13	13.19	12.39	11.21	9.62	9.69	9.10	9.11
CaO	0.01	0.00	0.00	0.00	0.00	0.00	0.00	0.00	0.01	0.05	0.03	0.01	0.07	0.05	0.00	0.00	0.04	0.00
Total	97.82	98.64	98.41	98.71	98.68	99.67	99.34	99.52	99.55	99.31	98.86	98.91	98.35	98.85	98.97	99.60	99.01	99.49
Ti	0.009	0.008	0.009	0.009	0.011	0.011	0.009	0.009	0.008	0.009	0.001	0.000	0.001	0.001	0.008	0.007	0.007	0.007
Al	0.415	0.410	0.410	0.412	0.506	0.510	0.490	0.494	0.490	0.494	1.153	1.143	1.248	1.165	0.479	0.480	0.450	0.451
Cr	1.441	1.436	1.437	1.432	1.340	1.329	1.379	1.378	1.362	1.351	0.741	0.737	0.642	0.685	1.350	1.370	1.394	1.394
Fe <sup>3+</sup>	0.125	0.137	0.134	0.139	0.132	0.140	0.113	0.109	0.132	0.138	0.104	0.119	0.108	0.147	0.155	0.135	0.142	0.141
Fe <sup>2+</sup>	0.528	0.530	0.539	0.530	0.522	0.506	0.526	0.520	0.515	0.506	0.416	0.407	0.447	0.485	0.532	0.529	0.547	0.553
Mn	0.000	0.001	0.000	0.002	0.000	0.003	0.002	0.003	0.001	0.004	0.003	0.003	0.005	0.004	0.003	0.001	0.002	0.005
Zn	0.000	0.005	0.000	0.005	0.000	0.006	0.000	0.006	0.000	0.005	0.000	0.007	0.000	0.009	0.000	0.003	0.005	0.000
Mg	0.481	0.472	0.470	0.472	0.488	0.495	0.481	0.481	0.492	0.492	0.581	0.584	0.547	0.502	0.473	0.474	0.451	0.450
Ca	0.000	0.000	0.000	0.000	0.000	0.000	0.000	0.000	0.000	0.002	0.001	0.000	0.002	0.002	0.000	0.000	0.001	0.000
Cr#	77.6	77.8	77.8	77.7	72.6	72.3	73.8	73.6	73.5	73.2	39.1	39.2	34.0	37.0	73.8	74.1	75.6	75.6
Mg#	47.6	47.1	46.6	47.1	48.3	49.5	47.8	48.0	48.9	49.3	58.2	58.9	55.0	50.8	47.1	47.2	45.2	44.8
Fe <sup>3+</sup> #	6.34	6.98	6.83	7.09	6.77	7.15	5.79	5.54	6.67	6.98	5.23	5.99	5.45	7.48	7.87	6.80	7.24	7.18

Total iron as FeO. Fe<sup>3+</sup> calculations on the basis of spinel stoichiometry; Mg#=100Mg/(Mg+Fe), Cr#=100Cr/(Cr+Al), Fe<sup>3+</sup>#=100Fe<sup>3+</sup>/(Fe<sup>3+</sup>+Cr+Al); c = grain core, r = grain rim.

**Table F-11.** Microprobe analyses and formulae of spinels from different ultramafic lithologies of the Krivaja-Konjuh ophiolite complex

Rock type	Chromitite																	
Sample-Nr.	d17-33a	d17-33b	d17-34a	d17-34b	d17-41a	d17-41b	d17-42a	d17-42b	d17-44a	d17-44b	d16-20b	d18-01a	d18-01b	d18-02a	d18-02b	d18-06a	d18-06b	d18-10a
Remark																		
TiO <sub>2</sub>	0.02	0.00	0.04	0.06	0.06	0.04	0.00	0.02	0.03	0.09	0.04	0.23	0.30	0.25	0.24	0.19	0.23	0.30
Al <sub>2</sub> O <sub>3</sub>	40.35	40.37	37.89	38.14	40.14	40.53	40.04	39.93	23.11	18.25	32.94	11.87	11.91	12.77	12.68	12.55	12.48	12.64
Cr <sub>2</sub> O <sub>3</sub>	23.74	23.26	25.68	25.89	23.03	22.91	23.75	23.55	33.74	38.06	28.88	56.47	56.05	53.59	54.15	55.48	55.21	53.97
Fe <sub>2</sub> O <sub>3</sub>																		
FeO	19.19	19.36	19.54	19.49	19.94	19.75	19.89	19.52	25.60	24.32	25.17	20.22	20.75	20.72	20.59	21.53	21.04	20.05
MnO	0.05	0.10	0.05	0.10	0.05	0.06	0.03	0.05	0.16	0.13	0.16	0.09	0.11	0.10	0.08	0.07	0.10	0.08
ZnO	0.42	0.00	0.38	0.00	0.51	0.00	0.54	0.00	0.26	0.40	0.40	0.00	0.14	0.00	0.24	0.00	0.20	0.00
MgO	14.93	14.73	14.50	14.29	14.38	14.28	14.46	14.26	11.25	11.36	11.21	10.75	10.71	10.25	10.44	10.32	10.06	10.89
CaO	0.05	0.07	0.02	0.01	0.00	0.00	0.00	0.01	0.05	0.04	0.05	0.00	0.00	0.02	0.00	0.00	0.02	0.00
Total	98.34	98.31	97.71	98.35	97.60	98.09	98.16	97.90	93.95	92.52	98.85	99.62	99.96	97.70	98.41	100.13	99.34	97.93
Ti	0.000	0.000	0.001	0.001	0.001	0.001	0.000	0.000	0.001	0.002	0.001	0.006	0.007	0.006	0.006	0.005	0.006	0.007
Al	1.362	1.365	1.301	1.304	1.368	1.376	1.359	1.361	0.885	0.723	1.165	0.457	0.457	0.500	0.493	0.481	0.483	0.492
Cr	0.537	0.527	0.591	0.594	0.527	0.522	0.541	0.538	0.867	1.011	0.685	1.459	1.444	1.407	1.412	1.427	1.433	1.409
Fe <sup>3+</sup>	0.100	0.108	0.107	0.100	0.102	0.100	0.100	0.100	0.246	0.262	0.147	0.073	0.084	0.080	0.083	0.083	0.072	0.084
Fe <sup>2+</sup>	0.360	0.357	0.369	0.372	0.380	0.375	0.379	0.372	0.450	0.422	0.485	0.480	0.481	0.495	0.485	0.503	0.505	0.469
Mn	0.001	0.002	0.001	0.003	0.001	0.001	0.001	0.001	0.005	0.004	0.004	0.002	0.003	0.003	0.002	0.002	0.003	0.002
Zn	0.000	0.009	0.000	0.008	0.000	0.011	0.000	0.011	0.000	0.006	0.009	0.000	0.003	0.000	0.006	0.000	0.005	0.000
Mg	0.638	0.630	0.630	0.618	0.620	0.613	0.621	0.615	0.545	0.569	0.502	0.523	0.520	0.507	0.513	0.500	0.493	0.536
Ca	0.002	0.002	0.001	0.000	0.000	0.000	0.000	0.000	0.002	0.001	0.002	0.000	0.000	0.001	0.000	0.000	0.001	0.000
Cr#	28.3	27.9	31.3	31.3	27.8	27.5	28.5	28.3	49.5	58.3	37.0	76.1	75.9	73.8	74.1	74.8	74.8	74.1
Mg#	63.9	63.8	63.0	62.4	62.0	62.0	62.1	62.3	54.8	57.4	50.8	52.2	51.9	50.6	51.4	49.9	49.4	53.3
Fe <sup>3+</sup> #	5.05	5.49	5.34	5.00	5.13	5.09	5.07	5.00	12.3	13.1	7.43	3.79	4.26	4.08	4.24	4.27	3.69	4.35

Total iron as FeO. Fe<sup>3+</sup> calculations on the basis of spinel stoichiometry; Mg#=100Mg/(Mg+Fe), Cr#=100Cr/(Cr+Al), Fe<sup>3+</sup>#=100Fe<sup>3+</sup>/(Fe<sup>3+</sup>+Cr+Al); c = grain core, r = grain rim.

Plagioclase

**Table G-1.** Microprobe analyses and formulae of plagioclase from different lithologies of the Krivaja-Konjuh ophiolite complex

Rock type	Plagioclase Iherzolite – Olivine websterite													
Sample-Nr.	gr12-35	gr12-36	gr12-47	gr12-48	m2-21	m2-22	m2-23	m2-27	d3-13	d3-9	d3-14	4a-15	1c-8	1c-10
Remark	r	c	c	r	c	r	a	r	r	c	c		a	a
SiO <sub>2</sub>	48.06	48.61	48.21	48.16	46.09	45.42	32.94	44.25	47.78	47.56	49.09	53.68	46.50	46.26
Al <sub>2</sub> O <sub>3</sub>	32.55	32.87	32.83	33.12	34.47	34.99	27.67	33.74	32.76	32.45	32.06	29.42	32.57	33.21
Fe <sub>2</sub> O <sub>3</sub>	0.21	0.16	0.18	0.24	0.13	0.12	0.91	0.15	0.30	0.20	0.14	0.11	0.21	0.26
BaO	0.00	0.00	0.00	0.00	0.00	0.00	0.00	0.00	0.00	0.00	0.00	0.00	0.00	0.00
CaO	15.79	15.69	15.77	15.85	18.31	18.45	29.33	20.13	16.10	15.71	15.08	11.94	16.74	16.81
Na <sub>2</sub> O	2.40	2.52	2.43	2.40	1.41	1.22	0.03	1.31	2.48	2.72	2.98	4.98	2.02	2.01
K <sub>2</sub> O	0.01	0.01	0.00	0.00	0.00	0.01	0.00	0.00	0.01	0.02	0.01	0.02	0.00	0.04
Total	99.01	99.85	99.41	99.77	100.42	100.20	90.87	99.58	99.44	98.67	99.37	100.15	98.03	98.59
Si	2.220	2.225	2.218	2.209	2.116	2.091	1.789	2.068	2.204	2.209	2.256	2.424	2.179	2.158
Al	1.773	1.773	1.780	1.790	1.865	1.898	1.772	1.859	1.780	1.777	1.737	1.566	1.799	1.826
Fe <sup>3+</sup>	0.007	0.006	0.006	0.008	0.004	0.004	0.037	0.005	0.010	0.007	0.005	0.004	0.007	0.009
Ba	0.000	0.000	0.000	0.000	0.000	0.000	0.000	0.000	0.000	0.000	0.000	0.000	0.000	0.000
Ca	0.782	0.769	0.777	0.779	0.901	0.910	1.707	1.008	0.796	0.782	0.743	0.578	0.840	0.840
Na	0.215	0.224	0.217	0.213	0.126	0.109	0.003	0.119	0.222	0.245	0.266	0.436	0.183	0.182
K	0.000	0.000	0.000	0.000	0.000	0.001	0.000	0.000	0.001	0.001	0.000	0.001	0.000	0.002
Or	0.04	0.02	0.03	0.02	0.05	0.18	0.01	0.02	0.13	0.11	0.02	0.16	0.02	0.25
Ab	21.6	22.5	21.8	21.5	12.3	10.7	0.2	10.6	21.8	23.8	26.3	43.0	17.9	17.8
An	78.4	77.4	78.2	78.5	87.7	89.3	99.8	89.4	78.2	76.0	73.6	56.9	82.1	82.0

Formulae of plagioclase calculated on the basis of 8 oxygens, FeO<sub>tot</sub> is expressed as Fe<sub>2</sub>O<sub>3</sub>, c = grain core, r = grain rim, a = plagioclase affected by alteration

Other phases

**Table H-1.** Microprobe analyses and formulae of minor phases from different ultramafic lithologies of the Krivaja-Konjuh ophiolite complex

Sample-Nr.	z4-11	z4-28	z4-29	z4-30	z4-31	u35-33b	u35-33	u35-54	u35-57	1c-34b	u19-43	d5-36	4a-34	u35-56	1c-22	u19-11	2a-43	2a-43a
Phase	Amph	Amph	Amph	Amph	Amph	Amph	Amph	Amph	Amph	Amph	Amph	Chl	Chl	Chl	Chl	Chl	Hib	Hib
Host Rock	Sp lherz.	Sp lherz.	Sp lherz.	Sp lherz.	Sp lherz.	Sp lherz.	Sp lherz.	Sp lherz.	Sp lherz.	Ol webst.	Dunite	Pl lherz.	Pl lherz.	Sp lherz.	Ol webst.	Dunite	Ol webst.	Ol webst.
SiO <sub>2</sub>	53.60	54.94	55.59	55.33	56.18	44.45	44.95	44.38	44.30	41.28	39.76	30.80	28.32	32.40	26.76	26.62	30.37	30.28
TiO <sub>2</sub>	0.36	0.39	0.23	0.15	0.09	1.45	1.44	1.53	1.45	0.11	1.11	0.02	0.01	0.09	0.01	0.02	0.01	0.00
Al <sub>2</sub> O <sub>3</sub>	4.38	3.43	2.95	2.14	2.01	11.57	11.56	12.06	12.10	13.76	12.55	13.02	16.26	17.70	21.06	18.49	22.08	22.64
Cr <sub>2</sub> O <sub>3</sub>	0.48	0.40	0.41	0.30	0.54	1.68	1.53	1.60	1.52	0.04	0.73	0.08	0.01	0.18	0.03	0.00	0.00	0.00
Fe <sub>2</sub> O <sub>3</sub>	1.35	0.00	0.27	0.00	0.00	0.00	0.00	0.00	0.00	6.53	9.66	0.00	0.00	0.00	0.00	0.00	1.10	0.93
FeO	1.20	3.52	3.09	3.40	3.60	4.17	4.23	4.00	4.24	0.00	3.67	17.10	21.07	9.89	18.45	26.33	0.00	0.00
MnO	0.00	0.12	0.15	0.10	0.13	0.02	0.03	0.10	0.05	0.13	0.11	0.39	0.66	0.95	0.20	1.26	0.05	0.00
MgO	22.32	21.94	22.50	22.14	23.25	17.90	18.14	17.67	17.94	23.76	17.78	23.92	19.49	24.13	19.00	12.09	0.09	0.00
CaO	12.74	12.16	12.15	12.20	10.85	12.22	12.36	12.10	12.15	9.36	8.99	0.13	0.43	1.91	0.28	0.49	38.08	38.06
Na <sub>2</sub> O	0.65	0.49	0.40	0.52	0.31	2.76	2.74	2.55	2.62	1.37	2.63	0.05	0.05	0.16	0.15	0.05	0.05	0.01
K <sub>2</sub> O	0.02	0.02	0.00	0.15	0.00	0.08	0.08	0.10	0.09	0.02	0.34	0.02	0.00	0.03	0.01	0.00	0.01	0.01
H <sub>2</sub> O	2.17	2.17	2.18	2.15	2.17	2.08	2.10	2.08	2.08	2.10	2.05	11.58	11.41	12.31	11.58	10.93	6.08	6.10
Total	99.27	99.58	99.93	98.56	99.12	98.37	99.16	98.17	98.53	98.46	99.37	97.09	97.70	99.73	97.55	96.28	97.91	98.02
Si	7.420	7.600	7.647	7.731	7.766	6.409	6.426	6.398	6.371	5.883	5.817	3.189	2.977	3.157	2.771	2.920	2.993	2.976
Ti	0.037	0.040	0.024	0.016	0.009	0.157	0.154	0.165	0.156	0.012	0.122	0.002	0.001	0.006	0.001	0.002	0.000	0.000
Al	0.715	0.560	0.478	0.352	0.327	1.966	1.948	2.049	2.052	2.311	2.165	1.588	2.015	2.032	2.571	2.390	2.565	2.623
Cr	0.052	0.044	0.045	0.033	0.059	0.191	0.173	0.182	0.173	0.005	0.084	0.006	0.001	0.014	0.003	0.000	0.000	0.000
Fe <sup>3+</sup>	0.141	0.000	0.028	0.000	0.000	0.000	0.000	0.000	0.000	0.701	1.063	0.000	0.000	0.000	0.000	0.000	0.082	0.069
Fe <sup>2+</sup>	0.139	0.407	0.355	0.397	0.416	0.502	0.506	0.482	0.510	0.000	0.449	1.481	1.853	0.806	1.598	2.415	0.000	0.000
Mn	0.000	0.013	0.018	0.012	0.016	0.003	0.004	0.012	0.006	0.016	0.014	0.034	0.059	0.078	0.018	0.117	0.004	0.000
Mg	4.606	4.524	4.614	4.611	4.792	3.847	3.867	3.798	3.846	5.048	3.877	3.692	3.055	3.504	2.933	1.977	0.013	0.000
Ca	1.890	1.802	1.791	1.826	1.606	1.888	1.894	1.868	1.873	1.430	1.409	0.015	0.048	0.199	0.031	0.057	4.022	4.009
Na	0.174	0.132	0.106	0.140	0.082	0.772	0.761	0.713	0.730	0.378	0.746	0.009	0.011	0.030	0.031	0.011	0.009	0.001
K	0.003	0.004	0.001	0.026	0.000	0.014	0.014	0.019	0.017	0.003	0.063	0.002	0.000	0.004	0.002	0.000	0.001	0.001
OH <sup>-</sup>	2.000	2.000	2.000	2.000	2.000	2.000	2.000	2.000	2.000	2.000	2.000	8.000	8.000	8.000	8.000	8.000	4.000	4.000
Mg#	0.94	0.92	0.92	0.92	0.92	0.88	0.88	0.89	0.88	0.88	0.72	0.71	0.62	0.81	0.65	0.45		
Sum A	0.178	0.126	0.107	0.144	0.073	0.749	0.746	0.687	0.733	0.381	0.810							
Al <sup>IV</sup>	0.580	0.400	0.353	0.269	0.23	1.591	1.574	1.602	1.629	2.117	2.165							

Amphibole formulae calculated on the basis of 23 oxygens with fixed number of cations (15) and Fe<sup>3+</sup>/Fe<sup>2+</sup> adjustment. Chlorite formulae calculated on the basis of 14 oxygens and total iron as FeO. Hibschie formulae calculated on the basis of ideal stoichiometric proportion of 12 oxygens and 4OH<sup>-</sup>. Amph = amphibole, Chl = chlorite, Hib = hibschie, Sp lherz. = Sp lherzolite, Ol webst. = Ol websterite, Pl lherz. = Pl lherzolite, UM cum = cumulate texture ultramafic rocks

**Table H-2.** Microprobe analyses and formulae of minor phases from different ultramafic lithologies of the Krivaja-Konjuh ophiolite complex

Sample-Nr.	4a-44	4a-45	u19-16	4a-17	gr2-52	m2-30	u4-64	o2-19	z4-27	u35-6	1c-46b	u19-10	k1-6	r7-30
Phase	Pec	Pec	Prh	Srp	Srp	Srp	Srp	Srp	Srp	Srp	Srp	Srp	Srp	Srp
Host Rock	PI Iherz.	PI Iherz.	UM cum.	PI Iherz.	PI Iherz.	PI Iherz.	PI Iherz.	Sp Iherz.	Sp Iherz.	Sp Iherz.	OI webst.	Dunite	Dunite	Sp Iherz.
SiO <sub>2</sub>	52.73	45.90	43.22	35.96	38.99	34.23	40.15	37.04	39.58	37.65	40.58	39.77	39.43	41.01
TiO <sub>2</sub>	0.01	0.02	0.04	0.00	0.00	0.00	0.00	0.02	0.01	1.24	0.05	0.00	0.00	0.02
Al <sub>2</sub> O <sub>3</sub>	0.79	5.31	24.55	0.67	0.46	0.08	0.90	2.64	1.29	3.02	6.91	1.32	2.20	0.53
Cr <sub>2</sub> O <sub>3</sub>	0.08	0.03	0.01	0.02	0.00	0.00	0.01	0.17	0.02	0.85	0.45	0.00	0.02	0.00
Fe <sub>2</sub> O <sub>3</sub>	0.00	0.00	0.00	7.36	6.81	10.66	2.41	2.21	0.00	0.00	0.00	2.87	0.57	0.00
FeO	0.38	2.65	0.12	0.00	0.00	0.00	2.97	6.08	9.96	11.76	6.57	3.42	4.67	5.21
MnO	0.07	0.04	0.05	0.10	0.06	0.06	0.02	0.24	0.23	0.19	0.14	0.01	0.10	0.08
MgO	0.12	0.33	0.11	39.66	40.68	40.99	39.11	34.46	31.89	32.25	31.48	38.59	37.41	38.31
CaO	33.70	34.24	26.67	0.12	0.05	0.05	0.03	0.11	0.80	0.10	0.26	0.17	0.05	0.11
Na <sub>2</sub> O	8.53	5.78	0.02	0.00	0.00	0.02	0.03	0.00	0.03	0.00	0.04	0.00	0.02	0.00
K <sub>2</sub> O	0.01	0.01	0.00	0.02	0.00	0.00	0.00	0.02	0.01	0.00	0.01	0.00	0.00	0.00
H <sub>2</sub> O	2.68	2.58	4.54	12.06	12.61	12.15	12.46	11.84	11.86	12.14	12.58	12.48	12.27	12.39
Total	99.08	96.90	99.33	95.98	99.67	98.23	98.09	94.81	95.66	99.19	99.08	98.63	96.74	97.67
Si	2.951	2.667	2.857	1.788	1.854	1.689	1.932	1.876	2.001	1.860	1.934	1.911	1.927	1.985
Ti	0.000	0.001	0.002	0.000	0.000	0.000	0.000	0.001	0.000	0.046	0.002	0.000	0.000	0.001
Al	0.052	0.364	1.913	0.039	0.026	0.004	0.051	0.157	0.077	0.176	0.388	0.075	0.127	0.030
Cr	0.004	0.001	0.000	0.001	0.000	0.000	0.000	0.007	0.001	0.033	0.017	0.000	0.001	0.000
Fe <sup>3+</sup>	0.000	0.000	0.000	0.275	0.244	0.396	0.087	0.084	0.000	0.000	0.000	0.104	0.021	0.000
Fe <sup>2+</sup>	0.018	0.129	0.007	0.000	0.000	0.000	0.119	0.258	0.421	0.486	0.262	0.137	0.191	0.211
Mn	0.003	0.002	0.003	0.004	0.002	0.002	0.001	0.010	0.010	0.008	0.006	0.000	0.004	0.003
Mg	0.010	0.028	0.011	2.940	2.883	3.015	2.805	2.601	2.404	2.375	2.237	2.764	2.726	2.764
Ca	2.020	2.131	1.889	0.006	0.002	0.002	0.002	0.006	0.044	0.005	0.013	0.009	0.003	0.006
Na	0.926	0.651	0.002	0.000	0.000	0.002	0.003	0.000	0.003	0.000	0.003	0.000	0.002	0.000
K	0.001	0.001	0.000	0.001	0.000	0.000	0.000	0.001	0.000	0.000	0.000	0.000	0.000	0.000
OH <sup>-</sup>	1.000	1.000	2.000	4.000	4.000	4.000	4.000	4.000	4.000	4.000	4.000	4.000	4.000	4.000
Mg#	0.35	0.18	0.62	0.91	0.92	0.88	0.93	0.88	0.85	0.83	0.90	0.92	0.93	0.93

Pectolite formulae calculated on the basis of 8 oxygens. Prehnite formulae calculated on the basis of 10.5 oxygens and total iron as FeO. Serpentine formulae calculated on the basis of 7 oxygens. Pec = pectolite, Prh = prehnite, Srp = serpentine, Sp Iherz. = Sp Iherzolite, OI webst. = OI websterite, PI Iherz. = PI Iherzolite, UM cum = cumulate texture ultramafic rocks

## Metamorphic sole

### *Amphibole*

**Table I-1.** Microprobe analyses and formulae of amphibole from different metamorphic rock varieties of the Krivaja-Konjuh ophiolite complex

Rock type	Granoblastic amphibolite																	
Sample-Nr.	u30-9	u30-11	u30-28	u30-1	u30-6	u30-15	u30-22	u30-32	u30-2	u30-5	u30-14	u30-17	u30-21	u30-27	u30-34	u30-40	u30-41	u29-18
Remark				c	c	c	c	sp	r	r	r	r	r	r		c	r	c
SiO <sub>2</sub>	46.09	46.68	46.00	46.26	46.17	46.32	45.99	45.96	46.54	46.32	45.75	45.94	46.08	46.05	46.00	45.93	45.62	42.24
TiO <sub>2</sub>	0.14	0.12	0.12	0.14	0.12	0.15	0.13	0.09	0.11	0.14	0.16	0.14	0.16	0.14	0.12	0.14	0.17	0.11
Al <sub>2</sub> O <sub>3</sub>	15.67	15.73	15.62	15.20	15.52	15.69	15.56	15.86	15.34	15.50	15.99	15.47	15.61	15.81	15.63	15.71	15.51	17.44
Cr <sub>2</sub> O <sub>3</sub>	0.04	0.03	0.15	0.02	0.06	0.10	0.10	0.18	0.04	0.08	0.05	0.11	0.18	0.10	0.29	0.10	0.21	0.23
FeO	4.85	4.65	4.82	4.60	4.76	4.76	4.73	4.45	4.73	4.76	4.74	4.88	4.98	4.98	4.69	5.24	5.09	4.61
MnO	0.03	0.13	0.09	0.08	0.03	0.10	0.11	0.13	0.13	0.05	0.17	0.11	0.15	0.09	0.07	0.10	0.12	0.07
MgO	17.09	17.46	17.15	17.60	17.20	17.30	17.31	17.10	17.52	17.54	17.15	17.36	17.50	17.44	17.29	17.14	16.98	15.90
CaO	11.90	11.84	11.93	11.72	11.97	11.69	11.87	11.86	11.69	11.72	11.62	11.84	11.74	11.79	11.81	12.02	11.95	13.31
Na <sub>2</sub> O	1.74	1.70	1.68	1.58	1.76	1.70	1.60	1.77	1.68	1.64	1.52	1.67	1.63	1.64	1.67	1.75	1.74	2.43
K <sub>2</sub> O	0.04	0.03	0.03	0.05	0.04	0.04	0.06	0.05	0.05	0.05	0.16	0.05	0.04	0.03	0.03	0.06	0.05	0.29
Total	97.68	98.49	97.73	97.36	97.79	97.93	97.55	97.58	97.93	97.91	97.43	97.63	98.16	98.13	97.69	98.29	97.51	96.63
Si	6.457	6.477	6.444	6.486	6.466	6.466	6.443	6.442	6.496	6.464	6.421	6.435	6.418	6.412	6.440	6.408	6.416	6.038
Al <sup>IV</sup>	1.543	1.523	1.556	1.514	1.534	1.534	1.557	1.558	1.504	1.536	1.579	1.565	1.582	1.588	1.560	1.592	1.584	1.962
Al <sup>VI</sup>	1.045	1.049	1.023	0.997	1.027	1.047	1.011	1.062	1.020	1.012	1.066	0.989	0.980	1.007	1.019	0.991	0.986	0.975
Ti	0.015	0.012	0.013	0.015	0.013	0.015	0.013	0.010	0.012	0.015	0.017	0.015	0.017	0.015	0.012	0.014	0.017	0.012
Cr	0.005	0.003	0.016	0.002	0.007	0.011	0.012	0.020	0.005	0.009	0.005	0.012	0.020	0.011	0.032	0.011	0.024	0.026
Fe <sup>3+</sup>	0.000	0.000	0.030	0.049	0.000	0.000	0.063	0.000	0.000	0.033	0.030	0.074	0.101	0.093	0.027	0.076	0.058	0.211
Mg	3.570	3.611	3.582	3.678	3.591	3.601	3.615	3.573	3.645	3.649	3.589	3.624	3.633	3.619	3.608	3.565	3.559	3.388
Mn	0.003	0.015	0.011	0.010	0.004	0.011	0.013	0.016	0.015	0.006	0.020	0.013	0.018	0.010	0.008	0.012	0.014	0.008
Fe <sup>2+</sup>	0.362	0.308	0.326	0.250	0.358	0.314	0.273	0.320	0.304	0.275	0.273	0.274	0.232	0.245	0.294	0.331	0.341	0.341
Fe <sup>2+</sup>	0.206	0.231	0.209	0.240	0.199	0.241	0.219	0.202	0.248	0.248	0.253	0.224	0.248	0.242	0.229	0.204	0.199	0.000
Ca	1.786	1.760	1.791	1.760	1.796	1.748	1.781	1.781	1.748	1.752	1.747	1.776	1.752	1.758	1.771	1.796	1.801	2.039
Na	0.464	0.449	0.456	0.429	0.473	0.449	0.434	0.465	0.451	0.443	0.414	0.454	0.441	0.442	0.452	0.474	0.473	0.673
K	0.006	0.005	0.006	0.009	0.006	0.007	0.011	0.008	0.009	0.010	0.029	0.008	0.006	0.005	0.006	0.011	0.009	0.053
Mg#	0.86	0.87	0.87	0.88	0.87	0.87	0.88	0.87	0.87	0.87	0.87	0.88	0.88	0.88	0.87	0.87	0.87	0.91

Amphibole formulae calculated on the basis of 23 oxygens with fixed number of cations (15) and Fe<sup>3+</sup>/Fe<sup>2+</sup> adjustment. Mg# = Mg/(Mg+Fe<sup>2+</sup>). c = grain core. r = grain rim. sp = inclusion in spinel



**Table I-2.** Microprobe analyses and formulae of amphibole from different metamorphic rock varieties of the Krivaja-Konjuh ophiolite complex

Rock type	Granoblastic amphibolite																	
Sample-Nr.	u29-29	u29-41	u29-50	u29-61	u29-64	u29-19	u29-25	u29-26	u29-30	u29-42	u29-46	u29-49	u29-56	u29-58	u29-65	11c-24	11c-1	11c-25
Remark	c	c	c	c	c	r	r	r	r	r	r	r	r	r	r	sec		
SiO <sub>2</sub>	42.38	42.72	41.36	42.15	42.14	41.30	41.68	41.21	42.31	41.93	41.59	41.56	40.28	42.08	42.01	46.76	46.25	48.27
TiO <sub>2</sub>	0.10	0.10	0.13	0.18	0.14	0.15	0.09	0.08	0.10	0.12	0.13	0.08	0.12	0.12	0.10	0.05	0.61	0.28
Al <sub>2</sub> O <sub>3</sub>	16.73	17.67	17.91	17.62	17.49	17.59	17.30	17.50	16.95	17.52	20.22	17.80	18.15	17.58	18.03	5.97	9.74	8.15
Cr <sub>2</sub> O <sub>3</sub>	1.27	0.35	0.33	0.21	0.68	0.51	0.63	0.69	0.66	0.60	0.58	0.39	0.62	0.34	0.32	0.04	0.09	0.01
Fe <sub>2</sub> O <sub>3</sub>																		
FeO	4.54	4.23	4.49	4.47	4.28	4.57	4.52	4.76	4.66	4.36	4.14	4.37	4.92	4.20	4.38	11.07	12.45	12.10
MnO	0.05	0.10	0.00	0.03	0.05	0.03	0.01	0.05	0.07	0.10	0.05	0.09	0.05	0.08	0.06	0.25	0.19	0.18
MgO	15.67	15.63	15.70	16.14	15.99	15.66	15.78	15.80	15.96	15.60	13.02	15.85	15.48	16.12	15.71	14.99	14.09	14.93
CaO	13.03	13.26	13.34	13.12	13.27	13.22	13.04	13.41	13.17	13.18	13.05	13.18	13.19	13.21	12.95	17.23	11.75	12.03
Na <sub>2</sub> O	2.29	2.34	2.72	2.58	2.41	2.64	2.70	2.65	2.50	2.36	2.66	2.72	2.70	2.66	2.37	0.43	1.90	1.51
K <sub>2</sub> O	0.28	0.30	0.33	0.33	0.27	0.35	0.29	0.36	0.27	0.32	0.56	0.32	0.69	0.34	0.31	0.00	0.05	0.02
Total	96.34	96.68	96.31	96.82	96.72	96.01	96.04	96.50	96.66	96.08	96.00	96.35	96.20	96.72	96.23	96.79	97.16	97.52
Si	6.092	6.102	5.950	6.017	6.016	5.962	6.016	5.921	6.059	6.034	5.992	5.972	5.831	6.016	6.025	6.743	6.773	6.994
Al <sup>IV</sup>	1.908	1.898	2.050	1.983	1.984	2.038	1.984	2.079	1.941	1.966	2.008	2.028	2.169	1.984	1.975	1.015	1.227	1.006
Al <sup>VI</sup>	0.927	1.076	0.987	0.981	0.958	0.955	0.958	0.885	0.920	1.005	1.425	0.987	0.927	0.979	1.073	0.000	0.453	0.386
Ti	0.010	0.010	0.014	0.019	0.015	0.017	0.010	0.009	0.011	0.013	0.014	0.009	0.013	0.013	0.011	0.005	0.067	0.030
Cr	0.144	0.040	0.038	0.023	0.077	0.058	0.072	0.079	0.075	0.068	0.066	0.044	0.071	0.038	0.037	0.004	0.011	0.001
Fe <sup>3+</sup>	0.127	0.060	0.178	0.166	0.201	0.190	0.125	0.294	0.180	0.151	0.000	0.163	0.260	0.142	0.130	1.334	0.082	0.129
Mg	3.358	3.328	3.366	3.434	3.403	3.371	3.396	3.385	3.406	3.345	2.797	3.395	3.340	3.436	3.358	3.222	3.077	3.226
Mn	0.006	0.012	0.000	0.004	0.006	0.003	0.001	0.006	0.008	0.012	0.007	0.011	0.006	0.009	0.007	0.030	0.023	0.022
Fe <sup>2+</sup>	0.419	0.446	0.363	0.367	0.311	0.361	0.421	0.277	0.378	0.373	0.498	0.361	0.336	0.360	0.385	0.000	1.288	1.205
Fe <sup>2+</sup>	0.000	0.000	0.000	0.000	0.000	0.000	0.000	0.000	0.000	0.000	0.000	0.000	0.000	0.000	0.010	0.000	0.156	0.133
Ca	2.007	2.029	2.056	2.007	2.030	2.045	2.016	2.065	2.021	2.032	2.014	2.030	2.046	2.023	1.990	2.662	1.844	1.867
Na	0.637	0.648	0.759	0.715	0.668	0.738	0.755	0.737	0.695	0.657	0.744	0.758	0.757	0.737	0.658	0.120	0.540	0.425
K	0.052	0.054	0.061	0.060	0.049	0.064	0.053	0.066	0.049	0.058	0.103	0.058	0.127	0.062	0.056	0.000	0.008	0.003
Mg#	0.89	0.88	0.90	0.90	0.92	0.90	0.89	0.92	0.90	0.90	0.85	0.90	0.91	0.91	0.89	1.00	0.68	0.71

Amphibole formulae calculated on the basis of 23 oxygens with fixed number of cations (15) and Fe<sup>3+</sup>/Fe<sup>2+</sup> adjustment. Mg# = Mg/(Mg+Fe<sup>2+</sup>). c = grain core. r = grain rim. sec = secondary amphibole

**Table I-3.** Microprobe analyses and formulae of amphibole from different metamorphic rock varieties of the Krivaja-Konjuh ophiolite complex

Rock type	Granoblastic amphibolite																	
Sample-Nr.	11c-27	11c-29	11c-2	11c-12	11c-19	11c-20	11c-21	11c-3	11c-7	11c-11	11c-15	11c-22	r8-1	r8-12	r8-17	r8-21	r8-24	r8-2
Remark			c	c	c	c	c	r	r	r	r	r	c	c	c	c	c	r
SiO <sub>2</sub>	45.58	45.74	46.06	46.07	45.83	32.67	44.73	45.62	46.14	45.73	45.86	46.60	48.07	48.18	49.02	45.53	47.79	47.81
TiO <sub>2</sub>	0.38	0.45	0.58	0.50	0.54	0.45	0.36	0.52	0.50	0.51	0.58	0.48	1.40	1.14	0.97	1.23	1.41	1.31
Al <sub>2</sub> O <sub>3</sub>	10.28	10.07	9.56	9.81	9.97	9.21	9.35	9.66	10.11	10.03	10.02	9.45	6.94	6.56	5.81	14.98	7.10	6.92
Cr <sub>2</sub> O <sub>3</sub>	0.00	0.01	0.10	0.08	0.12	0.08	0.09	0.11	0.11	0.09	0.25	0.08	0.15	0.07	0.09	0.06	0.09	0.13
Fe <sub>2</sub> O <sub>3</sub>																		
FeO	13.37	12.69	12.80	12.94	12.75	12.32	12.68	13.30	13.05	13.06	13.12	11.88	14.08	13.78	13.91	6.26	14.09	13.90
MnO	0.23	0.10	0.15	0.24	0.10	0.20	0.19	0.21	0.18	0.25	0.21	0.16	0.22	0.27	0.24	0.19	0.26	0.31
MgO	13.67	13.50	14.04	13.79	13.72	13.81	14.69	13.92	13.57	13.59	13.57	14.35	13.63	13.85	14.06	9.28	13.37	13.78
CaO	11.70	11.95	11.78	11.81	11.77	11.23	10.53	11.80	12.14	11.76	11.82	12.10	11.60	11.73	11.98	19.89	11.86	11.93
Na <sub>2</sub> O	1.81	1.88	1.71	1.68	1.85	1.79	1.49	1.85	1.83	1.91	1.86	1.70	1.19	1.12	0.95	0.41	1.08	1.16
K <sub>2</sub> O	0.03	0.07	0.04	0.05	0.05	0.04	0.04	0.05	0.07	0.04	0.05	0.05	0.08	0.11	0.06	0.09	0.11	0.10
Total	97.08	96.47	96.81	96.96	96.72	96.42	94.18	97.07	97.70	97.00	97.35	96.86	97.36	96.80	97.07	97.91	97.17	97.34
Si	6.686	6.755	6.760	6.755	6.747	6.776	6.708	6.697	6.731	6.725	6.721	6.814	7.060	7.101	7.189	6.524	7.033	7.013
Al <sup>IV</sup>	1.314	1.245	1.240	1.245	1.253	1.219	1.292	1.303	1.269	1.275	1.279	1.186	0.940	0.899	0.811	1.476	0.967	0.987
Al <sup>VI</sup>	0.463	0.508	0.414	0.450	0.477	0.430	0.360	0.368	0.470	0.464	0.451	0.442	0.261	0.240	0.193	1.053	0.264	0.209
Ti	0.042	0.050	0.063	0.055	0.060	0.074	0.041	0.058	0.055	0.056	0.064	0.053	0.155	0.127	0.107	0.132	0.156	0.145
Cr	0.000	0.001	0.011	0.010	0.013	0.012	0.011	0.012	0.013	0.011	0.029	0.009	0.017	0.008	0.010	0.007	0.010	0.015
Fe <sup>3+</sup>	0.248	0.084	0.195	0.189	0.105	0.200	0.400	0.272	0.149	0.135	0.135	0.140	0.000	0.057	0.115	0.020	0.052	0.126
Mg	2.988	2.971	3.071	3.014	3.011	3.045	3.283	3.047	2.951	2.979	2.966	3.129	2.984	3.042	3.074	1.981	2.933	3.012
Mn	0.029	0.013	0.018	0.030	0.013	0.019	0.024	0.026	0.022	0.031	0.027	0.020	0.027	0.033	0.029	0.024	0.033	0.039
Fe <sup>2+</sup>	1.230	1.374	1.227	1.252	1.320	1.380	0.882	1.217	1.340	1.324	1.329	1.207	1.555	1.492	1.473	0.729	1.553	1.455
Fe <sup>2+</sup>	0.162	0.109	0.148	0.145	0.144	0.160	0.309	0.144	0.103	0.147	0.144	0.105	0.174	0.149	0.118	0.000	0.130	0.124
Ca	1.838	1.891	1.852	1.855	1.856	1.715	1.691	1.856	1.897	1.853	1.856	1.895	1.825	1.851	1.882	3.053	1.870	1.876
Na	0.513	0.539	0.486	0.478	0.528	0.509	0.433	0.527	0.516	0.545	0.527	0.481	0.337	0.320	0.269	0.115	0.309	0.329
K	0.006	0.014	0.007	0.009	0.009	0.008	0.007	0.009	0.012	0.007	0.010	0.009	0.016	0.020	0.011	0.016	0.020	0.019
Mg#	0.68	0.67	0.69	0.68	0.67	0.66	0.73	0.69	0.67	0.67	0.67	0.70	0.63	0.65	0.66	0.73	0.64	0.66

Amphibole formulae calculated on the basis of 23 oxygens with fixed number of cations (15) and Fe<sup>3+</sup>/Fe<sup>2+</sup> adjustment. Mg# = Mg/(Mg+Fe<sup>2+</sup>). c = grain core. r = grain rim

**Table I-4.** Microprobe analyses and formulae of amphibole from different metamorphic rock varieties of the Krivaja-Konjuh ophiolite complex

Rock type	Granoblastic amphibolite																	
Sample-Nr.	r8-6	r8-8	r8-11	r8-16	r8-22	r8-23	r8-25	r8-30	r8-31	r8-32	u23-27	u23-1	u23-11	u23-14	u23-17	u23-28	u23-2	u23-6
Remark	r	r	r	r	r	r	r	r	r	r		c	c	c	c	c	r	r
SiO <sub>2</sub>	47.56	47.64	48.79	47.81	49.57	49.64	47.91	47.94	47.97	47.64	48.55	47.26	48.06	48.37	47.31	48.24	47.79	47.88
TiO <sub>2</sub>	1.29	1.47	1.10	1.19	0.72	0.18	1.49	1.26	1.10	1.36	0.36	0.36	0.31	0.34	0.34	0.34	0.31	0.31
Al <sub>2</sub> O <sub>3</sub>	6.67	7.09	6.19	6.94	5.53	3.80	7.12	6.85	6.05	6.92	10.20	11.40	11.45	10.54	11.36	10.21	10.67	10.48
Cr <sub>2</sub> O <sub>3</sub>	0.13	0.08	0.09	0.02	0.07	0.00	0.07	0.11	0.05	0.09	0.10	0.35	0.20	0.32	0.38	0.24	0.35	0.20
Fe <sub>2</sub> O <sub>3</sub>											0.00	0.00	0.00	0.00	0.00	0.00	0.00	0.00
FeO	13.42	13.74	14.00	14.14	13.23	22.26	13.89	13.57	13.23	13.87	5.82	6.50	6.57	6.09	6.68	6.27	6.56	6.01
MnO	0.30	0.24	0.29	0.23	0.29	0.34	0.31	0.22	0.25	0.36	0.11	0.10	0.15	0.18	0.08	0.15	0.12	0.24
MgO	13.74	13.36	13.77	13.37	14.21	8.42	13.41	13.69	13.40	13.55	17.40	16.70	17.11	17.21	16.84	17.19	16.91	17.20
CaO	11.95	11.75	11.92	11.86	12.14	12.11	11.87	12.13	12.15	12.02	12.01	11.96	12.01	11.91	11.92	11.84	12.14	11.88
Na <sub>2</sub> O	1.06	1.14	1.00	1.15	0.87	0.25	1.08	1.01	1.36	1.16	1.52	1.58	1.57	1.39	1.59	1.43	1.51	1.47
K <sub>2</sub> O	0.09	0.08	0.08	0.10	0.08	0.06	0.12	0.09	0.08	0.08	0.10	0.12	0.12	0.12	0.13	0.12	0.12	0.11
Total	96.21	96.58	97.23	96.80	96.70	97.05	97.26	96.87	96.82	97.05	96.16	96.33	97.55	96.49	96.63	96.03	96.46	95.78
Si	7.045	7.048	7.159	7.062	7.277	7.546	7.041	7.051	7.027	7.014	6.932	6.774	6.795	6.894	6.766	6.914	6.842	6.879
Al <sup>IV</sup>	0.955	0.952	0.841	0.938	0.723	0.454	0.959	0.949	0.973	0.986	1.068	1.226	1.205	1.106	1.234	1.086	1.158	1.121
Al <sup>VI</sup>	0.210	0.284	0.230	0.269	0.233	0.226	0.274	0.237	0.277	0.215	0.648	0.700	0.704	0.665	0.680	0.638	0.643	0.653
Ti	0.144	0.163	0.121	0.132	0.079	0.020	0.164	0.139	0.140	0.151	0.039	0.039	0.033	0.037	0.037	0.037	0.033	0.033
Cr	0.016	0.010	0.010	0.002	0.008	0.000	0.008	0.013	0.007	0.010	0.011	0.040	0.022	0.036	0.043	0.027	0.039	0.023
Fe <sup>3+</sup>	0.121	0.000	0.057	0.055	0.061	0.102	0.017	0.114	0.043	0.114	0.000	0.000	0.000	0.000	0.000	0.000	0.000	0.000
Mg	3.034	2.947	3.011	2.944	3.110	1.908	2.938	3.002	3.023	2.975	3.704	3.568	3.606	3.657	3.591	3.674	3.609	3.684
Mn	0.037	0.030	0.035	0.028	0.036	0.044	0.038	0.028	0.045	0.045	0.013	0.012	0.018	0.022	0.010	0.019	0.014	0.029
Fe <sup>2+</sup>	1.439	1.566	1.535	1.569	1.472	2.699	1.560	1.467	1.525	1.490	0.585	0.642	0.617	0.584	0.639	0.605	0.663	0.577
Fe <sup>2+</sup>	0.103	0.133	0.125	0.123	0.091	0.028	0.130	0.088	0.121	0.105	0.110	0.137	0.160	0.142	0.159	0.145	0.123	0.145
Ca	1.897	1.862	1.875	1.877	1.909	1.972	1.870	1.912	1.855	1.895	1.837	1.836	1.820	1.819	1.827	1.819	1.862	1.829
Na	0.304	0.321	0.286	0.328	0.247	0.073	0.309	0.289	0.308	0.330	0.367	0.413	0.410	0.347	0.427	0.360	0.404	0.384
K	0.017	0.015	0.016	0.019	0.014	0.012	0.022	0.017	0.015	0.014	0.018	0.022	0.022	0.022	0.024	0.023	0.022	0.019
Mg#	0.66	0.63	0.64	0.64	0.67	0.41	0.63	0.66	0.62	0.65	0.84	0.82	0.82	0.83	0.82	0.83	0.82	0.84

Amphibole formulae calculated on the basis of 23 oxygens with fixed number of cations (15) and Fe<sup>3+</sup>/Fe<sup>2+</sup> adjustment. Mg# = Mg/(Mg+Fe<sup>2+</sup>). c = grain core. r = grain rim

**Table I-5.** Microprobe analyses and formulae of amphibole from different metamorphic rock varieties of the Krivaja-Konjuh ophiolite complex

Rock type	Granoblastic amphibolite – Garnet-diopside amphibolite																	
Sample-Nr.	u23-7	u23-10	u23-12	u23-18	u23-29	u23-35	cc1-39	cc1-5	cc1-14	cc1-53	cc1-61	cc1-51	cc1-9	cc1-11	cc1-13	cc1-26	cc1-29	cc1-32
Remark	r	r	r	r	r	r	r.cpx				c	k.c.	r	r	r	r	r	r
SiO <sub>2</sub>	48.25	47.42	48.76	47.15	47.70	47.18	43.88	45.15	44.96	43.50	43.70	44.47	43.81	44.00	44.42	42.37	42.19	43.87
TiO <sub>2</sub>	0.30	0.31	0.33	0.33	0.36	0.33	0.71	0.60	0.92	1.19	1.51	0.81	1.23	1.08	0.77	0.42	0.47	0.77
Al <sub>2</sub> O <sub>3</sub>	10.41	11.60	10.78	11.40	9.97	11.04	11.87	10.85	10.37	11.87	12.22	12.10	11.28	11.78	11.42	13.56	13.59	11.99
Cr <sub>2</sub> O <sub>3</sub>	0.22	0.19	0.22	0.40	0.21	0.15	0.04	0.07	0.08	0.05	0.10	0.12	0.07	0.12	0.10	0.12	0.19	0.07
Fe <sub>2</sub> O <sub>3</sub>	0.00	0.00	0.00	0.00	0.00	0.00												
FeO	6.61	6.58	6.04	6.70	6.36	6.54	11.43	11.90	11.62	11.11	10.69	11.29	12.02	10.49	12.27	11.27	11.53	11.34
MnO	0.12	0.14	0.16	0.12	0.13	0.17	0.15	0.12	0.13	0.19	0.16	0.21	0.16	0.15	0.17	0.23	0.21	0.09
MgO	17.41	17.14	17.32	17.04	17.25	16.98	14.36	14.39	14.89	14.27	14.31	14.70	14.02	13.91	13.74	14.01	14.07	14.62
CaO	11.93	11.95	11.76	12.09	12.06	12.00	11.62	11.33	11.19	11.35	11.23	11.24	11.61	11.30	11.21	11.89	11.37	11.61
Na <sub>2</sub> O	1.38	1.59	1.36	1.49	1.50	1.54	1.86	1.72	1.89	2.19	2.24	2.33	1.96	1.79	2.08	1.83	2.71	2.11
K <sub>2</sub> O	0.11	0.14	0.11	0.09	0.08	0.13	0.05	0.05	0.04	0.07	0.10	0.03	0.04	0.05	0.06	0.05	0.06	0.03
Total	96.72	97.05	96.84	96.81	95.63	96.07	95.96	96.17	96.07	95.80	96.25	97.30	96.20	94.66	96.24	96.99	96.39	96.49
Si	6.876	6.746	6.909	6.722	6.882	6.782	6.455	6.634	6.615	6.440	6.440	6.475	6.468	6.566	6.569	6.965	6.223	6.424
Al <sup>IV</sup>	1.124	1.254	1.091	1.278	1.118	1.218	1.545	1.366	1.385	1.560	1.560	1.525	1.532	1.434	1.431	1.535	1.777	1.576
Al <sup>VI</sup>	0.623	0.691	0.708	0.637	0.578	0.653	0.512	0.513	0.413	0.511	0.562	0.551	0.430	0.638	0.559	0.541	0.586	0.494
Ti	0.032	0.034	0.035	0.036	0.039	0.035	0.079	0.066	0.102	0.133	0.168	0.089	0.136	0.121	0.085	0.052	0.052	0.085
Cr	0.025	0.021	0.025	0.045	0.024	0.017	0.005	0.008	0.009	0.006	0.012	0.014	0.008	0.014	0.011	0.014	0.022	0.008
Fe <sup>3+</sup>	0.012	0.012	0.000	0.095	0.002	0.024	0.333	0.216	0.215	0.134	0.000	0.118	0.253	0.013	0.081	0.145	0.279	0.300
Mg	3.698	3.635	3.658	3.622	3.710	3.638	3.149	3.152	3.266	3.149	3.144	3.190	3.085	3.093	3.029	3.041	3.095	3.193
Mn	0.014	0.017	0.019	0.015	0.016	0.021	0.018	0.015	0.016	0.024	0.020	0.026	0.020	0.018	0.022	0.025	0.026	0.011
Fe <sup>2+</sup>	0.596	0.591	0.554	0.550	0.630	0.612	0.904	1.030	0.979	1.042	1.095	1.011	1.068	1.102	1.213	0.987	0.939	0.909
Fe <sup>2+</sup>	0.179	0.179	0.162	0.154	0.135	0.151	0.168	0.216	0.235	0.200	0.223	0.246	0.164	0.194	0.224	0.252	0.203	0.179
Ca	1.821	1.821	1.786	1.846	1.865	1.849	1.832	1.784	1.765	1.800	1.774	1.754	1.836	1.806	1.776	1.795	1.797	1.821
Na	0.380	0.438	0.321	0.412	0.421	0.430	0.529	0.489	0.538	0.630	0.636	0.658	0.562	0.517	0.598	0.640	0.775	0.599
K	0.020	0.025	0.019	0.017	0.015	0.023	0.009	0.008	0.007	0.012	0.018	0.005	0.008	0.010	0.012	0.021	0.011	0.005
Mg#	0.83	0.83	0.84	0.84	0.83	0.83	0.75	0.72	0.73	0.72	0.70	0.72	0.71	0.70	0.68	0.77	0.73	0.75

Amphibole formulae calculated on the basis of 23 oxygens with fixed number of cations (15) and Fe<sup>3+</sup>/Fe<sup>2+</sup> adjustment. Mg# = Mg/(Mg+Fe<sup>2+</sup>). c = grain core. r = grain rim. r.cpx = rim around clinopyroxene. k.c = amphibole in garnet kelfitic corona

**Table I-6.** Microprobe analyses and formulae of amphibole from different metamorphic rock varieties of the Krivaja-Konjuh ophiolite complex

Rock type	Garnet-diopside amphibolite																	
Sample-Nr.	cc1-57	cc1-62	cc1-72	cc1-76	cc1-77	cc1-82	cc1-85	mk2-19	mk2-20	mk2-28	mk2-30	mk2-33	mk2-35	mk2-4	mk2-8	mk2-46	mk2-3	mk2-6
Remark	r	r	r	r	r	r	r	cpx, grt	cpx, grt					c	c	cpx	r	r
SiO <sub>2</sub>	45.32	42.77	44.74	44.96	46.49	45.22	44.95	44.18	44.60	43.34	42.78	43.04	45.50	43.87	43.76	43.31	44.12	43.56
TiO <sub>2</sub>	1.62	1.73	0.61	1.36	1.23	1.41	1.57	1.49	1.42	0.80	0.98	1.09	0.90	1.41	1.42	1.91	1.44	1.43
Al <sub>2</sub> O <sub>3</sub>	10.96	13.25	11.09	10.89	9.97	11.12	11.06	12.59	12.17	12.12	11.85	11.95	9.65	10.57	11.61	12.46	10.75	11.57
Cr <sub>2</sub> O <sub>3</sub>	0.08	0.07	0.09	0.14	0.17	0.08	0.05	0.10	0.15	0.11	0.19	0.11	0.03	0.15	0.02	0.11	0.06	0.09
Fe <sub>2</sub> O <sub>3</sub>																		
FeO	9.60	10.71	11.72	9.67	8.94	9.68	9.70	10.70	10.61	11.45	11.66	12.59	11.37	11.92	12.09	11.02	11.96	12.06
MnO	0.12	0.10	0.15	0.03	0.11	0.08	0.10	0.08	0.06	0.33	0.38	0.28	0.33	0.15	0.16	0.12	0.13	0.17
MgO	14.88	13.76	14.31	15.69	15.90	15.17	15.46	14.24	14.12	14.22	14.12	13.50	14.96	14.04	13.97	13.80	14.05	13.99
CaO	11.91	11.26	11.27	11.89	11.92	11.64	11.58	11.29	11.30	11.43	11.13	11.72	11.52	12.03	11.32	11.18	11.79	11.44
Na <sub>2</sub> O	1.88	2.36	2.09	2.04	1.91	2.01	2.17	2.08	2.08	2.28	2.40	2.30	1.98	2.27	2.41	2.27	2.19	2.40
K <sub>2</sub> O	0.05	0.07	0.04	0.07	0.07	0.08	0.06	0.03	0.04	0.06	0.03	0.02	0.06	0.05	0.02	0.07	0.07	0.03
Total	96.41	96.07	96.10	96.73	96.68	96.48	96.68	96.79	96.55	96.14	95.51	96.60	96.28	96.45	96.77	96.26	96.54	96.75
Si	6.619	6.322	6.601	6.537	6.743	6.601	6.556	6.457	6.527	6.398	6.375	6.362	6.692	6.489	6.454	6.395	6.514	6.426
Al <sup>IV</sup>	1.381	1.678	1.399	1.463	1.257	1.399	1.444	1.543	1.473	1.602	1.625	1.638	1.308	1.511	1.546	1.605	1.486	1.574
Al <sup>VI</sup>	0.506	0.630	0.528	0.403	0.446	0.514	0.456	0.626	0.627	0.507	0.455	0.443	0.364	0.332	0.471	0.563	0.384	0.437
Ti	0.177	0.193	0.068	0.148	0.134	0.155	0.172	0.164	0.156	0.089	0.110	0.121	0.099	0.156	0.158	0.212	0.160	0.159
Cr	0.010	0.008	0.011	0.016	0.019	0.009	0.006	0.012	0.017	0.012	0.022	0.013	0.004	0.018	0.002	0.013	0.007	0.011
Fe <sup>3+</sup>	0.000	0.000	0.121	0.160	0.000	0.000	0.016	0.000	0.000	0.242	0.230	0.276	0.167	0.187	0.065	0.000	0.138	0.115
Mg	3.239	3.033	3.147	3.401	3.438	3.301	3.361	3.103	3.081	3.130	3.136	2.975	3.279	3.095	3.071	3.038	3.091	3.077
Mn	0.015	0.012	0.018	0.003	0.013	0.010	0.013	0.010	0.007	0.041	0.048	0.035	0.041	0.018	0.019	0.015	0.017	0.021
Fe <sup>2+</sup>	1.053	1.124	1.107	0.868	0.949	1.010	0.976	1.085	1.112	0.979	1.000	1.137	1.046	1.193	1.214	1.159	1.204	1.180
Fe <sup>2+</sup>	0.119	0.200	0.218	0.148	0.135	0.171	0.191	0.223	0.187	0.192	0.223	0.144	0.185	0.094	0.212	0.202	0.135	0.192
Ca	1.864	1.783	1.782	1.852	1.852	1.820	1.809	1.769	1.771	1.808	1.777	1.856	1.815	1.906	1.788	1.769	1.865	1.808
Na	0.517	0.658	0.596	0.574	0.523	0.560	0.612	0.581	0.550	0.652	0.694	0.660	0.564	0.652	0.688	0.621	0.626	0.687
K	0.010	0.013	0.008	0.013	0.013	0.014	0.011	0.005	0.008	0.011	0.006	0.003	0.012	0.010	0.005	0.012	0.013	0.006
Mg#	0.73	0.70	0.70	0.77	0.76	0.74	0.74	0.70	0.70	0.73	0.72	0.70	0.73	0.71	0.68	0.69	0.70	0.69

Amphibole formulae calculated on the basis of 23 oxygens with fixed number of cations (15) and Fe<sup>3+</sup>/Fe<sup>2+</sup> adjustment. Mg# = Mg/(Mg+Fe<sup>2+</sup>). c = grain core. r = grain rim. cpx, grt = inclusion in clinopyroxene in garnet. cpx = inclusion in clinopyroxene

**Table I-7.** Microprobe analyses and formulae of amphibole from different metamorphic rock varieties of the Krivaja-Konjuh ophiolite complex

Rock type	Garnet-diopside amphibolite																	
Sample-Nr.	mk2-23	mk2-24	gr7-70	gr7-39	gr7-47	gr7-48	gr7-60	gr7-69	gr7-9	gr7-37	gr7-8	gr7-33	gr7-6	gr7-32	gr7-42	gr7-44	gr7-45	gr7-49
Remark	r	r		c	c	c	c	c	k.c.	k.c.	k.c.	k.c.	r.cpx	r.cpx	r	r	r	r
SiO <sub>2</sub>	43.11	43.88	42.46	43.13	42.93	42.66	43.43	43.75	42.71	42.06	41.26	41.30	42.27	40.97	42.76	42.04	42.14	41.28
TiO <sub>2</sub>	0.97	0.80	0.93	0.92	1.10	0.93	1.37	1.13	0.97	0.86	0.19	0.16	0.60	0.45	0.94	1.06	1.14	1.28
Al <sub>2</sub> O <sub>3</sub>	12.12	11.65	13.55	12.23	13.22	13.18	12.94	13.35	12.51	13.45	14.32	14.43	13.04	14.72	12.11	13.99	13.81	13.37
Cr <sub>2</sub> O <sub>3</sub>	0.03	0.05	0.27	0.16	0.24	0.17	0.16	0.29	0.32	0.30	0.16	0.07	0.23	0.28	0.17	0.29	0.25	0.29
Fe <sub>2</sub> O <sub>3</sub>																		
FeO	12.07	12.06	6.86	8.65	8.63	8.17	7.50	6.48	10.11	8.40	10.40	9.52	9.58	8.77	8.78	8.57	8.69	9.83
MnO	0.28	0.38	0.00	0.07	0.05	0.09	0.09	0.05	0.13	0.10	0.12	0.16	0.10	0.12	0.13	0.03	0.04	0.10
MgO	13.70	14.02	16.34	16.10	15.65	15.97	15.98	16.27	15.19	15.33	14.40	15.00	15.11	14.98	15.93	15.02	15.19	15.41
CaO	11.26	11.20	11.61	11.46	11.58	11.33	11.41	11.69	11.34	11.38	11.44	11.63	11.56	11.56	11.55	11.87	11.80	11.61
Na <sub>2</sub> O	2.42	2.18	2.83	2.70	2.74	2.89	2.82	2.96	2.59	2.71	2.95	2.93	2.69	3.00	2.60	2.67	2.80	2.78
K <sub>2</sub> O	0.03	0.01	0.05	0.01	0.04	0.03	0.05	0.06	0.04	0.03	0.02	0.02	0.04	0.06	0.03	0.03	0.05	0.06
Total	95.99	96.21	94.90	95.44	96.17	95.42	95.75	96.03	95.92	94.61	95.27	95.21	95.21	94.91	95.01	95.55	95.89	95.99
Si	6.404	6.481	6.252	6.347	6.281	6.280	6.356	6.357	6.294	6.250	6.132	6.109	6.261	6.082	6.322	6.192	6.194	6.074
Al <sup>IV</sup>	1.596	1.519	1.748	1.653	1.719	1.720	1.644	1.643	1.706	1.750	1.868	1.891	1.739	1.918	1.678	1.808	1.806	1.926
Al <sup>VI</sup>	0.527	0.510	0.603	0.468	0.560	0.568	0.588	0.643	0.466	0.605	0.640	0.626	0.537	0.657	0.432	0.621	0.586	0.392
Ti	0.109	0.089	0.103	0.102	0.121	0.103	0.151	0.124	0.108	0.096	0.022	0.018	0.067	0.050	0.105	0.117	0.126	0.141
Cr	0.004	0.005	0.032	0.018	0.028	0.020	0.018	0.033	0.037	0.035	0.019	0.008	0.026	0.033	0.020	0.034	0.029	0.034
Fe <sup>3+</sup>	0.144	0.199	0.090	0.189	0.104	0.098	0.000	0.000	0.239	0.131	0.312	0.377	0.262	0.253	0.266	0.152	0.131	0.414
Mg	3.033	3.087	3.587	3.532	3.414	3.505	3.487	3.524	3.336	3.397	3.191	3.308	3.337	3.316	3.511	3.298	3.328	3.381
Mn	0.035	0.047	0.000	0.008	0.006	0.011	0.012	0.006	0.017	0.012	0.015	0.020	0.012	0.015	0.017	0.003	0.004	0.012
Fe <sup>2+</sup>	1.148	1.063	0.586	0.683	0.768	0.695	0.743	0.670	0.796	0.724	0.802	0.644	0.759	0.676	0.649	0.776	0.795	0.625
Fe <sup>2+</sup>	0.207	0.227	0.169	0.193	0.185	0.213	0.174	0.117	0.210	0.188	0.179	0.156	0.165	0.161	0.171	0.127	0.142	0.170
Ca	1.793	1.773	1.831	1.807	1.815	1.787	1.789	1.820	1.790	1.812	1.821	1.844	1.835	1.839	1.829	1.873	1.858	1.830
Na	0.697	0.624	0.808	0.771	0.778	0.823	0.762	0.771	0.741	0.781	0.850	0.840	0.773	0.864	0.745	0.761	0.798	0.792
K	0.006	0.002	0.010	0.003	0.008	0.005	0.010	0.011	0.007	0.006	0.005	0.005	0.008	0.011	0.006	0.006	0.009	0.011
Mg#	0.69	0.71	0.83	0.80	0.78	0.79	0.79	0.82	0.77	0.79	0.76	0.81	0.78	0.80	0.81	0.78	0.78	0.81

Amphibole formulae calculated on the basis of 23 oxygens with fixed number of cations (15) and Fe<sup>3+</sup>/Fe<sup>2+</sup> adjustment. Mg# = Mg/(Mg+Fe<sup>2+</sup>). c = grain core. r = grain rim. k.c = amphibole in garnet kelfitic corona. r.cpx = rim around clinopyroxene

**Table I-8.** Microprobe analyses and formulae of amphibole from different metamorphic rock varieties of the Krivaja-Konjuh ophiolite complex

Rock type	Garnet-diopside amphibolite																	
Sample-Nr.	gr7-52	gr7-61	gr7-65	gr7-66	gr7-10	gr7-14	gr7-36	gr7-59	v1-21	v1-29	v1-38	v1-54	v1-65	v1-78	v1-33	v1-52	v1-21b	v1-23
Remark	r	r	r	r	k.c.	k.c.	k.c.	r.cpx	c	c	c	c	c	c	cpx	cpx	r	r
SiO <sub>2</sub>	50.55	43.31	43.54	44.56	41.29	40.65	40.90	43.11	43.69	43.86	43.42	46.37	46.28	46.71	46.15	46.37	42.69	44.12
TiO <sub>2</sub>	0.27	1.49	1.09	0.70	1.37	1.23	0.72	1.69	0.22	0.27	0.68	0.70	0.69	0.71	0.60	0.79	0.30	0.24
Al <sub>2</sub> O <sub>3</sub>	5.46	12.55	13.12	12.03	13.50	13.98	14.56	13.16	12.99	12.71	12.34	10.04	10.60	10.08	11.59	9.74	13.30	12.02
Cr <sub>2</sub> O <sub>3</sub>	0.23	0.16	0.28	0.24	0.34	0.37	0.41	0.24	0.15	0.08	0.13	0.13	0.09	0.10	0.05	0.17	0.15	0.14
Fe <sub>2</sub> O <sub>3</sub>																		
FeO	8.48	7.81	6.63	6.32	10.34	10.05	9.08	7.62	11.07	10.79	10.70	9.99	9.77	9.32	9.48	9.44	11.24	10.72
MnO	0.09	0.06	0.00	0.04	0.13	0.15	0.05	0.09	0.29	0.37	0.32	0.18	0.12	0.12	0.15	0.11	0.53	0.33
MgO	16.07	16.03	16.56	16.82	14.05	14.00	14.94	16.05	15.09	15.30	15.02	16.34	16.14	16.67	15.46	15.80	15.06	15.27
CaO	13.33	11.60	12.15	12.26	11.74	11.78	11.36	11.57	10.84	11.13	11.07	11.29	11.40	11.81	11.67	11.68	10.97	11.07
Na <sub>2</sub> O	0.86	2.70	2.71	2.41	2.61	2.86	2.85	2.80	2.25	2.28	2.34	1.82	1.88	1.85	1.78	1.93	2.50	2.18
K <sub>2</sub> O	0.01	0.04	0.02	0.05	0.03	0.03	0.02	0.01	0.05	0.03	0.04	0.03	0.05	0.03	0.08	0.03	0.03	0.04
Total	95.35	95.76	96.09	95.41	95.40	95.09	94.90	96.32	96.63	96.80	96.04	96.88	97.02	97.40	97.00	96.07	96.75	96.12
Si	7.374	6.352	6.323	6.490	6.145	6.076	6.073	6.284	6.369	6.377	6.383	6.701	6.680	6.699	6.663	6.777	6.232	6.461
Al <sup>IV</sup>	0.626	1.648	1.677	1.510	1.855	1.924	1.927	1.716	1.631	1.623	1.617	1.299	1.320	1.301	1.337	1.223	1.768	1.539
Al <sup>VI</sup>	0.313	0.522	0.568	0.556	0.514	0.538	0.622	0.545	0.602	0.555	0.520	0.412	0.484	0.403	0.635	0.455	0.520	0.534
Ti	0.029	0.164	0.119	0.077	0.153	0.138	0.081	0.185	0.024	0.029	0.075	0.076	0.075	0.076	0.065	0.087	0.033	0.026
Cr	0.026	0.019	0.032	0.027	0.040	0.043	0.048	0.028	0.017	0.010	0.015	0.015	0.010	0.012	0.005	0.020	0.017	0.016
Fe <sup>3+</sup>	0.000	0.001	0.072	0.085	0.235	0.233	0.271	0.000	0.318	0.350	0.258	0.204	0.141	0.215	0.054	0.021	0.453	0.309
Mg	3.495	3.506	3.585	3.653	3.117	3.119	3.308	3.487	3.280	3.316	3.293	3.520	3.474	3.563	3.327	3.442	3.277	3.333
Mn	0.011	0.007	0.000	0.005	0.016	0.018	0.007	0.010	0.035	0.045	0.040	0.022	0.015	0.015	0.018	0.013	0.065	0.041
Fe <sup>2+</sup>	1.034	0.781	0.624	0.598	0.925	0.910	0.664	0.744	0.725	0.695	0.800	0.750	0.802	0.717	0.896	0.961	0.635	0.740
Fe <sup>2+</sup>	0.000	0.177	0.110	0.087	0.127	0.113	0.192	0.184	0.308	0.267	0.257	0.252	0.237	0.185	0.195	0.171	0.285	0.264
Ca	2.083	1.823	1.890	1.913	1.873	1.887	1.808	1.807	1.692	1.733	1.743	1.748	1.763	1.815	1.805	1.829	1.715	1.736
Na	0.244	0.769	0.764	0.681	0.754	0.829	0.821	0.781	0.636	0.643	0.667	0.510	0.526	0.515	0.499	0.546	0.706	0.619
K	0.003	0.008	0.004	0.008	0.006	0.005	0.004	0.002	0.010	0.006	0.008	0.005	0.010	0.005	0.014	0.006	0.005	0.008
Mg#	0.77	0.79	0.83	0.84	0.75	0.75	0.79	0.79	0.76	0.78	0.76	0.78	0.77	0.80	0.75	0.75	0.78	0.77

Amphibole formulae calculated on the basis of 23 oxygens with fixed number of cations (15) and Fe<sup>3+</sup>/Fe<sup>2+</sup> adjustment. Mg# = Mg/(Mg+Fe<sup>2+</sup>). c = grain core. r = grain rim. k.c = amphibole in garnet kelfitic corona. r.cpx = rim around clinopyroxene. cpx = inclusion in clinopyroxene

**Table I-9.** Microprobe analyses and formulae of amphibole from different metamorphic rock varieties of the Krivaja-Konjuh ophiolite complex

Rock type	Garnet-diopside amphibolite																	
Sample-Nr.	v1-24	v1-25d	v1-27	v1-36	v1-39	v1-41	v1-53	v1-57	v1-61	v1-64	v1-66	v1-79	v1-81	du5-12a	du5-45	du5-8	du5-34	du5-39
Remark	r	r	r	r	r	r	r	r	r	r	r	r	r		k.c.	c	c	c
SiO <sub>2</sub>	45.03	44.63	44.08	43.85	43.63	51.74	46.54	46.10	46.77	46.64	46.32	46.98	46.16	43.09	43.40	43.72	43.25	42.51
TiO <sub>2</sub>	0.22	0.22	0.29	0.50	0.66	0.08	0.68	0.82	0.77	0.73	0.68	0.73	0.77	1.08	0.99	1.10	1.23	1.35
Al <sub>2</sub> O <sub>3</sub>	11.86	11.91	11.93	12.24	11.86	2.52	9.36	9.93	9.70	10.21	10.05	10.37	10.07	14.02	13.28	14.49	14.07	14.24
Cr <sub>2</sub> O <sub>3</sub>	0.09	0.08	0.05	0.12	0.05	0.02	0.16	0.16	0.08	0.12	0.11	0.07	0.05	0.12	0.11	0.03	0.06	0.04
Fe <sub>2</sub> O <sub>3</sub>																		
FeO	10.39	10.95	11.05	10.72	11.32	12.08	9.97	9.89	10.13	9.29	9.50	9.07	9.62	12.45	12.05	10.94	11.82	11.33
MnO	0.25	0.22	0.27	0.42	0.35	0.40	0.18	0.12	0.15	0.10	0.12	0.10	0.12	0.08	0.14	0.03	0.17	0.18
MgO	15.52	15.29	15.09	16.91	14.92	17.86	16.04	16.20	15.93	16.35	16.05	16.58	16.42	12.96	13.14	13.30	13.16	12.76
CaO	11.12	11.66	11.16	10.39	11.34	11.36	11.79	11.51	11.52	11.80	11.77	11.45	11.76	11.86	11.69	11.89	11.64	11.83
Na <sub>2</sub> O	1.94	2.03	2.16	1.89	2.29	0.28	1.84	1.85	1.78	1.79	1.77	1.91	1.82	2.20	2.17	1.95	2.03	2.19
K <sub>2</sub> O	0.02	0.02	0.02	0.03	0.02	0.01	0.04	0.03	0.03	0.05	0.01	0.02	0.05	0.09	0.10	0.08	0.13	0.13
Total	96.43	97.00	96.08	97.05	96.43	96.34	96.61	96.61	96.86	97.08	96.40	97.27	96.83	97.96	97.07	97.52	97.57	96.55
Si	6.545	6.467	6.462	6.300	6.398	7.461	6.761	6.688	6.775	6.714	6.723	6.746	6.667	6.273	6.371	6.344	6.303	6.272
A <sup>IV</sup>	1.455	1.533	1.538	1.700	1.602	0.428	1.239	1.312	1.225	1.286	1.277	1.254	1.333	1.727	1.629	1.656	1.697	1.728
Al <sup>VI</sup>	0.576	0.501	0.524	0.373	0.448	0.000	0.364	0.386	0.432	0.447	0.442	0.501	0.381	0.679	0.668	0.821	0.719	0.748
Ti	0.024	0.023	0.031	0.054	0.073	0.009	0.075	0.090	0.084	0.079	0.075	0.078	0.084	0.119	0.109	0.120	0.135	0.150
Cr	0.010	0.009	0.005	0.014	0.006	0.002	0.018	0.019	0.009	0.013	0.013	0.008	0.005	0.014	0.013	0.003	0.007	0.005
Fe <sup>3+</sup>	0.269	0.401	0.330	0.675	0.348	0.550	0.183	0.203	0.110	0.159	0.172	0.054	0.261	0.159	0.095	0.029	0.104	0.025
Mg	3.364	3.302	3.298	3.622	3.261	3.840	3.474	3.502	3.441	3.509	3.471	3.549	3.535	2.813	2.875	2.877	2.859	2.808
Mn	0.031	0.027	0.033	0.051	0.043	0.049	0.022	0.015	0.018	0.012	0.015	0.012	0.014	0.009	0.018	0.003	0.021	0.022
Fe <sup>2+</sup>	0.726	0.736	0.779	0.211	0.821	0.551	0.864	0.785	0.906	0.780	0.811	0.796	0.720	1.207	1.223	1.147	1.154	1.243
Fe <sup>2+</sup>	0.268	0.189	0.246	0.401	0.219	0.355	0.165	0.211	0.211	0.179	0.170	0.239	0.181	0.150	0.162	0.152	0.183	0.130
Ca	1.732	1.811	1.754	1.599	1.781	1.755	1.835	1.789	1.789	1.821	1.830	1.761	1.819	1.850	1.838	1.848	1.817	1.870
Na	0.547	0.571	0.613	0.526	0.651	0.079	0.517	0.520	0.499	0.500	0.498	0.531	0.509	0.620	0.617	0.549	0.573	0.627
K	0.004	0.004	0.003	0.005	0.003	0.001	0.007	0.006	0.006	0.009	0.003	0.003	0.008	0.017	0.019	0.014	0.023	0.024
Mg#	0.77	0.78	0.76	0.86	0.76	0.81	0.77	0.78	0.75	0.79	0.78	0.77	0.80	0.67	0.67	0.69	0.68	0.67

Amphibole formulae calculated on the basis of 23 oxygens with fixed number of cations (15) and Fe<sup>3+</sup>/Fe<sup>2+</sup> adjustment. Mg# = Mg/(Mg+Fe<sup>2+</sup>). c = grain core. r = grain rim. k.c = amphibole in garnet kelfitic corona



**Table I-10.** Microprobe analyses and formulae of amphibole from different metamorphic rock varieties of the Krivaja-Konjuh ophiolite complex

Rock type	Garnet-diopside amphibolite																	
Sample-Nr.	du5-33	du5-7	du5-40	u22-17	u22-6	u22-11	u22-13	u22-28	u22-31	u22-56	u22-3	u22-5	u22-15	u22-2	u22-49	u22-19	u22-20	u22-30
Remark	r	r	r		c	c	k.c.	k.c.	k.c.	k.c.		r	r	sec	sec			
SiO <sub>2</sub>	42.26	43.79	43.43	44.25	43.89	43.34	40.76	40.41	42.41	41.64	41.24	43.61	43.91	43.21	41.85	44.15	43.61	43.56
TiO <sub>2</sub>	1.30	1.13	1.98	0.57	0.41	0.37	0.09	0.33	0.07	0.18	0.13	0.35	0.27	0.11	0.53	0.52	0.49	0.34
Al <sub>2</sub> O <sub>3</sub>	14.57	14.49	12.97	13.55	14.08	13.76	16.76	17.14	15.93	16.71	17.12	13.90	13.67	15.43	13.79	14.24	13.71	13.44
Cr <sub>2</sub> O <sub>3</sub>	0.08	0.01	0.02	0.23	0.15	0.13	0.20	0.13	0.16	0.13	0.20	0.19	0.08	0.06	0.19	0.16	0.10	0.04
Fe <sub>2</sub> O <sub>3</sub>																		
FeO	11.90	10.65	11.41	8.73	9.09	9.49	9.98	9.94	8.63	9.70	10.58	9.20	9.28	9.26	9.72	8.54	8.69	9.38
MnO	0.13	0.07	0.12	0.19	0.15	0.11	0.36	0.15	0.31	0.16	0.34	0.15	0.19	0.27	0.14	0.16	0.11	0.12
MgO	12.74	13.24	13.30	16.07	15.59	15.52	14.76	13.61	15.47	14.62	14.88	15.88	15.87	15.10	17.20	15.75	15.96	15.58
CaO	11.71	11.68	12.08	11.46	11.28	11.53	11.27	11.50	11.54	11.13	10.67	11.23	11.23	11.63	9.33	11.58	11.50	11.49
Na <sub>2</sub> O	2.15	1.97	2.00	2.47	2.56	2.51	3.33	2.97	2.63	2.91	3.17	2.54	2.64	2.59	1.95	2.59	2.64	2.72
K <sub>2</sub> O	0.11	0.09	0.11	0.02	0.05	0.03	0.01	0.04	0.01	0.03	0.01	0.04	0.01	0.01	0.01	0.05	0.05	0.02
Total	96.96	97.11	97.42	97.54	97.24	96.78	97.51	96.21	97.16	97.21	98.35	97.08	97.15	97.67	94.72	97.72	96.87	96.69
Si	6.210	6.371	6.347	6.351	6.333	6.284	5.909	5.942	6.101	6.032	5.923	6.295	6.339	6.204	6.123	6.331	6.308	6.334
Al <sup>IV</sup>	1.790	1.629	1.653	1.649	1.667	1.716	2.091	2.058	1.899	1.968	2.077	1.705	1.661	1.796	1.877	1.669	1.692	1.666
Al <sup>VI</sup>	0.733	0.855	0.581	0.643	0.727	0.635	0.772	0.912	0.802	0.886	0.822	0.660	0.665	0.815	0.500	0.738	0.645	0.636
Ti	0.144	0.124	0.217	0.062	0.045	0.040	0.010	0.036	0.008	0.020	0.014	0.038	0.029	0.012	0.058	0.056	0.053	0.037
Cr	0.009	0.001	0.002	0.026	0.017	0.015	0.022	0.015	0.019	0.015	0.023	0.021	0.009	0.006	0.022	0.018	0.012	0.005
Fe <sup>3+</sup>	0.126	0.000	0.047	0.167	0.108	0.275	0.337	0.205	0.328	0.205	0.318	0.231	0.187	0.228	0.683	0.074	0.181	0.181
Mg	2.792	2.871	2.898	3.438	3.353	3.354	3.191	2.984	3.317	3.157	3.187	3.417	3.416	3.233	3.736	3.366	3.442	3.376
Mn	0.016	0.008	0.015	0.023	0.019	0.014	0.044	0.018	0.038	0.020	0.041	0.018	0.023	0.032	0.000	0.020	0.014	0.015
Fe <sup>2+</sup>	1.180	1.141	1.239	0.642	0.732	0.667	0.623	0.829	0.489	0.697	0.596	0.615	0.670	0.674	0.000	0.729	0.654	0.749
Fe <sup>2+</sup>	0.156	0.155	0.109	0.239	0.256	0.209	0.250	0.189	0.222	0.272	0.357	0.264	0.263	0.211	0.506	0.221	0.217	0.210
Ca	1.844	1.821	1.891	1.761	1.744	1.791	1.750	1.811	1.778	1.728	1.643	1.736	1.737	1.789	1.463	1.779	1.783	1.790
Na	0.613	0.533	0.567	0.688	0.717	0.705	0.936	0.847	0.732	0.817	0.884	0.710	0.738	0.721	0.554	0.720	0.740	0.766
K	0.021	0.017	0.021	0.003	0.008	0.006	0.002	0.007	0.003	0.005	0.003	0.007	0.002	0.002	0.002	0.008	0.009	0.004
Mg#	0.68	0.69	0.68	0.80	0.77	0.79	0.79	0.75	0.82	0.76	0.77	0.80	0.79	0.79	0.88	0.78	0.80	0.78

Amphibole formulae calculated on the basis of 23 oxygens with fixed number of cations (15) and Fe<sup>3+</sup>/Fe<sup>2+</sup> adjustment. Mg# = Mg/(Mg+Fe<sup>2+</sup>). c = grain core. r = grain rim. k.c = amphibole in garnet kelfitic corona. sec = secondary amphibole

**Table I-11.** Microprobe analyses and formulae of amphibole from different metamorphic rock varieties of the Krivaja-Konjuh ophiolite complex

Rock type	Garnet-diopside amphibolite – Garnet-diopside-hypersthene amphibolite																	
Sample-Nr.	u22-46	u22-57	u22-59	x1-16	x1-17	x1-36	x1-49	x1-15	x1-18	x1-29	x1-31	x1-33	x1-50	x1-51	x1-52	u40-1	u40-42	u40-69
Remark				c	c	c	c	r	r	r	r	r	r	r	r	c	c	c
SiO <sub>2</sub>	43.87	43.30	44.26	43.18	43.88	44.50	43.71	42.84	44.04	44.41	46.01	44.08	44.78	43.81	44.77	43.67	43.03	43.08
TiO <sub>2</sub>	0.43	0.27	0.48	0.74	1.04	1.28	1.21	0.69	1.03	1.26	1.19	1.32	1.20	1.27	1.27	1.27	1.04	1.43
Al <sub>2</sub> O <sub>3</sub>	13.09	14.86	13.94	13.25	11.86	11.48	11.84	12.74	12.26	11.19	10.29	11.46	10.74	11.39	10.42	12.24	12.36	12.08
Cr <sub>2</sub> O <sub>3</sub>	0.27	0.30	0.16	0.06	0.01	0.05	0.02	0.01	0.05	0.06	0.12	0.07	0.07	0.05	0.09	0.09	0.01	0.12
Fe <sub>2</sub> O <sub>3</sub>																		
FeO	9.03	8.75	7.82	11.19	11.67	11.05	12.20	12.36	10.18	11.40	10.72	11.38	11.61	12.08	10.81	11.67	12.40	11.81
MnO	0.13	0.09	0.15	0.25	0.21	0.18	0.16	0.35	0.16	0.15	0.13	0.15	0.11	0.16	0.12	0.20	0.17	0.17
MgO	16.11	15.74	16.30	13.80	14.29	14.46	13.67	14.40	14.31	14.16	14.96	14.13	14.21	14.04	14.36	14.45	14.11	14.05
CaO	11.55	11.45	11.64	11.47	11.45	11.31	11.65	10.95	11.95	11.76	11.58	11.68	11.73	11.66	11.56	11.10	11.52	11.13
Na <sub>2</sub> O	2.60	2.75	2.54	2.46	2.33	2.27	2.25	2.41	2.31	2.20	2.01	2.28	2.02	2.19	2.05	2.41	2.37	2.39
K <sub>2</sub> O	0.03	0.02	0.03	0.02	0.02	0.03	0.07	0.04	0.03	0.05	0.02	0.04	0.05	0.05	0.01	0.04	0.00	0.01
Total	97.11	97.53	97.31	96.41	96.75	96.60	96.78	96.79	96.30	96.64	97.04	96.58	96.52	96.70	95.45	97.12	97.01	96.25
Si	6.333	6.223	6.347	6.362	6.442	6.537	6.441	6.287	6.471	6.534	6.702	6.492	6.589	6.450	6.648	6.391	6.311	6.375
Al <sup>IV</sup>	1.667	1.777	1.653	1.638	1.558	1.463	1.559	1.713	1.529	1.466	1.298	1.508	1.411	1.550	1.352	1.609	1.689	1.625
Al <sup>VI</sup>	0.561	0.740	0.702	0.662	0.495	0.525	0.497	0.491	0.595	0.474	0.469	0.481	0.452	0.427	0.471	0.503	0.447	0.481
Ti	0.047	0.029	0.052	0.082	0.114	0.142	0.135	0.076	0.113	0.139	0.131	0.146	0.133	0.141	0.142	0.140	0.115	0.160
Cr	0.031	0.034	0.019	0.007	0.002	0.005	0.003	0.001	0.005	0.007	0.014	0.008	0.008	0.006	0.011	0.010	0.001	0.014
Fe <sup>3+</sup>	0.248	0.174	0.118	0.098	0.166	0.000	0.136	0.376	0.040	0.071	0.000	0.068	0.102	0.203	0.000	0.127	0.337	0.123
Mg	3.468	3.372	3.483	3.030	3.129	3.167	3.003	3.150	3.135	3.105	3.249	3.103	3.116	3.081	3.178	3.153	3.085	3.099
Mn	0.016	0.010	0.018	0.031	0.025	0.023	0.019	0.043	0.019	0.019	0.016	0.018	0.014	0.020	0.015	0.025	0.021	0.021
Fe <sup>2+</sup>	0.629	0.641	0.608	1.090	1.069	1.139	1.208	0.863	1.092	1.185	1.121	1.176	1.176	1.123	1.184	1.042	0.993	1.103
Fe <sup>2+</sup>	0.213	0.237	0.211	0.190	0.198	0.218	0.160	0.278	0.119	0.147	0.184	0.158	0.151	0.161	0.159	0.259	0.190	0.236
Ca	1.787	1.763	1.789	1.810	1.802	1.780	1.840	1.722	1.881	1.853	1.807	1.842	1.849	1.839	1.840	1.741	1.810	1.764
Na	0.727	0.767	0.705	0.703	0.663	0.646	0.642	0.687	0.657	0.627	0.559	0.652	0.576	0.624	0.587	0.683	0.674	0.687
K	0.006	0.004	0.005	0.004	0.003	0.006	0.013	0.007	0.005	0.009	0.004	0.008	0.009	0.009	0.002	0.007	0.000	0.001
Mg#	0.80	0.79	0.81	0.70	0.71	0.70	0.69	0.73	0.72	0.70	0.71	0.70	0.70	0.71	0.70	0.71	0.72	0.70

Amphibole formulae calculated on the basis of 23 oxygens with fixed number of cations (15) and Fe<sup>3+</sup>/Fe<sup>2+</sup> adjustment. Mg# = Mg/(Mg+Fe<sup>2+</sup>). c = grain core. r = grain rim

**Table I-12.** Microprobe analyses and formulae of amphibole from different metamorphic rock varieties of the Krivaja-Konjuh ophiolite complex

Rock type	Garnet-diopside-hypersthene amphibolite																	
Sample-Nr.	u40-2	u40-6	u40-8	u40-22	u40-41	u40-45	u40-68	v4-6	v4-23	v4-39	v4-41	v4-49	v4-55	v4-3	v4-4	v4-8	v4-10	v4-17
Remark	r	r	r	r	r	r	r	c	c	c	c	c	c	r	r	r	r	r
SiO <sub>2</sub>	43.28	43.05	43.14	43.54	43.28	43.80	43.19	45.31	44.85	44.19	43.39	45.04	44.85	43.97	45.63	45.10	46.66	45.68
TiO <sub>2</sub>	1.32	1.46	1.52	1.30	1.33	0.98	1.51	0.30	0.47	0.34	0.77	0.45	0.48	0.42	0.32	0.40	0.37	0.29
Al <sub>2</sub> O <sub>3</sub>	12.34	11.99	12.20	12.28	12.11	11.50	12.03	11.92	12.33	11.48	12.72	12.22	12.94	12.86	11.04	12.32	10.11	12.33
Cr <sub>2</sub> O <sub>3</sub>	0.04	0.04	0.03	0.06	0.02	0.04	0.09	0.10	0.16	0.23	0.18	0.07	0.15	0.08	0.15	0.12	0.10	0.10
Fe <sub>2</sub> O <sub>3</sub>																		
FeO	11.19	11.33	11.24	10.93	11.99	11.89	11.50	9.35	9.03	11.19	10.64	9.14	9.17	9.70	9.15	9.13	8.38	8.64
MnO	0.14	0.16	0.15	0.18	0.19	0.24	0.25	0.17	0.14	0.18	0.36	0.21	0.08	0.15	0.12	0.17	0.11	0.17
MgO	14.68	14.42	14.17	14.49	13.94	14.47	14.14	16.04	15.80	14.43	14.69	15.95	15.43	15.43	16.16	15.90	16.79	16.25
CaO	11.06	11.27	11.24	11.53	11.45	11.40	11.46	11.73	11.76	11.34	11.03	11.48	11.55	11.93	11.77	11.71	11.93	12.13
Na <sub>2</sub> O	2.48	2.40	2.52	2.55	2.39	2.28	2.39	2.20	2.27	2.15	2.50	2.30	2.41	2.39	2.07	2.26	2.00	2.14
K <sub>2</sub> O	0.03	0.03	0.03	0.02	0.01	0.03	0.02	0.05	0.04	0.07	0.05	0.06	0.04	0.05	0.04	0.03	0.05	0.05
Total	96.57	96.13	96.24	96.87	96.71	96.64	96.58	97.17	96.85	95.59	96.34	96.91	97.09	96.94	96.45	97.13	96.51	97.79
Si	6.361	6.363	6.383	6.386	6.378	6.438	6.366	6.528	6.488	6.541	6.379	6.513	6.489	6.372	6.616	6.502	6.740	6.519
Al <sup>IV</sup>	1.639	1.637	1.617	1.614	1.622	1.562	1.634	1.472	1.512	1.459	1.621	1.487	1.511	1.628	1.384	1.498	1.260	1.481
Al <sup>VI</sup>	0.498	0.451	0.510	0.509	0.481	0.431	0.456	0.552	0.591	0.544	0.584	0.596	0.695	0.568	0.502	0.595	0.460	0.593
Ti	0.146	0.162	0.169	0.143	0.147	0.109	0.167	0.033	0.051	0.038	0.086	0.049	0.052	0.045	0.035	0.043	0.040	0.031
Cr	0.005	0.004	0.003	0.007	0.002	0.005	0.011	0.011	0.018	0.027	0.021	0.008	0.017	0.009	0.018	0.014	0.012	0.012
Fe <sup>3+</sup>	0.131	0.165	0.036	0.081	0.158	0.252	0.145	0.219	0.156	0.180	0.123	0.128	0.009	0.282	0.206	0.166	0.138	0.213
Mg	3.216	3.178	3.126	3.167	3.061	3.170	3.108	3.446	3.408	3.184	3.220	3.438	3.327	3.333	3.493	3.418	3.615	3.457
Mn	0.017	0.020	0.019	0.022	0.023	0.030	0.031	0.021	0.017	0.022	0.045	0.025	0.009	0.018	0.014	0.021	0.014	0.020
Fe <sup>2+</sup>	0.986	1.020	1.136	1.070	1.127	1.004	1.083	0.719	0.759	1.004	0.923	0.756	0.890	0.746	0.733	0.744	0.722	0.674
Fe <sup>2+</sup>	0.258	0.215	0.218	0.189	0.192	0.206	0.190	0.189	0.177	0.201	0.263	0.222	0.210	0.148	0.172	0.191	0.153	0.145
Ca	1.742	1.785	1.782	1.811	1.808	1.794	1.810	1.811	1.823	1.799	1.737	1.778	1.790	1.852	1.828	1.809	1.847	1.855
Na	0.707	0.688	0.723	0.726	0.684	0.651	0.684	0.616	0.637	0.618	0.713	0.645	0.677	0.671	0.582	0.631	0.561	0.593
K	0.005	0.005	0.006	0.004	0.003	0.006	0.004	0.010	0.007	0.013	0.010	0.011	0.008	0.008	0.007	0.006	0.009	0.010
Mg#	0.72	0.72	0.70	0.72	0.70	0.72	0.71	0.79	0.78	0.73	0.73	0.78	0.75	0.79	0.79	0.79	0.81	0.81

Amphibole formulae calculated on the basis of 23 oxygens with fixed number of cations (15) and Fe<sup>3+</sup>/Fe<sup>2+</sup> adjustment. Mg# = Mg/(Mg+Fe<sup>2+</sup>). c = grain core. r = grain rim

**Table I-13.** Microprobe analyses and formulae of amphibole from different metamorphic rock varieties of the Krivaja-Konjuh ophiolite complex

Rock type	Garnet-diopside-hypersthene amphibolite – Diopside-amphibolite gneiss																	
Sample-Nr.	v4-18	v4-35	v4-36	v2-42	v2-48	v4-50	v4-54	10d-19	10d-24	10d-34b	10d-40	10d-42	10d-58	10d-1	10d-4	10d-7	10d-9	11d-12
Remark	r	r	r	r	r	r	r							c	c	c	c	c
SiO <sub>2</sub>	48.11	45.21	49.52	43.36	44.88	45.43	44.63	39.30	43.94	40.03	39.94	39.65	39.75	38.93	40.16	38.78	39.17	38.82
TiO <sub>2</sub>	0.12	0.38	0.16	0.72	0.49	0.47	0.51	2.81	0.16	2.30	2.10	2.17	2.84	2.72	0.25	4.15	2.89	2.64
Al <sub>2</sub> O <sub>3</sub>	9.00	10.84	7.33	12.82	11.80	11.96	12.18	14.23	10.24	13.98	14.73	13.53	13.76	14.83	13.07	14.05	14.05	13.56
Cr <sub>2</sub> O <sub>3</sub>	0.07	0.14	0.05	0.14	0.12	0.15	0.15	0.02	0.06	0.04	0.08	0.04	0.06	0.04	0.02	0.03	0.05	0.05
Fe <sub>2</sub> O <sub>3</sub>																		
FeO	8.91	11.36	9.42	10.73	9.08	8.80	8.94	15.64	19.36	15.01	14.80	15.28	15.96	15.15	24.57	16.47	15.13	15.85
MnO	0.13	0.24	0.25	0.39	0.12	0.11	0.09	0.23	0.27	0.30	0.25	0.29	0.22	0.23	0.16	0.25	0.27	0.26
MgO	17.32	15.07	17.09	15.00	16.15	15.92	15.86	9.81	9.47	10.45	9.60	10.46	10.06	9.61	4.79	9.73	9.92	10.22
CaO	12.17	11.55	11.62	10.96	11.52	11.60	11.37	11.91	11.74	12.11	12.70	11.82	11.51	12.25	11.76	10.69	11.67	11.86
Na <sub>2</sub> O	1.79	2.02	1.32	2.35	2.19	2.17	2.35	3.02	1.92	2.55	2.46	2.74	2.92	2.93	1.72	2.77	2.86	2.90
K <sub>2</sub> O	0.02	0.07	0.03	0.04	0.05	0.04	0.05	0.19	0.19	0.24	0.16	0.18	0.21	0.15	0.32	0.15	0.18	0.19
Total	97.65	96.87	96.78	96.50	96.40	96.64	96.12	97.16	97.35	96.99	96.82	96.18	97.29	96.83	96.81	97.08	96.19	96.36
Si	6.854	6.589	7.120	6.344	6.513	6.577	6.508	5.958	6.637	6.028	6.025	6.035	6.015	5.910	6.263	5.891	5.980	5.926
Al <sup>IV</sup>	1.146	1.411	0.880	1.656	1.487	1.423	1.492	2.042	1.363	1.972	1.975	1.965	1.985	2.090	1.737	2.109	2.020	2.074
Al <sup>VI</sup>	0.365	0.451	0.361	0.554	0.532	0.618	0.601	0.500	0.461	0.509	0.643	0.462	0.469	0.564	0.665	0.407	0.508	0.365
Ti	0.013	0.041	0.018	0.079	0.053	0.051	0.056	0.320	0.018	0.260	0.238	0.249	0.323	0.311	0.030	0.474	0.332	0.303
Cr	0.008	0.016	0.005	0.017	0.013	0.017	0.018	0.002	0.008	0.004	0.009	0.005	0.007	0.004	0.002	0.003	0.006	0.007
Fe <sup>3+</sup>	0.248	0.277	0.105	0.253	0.209	0.070	0.088	0.000	0.260	0.149	0.097	0.156	0.000	0.009	0.428	0.000	0.000	0.200
Mg	3.678	3.275	3.663	3.271	3.494	3.435	3.449	2.217	2.133	2.345	2.159	2.373	2.270	2.175	1.114	2.203	2.258	2.327
Mn	0.016	0.029	0.031	0.048	0.015	0.014	0.011	0.030	0.034	0.038	0.032	0.038	0.028	0.030	0.021	0.032	0.034	0.034
Fe <sup>2+</sup>	0.671	0.911	0.817	0.778	0.684	0.796	0.778	1.930	2.086	1.695	1.771	1.717	1.902	1.906	2.740	1.880	1.861	1.764
Fe <sup>2+</sup>	0.142	0.197	0.210	0.282	0.209	0.200	0.224	0.053	0.099	0.046	0.000	0.072	0.118	0.008	0.035	0.212	0.071	0.060
Ca	1.858	1.803	1.790	1.718	1.791	1.800	1.776	1.935	1.901	1.954	2.052	1.928	1.866	1.992	1.965	1.740	1.909	1.940
Na	0.495	0.572	0.368	0.668	0.617	0.609	0.666	0.875	0.562	0.744	0.721	0.809	0.840	0.861	0.520	0.768	0.827	0.859
K	0.003	0.013	0.006	0.007	0.009	0.008	0.009	0.036	0.037	0.047	0.030	0.035	0.040	0.029	0.063	0.030	0.035	0.036
Mg#	0.82	0.75	0.78	0.76	0.80	0.78	0.77	0.53	0.49	0.57	0.55	0.57	0.53	0.53	0.29	0.51	0.54	0.56

Amphibole formulae calculated on the basis of 23 oxygens with fixed number of cations (15) and Fe<sup>3+</sup>/Fe<sup>2+</sup> adjustment. Mg# = Mg/(Mg+Fe<sup>2+</sup>). c = grain core. r = grain rim

**Table I-14.** Microprobe analyses and formulae of amphibole from different metamorphic rock varieties of the Krivaja-Konjuh ophiolite complex

Rock type	Diopside-amphibolite gneiss																	
Sample-Nr.	10d-17	10d-25	10d-30	10d-36	10d-41a	10d-2	10d-3	10d-8	10d-10	10d-11	10d-18	10d-23	10d-31	10d-35	10d-41	10d-47	10d-50	10d-52
Remark	c	c	c	c	c	r	r	r	r	r	r	r	r	r	r	r	r	r
SiO <sub>2</sub>	51.26	40.42	39.52	39.04	51.48	39.03	40.67	39.19	39.12	39.05	51.39	41.08	39.69	39.18	49.16	39.90	39.64	39.40
TiO <sub>2</sub>	0.03	2.31	2.39	2.58	0.15	2.85	0.33	2.79	2.84	2.83	0.04	1.41	2.37	2.57	0.10	2.32	2.81	2.82
Al <sub>2</sub> O <sub>3</sub>	0.45	13.32	14.24	14.50	4.15	14.12	11.88	14.53	14.06	13.90	0.41	12.79	14.03	14.25	7.25	13.71	13.77	13.52
Cr <sub>2</sub> O <sub>3</sub>	0.04	0.05	0.01	0.03	0.09	0.07	0.00	0.02	0.06	0.07	0.03	0.04	0.06	0.05	0.04	0.09	0.06	0.12
Fe <sub>2</sub> O <sub>3</sub>																		
FeO	27.38	15.18	15.25	15.20	12.70	15.83	25.26	16.03	15.60	15.84	27.38	15.45	15.31	14.55	12.97	16.21	16.64	16.05
MnO	0.42	0.22	0.28	0.37	0.15	0.26	0.11	0.34	0.31	0.24	0.51	0.23	0.35	0.28	0.24	0.20	0.19	0.22
MgO	5.92	10.75	10.28	10.35	14.88	10.01	4.70	9.84	10.05	10.10	6.23	11.11	10.40	10.33	13.47	9.86	9.66	10.06
CaO	12.07	12.02	11.76	11.87	12.48	11.97	11.52	11.94	11.94	11.69	12.10	12.37	12.00	11.75	12.42	11.70	11.73	11.73
Na <sub>2</sub> O	0.13	2.62	2.82	3.01	0.92	3.20	1.55	3.01	2.99	3.08	0.10	2.47	2.92	2.99	1.48	2.91	2.67	2.93
K <sub>2</sub> O	0.04	0.21	0.19	0.21	0.05	0.17	0.30	0.18	0.14	0.20	0.02	0.15	0.20	0.21	0.12	0.17	0.18	0.19
Total	97.71	97.09	96.74	97.15	97.05	97.50	96.32	97.86	97.12	96.99	98.23	97.10	97.33	96.15	97.23	97.07	97.35	97.04
Si	7.937	6.083	5.987	5.900	7.501	5.909	6.388	5.903	5.930	5.938	7.905	6.151	5.982	5.972	7.189	6.055	6.002	5.986
Al <sup>IV</sup>	0.063	1.917	2.013	2.100	0.499	2.091	1.612	2.097	2.070	2.062	0.074	1.849	2.018	2.028	0.811	1.945	1.998	2.014
Al <sup>VI</sup>	0.019	0.445	0.529	0.482	0.214	0.428	0.587	0.483	0.441	0.429	0.000	0.408	0.474	0.532	0.439	0.508	0.458	0.407
Ti	0.003	0.261	0.273	0.294	0.016	0.325	0.039	0.316	0.324	0.324	0.005	0.159	0.269	0.295	0.011	0.264	0.320	0.322
Cr	0.005	0.006	0.001	0.003	0.010	0.009	0.000	0.002	0.007	0.008	0.004	0.004	0.008	0.005	0.004	0.011	0.008	0.015
Fe <sup>3+</sup>	0.000	0.141	0.072	0.105	0.000	0.034	0.417	0.068	0.067	0.031	0.067	0.372	0.109	0.000	0.000	0.008	0.073	0.048
Mg	1.366	2.412	2.321	2.331	3.232	2.259	1.102	2.210	2.271	2.290	1.428	2.480	2.338	2.347	2.936	2.230	2.180	2.280
Mn	0.055	0.028	0.036	0.047	0.018	0.033	0.015	0.043	0.040	0.031	0.067	0.029	0.045	0.036	0.030	0.026	0.024	0.028
Fe <sup>2+</sup>	3.545	1.708	1.769	1.738	1.509	1.913	2.841	1.878	1.849	1.887	3.429	1.547	1.758	1.785	1.581	1.953	1.936	1.901
Fe <sup>2+</sup>	0.000	0.063	0.091	0.078	0.039	0.058	0.061	0.073	0.062	0.096	0.026	0.015	0.062	0.069	0.005	0.097	0.097	0.091
Ca	2.002	1.937	1.909	1.922	1.948	1.942	1.939	1.927	1.938	1.904	1.995	1.985	1.938	1.919	1.946	1.903	1.903	1.909
Na	0.038	0.764	0.829	0.882	0.245	0.938	0.471	0.878	0.879	0.908	0.031	0.718	0.852	0.871	0.372	0.856	0.784	0.864
K	0.007	0.039	0.037	0.041	0.010	0.033	0.059	0.034	0.027	0.038	0.004	0.028	0.038	0.041	0.022	0.033	0.035	0.036
Mg#	0.28	0.58	0.56	0.56	0.68	0.53	0.28	0.53	0.54	0.54	0.29	0.61	0.56	0.56	0.65	0.52	0.52	0.53

Amphibole formulae calculated on the basis of 23 oxygens with fixed number of cations (15) and Fe<sup>3+</sup>/Fe<sup>2+</sup> adjustment. Mg# = Mg/(Mg+Fe<sup>2+</sup>). c = grain core. r = grain rim

## Garnet

Table J-1. Microprobe analyses and formulae of garnet from different metamorphic rock varieties of the Krivaja-Konjuh ophiolite complex

Rock type	Garnet-diopside amphibolite																	
Sample-Nr.	cc1-1	cc1-2	cc1-4	cc1-28	cc1-31	cc1-33	cc1-35	cc1-37	cc1-40	cc1-49	cc1-50	cc1-63	cc1-64	mk2-14	mk2-18	mk2-36	mk2-37	mk2-41
Remark	c	r	r	r	r	r	r	r	c	c	r	r	c			c	r	
SiO <sub>2</sub>	38.64	38.77	39.09	39.27	39.00	39.10	38.86	39.31	38.69	39.22	39.43	39.79	39.20	39.67	39.76	39.79	39.82	39.93
TiO <sub>2</sub>	0.19	0.04	0.09	0.06	0.05	0.03	0.06	0.07	0.24	0.15	0.11	0.03	0.18	0.17	0.07	0.16	0.12	0.09
Al <sub>2</sub> O <sub>3</sub>	21.70	21.92	21.99	21.83	22.05	22.08	22.05	22.01	21.56	21.97	22.03	22.16	21.91	21.98	22.04	21.44	21.66	21.73
Fe <sub>2</sub> O <sub>3</sub>																		
FeO	18.57	18.83	19.18	19.18	19.56	19.28	18.85	18.57	19.45	18.75	18.51	18.96	18.30	19.97	19.20	19.15	19.25	19.37
MnO	1.35	0.73	0.56	0.58	0.63	0.59	0.47	0.58	0.48	0.72	0.57	0.61	0.58	0.79	0.88	0.78	0.79	0.86
MgO	7.75	9.52	9.55	9.73	9.40	9.62	9.41	9.56	8.03	8.42	9.15	9.62	8.91	11.19	11.33	11.14	11.17	11.30
CaO	11.07	9.13	9.19	9.25	9.15	9.12	9.91	9.51	10.85	10.98	10.39	9.06	10.76	6.72	6.59	6.75	6.63	6.33
Total	99.35	98.98	99.74	100.20	99.97	99.86	99.68	99.76	99.40	100.24	100.25	100.30	99.85	100.59	99.94	99.29	99.44	99.67
Si	2.958	2.954	2.957	2.957	2.948	2.954	2.940	2.969	2.957	2.963	2.968	2.991	2.965	2.965	2.984	3.010	3.006	3.008
Ti	0.011	0.002	0.005	0.003	0.003	0.002	0.004	0.004	0.014	0.008	0.006	0.002	0.010	0.009	0.004	0.009	0.007	0.005
Al	1.958	1.968	1.960	1.937	1.965	1.966	1.966	1.960	1.942	1.957	1.955	1.963	1.953	1.936	1.949	1.912	1.927	1.928
Fe <sup>3+</sup>	0.100	0.118	0.113	0.125	0.126	0.121	0.142	0.089	0.119	0.101	0.096	0.051	0.098	0.112	0.073	0.046	0.051	0.046
Fe <sup>2+</sup>	1.089	1.082	1.100	1.083	1.111	1.096	1.050	1.084	1.124	1.083	1.070	1.141	1.059	1.136	1.132	1.166	1.165	1.174
Mn	0.088	0.047	0.036	0.037	0.040	0.037	0.030	0.037	0.031	0.046	0.036	0.039	0.037	0.050	0.056	0.050	0.050	0.055
Mg	0.884	1.082	1.077	1.092	1.059	1.084	1.061	1.076	0.915	0.949	1.026	1.078	1.004	1.247	1.268	1.256	1.257	1.269
Ca	0.908	0.745	0.745	0.746	0.741	0.738	0.803	0.770	0.888	0.889	0.838	0.730	0.872	0.538	0.530	0.547	0.536	0.511
Py	29.79	36.59	36.42	36.91	35.90	36.66	36.03	36.28	30.93	31.98	34.55	36.08	33.79	41.97	42.47	41.62	41.79	42.18
Al	36.68	36.59	37.20	36.61	37.64	37.10	35.67	36.55	38.00	36.50	36.01	38.20	35.62	38.24	37.91	38.62	38.72	39.02
Sp	2.95	1.60	1.20	1.25	1.36	1.27	1.02	1.24	1.05	1.55	1.22	1.30	1.25	1.68	1.88	1.65	1.68	1.82
And	4.95	5.79	5.57	6.13	6.15	5.94	6.94	4.39	5.89	5.02	4.73	2.55	4.88	5.46	3.61	2.33	2.56	2.33
Uv	0.22	0.10	0.21	0.87	0.37	0.11	0.22	0.40	0.21	0.06	0.15	0.17	0.00	0.27	0.19	0.21	0.00	0.09
Mel	0.54	0.10	0.26	0.16	0.15	0.09	0.17	0.20	0.67	0.41	0.31	0.09	0.51	0.45	0.19	0.46	0.34	0.27
Gr	24.86	19.22	19.14	18.07	18.44	18.83	19.94	20.96	23.26	24.48	23.03	21.62	23.95	11.92	13.76	15.11	14.92	14.29
Mg#	0.45	0.50	0.49	0.50	0.49	0.50	0.50	0.50	0.45	0.47	0.49	0.49	0.49	0.52	0.53	0.52	0.52	0.52

Total iron as FeO. Mg# = Mg/(Mg+Fe<sup>2+</sup>). c = grain core. r = grain rim

**Table J-2.** Microprobe analyses and formulae of garnet from different metamorphic rock varieties of the Krivaja-Konjuh ophiolite complex

Rock type	Garnet-diopside amphibolite																	
Sample-Nr.	gr7-1	gr7-2	gr7-16	gr7-20	gr7-23	gr7-27	gr7-28	v1-1	v1-2	v1-8	v1-11	v1-14	v1-16	v1-18	v1-19	v1-19b	v1-86	v1-91
Remark	c	r	r	r	r	c	r	c	r	r	r	r	r	r	k.c.	k.c.	c	r
SiO <sub>2</sub>	40.21	40.47	40.72	40.71	40.57	39.95	40.70	40.05	39.99	39.89	39.92	40.22	39.59	40.05	41.95	35.89	39.85	39.74
TiO <sub>2</sub>	0.07	0.02	0.05	0.04	0.04	0.11	0.03	0.02	0.05	0.02	0.05	0.05	0.04	0.05	0.04	0.02	0.17	0.10
Al <sub>2</sub> O <sub>3</sub>	21.69	21.26	21.62	21.25	21.76	21.51	21.77	22.23	22.58	22.37	22.36	22.18	22.31	22.47	14.33	21.73	22.16	21.92
Cr <sub>2</sub> O <sub>3</sub>	0.18	0.31	0.08	0.27	0.22	0.13	0.13	0.09	0.06	0.11	0.06	0.10	0.10	0.10	0.07	0.11	0.09	0.10
Fe <sub>2</sub> O <sub>3</sub>																		
FeO	15.34	14.39	14.45	14.66	14.95	15.78	13.98	17.54	17.76	18.04	18.38	18.19	17.83	18.07	18.43	19.29	18.55	18.09
MnO	0.46	0.30	0.30	0.22	0.35	0.38	0.17	0.71	0.66	0.80	0.77	0.85	0.80	0.82	0.94	0.74	1.03	0.96
MgO	12.19	12.97	13.02	13.23	13.49	11.85	13.87	12.84	12.92	13.01	12.54	12.67	12.75	12.85	22.84	22.82	12.10	12.06
CaO	9.43	9.30	8.66	9.06	8.18	9.36	8.26	6.07	6.16	5.94	6.08	5.73	6.16	5.94	0.25	0.20	6.82	6.58
Total	99.58	99.01	98.90	99.45	99.57	99.08	98.91	99.57	100.17	100.20	100.18	100.01	99.58	100.35	98.86	100.82	100.79	99.56
Si	2.993	3.015	3.035	3.019	3.002	2.994	3.019	2.986	2.963	2.957	2.968	2.994	2.955	2.967	3.066	2.550	2.954	2.978
Ti	0.004	0.001	0.003	0.002	0.002	0.006	0.002	0.001	0.003	0.001	0.003	0.003	0.002	0.003	0.002	0.001	0.009	0.006
Al	1.903	1.867	1.899	1.857	1.898	1.901	1.903	1.954	1.972	1.954	1.959	1.946	1.963	1.962	1.234	1.819	1.936	1.936
Fe <sup>3+</sup>	0.094	0.084	0.020	0.084	0.082	0.092	0.050	0.070	0.093	0.124	0.095	0.055	0.119	0.095	0.627	1.075	0.133	0.093
Fe <sup>2+</sup>	0.861	0.813	0.880	0.825	0.844	0.897	0.817	1.024	1.008	0.995	1.048	1.077	0.994	1.025	0.499	0.071	1.017	1.041
Mn	0.029	0.019	0.019	0.014	0.022	0.024	0.011	0.045	0.041	0.050	0.048	0.054	0.050	0.051	0.058	0.044	0.065	0.061
Mg	1.352	1.440	1.447	1.462	1.488	1.324	1.533	1.427	1.428	1.438	1.390	1.406	1.418	1.419	2.488	2.416	1.337	1.348
Ca	0.752	0.742	0.691	0.720	0.648	0.751	0.656	0.485	0.489	0.472	0.485	0.457	0.493	0.472	0.019	0.015	0.542	0.528
Py	45.16	47.79	47.64	48.40	49.56	44.18	50.82	47.88	48.13	48.66	46.79	46.97	47.99	47.84	81.17	94.86	45.17	45.25
Al	28.76	26.97	28.97	27.32	28.11	29.93	27.08	34.35	33.98	33.67	35.26	35.98	33.63	34.54	16.29	2.80	34.34	34.97
Sp	0.97	0.62	0.63	0.46	0.74	0.81	0.35	1.50	1.39	1.70	1.63	1.80	1.71	1.73	1.90	1.74	2.19	2.05
And	4.67	4.24	1.05	4.27	4.10	4.61	2.56	3.47	4.56	6.07	4.68	2.76	5.81	4.67	32.48	43.86	6.55	4.61
Uv	0.51	0.92	0.25	0.82	0.65	0.39	0.38	0.27	0.17	0.31	0.19	0.30	0.27	0.28	0.20	0.26	0.27	0.28
Mel	0.20	0.05	0.13	0.12	0.11	0.32	0.09	0.05	0.14	0.06	0.14	0.13	0.12	0.14	0.11	0.04	0.46	0.29
Gr	19.72	19.41	21.33	18.62	16.74	19.77	18.72	12.49	11.63	9.53	11.30	12.06	10.47	10.81	1.01	1.04	11.02	12.55
Mg#	0.61	0.64	0.62	0.64	0.64	0.60	0.65	0.58	0.59	0.59	0.57	0.57	0.59	0.58	0.83	0.97	0.57	0.56

Total iron as FeO. Mg# = Mg/(Mg+Fe<sup>2+</sup>). c = grain core. r = grain rim. k.c. = remnant of garnet in kelfitic corona

**Table J-3.** Microprobe analyses and formulae of garnet from different metamorphic rock varieties of the Krivaja-Konjuh ophiolite complex

Rock type	Garnet-diopside amphibolite																	
Sample-Nr.	v1-92	v1-93	v1-97	v1-102	du5-1	du5-2	du5-3	du5-4	du5-11	du5-13	du5-16	du5-18	du5-20a	du5-23	du5-24	du5-29	du5-32	du5-41
Remark	c	r		k.c.	c	r	r	c	r	r	r	r	r	c	r	r	r	r
SiO <sub>2</sub>	39.34	39.38	39.74	37.09	39.70	39.41	38.97	39.16	38.94	38.16	39.23	38.94	39.01	39.38	38.95	38.93	38.84	38.91
TiO <sub>2</sub>	0.08	0.07	0.06	0.03	0.10	0.09	0.08	0.04	0.13	0.07	0.05	0.09	0.10	0.08	0.07	0.07	0.08	0.07
Al <sub>2</sub> O <sub>3</sub>	22.23	22.18	22.30	21.40	22.23	22.11	22.01	22.36	22.61	21.67	22.19	21.95	22.08	22.04	21.75	21.91	22.11	21.93
Cr <sub>2</sub> O <sub>3</sub>	0.15	0.08	0.04	0.20	0.00	0.11	0.06	0.03	0.06	0.12	0.18	0.10	0.09	0.11	0.03	0.18	0.00	0.00
Fe <sub>2</sub> O <sub>3</sub>																		
FeO	17.91	17.71	18.65	17.35	19.28	19.41	20.75	20.18	19.08	18.18	19.63	19.96	19.46	19.05	19.62	19.48	19.35	19.10
MnO	0.87	0.83	1.00	1.20	0.63	0.66	0.62	0.86	0.51	0.65	0.69	0.74	0.58	0.80	0.78	0.72	0.66	0.78
MgO	12.18	12.26	12.33	23.58	7.19	7.19	6.18	6.91	6.54	6.45	6.78	6.57	7.11	7.14	6.64	6.57	6.59	7.23
CaO	6.79	6.84	6.14	0.19	12.09	11.84	12.25	11.79	12.59	14.50	12.24	12.09	12.09	12.11	12.27	12.29	12.24	12.35
Total	99.56	99.37	100.27	101.04	101.24	100.82	100.93	101.33	100.48	99.81	101.01	100.46	100.52	100.71	100.13	100.13	99.89	100.37
Si	2.944	2.950	2.957	2.617	2.987	2.979	2.962	2.953	2.956	2.914	2.966	2.965	2.958	2.980	2.974	2.972	2.969	2.952
Ti	0.004	0.004	0.003	0.002	0.006	0.005	0.004	0.002	0.007	0.004	0.003	0.005	0.006	0.004	0.004	0.004	0.005	0.004
Al	1.961	1.958	1.955	1.780	1.971	1.970	1.972	1.987	2.023	1.950	1.977	1.969	1.973	1.965	1.957	1.971	1.992	1.961
Fe <sup>3+</sup>	0.136	0.131	0.122	0.971	0.044	0.056	0.095	0.101	0.050	0.208	0.078	0.088	0.094	0.061	0.087	0.067	0.062	0.129
Fe <sup>2+</sup>	0.985	0.978	1.038	0.053	1.168	1.171	1.224	1.171	1.161	0.953	1.163	1.183	1.140	1.145	1.166	1.177	1.175	1.083
Mn	0.055	0.053	0.063	0.072	0.040	0.042	0.040	0.055	0.033	0.042	0.044	0.048	0.037	0.052	0.051	0.047	0.043	0.050
Mg	1.359	1.370	1.368	2.480	0.807	0.810	0.700	0.777	0.740	0.734	0.764	0.746	0.803	0.805	0.756	0.747	0.751	0.817
Ca	0.544	0.549	0.489	0.014	0.975	0.959	0.997	0.953	1.024	1.186	0.991	0.986	0.982	0.982	1.004	1.005	1.003	1.004
Py	46.18	46.43	46.23	94.71	26.98	27.16	23.63	26.28	25.02	25.17	25.80	25.16	27.11	26.98	25.41	25.12	25.28	27.67
Al	33.46	33.17	35.10	2.02	39.08	39.28	41.34	39.62	39.24	32.70	39.25	39.94	38.49	38.38	39.18	39.54	39.54	36.66
Sp	1.88	1.79	2.13	2.74	1.35	1.41	1.35	1.86	1.11	1.45	1.48	1.62	1.25	1.73	1.70	1.57	1.44	1.69
And	6.62	6.41	5.99	40.80	2.22	2.77	4.67	4.96	2.48	10.00	3.84	4.32	4.62	3.01	4.29	3.31	3.06	6.30
Uv	0.43	0.23	0.13	0.48	0.00	0.33	0.17	0.09	0.19	0.34	0.53	0.30	0.26	0.34	0.10	0.54	0.00	0.00
Mel	0.21	0.20	0.17	0.07	0.29	0.25	0.22	0.10	0.36	0.20	0.13	0.24	0.29	0.21	0.19	0.19	0.24	0.19
Gr	11.22	11.77	10.25	-40.81	30.08	28.80	28.62	27.08	31.60	30.14	28.96	28.43	27.99	29.35	29.14	29.73	30.45	27.50
Mg#	0.58	0.58	0.57	0.98	0.41	0.41	0.36	0.40	0.39	0.43	0.40	0.39	0.41	0.41	0.39	0.39	0.39	0.43

Total iron as FeO. Mg# = Mg/(Mg+Fe<sup>2+</sup>). c = grain core. r = grain rim. k.c. = remnant of garnet in kelfitic corona



**Table J-4.** Microprobe analyses and formulae of garnet from different metamorphic rock varieties of the Krivaja-Konjuh ophiolite complex

Rock type	Garnet-diopside amphibolite – Garnet-diopside-hypersthene amphibolite																	
Sample-Nr.	u22-25	u22-26	u22-35	u22-37	u22-41	u22-42	u22-50	u22-52	u22-54	u22-55	u22-62	u22-64	u22-65	x1-1	x1-4	x1-13	x1-14	x1-37
Remark	c	r	r	r	c	r	r	r	c	r	r	r	c	c	r	r	r	c
SiO <sub>2</sub>	39.93	40.17	40.15	40.70	40.47	40.59	40.36	40.71	40.32	40.88	40.49	40.00	39.79	39.79	39.62	39.53	39.96	40.09
TiO <sub>2</sub>	0.09	0.09	0.04	0.01	0.06	0.05	0.05	0.05	0.08	0.02	0.09	0.06	0.02	0.13	0.06	0.07	0.04	0.11
Al <sub>2</sub> O <sub>3</sub>	22.92	23.17	22.82	23.20	23.12	23.01	22.94	23.10	22.94	22.99	22.94	23.01	23.04	22.13	22.56	22.49	22.19	22.23
Cr <sub>2</sub> O <sub>3</sub>	0.08	0.21	0.23	0.00	0.12	0.15	0.14	0.07	0.09	0.20	0.08	0.11	0.21	0.05	0.04	0.03	0.07	0.20
Fe <sub>2</sub> O <sub>3</sub>																		
FeO	14.89	14.38	14.04	13.85	14.49	14.04	13.83	14.38	15.04	14.25	13.82	13.95	15.78	18.67	18.57	19.52	18.86	18.85
MnO	0.48	0.34	0.34	0.29	0.43	0.37	0.32	0.39	0.45	0.37	0.44	0.41	0.50	0.82	0.69	0.82	0.66	0.67
MgO	13.43	14.04	13.96	14.06	13.60	14.27	14.03	14.07	13.45	13.97	13.92	13.72	13.21	11.22	11.78	11.54	11.57	11.95
CaO	7.97	8.54	8.57	8.67	8.04	8.15	8.33	8.39	8.08	8.29	8.29	8.12	8.09	6.62	6.11	6.02	6.12	6.14
Total	99.79	100.94	100.16	100.78	100.31	100.67	100.02	101.15	100.45	100.96	100.06	99.38	100.66	99.43	99.42	100.02	99.47	100.11
Si	2.944	2.918	2.939	2.956	2.964	2.952	2.956	2.951	2.953	2.971	2.966	2.951	2.917	2.998	2.976	2.961	3.006	2.992
Ti	0.005	0.005	0.002	0.001	0.003	0.002	0.003	0.003	0.004	0.001	0.005	0.003	0.001	0.007	0.003	0.004	0.002	0.006
Al	1.992	1.983	1.968	1.986	1.994	1.972	1.979	1.974	1.981	1.969	1.981	2.001	1.991	1.965	1.997	1.986	1.968	1.961
Fe <sup>3+</sup>	0.105	0.160	0.138	0.101	0.066	0.113	0.099	0.113	0.102	0.076	0.074	0.085	0.164	0.026	0.044	0.085	0.012	0.043
Fe <sup>2+</sup>	0.813	0.713	0.721	0.740	0.822	0.741	0.748	0.758	0.820	0.790	0.773	0.775	0.803	1.150	1.122	1.138	1.174	1.133
Mn	0.030	0.021	0.021	0.018	0.026	0.023	0.020	0.024	0.028	0.023	0.027	0.026	0.031	0.052	0.044	0.052	0.042	0.042
Mg	1.476	1.520	1.524	1.523	1.486	1.549	1.532	1.521	1.469	1.514	1.520	1.509	1.443	1.258	1.319	1.288	1.297	1.330
Ca	0.629	0.665	0.672	0.674	0.631	0.635	0.653	0.651	0.634	0.645	0.651	0.642	0.635	0.535	0.492	0.483	0.493	0.491
Py	50.07	52.07	51.86	51.53	50.11	52.55	51.87	51.48	49.77	50.93	51.15	51.12	49.54	42.01	44.31	43.51	43.15	44.39
Al	27.56	24.43	24.56	25.05	27.72	25.13	25.33	25.67	27.79	26.58	26.02	26.26	27.57	38.40	37.71	38.42	39.06	37.82
Sp	1.01	0.72	0.71	0.59	0.89	0.78	0.68	0.81	0.95	0.77	0.91	0.87	1.07	1.74	1.47	1.77	1.39	1.41
And	5.15	7.72	6.71	4.96	3.23	5.55	4.84	5.55	4.98	3.74	3.65	4.18	7.88	1.33	2.22	4.29	0.64	2.15
Uv	0.21	0.57	0.64	0.00	0.33	0.43	0.40	0.20	0.24	0.56	0.23	0.32	0.59	0.14	0.12	0.09	0.22	0.00
Mel	0.25	0.24	0.11	0.03	0.15	0.12	0.13	0.13	0.21	0.06	0.23	0.17	0.06	0.37	0.16	0.20	0.11	0.29
Gr	15.74	14.24	15.41	17.84	17.56	15.46	16.75	16.16	16.06	17.35	17.81	17.09	13.28	16.03	14.01	11.73	15.44	13.93
Mg#	0.64	0.68	0.68	0.67	0.64	0.68	0.67	0.67	0.64	0.66	0.66	0.66	0.64	0.52	0.54	0.53	0.52	0.54

Total iron as FeO. Mg# = Mg/(Mg+Fe<sup>2+</sup>). c = grain core. r = grain rim

**Table J-5.** Microprobe analyses and formulae of garnet from different metamorphic rock varieties of the Krivaja-Konjuh ophiolite complex

Rock type	Garnet-diopside-hypersthene amphibolite – Plagioclase-garnet-diopside gneiss																	
Sample-Nr.	x1-38	x1-42	x1-57	x1-60	x1-62	u40-27	u40-28	u40-53	u40-54	u40-58	u40-60	u40-62	v4-28	v4-29	z1c-1	z1c-2	z1c-5	z1c-6
Remark	r	r	c	c	c	c	r	c	r	r	r	r	c	r	c	r	r	r
SiO <sub>2</sub>	39.85	40.26	40.45	40.07	39.84	39.41	39.59	39.59	39.65	39.50	39.54	39.83	40.79	40.50	37.73	38.20	38.39	38.31
TiO <sub>2</sub>	0.16	0.12	0.10	0.16	0.08	0.13	0.02	0.09	0.12	0.10	0.11	0.11	0.03	0.04	0.14	0.07	0.12	0.10
Al <sub>2</sub> O <sub>3</sub>	22.16	22.49	22.51	22.11	22.37	22.22	22.56	22.23	22.14	22.52	22.35	22.51	22.70	22.64	21.08	20.97	21.22	21.13
Cr <sub>2</sub> O <sub>3</sub>	0.02	0.05	0.08	0.04	0.06	0.01	0.00	0.09	0.13	0.05	0.08	0.06	0.15	0.15	0.05	0.05	0.05	0.01
Fe <sub>2</sub> O <sub>3</sub>																		
FeO	17.96	18.29	18.83	18.94	18.69	18.49	18.55	18.52	18.71	18.51	18.68	18.59	15.72	15.89	24.91	24.02	23.99	24.15
MnO	0.70	0.71	0.62	0.63	0.70	1.17	0.82	0.84	0.68	0.75	0.67	0.78	0.79	0.91	2.18	1.15	1.31	1.46
MgO	11.92	11.80	11.85	11.84	12.58	10.99	11.59	11.55	11.95	11.84	11.88	11.89	13.51	13.28	5.58	7.42	7.90	7.29
CaO	6.21	6.09	6.11	6.41	5.94	7.61	6.55	6.74	6.40	6.39	6.24	6.55	6.26	6.39	8.64	7.26	7.37	7.17
Total	99.00	99.86	100.56	100.20	100.25	100.05	99.69	99.66	99.78	99.68	99.56	100.32	99.97	99.81	100.33	99.15	100.34	99.61
Si	3.003	3.008	3.007	2.991	2.960	2.955	2.968	2.972	2.969	2.958	2.966	2.966	3.010	2.998	2.930	2.969	2.943	2.967
Ti	0.009	0.007	0.006	0.009	0.004	0.007	0.001	0.005	0.007	0.006	0.006	0.006	0.002	0.002	0.008	0.004	0.007	0.006
Al	1.968	1.981	1.972	1.945	1.959	1.963	1.993	1.966	1.954	1.988	1.976	1.975	1.975	1.976	1.930	1.921	1.917	1.929
Fe <sup>3+</sup>	0.011	0.000	0.000	0.053	0.107	0.113	0.071	0.075	0.089	0.085	0.076	0.076	0.000	0.017	0.193	0.130	0.181	0.125
Fe <sup>2+</sup>	1.120	1.143	1.171	1.129	1.054	1.046	1.091	1.087	1.082	1.074	1.096	1.082	0.970	0.966	1.425	1.431	1.357	1.439
Mn	0.044	0.045	0.039	0.040	0.044	0.074	0.052	0.053	0.043	0.048	0.043	0.049	0.049	0.057	0.143	0.076	0.085	0.096
Mg	1.339	1.314	1.313	1.318	1.394	1.228	1.296	1.293	1.334	1.321	1.329	1.319	1.486	1.465	0.647	0.860	0.902	0.842
Ca	0.502	0.488	0.487	0.513	0.473	0.611	0.526	0.542	0.514	0.513	0.502	0.522	0.495	0.507	0.719	0.605	0.605	0.595
Py	44.56	43.95	43.63	43.93	47.02	41.50	43.69	43.45	44.87	44.70	44.74	44.39	49.53	48.91	22.04	28.93	30.60	28.32
Al	37.27	38.22	38.89	37.65	35.55	35.35	36.81	36.54	36.41	36.34	36.92	36.38	32.33	32.25	48.58	48.16	45.99	48.43
Sp	1.48	1.51	1.31	1.33	1.48	2.51	1.76	1.79	1.44	1.61	1.44	1.66	1.63	1.90	4.88	2.56	2.89	3.22
And	0.59	0.00	0.00	2.68	5.33	5.57	3.51	3.74	4.43	4.17	3.74	3.77	0.00	0.85	9.38	6.44	8.86	6.19
Uv	0.06	0.16	0.25	0.11	0.18	0.04	0.00	0.26	0.37	0.15	0.22	0.18	0.40	0.45	0.15	0.15	0.14	0.02
Mel	0.49	0.35	0.29	0.45	0.21	0.37	0.05	0.26	0.33	0.29	0.31	0.31	0.10	0.10	0.39	0.20	0.32	0.28
Gr	15.55	15.81	15.64	13.85	10.23	14.67	14.19	13.96	12.14	12.76	12.63	13.32	16.00	15.53	14.59	13.56	11.19	13.54
Mg#	0.54	0.53	0.53	0.54	0.57	0.54	0.54	0.54	0.55	0.55	0.55	0.55	0.61	0.60	0.31	0.38	0.40	0.37

Total iron as FeO. Mg#=Mg/(Mg+Fe<sup>2+</sup>). c = grain core. r = grain rim

**Table J-6.** Microprobe analyses and formulae of garnet from different metamorphic rock varieties of the Krivaja-Konjuh ophiolite complex

Rock type	Plagioclase-garnet-diopside gneiss								
Sample-Nr.	z1c-8	z1c-26	z1c-27	z1c-42	z1c-43	z1c-44	z1c-45	z1c-54	z1c-63
Remark	r	c	r	r	r	c	r	r	r
SiO <sub>2</sub>	38.09	38.72	38.46	38.34	38.02	38.27	38.81	38.61	38.38
TiO <sub>2</sub>	0.13	0.07	0.09	0.09	0.11	0.10	0.06	0.10	0.06
Al <sub>2</sub> O <sub>3</sub>	20.84	21.52	21.60	21.16	20.92	21.30	21.50	21.37	21.47
Cr <sub>2</sub> O <sub>3</sub>	0.01	0.03	0.00	0.09	0.01	0.00	0.00	0.06	0.01
Fe <sub>2</sub> O <sub>3</sub>									
FeO	24.49	24.02	23.86	23.53	24.10	23.91	23.61	23.88	23.67
MnO	1.36	0.77	1.02	1.18	1.26	0.75	0.95	1.22	1.11
MgO	6.51	8.43	8.56	7.57	7.10	7.70	8.57	8.61	8.96
CaO	8.03	6.49	6.10	7.73	7.68	7.57	6.89	6.35	6.08
Total	99.47	100.07	99.70	99.68	99.20	99.64	100.37	100.23	99.75
Si	2.966	2.966	2.955	2.959	2.959	2.952	2.960	2.953	2.942
Ti	0.008	0.004	0.005	0.005	0.006	0.006	0.003	0.006	0.004
Al	1.913	1.943	1.956	1.925	1.918	1.936	1.933	1.926	1.940
Fe <sup>3+</sup>	0.139	0.117	0.124	0.141	0.154	0.153	0.141	0.158	0.168
Fe <sup>2+</sup>	1.456	1.422	1.409	1.377	1.414	1.389	1.365	1.370	1.349
Mn	0.090	0.050	0.066	0.077	0.083	0.049	0.061	0.079	0.072
Mg	0.756	0.962	0.981	0.871	0.823	0.885	0.974	0.982	1.024
Ca	0.670	0.533	0.502	0.639	0.640	0.626	0.563	0.521	0.500
Py	25.45	32.43	33.16	29.37	27.82	30.01	32.87	33.27	34.76
Al	48.99	47.93	47.62	46.47	47.77	47.11	46.07	46.41	45.83
Sp	3.01	1.69	2.23	2.60	2.80	1.67	2.06	2.67	2.45
And	6.90	5.75	6.11	6.95	7.59	7.50	6.92	7.73	8.19
Uv	0.04	0.10	0.00	0.28	0.03	0.00	0.00	0.17	0.04
Mel	0.38	0.21	0.24	0.24	0.30	0.28	0.16	0.29	0.17
Gr	15.23	11.90	10.64	14.09	13.70	13.43	11.93	9.46	8.57
Mg#	0.34	0.40	0.41	0.39	0.37	0.39	0.42	0.42	0.43

Total iron as FeO. Mg# = Mg/(Mg+Fe<sup>2+</sup>). c = grain core. r = grain rim

Plagioclase

Table K-1. Microprobe analyses and formulae of plagioclase from different metamorphic rock varieties of the Krivaja-Konjuh ophiolite complex

Rock type	Granoblastic amphibolite																	
Sample-Nr.	u30-7	u30-10	u30-12	u30-13	u30-16	u29-5	u29-6	u29-13	u29-16	u29-17	u29-23	u29-24	u29-27	u29-39	u29-45	u29-47	u29-55	u29-57
Remark	r	c			r	c	r		c	r	c					r	c	r
SiO <sub>2</sub>	43.74	43.40	43.63	43.07	43.60	42.85	42.41	42.21	42.45	42.17	42.54	42.13	42.41	42.52	42.44	42.54	42.50	42.57
Al <sub>2</sub> O <sub>3</sub>	36.49	36.62	36.54	36.31	36.35	36.29	36.39	36.34	36.57	36.69	36.54	36.82	36.32	36.53	36.58	36.79	36.21	36.40
Fe <sub>2</sub> O <sub>3</sub>	0.03	0.00	0.00	0.04	0.02	0.05	0.07	0.06	0.04	0.02	0.05	0.06	0.08	0.18	0.11	0.06	0.07	0.06
BaO	0.00	0.00	0.00	0.00	0.00	0.01	0.01	0.01	0.00	0.00	0.01	0.00	0.00	0.00	0.03	0.02	0.00	0.00
CaO	19.96	19.55	19.97	19.56	19.88	20.20	20.38	20.13	20.39	20.07	20.25	20.16	20.50	20.11	20.48	20.17	20.09	20.24
Na <sub>2</sub> O	0.26	0.28	0.23	0.34	0.26	0.08	0.01	0.03	0.03	0.05	0.03	0.02	0.01	0.03	0.01	0.01	0.04	0.02
K <sub>2</sub> O	0.01	0.00	0.00	0.00	0.01	0.00	0.00	0.00	0.02	0.01	0.00	0.01	0.00	0.02	0.00	0.00	0.00	0.01
Total	100.50	99.85	100.36	99.32	100.12	99.47	99.27	98.78	99.51	99.01	99.43	99.20	99.33	99.39	99.65	99.59	98.90	99.31
Si	2.015	2.010	2.012	2.007	2.016	1.997	1.983	1.983	1.980	1.975	1.985	1.970	1.983	1.984	1.978	1.981	1.992	1.988
Al	1.981	1.999	1.986	1.995	1.981	1.993	2.005	2.012	2.011	2.025	2.009	2.030	2.001	2.009	2.010	2.019	2.001	2.004
Fe <sup>3+</sup>	0.001	0.000	0.000	0.001	0.001	0.002	0.002	0.002	0.001	0.001	0.002	0.002	0.003	0.006	0.004	0.002	0.002	0.002
Ba	0.000	0.000	0.000	0.000	0.000	0.000	0.000	0.000	0.000	0.000	0.000	0.000	0.000	0.000	0.001	0.000	0.000	0.000
Ca	0.985	0.970	0.987	0.977	0.985	1.009	1.021	1.013	1.019	1.007	1.012	1.010	1.027	1.006	1.023	1.006	1.009	1.013
Na	0.024	0.025	0.020	0.031	0.023	0.008	0.001	0.003	0.003	0.004	0.003	0.002	0.001	0.002	0.001	0.000	0.003	0.002
K	0.001	0.000	0.000	0.000	0.001	0.000	0.000	0.000	0.001	0.001	0.000	0.001	0.000	0.001	0.000	0.000	0.000	0.001
Or	0.06	0.00	0.00	0.00	0.07	0.00	0.00	0.00	0.11	0.06	0.02	0.07	0.00	0.10	0.00	0.00	0.00	0.06
Ab	2.34	2.48	2.02	3.05	2.28	0.75	0.11	0.29	0.28	0.44	0.27	0.21	0.11	0.23	0.11	0.04	0.32	0.21
An	97.6	97.5	98.0	97.0	97.7	99.3	99.9	99.7	99.6	99.5	99.7	99.7	99.9	99.7	99.9	100.0	99.7	99.7

Formulae of plagioclase calculated on the basis of 8 oxygens, FeO<sub>tot</sub> is expressed as Fe<sub>2</sub>O<sub>3</sub>, c = grain core, r = grain rim

**Table K-2.** Microprobe analyses and formulae of plagioclase from different metamorphic rock varieties of the Krivaja-Konjuh ophiolite complex

Rock type	Granoblastic amphibolite																	
Sample-Nr	u29-59	11c-30	r8-4	r8-5	r8-7	r8-13	r8-14	r8-15	r8-28	r8-29	r8-36	u23-3	u23-4	u23-5	u23-8	u23-9	u23-13	u23-15
Remark		ab	r	c	r	r	c	r	r	r	c	r	c	r	r	r	r	r
SiO <sub>2</sub>	42.19	66.93	53.25	64.84	56.65	60.93	54.64	55.14	54.69	53.80	53.63	45.64	46.15	45.91	45.61	45.79	45.74	45.88
Al <sub>2</sub> O <sub>3</sub>	36.18	19.99	29.36	21.99	27.41	24.89	29.28	28.89	28.40	29.07	28.95	34.61	34.98	34.99	34.91	33.07	34.95	34.94
Fe <sub>2</sub> O <sub>3</sub>	0.08	0.13	0.29	0.00	0.13	0.13	0.12	0.20	0.16	0.24	0.21	0.07	0.02	0.04	0.00	0.07	0.06	0.02
BaO	0.00	0.00	0.00	0.00	0.00	0.00	0.00	0.00	0.00	0.00	0.00	0.00	0.00	0.00	0.00	0.00	0.00	0.00
CaO	20.47	0.00	11.74	3.02	8.80	4.44	11.12	10.95	11.13	11.36	11.50	18.21	17.63	17.57	17.65	16.38	17.89	17.74
Na <sub>2</sub> O	0.04	11.13	5.14	10.28	7.96	8.30	5.31	5.43	5.54	5.34	5.34	1.45	1.39	1.48	1.47	2.09	1.49	1.39
K <sub>2</sub> O	0.00	0.11	0.04	0.08	0.08	0.75	0.04	0.04	0.03	0.04	0.05	0.01	0.00	0.00	0.00	0.01	0.00	0.01
Total	98.95	98.29	99.82	100.20	101.03	99.44	100.49	100.66	99.94	99.86	99.68	99.99	100.16	99.99	99.64	97.43	100.13	99.97
Si	1.981	2.971	2.416	2.853	2.530	2.719	2.452	2.470	2.471	2.436	2.435	2.105	2.117	2.111	2.106	2.158	2.104	2.111
Al	2.002	1.046	1.570	1.140	1.443	1.309	1.549	1.525	1.512	1.552	1.549	1.881	1.891	1.896	1.900	1.837	1.894	1.894
Fe <sup>3+</sup>	0.003	0.004	0.010	0.000	0.004	0.004	0.004	0.007	0.005	0.008	0.007	0.002	0.001	0.001	0.000	0.003	0.002	0.001
Ba	0.000	0.000	0.000	0.000	0.000	0.000	0.000	0.000	0.000	0.000	0.000	0.000	0.000	0.000	0.000	0.000	0.000	0.000
Ca	1.030	0.000	0.571	0.142	0.421	0.212	0.535	0.526	0.539	0.551	0.559	0.900	0.866	0.865	0.873	0.827	0.881	0.874
Na	0.003	0.958	0.453	0.877	0.689	0.718	0.462	0.471	0.485	0.469	0.470	0.129	0.123	0.132	0.132	0.191	0.132	0.124
K	0.000	0.006	0.002	0.004	0.005	0.043	0.002	0.002	0.002	0.002	0.003	0.000	0.000	0.000	0.000	0.001	0.000	0.001
Or	0.01	0.62	0.24	0.42	0.41	4.40	0.20	0.22	0.15	0.23	0.30	0.05	0.00	0.00	0.00	0.08	0.00	0.06
Ab	0.32	99.4	44.1	85.7	61.8	73.8	46.2	47.2	47.3	45.9	45.5	12.6	12.5	13.3	13.1	18.8	13.1	12.4
An	99.7	0.01	55.6	13.9	37.8	21.8	53.6	52.6	52.5	53.9	54.2	87.4	87.5	86.7	86.9	81.2	86.9	87.5

Formulae of plagioclase calculated on the basis of 8 oxygens, FeO<sub>tot</sub> is expressed as Fe<sub>2</sub>O<sub>3</sub>, c = grain core, r = grain rim, ab = albite

**Table K-3.** Microprobe analyses and formulae of plagioclase from different metamorphic rock varieties of the Krivaja-Konjuh ophiolite complex

Rock type	Granoblastic amphibolite – Garnet-diopside amphibolite																	
Sample-Nr	u23-16	u23-19	u23-30	u23-32	u23-33	u23-34	u23-36	cc1-6	cc1-7	cc1-8	cc1-10	cc1-12	cc1-43	cc1-44	cc1-52	cc1-54	cc1-56	cc1-58
Remark	c	r	r	r	c	c	r	r	c	r	r	r	c	r	a	c	r	r
SiO <sub>2</sub>	45.24	45.44	45.83	45.85	45.42	45.72	45.10	54.80	54.11	52.83	55.08	50.08	54.69	51.84	47.85	53.90	53.80	54.00
Al <sub>2</sub> O <sub>3</sub>	34.66	35.13	34.21	34.69	34.39	34.58	34.54	28.13	28.48	29.07	28.08	31.38	28.45	29.99	31.91	28.61	29.07	28.19
Fe <sub>2</sub> O <sub>3</sub>	0.00	0.10	0.07	0.02	0.07	0.03	0.05	0.21	0.16	0.19	0.16	0.33	0.15	0.22	0.31	0.17	0.15	0.27
BaO	0.00	0.00	0.00	0.00	0.00	0.00	0.00	0.00	0.00	0.00	0.00	0.00	0.00	0.00	0.00	0.00	0.00	0.00
CaO	17.75	18.06	17.45	17.81	17.84	18.29	18.16	10.57	10.71	11.12	10.25	14.21	10.56	12.29	14.25	10.93	11.11	11.21
Na <sub>2</sub> O	1.38	1.28	1.67	1.42	1.37	1.40	1.38	6.01	5.55	5.25	6.10	3.90	5.75	4.72	3.34	5.56	5.47	5.50
K <sub>2</sub> O	0.00	0.01	0.04	0.02	0.00	0.00	0.00	0.00	0.01	0.03	0.01	0.01	0.01	0.04	0.08	0.01	0.04	0.02
Total	99.02	100.01	99.27	99.81	99.09	100.02	99.23	99.72	99.01	98.48	99.68	99.92	99.61	99.09	97.73	99.18	99.64	99.18
Si	2.103	2.093	2.125	2.114	2.111	2.107	2.096	2.481	2.465	2.425	2.491	2.289	2.476	2.374	2.239	2.454	2.440	2.462
Al	1.899	1.907	1.869	1.885	1.883	1.878	1.892	1.501	1.529	1.573	1.497	1.690	1.518	1.618	1.759	1.536	1.554	1.514
Fe <sup>3+</sup>	0.000	0.003	0.003	0.001	0.002	0.001	0.002	0.007	0.006	0.007	0.006	0.011	0.005	0.007	0.011	0.006	0.005	0.009
Ba	0.000	0.000	0.000	0.000	0.000	0.000	0.000	0.000	0.000	0.000	0.000	0.000	0.000	0.000	0.000	0.000	0.000	0.000
Ca	0.884	0.891	0.867	0.880	0.888	0.903	0.904	0.512	0.523	0.547	0.497	0.696	0.512	0.603	0.714	0.533	0.540	0.548
Na	0.124	0.114	0.150	0.126	0.123	0.125	0.125	0.528	0.490	0.467	0.535	0.346	0.504	0.419	0.303	0.491	0.481	0.486
K	0.000	0.001	0.002	0.001	0.000	0.000	0.000	0.000	0.000	0.002	0.000	0.001	0.001	0.002	0.005	0.000	0.002	0.001
Or	0.00	0.06	0.21	0.12	0.00	0.01	0.00	0.01	0.05	0.17	0.04	0.07	0.08	0.23	0.48	0.04	0.23	0.10
Ab	12.3	11.3	14.7	12.6	12.2	12.2	12.1	50.7	48.4	46.0	51.8	33.2	49.6	40.9	29.6	47.9	47.0	47.0
An	87.7	88.6	85.1	87.3	87.8	87.8	87.9	49.3	51.6	53.9	48.1	66.8	50.3	58.9	69.9	52.0	52.8	52.9

Formulae of plagioclase calculated on the basis of 8 oxygens, FeO<sub>tot</sub> is expressed as Fe<sub>2</sub>O<sub>3</sub>, c = grain core, r = grain rim, a = altered

**Table K-4.** Microprobe analyses and formulae of plagioclase from different metamorphic rock varieties of the Krivaja-Konjuh ophiolite complex

Rock type	Garnet-diopside amphibolite																	
Sample-Nr	cc1-79	cc1-80	cc1-84	cc1-86	mk2-1	mk2-2	mk2-7	mk2-25	mk2-26	mk2-29	mk2-34	gr7-3	gr7-4	gr7-11	gr7-15	gr7-35	gr7-40	gr7-43
Remark	r	c			r	c	r	r	r			grt	grt					r
SiO <sub>2</sub>	54.72	55.36	51.53	54.60	51.07	49.46	52.49	49.41	47.53	46.52	46.59	52.75	52.00	46.99	49.52	45.23	51.08	48.99
Al <sub>2</sub> O <sub>3</sub>	28.20	27.94	29.82	27.82	31.46	32.03	30.49	32.40	33.78	34.69	32.86	29.72	30.18	32.50	32.31	30.99	31.06	32.02
Fe <sub>2</sub> O <sub>3</sub>	0.15	0.13	0.14	0.19	0.30	0.16	0.32	0.29	0.37	0.29	2.00	0.18	0.13	0.23	0.17	0.34	0.09	0.17
BaO	0.00	0.00	0.00	0.00	0.00	0.00	0.00	0.00	0.00	0.00	0.00	0.00	0.00	0.00	0.00	0.00	0.00	0.00
CaO	10.51	10.02	10.35	10.48	14.02	14.68	12.41	14.81	16.38	17.10	15.30	12.79	13.05	16.53	15.16	17.97	13.57	15.01
Na <sub>2</sub> O	5.85	6.23	4.31	5.84	3.79	3.07	4.45	3.02	2.11	1.87	2.42	4.19	4.10	1.93	2.75	1.31	3.60	2.87
K <sub>2</sub> O	0.02	0.02	1.18	0.01	0.01	0.00	0.02	0.02	0.01	0.01	0.00	0.00	0.02	0.00	0.00	0.02	0.00	0.00
Total	99.44	99.69	97.33	98.93	100.64	99.40	100.17	99.95	100.18	100.48	99.18	99.62	99.48	98.17	99.91	95.85	99.40	99.06
Si	2.482	2.501	2.398	2.489	2.311	2.268	2.374	2.256	2.175	2.129	2.163	2.398	2.371	2.195	2.260	2.178	2.333	2.257
Al	1.507	1.488	1.635	1.495	1.678	1.731	1.625	1.743	1.822	1.871	1.798	1.592	1.622	1.789	1.738	1.758	1.671	1.739
Fe <sup>3+</sup>	0.005	0.005	0.005	0.006	0.010	0.006	0.011	0.010	0.013	0.010	0.070	0.006	0.004	0.008	0.006	0.012	0.003	0.006
Ba	0.000	0.000	0.000	0.000	0.000	0.000	0.000	0.000	0.000	0.000	0.000	0.000	0.000	0.000	0.000	0.000	0.000	0.000
Ca	0.510	0.485	0.516	0.512	0.680	0.721	0.602	0.725	0.803	0.838	0.761	0.623	0.638	0.827	0.742	0.927	0.664	0.741
Na	0.514	0.545	0.389	0.516	0.332	0.273	0.390	0.267	0.187	0.166	0.218	0.370	0.362	0.174	0.243	0.122	0.319	0.257
K	0.001	0.001	0.070	0.001	0.000	0.000	0.001	0.001	0.001	0.001	0.000	0.000	0.001	0.000	0.000	0.001	0.000	0.000
Or	0.10	0.13	7.20	0.07	0.04	0.02	0.10	0.11	0.06	0.07	0.02	0.00	0.13	0.00	0.00	0.11	0.02	0.01
Ab	50.1	52.9	39.9	50.2	32.8	27.4	39.3	26.9	18.9	16.5	22.3	37.2	36.2	17.4	24.7	11.6	32.4	25.7
An	49.8	47.0	52.9	49.7	67.1	72.5	60.6	73.0	81.1	83.4	77.7	62.8	63.7	82.6	75.3	88.3	67.5	74.3

Formulae of plagioclase calculated on the basis of 8 oxygens, FeO<sub>tot</sub> is expressed as Fe<sub>2</sub>O<sub>3</sub>, c = grain core, r = grain rim, grt = inclusion in garnet

**Table K-5.** Microprobe analyses and formulae of plagioclase from different metamorphic rock varieties of the Krivaja-Konjuh ophiolite complex

Rock type	Garnet-diopside amphibolite																	
Sample-Nr	gr7-46	gr7-50	gr7-51	gr7-56	gr7-62	gr7-67	gr7-68	v1-5	v1-20	v1-22	v1-26	v1-26b	v1-31	v1-37	v1-46	v1-55	v1-56	v1-58
Remark	r	r	r	c		r	r		c	k.c.	amp	amp	r			r	c	r
SiO <sub>2</sub>	49.35	49.52	49.52	47.96	48.38	50.44	49.28	48.71	46.06	46.05	47.51	46.23	45.53	45.54	45.29	49.04	50.07	50.75
Al <sub>2</sub> O <sub>3</sub>	32.19	31.71	31.57	32.38	32.52	31.57	32.17	31.84	34.64	33.93	33.31	34.32	34.94	35.01	34.52	31.50	31.48	31.20
Fe <sub>2</sub> O <sub>3</sub>	0.15	0.10	0.12	0.04	0.19	0.12	0.11	0.32	0.25	0.76	0.42	0.41	0.33	0.52	0.24	0.21	0.19	0.26
BaO	0.00	0.00	0.00	0.00	0.00	0.00	0.00	0.00	0.00	0.00	0.00	0.00	0.00	0.00	0.00	0.00	0.00	0.00
CaO	14.95	14.91	14.93	16.17	15.91	14.29	15.08	15.25	17.45	17.63	16.04	17.01	17.81	15.32	17.39	15.06	14.49	13.74
Na <sub>2</sub> O	2.85	2.75	2.78	2.27	2.46	3.34	2.81	3.00	1.53	1.46	2.37	1.64	1.30	0.99	1.41	3.15	3.59	4.00
K <sub>2</sub> O	0.00	0.01	0.00	0.02	0.01	0.00	0.00	0.00	0.01	0.01	0.00	0.00	0.01	1.34	0.18	0.01	0.00	0.00
Total	99.47	99.00	98.93	98.84	99.47	99.75	99.45	99.13	99.94	99.84	99.66	99.61	99.94	98.72	99.04	98.97	99.82	99.95
Si	2.262	2.279	2.281	2.221	2.226	2.301	2.260	2.248	2.120	2.126	2.186	2.133	2.099	2.121	2.107	2.265	2.289	2.313
Al	1.739	1.720	1.714	1.767	1.763	1.697	1.739	1.732	1.879	1.847	1.806	1.866	1.898	1.922	1.892	1.715	1.696	1.676
Fe <sup>3+</sup>	0.005	0.003	0.004	0.001	0.007	0.004	0.004	0.011	0.009	0.026	0.015	0.014	0.012	0.018	0.009	0.007	0.006	0.009
Ba	0.000	0.000	0.000	0.000	0.000	0.000	0.000	0.000	0.000	0.000	0.000	0.000	0.000	0.000	0.000	0.000	0.000	0.000
Ca	0.734	0.735	0.737	0.802	0.784	0.698	0.741	0.754	0.860	0.872	0.791	0.841	0.880	0.765	0.867	0.745	0.710	0.671
Na	0.253	0.245	0.248	0.203	0.220	0.295	0.250	0.269	0.137	0.131	0.212	0.147	0.116	0.089	0.127	0.282	0.318	0.353
K	0.000	0.000	0.000	0.001	0.000	0.000	0.000	0.000	0.001	0.001	0.000	0.000	0.001	0.080	0.011	0.000	0.000	0.000
Or	0.00	0.04	0.00	0.13	0.04	0.00	0.01	0.00	0.08	0.08	0.00	0.00	0.08	8.55	1.07	0.04	0.00	0.00
Ab	25.6	25.0	25.2	20.2	21.9	29.7	25.2	26.3	13.7	13.0	21.1	14.9	11.7	9.51	12.7	27.4	31.0	34.5
An	74.4	75.0	74.8	79.7	78.1	70.3	74.8	73.7	86.2	86.9	78.9	85.1	88.3	81.9	86.3	72.5	69.0	65.5

Formulae of plagioclase calculated on the basis of 8 oxygens, FeO<sub>tot</sub> is expressed as Fe<sub>2</sub>O<sub>3</sub>, c = grain core, r = grain rim, k.c. = part of garnet kelfitic corona, amp = inclusion in amphibole



**Table K-6.** Microprobe analyses and formulae of plagioclase from different metamorphic rock varieties of the Krivaja-Konjuh ophiolite complex

Rock type	Garnet-diopside amphibolite																	
Sample-Nr	v1-59	v1-62	v1-63	v1-67	v1-80	v1-82	v1-83	v1-87	v1-88	v1-94	v1-95	u22-29	u22-22	u22-39	u22-12	u22-4	u22-16	u22-18
Remark	grt	c	r	r	amp	amp	amp	grt	grt	grt	grt		c	c	k.c.	k.c.	r	r
SiO <sub>2</sub>	50.83	50.18	48.70	47.92	48.61	47.55	48.15	50.53	50.86	49.00	50.18	49.46	50.56	50.93	48.37	44.64	49.49	46.65
Al <sub>2</sub> O <sub>3</sub>	31.18	31.40	32.21	32.91	33.00	33.21	32.54	31.49	31.33	31.88	31.44	32.49	31.83	31.25	33.00	35.59	32.54	33.53
Fe <sub>2</sub> O <sub>3</sub>	0.38	0.16	0.21	0.19	0.25	0.24	0.22	0.32	0.37	0.58	0.26	0.35	0.18	0.17	0.24	0.30	0.28	0.25
BaO	0.00	0.00	0.00	0.00	0.00	0.00	0.00	0.00	0.00	0.00	0.00							
CaO	13.19	14.05	15.21	15.72	15.52	16.09	15.60	13.94	13.83	15.48	14.01	15.43	14.31	13.28	15.99	18.71	15.50	14.52
Na <sub>2</sub> O	4.05	3.55	3.16	2.62	2.66	2.41	2.82	3.71	3.76	3.07	3.52	2.77	3.57	3.99	2.60	0.99	2.91	2.38
K <sub>2</sub> O	0.00	0.08	0.00	0.00	0.00	0.02	0.00	0.01	0.04	0.00	0.07	0.01	0.00	0.01	0.01	0.01	0.01	1.50
Total	99.63	99.41	99.49	99.37	100.04	99.52	99.32	100.01	100.18	100.01	99.47	100.50	100.46	99.63	100.21	100.23	100.73	98.82
Si	2.320	2.299	2.240	2.208	2.221	2.191	2.220	2.302	2.312	2.246	2.298	2.248	2.293	2.323	2.211	2.058	2.246	2.174
Al	1.678	1.696	1.746	1.787	1.777	1.803	1.768	1.691	1.678	1.722	1.697	1.741	1.701	1.680	1.778	1.934	1.741	1.841
Fe <sup>3+</sup>	0.013	0.006	0.007	0.007	0.009	0.008	0.008	0.011	0.013	0.020	0.009	0.012	0.006	0.006	0.008	0.010	0.010	0.009
Ba	0.000	0.000	0.000	0.000	0.000	0.000	0.000	0.000	0.000	0.000	0.000	0.000	0.000	0.000	0.000	0.000	0.000	0.000
Ca	0.645	0.690	0.749	0.776	0.760	0.794	0.770	0.680	0.673	0.760	0.687	0.751	0.695	0.649	0.783	0.924	0.754	0.725
Na	0.358	0.315	0.282	0.234	0.236	0.215	0.252	0.328	0.331	0.273	0.313	0.244	0.314	0.353	0.230	0.089	0.256	0.215
K	0.000	0.004	0.000	0.000	0.000	0.001	0.000	0.001	0.002	0.000	0.004	0.001	0.000	0.001	0.001	0.000	0.001	0.089
Or	0.01	0.43	0.00	0.00	0.00	0.13	0.00	0.07	0.21	0.01	0.39	0.00	1.42	0.08	0.01	0.06	0.06	0.03
Ab	35.7	31.2	27.3	23.2	23.7	21.3	24.6	32.5	32.9	26.4	31.1	24.5	31.1	35.2	22.7	8.75	25.3	20.9
An	64.3	68.4	72.7	76.8	76.3	78.6	75.4	67.4	66.9	73.6	68.5	75.4	68.9	64.7	77.2	91.2	74.6	70.5

Formulae of plagioclase calculated on the basis of 8 oxygens, FeO<sub>tot</sub> is expressed as Fe<sub>2</sub>O<sub>3</sub>, c = grain core, r = grain rim, k.c. = part of garnet kelfitic corona, amp = inclusion in amphibole, grt = inclusion in garnet

**Table K-7.** Microprobe analyses and formulae of plagioclase from different metamorphic rock varieties of the Krivaja-Konjuh ophiolite complex

Rock type	Garnet-diopside amphibolite – Garnet-diopside-hypersthene amphibolite																	
Sample-Nr	u22-21	u22-38	x1-9	x1-10	x1-30	x1-32	x1-34	x1-35	x1-44	x1-45	x1-53	x1-54	x1-55	x1-56	u40-3	u40-5	u40-7	u40-9
Remark	r	r	c	r	r	r	r	c	r	c	r	r	r	c	r	r	r	c
SiO <sub>2</sub>	47.96	50.49	46.87	45.95	51.32	52.08	51.82	53.18	45.70	46.32	53.32	51.83	50.79	50.70	47.13	47.42	51.39	47.40
Al <sub>2</sub> O <sub>3</sub>	33.27	31.66	33.77	34.18	30.89	30.11	30.64	30.12	34.55	34.48	29.74	30.00	31.38	31.50	33.78	33.41	30.85	33.48
Fe <sub>2</sub> O <sub>3</sub>	0.37	0.15	0.35	1.08	0.53	0.29	0.25	0.20	0.45	0.43	0.26	0.24	0.23	0.21	0.31	0.29	0.23	0.16
BaO	0.00	0.00	0.00	0.00	0.00	0.00	0.00	0.00	0.00	0.00	0.00	0.00	0.00	0.00				
CaO	15.89	14.22	17.31	17.25	13.25	12.54	13.11	12.06	18.11	17.19	12.07	12.27	14.00	14.05	16.57	16.09	13.16	15.93
Na <sub>2</sub> O	2.64	3.61	1.73	1.59	3.88	4.48	4.05	4.78	1.44	1.57	4.76	4.67	3.75	3.71	2.20	2.42	4.00	2.37
K <sub>2</sub> O	0.01	0.02	0.00	0.00	0.00	0.00	0.02	0.00	0.00	0.00	0.00	0.02	0.01	0.00	0.02	0.00	0.00	0.01
Total	100.13	100.15	100.03	100.06	99.85	99.50	99.88	100.34	100.25	99.99	100.15	99.04	100.15	100.17	100.01	99.63	99.62	99.36
Si	2.196	2.297	2.154	2.118	2.336	2.374	2.355	2.398	2.104	2.129	2.409	2.374	2.309	2.305	2.164	2.182	2.342	2.185
Al	1.795	1.697	1.829	1.857	1.657	1.618	1.641	1.601	1.875	1.868	1.584	1.619	1.682	1.688	1.828	1.812	1.657	1.819
Fe <sup>3+</sup>	0.013	0.005	0.012	0.038	0.018	0.010	0.009	0.007	0.016	0.015	0.009	0.008	0.008	0.007	0.011	0.010	0.008	0.006
Ba	0.000	0.000	0.000	0.000	0.000	0.000	0.000	0.000	0.000	0.000	0.000	0.000	0.000	0.000	0.000	0.000	0.000	0.000
Ca	0.779	0.693	0.852	0.852	0.646	0.612	0.638	0.583	0.893	0.847	0.584	0.602	0.682	0.684	0.815	0.794	0.642	0.787
Na	0.234	0.319	0.154	0.142	0.342	0.396	0.357	0.418	0.128	0.140	0.417	0.415	0.331	0.327	0.196	0.216	0.354	0.212
K	0.000	0.001	0.000	0.000	0.000	0.000	0.001	0.000	0.000	0.000	0.000	0.001	0.000	0.000	0.001	0.000	0.000	0.001
Or	0.03	0.10	0.00	0.00	0.00	0.00	0.01	0.10	0.01	0.02	0.00	0.01	0.14	0.05	0.00	0.12	0.01	0.00
Ab	23.1	31.5	15.3	14.3	34.6	39.3	35.8	41.8	12.5	14.2	41.6	40.7	32.6	32.3	19.3	21.4	35.5	21.2
An	76.9	68.4	84.7	85.7	65.4	60.7	64.1	58.2	87.4	85.8	58.3	59.1	67.3	67.7	80.6	78.6	64.5	78.7

Formulae of plagioclase calculated on the basis of 8 oxygens, FeO<sub>tot</sub> is expressed as Fe<sub>2</sub>O<sub>3</sub>, c = grain core, r = grain rim

**Table K-8.** Microprobe analyses and formulae of plagioclase from different metamorphic rock varieties of the Krivaja-Konjuh ophiolite complex

Rock type	Garnet-diopside-hypersthene amphibolite																	
Sample-Nr	u40-12	u40-13	u40-29	u40-30	u40-43	u40-44	u50-51	u50-52	u40-65	v4-1	v4-2	v4-5	v4-9	v4-11	v4-12	v4-24	v4-25	v4-34
Remark	r	c	grt	grt	r	r	k.c.	k.c.		c	r	r	r	r	amp	c	r	
SiO <sub>2</sub>	49.60	51.27	51.86	51.92	46.86	47.00	45.07	45.54	44.96	47.41	46.97	46.46	46.70	46.95	46.70	47.36	45.82	46.46
Al <sub>2</sub> O <sub>3</sub>	32.01	31.04	30.11	29.81	32.96	33.59	34.68	34.91	35.82	33.55	33.69	32.61	33.84	33.50	33.84	34.34	34.66	34.08
Fe <sub>2</sub> O <sub>3</sub>	0.23	0.19	0.60	0.37	0.40	0.39	0.30	0.54	0.36	0.12	0.29	0.31	0.31	0.26	0.34	0.29	0.36	0.21
BaO	0.00	0.00	0.00	0.00	0.00	0.00	0.00	0.00	0.00	0.00	0.00	0.00	0.00	0.00	0.00	0.00	0.00	0.00
CaO	14.41	13.08	12.31	12.48	16.86	16.43	18.19	17.73	18.59	16.53	17.22	17.39	17.11	16.89	17.21	16.60	17.24	17.49
Na <sub>2</sub> O	3.30	4.14	4.62	4.46	2.12	2.19	1.25	1.40	1.11	2.19	1.97	1.61	1.86	2.00	1.77	2.00	1.67	1.72
K <sub>2</sub> O	0.00	0.00	0.01	0.00	0.00	0.02	0.00	0.03	0.00	0.00	0.00	0.01	0.00	0.01	0.02	0.00	0.01	0.00
Total	99.56	99.72	99.52	99.04	99.20	99.61	99.49	100.15	100.84	99.81	100.14	98.38	99.82	99.61	99.88	100.58	99.76	99.95
Si	2.271	2.335	2.366	2.378	2.172	2.166	2.090	2.096	2.059	2.178	2.157	2.172	2.151	2.165	2.150	2.159	2.114	2.138
Al	1.728	1.666	1.620	1.609	1.801	1.825	1.896	1.894	1.934	1.817	1.824	1.797	1.837	1.821	1.836	1.845	1.885	1.849
Fe <sup>3+</sup>	0.008	0.006	0.021	0.013	0.014	0.013	0.011	0.019	0.012	0.004	0.010	0.011	0.011	0.009	0.012	0.010	0.012	0.007
Ba	0.000	0.000	0.000	0.000	0.000	0.000	0.000	0.000	0.000	0.000	0.000	0.000	0.000	0.000	0.000	0.000	0.000	0.000
Ca	0.707	0.638	0.602	0.613	0.838	0.812	0.904	0.875	0.912	0.814	0.847	0.871	0.844	0.835	0.849	0.811	0.852	0.862
Na	0.293	0.365	0.409	0.396	0.191	0.196	0.112	0.125	0.099	0.195	0.176	0.146	0.166	0.179	0.158	0.177	0.150	0.154
K	0.000	0.000	0.001	0.000	0.000	0.001	0.000	0.002	0.000	0.000	0.000	0.001	0.000	0.000	0.001	0.000	0.001	0.000
Or	0.00	0.01	0.07	0.01	0.00	0.13	0.00	0.18	0.02	0.00	0.00	0.06	0.01	0.04	0.11	0.01	0.06	0.00
Ab	29.3	36.4	40.4	39.2	18.6	19.4	11.0	12.5	9.8	19.3	17.2	14.3	16.5	17.6	15.7	17.9	14.9	15.1
An	70.7	63.6	59.5	60.8	81.4	80.5	89.0	87.3	90.2	80.7	82.8	85.6	83.5	82.3	84.2	82.1	85.0	84.9

Formulae of plagioclase calculated on the basis of 8 oxygens, FeO<sub>tot</sub> is expressed as Fe<sub>2</sub>O<sub>3</sub>, c = grain core, r = grain rim, k.c. = part of garnet kelfitic corona, amp = inclusion in amphibole, grt = inclusion in garnet

**Table K-9.** Microprobe analyses and formulae of plagioclase from different metamorphic rock varieties of the Krivaja-Konjuh ophiolite complex

Rock type	Garnet-diopside-hypersthene amphibolite – Diopside-amphibolite gneiss – Plagioclase-garnet-diopside gneiss																	
Sample-Nr	v4-37	v4-38	v4-44	v4-45	v4-46	v4-47	v4-51	10d-33	10d-27	10d-26	10d-13	10d-14	10d-16	z1c-10	z1c-11	z1c-20	z1c-38	z1c-48
Remark	r	r	c	r	c	r	r	ab	c	ab	r	a	a	r	c		c	grt
SiO <sub>2</sub>	47.86	47.84	47.99	48.09	47.49	46.77	48.13	69.00	69.47	69.26	53.97	54.24	39.98	61.22	61.03	60.51	55.28	59.83
Al <sub>2</sub> O <sub>3</sub>	33.77	33.78	33.31	33.14	34.24	33.69	33.65	19.99	19.90	19.94	0.21	0.09	24.37	23.67	23.35	25.18	28.30	25.11
Fe <sub>2</sub> O <sub>3</sub>	0.47	0.16	0.19	0.22	0.21	0.24	0.18	0.17	0.13	0.18	0.30	0.50	3.34	0.21	0.62	0.16	0.12	0.24
BaO	0.00	0.00	0.00	0.00	0.00	0.00	0.00	0.00	0.00	0.00	0.00	0.00	0.00	0.00	0.00	0.00	0.00	0.00
CaO	16.23	16.03	15.94	15.83	16.67	16.67	16.44	0.14	0.21	0.14	34.08	33.39	24.70	5.73	5.51	6.34	10.01	6.25
Na <sub>2</sub> O	2.17	2.27	2.52	2.45	2.00	2.02	2.42	11.77	11.79	11.78	8.52	9.16	0.05	8.63	8.50	8.15	6.13	7.85
K <sub>2</sub> O	0.02	0.00	0.00	0.01	0.01	0.00	0.00	0.01	0.00	0.00	0.00	0.00	0.01	0.09	0.06	0.04	0.02	0.35
Total	100.51	100.07	99.95	99.73	100.63	99.38	100.82	101.08	101.49	101.30	97.08	97.37	92.44	99.56	99.06	100.37	99.86	99.61
Si	2.182	2.188	2.199	2.207	2.164	2.160	2.189	2.982	2.989	2.986	2.814	2.820	2.086	2.735	2.739	2.683	2.493	2.676
Al	1.815	1.820	1.799	1.792	1.839	1.834	1.803	1.018	1.009	1.013	0.013	0.005	1.499	1.246	1.236	1.316	1.504	1.324
Fe <sup>3+</sup>	0.016	0.006	0.007	0.008	0.007	0.008	0.006	0.005	0.004	0.006	0.012	0.020	0.131	0.007	0.021	0.005	0.004	0.008
Ba	0.000	0.000	0.000	0.000	0.000	0.000	0.000	0.000	0.000	0.000	0.000	0.000	0.000	0.000	0.000	0.000	0.000	0.000
Ca	0.793	0.785	0.783	0.778	0.814	0.825	0.801	0.006	0.010	0.006	1.904	1.860	1.381	0.274	0.265	0.301	0.483	0.299
Na	0.192	0.201	0.224	0.218	0.177	0.181	0.213	0.987	0.984	0.985	0.862	0.923	0.005	0.748	0.739	0.701	0.536	0.681
K	0.001	0.000	0.000	0.000	0.000	0.000	0.000	0.001	0.000	0.000	0.000	0.000	0.000	0.005	0.003	0.002	0.001	0.020
Or	0.10	0.00	0.00	0.05	0.04	0.00	0.00	0.06	0.00	0.01	0.00	0.00	0.03	0.51	0.34	0.20	0.13	1.97
Ab	19.5	20.4	22.3	21.8	17.8	18.0	21.0	99.3	99.0	99.4	31.2	33.2	0.4	72.8	73.4	69.8	52.5	68.1
An	80.4	79.6	77.7	78.1	82.1	82.0	79.0	0.7	1.0	0.6	68.8	66.8	99.6	26.7	26.3	30.0	47.4	29.9

Formulae of plagioclase calculated on the basis of 8 oxygens, FeO<sub>tot</sub> is expressed as Fe<sub>2</sub>O<sub>3</sub>, c = grain core, r = grain rim, a = altered, ab = albite, grt = inclusion in garnet

**Table K-10.** Microprobe analyses and formulae of plagioclase from different metamorphic rock varieties of the Krivaja-Konjuh ophiolite complex

Rock type	Plagioclase-garnet-diopside gneiss				
Sample-Nr	z1c-49	z1c-50	z1c-51	z1c-57	z1c-68a
Remark	grt	grt			
SiO <sub>2</sub>	58.94	62.03	55.13	56.35	53.26
Al <sub>2</sub> O <sub>3</sub>	26.24	23.76	28.39	27.98	29.74
Fe <sub>2</sub> O <sub>3</sub>	0.30	0.21	0.17	0.27	0.17
BaO	0.00	0.00	0.00	0.00	0.00
CaO	7.42	5.03	10.24	9.39	11.51
Na <sub>2</sub> O	7.62	9.06	6.00	6.47	4.93
K <sub>2</sub> O	0.04	0.03	0.03	0.02	0.24
Total	100.56	100.12	99.96	100.47	99.85
Si	2.620	2.750	2.485	2.521	2.413
Al	1.375	1.241	1.509	1.475	1.588
Fe <sub>3</sub>	0.010	0.007	0.006	0.009	0.006
Ba	0.000	0.000	0.000	0.000	0.000
Ca	0.353	0.239	0.494	0.450	0.559
Na	0.657	0.779	0.524	0.561	0.433
K	0.002	0.002	0.002	0.001	0.014
Or	0.24	0.17	0.19	0.12	1.37
Ab	64.9	76.4	51.4	55.4	43.1
An	34.9	23.4	48.4	44.4	55.5

Formulae of plagioclase calculated on the basis of 8 oxygens, FeO<sub>tot</sub> is expressed as Fe<sub>2</sub>O<sub>3</sub>, grt = inclusion in garnet

*Clinopyroxene*

**Table L-1.** Microprobe analyses and formulae of clinopyroxene from different metamorphic rock varieties of the Krivaja-Konjuh ophiolite complex

Rock type	Granoblastic amphibolite – Garnet-diopside amphibolite																	
Sample-Nr.	u29-28	u29-31	u29-32	u29-43	u29-44	u29-51	u29-52	u29-60	u29-62	u29-63	11c-13	11c-14	11c-17	11c-18	11c-23	11c-26	cc1-16	cc1-17
Remark		c	r	r	c	r	c		c	r	r	c	r	c	r		amp	c
SiO <sub>2</sub>	49.92	45.42	49.61	47.79	48.33	42.88	42.47	47.83	48.18	47.71	52.78	52.78	52.22	52.96	53.02	52.85	49.48	50.19
TiO <sub>2</sub>	0.08	0.29	0.18	0.29	0.28	0.00	0.00	0.42	0.49	0.51	0.09	0.09	0.09	0.02	0.04	0.04	0.48	0.50
Al <sub>2</sub> O <sub>3</sub>	6.57	11.30	6.43	7.66	8.02	36.85	36.55	8.38	8.00	8.70	1.93	1.93	1.95	0.51	1.04	1.80	5.08	5.25
Cr <sub>2</sub> O <sub>3</sub>	0.29	0.27	0.37	0.93	0.51	0.00	0.00	0.59	0.52	0.49	0.05	0.05	0.00	0.10	0.05	0.04	0.05	0.09
Fe <sub>2</sub> O <sub>3</sub>																		
FeO	2.33	3.62	2.36	3.15	3.01	0.08	0.07	2.53	2.86	2.81	8.08	8.36	8.17	7.41	6.90	7.72	6.94	6.79
MnO	0.09	0.05	0.10	0.01	0.08	0.00	0.00	0.07	0.07	0.08	0.17	0.20	0.30	0.24	0.24	0.24	0.05	0.05
MgO	14.27	12.41	14.56	13.62	13.38	0.00	0.00	13.64	13.55	13.63	13.94	13.97	13.82	13.95	14.19	14.05	13.40	13.26
CaO	25.39	25.47	25.50	25.51	25.62	20.35	20.54	25.45	25.32	25.43	22.82	22.83	23.00	24.35	24.13	23.12	22.37	22.19
Na <sub>2</sub> O	0.05	0.03	0.05	0.03	0.02	0.04	0.04	0.04	0.03	0.06	0.50	0.53	0.47	0.32	0.35	0.50	0.67	0.79
K <sub>2</sub> O	0.03	0.00	0.01	0.00	0.01	0.00	0.00	0.01	0.00	0.00	0.01	0.01	0.00	0.01	0.00	0.00	0.00	0.01
Total	99.01	98.86	99.18	99.00	99.25	100.20	99.67	98.96	99.01	99.40	100.36	100.74	100.02	99.86	99.95	100.35	98.53	99.11
Si	1.839	1.682	1.824	1.768	1.783	1.489	1.484	1.766	1.781	1.754	1.950	1.943	1.937	1.970	1.964	1.951	1.850	1.865
Al <sup>IV</sup>	0.161	0.318	0.176	0.232	0.217	0.511	0.516	0.234	0.219	0.246	0.050	0.057	0.063	0.022	0.036	0.049	0.150	0.135
Al <sup>VI</sup>	0.124	0.176	0.102	0.103	0.132	0.997	0.990	0.130	0.129	0.131	0.034	0.027	0.023	0.000	0.010	0.029	0.074	0.095
Fe <sup>3+</sup>	0.028	0.112	0.058	0.087	0.057	0.000	0.000	0.067	0.049	0.078	0.046	0.062	0.069	0.059	0.047	0.053	0.096	0.066
Ti	0.002	0.008	0.005	0.008	0.008	0.000	0.000	0.012	0.014	0.014	0.002	0.002	0.003	0.000	0.001	0.001	0.013	0.014
Cr	0.009	0.008	0.011	0.027	0.015	0.000	0.000	0.017	0.015	0.014	0.001	0.001	0.000	0.003	0.001	0.001	0.001	0.002
Mg	0.784	0.685	0.798	0.751	0.736	0.000	0.000	0.751	0.746	0.747	0.768	0.767	0.764	0.773	0.784	0.773	0.747	0.735
Fe <sup>2+</sup>	0.044	0.000	0.015	0.010	0.036	0.002	0.002	0.011	0.039	0.009	0.204	0.196	0.185	0.172	0.166	0.185	0.121	0.145
Mn	0.003	0.002	0.003	0.000	0.002	0.000	0.000	0.002	0.002	0.003	0.005	0.006	0.009	0.007	0.007	0.008	0.002	0.002
Ca	1.002	1.011	1.004	1.011	1.013	0.757	0.769	1.007	1.003	1.001	0.903	0.901	0.914	0.970	0.958	0.914	0.896	0.884
Na	0.003	0.002	0.004	0.002	0.001	0.003	0.003	0.003	0.002	0.004	0.036	0.038	0.033	0.023	0.025	0.036	0.049	0.057
K	0.001	0.000	0.001	0.000	0.001	0.000	0.000	0.000	0.000	0.000	0.000	0.001	0.000	0.001	0.000	0.000	0.000	0.000
Wo	53.9	55.9	53.5	54.4	54.9	99.7	99.7	54.8	54.5	54.5	46.9	46.6	47.1	49.0	48.8	47.3	48.1	48.3
En	42.1	37.9	42.5	40.4	39.9	0.00	0.00	40.9	40.6	40.6	39.9	39.7	39.4	39.0	39.9	40.0	40.1	40.1
Fs	4.03	6.32	4.04	5.35	5.22	0.34	0.35	4.42	4.95	4.86	13.2	13.7	13.5	12.0	11.3	12.7	11.7	11.6

Formulae of clinopyroxene calculated on the basis of 6 oxygens. c = grain core, r = grain rim, amp = inclusion in amphibole

**Table L-2.** Microprobe analyses and formulae of clinopyroxene from different metamorphic rock varieties of the Krivaja-Konjuh ophiolite complex

Rock type	Garnet-diopside amphibolite																	
Sample-Nr.	cc1-18	cc1-19	cc1-27	cc1-30	cc1-34	cc1-36	cc1-38	cc1-45	cc1-48	cc1-59	cc1-60	cc1-69	cc1-70	cc1-71	cc1-73	cc1-74	cc1-75	cc1-78
Remark	c	r	r	r	r	r	r		r	c	r	r	c	r			c	r
SiO <sub>2</sub>	50.27	50.78	49.56	50.37	49.36	50.00	49.57	51.69	49.94	50.13	50.28	49.94	52.43	50.44	51.87	51.22	50.77	50.28
TiO <sub>2</sub>	0.48	0.38	0.57	0.48	0.53	0.49	0.61	0.31	0.47	0.51	0.55	0.49	0.41	0.36	0.39	0.48	0.53	0.45
Al <sub>2</sub> O <sub>3</sub>	4.50	3.73	5.90	5.66	5.48	5.27	5.96	3.94	5.80	6.06	5.66	5.75	9.03	4.10	3.83	4.69	6.04	5.71
Cr <sub>2</sub> O <sub>3</sub>	0.06	0.07	0.07	0.05	0.09	0.10	0.12	0.09	0.05	0.06	0.04	0.07	0.07	0.10	0.17	0.04	0.08	0.03
Fe <sub>2</sub> O <sub>3</sub>																		
FeO	7.48	6.82	6.15	6.15	7.80	7.29	6.79	5.80	7.04	5.86	6.60	6.49	4.91	6.99	6.48	6.51	5.73	6.41
MnO	0.18	0.21	0.09	0.11	0.10	0.17	0.03	0.02	0.16	0.10	0.11	0.12	0.10	0.16	0.10	0.07	0.14	0.11
MgO	13.80	14.01	13.15	13.35	13.17	13.33	13.03	14.30	13.22	12.83	13.16	12.97	11.07	13.68	14.00	13.63	13.19	13.50
CaO	22.44	22.10	22.11	22.00	21.77	22.03	22.25	22.73	22.17	22.13	21.95	21.82	19.43	22.23	22.58	22.49	22.16	22.47
Na <sub>2</sub> O	0.59	0.57	0.82	0.95	0.64	0.68	0.74	0.83	0.68	1.10	0.92	0.95	2.21	0.58	0.69	0.79	1.06	0.79
K <sub>2</sub> O	0.00	0.01	0.00	0.00	0.00	0.01	0.00	0.00	0.01	0.00	0.00	0.00	0.04	0.00	0.01	0.01	0.01	0.01
Total	99.79	98.68	98.41	99.12	98.93	99.37	99.09	99.71	99.54	98.77	99.26	98.59	99.70	98.63	100.11	99.94	99.70	99.76
Si	1.859	1.897	1.851	1.865	1.844	1.857	1.844	1.901	1.850	1.863	1.864	1.863	1.904	1.887	1.909	1.886	1.868	1.852
Al <sup>IV</sup>	0.141	0.103	0.149	0.135	0.156	0.143	0.156	0.099	0.150	0.137	0.136	0.137	0.096	0.113	0.091	0.114	0.132	0.148
Al <sup>VI</sup>	0.055	0.061	0.111	0.113	0.085	0.087	0.105	0.071	0.103	0.128	0.111	0.116	0.291	0.067	0.075	0.090	0.130	0.100
Fe <sup>3+</sup>	0.099	0.061	0.063	0.062	0.085	0.075	0.067	0.068	0.068	0.058	0.059	0.059	0.000	0.065	0.039	0.053	0.046	0.078
Ti	0.013	0.011	0.016	0.013	0.015	0.014	0.017	0.008	0.013	0.014	0.015	0.014	0.011	0.010	0.011	0.013	0.015	0.013
Cr	0.002	0.002	0.002	0.001	0.003	0.003	0.003	0.003	0.001	0.002	0.001	0.002	0.002	0.003	0.005	0.001	0.002	0.001
Mg	0.761	0.780	0.732	0.737	0.733	0.738	0.722	0.784	0.730	0.711	0.727	0.721	0.600	0.763	0.768	0.749	0.724	0.741
Fe <sup>2+</sup>	0.132	0.152	0.129	0.128	0.159	0.151	0.144	0.111	0.150	0.124	0.146	0.143	0.149	0.153	0.160	0.147	0.130	0.119
Mn	0.006	0.007	0.003	0.003	0.003	0.005	0.001	0.001	0.005	0.003	0.003	0.004	0.003	0.005	0.003	0.002	0.004	0.003
Ca	0.889	0.884	0.885	0.873	0.871	0.877	0.887	0.895	0.880	0.881	0.872	0.872	0.756	0.891	0.890	0.888	0.874	0.887
Na	0.042	0.041	0.059	0.069	0.046	0.049	0.053	0.059	0.049	0.079	0.066	0.068	0.156	0.042	0.049	0.056	0.075	0.056
K	0.000	0.001	0.000	0.000	0.000	0.001	0.000	0.000	0.001	0.000	0.000	0.000	0.002	0.000	0.000	0.000	0.000	0.000
Wo	47.1	46.9	48.8	48.4	47.1	47.5	48.7	48.2	48.0	49.6	48.3	48.5	50.1	47.4	47.9	48.3	49.1	48.5
En	40.3	41.4	40.4	40.9	39.6	40.0	39.7	42.2	39.8	40.0	40.2	40.1	39.8	40.6	41.3	40.7	40.7	40.5
Fs	12.5	11.7	10.8	10.7	13.3	12.6	11.6	9.62	12.2	10.4	11.5	11.5	10.1	11.9	10.9	11.0	10.2	11.0

Formulae of clinopyroxene calculated on the basis of 6 oxygens. c = grain core, r = grain rim

**Table L-3.** Microprobe analyses and formulae of clinopyroxene from different metamorphic rock varieties of the Krivaja-Konjuh ophiolite complex

Rock type	Garnet-diopside amphibolite																	
Sample-Nr.	cc1-83	mk2-5	mk2-10	mk2-12	mk2-13	mk2-15	mk2-16	mk2-17	mk2-21	mk2-22	mk2-31	mk2-32	mk2-38	mk2-39	mk2-40	mk2-42	gr7-54	gr7-55
Remark			r	c	grt	grt	c	grt	c	r	r	c	c	k.c.		c	c	pl
SiO <sub>2</sub>	49.69	49.77	51.66	50.96	50.78	51.20	50.47	49.99	49.87	49.68	50.33	50.40	50.38	50.11	49.71	49.99	50.23	50.46
TiO <sub>2</sub>	0.63	0.40	0.26	0.53	0.55	0.46	0.48	0.52	0.38	0.40	0.28	0.26	0.69	0.59	0.68	0.56	0.44	0.33
Al <sub>2</sub> O <sub>3</sub>	6.52	4.49	3.13	5.17	5.28	5.10	5.22	5.43	4.67	4.63	4.34	4.39	5.44	5.34	5.44	5.20	7.29	6.10
Cr <sub>2</sub> O <sub>3</sub>	0.15	0.00	0.08	0.04	0.03	0.04	0.01	0.05	0.03	0.00	0.03	0.03	0.04	0.05	0.02	0.05	0.15	0.18
Fe <sub>2</sub> O <sub>3</sub>																		
FeO	6.38	8.23	7.27	7.90	7.27	7.35	7.05	8.42	7.98	7.95	7.94	8.47	7.42	7.54	7.67	7.55	4.41	4.55
MnO	0.04	0.20	0.19	0.13	0.14	0.09	0.18	0.20	0.35	0.38	0.47	0.36	0.17	0.20	0.07	0.16	0.05	0.01
MgO	12.91	13.81	14.14	13.82	13.60	13.44	13.32	13.78	12.99	13.03	13.12	13.21	13.31	13.52	13.46	13.07	13.29	13.95
CaO	22.01	21.09	23.05	20.65	21.87	21.52	21.73	20.43	21.81	22.24	21.92	21.44	21.53	21.41	21.54	21.85	22.18	22.25
Na <sub>2</sub> O	0.92	0.73	0.47	0.70	0.72	0.74	0.76	0.64	0.62	0.53	0.59	0.67	0.76	0.76	0.73	0.77	1.01	0.83
K <sub>2</sub> O	0.02	0.01	0.00	0.01	0.01	0.01	0.00	0.00	0.00	0.00	0.00	0.00	0.00	0.01	0.01	0.00	0.00	0.00
Total	99.26	98.72	100.25	99.90	100.24	99.94	99.21	99.47	98.70	98.85	99.03	99.23	99.74	99.53	99.31	99.20	99.05	98.66
Si	1.841	1.860	1.904	1.882	1.868	1.890	1.875	1.856	1.871	1.863	1.883	1.881	1.865	1.857	1.847	1.861	1.851	1.867
Al <sup>IV</sup>	0.159	0.140	0.096	0.118	0.132	0.110	0.125	0.144	0.129	0.137	0.117	0.119	0.135	0.143	0.153	0.139	0.149	0.133
Al <sup>VI</sup>	0.125	0.058	0.040	0.107	0.097	0.112	0.104	0.094	0.078	0.067	0.075	0.075	0.102	0.090	0.085	0.090	0.168	0.133
Fe <sup>3+</sup>	0.061	0.113	0.073	0.031	0.056	0.025	0.048	0.065	0.073	0.086	0.068	0.077	0.048	0.074	0.084	0.072	0.025	0.036
Ti	0.018	0.011	0.007	0.015	0.015	0.013	0.013	0.015	0.011	0.011	0.008	0.007	0.019	0.016	0.019	0.016	0.012	0.009
Cr	0.004	0.000	0.002	0.001	0.001	0.001	0.000	0.002	0.001	0.000	0.001	0.001	0.001	0.001	0.001	0.001	0.004	0.005
Mg	0.713	0.770	0.777	0.761	0.746	0.740	0.738	0.763	0.727	0.728	0.732	0.735	0.734	0.747	0.745	0.726	0.730	0.769
Fe <sup>2+</sup>	0.137	0.144	0.151	0.214	0.167	0.202	0.171	0.196	0.177	0.164	0.180	0.187	0.182	0.160	0.155	0.163	0.111	0.105
Mn	0.001	0.006	0.006	0.004	0.004	0.003	0.006	0.006	0.011	0.012	0.015	0.011	0.005	0.006	0.002	0.005	0.002	0.000
Ca	0.874	0.845	0.910	0.817	0.862	0.851	0.865	0.813	0.877	0.893	0.879	0.858	0.854	0.850	0.857	0.872	0.876	0.882
Na	0.066	0.053	0.033	0.050	0.051	0.053	0.055	0.046	0.045	0.038	0.043	0.049	0.054	0.054	0.053	0.056	0.072	0.060
K	0.001	0.001	0.000	0.000	0.001	0.001	0.000	0.000	0.000	0.000	0.000	0.000	0.000	0.001	0.000	0.000	0.000	0.000
Wo	48.9	45.0	47.5	44.7	46.9	46.7	47.3	44.1	47.0	47.4	46.9	45.9	46.8	46.3	46.5	47.4	50.2	49.2
En	39.9	41.0	40.5	41.7	40.6	40.6	40.4	41.4	39.0	38.7	39.0	39.3	40.3	40.6	40.4	39.5	41.9	42.9
Fs	11.1	14.0	12.0	13.6	12.4	12.6	12.3	14.5	14.0	13.9	14.0	14.8	12.9	13.1	13.0	13.1	7.94	7.92

Formulae of clinopyroxene calculated on the basis of 6 oxygens. c = grain core, r = grain rim, grt = inclusion in garnet, k.c. = clinopyroxene in garnet kelfitic corona, pl = inclusion in plagioclase



**Table L-4.** Microprobe analyses and formulae of clinopyroxene from different metamorphic rock varieties of the Krivaja-Konjuh ophiolite complex

Rock type	Garnet-diopside amphibolite																	
Sample-Nr.	gr7-57	gr7-58	gr7-63	gr7-64	v1-3	v1-4	v1-7	v1-10	v1-13	v1-15	v1-17	v1-25c	v1-28	v1-30	v1-32	v1-34	v1-42	v1-45
Remark	c	r	c	r	grt	grt			r	r	r	r	r	c	c	r	r	r
SiO <sub>2</sub>	49.61	51.20	49.48	49.66	51.59	51.30	51.03	51.40	51.25	51.19	50.92	50.66	50.50	51.25	51.30	50.27	50.92	51.01
TiO <sub>2</sub>	0.42	0.36	0.42	0.36	0.24	0.19	0.19	0.24	0.19	0.26	0.24	0.13	0.17	0.22	0.19	0.23	0.26	0.19
Al <sub>2</sub> O <sub>3</sub>	7.51	4.93	8.68	7.16	4.24	4.19	3.92	3.76	4.17	4.21	4.16	4.08	4.26	4.40	4.83	4.43	4.59	4.60
Cr <sub>2</sub> O <sub>3</sub>	0.09	0.11	0.12	0.12	0.03	0.04	0.09	0.08	0.05	0.03	0.04	0.09	0.09	0.08	0.03	0.06	0.04	0.07
Fe <sub>2</sub> O <sub>3</sub>																		
FeO	4.94	4.52	4.14	4.49	6.21	6.18	6.72	6.09	6.89	6.13	6.41	7.05	7.59	6.74	6.85	7.20	7.38	7.02
MnO	0.05	0.05	0.04	0.03	0.15	0.15	0.11	0.18	0.14	0.19	0.19	0.23	0.20	0.18	0.15	0.24	0.20	0.24
MgO	13.75	14.74	12.89	13.73	14.76	14.43	15.03	14.86	14.79	14.55	14.47	14.51	14.49	14.27	13.80	14.05	14.18	14.15
CaO	21.88	22.70	21.90	22.03	21.71	22.45	22.23	22.06	20.65	21.91	22.31	22.58	21.35	22.09	21.77	22.24	21.71	21.76
Na <sub>2</sub> O	0.88	0.58	1.21	0.85	0.67	0.54	0.48	0.47	0.54	0.53	0.58	0.49	0.48	0.64	0.75	0.47	0.59	0.62
K <sub>2</sub> O	0.00	0.01	0.00	0.00	0.01	0.00	0.01	0.00	0.00	0.01	0.01	0.00	0.01	0.00	0.00	0.00	0.00	0.00
Total	99.11	99.20	98.88	98.44	99.60	99.49	99.77	99.14	98.65	99.01	99.31	99.81	99.13	99.86	99.67	99.18	99.86	99.68
Si	1.826	1.885	1.822	1.840	1.899	1.894	1.878	1.904	1.908	1.898	1.883	1.868	1.877	1.887	1.894	1.868	1.879	1.883
Al <sup>IV</sup>	0.174	0.115	0.178	0.160	0.101	0.106	0.122	0.096	0.092	0.102	0.117	0.132	0.123	0.113	0.106	0.132	0.121	0.117
Al <sup>VI</sup>	0.152	0.099	0.199	0.152	0.083	0.077	0.047	0.068	0.091	0.082	0.065	0.045	0.063	0.078	0.104	0.062	0.078	0.084
Fe <sup>3+</sup>	0.058	0.034	0.039	0.046	0.053	0.056	0.096	0.047	0.027	0.042	0.080	0.113	0.083	0.065	0.045	0.089	0.070	0.065
Ti	0.012	0.010	0.012	0.010	0.007	0.005	0.005	0.007	0.005	0.007	0.007	0.003	0.005	0.006	0.005	0.006	0.007	0.005
Cr	0.002	0.003	0.003	0.004	0.001	0.001	0.003	0.002	0.001	0.001	0.001	0.003	0.003	0.002	0.001	0.002	0.001	0.002
Mg	0.754	0.809	0.707	0.758	0.810	0.794	0.824	0.820	0.821	0.804	0.798	0.797	0.803	0.783	0.759	0.778	0.780	0.779
Fe <sup>2+</sup>	0.094	0.105	0.088	0.094	0.139	0.135	0.110	0.142	0.187	0.148	0.118	0.105	0.152	0.142	0.166	0.135	0.158	0.152
Mn	0.002	0.002	0.001	0.001	0.005	0.005	0.003	0.006	0.004	0.006	0.006	0.007	0.006	0.005	0.005	0.007	0.006	0.008
Ca	0.863	0.896	0.864	0.875	0.856	0.888	0.876	0.875	0.824	0.871	0.884	0.892	0.850	0.872	0.861	0.886	0.858	0.861
Na	0.063	0.041	0.087	0.061	0.047	0.039	0.034	0.033	0.039	0.038	0.042	0.035	0.035	0.045	0.054	0.034	0.042	0.045
K	0.000	0.001	0.000	0.000	0.001	0.000	0.000	0.000	0.000	0.001	0.000	0.000	0.000	0.000	0.000	0.000	0.000	0.000
Wo	48.7	48.5	50.8	49.3	46.0	47.3	45.9	46.3	44.2	46.5	46.9	46.6	44.9	46.7	46.9	46.7	45.8	46.2
En	42.6	43.8	41.6	42.8	43.5	42.3	43.1	43.4	44.0	43.0	42.3	41.7	42.4	41.9	41.3	41.1	41.7	41.8
Fs	8.74	7.62	7.64	7.95	10.5	10.4	11.0	10.3	11.8	10.5	10.8	11.7	12.8	11.4	11.8	12.2	12.5	12.0

Formulae of clinopyroxene calculated on the basis of 6 oxygens. c = grain core, r = grain rim, grt = inclusion in garnet

**Table L-5.** Microprobe analyses and formulae of clinopyroxene from different metamorphic rock varieties of the Krivaja-Konjuh ophiolite complex

Rock type	Garnet-diopside amphibolite																	
Sample-Nr.	v1-48	v1-49	v1-50	v1-51	v1-60	v1-68	v1-69	v1-70	v1-73	v1-74	v1-77	v1-89	v1-90	v1-96	v1-98	v1-99	v1-100	du5-9
Remark	c	r	c	r	amp	c	c	r	r	r	r	grt	grt		k.c.	k.c.	r	c
SiO <sub>2</sub>	50.74	50.82	51.21	51.44	51.47	51.82	51.98	51.79	50.71	51.72	51.47	51.03	48.94	51.28	50.79	51.30	50.65	50.99
TiO <sub>2</sub>	0.21	0.28	0.16	0.22	0.10	0.20	0.13	0.15	0.12	0.13	0.15	0.45	0.41	0.40	0.49	0.18	0.19	0.50
Al <sub>2</sub> O <sub>3</sub>	4.03	4.23	4.54	3.54	3.15	3.56	3.25	3.01	4.06	3.63	2.60	4.46	5.97	4.12	4.32	3.09	4.06	5.34
Cr <sub>2</sub> O <sub>3</sub>	0.08	0.10	0.04	0.00	0.03	0.04	0.00	0.07	0.02	0.05	0.08	0.05	0.07	0.03	0.06	0.14	0.06	0.03
Fe <sub>2</sub> O <sub>3</sub>																		
FeO	7.54	7.68	6.14	6.43	6.53	6.84	6.62	6.41	6.73	6.23	5.90	6.86	7.96	6.52	6.52	6.31	7.33	6.56
MnO	0.23	0.30	0.15	0.20	0.17	0.18	0.23	0.19	0.24	0.22	0.23	0.22	0.23	0.09	0.14	0.17	0.54	0.12
MgO	14.51	14.18	14.28	14.63	14.84	14.75	14.69	14.69	14.82	14.63	15.23	14.55	14.12	14.68	14.44	14.64	14.54	12.94
CaO	21.21	21.96	21.87	22.26	21.58	22.16	22.37	22.42	21.57	22.36	22.72	21.87	19.82	22.27	21.71	22.90	22.10	23.13
Na <sub>2</sub> O	0.55	0.44	0.73	0.69	0.50	0.60	0.59	0.59	0.58	0.68	0.48	0.65	1.03	0.63	0.66	0.41	0.43	0.67
K <sub>2</sub> O	0.02	0.00	0.01	0.00	0.00	0.01	0.00	0.00	0.01	0.00	0.00	0.00	0.03	0.00	0.01	0.00	0.00	0.00
Total	99.09	100.00	99.14	99.40	98.37	100.13	99.87	99.32	98.84	99.64	98.86	100.14	98.58	100.02	99.16	99.14	99.88	100.28
Si	1.886	1.877	1.894	1.900	1.922	1.903	1.914	1.916	1.882	1.905	1.910	1.873	1.821	1.883	1.882	1.904	1.869	1.877
Al <sup>IV</sup>	0.114	0.123	0.106	0.100	0.078	0.097	0.086	0.084	0.118	0.095	0.090	0.127	0.179	0.117	0.118	0.096	0.131	0.123
Al <sup>VI</sup>	0.062	0.061	0.092	0.053	0.061	0.056	0.055	0.048	0.060	0.062	0.023	0.066	0.083	0.061	0.070	0.039	0.046	0.109
Fe <sup>3+</sup>	0.079	0.075	0.056	0.084	0.047	0.072	0.067	0.068	0.093	0.073	0.091	0.080	0.147	0.079	0.067	0.072	0.103	0.033
Ti	0.006	0.008	0.005	0.006	0.003	0.005	0.004	0.004	0.003	0.003	0.004	0.012	0.011	0.011	0.014	0.005	0.005	0.014
Cr	0.002	0.003	0.001	0.000	0.001	0.001	0.000	0.002	0.000	0.001	0.002	0.001	0.002	0.001	0.002	0.004	0.002	0.001
Mg	0.804	0.781	0.787	0.806	0.826	0.807	0.806	0.810	0.820	0.803	0.842	0.796	0.783	0.803	0.798	0.810	0.800	0.710
Fe <sup>2+</sup>	0.155	0.163	0.134	0.114	0.157	0.138	0.137	0.131	0.116	0.119	0.092	0.130	0.100	0.122	0.136	0.124	0.123	0.169
Mn	0.007	0.009	0.005	0.006	0.005	0.006	0.007	0.006	0.008	0.007	0.007	0.007	0.007	0.003	0.004	0.005	0.017	0.004
Ca	0.844	0.869	0.867	0.881	0.863	0.872	0.882	0.889	0.858	0.882	0.903	0.860	0.790	0.876	0.862	0.911	0.874	0.912
Na	0.040	0.031	0.053	0.049	0.036	0.042	0.042	0.042	0.042	0.048	0.035	0.046	0.075	0.045	0.048	0.030	0.030	0.048
K	0.001	0.000	0.000	0.000	0.000	0.000	0.000	0.000	0.000	0.000	0.000	0.000	0.001	0.000	0.000	0.000	0.000	0.000
Wo	44.7	45.8	46.9	46.6	45.5	46.0	46.5	46.7	45.3	46.8	46.6	45.9	43.2	46.5	46.2	47.4	45.6	49.9
En	42.5	41.2	42.6	42.6	43.5	42.6	42.4	42.6	43.3	42.6	43.5	42.5	42.8	42.7	42.7	42.2	41.7	38.8
Fs	12.8	13.0	10.5	10.8	11.0	11.4	11.1	10.7	11.4	10.6	9.8	11.6	13.9	10.8	11.1	10.5	12.7	11.3

Formulae of clinopyroxene calculated on the basis of 6 oxygens. c = grain core, r = grain rim, grt = inclusion in garnet, amp = inclusion in amphibole, k.c. = clinopyroxene in garnet kelfitic corona

**Table L-6.** Microprobe analyses and formulae of clinopyroxene from different metamorphic rock varieties of the Krivaja-Konjuh ophiolite complex

Rock type	Garnet-diopside amphibolite																	
Sample-Nr.	du5-10	du5-12	du5-14	du5-15	du5-17	du5-19	du5-25	du5-28	du5-30	du5-31	du5-37	du5-38	u22-7	u22-8	u22-9	u22-10	u22-32	u22-33
Remark	r	r	c	r	r	r	r	c	r	r	c	r	r	c	c	r	r	c
SiO <sub>2</sub>	51.10	51.54	51.87	51.50	51.54	50.49	50.42	50.93	50.64	50.53	51.08	50.64	50.22	50.03	50.49	51.79	49.93	49.79
TiO <sub>2</sub>	0.43	0.45	0.34	0.40	0.40	0.49	0.47	0.39	0.43	0.29	0.57	0.45	0.35	0.38	0.30	0.20	0.46	0.40
Al <sub>2</sub> O <sub>3</sub>	5.11	5.02	4.50	4.71	5.06	5.51	6.06	5.36	5.89	4.90	6.15	5.44	6.85	7.00	5.93	4.57	7.68	7.78
Cr <sub>2</sub> O <sub>3</sub>	0.05	0.06	0.06	0.12	0.12	0.07	0.08	0.05	0.14	0.04	0.00	0.04	0.19	0.19	0.19	0.07	0.07	0.09
Fe <sub>2</sub> O <sub>3</sub>																		
FeO	6.92	6.68	6.55	6.65	6.71	6.81	6.61	6.49	6.39	7.10	6.19	6.84	5.60	5.20	5.25	5.37	5.21	5.57
MnO	0.08	0.07	0.09	0.03	0.10	0.12	0.09	0.05	0.10	0.10	0.07	0.05	0.12	0.09	0.09	0.13	0.10	0.16
MgO	13.07	13.11	13.46	13.23	13.00	12.85	12.84	12.97	12.85	13.15	12.76	12.96	13.82	13.72	14.32	14.98	13.54	13.55
CaO	22.96	22.91	22.94	23.06	22.87	22.71	23.22	23.34	23.25	23.56	22.72	22.86	22.56	22.42	22.51	22.54	22.17	22.56
Na <sub>2</sub> O	0.52	0.60	0.57	0.69	0.62	0.66	0.59	0.78	0.71	0.35	0.74	0.45	0.73	0.79	0.73	0.64	0.89	0.86
K <sub>2</sub> O	0.00	0.00	0.02	0.00	0.00	0.01	0.00	0.01	0.01	0.00	0.00	0.00	0.00	0.00	0.01	0.00	0.01	0.00
Total	100.24	100.44	100.40	100.39	100.42	99.72	100.38	100.37	100.40	100.02	100.28	99.73	100.44	99.81	99.82	100.28	100.05	100.77
Si	1.885	1.896	1.907	1.894	1.897	1.870	1.855	1.871	1.860	1.870	1.878	1.878	1.832	1.833	1.849	1.889	1.824	1.808
Al <sup>IV</sup>	0.115	0.104	0.093	0.106	0.103	0.130	0.145	0.129	0.140	0.130	0.122	0.122	0.168	0.167	0.151	0.111	0.176	0.192
Al <sup>VI</sup>	0.107	0.113	0.102	0.098	0.117	0.111	0.117	0.103	0.115	0.084	0.144	0.116	0.126	0.136	0.105	0.085	0.155	0.141
Fe <sup>3+</sup>	0.019	0.007	0.012	0.033	0.005	0.037	0.042	0.060	0.047	0.055	0.000	0.012	0.069	0.061	0.076	0.059	0.058	0.088
Ti	0.012	0.012	0.009	0.011	0.011	0.014	0.013	0.011	0.012	0.008	0.016	0.013	0.010	0.010	0.008	0.005	0.013	0.011
Cr	0.002	0.002	0.002	0.004	0.004	0.002	0.002	0.001	0.004	0.001	0.000	0.001	0.006	0.006	0.005	0.002	0.002	0.002
Mg	0.719	0.719	0.738	0.725	0.713	0.710	0.704	0.710	0.704	0.726	0.699	0.717	0.751	0.750	0.782	0.814	0.737	0.733
Fe <sup>2+</sup>	0.194	0.198	0.189	0.172	0.202	0.173	0.161	0.140	0.149	0.165	0.190	0.200	0.102	0.099	0.085	0.105	0.101	0.081
Mn	0.002	0.002	0.003	0.001	0.003	0.004	0.003	0.001	0.003	0.003	0.002	0.002	0.004	0.003	0.003	0.004	0.003	0.005
Ca	0.908	0.903	0.904	0.908	0.902	0.901	0.915	0.918	0.915	0.934	0.895	0.908	0.881	0.880	0.883	0.881	0.868	0.878
Na	0.037	0.043	0.041	0.049	0.044	0.047	0.042	0.056	0.050	0.025	0.053	0.032	0.052	0.056	0.052	0.045	0.063	0.061
K	0.000	0.000	0.001	0.000	0.000	0.001	0.000	0.000	0.000	0.000	0.000	0.000	0.000	0.000	0.001	0.000	0.000	0.000
Wo	49.3	49.4	49.0	49.4	49.4	49.4	50.1	50.2	50.3	49.6	50.1	49.4	48.8	49.1	48.3	47.3	49.1	49.2
En	39.0	39.3	40.0	39.4	39.1	38.9	38.6	38.8	38.7	38.6	39.1	39.0	41.6	41.8	42.7	43.7	41.7	41.1
Fs	11.7	11.4	11.1	11.2	11.5	11.7	11.3	11.0	11.0	11.8	10.8	11.6	9.72	9.13	9.05	9.02	9.26	9.82

Formulae of clinopyroxene calculated on the basis of 6 oxygens. c = grain core, r = grain rim

**Table L-7.** Microprobe analyses and formulae of clinopyroxene from different metamorphic rock varieties of the Krivaja-Konjuh ophiolite complex

Rock type	Garnet-diopside amphibolite – Garnet-diopside-hypersthene amphibolite																	
Sample-Nr.	u22-34	u22-36	u22-40	u22-47	u22-48	u22-51	u22-60	u22-61	u22-63	x1-23	x1-24	x1-27	x1-6	x1-40	x1-59	x1-3	x1-5	x1-11
Remark	r	r											c	c	c	grt	r	r
SiO <sub>2</sub>	49.54	50.60	52.46	52.13	50.41	52.28	51.20	49.85	49.41	51.47	50.21	50.56	50.05	50.63	51.00	51.01	50.72	49.97
TiO <sub>2</sub>	0.46	0.21	0.23	0.04	0.37	0.18	0.25	0.25	0.37	0.18	0.31	0.29	0.54	0.49	0.37	0.34	0.49	0.43
Al <sub>2</sub> O <sub>3</sub>	7.60	5.58	4.47	3.39	6.68	3.96	6.81	7.30	7.51	3.31	4.56	4.47	5.51	5.38	4.88	4.55	5.23	4.82
Cr <sub>2</sub> O <sub>3</sub>	0.15	0.15	0.14	0.11	0.10	0.10	0.10	0.18	0.13	0.04	0.04	0.02	0.01	0.07	0.05	0.05	0.04	0.00
Fe <sub>2</sub> O <sub>3</sub>																		
FeO	5.61	5.79	5.31	5.26	5.83	4.52	4.55	5.09	5.54	7.39	7.62	7.61	7.36	7.55	6.81	8.51	6.88	7.19
MnO	0.15	0.12	0.14	0.12	0.17	0.08	0.12	0.11	0.10	0.28	0.20	0.26	0.16	0.21	0.12	0.18	0.17	0.35
MgO	13.58	14.48	14.93	15.34	13.91	15.31	13.94	13.99	13.57	13.88	13.37	13.26	13.07	12.99	13.63	14.80	13.28	13.49
CaO	22.15	22.83	22.49	22.56	22.75	22.86	22.69	22.46	22.46	22.39	21.95	22.08	22.12	21.64	21.93	18.89	22.17	22.26
Na <sub>2</sub> O	0.83	0.52	0.65	0.56	0.73	0.62	0.93	0.60	0.72	0.53	0.68	0.69	0.90	0.77	0.86	0.70	0.72	0.49
K <sub>2</sub> O	0.00	0.02	0.00	0.00	0.00	0.00	0.02	0.00	0.00	0.00	0.00	0.00	0.02	0.00	0.00	0.00	0.00	0.00
Total	100.06	100.30	100.82	99.51	100.95	99.91	100.61	99.83	99.82	99.46	98.94	99.22	99.75	99.72	99.64	99.91	99.69	99.00
Si	1.812	1.849	1.904	1.915	1.830	1.909	1.856	1.826	1.812	1.912	1.874	1.883	1.850	1.877	1.883	1.896	1.876	1.865
Al <sup>IV</sup>	0.188	0.151	0.096	0.085	0.170	0.091	0.144	0.174	0.188	0.088	0.126	0.117	0.150	0.123	0.117	0.104	0.124	0.135
Al <sup>VI</sup>	0.139	0.089	0.096	0.062	0.116	0.080	0.147	0.141	0.137	0.057	0.074	0.079	0.090	0.112	0.095	0.096	0.104	0.077
Fe <sup>3+</sup>	0.078	0.084	0.029	0.057	0.083	0.042	0.046	0.057	0.077	0.057	0.083	0.070	0.095	0.038	0.062	0.038	0.043	0.070
Ti	0.013	0.006	0.006	0.001	0.010	0.005	0.007	0.007	0.010	0.005	0.009	0.008	0.015	0.014	0.010	0.010	0.013	0.012
Cr	0.004	0.004	0.004	0.003	0.003	0.003	0.003	0.005	0.004	0.001	0.001	0.000	0.000	0.002	0.001	0.001	0.001	0.000
Mg	0.740	0.789	0.808	0.840	0.753	0.833	0.754	0.764	0.742	0.769	0.744	0.736	0.720	0.718	0.750	0.820	0.733	0.750
Fe <sup>2+</sup>	0.093	0.092	0.132	0.105	0.094	0.096	0.091	0.099	0.092	0.173	0.155	0.167	0.133	0.196	0.149	0.227	0.170	0.154
Mn	0.005	0.004	0.004	0.004	0.005	0.002	0.004	0.003	0.003	0.009	0.006	0.008	0.005	0.007	0.004	0.006	0.005	0.011
Ca	0.868	0.894	0.875	0.888	0.885	0.895	0.881	0.881	0.883	0.891	0.878	0.881	0.876	0.859	0.867	0.753	0.879	0.890
Na	0.059	0.037	0.046	0.040	0.051	0.044	0.066	0.042	0.051	0.038	0.049	0.050	0.065	0.055	0.062	0.050	0.052	0.035
K	0.000	0.001	0.000	0.000	0.000	0.000	0.001	0.000	0.000	0.000	0.000	0.000	0.001	0.000	0.000	0.000	0.000	0.000
Wo	48.6	48.0	47.3	46.9	48.6	47.9	49.6	48.8	49.1	46.9	47.0	47.3	47.9	47.3	47.4	40.8	48.0	47.4
En	41.5	42.3	43.7	44.4	41.4	44.6	42.4	42.3	41.3	40.5	39.9	39.5	39.4	39.5	41.0	44.5	40.0	40.0
Fs	9.93	9.72	9.05	8.72	10.0	7.52	8.04	8.86	9.62	12.6	13.1	13.2	12.7	13.2	11.7	14.7	11.9	12.6

Formulae of clinopyroxene calculated on the basis of 6 oxygens. c = grain core, r = grain rim, grt = inclusion in garnet

**Table L-8.** Microprobe analyses and formulae of clinopyroxene from different metamorphic rock varieties of the Krivaja-Konjuh ophiolite complex

Rock type	Garnet-diopside-hypersthene amphibolite																	
Sample-Nr.	x1-12	x1-39	x1-41	x1-58	x1-61	x1-2	u40-20	u40-11	u40-15	u40-16	u40-18	u40-19	u40-38	u40-63	u40-56	u40-10	u40-14	u40-17
Remark	r	r	r	r	r	grt		c	c	c	c	c	c	c	grt	r	r	r
SiO <sub>2</sub>	50.30	50.45	50.87	50.74	50.69	51.01	50.59	51.47	51.65	50.73	50.82	49.80	50.65	50.56	50.15	51.29	51.18	52.14
TiO <sub>2</sub>	0.40	0.37	0.25	0.45	0.48	0.51	0.33	0.26	0.33	0.37	0.32	0.36	0.20	0.53	0.74	0.26	0.34	0.17
Al <sub>2</sub> O <sub>3</sub>	5.19	4.87	4.55	4.99	4.90	4.84	4.27	3.56	4.26	4.14	3.97	4.47	4.24	5.25	5.40	3.46	4.27	2.37
Cr <sub>2</sub> O <sub>3</sub>	0.05	0.07	0.06	0.05	0.00	0.06	0.08	0.05	0.01	0.03	0.04	0.08	0.05	0.00	0.07	0.04	0.00	0.02
Fe <sub>2</sub> O <sub>3</sub>																		
FeO	7.40	7.61	7.72	6.75	7.01	7.58	7.52	7.04	7.16	7.34	6.93	7.35	8.17	6.98	6.66	6.73	7.01	6.75
MnO	0.14	0.26	0.23	0.09	0.07	0.19	0.25	0.19	0.24	0.26	0.20	0.22	0.26	0.14	0.08	0.22	0.19	0.12
MgO	13.40	13.21	13.60	13.39	13.60	14.18	13.80	13.98	14.09	13.91	13.92	13.87	13.80	13.50	13.66	14.52	14.18	14.77
CaO	22.11	22.10	21.84	21.97	22.04	20.26	22.34	22.27	22.18	22.45	21.86	21.89	22.06	21.85	22.02	22.40	22.01	22.84
Na <sub>2</sub> O	0.71	0.64	0.66	0.81	0.80	0.72	0.61	0.65	0.74	0.59	0.67	0.71	0.57	0.78	0.76	0.57	0.71	0.49
K <sub>2</sub> O	0.00	0.00	0.00	0.00	0.00	0.00	0.01	0.00	0.00	0.00	0.00	0.00	0.00	0.00	0.01	0.00	0.00	0.00
Total	99.69	99.58	99.78	99.24	99.60	99.28	99.80	99.48	100.65	99.82	98.72	98.75	100.00	99.59	99.55	99.48	99.88	99.66
Si	1.861	1.874	1.883	1.883	1.874	1.891	1.871	1.908	1.890	1.876	1.896	1.857	1.872	1.870	1.854	1.897	1.885	1.927
Al <sup>IV</sup>	0.139	0.126	0.117	0.117	0.126	0.109	0.129	0.092	0.110	0.124	0.104	0.143	0.128	0.130	0.146	0.103	0.115	0.073
Al <sup>VI</sup>	0.088	0.087	0.082	0.101	0.088	0.103	0.058	0.063	0.074	0.056	0.071	0.054	0.057	0.099	0.089	0.048	0.071	0.030
Fe <sup>3+</sup>	0.078	0.063	0.067	0.048	0.069	0.027	0.094	0.060	0.070	0.089	0.062	0.117	0.099	0.057	0.069	0.081	0.076	0.069
Ti	0.011	0.010	0.007	0.013	0.013	0.014	0.009	0.007	0.009	0.010	0.009	0.010	0.006	0.015	0.020	0.007	0.009	0.005
Cr	0.001	0.002	0.002	0.001	0.000	0.002	0.002	0.002	0.000	0.001	0.001	0.002	0.002	0.000	0.002	0.001	0.000	0.001
Mg	0.739	0.731	0.750	0.741	0.749	0.784	0.761	0.773	0.768	0.767	0.774	0.771	0.760	0.744	0.753	0.801	0.778	0.814
Fe <sup>2+</sup>	0.151	0.174	0.172	0.161	0.148	0.208	0.138	0.159	0.150	0.138	0.154	0.112	0.154	0.159	0.137	0.127	0.140	0.140
Mn	0.004	0.008	0.007	0.003	0.002	0.006	0.008	0.006	0.007	0.008	0.006	0.007	0.008	0.004	0.003	0.007	0.006	0.004
Ca	0.877	0.879	0.866	0.874	0.873	0.805	0.885	0.885	0.870	0.889	0.874	0.875	0.874	0.866	0.872	0.888	0.869	0.904
Na	0.051	0.046	0.047	0.058	0.057	0.052	0.044	0.046	0.052	0.042	0.048	0.051	0.041	0.056	0.054	0.041	0.051	0.035
K	0.000	0.000	0.000	0.000	0.000	0.000	0.000	0.000	0.000	0.000	0.000	0.000	0.000	0.000	0.001	0.000	0.000	0.000
Wo	47.4	47.4	46.5	47.8	47.4	44.0	46.9	47.0	46.6	47.0	46.7	46.5	46.1	47.3	47.6	46.6	46.5	46.8
En	40.0	39.4	40.3	40.6	40.7	42.8	40.3	41.1	41.2	40.5	41.4	41.0	40.1	40.6	41.1	42.1	41.6	42.2
Fs	12.6	13.2	13.2	11.6	11.9	13.2	12.7	11.9	12.1	12.4	11.9	12.6	13.8	12.0	11.4	11.3	11.9	11.0

Formulae of clinopyroxene calculated on the basis of 6 oxygens. c = grain core, r = grain rim, grt = inclusion in garnet

**Table L-9.** Microprobe analyses and formulae of clinopyroxene from different metamorphic rock varieties of the Krivaja-Konjuh ophiolite complex

Rock type	Garnet-diopside-hypersthene amphibolite																	
Sample-Nr.	u40-23	u40-37	u40-39	u40-59	u40-61	u40-55	u40-57	v4-7	v4-13	v4-14	v4-19	v4-22	v4-26	v4-27	v4-40	v2-43	v4-52	v4-53
Remark	r	r	r	r	r	grt	grt	amp	amp	amp	r	r	r	c	c	r	r	c
SiO <sub>2</sub>	50.05	50.25	50.16	49.78	50.62	50.58	50.41	52.47	52.20	51.97	53.01	53.61	51.89	51.91	52.81	52.45	52.46	51.02
TiO <sub>2</sub>	0.34	0.28	0.31	0.52	0.53	0.72	0.68	0.05	0.10	0.06	0.03	0.05	0.09	0.13	0.06	0.05	0.08	0.16
Al <sub>2</sub> O <sub>3</sub>	4.68	4.65	4.43	5.59	5.07	5.33	5.36	3.23	3.62	3.71	2.21	1.56	3.53	3.77	1.98	2.35	3.26	4.54
Cr <sub>2</sub> O <sub>3</sub>	0.04	0.00	0.06	0.05	0.08	0.10	0.04	0.06	0.04	0.09	0.04	0.04	0.00	0.07	0.07	0.08	0.00	0.02
Fe <sub>2</sub> O <sub>3</sub>																		
FeO	7.93	8.91	8.09	7.62	7.25	7.30	6.91	5.48	6.00	5.92	5.54	5.09	5.67	5.65	7.04	7.03	5.39	6.22
MnO	0.19	0.24	0.31	0.13	0.13	0.09	0.15	0.23	0.25	0.25	0.30	0.23	0.24	0.16	0.37	0.33	0.16	0.24
MgO	14.56	13.87	13.42	13.54	14.94	15.27	13.80	14.87	14.73	14.93	15.46	16.02	14.90	14.73	14.83	14.70	14.82	14.67
CaO	20.53	21.29	21.80	21.14	21.41	21.19	21.59	23.12	22.67	22.22	23.22	23.30	22.74	22.70	21.93	22.36	23.22	22.16
Na <sub>2</sub> O	0.76	0.60	0.60	0.85	0.66	0.59	0.74	0.54	0.59	0.52	0.47	0.35	0.52	0.53	0.53	0.52	0.49	0.77
K <sub>2</sub> O	0.01	0.00	0.00	0.00	0.00	0.00	0.00	0.00	0.00	0.01	0.00	0.00	0.01	0.00	0.01	0.01	0.00	0.00
Total	99.09	100.08	99.18	99.23	100.69	101.17	99.67	100.04	100.20	99.67	100.28	100.26	99.58	99.66	99.62	99.89	99.86	99.81
Si	1.857	1.857	1.871	1.848	1.845	1.835	1.862	1.923	1.912	1.912	1.939	1.958	1.910	1.911	1.955	1.936	1.927	1.872
Al <sup>IV</sup>	0.143	0.143	0.129	0.152	0.155	0.165	0.138	0.077	0.088	0.088	0.061	0.042	0.090	0.089	0.045	0.064	0.073	0.128
Al <sup>VI</sup>	0.061	0.060	0.066	0.092	0.063	0.062	0.095	0.063	0.069	0.073	0.034	0.026	0.063	0.074	0.041	0.038	0.068	0.068
Fe <sup>3+</sup>	0.117	0.111	0.087	0.091	0.107	0.102	0.057	0.048	0.054	0.046	0.058	0.037	0.059	0.044	0.037	0.059	0.036	0.105
Ti	0.009	0.008	0.009	0.015	0.015	0.020	0.019	0.001	0.003	0.002	0.001	0.001	0.003	0.004	0.002	0.001	0.002	0.004
Cr	0.001	0.000	0.002	0.001	0.002	0.003	0.001	0.002	0.001	0.003	0.001	0.001	0.000	0.002	0.002	0.002	0.000	0.001
Mg	0.805	0.764	0.746	0.749	0.812	0.826	0.760	0.813	0.804	0.819	0.843	0.872	0.818	0.808	0.818	0.809	0.811	0.802
Fe <sup>2+</sup>	0.129	0.165	0.166	0.146	0.114	0.119	0.156	0.120	0.130	0.136	0.111	0.118	0.116	0.130	0.181	0.158	0.130	0.086
Mn	0.006	0.008	0.010	0.004	0.004	0.003	0.005	0.007	0.008	0.008	0.009	0.007	0.007	0.005	0.012	0.010	0.005	0.007
Ca	0.816	0.843	0.871	0.840	0.836	0.824	0.854	0.908	0.890	0.876	0.910	0.912	0.897	0.895	0.869	0.884	0.914	0.871
Na	0.055	0.043	0.044	0.061	0.047	0.042	0.053	0.038	0.042	0.037	0.033	0.025	0.037	0.038	0.038	0.037	0.035	0.055
K	0.000	0.000	0.000	0.000	0.000	0.000	0.000	0.000	0.000	0.001	0.000	0.000	0.000	0.000	0.000	0.000	0.000	0.000
Wo	43.6	44.6	46.4	45.9	44.6	44.0	46.6	47.9	47.2	46.5	47.1	46.8	47.3	47.6	45.4	46.0	48.2	46.5
En	43.0	40.4	39.7	40.9	43.3	44.1	41.5	42.9	42.7	43.5	43.6	44.8	43.1	42.9	42.7	42.1	42.8	42.9
Fs	13.5	15.0	13.9	13.2	12.0	12.0	11.9	9.2	10.2	10.13	9.34	8.33	9.62	9.54	12.0	11.8	9.0	10.6

Formulae of clinopyroxene calculated on the basis of 6 oxygens. c = grain core, r = grain rim, grt = inclusion in garnet, amp = inclusion in amphibole

**Table L-10.** Microprobe analyses and formulae of clinopyroxene from different metamorphic rock varieties of the Krivaja-Konjuh ophiolite complex

Rock type	Diopside-amphibolite gneiss – Plagioclase-garnet-diopside gneiss																	
Sample-Nr.	10d-37	10d-39	10d-49	10d-51	10d-52a	10d-57	z1c-3	z1c-4	z1c-7	z1c-9	z1c-21	z1c-22	z1c-23	z1c-30	z1c-32	z1c-33	z1c-39	z1c-53
Remark							c	r	r	r	c	r	r	c	r	r	r	
SiO <sub>2</sub>	51.88	53.09	53.22	49.52	47.66	48.70	48.49	48.55	48.43	48.58	50.02	49.70	50.18	50.60	49.58	49.73	49.71	51.90
TiO <sub>2</sub>	0.07	0.02	0.07	0.70	1.21	0.28	0.75	0.60	0.59	0.67	0.69	0.78	0.46	0.51	0.77	0.54	0.55	0.51
Al <sub>2</sub> O <sub>3</sub>	2.83	0.99	1.07	4.33	5.82	5.00	6.25	6.07	5.73	6.13	4.38	4.50	3.38	4.43	4.92	4.59	5.18	3.81
Cr <sub>2</sub> O <sub>3</sub>	0.00	0.00	0.01	0.14	0.09	0.00	0.00	0.02	0.00	0.03	0.00	0.01	0.00	0.03	0.06	0.09	0.01	0.00
Fe <sub>2</sub> O <sub>3</sub>																		
FeO	14.14	7.60	8.43	9.49	10.12	13.04	12.91	12.63	12.47	12.87	8.70	8.79	8.34	9.44	8.80	9.93	10.09	7.39
MnO	0.28	0.29	0.33	0.25	0.18	0.21	0.27	0.30	0.29	0.25	0.37	0.31	0.31	0.37	0.40	0.42	0.30	0.22
MgO	7.50	13.44	13.03	12.21	10.77	12.06	10.05	10.95	11.18	10.34	13.03	12.94	13.75	13.14	12.61	13.16	12.43	13.36
CaO	22.25	24.39	23.83	22.52	22.37	19.40	18.92	19.01	19.20	18.91	21.48	21.34	21.63	20.81	21.45	20.01	20.09	22.18
Na <sub>2</sub> O	1.24	0.44	0.66	1.10	1.22	0.61	1.50	1.19	1.19	1.35	0.70	0.67	0.64	0.75	0.78	0.75	0.81	0.81
K <sub>2</sub> O	0.00	0.00	0.01	0.00	0.00	0.01	0.01	0.02	0.03	0.00	0.01	0.00	0.00	0.01	0.00	0.01	0.00	0.00
Total	100.19	100.26	100.65	100.26	99.43	99.29	99.15	99.33	99.12	99.12	99.37	99.04	98.68	100.09	99.37	99.21	99.18	100.16
Si	1.981	1.968	1.969	1.836	1.790	1.841	1.836	1.832	1.829	1.840	1.868	1.864	1.882	1.878	1.853	1.863	1.866	1.916
Al <sup>IV</sup>	0.019	0.032	0.031	0.164	0.210	0.159	0.164	0.168	0.171	0.160	0.132	0.136	0.118	0.122	0.147	0.137	0.134	0.084
Al <sup>VI</sup>	0.108	0.011	0.016	0.026	0.048	0.063	0.115	0.102	0.085	0.114	0.061	0.063	0.032	0.071	0.070	0.065	0.095	0.081
Fe <sup>3+</sup>	0.000	0.051	0.059	0.174	0.179	0.125	0.117	0.119	0.141	0.106	0.083	0.077	0.107	0.077	0.088	0.094	0.066	0.033
Ti	0.002	0.001	0.002	0.019	0.034	0.008	0.021	0.017	0.017	0.019	0.019	0.022	0.013	0.014	0.022	0.015	0.016	0.014
Cr	0.000	0.000	0.000	0.004	0.003	0.000	0.000	0.001	0.000	0.001	0.000	0.000	0.000	0.001	0.002	0.003	0.000	0.000
Mg	0.427	0.743	0.718	0.675	0.603	0.679	0.568	0.616	0.630	0.584	0.725	0.723	0.769	0.727	0.703	0.735	0.696	0.735
Fe <sup>2+</sup>	0.451	0.185	0.201	0.120	0.138	0.287	0.292	0.280	0.253	0.301	0.189	0.199	0.155	0.216	0.187	0.217	0.250	0.195
Mn	0.009	0.009	0.010	0.008	0.006	0.007	0.009	0.010	0.009	0.008	0.012	0.010	0.010	0.012	0.013	0.013	0.010	0.007
Ca	0.910	0.969	0.945	0.895	0.900	0.786	0.768	0.768	0.777	0.767	0.860	0.858	0.869	0.828	0.859	0.803	0.808	0.877
Na	0.092	0.032	0.048	0.079	0.088	0.045	0.110	0.087	0.087	0.099	0.050	0.048	0.046	0.054	0.056	0.055	0.059	0.058
K	0.000	0.000	0.000	0.000	0.000	0.000	0.000	0.001	0.002	0.000	0.000	0.000	0.000	0.001	0.000	0.000	0.000	0.000
Wo	50.6	49.5	48.8	47.8	49.3	41.7	43.8	42.9	42.9	43.4	46.0	46.0	45.5	44.5	46.5	43.1	44.2	47.5
En	23.7	38.0	37.1	36.1	33.0	36.1	32.4	34.4	34.8	33.0	38.8	38.8	40.3	39.1	38.0	39.5	38.0	39.8
Fs	25.6	12.5	14.0	16.1	17.7	22.2	23.8	22.8	22.3	23.5	15.2	15.3	14.2	16.4	15.6	17.4	17.8	12.7

Formulae of clinopyroxene calculated on the basis of 6 oxygens. c = grain core, r = grain rim

**Table L-11.** Microprobe analyses and formulae of clinopyroxene from different metamorphic rock varieties of the Krivaja-Konjuh ophiolite complex

Rock type	Plagioclase-garnet-diopside gneiss							
Sample-Nr.	z1c-55	z1c-58	z1c-60	z1c-70	z1c-72	z1c-72a	z1c-75	z1c-77
Remark					c	r		
SiO <sub>2</sub>	50.59	50.17	50.93	50.18	50.33	51.15	49.73	50.91
TiO <sub>2</sub>	0.57	0.58	0.54	0.56	0.59	0.51	0.65	0.51
Al <sub>2</sub> O <sub>3</sub>	4.06	4.37	4.01	4.20	4.39	3.98	4.50	4.05
Cr <sub>2</sub> O <sub>3</sub>	0.03	0.05	0.00	0.02	0.04	0.00	0.00	0.00
Fe <sub>2</sub> O <sub>3</sub>								
FeO	9.33	9.27	8.55	9.03	8.62	8.38	9.43	7.83
MnO	0.31	0.36	0.32	0.27	0.43	0.34	0.30	0.25
MgO	12.80	12.61	13.35	13.17	12.81	13.15	12.91	13.39
CaO	20.91	20.87	22.04	21.38	21.51	21.53	20.88	21.90
Na <sub>2</sub> O	0.71	0.76	0.73	0.66	0.72	0.76	0.77	0.79
K <sub>2</sub> O	0.00	0.01	0.02	0.00	0.01	0.00	0.02	0.00
Total	99.30	99.05	100.48	99.46	99.43	99.81	99.18	99.63
Si	1.896	1.885	1.879	1.873	1.880	1.900	1.863	1.889
Al <sup>IV</sup>	0.104	0.115	0.121	0.127	0.120	0.100	0.137	0.111
Al <sup>VI</sup>	0.075	0.078	0.053	0.057	0.073	0.074	0.061	0.067
Fe <sup>3+</sup>	0.048	0.059	0.092	0.085	0.065	0.052	0.096	0.073
Ti	0.016	0.016	0.015	0.016	0.017	0.014	0.018	0.014
Cr	0.001	0.001	0.000	0.001	0.001	0.000	0.000	0.000
Mg	0.715	0.706	0.734	0.733	0.713	0.728	0.721	0.741
Fe <sup>2+</sup>	0.244	0.232	0.172	0.197	0.204	0.208	0.199	0.171
Mn	0.010	0.011	0.010	0.008	0.013	0.011	0.010	0.008
Ca	0.839	0.840	0.871	0.855	0.861	0.857	0.838	0.871
Na	0.052	0.055	0.052	0.048	0.052	0.055	0.056	0.057
K	0.000	0.000	0.001	0.000	0.000	0.000	0.001	0.000
Wo	45.2	45.4	46.4	45.5	46.4	46.2	45.0	46.7
En	38.5	38.2	39.1	39.0	38.4	39.2	38.7	39.8
Fs	16.3	16.4	14.6	15.5	15.2	14.6	16.4	13.5

Formulae of clinopyroxene calculated on the basis of 6 oxygens. c = grain core, r = grain rim



Orthopyroxene

**Table M-1.** Microprobe analyses and formulae of orthopyroxene from different metamorphic rock varieties of the Krivaja-Konjuh ophiolite complex

Rock type	Garnet-diopside amphibolite																	
Sample-Nr.	mk2-27	mk2-9	mk2-47	mk2-48	mk2-43	mk2-45	gr7-53	v1-12c	v1-101	v1-25b	v1-71	v1-84	v1-27b	v1-6	v1-9	v1-25	v1-35	v1-40
Remark		c	m	m	m	m			k.c.	c	c	c	mca	m	m	r	r	r
SiO <sub>2</sub>	52.75	50.53	53.75	53.73	51.93	53.10	53.34	53.26	51.36	52.75	53.10	52.99	51.92	53.04	52.88	51.98	52.18	52.18
TiO <sub>2</sub>	0.07	0.37	0.11	0.08	0.17	0.21	0.04	0.03	0.01	0.01	0.06	0.02	0.05	0.02	0.02	0.01	0.07	0.08
Al <sub>2</sub> O <sub>3</sub>	1.71	4.07	2.13	2.06	5.06	2.13	3.72	2.36	5.21	2.79	2.66	2.52	3.64	3.33	3.28	3.17	2.95	2.44
Cr <sub>2</sub> O <sub>3</sub>	0.10	0.01	0.07	0.02	0.05	0.07	0.10	0.10	0.01	0.02	0.07	0.08	0.06	0.11	0.14	0.00	0.00	0.09
FeO	17.49	7.85	15.50	16.51	14.63	15.48	13.13	16.18	14.73	17.41	16.13	16.79	16.99	15.62	15.97	17.99	17.02	17.80
MnO	1.06	0.29	1.47	1.73	1.38	1.47	0.10	1.49	1.26	0.70	0.37	0.43	0.62	0.31	0.32	0.55	0.67	0.67
MgO	25.22	13.33	26.71	26.14	22.97	26.18	28.77	26.78	26.48	25.76	27.17	27.13	24.64	26.79	26.62	25.53	25.75	25.46
CaO	0.54	22.21	0.69	0.48	1.77	0.41	0.55	0.40	0.29	0.51	0.57	0.39	0.69	0.52	0.52	0.55	0.48	0.51
Na <sub>2</sub> O	0.00	0.55	0.00	0.02	0.14	0.00	0.01	0.00	0.00	0.00	0.03	0.00	0.08	0.02	0.00	0.01	0.00	0.00
K <sub>2</sub> O	0.00	0.00	0.00	0.01	0.01	0.00	0.00	0.02	0.00	0.01	0.01	0.01	0.01	0.02	0.01	0.01	0.01	0.00
Total	98.94	99.20	100.42	100.76	98.12	99.04	99.76	100.63	99.34	99.94	100.17	100.34	98.69	99.76	99.76	99.80	99.12	99.12
Si	1.943	1.886	1.934	1.936	1.914	1.940	1.898	1.914	1.856	1.915	1.908	1.904	1.911	1.913	1.910	1.892	1.907	1.912
Al <sup>IV</sup>	0.057	0.114	0.066	0.064	0.086	0.060	0.102	0.086	0.144	0.085	0.092	0.096	0.089	0.087	0.090	0.108	0.093	0.088
Al <sup>VI</sup>	0.017	0.065	0.024	0.023	0.133	0.032	0.054	0.014	0.078	0.035	0.021	0.011	0.069	0.054	0.050	0.027	0.035	0.018
Fe <sup>3+</sup>	0.033	0.067	0.034	0.037	0.000	0.015	0.043	0.069	0.065	0.049	0.069	0.082	0.022	0.032	0.035	0.081	0.055	0.066
Ti	0.002	0.010	0.003	0.002	0.005	0.006	0.001	0.001	0.000	0.000	0.002	0.000	0.001	0.000	0.001	0.000	0.002	0.001
Cr	0.003	0.000	0.002	0.001	0.002	0.002	0.003	0.003	0.000	0.001	0.002	0.002	0.002	0.003	0.004	0.000	0.000	0.003
Mg	1.385	0.742	1.433	1.404	1.262	1.426	1.526	1.434	1.426	1.394	1.455	1.454	1.352	1.440	1.433	1.385	1.403	1.392
Fe <sup>2+</sup>	0.505	0.179	0.433	0.460	0.451	0.458	0.347	0.417	0.380	0.480	0.416	0.423	0.501	0.439	0.447	0.466	0.465	0.480
Mn	0.033	0.009	0.045	0.053	0.043	0.046	0.003	0.045	0.038	0.021	0.011	0.013	0.019	0.009	0.010	0.017	0.021	0.021
Ca	0.021	0.888	0.027	0.018	0.070	0.016	0.021	0.016	0.011	0.020	0.022	0.015	0.027	0.020	0.020	0.021	0.019	0.020
Na	0.000	0.039	0.000	0.001	0.010	0.000	0.001	0.000	0.000	0.000	0.002	0.000	0.006	0.001	0.000	0.001	0.000	0.000
K	0.000	0.000	0.000	0.000	0.000	0.000	0.000	0.001	0.000	0.000	0.000	0.000	0.000	0.001	0.000	0.000	0.001	0.000
Wo	1.08	47.14	1.35	0.93	3.83	0.82	1.08	7.73	0.78	0.59	1.01	1.11	0.75	1.41	1.03	1.02	1.08	0.96
En	70.0	39.4	72.7	71.2	69.1	72.7	78.6	72.4	74.2	71.0	73.8	73.2	70.4	74.2	73.7	70.3	71.5	70.3
Fs	28.9	13.5	25.9	27.9	27.0	26.4	20.3	26.8	25.2	28.0	25.1	26.1	28.2	24.8	25.3	28.6	27.6	28.6

Formulae of orthopyroxene calculated on the basis of 6 oxygens. c = grain core, r = grain rim, m = orthopyroxene margin around clinopyroxene, mca = orthopyroxene margin between clinopyroxene and amphibole, k.c. = orthopyroxene in garnet kelfittic corona

**Table M-2.** Microprobe analyses and formulae of orthopyroxene from different metamorphic rock varieties of the Krivaja-Konjuh ophiolite complex

Rock type	Garnet-diopside amphibolite – Garnet-diopside-hypersthene amphibolite																	
Sample-Nr.	v1-41b	v1-43	v1-44	v1-47	v1-72	v1-75	v1-76	v1-85	x1-22	x1-25	x1-26	x1-28	x1-19	x1-46	x1-20	x1-43	u40-4	u40-31
Remark	r	r	r	r	r	r	r	r					c	c	r	r		
SiO <sub>2</sub>	52.45	52.17	51.43	52.07	53.21	53.37	53.38	52.62	51.71	52.26	52.91	52.05	52.54	52.10	52.93	51.88	52.24	51.55
TiO <sub>2</sub>	0.04	0.05	0.06	0.04	0.05	0.04	0.08	0.00	0.07	0.01	0.06	0.06	0.07	0.02	0.01	0.07	0.05	0.04
Al <sub>2</sub> O <sub>3</sub>	2.93	3.24	3.82	3.40	2.46	2.24	2.05	2.35	3.50	3.22	2.85	3.59	3.07	4.69	2.55	4.76	2.67	3.31
Cr <sub>2</sub> O <sub>3</sub>	0.06	0.09	0.12	0.14	0.05	0.11	0.03	0.09	0.00	0.03	0.03	0.02	0.03	0.04	0.00	0.02	0.02	0.02
Fe <sub>2</sub> O <sub>3</sub>																		
FeO	18.29	17.50	16.52	16.75	16.40	16.49	16.14	16.50	18.44	18.23	17.87	17.92	17.91	16.05	17.68	15.90	16.75	18.20
MnO	0.78	0.63	1.10	0.71	0.39	0.50	0.40	0.26	0.44	0.48	0.50	0.47	0.61	1.07	0.52	0.90	0.48	0.82
MgO	25.69	25.43	25.73	26.14	26.95	27.17	27.35	26.56	24.56	24.30	24.87	24.06	24.52	25.44	25.45	25.36	26.17	24.56
CaO	0.51	0.51	0.29	0.50	0.60	0.52	0.50	0.57	0.52	0.55	0.58	1.23	0.62	0.34	0.45	0.30	0.39	0.53
Na <sub>2</sub> O	0.01	0.01	0.01	0.01	0.01	0.00	0.02	0.02	0.02	0.03	0.00	0.02	0.02	0.00	0.01	0.00	0.01	0.01
K <sub>2</sub> O	0.01	0.00	0.01	0.00	0.01	0.00	0.00	0.02	0.00	0.01	0.00	0.00	0.01	0.00	0.00	0.00	0.01	0.00
Total	100.76	99.62	99.07	99.76	100.12	100.44	99.94	98.98	99.27	99.11	99.67	99.41	99.38	99.75	99.60	99.19	98.79	99.05
Si	1.893	1.902	1.879	1.887	1.916	1.916	1.923	1.918	1.899	1.924	1.935	1.911	1.928	1.890	1.932	1.891	1.911	1.898
Al <sup>IV</sup>	0.107	0.098	0.121	0.113	0.084	0.084	0.077	0.082	0.101	0.076	0.065	0.089	0.072	0.110	0.068	0.109	0.089	0.102
Al <sup>VI</sup>	0.018	0.041	0.043	0.033	0.021	0.011	0.010	0.019	0.051	0.064	0.057	0.066	0.061	0.090	0.041	0.095	0.026	0.042
Fe <sup>3+</sup>	0.086	0.053	0.073	0.075	0.060	0.067	0.064	0.062	0.047	0.012	0.004	0.020	0.007	0.018	0.027	0.009	0.060	0.058
Ti	0.001	0.001	0.002	0.001	0.001	0.001	0.002	0.000	0.002	0.000	0.002	0.002	0.002	0.001	0.000	0.002	0.001	0.001
Cr	0.002	0.003	0.003	0.004	0.001	0.003	0.001	0.003	0.000	0.001	0.001	0.001	0.001	0.001	0.000	0.001	0.001	0.001
Mg	1.382	1.382	1.401	1.413	1.447	1.454	1.469	1.443	1.345	1.334	1.355	1.317	1.341	1.375	1.384	1.378	1.428	1.348
Fe <sup>2+</sup>	0.466	0.481	0.432	0.433	0.434	0.428	0.423	0.441	0.520	0.549	0.543	0.531	0.542	0.469	0.513	0.475	0.452	0.503
Mn	0.024	0.019	0.034	0.022	0.012	0.015	0.012	0.008	0.014	0.015	0.016	0.015	0.019	0.033	0.016	0.028	0.015	0.026
Ca	0.020	0.020	0.011	0.019	0.023	0.020	0.019	0.022	0.021	0.022	0.023	0.048	0.025	0.013	0.018	0.012	0.015	0.021
Na	0.001	0.001	0.000	0.000	0.001	0.000	0.001	0.001	0.001	0.002	0.000	0.001	0.001	0.000	0.001	0.000	0.001	0.001
K	0.001	0.000	0.000	0.000	0.000	0.000	0.000	0.001	0.000	0.000	0.000	0.000	0.000	0.000	0.000	0.000	0.001	0.000
Wo	0.99	1.01	0.57	0.99	1.17	1.01	0.96	1.12	2.40	1.06	1.12	1.17	2.50	1.27	0.68	0.89	0.62	0.77
En	69.9	70.7	71.8	72.0	73.2	73.3	73.9	73.0	69.1	69.0	69.9	68.2	69.3	72.1	70.7	72.4	72.5	69.0
Fs	29.1	28.3	27.6	27.0	25.6	25.7	25.1	25.9	29.8	29.8	29.0	29.3	29.4	27.2	28.4	26.9	26.8	30.0

Formulae of orthopyroxene calculated on the basis of 6 oxygens. c = grain core, r = grain rim

**Table M-3.** Microprobe analyses and formulae of orthopyroxene from different metamorphic rock varieties of the Krivaja-Konjuh ophiolite complex

Rock type	Garnet-diopside-hypersthene amphibolite																
Sample-Nr.	u40-32	u40-33	u40-46	40-64	u40-67	u40-26	u40-35	u40-48	u40-49	u40-21	u40-25	u40-36	u40-40	v4-15	v4-16	v4-20	v4-21
Remark						c	c	k.c.	k.c.	r	r	r	r	c	r	r	r
SiO <sub>2</sub>	52.59	51.84	52.33	50.57	51.01	52.02	52.00	50.68	51.90	52.43	52.19	51.94	52.71	53.55	54.25	53.43	54.05
TiO <sub>2</sub>	0.04	0.08	0.06	0.05	0.05	0.11	0.07	0.03	0.02	0.06	0.10	0.03	0.02	0.04	0.01	0.06	0.02
Al <sub>2</sub> O <sub>3</sub>	1.84	3.28	4.03	6.08	5.43	2.70	3.22	5.40	3.93	2.40	2.86	2.81	2.22	3.08	2.38	3.06	2.28
Cr <sub>2</sub> O <sub>3</sub>	0.02	0.07	0.06	0.18	0.16	0.00	0.02	0.11	0.02	0.03	0.04	0.02	0.01	0.03	0.04	0.03	0.02
Fe <sub>2</sub> O <sub>3</sub>																	
FeO	18.76	17.97	15.98	16.30	15.63	18.33	18.09	16.21	15.60	18.27	18.34	18.33	18.73	14.59	14.63	14.19	14.35
MnO	0.78	0.73	0.98	0.79	0.72	0.43	0.82	1.20	1.13	0.43	0.58	0.71	0.67	0.44	0.41	0.49	0.44
MgO	24.82	24.76	25.95	25.44	25.19	25.27	24.77	25.05	26.45	25.29	25.22	24.22	25.12	27.16	27.95	26.30	27.76
CaO	0.47	0.48	0.36	0.33	0.26	0.51	0.56	0.33	0.29	0.47	0.57	0.59	0.55	0.52	0.46	0.51	0.53
Na <sub>2</sub> O	0.01	0.00	0.02	0.01	0.00	0.01	0.02	0.00	0.01	0.00	0.00	0.03	0.01	0.00	0.03	0.03	0.00
K <sub>2</sub> O	0.00	0.00	0.00	0.01	0.00	0.00	0.01	0.00	0.01	0.00	0.01	0.00	0.02	0.02	0.01	0.02	0.00
Total	99.32	99.21	99.76	99.75	98.43	99.37	99.57	99.00	99.36	99.36	99.91	98.67	100.07	99.42	100.16	98.10	99.44
Si	1.936	1.904	1.895	1.830	1.871	1.906	1.904	1.853	1.882	1.921	1.903	1.924	1.923	1.932	1.939	1.950	1.946
Al <sup>IV</sup>	0.064	0.096	0.105	0.170	0.129	0.094	0.096	0.147	0.118	0.079	0.097	0.076	0.077	0.068	0.061	0.050	0.054
Al <sup>VI</sup>	0.016	0.046	0.067	0.090	0.105	0.022	0.043	0.085	0.049	0.025	0.026	0.046	0.018	0.063	0.040	0.081	0.043
Fe <sup>3+</sup>	0.046	0.043	0.035	0.073	0.017	0.066	0.051	0.057	0.069	0.050	0.065	0.030	0.060	0.003	0.022	0.000	0.010
Ti	0.001	0.002	0.001	0.001	0.001	0.003	0.002	0.001	0.000	0.002	0.003	0.001	0.001	0.001	0.000	0.002	0.000
Cr	0.001	0.002	0.002	0.005	0.004	0.000	0.001	0.003	0.001	0.001	0.001	0.000	0.000	0.001	0.001	0.001	0.001
Mg	1.362	1.356	1.401	1.373	1.377	1.380	1.352	1.365	1.429	1.382	1.371	1.337	1.366	1.461	1.489	1.430	1.490
Fe <sup>2+</sup>	0.531	0.509	0.449	0.420	0.462	0.495	0.503	0.438	0.404	0.510	0.494	0.538	0.511	0.437	0.416	0.433	0.423
Mn	0.024	0.023	0.030	0.024	0.022	0.013	0.025	0.037	0.035	0.013	0.018	0.022	0.021	0.013	0.012	0.015	0.014
Ca	0.018	0.019	0.014	0.013	0.010	0.020	0.022	0.013	0.011	0.018	0.022	0.023	0.022	0.020	0.018	0.020	0.020
Na	0.001	0.000	0.001	0.001	0.000	0.000	0.001	0.000	0.001	0.000	0.000	0.002	0.001	0.000	0.002	0.002	0.000
K	0.000	0.000	0.000	0.000	0.000	0.000	0.000	0.000	0.000	0.000	0.000	0.000	0.001	0.001	0.000	0.001	0.000
Wo	0.93	0.97	0.98	0.72	0.68	0.55	1.01	1.13	0.68	0.59	0.93	1.13	1.20	1.09	1.03	0.90	1.05
En	68.7	69.6	72.6	72.1	72.9	69.9	69.2	71.4	73.4	70.0	69.6	68.6	69.0	75.5	76.1	75.3	76.2
Fs	30.4	29.5	26.6	27.2	26.6	29.1	29.7	27.9	26.0	29.0	29.3	30.2	29.9	23.4	23.0	23.6	22.8

Formulae of orthopyroxene calculated on the basis of 6 oxygens. c = grain core, r = grain rim, k.c. = orthopyroxene in garnet kelfitic corona

Other phases

**Table N-1.** Microprobe analyses and formulae of minor phases from different metamorphic rock varieties of the Krivaja-Konjuh ophiolite complex

Sample-Nr.	u30-3	u30-4	u30-20	u30-25	u30-26	u30-29	u30-44	u29-10	u29-11	u29-14	u29-15	u29-21	u29-22	11c-31	11c-32	11c-34	11c-35	11c-38
Phase	Czo	Czo	Czo	Czo	Czo	Czo (r)	Czo	Czo (c)	Czo (r)	Czo (r)	Czo (c)	Czo (r)	Czo (c)	Czo	Czo	Czo	Czo	Czo
Host Rock	Gr. Am.	Gr. Am.	Gr. Am.	Gr. Am.	Gr. Am.	Gr. Am.	Gr. Am..	Gr. Am.	Gr. Am.	Gr. Am.	Gr. Am.	Gr. Am.	Gr. Am.	Gr. Am.	Gr. Am.	Gr. Am.	Gr. Am.	Gr. Am.
SiO <sub>2</sub>	40.58	40.20	39.69	40.17	39.83	39.34	39.82	37.80	38.73	38.98	39.09	39.09	38.91	37.75	39.29	37.92	38.95	38.62
TiO <sub>2</sub>	0.01	0.00	0.00	0.00	0.00	0.00	0.00	0.04	0.00	0.02	0.00	0.01	0.02	0.09	0.08	0.14	0.04	0.07
Al <sub>2</sub> O <sub>3</sub>	33.32	33.82	33.11	33.51	33.97	32.84	33.35	31.88	32.83	32.67	32.72	32.90	32.86	26.30	30.48	28.03	32.93	29.42
Cr <sub>2</sub> O <sub>3</sub>	0.00	0.00	0.00	0.02	0.00	0.00	0.00	0.10	0.10	0.14	0.17	0.10	0.25	0.00	0.00	0.00	0.00	0.00
Fe <sub>2</sub> O <sub>3</sub>																		
FeO	0.07	0.10	0.78	0.05	0.05	0.19	0.38	0.78	0.72	1.01	0.70	0.73	0.70	8.72	4.02	6.73	1.00	5.48
MnO	0.01	0.00	0.00	0.00	0.00	0.00	0.00	0.03	0.00	0.05	0.00	0.00	0.04	0.04	0.02	0.00	0.01	0.00
NiO	0.00	0.00	0.00	0.00	0.00	0.00	0.00	0.00	0.00	0.00	0.00	0.00	0.00	0.00	0.00	0.00	0.00	0.00
MgO	0.00	0.00	0.00	0.01	0.00	0.00	0.00	0.06	0.06	0.08	0.10	0.06	0.08	0.05	0.06	0.07	0.01	0.04
CaO	24.22	23.90	23.84	24.44	24.54	24.56	24.47	25.76	24.89	24.54	24.53	24.67	24.64	24.01	24.43	23.87	24.71	24.35
Na <sub>2</sub> O	0.09	0.27	0.11	0.12	0.09	0.06	0.10	0.02	0.00	0.00	0.02	0.01	0.01	0.00	0.00	0.02	0.00	0.00
K <sub>2</sub> O	0.00	0.00	0.02	0.00	0.00	0.00	0.00	0.01	0.00	0.02	0.00	0.00	0.00	0.00	0.02	0.00	0.00	0.01
Total	98.30	98.28	97.55	98.33	98.48	96.98	98.12	96.45	97.33	97.49	97.32	97.58	97.50	96.98	98.40	96.77	97.64	97.98
Si	3.052	3.025	3.020	3.026	2.997	3.010	3.010	2.938	2.965	2.978	2.988	2.980	2.972	2.969	2.996	2.967	2.970	2.973
Ti	0.000	0.000	0.000	0.000	0.000	0.000	0.000	0.002	0.000	0.001	0.000	0.001	0.001	0.005	0.004	0.008	0.002	0.004
Al	2.954	2.999	2.969	2.974	3.012	2.962	2.971	2.921	2.962	2.941	2.948	2.957	2.958	2.438	2.740	2.585	2.960	2.669
Cr	0.000	0.000	0.000	0.001	0.000	0.000	0.000	0.006	0.006	0.008	0.010	0.006	0.015	0.000	0.000	0.000	0.000	0.000
Fe <sup>3+</sup>	0.000	0.000	0.011	0.000	0.003	0.012	0.024	0.050	0.046	0.064	0.044	0.047	0.045	0.574	0.256	0.441	0.064	0.353
Fe <sup>2+</sup>	0.005	0.006	0.039	0.003	0.000	0.000	0.000	0.000	0.000	0.000	0.000	0.000	0.000	0.000	0.000	0.000	0.000	0.000
Mn	0.001	0.000	0.000	0.000	0.000	0.000	0.000	0.002	0.000	0.003	0.000	0.000	0.003	0.003	0.001	0.000	0.000	0.000
Ni	0.000	0.000	0.000	0.000	0.000	0.000	0.000	0.000	0.000	0.000	0.000	0.000	0.000	0.000	0.001	0.000	0.000	0.000
Mg	0.000	0.000	0.000	0.001	0.000	0.000	0.000	0.007	0.006	0.009	0.011	0.007	0.009	0.006	0.007	0.008	0.001	0.004
Ca	1.952	1.927	1.943	1.972	1.978	2.013	1.982	2.145	2.041	2.008	2.009	2.016	2.016	2.023	1.996	2.001	2.019	2.009
Na	0.012	0.039	0.017	0.018	0.014	0.008	0.015	0.002	0.000	0.000	0.003	0.002	0.002	0.000	0.000	0.003	0.000	0.000
K	0.000	0.000	0.002	0.000	0.000	0.000	0.000	0.000	0.000	0.002	0.000	0.000	0.000	0.000	0.002	0.000	0.000	0.001
OH	1.000	1.000	1.000	1.000	1.000	1.000	1.000	1.000	1.000	1.000	1.000	1.000	1.000	1.000	1.000	1.000	1.000	1.000
Fe#	0.03	0.02	0.41	0.04	0.11	0.41	0.83	1.71	1.52	2.11	1.53	1.61	1.52	19.11	8.54	14.6	2.13	11.7

Clinozoisite/epidote formulae calculated on the basis of 12.5 oxygens and total iron as Fe<sup>3+</sup>. Fe# = 100Fe<sup>3+</sup>/(Fe<sup>3+</sup>+Al). Czo = clinozoisite, c = grain core, r = grain rim, Gr. Am. = granoblastic amphibolite

**Table N-2.** Microprobe analyses and formulae of minor phases from different metamorphic rock varieties of the Krivaja-Konjuh ophiolite complex

Sample-Nr.	11c-39	11c-42	11c-55	11c-4	11c-5	11c-6	11c-8	11c-9	11c-16	11c-28	r8-18	r8-19	u23-23	10d-6	10d-48	10d-53	u30-37	u30-30
Phase	Czo	Czo	Czo	Prh	Prh	Prh	Prh	Prh	Prh	Prh	Prh	Prh	Prh	Prh	Prh	Prh	Spr	Spr
Host Rock	Gr. Am.	Gr. Am.	Gr. Am.	Gr. Am.	Gr. Am.	Gr. Am.	Gr. Am..	Gr. Am.	Gr. Am.	Gr. Am.	Gr. Am.	Gr. Am.	Gr. Am.	DiA.S	DiA.S	DiA.S	Gr. Am.	Gr. Am.
SiO <sub>2</sub>	38.30	38.31	38.30	43.18	44.02	42.01	41.68	43.84	43.58	43.64	43.78	43.43	43.28	43.41	43.74	43.86	13.01	12.79
TiO <sub>2</sub>	0.12	0.07	0.00	0.00	0.00	0.00	0.00	0.00	0.00	0.00	0.04	0.10	0.06	0.14	0.00	0.02	0.00	0.00
Al <sub>2</sub> O <sub>3</sub>	27.53	27.74	27.91	24.37	24.16	24.96	25.61	24.42	24.19	24.14	24.06	23.04	24.47	24.12	23.84	24.20	64.57	64.68
Cr <sub>2</sub> O <sub>3</sub>	0.00	0.04	0.00	0.00	0.00	0.00	0.00	0.00	0.00	0.00	0.03	0.04	0.06	0.01	0.02	0.01	0.39	0.49
Fe <sub>2</sub> O <sub>3</sub>																		
FeO	7.13	7.25	7.18	0.09	0.05	0.40	0.35	0.12	0.02	0.11	0.57	0.64	0.28	0.36	0.39	0.17	3.87	4.03
MnO	0.07	0.03	0.00	0.00	0.00	0.00	0.00	0.00	0.00	0.00	0.06	0.11	0.04	0.07	0.00	0.00	0.07	0.08
NiO	0.00	0.00	0.00	0.00	0.00	0.00	0.00	0.00	0.00	0.00	0.00	0.00	0.00	0.00	0.00	0.00	0.12	0.11
MgO	0.06	0.02	0.00	0.00	0.00	0.00	0.00	0.00	0.00	0.00	0.01	0.03	0.02	0.00	0.03	0.00	18.76	18.51
CaO	23.82	24.01	23.77	26.55	26.53	26.13	25.28	26.68	26.73	26.24	26.77	26.53	26.89	27.02	26.42	27.21	0.03	0.03
Na <sub>2</sub> O	0.00	0.00	0.00	0.07	0.07	0.09	0.12	0.23	0.12	0.17	0.11	0.09	0.01	0.02	0.04	0.09	0.01	0.00
K <sub>2</sub> O	0.00	0.00	0.00	0.00	0.00	0.00	0.00	0.00	0.00	0.02	0.01	0.00	0.02	0.00	0.00	0.00	0.01	0.02
Total	97.03	97.47	97.16	94.27	94.85	93.61	93.04	95.30	94.65	94.33	95.43	94.00	95.12	95.14	94.47	95.56	100.83	100.73
Si	2.991	2.980	2.984	3.005	3.040	2.948	2.934	3.017	3.021	3.032	3.015	3.041	2.990	3.000	3.038	3.016	1.508	1.485
Ti	0.007	0.004	0.000	0.000	0.000	0.000	0.000	0.000	0.000	0.000	0.002	0.005	0.003	0.007	0.000	0.001	0.000	0.000
Al	2.534	2.543	2.563	1.999	1.966	2.064	2.124	1.981	1.976	1.976	1.953	1.902	1.993	1.964	1.952	1.961	8.818	8.851
Cr	0.000	0.003	0.000	0.000	0.000	0.000	0.000	0.000	0.000	0.000	0.002	0.002	0.003	0.001	0.001	0.000	0.035	0.045
Fe <sup>3+</sup>	0.466	0.472	0.468	0.000	0.000	0.024	0.021	0.007	0.000	0.000	0.026	0.015	0.016	0.021	0.000	0.010	0.133	0.137
Fe <sup>2+</sup>	0.000	0.000	0.000	0.005	0.003	0.000	0.000	0.000	0.001	0.006	0.006	0.023	0.000	0.000	0.022	0.000	0.241	0.254
Mn	0.004	0.002	0.000	0.000	0.000	0.000	0.000	0.000	0.000	0.000	0.003	0.006	0.002	0.004	0.000	0.000	0.007	0.008
Ni	0.000	0.000	0.000	0.000	0.000	0.000	0.000	0.000	0.000	0.000	0.000	0.000	0.000	0.000	0.000	0.000	0.011	0.010
Mg	0.007	0.002	0.000	0.000	0.000	0.000	0.000	0.000	0.000	0.000	0.001	0.003	0.002	0.000	0.003	0.000	3.241	3.204
Ca	1.993	2.001	1.984	1.980	1.963	1.965	1.906	1.967	1.985	1.953	1.976	1.991	1.990	2.001	1.966	2.004	0.003	0.003
Na	0.000	0.000	0.000	0.009	0.010	0.012	0.016	0.031	0.016	0.023	0.014	0.012	0.001	0.002	0.005	0.011	0.001	0.000
K	0.000	0.000	0.000	0.000	0.000	0.000	0.000	0.000	0.000	0.002	0.001	0.000	0.002	0.000	0.000	0.000	0.001	0.002
OH	1.000	1.000	1.000	1.000	1.000	1.000	1.000	1.000	1.000	1.000	1.000	1.000	1.000	1.000	1.000	1.000		
Mg#																	89.6	89.1
Fe#	15.5	15.6	15.4															

Clinzoisite/epidote formulae calculated on the basis of 12.5 oxygens and total iron as Fe<sup>3+</sup>. Prehnite formulae calculated on the basis of 11 oxygens. Sapphirine formulae calculated on the basis of 20 oxygens and fixed number of cations (14). Fe# = 100Fe<sup>3+</sup>/(Fe<sup>3+</sup>+Al), Mg# = 100Mg/(Mg+Fe<sub>uk</sub>). Czo = clinzoisite, Gr. Am. = granoblastic amphibolite, DiAS = diopside amphibolite gneiss

**Table N-3.** Microprobe analyses and formulae of minor phases from different metamorphic rock varieties of the Krivaja-Konjuh ophiolite complex

Sample-Nr.	u30-31	u30-1	u30-5	u29-3	u29-4	u29-6b	u29-35	u29-36	u29-37	u29-40	u30-36	u30-42	u30-43	z1c-24	z1c-25	z1c-37	z1c-62	z1c-73
Phase	spr (r)	spr (c)	spr (r)	sp (m)	sp (m)	sp	sp (m)	sp (m)	sp (m)	sp	sp	sp	sp	us	us	us	us	us
Host Rock	Gr. Am.	Gr. Am.	Gr. Am.	Gr. Am.	Gr. Am.	Gr. Am.	Gr. Am..	Gr. Am.	Gr. Am.	Gr. Am.	Gr. Am.	Gr. Am.	Gr. Am.	PGDS	PGDS	PGDS	PGDS	PGDS
SiO <sub>2</sub>	13.07	13.05	13.27	0.00	0.00	0.00	0.00	0.00	0.00	0.00	0.01	0.00	0.01	0.04	0.10	0.05	0.15	0.00
TiO <sub>2</sub>	0.03	0.00	0.04	0.00	0.00	0.00	0.00	0.00	0.00	0.00	0.00	0.00	0.01	11.95	10.46	8.58	15.03	8.76
Al <sub>2</sub> O <sub>3</sub>	64.20	64.79	64.21	66.13	66.01	55.42	66.56	66.08	65.79	55.14	64.56	64.76	64.63	2.44	2.92	3.46	1.13	3.20
Cr <sub>2</sub> O <sub>3</sub>	0.51	0.10	0.64	0.37	0.41	10.51	0.19	0.18	0.52	11.38	1.79	2.24	2.72	0.13	0.13	0.08	0.24	0.19
Fe <sub>2</sub> O <sub>3</sub>																		
FeO	3.78	3.96	3.57	12.61	13.59	19.12	12.39	13.39	13.52	16.67	15.57	13.65	13.92	77.88	77.91	80.62	75.98	80.19
MnO	0.09	0.09	0.03	0.30	0.33	0.45	0.32	0.29	0.36	0.32	0.16	0.07	0.07	0.49	0.34	0.48	0.51	0.35
NiO	0.17	0.19	0.21	0.05	0.09	0.36	0.12	0.09	0.16	0.12	0.50	0.40	0.37	0.00	0.00	0.05	0.01	0.06
MgO	18.60	18.65	18.43	19.56	19.23	13.66	20.01	19.87	19.22	16.36	17.20	18.90	18.82	0.04	0.04	0.42	0.09	0.42
CaO	0.04	0.05	0.04	0.00	0.05	0.31	0.00	0.00	0.04	0.20	0.08	0.03	0.02	0.19	0.22	0.06	0.08	0.03
Na <sub>2</sub> O	0.00	0.00	0.02	0.00	0.00	0.00	0.00	0.00	0.00	0.00	0.01	0.01	0.00	0.01	0.00	0.02	0.02	0.02
K <sub>2</sub> O	0.00	0.00	0.01	0.00	0.00	0.00	0.00	0.00	0.00	0.00	0.00	0.00	0.00	0.00	0.00	0.01	0.00	0.00
Total	100.48	100.87	100.47	99.03	99.69	99.83	99.58	99.91	99.60	100.19	99.88	100.05	100.56	93.17	92.11	93.82	93.23	93.21
Si	1.521	1.512	1.545	0.000	0.000	0.000	0.000	0.000	0.000	0.000	0.000	0.000	0.000	0.001	0.004	0.002	0.006	0.000
Ti	0.002	0.000	0.004	0.000	0.000	0.000	0.000	0.000	0.000	0.000	0.000	0.000	0.000	0.346	0.305	0.244	0.439	0.251
Al	8.806	8.844	8.811	1.978	1.969	1.766	1.975	1.961	1.965	1.727	1.954	1.939	1.930	0.111	0.134	0.154	0.052	0.144
Cr	0.047	0.009	0.059	0.007	0.008	0.225	0.004	0.004	0.010	0.239	0.036	0.045	0.054	0.004	0.004	0.002	0.007	0.006
Fe <sup>3+</sup>	0.101	0.125	0.037	0.015	0.023	0.010	0.021	0.036	0.025	0.034	0.009	0.017	0.015	1.190	1.244	1.354	1.052	1.349
Fe <sup>2+</sup>	0.267	0.258	0.310	0.253	0.265	0.423	0.240	0.246	0.262	0.336	0.325	0.273	0.280	1.320	1.286	1.199	1.417	1.210
Mn	0.009	0.009	0.003	0.006	0.007	0.010	0.007	0.006	0.008	0.007	0.003	0.002	0.001	0.016	0.011	0.016	0.017	0.011
Ni	0.015	0.017	0.020	0.001	0.002	0.008	0.002	0.002	0.003	0.003	0.010	0.008	0.008	0.000	0.000	0.002	0.000	0.002
Mg	3.227	3.219	3.199	0.740	0.725	0.551	0.751	0.746	0.726	0.648	0.658	0.716	0.711	0.002	0.002	0.024	0.005	0.024
Ca	0.004	0.006	0.005	0.000	0.001	0.009	0.000	0.000	0.001	0.006	0.002	0.001	0.000	0.008	0.009	0.002	0.003	0.001
Na	0.000	0.001	0.005	0.000	0.000	0.000	0.000	0.000	0.000	0.000	0.000	0.001	0.000	0.001	0.000	0.001	0.001	0.001
K	0.000	0.000	0.001	0.000	0.000	0.000	0.000	0.000	0.000	0.000	0.000	0.000	0.000	0.000	0.000	0.001	0.000	0.000
Cr#				32.9	26.3	95.9	15.5	9.1	29.6	87.5	79.8	72.4	78.1	0.33	0.36	0.25	0.73	0.46
Mg#	89.8	89.4	90.2	74.5	73.3	56.6	75.8	75.2	73.5	65.8	66.9	72.4	71.8	0.23	0.25	1.96	0.45	1.95
Fe#				0.83	1.22	0.54	1.04	1.81	1.23	1.72	0.53	0.94	0.83	91.2	90.0	89.6	94.7	90.0

Sapphirine formulae calculated on the basis of 20 oxygens and fixed number of cations (14). Mg# = 100Mg/(Mg+Fe<sub>uk</sub>). In spinel total iron as FeO. Fe<sup>3+</sup> calculations on the basis of spinel stoichiometry; Mg# = 100Mg/(Mg+Fe), Cr# = 100Cr/(Cr+Al), Fe<sup>3+</sup># = 100Fe<sup>3+</sup>/(Fe<sup>3+</sup>+Cr+Al); c = grain core, r = grain rim, m = spinel margin around corundum, spr = sapphirine, sp = spinel, us = ulvöspinel, Gr. Am. = granoblastic amphibolite, PGDS = plagioclase-garnet-diopside gneiss

**Table N-4.** Microprobe analyses and formulae of minor phases from different metamorphic rock varieties of the Krivaja-Konjuh ophiolite complex

Sample-Nr.	u40-47	u40-50	u40-60b	u40-66	v4-32	11c-44	11c-49	11c-43	11c-50	r8-34	r8-35	cc1-24	cc1-25	cc1-66	cc1-68	10d-54	10d-46	10d-55
Phase	mt	mt	mt	mt	mt	ilm (c)	ilm (c)	ilm (r)	ilm (r)	ilm (c)	ilm (r)	ilm (c)	ilm (r)	ilm (c)	ilm (r)	ilm (c)	ilm (t)	ilm (r)
Host Rock	GDHA	GDHA	GDHA	GDHA	GDHA	Gr. Am.	Gr. Am..	Gr. Am.	Gr. Am.	Gr. Am.	Gr. Am.	GDA	GDA	GDA	GDA	DiAS	DiAS	DiAS
SiO <sub>2</sub>	0.05	0.02	1.47	0.09	0.01	0.00	0.41	0.02	0.14	0.02	1.04	0.00	0.00	0.00	0.00	0.04	0.03	0.03
TiO <sub>2</sub>	0.37	0.76	0.14	0.23	0.08	50.94	52.26	51.53	51.82	49.40	49.16	53.27	53.37	51.81	51.08	48.69	49.01	48.75
Al <sub>2</sub> O <sub>3</sub>	2.43	0.76	1.24	0.46	0.53	0.00	0.00	0.00	0.00	0.00	0.03	0.00	0.00	0.00	0.00	0.00	0.00	0.00
Cr <sub>2</sub> O <sub>3</sub>	0.24	0.18	0.17	0.29	0.24	0.06	0.09	0.09	0.08	0.04	0.06	0.07	0.06	0.06	0.08	0.05	0.13	0.03
Fe <sub>2</sub> O <sub>3</sub>																		
FeO	88.25	90.45	88.20	90.23	89.86	44.36	44.65	43.93	42.49	46.13	45.64	42.80	42.87	45.76	46.77	46.50	47.51	48.61
MnO	0.31	0.57	0.00	0.09	0.43	1.89	1.86	1.86	3.26	2.04	2.08	0.24	0.24	1.36	1.45	1.09	1.26	1.19
NiO	0.00	0.00	0.00	0.00	0.07	0.06	0.00	0.03	0.00	0.00	0.04	0.00	0.00	0.00	0.00	0.08	0.03	0.00
MgO	0.22	0.24	0.33	0.16	0.21	0.06	0.08	0.08	0.08	0.06	0.08	2.57	2.32	0.14	0.15	0.27	0.30	0.36
CaO	0.23	0.14	0.23	0.16	0.18	0.08	0.41	0.26	0.73	0.04	0.77	0.00	0.10	0.00	0.07	0.03	0.25	0.04
Na <sub>2</sub> O	0.00	0.00	0.02	0.01	0.01	0.00	0.02	0.01	0.00	0.00	0.03	0.00	0.00	0.00	0.00	0.02	0.00	0.03
K <sub>2</sub> O	0.00	0.00	0.00	0.00	0.00	0.00	0.00	0.00	0.01	0.01	0.01	0.00	0.00	0.00	0.00	0.02	0.00	0.01
Total	92.10	93.11	91.81	91.72	91.62	97.46	99.78	97.82	98.61	97.75	98.94	98.95	98.96	99.13	99.58	96.76	98.50	99.05
Si	0.002	0.001	0.057	0.004	0.000	0.000	0.010	0.001	0.003	0.001	0.026	0.000	0.000	0.000	0.000	0.001	0.001	0.001
Ti	0.011	0.022	0.004	0.007	0.002	0.991	0.991	0.999	0.994	0.957	0.935	1.001	1.004	0.991	0.971	0.950	0.939	0.928
Al	0.110	0.034	0.056	0.021	0.024	0.000	0.000	0.000	0.000	0.000	0.001	0.000	0.000	0.000	0.000	0.000	0.000	0.000
Cr	0.007	0.005	0.005	0.009	0.007	0.001	0.002	0.002	0.002	0.001	0.001	0.001	0.001	0.001	0.002	0.001	0.003	0.001
Fe <sup>3+</sup>	1.858	1.915	1.818	1.950	1.963	0.016	0.000	0.000	0.003	0.085	0.077	0.000	0.000	0.017	0.056	0.098	0.118	0.144
Fe <sup>2+</sup>	0.980	0.985	1.029	0.990	0.965	0.944	0.941	0.947	0.903	0.908	0.889	0.895	0.897	0.956	0.933	0.911	0.894	0.885
Mn	0.010	0.018	0.000	0.003	0.014	0.042	0.040	0.040	0.071	0.045	0.045	0.005	0.005	0.029	0.031	0.024	0.027	0.026
Ni	0.000	0.000	0.000	0.000	0.002	0.001	0.000	0.001	0.000	0.000	0.001	0.000	0.000	0.000	0.000	0.002	0.001	0.000
Mg	0.012	0.014	0.019	0.010	0.012	0.002	0.003	0.003	0.003	0.002	0.003	0.096	0.087	0.005	0.006	0.010	0.011	0.013
Ca	0.010	0.006	0.010	0.007	0.008	0.002	0.011	0.007	0.020	0.001	0.021	0.000	0.003	0.000	0.002	0.001	0.007	0.001
Na	0.000	0.000	0.002	0.001	0.001	0.000	0.001	0.001	0.000	0.000	0.001	0.000	0.000	0.000	0.000	0.001	0.000	0.001
K	0.000	0.000	0.000	0.000	0.000	0.000	0.000	0.000	0.000	0.000	0.000	0.000	0.000	0.000	0.000	0.001	0.000	0.000
Cr#	0.44	0.33	0.34	0.47	0.46													
Mg#	1.33	1.46	1.86	1.05	1.38													
Fe#	94.1	98.0	96.7	98.5	98.4													

In spinel (magnetite) total iron as FeO. Fe<sup>3+</sup> calculations on the basis of spinel stoichiometry; Mg#=100Mg/(Mg+Fe), Cr#=100Cr/(Cr+Al), Fe<sup>3+</sup>#=100Fe<sup>3+</sup>/(Fe<sup>3+</sup>+Cr+Al); Ilmenite formulas calculated on the basis of 3 oxygens. c = grain core, r = grain rim, t = inclusion in titanite, mt = magnetite, ilm = ilmenite, Gr. Am. = granoblastic amphibolite, GDHA = garnet-diopside-hypersthene amphibolite, GDA = garnet-diopside amphibolite, DiAS = diopside amphibolite gneiss

**Table N-5.** Microprobe analyses and formulae of minor phases from different metamorphic rock varieties of the Krivaja-Konjuh ophiolite complex

Sample-Nr.	z1c-29	z1c-47	z1c-16	z1c-28	z1c-46	z1c-12	z1c-13	z1c-66	z1c-67	10d-22	10d-28	10d-38	10d-44	10d-45	10d-56	du5-5	du5-6	du5-21
Phase	ilm (c)	ilm (c)	ilm (g)	ilm (r)	ilm (r)	ttn (g)	ttn (g)	ttn (g)	ttn (g)	ttn	ttn	ttn	ttn (c)	ttn (r)	ttn	ttn (c)	ttn (r)	ttn (c)
Host Rock	PGDS	PGDS	PGDS	PGDS	PGDS	PGDS	PGDS	PGDS	PGDS	DiAS	DiAS	DiAS	DiAS	DiAS	DiAS	GDA	GDA	GDA
SiO <sub>2</sub>	0.03	0.02	0.03	0.02	0.01	30.54	29.91	30.32	29.71	39.17	30.12	30.32	29.98	30.16	29.94	30.41	30.66	29.78
TiO <sub>2</sub>	52.23	52.02	48.68	52.19	51.78	38.01	38.14	37.96	38.69	18.10	37.14	36.11	38.50	38.10	38.80	38.98	38.28	37.57
Al <sub>2</sub> O <sub>3</sub>	0.00	0.00	0.00	0.00	0.00	1.09	1.16	1.25	1.15	14.61	1.62	3.06	1.06	1.04	0.92	1.24	1.41	1.59
Cr <sub>2</sub> O <sub>3</sub>	0.00	0.01	0.12	0.01	0.04	0.02	0.00	0.04	0.04	0.04	0.02	0.02	0.01	0.00	0.03	0.03	0.00	0.03
Fe <sub>2</sub> O <sub>3</sub>																		
FeO	43.55	44.10	46.28	43.86	44.21	0.90	1.58	0.70	0.78	5.35	0.85	0.87	0.58	0.62	0.50	0.58	0.67	0.55
MnO	0.68	0.37	0.57	0.72	0.36	0.15	0.13	0.01	0.02	0.10	0.08	0.03	0.05	0.01	0.01	0.00	0.04	0.00
NiO	0.01	0.04	0.07	0.02	0.00	0.00	0.00	0.00	0.00	0.00	0.00	0.00	0.00	0.00	0.00	0.00	0.00	0.00
MgO	2.23	2.52	1.89	2.19	2.59	0.18	0.09	0.14	0.06	2.71	0.07	0.00	0.02	0.01	0.00	0.00	0.00	0.03
CaO	0.00	0.01	0.17	0.01	0.01	28.17	27.69	28.74	28.16	19.50	28.05	28.79	28.57	28.49	28.58	28.45	28.67	28.23
Na <sub>2</sub> O	0.00	0.00	0.00	0.00	0.00	0.02	0.00	0.00	0.00	0.22	0.04	0.02	0.02	0.02	0.00	0.01	0.01	0.01
K <sub>2</sub> O	0.04	0.00	0.02	0.00	0.00	0.00	0.00	0.00	0.00	0.00	0.01	0.02	0.00	0.01	0.00	0.02	0.00	0.00
Total	98.77	99.10	97.84	99.01	98.98	99.08	98.70	99.17	98.62	99.80	97.99	99.22	98.78	98.45	98.77	99.73	99.73	97.78
Si	0.001	0.001	0.001	0.000	0.000	1.005	0.990	0.998	0.984	1.199	1.002	0.995	0.992	1.000	0.990	0.994	1.002	0.993
Ti	0.986	0.976	0.927	0.983	0.972	0.941	0.949	0.940	0.964	0.417	0.929	0.891	0.958	0.950	0.965	0.959	0.941	0.942
Al	0.000	0.000	0.000	0.000	0.000	0.042	0.045	0.049	0.045	0.527	0.063	0.118	0.041	0.041	0.036	0.048	0.054	0.063
Cr	0.000	0.000	0.002	0.000	0.001	0.001	0.000	0.001	0.001	0.001	0.000	0.001	0.000	0.000	0.001	0.001	0.000	0.001
Fe <sup>3+</sup>	0.028	0.046	0.143	0.033	0.055	0.025	0.044	0.019	0.022	0.137	0.024	0.024	0.016	0.017	0.014	0.016	0.018	0.015
Fe <sup>2+</sup>	0.886	0.874	0.836	0.886	0.868	0.000	0.000	0.000	0.000	0.000	0.000	0.000	0.000	0.000	0.000	0.000	0.000	0.000
Mn	0.014	0.008	0.012	0.015	0.008	0.004	0.004	0.000	0.001	0.002	0.002	0.001	0.001	0.000	0.000	0.000	0.001	0.000
Ni	0.000	0.001	0.002	0.000	0.000	0.000	0.000	0.000	0.000	0.000	0.000	0.000	0.000	0.000	0.000	0.000	0.000	0.000
Mg	0.083	0.094	0.071	0.082	0.096	0.009	0.004	0.007	0.003	0.124	0.003	0.000	0.001	0.001	0.000	0.000	0.000	0.001
Ca	0.000	0.000	0.005	0.000	0.000	0.993	0.982	1.014	0.999	0.639	1.000	1.012	1.012	1.012	1.013	0.997	1.004	1.009
Na	0.000	0.000	0.000	0.000	0.000	0.002	0.000	0.000	0.000	0.013	0.003	0.001	0.001	0.001	0.000	0.001	0.001	0.000
K	0.001	0.000	0.001	0.000	0.000	0.000	0.000	0.000	0.000	0.000	0.000	0.001	0.000	0.000	0.000	0.001	0.000	0.000

Ilmenite formulas calculated on the basis of 3 oxygens. Titanite formulae calculated on the basis of 5 oxygens and total iron as Fe<sup>3+</sup>. c = grain core, r = grain rim, g = inclusion in garnet, ilm = ilmenite, ttn = titanite, PGDS = plagioclase-garnet-diopside gneiss, DiAS = diopside amphibolite gneiss, GDA = garnet-diopside amphibolite



**Table N-6.** Microprobe analyses and formulae of minor phases from different metamorphic rock varieties of the Krivaja-Konjuh ophiolite complex

Sample-Nr.	du5-22	du5-26	du5-27	du5-35	du5-36	cc1-3	cc1-42b	cc1-55	r8-20	r8-21a	r8-27	u23-20	u23-21	u23-24	11c-48	11c-51	u29-1	u29-33
Phase	ttn (r)	ttn (c)	ttn (r)	ttn (c)	ttn (r)	ttn (g)	ttn (g)	ttn (g)	tta (a)	ttn (a)	ttn	ttn	ttn	ttn	ttn	crn (r)	crn (c)	crn (c)
Host Rock	GDA	GDA	GDA	GDA	GDA	GDA	GDA	GDA	Gr. Am.	Gr. Am.	Gr. Am.	Gr. Am.	Gr. Am.	Gr. Am.	Gr. Am.	Gr. Am.	Gr. Am.	Gr. Am.
SiO <sub>2</sub>	30.21	30.39	30.30	30.02	30.27	29.55	29.78	30.21	30.23	31.78	30.71	30.42	29.91	30.77	30.14	30.48	0.02	0.00
TiO <sub>2</sub>	37.43	38.74	38.65	38.02	37.58	37.91	38.21	38.25	36.79	33.00	33.45	33.95	33.11	33.77	35.07	37.71	0.00	0.01
Al <sub>2</sub> O <sub>3</sub>	1.63	1.25	1.32	1.68	1.62	1.26	1.19	1.05	1.31	3.46	3.05	3.92	7.07	3.95	2.34	1.18	100.52	100.62
Cr <sub>2</sub> O <sub>3</sub>	0.06	0.03	0.00	0.02	0.00	0.00	0.01	0.01	0.01	0.02	0.01	0.38	0.59	0.79	0.08	0.09	0.50	0.28
Fe <sub>2</sub> O <sub>3</sub>																		
FeO	0.66	0.49	0.71	0.54	0.59	0.66	0.82	0.72	2.18	2.77	1.84	0.66	1.24	0.38	1.59	0.62	0.16	0.26
MnO	0.04	0.00	0.01	0.00	0.00	0.01	0.00	0.01	0.13	0.06	0.02	0.02	0.03	0.00	0.02	0.04	0.02	0.00
NiO	0.00	0.00	0.00	0.00	0.00	0.01	0.00	0.00	0.00	0.00	0.00	0.00	0.00	0.00	0.07	0.00	0.00	0.00
MgO	0.02	0.24	0.01	0.03	0.02	0.02	0.02	0.01	0.09	0.37	0.00	0.44	0.45	0.00	0.00	0.13	0.00	0.04
CaO	28.17	28.75	28.68	28.16	28.06	28.30	28.37	28.12	28.58	26.73	28.51	27.91	25.32	28.96	28.19	28.18	0.01	0.00
Na <sub>2</sub> O	0.00	0.00	0.02	0.00	0.01	0.01	0.01	0.00	0.00	0.02	0.03	0.01	0.01	0.00	0.03	0.00	0.00	0.00
K <sub>2</sub> O	0.00	0.00	0.01	0.01	0.00	0.00	0.02	0.01	0.01	0.00	0.02	0.00	0.01	0.00	0.00	0.00	0.00	0.01
Total	98.23	99.89	99.71	98.49	98.14	97.73	98.44	98.38	99.32	98.22	97.64	97.71	97.73	98.63	97.52	98.42	101.24	101.22
Si	1.002	0.993	0.992	0.993	1.004	0.988	0.988	1.001	0.996	1.045	1.023	1.009	0.982	1.014	1.008	1.009	0.000	0.000
Ti	0.934	0.952	0.951	0.946	0.937	0.953	0.954	0.953	0.912	0.816	0.838	0.847	0.818	0.837	0.882	0.939	0.000	0.000
Al	0.064	0.048	0.051	0.066	0.063	0.050	0.047	0.041	0.051	0.134	0.120	0.153	0.274	0.153	0.092	0.046	1.990	1.992
Cr	0.002	0.001	0.000	0.000	0.000	0.000	0.000	0.000	0.000	0.001	0.000	0.010	0.015	0.021	0.002	0.002	0.007	0.004
Fe <sup>3+</sup>	0.018	0.013	0.019	0.015	0.016	0.018	0.023	0.020	0.060	0.076	0.051	0.018	0.034	0.010	0.044	0.017	0.002	0.004
Fe <sup>2+</sup>	0.000	0.000	0.000	0.000	0.000	0.000	0.000	0.000	0.000	0.000	0.000	0.000	0.000	0.000	0.000	0.000	0.000	0.000
Mn	0.001	0.000	0.000	0.000	0.000	0.000	0.000	0.000	0.004	0.002	0.001	0.001	0.001	0.000	0.001	0.001	0.000	0.000
Ni	0.000	0.000	0.000	0.000	0.000	0.000	0.000	0.000	0.000	0.000	0.000	0.000	0.000	0.000	0.002	0.000	0.000	0.000
Mg	0.001	0.011	0.001	0.001	0.001	0.001	0.001	0.000	0.004	0.018	0.000	0.022	0.022	0.000	0.000	0.006	0.000	0.001
Ca	1.001	1.006	1.006	0.998	0.997	1.014	1.009	0.999	1.009	0.942	1.018	0.992	0.891	1.022	1.010	0.999	0.000	0.000
Na	0.000	0.000	0.001	0.000	0.001	0.001	0.001	0.000	0.000	0.002	0.002	0.001	0.001	0.000	0.002	0.000	0.000	0.000
K	0.000	0.000	0.000	0.001	0.000	0.000	0.001	0.000	0.000	0.000	0.001	0.000	0.000	0.000	0.000	0.000	0.000	0.000

Titanite formulae calculated on the basis of 5 oxygens and total iron as Fe<sup>3+</sup>. Corundum formulae calculated on the basis of 3 oxygens. c = grain core, r = grain rim, g = inclusion in garnet, a = inclusion in amphibole, ttn = titanite, crn = corundum, Gr. Am. = granoblastic amphibolite, GDA = garnet-diopside amphibolite

**Table N-7.** Microprobe analyses and formulae of minor phases from different metamorphic rock varieties of the Krivaja-Konjuh ophiolite complex

Sample-Nr.	u29-2	u29-34	u29-7	u29-8	u29-9	u29-38	11c-53	11c-54	11c-56	u22-43	u22-45	cc1-67	cc1-41	cc1-81	cc1-22	cc1-46	du5-44	du5-46
Phase	crn (r)	crn (r)	ct	ct	ct	ct	chl	chl	chl	chl(k.c.)	chl(k.c.)	rt	rt (cpx)	rt (cpx)	rt (c)	rt (c)	xo	xo
Host Rock	Gr. Am.	Gr. Am.	Gr. Am.	Gr. Am.	Gr. Am.	Gr. Am.	Gr. Am.	Gr. Am.	Gr. Am.	GDA	GDA	GDA	GDA	GDA	GDA	GDA	GDA	GDA
SiO <sub>2</sub>	0.03	0.01	15.68	15.64	16.99	15.56	26.35	26.20	26.19	30.57	30.90	0.04	0.06	0.03	0.02	0.02	48.40	49.35
TiO <sub>2</sub>	0.00	0.00	0.02	0.05	0.02	0.03	0.06	0.02	0.03	0.03	0.01	98.88	98.71	98.19	99.02	99.50	0.03	0.03
Al <sub>2</sub> O <sub>3</sub>	100.30	100.67	44.87	44.62	42.15	45.43	20.50	20.48	19.85	17.28	17.27	0.00	0.00	0.00	0.00	0.00	2.24	1.16
Cr <sub>2</sub> O <sub>3</sub>	0.47	0.32	0.11	0.09	0.03	0.30	0.00	0.00	0.00	0.27	0.18	0.16	0.12	0.26	0.15	0.14	0.00	0.00
Fe <sub>2</sub> O <sub>3</sub>																		
FeO	0.15	0.25	2.23	2.39	2.23	2.60	22.77	23.50	21.09	19.78	18.47	0.33	0.50	0.61	0.24	0.31	1.67	0.50
MnO	0.00	0.00	0.04	0.00	0.02	0.04	0.20	0.21	0.15	0.23	0.17	0.00	0.00	0.00	0.03	0.00	0.00	0.00
NiO	0.00	0.00	0.00	0.00	0.09	0.00	0.00	0.00	0.03	0.00	0.00	0.00	0.00	0.00	0.00	0.05		
MgO	0.00	0.00	18.01	18.36	18.61	18.34	16.87	16.89	17.59	19.04	19.39	0.02	0.01	0.00	0.00	0.00	2.03	2.01
CaO	0.00	0.03	12.94	12.89	11.92	12.85	0.11	0.19	0.09	0.33	0.46	0.08	0.40	0.45	0.01	0.05	43.57	46.10
Na <sub>2</sub> O	0.02	0.02	0.17	0.26	0.35	0.17	0.00	0.00	0.00	0.03	0.01	0.02	0.00	0.00	0.00	0.00	0.00	0.00
K <sub>2</sub> O	0.00	0.00	0.00	0.00	0.00	0.01	0.00	0.00	0.01	0.04	0.01	0.01	0.00	0.00	0.02	0.01	0.00	0.00
Total	100.96	101.30	94.06	94.30	92.41	95.31	86.85	87.48	85.05	87.59	86.86	99.54	99.80	99.54	99.50	100.08	97.95	97.16
Si	0.000	0.000	1.123	1.117	1.234	1.101	2.763	2.740	2.785	3.111	3.145	0.001	0.001	0.000	0.000	0.000	5.709	5.889
Ti	0.000	0.000	0.001	0.003	0.001	0.001	0.005	0.002	0.002	0.002	0.001	0.995	0.991	0.989	0.996	0.995	0.002	0.002
Al	1.991	1.991	3.787	3.755	3.610	3.791	2.533	2.525	2.488	2.073	2.072	0.000	0.000	0.000	0.000	0.000	0.312	0.163
Cr	0.006	0.004	0.006	0.005	0.002	0.017	0.000	0.000	0.000	0.022	0.014	0.002	0.001	0.003	0.002	0.001	0.000	0.000
Fe <sup>3+</sup>	0.002	0.004	0.000	0.036	0.000	0.010	0.000	0.000	0.000	0.000	0.000	0.004	0.006	0.007	0.003	0.003	0.164	0.050
Fe <sup>2+</sup>	0.000	0.000	0.133	0.107	0.136	0.144	1.997	2.056	1.876	1.683	1.572						0.000	0.000
Mn	0.000	0.000	0.002	0.000	0.001	0.002	0.017	0.018	0.013	0.019	0.015	0.000	0.000	0.000	0.000	0.000	0.001	0.001
Ni	0.000	0.000	0.000	0.000	0.005	0.000	0.000	0.000	0.003	0.000	0.000	0.000	0.000	0.000	0.000	0.001		
Mg	0.000	0.000	1.923	1.955	2.016	1.935	2.638	2.634	2.789	2.889	2.942	0.000	0.000	0.000	0.000	0.000	0.356	0.001
Ca	0.000	0.000	0.993	0.986	0.928	0.974	0.012	0.021	0.010	0.036	0.050	0.001	0.006	0.006	0.000	0.001	5.506	5.894
Na	0.000	0.001	0.023	0.036	0.049	0.023	0.001	0.000	0.001	0.006	0.002	0.001	0.000	0.000	0.000	0.000	0.000	0.000
K	0.000	0.000	0.000	0.000	0.000	0.000	0.000	0.000	0.001	0.005	0.002	0.000	0.000	0.000	0.000	0.000	0.000	0.001
OH	0.000	0.000	2.000	2.000	2.000	2.000	8.000	8.000	8.000	8.000	8.000						2.000	2.000
Mg#			93.5	93.2	93.7	92.6	56.9	56.2	59.8	63.2	65.2							

Corrundum formulae calculated on the basis of 3 oxygens. Clintonite formulae calculated on the basis of 11 oxygens and fixed number of cations (11). Chlorite formulae calculated on the basis of 14 oxygens and total iron as Fe<sup>2+</sup>. Mg# = 100Mg/(Mg+Fe<sub>kl</sub>). Rutile formulae calculated on the basis of 2 oxygens and total iron as Fe<sup>3+</sup>. r = grain rim, k.c. = chlorite from garnet kelfitic corona, cpx = rutile inclusion in clinopyroxene, crn = corundum, ct = clintonite, chl = chlorite, xo = xonotlite, Gr. Am. = granoblastic amphibolite, GDA = garnet-diopside amphibolite

## APPENDIX D. Bulk-rock geochemistry

### Ultramafic rocks

**Table X-1.** Geochemical analyses of macroelements and CIPW normative composition in different ultramafic lithologies from the Krivaja-Konjuh ophiolite complex.

Sample	O2	Z2	Z4	U35	GR2	GR12	M2	U4	4A	R7	K1	U19	2A	1C	R6	1B	2B
Rock type	Sp Lh	Sp Lh	Sp Lh	Sp Lh	Pl Lh	Pl Lh	Pl Lh	Pl Lh	Pl Lh	Pl Lh	Dun	Dun	Ol web	Ol web	Per	Per	Per
SiO <sub>2</sub>	42.97	42.17	41.75	40.705	41.51	41.92	42.9	42.6	39.89	42.13	36.54	37.07	45.93	42.74	41.59	41.47	41.4
TiO <sub>2</sub>	0.07	0.05	0.05	0.06	0.08	0.07	0.06	0.06	0.04	0.08	0.03	0.08	0.18	0.15	0.08	0.08	0.09
Al <sub>2</sub> O <sub>3</sub>	2.65	2.19	2.49	2.89	3.17	2.45	2.31	2.55	1.67	2.99	5.15	5.8	6.89	7.72	2.82	3.19	2.99
Cr <sub>2</sub> O <sub>3</sub>	0.36	0.36	0.38	0.37	0.40	0.38	0.39	0.36	0.31	0.36	0.54	0.31	0.49	0.71	0.34	0.37	0.40
FeO	7.60	7.64	7.52	7.82	7.34	7.62	7.79	7.44	7.69	7.43	8.74	8.42	5.30	5.91	7.33	7.63	7.60
MnO	0.12	0.12	0.12	0.12	0.12	0.12	0.13	0.12	0.11	0.12	0.14	0.13	0.12	0.12	0.12	0.12	0.12
MgO	35.44	36.71	35.29	35.79	35.5	36.77	37.08	35.77	38.32	34.76	33.21	31.88	25.23	28.07	36.05	35.6	35.09
CaO	2.66	2.09	2.94	2.66	3.31	2.21	2.51	2.7	1.32	2.68	2.46	4.55	9.41	6.15	2.95	3.02	2.26
Na <sub>2</sub> O	0.14	0.06	0.09	0.11	0.2	0.17	0.12	0.12	0.05	0.14	<0.01	0.02	0.19	0.13	0.16	0.17	0.14
K <sub>2</sub> O	<0.01	<0.01	<0.01	<0.01	<0.01	<0.01	<0.01	<0.01	<0.01	<0.01	<0.01	<0.01	<0.01	0.01	<0.01	<0.01	<0.01
P <sub>2</sub> O <sub>5</sub>	0.02	0.02	<0.01	0.02	0.01	0.01	0.02	0.02	0.02	0.01	0.02	0.03	0.01	0.01	<0.01	<0.01	0.01
H <sub>2</sub> O	5.89	6.39	7.03	7.33	6.24	6.26	4.67	6.27	8.23	7.19	10.98	9.62	4.44	6.43	6.53	6.19	7.82
CO <sub>2</sub>	0.27	0.37	0.53	0.23	0.30	0.20	0.17	0.17	0.43	0.37	0.20	0.20	0.30	0.43	0.23	0.23	0.30
Total	98.23	98.21	98.23	98.14	98.25	98.22	98.21	98.24	98.11	98.30	98.13	98.20	98.65	98.62	98.24	98.15	98.29
Mg#	89.3	89.5	89.3	89.1	89.6	89.6	89.5	89.6	89.9	89.3	87.1	87.1	89.5	89.4	89.8	89.3	89.2
il	0.13	0.09	0.09	0.11	0.15	0.13	0.11	0.11	0.08	0.15	0.06	0.15	0.34	0.28	0.15	0.15	0.17
or	0.06	0.06	0.06	0.06	0.06	0.06	0.06	0.06	0.06	0.06	0.06	0.06	0.06	0.06	0.06	0.06	0.06
ab	1.18	0.51	0.76	0.93	1.69	1.44	1.02	1.02	0.42	1.18	0.08	0.17	1.61	1.10	1.35	1.44	1.18
an	6.57	5.68	6.36	7.36	7.72	5.89	5.73	6.39	3.70	7.50	10.81	15.71	17.92	20.45	6.95	7.91	7.50
mt	1.84	1.85	1.82	1.89	1.77	1.84	1.88	1.80	1.86	1.80	2.11	2.04	1.28	1.43	1.77	1.84	1.84
c									0.22		1.16						
di <sub>wo</sub>	2.00	0.93	2.01	1.77	2.81	1.56	2.30	2.42		1.42		2.26	11.19	3.04	2.58	2.32	0.73
di <sub>en</sub>	1.58	0.73	1.59	1.40	2.23	1.24	1.82	1.92		1.12		1.75	8.87	2.41	2.04	1.83	0.58
di <sub>fs</sub>	0.20	0.09	0.20	0.18	0.27	0.15	0.22	0.23		0.14		0.27	1.05	0.29	0.24	0.23	0.07
hy <sub>en</sub>	26.95	26.75	24.77	18.99	18.17	22.16	23.57	24.87	21.11	26.28	12.39	5.58	24.08	24.26	19.50	18.93	24.74
hy <sub>fs</sub>	3.33	3.22	3.06	2.40	2.16	2.65	2.87	2.99	2.45	3.24	1.89	0.85	2.86	2.91	2.28	2.34	3.08
qz																	
ol <sub>fo</sub>	41.87	44.81	43.12	48.18	47.67	47.78	46.93	43.66	52.09	41.47	49.28	50.51	20.95	30.31	47.83	47.59	43.51
ol <sub>fa</sub>	5.71	5.95	5.86	6.70	6.26	6.30	6.29	5.79	6.67	5.63	8.31	8.48	2.74	4.01	6.18	6.48	5.97

Sp Lh=spinel lherzolite. Pl Lh=plagioclase lherzolite. Dun=Dunite. Ol web=olivine websterite. Per=peridotite of unknown mineral composition. Values are in wt% (oxides) and ppm (elements).

**Table X-2.** Geochemical analyses of microelements and REE in different ultramafic lithologies from the Krivaja-Konjuh ophiolite complex.

Sample	O2	Z2	Z4	U35	GR2	GR12	M2	U4	4A	R7	K1	U19	2A	1C	R6	1B	2B
Rock type	Sp Lh	Sp Lh	Sp Lh	Sp Lh	Pl Lh	Pl Lh	Pl Lh	Pl Lh	Pl Lh	Pl Lh	Dun	Dun	Ol web	Ol web	Per	Per	Per
Cs	<0.10	<0.10	<0.10	<0.10	0.4	<0.10	0.1	0.7	0.2	<0.10	<0.10	<0.10	2.7	2	<0.10	<0.10	0.2
Rb	0.2	0.2	0.5	0.2	0.5	0.3	0.4	0.5	0.5	0.3	0.6	0.2	1.7	2.2	0.2	0.4	0.3
Ba	2	2	<1	<1	4	2	<1	<1	1	2	4	3	2	7	<1	1	2
Th	<0.2	<0.2	<0.2	<0.2	<0.2	<0.2	<0.2	<0.2	<0.2	<0.2	<0.2	<0.2	<0.2	<0.2	<0.2	<0.2	<0.2
U	<0.1	<0.1	<0.1	<0.1	<0.1	<0.1	<0.1	<0.1	<0.1	<0.1	<0.1	<0.1	<0.1	<0.1	<0.1	<0.1	<0.1
Sr	0.7	3.4	2.2	3.4	13.2	8	<0.5	1.5	6.2	1.4	2.5	36.4	11	14.2	1.8	1	3.6
Nb	0.2	<0.1	0.2	0.8	0.1	<0.1	<0.1	<0.1	0.1	<0.1	0.2	<0.1	<0.1	0.2	<0.1	<0.1	<0.1
Zr	1.4	1	2	1	1.2	1.1	1.2	1.9	3.4	1.5	1.3	1.5	4.3	1.2	1.6	1.3	1.9
Hf	<0.1	<0.1	<0.1	<0.1	0.1	<0.1	0.1	<0.1	<0.1	0.1	<0.1	0.1	0.1	<0.1	<0.1	<0.1	<0.1
Pb	0.1	0.1	0.2	0.2	0.3	<0.1	<0.1	0.2	0.2	1	<0.1	0.1	0.2	0.1	0.1	0.1	0.2
Y	2.1	1.5	1.9	2	2.2	1.7	1.7	1.8	1.3	2.1	0.4	0.9	6.8	5.9	2.3	2.7	2.3
Co	104	100	100	103	91	94	97	93	106	92	96	100	59	62	96	96	98
Ni	2078	1956	1947	1976	1817	1892	1987	1868	2294	1825	1943	1586	1215	928	1886	1884	1924
V	64	61	71	67	73	61	69	73	42	72	28	28	203	196	72	74	65
Sc	13	12	14	13	14	13	13	14	9	14	5	6	36	35	14	14	13
Cu	26	15	25	22	28	18	28	28	17	23	12	17	176	54	23	35	25
Zn	18	20	19	25	26	24	23	24	27	16	33	35	12	11	16	25	27
Ga	2.2	2	2.2	2.6	2.9	2.6	2.4	2.4	1.5	2.9	2.9	3.9	4.9	7	2.7	2.9	2.7
La	0.1	0.3	<0.1	<0.1	<0.10	0.3	0.2	0.3	<0.1	0.3	0.2	0.4	<0.1	<0.1	0.3	<0.1	<0.1
Ce	<0.1	<0.1	<0.1	<0.1	0.2	0.3	0.3	0.3	<0.1	0.3	0.2	0.9	0.2	<0.1	0.4	<0.1	<0.1
Pr	<0.02	<0.02	<0.02	<0.02	0.03	0.06	0.05	0.05	0.03	0.07	0.04	0.11	0.08	0.03	0.07	<0.02	<0.02
Nd	<0.3	<0.3	<0.3	<0.3	<0.3	<0.3	<0.3	<0.3	<0.3	<0.3	<0.3	0.4	0.5	<0.3	<0.3	<0.3	<0.3
Sm	0.09	<0.05	0.08	0.1	0.15	0.08	<0.05	0.07	0.1	0.11	<0.05	0.06	0.41	0.25	0.12	0.09	0.12
Eu	0.05	0.02	0.03	0.04	0.06	0.05	0.04	0.03	0.03	0.06	0.04	0.12	0.18	0.13	0.07	0.07	0.06
Gd	0.23	0.13	0.15	0.16	0.28	0.27	0.23	0.24	0.13	0.29	<0.05	0.15	0.78	0.53	0.38	0.28	0.24
Tb	0.05	0.03	0.04	0.05	0.05	0.04	0.04	0.04	0.03	0.06	0.02	0.03	0.16	0.14	0.06	0.06	0.06
Dy	0.32	0.22	0.35	0.33	0.42	0.35	0.31	0.33	0.18	0.39	0.12	0.15	1.11	0.94	0.43	0.55	0.45
Ho	0.08	0.05	0.07	0.06	0.09	0.07	0.08	0.08	0.04	0.08	<0.02	0.04	0.26	0.23	0.09	0.1	0.08
Er	0.26	0.16	0.25	0.24	0.34	0.22	0.21	0.23	0.14	0.29	0.05	0.1	0.78	0.74	0.31	0.34	0.29
Tm	0.04	0.03	0.04	0.03	0.05	0.03	0.04	0.03	0.02	0.04	<0.01	0.02	0.13	0.12	0.05	0.05	0.04
Yb	0.26	0.16	0.23	0.25	0.27	0.28	0.23	0.24	0.12	0.28	0.07	0.17	0.8	0.75	0.3	0.33	0.27
Lu	0.04	0.03	0.04	0.04	0.05	0.05	0.04	0.05	0.03	0.05	0.01	0.03	0.11	0.11	0.06	0.05	0.05

Sp Lh=spinel lherzolite. Pl Lh=plagioclase lherzolite. Dun=dunite. Ol web=olivine websterite. Per=peridotite of unknown mineral composition. All values are in ppm.

Metamorphic rocks

**Table Y-1.** Geochemical analyses of macroelements and CIPW normative composition in different metamorphic lithologies from the Krivaja-Konjuh ophiolite complex.

Sample	U30	U29	11C	R8	U23	CC1	MK2	GR7	V1	DU5	U22	X1	U40	V4	10D	Z1C	YU145	YU137
Rock type	Gr. Am.	Gr. Am.	Gr. Am.	Gr. Am.	Gr. Am.	G-D A	G-D A	G-D A	G-D A	G-D A	G-D A	G-D-H	G-D-H	G-D-H	D-A-S	PGDS	O.S.	O.S.
SiO <sub>2</sub>	41.99	39.70	47.32	50.10	46.05	48.21	47.13	46.31	47.39	41.67	45.38	47.89	47.59	45.21	42.65	45.57	46.80	49.40
TiO <sub>2</sub>	0.09	0.06	0.64	0.92	0.22	0.55	0.48	0.28	0.27	1.26	0.31	0.44	0.40	0.24	1.34	2.21	0.17	1.48
Al <sub>2</sub> O <sub>3</sub>	17.71	27.47	15.07	14.88	15.97	16.91	14.76	17.53	15.26	15.37	16.04	14.40	14.02	16.19	12.61	13.12	18.90	14.80
Cr <sub>2</sub> O <sub>3</sub>	0.72	0.26	0.04	0.06	0.14	0.07	0.05	0.10	0.05	0.06	0.12	0.06	0.06	0.08	0.03	0.01	0.07	0.03
FeO	5.08	2.69	8.45	8.38	4.99	6.44	7.93	5.74	7.32	11.21	5.55	7.94	8.30	7.07	10.31	14.50	4.99	10.04
MnO	0.07	0.05	0.12	0.16	0.09	0.09	0.15	0.09	0.18	0.21	0.11	0.16	0.17	0.13	0.20	0.24	0.10	0.20
MgO	20.00	9.49	8.64	8.37	13.35	9.35	10.77	10.70	11.75	11.01	12.22	11.53	11.81	13.27	8.44	8.89	11.30	8.36
CaO	9.12	15.99	13.37	10.12	14.24	13.49	14.04	15.35	13.87	15.02	14.73	13.85	13.58	12.06	19.30	9.45	13.90	9.68
Na <sub>2</sub> O	1.11	1.33	2.58	3.67	1.32	2.69	2.07	1.62	1.60	1.21	1.83	1.84	1.78	2.32	1.40	2.73	1.76	3.53
K <sub>2</sub> O	0.03	0.22	0.19	0.22	0.09	0.04	0.02	0.03	0.03	0.06	0.18	0.03	0.03	0.05	0.07	0.17	0.10	0.29
P <sub>2</sub> O <sub>5</sub>	0.02	0.01	0.04	0.17	0.01	0.03	0.03	0.02	0.02	0.09	0.01	0.01	0.02	0.01	0.13	0.19	0	0.15
H <sub>2</sub> O <sup>-</sup>	2.90	2.10	2.30	1.80	2.70	1.10	1.30	1.30	1.20	1.30	2.60	0.70	0.90	2.30	2.10	1.00	1.99	1.61
CO <sub>2</sub>	0	0	0	0	0	0	0	0	0	0	0	0	0	0	0	0	0.04	0.05
Total	98.12	99.11	98.72	98.79	99.03	98.90	98.68	98.97	98.89	98.41	98.96	98.79	98.60	98.85	98.55	98.07	100.05	99.59
Mg#	87.5	86.2	64.5	64.0	82.6	72.1	70.7	76.8	74.1	63.6	79.6	72.1	71.7	77.0	59.3	52.2	80.1	59.7
il	0.18	0.12	1.26	1.80	0.43	1.07	0.93	0.54	0.52	2.46	0.61	0.85	0.78	0.47	2.63	4.31	0.33	2.87
or	0.19		1.16	1.34	0.55	0.24	0.12	0.18	0.18		1.10	0.18	0.18	0.31		1.03	0.60	1.75
ab	8.91		18.24	31.97	10.69	19.32	15.04	9.57	13.84		6.50	15.85	15.39	12.15		23.74	13.26	30.45
an	45.38	70.41	30.01	24.17	38.78	34.67	31.71	41.40	35.14	37.34	36.31	31.50	30.84	34.77	28.89	23.68	44.21	24.14
mt	1.29	0.67	2.12	2.09	1.25	1.59	1.97	1.42	1.81	2.78	1.39	1.95	2.05	1.77	2.58	3.60	1.23	2.47
c																		
di <sub>wo</sub>	0.82		16.04	11.01	14.38	13.98	16.50	15.18	14.65	15.83	16.45	16.03	15.82	11.30	22.52	9.70	10.89	9.94
di <sub>en</sub>	0.63		9.93	8.81	10.73	9.47	10.92	10.71	12.42	9.80	11.94	11.87	12.30	7.95	13.29	7.75	7.91	8.17
di <sub>fs</sub>	0.09		5.16	4.52	2.23	3.43	4.39	3.17	4.37	5.10	2.98	4.49	4.79	2.38	8.11	6.10	1.97	4.79
hy <sub>en</sub>				1.97					2.44			1.12	1.76			2.51		2.23
hy <sub>fs</sub>				1.01					0.86			0.42	0.68			1.98		1.31
qz																		
ol <sub>fo</sub>	36.18	17.07	8.66	8.87	16.65	10.03	11.62	11.60	12.26	12.88	13.74	12.17	12.45	18.39	5.93	10.51	14.56	9.15
ol <sub>fa</sub>	5.77	3.04	4.96	5.02	3.81	4.00	5.14	3.78	4.76	7.38	3.78	5.07	5.35	6.07	3.99	9.12	3.99	5.91
ne	0.51	6.28	2.37		0.49	2.13	1.58	2.41		5.70	5.18			4.42	6.64		1.04	

Gr. Am.=granoblastic amphibolite. G-D A=Grt-Di Amphibolite. G-D-H=Grt-Di-Hy Amphibolite. D-A-S=Diopside Amphibolite gneiss. PGDS=Pl-Grt-Di gneiss. O.S.=old samples. Total Fe as FeO. Values are in wt% (oxides) and ppm (elements).

**Table Y-2.** Geochemical analyses of microelements and REE in different metamorphic lithologies from the Krivaja-Konjuh ophiolite complex.

Sample	U30	U29	11C	R8	U23	CC1	MK2	GR7	V1	DU5	U22	X1	U40	V4	10D	Z1C	YU145	YU137
Rock type	Gr. Am.	Gr. Am.	Gr. Am.	Gr. Am.	Gr. Am.	G-D A	G-D A	G-D A	G-D A	G-D A	G-D A	G-D-H	G-D-H	G-D-H	D-A-S	PGDS	O.S.	O.S.
Cs	<0.1	<0.1	1.0	<0.1	<0.1	<0.1	<0.1	<0.1	<0.1	<0.1	0.2	<0.1	<0.1	<0.1	2.8	2.7	<0.1	n.a.
Rb	0.6	2.1	3.3	1.3	0.9	0.4	<0.1	0.5	0.6	0.5	3.5	0.3	0.4	0.2	0.9	3.6	1	0.1
Ba	3	26	201	18	8	8	2	9	3	4	12	1	2	3	24	25	18	107
Th	<0.2	<0.2	<0.2	<0.2	<0.2	<0.2	<0.2	<0.2	<0.2	<0.2	<0.2	<0.2	<0.2	<0.2	0.9	<0.2	<0.1	n.a.
U	<0.1	<0.1	<0.1	<0.1	<0.1	<0.1	<0.1	<0.1	<0.1	<0.1	<0.1	<0.1	<0.1	<0.1	0.2	0.1	<0.1	n.a.
Sr	30.5	333.4	231.7	166.4	112.7	120.9	94.6	121.7	68.4	52.6	182.6	78.3	74.9	80.4	149.2	158.9	138.0	40.0
Nb	<0.1	0.2	1.0	2.3	1.1	0.9	<0.1	<0.1	<0.1	2.2	<0.1	<0.4	<0.2	<0.1	<6.3	<5.5	0.4	3.6
Zr	3.9	1.0	25.1	59.9	12.8	20.1	6.5	4.3	3.4	52.9	7.5	8.2	5.8	5.6	55.1	100.4	3.0	66.0
Hf	<0.1	<0.1	0.9	1.7	0.4	0.7	0.2	0.1	0.1	1.4	0.2	0.3	0.1	0.2	1.9	2.8	0.1	n.a.
Pb	<0.1	0.7	0.1	0.3	0.2	0.2	0.2	0.4	0.2	0.1	0.2	<0.1	<0.1	0.1	0.3	0.1	n.a.	n.a.
Y	1.9	1.8	18.9	25.6	5.8	11.1	10.0	6.1	8.6	33.3	6.3	9.8	10.3	5.2	27.8	45.8	4	38.0
Co	63.0	30.4	44.2	38.0	43.2	36.3	48.5	40.9	47.1	54.7	37.9	44.4	46.9	53.7	43.8	57.3	n.a.	n.a.
Ni	153.8	35.2	35.2	25.1	75.9	34.9	65.5	99.8	69.8	56.7	38.7	51.3	56.1	61.8	60.6	47.8	269.0	68.0
V	57	41	288	215	103	184	257	167	176	348	183	240	234	122	352	515	n.a.	n.a.
Sc	8	6	39	33	24	33	46	33	43	47	40	47	47	26	45	52	21	n.a.
Cu	2.6	3.8	46.2	14.8	35.6	49.2	178.0	119.3	58.9	68.7	40.4	79.3	78.7	73.5	114.0	106.5	n.a.	n.a.
Zn	4	1	8	5	4	7	9	6	6	14	7	5	5	8	25	94	34	92
Ga	8.8	11.7	14.1	14.5	9.6	12.4	13.8	13.0	11.1	14.7	10.9	12.1	12.3	11.9	14.0	19.3	n.a.	n.a.
La	0.3	<0.1	0.9	3.3	1.3	1.8	0.3	0.2	0.4	2.7	0.5	0.2	0.3	0.3	11.9	2.8	0.2	n.a.
Ce	0.8	0.2	2.8	9.4	3.8	4.8	1.2	0.9	0.7	8.6	0.9	0.9	1.1	1.2	27.7	12.3	1	n.a.
Pr	0.12	0.04	0.54	1.52	0.53	0.79	0.25	0.21	0.17	1.52	0.19	0.21	0.20	0.22	3.5	2.3	n.a.	n.a.
Nd	0.6	<0.3	3.7	8.5	2.1	4.3	1.8	1.4	0.8	8.8	1.2	1.7	1.6	1.3	16.5	13.3	<1	n.a.
Sm	0.16	0.13	1.52	2.74	0.74	1.58	0.79	0.61	0.55	3.35	0.62	0.64	0.81	0.46	3.95	5.03	0.23	n.a.
Eu	0.17	0.16	0.61	0.98	0.33	0.71	0.5	0.39	0.34	1.21	0.33	0.45	0.44	0.35	1.21	1.69	0.13	n.a.
Gd	0.26	0.21	2.33	3.72	0.87	1.99	1.3	0.91	1	4.86	0.94	1.35	1.3	0.79	4.69	7.23	<0.5	n.a.
Tb	0.06	0.04	0.49	0.72	0.16	0.37	0.27	0.18	0.19	0.96	0.2	0.28	0.27	0.15	0.86	1.37	<0.1	n.a.
Dy	0.4	0.37	3.27	4.38	1.01	2.08	1.65	1.12	1.53	5.96	1.19	1.85	1.85	0.88	5.19	8.57	n.a.	n.a.
Ho	0.06	0.07	0.75	0.97	0.22	0.42	0.37	0.23	0.36	1.34	0.24	0.42	0.41	0.21	1.14	1.96	0.13	n.a.
Er	0.21	0.19	2.36	2.69	0.71	1.16	1	0.64	1.06	3.89	0.76	1.23	1.29	0.66	3.33	5.59	n.a.	n.a.
Tm	0.03	0.03	0.38	0.45	0.12	0.17	0.16	0.11	0.16	0.64	0.12	0.2	0.2	0.09	0.53	0.89	<0.05	n.a.
Yb	0.18	0.22	2.27	2.71	0.65	1.05	1.05	0.63	1.06	3.84	0.72	1.17	1.24	0.55	3.16	5.32	0.36	n.a.
Lu	0.03	0.03	0.36	0.39	0.10	0.16	0.16	0.09	0.18	0.60	0.10	0.18	0.19	0.08	0.48	0.82	0.06	n.a.

Gr. Am.=granoblastic amphibolite. G-D A=Grt-Di Amphibolite. G-D-H=Grt-Di-Hy Amphibolite. D-A-S=Diopside Amphibolite gneiss. PGDS=Pl-Grt-Di gneiss. O.S.=old samples. Total Fe as FeO. All values are in ppm.

## DANKSAGUNG

Für meine Doktorarbeit schulde ich vielen Menschen einen herzlichen Dank. Zunächst möchte ich ein besonderes Wort des Dankes an meinen Doktorvater, Prof. Dr. **Rainer Altherr**, richten, für die Gelegenheit die er mir gegeben hat meine Doktorarbeit in Deutschland abzuschliessen, sowie an der Gastfreundschaft, Unterstützung und Hilfs- und Gesprächsbereitschaft während meines Aufenthaltes am Institut für Geowissenschaften in Heidelberg.

Anschliessend möchte ich mich bei Prof. Dr. **Boško Lugović** von der Universität Zagreb bedanken, für die Hilfe während der Entwicklung dieser Dissertation, sowie für die mehrjährige wissenschaftliche Zusammenarbeit.

Ein großes Dankeschön geht an Dozentin Dr. **Vesnica Garašić** von der Universität Zagreb für die fachliche Hilfe, Beratung und Erstellung Ihres Gutachtens dieser Dissertation, sowie für die Aufmerksamkeit und Unterstützung in schwierigen Momenten.

Für den tadellosen Betrieb des EMPA- und Röntgenfluoreszenz-Labors geht ein besonderer Dank an Dr. **Hans-Peter Meyer**. Ich bedanke mich an **Alexander Varychev** für seine Geduld, sowie für die Zeit die er genommen hat mich zum Benutzen des SEMs zu belehren. Frau **Ilona Finn** und Herrn **Oliver Wieland** danke ich herzlich für die Herstellung perfekter Dünnschliffpräparate. Danken möchte ich auch Frau **Ilse Glass** für die Zeit, die sie genommen hat, mir die Herstellung von XRF-Präparaten zu erklären. Ein herzlicher Dank geht auch an **Mario Valent**, der unzählige mikroskopische Präparate hergestellt hat, sowie an **Nada Čegec** und **Branka Prša** für die sorgfältige Arbeit an der Trennung.

Den herzlichsten Dank hat Dr. **Elvir Babajić** von der Universität Tuzla verdient, der mir selbstlos während der Feldarbeit geholfen hat, vor allem im organisatorischen und logistischen Sinne.

Ich danke Prof. Dr. **Vladica Cvetković** von der Universität Belgrad für die „fruchtbaren Gespräche“, die mir bei der Ausarbeitung der Abschlussteile dieser Arbeit beträchtlich geholfen haben. Von der Universität Zagreb bedanke ich mich Prof. Dr. **Ivan Dragičević** für die Beratung der Regionalgeologie Bosniens und Prof. Dr. **Goran Durn** für seine Unterstützung.

Von Freunden und Kollegen möchte ich **Sonja** und **Goran** besonders hervorheben. Sonja war immer für mich da und half mir in vieler Hinsicht, vor allem in der Anfangsphase meines Aufenthalts in Deutschland. Mit Goran bin ich durch halb Bosnien gereist, wo ich den Kofferraum seines Autos mit über 200kg Peridotiten beladen habe.

Mein Dank gilt weiterhin **Uroš**, **Marta**, **Ana** und **Alan** für die Unterstützung während der mehrjährigen Zusammenarbeit.

Ich bedanke mich zudem bei allen Mitarbeitern des Institutes für Geowissenschaften in Heidelberg, sowie von der Fakultät für Bergbau, Geologie und Erdöl in Zagreb, wo ich studiert habe und als Lehrkraft tätig bin. Für die finanzielle Unterstützung bedanke ich mich dem Ministerium für Wissenschaft, Bildung und Sport Kroatiens, Deutschen Akademischen Austausch Dienst, sowie auch dem Ministerium für Bildung und Wissenschaft der Föderation Bosnien-Herzegowina.

Nicht zuletzt danke ich meinen **Eltern**, meiner **Schwester** und meiner **Liebe**, die mich stets bestärkt hat, wenn ich an mir gezweifelt habe. Ohne sie gäbe es kein Licht am Ende des Tunnels.





## **EIDESSTATTLICHE ERKLÄRUNG**

Hiermit erkläre ich, Branimir Šegvić, geboren am 08.08.1977 in Zadar, Kroatien, an Eides statt, dass ich die vorgelegte Dissertation selbst verfasst und mich dabei keiner anderen als der von mir ausdrücklich bezeichneten Quellen und Hilfen bedient habe.

Ich, Branimir Šegvić, geboren am 08.08.1977 in Zadar, Kroatien, erkläre zudem an Eides statt, dass ich an keiner anderen Stelle ein Prüfungsverfahren beantragt habe, dass ich die Dissertation nicht in dieser oder anderer Form bereits anderweitig als Prüfungsarbeit verwendet habe und dass ich sie an keiner anderen Fakultät als Dissertation vorgelegt habe.

Heidelberg, den 03.12.2009